Genetic approaches to understand peroxiredoxin-mediated H_2O_2 signalling mechanisms

Zoe Elizabeth Underwood

Thesis submitted for the degree of Doctor of Philosophy

Faculty of Medical Sciences

Institute for Cell and Molecular Biosciences

Newcastle University

September 2018

Declaration

I certify that this thesis contains my own work, except where acknowledged, and that no part of this material has been previously submitted for a degree or any other qualification at this or any other University.

The work in this thesis is also supported by the publications:

Veal EA, Underwood ZE, Tomalin LE, Morgan BA, Pillay CS. Hyperoxidation of Peroxiredoxins: Gain or Loss of Function? *Antioxidants & Redox Signaling* 2018 28(7):574-590.

Tomalin LE, Day AM, Underwood ZE, Smith GR, Dalle Pezze P, Rallis C, Patel W, Dickinson BC, Bahler J, Brewer TF, Chang CJ, Shanley DP, Veal EA. Increasing extracellular H_2O_2 produces a bi-phasic response in intracellular H_2O_2, with peroxiredoxin hyperoxidation only triggered once the cellular H_2O_2-buffering capacity is overwhelmed. *Free Radical Biology & Medicine* 2016 95:333-48.

Acknowledgements

I would firstly like to thank my supervisor, Elizabeth Veal, for her invaluable insight and guidance over the past four years. I would also like to acknowledge the Biotechnology and Biological Sciences Research Council (BBSRC) for funding this research. In addition, I would like to thank my secondary supervisor David Lydall, and my panel Alberto Sanz and Nick Watkins.

I would also like to thank Peter Banks and Adrian Blackburn in the High Throughput Screening Facility at Newcastle University, for use of the robotics and the statistical analysis performed for the SGA and QFA analysis in this thesis. Additionally, I would like to thank Alex Laude in the Bio-Imaging Unit for his expertise and use of the confocal microscope. As well as, Francesco Bruni in the Wellcome Trust Centre for Mitochondrial Research for his advice and supervision in mitochondrial fractionation techniques.

In addition, I would like to thank all the supervisors and members of the Quinn, Veal, Morgan and Whitehall labs, past and present, for discussion and advice throughout this project. Thanks to Alison, Lewis, Johny, Heather, Clare, Anu, Faye M, Pippa, Melanie, Alex, Slava, Callum, Yasmin, Martin and Grace for all of the cake and fun times over the last 4 years. Special thanks to Faye and Hannah for their friendship, support and encouragement throughout.

Finally, thanks to my Mum, Dad, Nan, Grandad, Gran, and my brother Simon, for their continuous love and support and for always believing I could succeed.

Abstract

Hydrogen peroxide (H_2O_2) is a potentially toxic bi-product of aerobic metabolism. Whilst high concentrations cause the cellular damage observed in many diseases and ageing, low levels of H_2O_2 have been shown to be important for normal health and longevity. How organisms sense H_2O_2, and use it to signal positive responses is therefore of great interest. This project focused on using genetic techniques in 2 model eukaryotes, *Schizosaccharomyces pombe* and *Caenorhabditis elegans*, to address these questions and to elucidate mechanisms by which peroxiredoxins (Prx) affect H_2O_2 signal transduction.

We have investigated whether a roGFP2-PRDX-2 fusion protein, expressed in *C. elegans*, was suitable to detect *in vivo* changes in intracellular H_2O_2 levels. Unfortunately, our data suggests that, although this roGFP2-PRDX-2 sensor shows some specificity for H_2O_2, it is insufficiently sensitive to detect small differences in endogenous H_2O_2. However, preliminary data using this sensor does suggest that there is an increase in H_2O_2 in anterior intestinal cells in response to infection with the fungal pathogen, *Candida albicans*.

We have also investigated the role of cytosolic family 2-Cys Prx in mitochondrial function, providing further evidence for mitochondrial defects in *tpx1*Δ mutant *S. pombe*, and *prdx-2*(*gk169*) mutant *C. elegans*, and identifying the presence of a pool of Tpx1 in the mitochondrial intermembrane space (IMS). We present evidence suggesting that a direct role in the IMS may contribute to the function of Tpx1 in H_2O_2 resistance, and H_2O_2-induced activation of Pap1.

The highly abundant 2-Cys Prx detoxify H_2O_2, but are also involved in initiating signal transduction. *S. pombe* has a single 2-Cys Prx, Tpx1, which is essential for transcriptional responses to H_2O_2. Tpx1 has multiple roles in promoting H_2O_2 signal transduction; for example, acting as a direct redox transducer to promote activation of the p38-related MAPK, Sty1, and also by promoting the oxidation of thioredoxins, to activate the transcription factor Pap1. To identify new candidate H_2O_2 regulated proteins, we have used high-throughput genetic screening of a library of mutants of non-essential *S. pombe* genes in two genetic backgrounds; $tpx1^{C169S}$, in which the thioredoxin peroxidase activity of Tpx1 is disrupted, but Sty1 regulation unaffected, and the deletion mutant; *tpx1*Δ.

From synthetic genetic array (SGA) analysis of the *tpx1*^{C169S} mutant we identified 31 candidate genes that are important for growth in the absence of thioredoxin peroxidase activity. Notably, orthologues of 6 of these genes also exhibit a synthetic sick interaction with the Prx mutant *tsa1*Δ in *S. cerevisiae*, suggesting that these pathways may have a conserved essential function in the absence of the thioredoxin peroxidase activity. Moreover, SGA analysis of *tpx1*Δ also identified 21 candidate genes important for growth in a *tpx1*Δ. Interestingly, less overlap was observed between the SGA analysis of *tpx1*Δ with *tsa1*Δ.

Our screening additionally identified 5 candidate genes where loss of function partially suppressed the growth defects associated with loss of *tpx1*. These included the single *S. pombe* cAMP-dependent protein kinase, *pka1*, and the COP9/signalosome complex protease subunit, *csn5*. Here we show that both proteins undergo oxidation, through the formation of direct protein-protein disulphide complexes with Tpx1, in response to 0.2 mM H_2O_2, thereby validating this approach as a means to identify new candidate H_2O_2-regulated proteins.

Finally, this screening identified that the glutaredoxin, Grx1, was important for growth and H_2O_2-dependent activation of Sty1 in *tpx1*^{C169S}-mutant cells. Further investigation suggested that Tpx1^{C169S} is constitutively glutathionylated in the absence of Grx1. This supports the hypothesis that a redox-active peroxidatic cysteine is important for Tpx1's signalling roles, as well as raising the possibility that Tpx1^{C169S} may function as a glutathione peroxidase.

In summary, this study has provided new targets and tools, as well as mechanistic insight, into the role of H_2O_2 and Prx in responses to peroxide.

Contents

List of Figures ..... **xv**

List of Tables ..... **xx**

List of Abbreviations ..... **xxi**

Chapter 1. Introduction **1**

1.1 Reactive Oxygen Species 1

1.1.1 Sources of ROS 1

1.1.2 Antioxidant defences 2

1.1.2.1 Superoxide dismutase 2

1.1.2.2 Catalase 2

1.1.2.3 Glutathione peroxidase 2

1.1.2.4 Thioredoxin peroxidase 3

1.1.2.5 Thioredoxin 3

1.1.2.6 Glutathione 3

1.1.3 Oxidative stress 6

1.1.4 Oxidative stress in ageing 6

1.2 ROS and signal transduction 7

1.2.1 Mechanism of thiol oxidation/disulphide formation 9

1.2.2 H_2O_2 as a signalling molecule 10

1.2.3 Adaptive responses to H_2O_2 11

1.2.4 Positive signalling at low H_2O_2 concentrations 14

1.3 Role of 2-Cys Prx in H_2O_2 sensing and signalling 15

1.3.1 The 3 classes of peroxiredoxins 15

1.3.2 Peroxiredoxins as antioxidants 17

1.3.3 Peroxiredoxins as chaperone proteins 17

1.3.4 Peroxiredoxins as signal transducers 20

1.3.5 Peroxiredoxins promote the oxidation of thioredoxins 22

1.4 Maintaining protein thiol oxidation in subcellular compartments 24

1.4.1 Maintaining protein thiol oxidation in the ER 24

1.4.2 Maintaining protein thiol oxidation in the mitochondria 25

1.4.3 Maintaining protein thiol oxidation in the cytoplasm 26

1.5 Detection of intracellular levels of H_2O_2 *in vivo* 26

1.5.1 The use of HyPer in the detection of *in vivo* levels of H_2O_2 27
1.5.2 The use of roGFP in detection of glutathione redox potential and H_2O_2 28
1.5.3 Improving the specificity of H_2O_2 sensor for *C. elegans* 29
1.6 Summary and Aims 29
1.6.1 *S. pombe* and *C. elegans* as models for investigating H_2O_2 signalling 29
1.6.2 Aims 30
Chapter 2. Materials and Methods 33
2.1 Fission yeast techniques 33
2.1.1 *S. pombe* strains and growth conditions 33
2.1.2 Yeast mating 39
2.1.3 Tetrad dissection 39
2.1.4 Random sporulation 39
2.1.5 Yeast genomic DNA extraction 40
2.1.6 Chemical transformation of DNA into *S. pombe* 40
2.1.7 Cell size analysis 41
2.2 Phenotypic Tests 41
2.2.1 High-throughput genetic screening 41
2.2.1.1 Synthetic Genetic Array (SGA) 41
2.2.1.2 SGA Analysis 42
2.2.1.3 Quantitative Fitness Analysis (QFA) 42
2.2.1.4 QFA Analysis 42
2.2.2 Halo Tests 46
2.2.3 Spot Tests 46
2.3 *C. elegans* Techniques 46
2.3.1 *C. elegans* strains 46
2.3.2 Growth and maintenance of *C. elegans* 47
2.3.3 Treatment of *C. elegans* with exogenous reagents 48
2.3.4 Starvation of *C. elegans* 48
2.3.5 Infection of *C. elegans* with *C. albicans* 48
2.4 Molecular biology techniques 48
2.4.1 Polymerase chain reaction 48
2.4.1.1 PCR to confirm gene deletion strains 49
2.4.1.2 PCR for sequencing 49
2.4.1.3 PCR to confirm mating type 49
2.4.1.4 PCR amplification of natMX6 cassette 49

2.4.1.5 Amplification of IMS targeting sequence 50
2.4.2 Oligonucleotide primer sequences 50
2.4.3 Agarose gel electrophoresis 52
2.4.4 DNA extraction 53
2.4.5 DNA sequencing 53
2.4.6 Bacterial growth conditions and transformations 53
2.4.7 Plasmid DNA extraction 53
2.4.8 Cloning an IMS targeting sequence into pRep1Tpx1 53
2.4.8.1 Restriction endonuclease digestion, phosphatase treatment and DNA ligation reactions 53
2.4.8.2 SURE competent cell transformation 54
2.4.8.3 Checking transformation colonies 54
2.5 Protein Analysis 56
2.5.1 Examination of levels of Sty1 phosphorylation in *S. pombe* 56
2.5.2 Preparation of whole cell lysates 56
2.5.2.1 Protein oxidation analysis using NEM and AMS 56
2.5.2.2 Protein oxidation analysis of glutathionylated residues 57
2.5.2.3 Protein oxidation using IAA (Pap1 oxidation assay) 58
2.5.3 Mitochondrial Isolation and Subfractionation 58
2.5.3.1 Isolation of *S. pombe* mitochondria 58
2.5.3.2 Subfractionation of *S. pombe* mitochondria 60
2.5.4 SDS-PAGE and Western blotting 60
2.6 Microscopy 62
2.6.1 Fluorescence microscopy 62
2.6.1.1 *S. pombe* cell size, morphology and nuclei staining 62
2.6.1.2 Examination of *C. elegans* by fluorescent microscopy 62
2.6.2 Confocal microscopy 62
2.6.2.1 Imaging mitochondria and Pap1 in *S. pombe* 63
2.6.2.2 Imaging mitochondria in *C. elegans* 63
2.6.2.3 Measurement of roGFP2 oxidation in *C. elegans* 63
2.7 Experimental replication 64
Chapter 3. Validation of the N-roGFP2::*prdx-2* genetic *in vivo* H_2O_2 sensor to detect endogenous changes in intracellular H_2O_2 65
3.1 Introduction 65
3.2 Results 67

3.2.1 N-roGFP2::*prdx-2* and C-roGFP2::*prdx-2* reporters are expressed in the cytosol, whereas the C-roGFP2::*prdx-3* reporter has mitochondrial expression.....67

3.2.2 Maintenance at different temperatures did not affect the oxidation/reduction ratio of N-roGFP2::*prdx-2* in the anterior intestine.....68

3.2.3 The oxidation of N-roGFP2::*prdx-2* is specific for H_2O_2.....71

3.2.4 Treatment with 1 or 5 mM extracellular H_2O_2 causes an increase in the oxidation/reduction ratio of N-roGFP2::*prdx-2* in the anterior intestine 73

3.2.5 Starvation of *C. elegans* did not affect the oxidation/reduction ratio of N-roGFP2::*prdx-2* in the anterior intestine.....75

3.2.6 Consistent differences in the oxidation/reduction ratio of N-roGFP2::*prdx-2* could not be detected between larval stages.....77

3.2.7 Exposure to the fungal pathogen *C. albicans* causes an increase in the oxidation/reduction ratio of N-roGFP2::*prdx-2* in the anterior intestine 79

3.3 Discussion 81

Chapter 4. Investigating the role of cytosolic family 2-Cys Prx in mitochondrial function 85

4.1 Introduction 85

4.2 Results 86

4.2.1 *tpx1*Δ mutant *S. pombe* and *prdx-2(gk169)* mutant *C. elegans* have mitochondrial defects 86

4.2.1.1 *prdx-2(gk169) C. elegans* have fragmented mitochondria compared with wild-type *C. elegans* 86

4.2.1.2 *tpx1*Δ mutant *S. pombe* have reduced growth on non-fermentable carbon source 88

4.2.2 Pap1 is localised to the mitochondria and this localisation is dependent on the presence of Tpx1 in *S. pombe*.....89

4.2.2.1 Tpx1 and Pap1 are localised to *S. pombe* mitochondrial intermembrane space.....89

4.2.2.2 Pap1 requires Tpx1 for mitochondrial localisation.....94

4.2.2.3 The Tpx1 resolving cysteine (169) is not required for Tpx1 or Pap1 localisation to the mitochondria.....96

4.2.3 From confocal microscopy analysis it is unclear whether Pap1 is localised to the mitochondria and whether this localisation is dependent on the presence of Tpx1 98

4.2.4 Targeting Tpx1 to the mitochondrial intermembrane space can rescue the growth, and H_2O_2 resistance of *tpx1*Δ mutant *S. pombe* cells 100

4.2.4.1 Targeting a low level of Tpx1 to the mitochondrial intermembrane space can rescue the growth of *tpx1*Δ mutant *S. pombe* cells on minimal media.....100

4.2.4.2 Targeting Tpx1 to the mitochondrial intermembrane space can rescue the H_2O_2 resistance of *tpx1*Δ mutant *S. pombe* cells 103

4.2.4.3 The targeting of *S. cerevisiae* Gpx3 to the mitochondrial intermembrane space does not rescue the growth of *tpx1*Δ mutant *S. pombe* cells 105

4.3 Discussion 107

Chapter 5. High through-put genetic screening of *tpx1* mutants revealed new candidate H_2O_2 regulated proteins 111

5.1 Introduction 111

5.2 Results 112

5.2.1 SGA analysis of the peroxidase defective $tpx1^{C169S}$ *S. pombe* identified 31 genes important for growth in $tpx1^{C169S}$ 112

5.2.1.1 Construction of nourseothricin-resistant $tpx1^{+}$, $tpx1^{C169S}$ and *tpx1*Δ strains 112

5.2.1.2 Nourseothricin-resistance is closely linked to the $tpx1^{C169S}$ mutation 115

5.2.1.3 Replacing the *leu2* gene with a natMX6 cassette had no effect on the growth or H_2O_2 sensitivity of $tpx1^{+}$ and $tpx1^{C169S}$ strains 116

5.2.1.4 SGA analysis identified 31 candidate genes important for growth when the Tpx1 peroxidase activity is removed 117

5.2.2 QFA analysis of the peroxidase defective $tpx1^{C169S}$ *S. pombe* 121

5.2.2.1 Cells required a 16 h dilution period to reach exponential growth phase. 121

5.2.2.2 The conditions of 500 µM H_2O_2, 750 µM H_2O_2 and 250 µM tBOOH were chosen for the detection of sensitivity suppressors 123

5.2.2.3 QFA identified 26 gene mutants as putative suppressors of the $tpx1^{C169S}$ H_2O_2 sensitivity phenotype 126

5.2.2.4 Reconstruction of 7 of these strains revealed that the suppression of H_2O_2 stress sensitivity was not caused by the candidate gene 130

5.2.2.5 Increased resistance of 3 isolates of $tpx1^{C169S}cgi121\Delta$ was caused by the loss of the C169S point mutation in $tpx1^{+}$ 134

5.2.2.6 Estimating the rate of loss of the $tpx1^{C169S}$ mutation 136

5.2.2.7 Median QFA revealed an additional 15 candidate genes as suppressors of the H_2O_2 sensitivity of $tpx1^{C169S}$ 137

5.2.2.8 Reconstruction of the $tpx1^{C169S}arg4\Delta$ strain revealed the suppression of $tpx1^{C169S}$ H_2O_2 sensitivity was not due to the deletion of *arg4* 138

5.2.2.9 H_2O_2 resistance of the $tpx1^{C169S}cgi121\Delta$ isolate 4 strain does not follow the deletion of *cgi121* 139

5.2.2.10 Pap1 oxidation in response to 0.2 mM H_2O_2 is restored in the $tpx1^{C169S}cgi121^{+}$ strain 141

5.2.2.11 Identification of $tpx1^{C169S}$-containing strains with increased H_2O_2 resistance despite absence of H_2O_2-inducible Pap1 oxidation 146

5.2.3 SGA analysis of *tpx1*Δ identified candidate H_2O_2 regulated proteins.....152
5.2.3.1 Replacing *ura4*$^+$ with a nat(MX6) cassette has no effect on growth of *tpx1*Δ strain.....152
5.2.3.2 SGA analysis of *tpx1*Δ identified candidate genes important for the growth of *tpx1*Δ.....153
5.2.3.3 SGA analysis of *tpx1*Δ identified candidate genes that suppressed the growth defect of *tpx1*Δ.....156
5.2.3.4 Ten of the double mutants generated from *tpx1*Δ SGA analyses suppressed the growth defect and H_2O_2 sensitivity of *tpx1*Δ.....160
5.2.3.5 Deletion of five of the candidate genes suppressed the growth defect, and H_2O_2 sensitivity, of *tpx1*Δ when manually re-crossed.....161
5.2.4 Investigating whether Pka1 is regulated by H_2O_2/Tpx1.....165
5.2.4.1 Investigating the genetic interaction of *tpx1* and *pka1*.....165
5.2.4.2 Investigating whether Pka1 undergoes oxidation in response to 0.2 mM H_2O_2, and whether this is via interaction with Tpx1.....171
5.2.5 Investigating whether Csn5 is regulated by H_2O_2/Tpx1.....177
5.2.5.1 Investigating the genetic interaction of *csn5* and *tpx1*.....177
5.2.5.2 Investigating whether Csn5 undergoes oxidation in response to 0.2 mM H_2O_2, and whether this is via interaction with Tpx1.....179
5.3 Discussion.....187
Chapter 6. *Grx1* is important for the growth and signalling of *tpx1*^{C169S}.....197
6.1 Introduction.....197
6.2 Results.....198
6.2.1 Deletion of *grx1* in a *tpx1*^{C169S} reduces cell viability, growth, and affects cell morphology.....198
6.2.1.1 Deletion of *grx1* in a *tpx1*^{C169S} is synthetic lethal.....198
6.2.1.2 The *tpx1*^{C169S}*grx1*Δ has morphological defects compared to *tpx1*$^+$, *tpx1*^{C169S} and *grx1*Δ cells.....199
6.2.1.3 The *tpx1*^{C169S}*grx1*Δ has reduced growth compared to *tpx1*^{C169S} and *grx1*Δ.....201
6.2.2 Deletion of *grx1* affects the signalling of *tpx1*^{C169S}.....202
6.2.2.1 Deleting *grx1* in a *tpx1*^{C169S} strain removes the ability of Pap1 and Tpx1 to form high molecular weight complexes.....202
6.2.2.2 The *tpx1*^{C169S}*grx1*Δ strain is resistant to tBOOH-induced hyperoxidation of the Tpx1 peroxidatic cysteine.....205
6.2.2.3 Detection of a glutathionylated residue by SDS-PAGE separation.....207
6.2.2.4 Deleting *grx1* removes *tpx1*^{C169S} ability to support H_2O_2-dependent activation of the Sty1 MAPK.....209

6.3 Discussion 212
Chapter 7. Final Discussion 215
7.1 Summarising key findings from this study 215
7.2 Future perspectives 217
7.3 Concluding remarks 219
Bibliography 221

List of Figures

Figure 1.1 ROS detoxification enzymes 5
Figure 1.2 Concentration-dependent biological effects of H_2O_2 8
Figure 1.3 Cysteine thiol oxidation 9
Figure 1.4 Adaptive responses to different concentrations of H_2O_2 in *S. pombe* 13
Figure 1.5 Mechanism of peroxiredoxins 16
Figure 1.6 Proposed roles for Prx hyperoxidation: H_2O_2 signalling, thioredoxin activity and increased chaperone activity 19
Figure 1.7 Peroxiredoxins as signal transducers 21
Figure 1.8 Tpx1 promotes the oxidation of Txl1 23
Figure 2.1 SGA and QFA Methodology 45
Figure 2.2 Cloning an IMS targeting sequence into pRep1Tpx1 55
Figure 3.1 Mechanism of the N-roGFP2::*prdx-2* as a H_2O_2 sensor 66
Figure 3.2 N-roGFP2::*prdx-2*, C-roGFP2::*prdx-2* and C-roGFP2::*prdx-3* reporters are expressed in multiple *C. elegans* tissues 67
Figure 3.3 Effect of temperature, NEM and H_2O_2 treatment on the ratio of roGFP2^{ox}/roGFP2^{red} in anterior intestinal cells 70
Figure 3.4 5 mM H_2O_2 significantly increased the ratio of roGFP2^{ox}/roGFP2^{red}, whereas treatment with diamide, or DTT did not alter the ratio of roGFP2^{ox}/roGFP2^{red} relative to NEM 72
Figure 3.5 Exposure to 1 or 5 mM extracellular H_2O_2 was required to cause an increase in the ratio of roGFP2^{ox}/roGFP2^{red} in anterior intestinal cells, relative to NEM 74
Figure 3.6 Fasting for up to 8 hours did not alter the ratio of roGFP2^{ox}/roGFP2^{red} in anterior intestinal cells 76
Figure 3.7 No consistent qualitative differences were observed between *C. elegans* expressing N-roGFP2::*prdx-2* at different larval stages 78
Figure 3.8 A substantial increase in the ratio of roGFP2^{ox}/roGFP2^{red} was detected in anterior intestinal cells following 24 h infection with the fungal pathogen *Candida albicans*, compared with *E. coli* 80
Figure 4.1 The effect of loss of PRDX-2 on mitochondrial morphology compared with wild-type *C. elegans* 87

Figure 4.2 Growth of wild-type and *tpx1*Δ mutant on fermentable and non-fermentable carbon sources 88
Figure 4.3 Tpx1 and Pap1 co-purify with mitochondria 90
Figure 4.4 Tpx1 and Pap1 are present in the mitochondrial intermembrane space 92
Figure 4.5 Pap1 requires Tpx1 for mitochondrial localisation. 95
Figure 4.6 Effect of substitution of resolving cysteine of Tpx1 on the mitochondrial pools of Tpx1 and Pap1 97
Figure 4.7 Confocal microscopy analysis of wild type and *tpx1*Δ *S. pombe* expressing RFP-tagged Cox4 and GFP-tagged Pap1 99
Figure 4.8 The effect of expression of wild-type and IMS-targeted Tpx1 on the growth of wild-type and *tpx1*Δ mutant *S. pombe* 102
Figure 4.9 Targeting Tpx1 to the mitochondria increased H_2O_2 resistance of *tpx1*Δ cells. 104
Figure 4.10 Spot test analysis of the growth and H_2O_2 resistance of $tpx1^+$ or *tpx1*Δ cells with and without targeting *S. cerevisiae* Gpx3 to the mitochondria 106
Figure 5.1 Construction of nourseothricin-resistant $tpx1^+$ (ZU10), $tpx1^{C169S}$ (ZU11) [A] and *tpx1*Δ (ZU12) [B] strains 114
Figure 5.2 The nourseothricin-resistant phenotype is closely linked to sensitivity to H_2O_2 115
Figure 5.3 Replacing the *leu2* gene with a natMX6 cassette did not have a significant effect on the growth or H_2O_2 sensitivity of $tpx1^+$ and $tpx1^{C169S}$ strains 116
Figure 5.4 Fitness of the Bioneer deletion library crossed with $tpx1^+$ (x-axis) plotted against the fitness of the Bioneer deletion library crossed with $tpx1^{C169S}$ mutation (y-axis) from SGA replicate 1 118
Figure 5.5 Fitness of the Bioneer deletion library crossed with $tpx1^+$ (x-axis) plotted against the fitness of the Bioneer deletion library crossed with $tpx1^{C169S}$ mutation (y-axis) from SGA replicate 2 119
Figure 5.6 Growth curves and corresponding spot tests of 7 *S. pombe* single deletion strains from library plate 1 (Bioneer) generated following a 16 h dilution period in liquid culture in a test run 122
Figure 5.7 Fitness graphs generated from the $tpx1^{C169S}$ QFA test screen using 250 µM H_2O_2, 500 µM H_2O_2, 750 µM H_2O_2, 500 µM tBOOH and 750 µM tBOOH stress conditions 125

Figure 5.8 Example QFA graph: comparison of the fitness of 384 strains (library plate 5) of the *tpx1*^{C169S} SGA in the presence or absence of 500 µM H_2O_2.....126
Figure 5.9 Example halo test: SGA generated strains with increased and reduced resistance to H_2O_2 compared with the *tpx1*^{C169S} (ZU11) starting strain.....128
Figure 5.10 Halo test analysis of SGA-generated strains [A and D], as well as halo test and spot test analysis of isogenic strains (in purple) generated from manually re-crossing *tpx1*^{C169S} with *uds1*Δ [B and C], or *hsr1*Δ [E and F] 131
Figure 5.11 Halo test and spot test analysis of all 4 isolates of SGA-generated *tpx1*^{C169S}*cgi121*Δ [A and B], as well as a halo test performed on isogenic strains (in purple) generated from re-crossing *cgi121*Δ (Bioneer) with *tpx1*^{C169S} (ZU11) [C].....133
Figure 5.12 Amplification of *tpx1* by PCR using a primer directed to an nmtend sequence as an indication of genotype 135
Figure 5.13 Spot test analysis performed on isogenic strains (tetrad in purple) generated from manually crossing *tpx1*^{C169S} (ZU11) with *arg4*Δ (Bioneer) with and without H_2O_2 139
Figure 5.14 Analysis of the H_2O_2 resistance of the *tpx1*^{C169S}*cgi121*$^{+}$ (ZU30) strain 141
Figure 5.15 Analysis of Tpx1 and Pap1 oxidation in the *tpx1*^{C169S}*cgi121*$^{+}$ (ZU30) strain 142
Figure 5.16 Effect of loss of Txl1 on the [A] H_2O_2 resistance and [B] H_2O_2-induced oxidation of Pap1 in tpx1^{C169S} mutant cells 144
Figure 5.17 Analysis of the oxidation of Tpx1 and Pap1 in the *tpx1*^{C169S}*cgi121*$^{+}$ (ZU30) strain.....145
Figure 5.18 Analysis of the oxidation of Pap1 and Tpx1 in H_2O_2-resistant isolates identified by screen.....149
Figure 5.19 Spot test analysis on the H_2O_2 resistant strains that retained the C169S mutation. [A] Spot test analysis of the 5 strains predicted to have increased H_2O_2 resistance and retained the C169S mutation.....151
Figure 5.20 Spot test analysis of the growth of *tpx1*Δ (VXOO) and nourseothricin-resistant *tpx1*Δ (ZU12).....153
Figure 5.21 Fitness of the Bioneer deletion library crossed with the first *tpx1*Δ SGA (y-axis), compared to the fitness of the Bioneer deletion library crossed with the *tpx1*$^{+}$ wild-type strain *ura1* (x-axis).....154

Figure 5.22 Fitness of the Bioneer deletion library crossed with the first *tpx1*Δ SGA (y-axis), compared to the fitness of the Bioneer deletion library crossed with the *tpx1*$^{+}$ wild-type strain *ura1* (x-axis) 157
Figure 5.23 Fitness of the Bioneer deletion library crossed with the second *tpx1*Δ SGA (y-axis), compared to the fitness of the Bioneer deletion library crossed with the *tpx1*$^{+}$ wild-type strain *ura1* (x-axis) 158
Figure 5.24 Spot test analysis of the 9 strains identified from the *tpx1*Δ SGA suppressor analysis 160
Figure 5.25 Spot test analysis of the 5 re-crossed suppressor strains to compare growth 162
Figure 5.26 Spot test analysis of the 5 re-crossed suppressor strains to compare H_2O_2 resistance 164
Figure 5.27 Growth curve [A] and spot test [B] analysis of isogenic strains (tetrad in purple) generated from manually crossing *tpx1*Δ (ZU12) with *pka1*Δ 168
Figure 5.28 Analysis of H_2O_2 resistance of isogenic strains generated from manually crossing *tpx1*Δ (ZU12) with *pka1*Δ (Bioneer) 170
Figure 5.29 H_2O_2 does not affect the mobility of Myc-tagged Pka1 172
Figure 5.30 Overexpression of Tpx1, or the trapping mutant Tpx1^{C169S}, promoted H_2O_2 induced oxidation of Pka1 174
Figure 5.31 Pka1 forms a mixed disulphide with Tpx1 in response to 0.2 mM H_2O_2 176
Figure 5.32 Growth curve [A] and spot test [B and C] analysis of strains revealed that deleting *csn5* in a *tpx1*Δ may slightly improve growth and H_2O_2 resistance 178
Figure 5.33 High molecular weight oxidised forms of endogenous Csn5 were detected following exposure to 0.2 mM H_2O_2 180
Figure 5.34 Overexpression of Tpx1, or the trapping mutant Tpx1^{C169S}, promoted H_2O_2 induced oxidation of Csn5 182
Figure 5.35 Csn5 forms a mixed disulphide with Tpx1 in response to 0.2 mM H_2O_2 184
Figure 5.36 H_2O_2 induced oxidation of Csn1 was not detected with endogenous levels of Tpx1, or with overexpression of Tpx1 or the trapping mutant Tpx1^{C169S} 186
Figure 5.37 Predicted model of the regulation of Pka1 by Tpx1. 191
Figure 5.38 Multiple sequence alignment of the orthologues of cAMP-dependent protein kinase: Pka1 (*S. pombe*), TPK1, TPK2, TPK3 and BCY1 (*S. cerevisiae*) and PRKACA (human) 193

Figure 5.39 Multiple sequence alignment of the orthologues of COP9 signalosome complex protease subunit 5: Csn5 (*S. pombe*), RRI1 (*S. cerevisiae*) and COPS5 (human) 196
Figure 6.1 Morphology of *tpx1*$^{+}$, *tpx1*^{C169S}, *grx1*Δ and *tpx1*^{C169S}*grx1*Δ cells 200
Figure 6.2 Loss of *grx1* reduced the viability of *tpx1*^{C169S} strain.....201
Figure 6.3 A short exposure [A] and long exposure [B] of the western blot analysis of Pap1 and Tpx1 oxidation in *tpx1*^{C169S}*grx1*Δ strains in response to 0.2 mM H_2O_2 204
Figure 6.4 Western blot analysis of Tpx1 and hyperoxidised Tpx1 in *tpx1*^{C169S}*grx1*Δ strains in response to 1 mM tBOOH.....206
Figure 6.5 Detection of a glutathionylated residue by SDS-PAGE separation 208
Figure 6.6 Western blot analysis of Sty1 phosphorylation in *tpx1*^{C169S}*grx1*Δ strains compared with *tpx1*$^{+}$ or *tpx1*^{C169S} in response to 6 mM H_2O_2.....211

List of Tables

Table 2.1 *S. pombe* strains used in this study 39
Table 2.2 Plasmids used in this study 41
Table 2.3 *C. elegans* strains used in this study 47
Table 2.4 *E. coli* strains used in this study 48
Table 2.5 *C. albicans* strain used in this study 48
Table 2.6 Oligonucleotide primers used in this study 52
Table 2.7 Antibodies used in this study 62
Table 5.1 Gene names and descriptions for the 31 candidate genes with the highest negative GIS from 2 independent *tpx1*^{C169S} SGA screens 120
Table 5.2 The 26 SGA strains that displayed higher H_2O_2 resistance by halo test, compared with the *tpx1*^{C169S} (ZU11) starting strain 129
Table 5.3 Estimation of the potential 'reversion rate' of *tpx1*^{C169S}*mug134*Δ strains to wild-type *tpx1*$^{+}$ 136
Table 5.4 Median suppressor analysis of the *tpx1*^{C169S} QFA generated an additional 15 candidate genes predicted to contribute (upon deletion) to the H_2O_2 sensitivity of the *tpx1*^{C169S} (ZU11) 138
Table 5.5 Growth analysis of spores from backcrossing the *tpx1*^{C169S}*cgi121*Δ isolate 4 (ZU24) with *tpx1*^{C169S} (ZU11) 140
Table 5.6 Gene names and descriptions for the 21 candidate genes that enhance the *tpx1*Δ growth defect (highest negative GIS) 155
Table 5.7 Gene names and descriptions of the 8 candidate genes which consistently suppressed the growth defect of *tpx1*Δ 159
Table 5.8 Genotype analysis of 26 tetrads generated from re-crossing *tpx1*Δ (ZU12) with *pka1*Δ (Bioneer) 166
Table 6.1 Analysis of the ability to form a colony and genotype of 10 dissected tetrads from a cross between *tpx1*^{C169S} and *grx1*Δ 198

List of Abbreviations

Ade	Adenine
Amp	Ampicillin
AMS	4-acetamido-4’-maleimidylstilbene-2,2’-disulphonic acid
AP	Alkaline phosphatase
AP-1	Activating protein-1
ASK1	Apoptosis signal-regulating kinase
Atf1	Activating transcription factor 1
ATP	Adenosine triphosphate
BHI	Brain Heart Infusion
β-me	β-mercaptoethanol
Bp	Base pair
BSA	Bovine serum albumin
bZIP	Basic leucine zipper
C. albicans	*Candida albicans*
C. elegans	*Caenorhabditis elegans*
cAMP	Cyclic adenosine monophosphate
cpYFP	Circularly permutated yellow fluorescent protein
Crm1	Chromosome region maintenance 1
Cu	Copper
Cys	Cysteine
Cys-SH	Reduced cysteine
Cys-SOH	Cysteine sulphenic acid
Cys-SO_2H	Cysteine sulphinic acid
Cys-SO_3H	Cysteine sulphonic acid
°C	Degrees Celsius
Δ	Gene deletion
D. melanogaster	*Drosophila melanogaster*
DAPI	4’,6-diamidino-2-phenylindole

DIC	Differential Interference Contrast
DMSO	Dimethyl sulphoxide
DNA	Deoxyribonucleic acid
dNTP	Deoxyribonucleotide triphosphate
DTT	Dithiothreitol
DUOX	Dual oxidase
E. coli	*Escherichia coli*
EDTA	Ethylenediaminetetraacetic acid
EGTA	Ethylene glycol-bis(2-aminoethylether)-N,N,N’,N’-tetraacetic acid
EMM	Edinburgh minimal media
EMM1/2G	Edinburgh minimal media with half glutamate
ER	Endoplasmic reticulum
Ero1	ER oxidoreductin 1
ETC	Electron transport chain
EtOH	Ethanol
FAD	Flavin adenine dinucleotide
Fe	Iron
g	Gram
GAPDH	Glyceraldehyde-3-phosphate dehydrogenase
gDNA	Genomic DNA
GIS	Genetic Interaction Score
GFP	Green fluorescent protein
Gpx	Glutathione peroxidase
Grx	Glutaredoxin
GSH	Reduced glutathione
GSSG	Oxidised glutathione dimer
GST	Glutathione-*S*-transferase
H_2O	Water
H_2O_2	Hydrogen peroxide
HB	Homogenization buffer

HMW	High molecular weight
HO·	Hydroxyl radicals
HRP	Horseradish peroxidase
Hsp	Heat shock protein
HTSF	High Throughput Screening Facility
IAA	Iodoacetamide
IGF-1	Insulin-like growth factor 1
IMM	Inner mitochondrial membrane
IMS	Intermembrane space
IPTG	Isopropyl β-D-1-thiogalactopyranoside
JNK	c-Jun N-terminal kinase
Kan	Kanamycin
Kb	Kilobase
kDa	Kilodalton
LB	Luria broth
Leu	Leucine
LiAc	Lithium Acetate
M	Molar
MAP	Mitogen activated protein
MAPK	Mitogen activated protein kinase
MAPKKK	Mitogen activated protein kinase kinase kinase
MeOH	Methanol
MFRTA	Mitochondrial Free Radical Theory of Ageing
$MgCl_2$	Magnesium chloride
MIA	Mitochondrial intermembrane space assembly machinery
µg	Microgram
µl	Microlitre
µM	Micromolar
mg	Milligram
mM	Millimolar

Min(s)	Minute(s)
Mn	Manganese
MP	Mitoplast
mRNA	Messenger RNA
MTS	Mitochondrial targeting sequence
mtUPR	Mitochondrial unfolded protein response
MW	Molecular weight
Mxr1	Methionine sulfoxide reductase
N_2	Liquid nitrogen
Na_2CO_3	Sodium carbonate
Na_3VO_4	Sodium vanadate
NAC	*N*-acetyl cysteine
NaCl	Sodium chloride
NADPH	Nicotinamide adenine dinucleotide phosphate
NAF	Sodium fluoride
NAT	Nourseothricin
NEM	*N*-Ethylmaleimide
NES	Nuclear export signal
NGM-L	Nematode Growth Media-Lite
NLS	Nuclear Localisation Signal
nm	Nanometer
nM	Nanomolar
Nox	NADPH oxidase
O_2	Molecular oxygen
$O_2{\cdot}^-$	Superoxide anion
OD	Optical Density
OM	Outer membrane
Orp1	Oxidant receptor peroxidase-1
Ox	Oxidation
OxICAT	Oxidative isotope-coded affinity tags

PAGE	Polyacrylamide gel electrophoresis
Pap1	*Pombe* AP-1 like
PBS	Phosphate-buffered saline
PCR	Polymerase Chain Reaction
PDI	Protein disulphide isomerase
PEG	Polyethylene glycol
PerR	Peroxide regulon repressor
Pf3-Ac	Acetylated peroxyflour-3
PLB	*Pombe* lysis buffer
PMSF	Phenylmethylsulfonyl fluoride
PRDX-2	Peroxiredoxin-2
Prx	Peroxiredoxin
PTEN	Phosphatase and tensin homolog
PTP	Protein tyrosine phosphatase
QFA	Quantitative Fitness Analysis
Red	Reduction
RFP	Red Fluorescent Protein
RNA	Ribonucleic acid
RNR	Ribonucleotide reductase
roGFP	Reduction-oxidation GFP
ROS	Reactive oxygen species
rpm	Revolutions per minute
S. cerevisiae	*Saccharomyces cerevisiae*
S. pombe	*Schizosaccharomyces pombe*
SDS	Sodium dodecyl sulphate
SGA	Synthetic Genetic Array
SH	Thiol
S^-	Thiolate
SM	Shaved mitochondria
SO^-	Sulphenate group

SO_2^-	Sulphinate group
SO_3^-	Sulphonate group
SOD	Superoxide dismutase
Srx	Sulfiredoxin
ssDNA	Salmon sperm DNA
STAT3	Signal transducer and activator of transcription 3
Str	Streptomycin
t-BOOH	*tert*-butyl hydroperoxide
TBST	Tris-buffered saline tween
TCA	Tricholoracetic acid
TE	Tris-EDTA
TF	Transcription factor
TIM	Translocase of the inner mitochondrial membrane
TOM	Translocase of the outer membrane
Tpx	Thioredoxin peroxidase
Trr	Thioredoxin reductase
Trx	Thioredoxin
Txl	Thioredoxin-like protein
Tyr	Tyrosine
Ura	Uracil
UV	Ultraviolet
VEGFR	Vascular endothelial growth factor receptor
v/v	Volume/volume
WT	Wild-type
w/v	Weight/volume
Yap1	Yeast AP-1
YE5S	Yeast extract media with five supplements
Zn	Zinc
1-Cys Prx	1-cysteine peroxiredoxin
2-Cys Prx	2-cysteine peroxiredoxin

Chapter 1

Chapter 1. Introduction

1.1 Reactive Oxygen Species

Reactive oxygen species (ROS) are formed by the incomplete reduction of oxygen, and are an unavoidable by-product of many cellular processes. ROS are highly reactive and cause cell damage by reacting indiscriminately with cellular components, such as: DNA, lipids and proteins (Halliwell, 1999). High levels of ROS have been associated with the pathology of many different diseases, and the ageing process (Bokov *et al.*, 2004). Cells therefore possess ROS detoxifying enzymes and defences in order to maintain intracellular ROS homeostasis. The ability of ROS to also act as signalling molecules has recently been recognised and has led to an exciting field of research in redox signalling. The upregulation of anti-oxidant gene expression in response to high levels of ROS has been well studied in many organisms (D'Autréaux and Toledano, 2007). This has led to the identification of proteins vital for sensing low levels of ROS, as well as downstream redox signalling pathways. Intriguingly, low levels of ROS can initiate a number of beneficial effects that are important for normal health and longevity (Sanz, 2016).

1.1.1 Sources of ROS

The incomplete reduction of oxygen leads to the formation of the highly reactive, ROS: the superoxide anion (O_2^-), hydrogen peroxide (H_2O_2) and the hydroxyl radical ($HO^{\cdot}$). The largest contributor of O_2^- production in the cell is from the mitochondria, particularly from complex I and III of the electron transport chain (ETC) (Brand, 2010). Electrons released during adenosine triphosphate (ATP) production reduce molecular oxygen to generate the highly volatile O_2^-. In addition, O_2^- is also produced by nicotinamide adenine dinucleotide phosphate (NADPH) oxidases as a host defence mechanism (Holmström and Finkel, 2014). O_2^- is highly unstable and the superoxide dismutase (SOD) enzyme quickly converts O_2^- to the more stable hydrogen peroxide molecule (H_2O_2). In the presence of metal ions, H_2O_2 is reduced to $HO^{\cdot}$ by metal-catalysed Fenton chemistry (Imlay, 2003). $HO^{\cdot}$ is highly reactive and indiscriminate with its targets. ROS are also produced endogenously by a large number of enzymes, such as: lipoxygenase, xanthine oxidase, cyclooxygenase, cytochrome P450 monooxygenase and nitric oxide synthase (D'Autréaux and Toledano, 2007). As well as during oxidative protein folding in compartments such

as the endoplasmic reticulum (ER). Exogenous sources of ROS also contribute to ROS levels within the cell, such as exposure to xenobiotics and UV radiation (Halliwell, 2007).

1.1.2 Antioxidant defences

In order to prevent the damage caused by high levels of ROS, cells possess a number of mechanisms in order to maintain intracellular ROS homeostasis. These can be separated into two categories: ROS detoxifying enzymes, and non-enzymatic ROS scavengers. ROS detoxifying enzymes consist of: superoxide dismutase, catalase and thiol peroxidases (glutathione peroxidase and thioredoxin peroxidase) (figure 1.1). In addition, glutathione, and thioredoxins, act as important electron donors to the thiol peroxidases. Other non-enzymatic antioxidants include vitamin C (ascorbic acid) or vitamin E (Evans and Halliwell, 2001).

1.1.2.1 Superoxide dismutase

SOD converts two O_2^- to the more stable H_2O_2, and oxygen (O_2). SOD is the most powerful antioxidant in the cell and is expressed at high concentrations. There are various forms of SOD, dependent on the type of metal ion required as a cofactor for its activity (iron (Fe), zinc (Zn), copper (Cu) and manganese (Mn)). Eukaryotes express Mn-SOD in the mitochondria, and ubiquitously express Cu/Zn-SOD in the cytosol (Fridovich, 1995; Ighodaro and Akinloye, 2017).

1.1.2.2 Catalase

Catalase is a large, abundant and ubiquitously expressed protein found in all living tissues, that requires iron or manganese as a cofactor for its activity. Catalase breaks down the H_2O_2 formed by SOD, into water (H_2O) and O_2. Catalase is highly efficient and mainly present in the peroxisomes of cells (Chelikani *et al.*, 2004). Interestingly, catalase is not present in the mitochondria of mammalian cells indicating that the conversion of H_2O_2 to H_2O is performed by alternate enzymes, such as glutathione peroxidases or mitochondrial peroxiredoxins (Ighodaro and Akinloye, 2017).

1.1.2.3 Glutathione peroxidase

Glutathione peroxidases (GPx) are highly abundant, ubiquitous enzymes which reduce H_2O_2 to H_2O (Góth *et al.*, 2004). In addition, phospholipid hydroperoxide Gpxs also have an important role in preventing the lipid peroxidation process by breaking down lipid

peroxides (Gill and Tuteja, 2010). Gpx possess a thioredoxin fold domain and act as an oxidoreductase by being coupled to glutathione, glutathione reductase and NADPH (figure 1.1C) (Ighodaro and Akinloye, 2017; Brigelius-Flohé and Maiorino, 2013).

1.1.2.4 Thioredoxin peroxidase

Thioredoxin peroxidases, also known as peroxiredoxins, also reduce H_2O_2 to H_2O, but utilise thioredoxin as a reductant. Peroxiredoxins are highly abundant (accounting for up to 1% of soluble cellular proteins) and have a high affinity for H_2O_2, providing an important barrier against increases in intracellular H_2O_2 levels (Chae *et al.*, 1999). Peroxiredoxins are coupled to thioredoxin, as well as thioredoxin reductase, and NADPH (figure 1.1B). In addition, peroxiredoxins have also been shown to possess chaperone activity (Jang *et al.*, 2004).

1.1.2.5 Thioredoxin

Thioredoxin is a small (~12 kDa) broad specificity oxidoreductase. Thioredoxins have 2 conserved cysteine residues at the active site motif (CGPC), and have a 'thioredoxin fold' structure (Eklund *et al.*, 1991). There are also many thioredoxin-like proteins and proteins with thioredoxin-like domains (CXXC) which have yet to be characterised (Nakao *et al.*, 2015). Thioredoxins reduce the disulphide bonds of a wide range of substrates, and are subsequently reduced and recycled by thioredoxin reductases, utilising electrons from NADPH (Pan and Bardwell, 2006). Thioredoxin is critical for many cellular processes, such as DNA synthesis, where it acts as the primary electron donor for ribonucleotide reductase (RNR); the key enzyme for deoxyribonucleotide synthesis (Laurent TC, 1964; Boronat *et al.*, 2017).

1.1.2.6 Glutathione

In addition to the thioredoxin system (1.1.2.5), the glutathione system is another important antioxidant system consisting of: glutathione, glutaredoxin (Grx), glutathione reductase and NADPH. Glutathione is a very abundant (millimolar concentrations) tripeptide (γ-glutamyl-cysteinylglycine), and proposed to be a major redox buffer in cells (Kalinina *et al.*, 2014). The reduced glutathione (GSH) to oxidised glutathione (GSSG) ratio (GSSG/2GSH) is often used as a measure of the oxidative environment in cells (Herrero *et al.*, 2008). GSH scavenges free radicals, as well as acts as a substrate for Gpx, glutathione transferase (GST) and Grx. For example, in the reduction of disulphide bonds,

GSH reduces Grx, and glutathione reductase recycles GSSG back to GSH, using electrons from NADPH (figure 1.1C) (Hanschmann *et al.*, 2013). Glutathione and glutaredoxins can also regulate protein function in response to stress by the reversible post-translational modification S-glutathionylation (Mieyal *et al.*, 2008). There is a crossover between the glutathione and the thioredoxin antioxidant systems, as glutathione can reduce thioredoxin, and the thioredoxin system has been reported to reduce glutathione (Du *et al.*, 2012; Tan *et al.*, 2010; Lu and Holmgren, 2014). Additionally, glutathione has other non-redox functions such as, in the solubilisation of potentially toxic xenobiotics, as well as in prostaglandin biosynthesis and iron sulphur cluster formation (Lushchak, 2012).

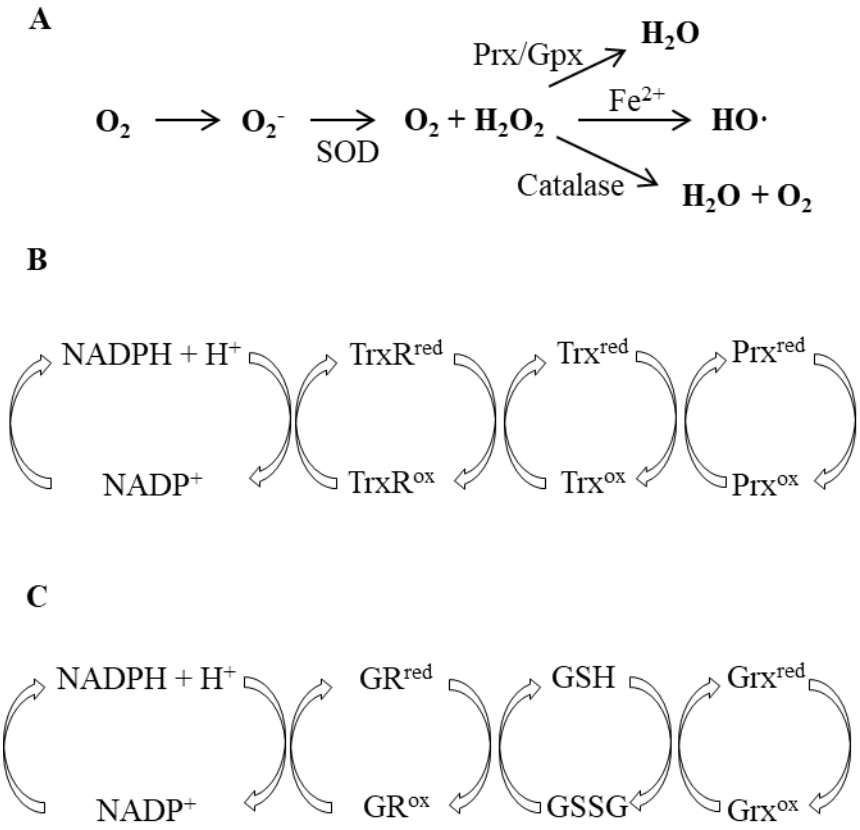

Figure 1.1 ROS detoxification enzymes. [A] ROS reactions. The incomplete reduction of an oxygen molecule (O_2) leads to the formation of a superoxide anion (O_2^-). Superoxide dismutase (SOD) converts the O_2^- to the more stable hydrogen peroxide (H_2O_2). In the presence of metal ions H_2O_2 is reduced to a hydroxyl radical (HO·). Peroxiredoxins and glutathione peroxidases detoxify H_2O_2 to H_2O. Catalase also breaks down H_2O_2 to H_2O and O_2. **[B] The thioredoxin system.** Oxidised peroxiredoxins (Prx^{ox}) are reduced by thioredoxins (Trx), which are subsequently reduced by thioredoxin reductases (TrxR), using electrons from NADPH. **[C] The glutathione system.** Oxidised glutaredoxins (Grx^{ox}) are reduced by glutathione (GSH), which is reduced by glutathione reductase (GR), using the electrons from NADPH.

1.1.3 Oxidative stress

Oxidative stress occurs if levels of ROS rapidly increase and overwhelm the protective mechanisms mentioned above. This oxidative environment results in the oxidation and damage of important cellular components, such as DNA, lipids and proteins. The majority of damage is caused by the highly toxic and indiscriminate $HO^{\cdot}$ (D'Autréaux and Toledano, 2007). The cellular damage caused by oxidative stress has been implicated in the cause and progression of a vast range of diseases, including atherosclerosis, diabetes, cancer, neurodegenerative and cardiovascular disorders (Finkel and Holbrook, 2000; Giustarini *et al.*, 2009).

1.1.4 Oxidative stress in ageing

The role of ROS in ageing has been a controversial topic for many years. The mitochondrial free radical theory of ageing (MFRTA) hypothesised that accumulated macromolecular damage caused by ROS was a direct cause of ageing (Harman, 1956; Harman, 1972). Indeed, in support of this theory, many studies described an increase in protein oxidation in aged tissues (Oliver CN, 1987; Smith *et al.*, 1991). Additionally, animal models provided further support for this theory; such as, the *C. elegans age-1* mutant strain, which presented increased SOD and catalase activity, and an increased lifespan compared to wild-type strains (Larsen, 1993). Additionally, the mice model Sod1-/-; revealed that mice deficient in the SOD1 enzyme had reduced lifespan (Elchuri *et al.*, 2004). However, the MFRTA has since been challenged by contradictory evidence in a number of important animal models. For example, while studies of the naked mole rats have revealed them to be the longest living rodents, they also exhibit higher levels of oxidative damage than mice (Andziak and Buffenstein, 2006). In addition, *C. elegans* and mice models in which the mitochondrial enzyme coenzyme Q is inactivated (*clk-1* and *mclk1* mutants, respectively) also exhibited an increase in lifespan (Liu *et al.*, 2005; Zheng *et al.*, 2010). It was also found that the deletion of *sod-2* in *C. elegans* resulted in increased lifespan, despite increased oxidative damage (Van Raamsdonk and Hekimi, 2009). Additionally, the long-lived *nuo-6* and *isp-1 C. elegans* mutants lost their increased longevity phenotype following treatment with the antioxidant *N*-acetyl cysteine (NAC) (Yang and Hekimi, 2010). Whereas, treatment of *C. elegans* with low doses of the pro-oxidant paraquat extended lifespan (Yang and Hekimi, 2010; Schmeisser *et al.*, 2013). In *Drosophila*, the knock down of components of ETC complex I caused an

increase in ROS, induction of mitochondrial unfolded protein response (mtUPR), and prolonged lifespan (Owusu-Ansah *et al.*, 2013). Additionally, overexpression of *Sod1* and *Sod2* in flies resulted in extension of lifespan (Parkes *et al.*, 1998; Sun *et al.*, 2002). Mutation of *dj-1β*, which resulted in increased mitochondrial H_2O_2 in flies, also exhibited increased longevity (Stefanatos *et al.*, 2012). As well as, the administration of 10 mM H_2O_2 supplemented food (Sohal, 1988). Calorie restriction has increased ROS and lifespan in a number of model organisms (Ristow and Zarse, 2010).

Investigations using H_2O_2 sensors have also revealed interesting insights into the role of ROS in the ageing process. Use of the HyPer sensor reported a negative correlation between high *in vivo* H_2O_2 levels and lifespan (Knoefler *et al.*, 2012). For instance, long-lived *daf-2* mutant *C. elegans*, bearing mutations in the insulin/IGF-1-like receptor, recover from a high exposure to ROS during development, and subsequently experience lower steady-state redox levels during the reproductive period; supporting the theory that events early in life may dictate lifespan (Knoefler *et al.*, 2012). Additionally, the roGFP2-Orp1 sensor has been used in *Drosophila*, where it was reported that an increase in life span was accompanied by increased H_2O_2 levels; female *Drosophila* reported higher cytosolic H_2O_2 levels in gut enterocytes than males, and females had on average a longer lifespan than males (Albrecht *et al.*, 2011).

1.2 ROS and signal transduction

Although the exact relationship between ROS and ageing remains unclear, it is now widely accepted that, despite causing damage at high concentrations, low concentrations of ROS can be vital for normal health and longevity (figure 1.2). Additionally, ROS can elicit a number of beneficial adaptive responses to stress, collectively known as hormesis (Mattson, 2008). Thus there is considerable interest in understanding how cells/organisms utilise the signalling function of ROS and also protect themselves against ROS-induced macromolecular damage. Some of the key mechanisms involved in ROS-signalling are outlined below.

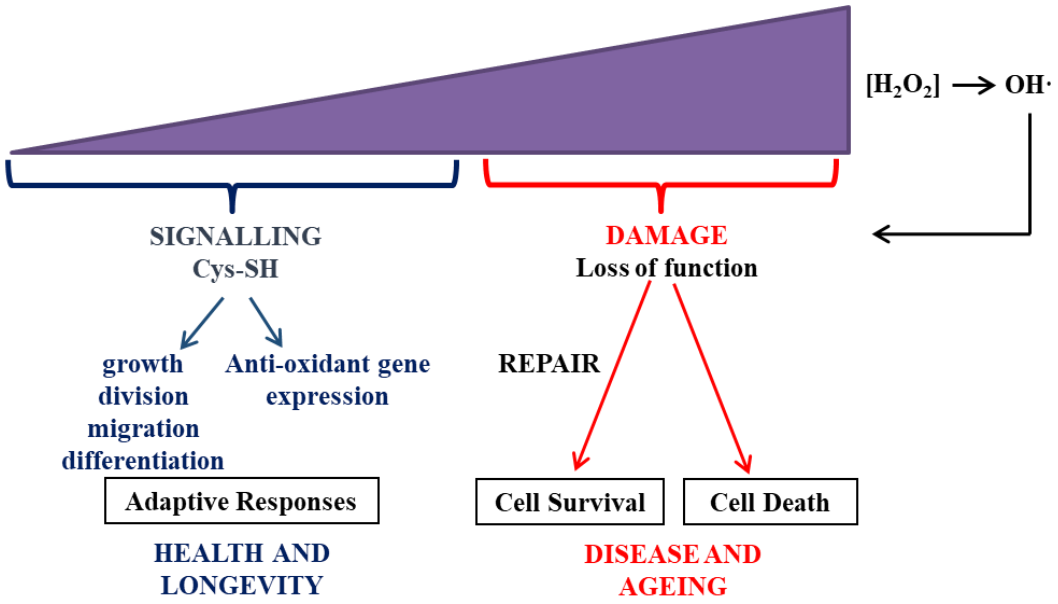

Figure 1.2 Concentration-dependent biological effects of H_2O_2. If H_2O_2 is sufficient to evade peroxide-removing systems, it can react with Fe^{2+}/Cu^{+}, generating hydroxyl radicals (OH·), causing oxidative damage associated with many diseases and ageing. However, low levels of H_2O_2 have signalling functions that are important for maintaining normal health and longevity, as well as maintaining ROS homeostasis.

1.2.1 Mechanism of thiol oxidation/disulphide formation

Cysteine residues can ionize to form thiolates (S^-) (Marinho *et al.*, 2014). In a sulphur-mediated nucleophilic attack, thiolates react with H_2O_2 to form a sulphenate group (SO^-), and release H_2O (figure 1.3). The sulphenate group is highly reactive and can resolve to form an intramolecular or intermolecular disulphide bond with another cysteine residue (Forman *et al.*, 2010). This disulphide bond can then be reduced by the thioredoxin or the glutathione systems. The sulphenate group can also be further oxidised by H_2O_2 to form a sulphinate (SO_2^-) group, which can be reversed by sulfiredoxin (Srx). Additionally, the sulphinate group can undergo further oxidation to a sulphonate (SO_3^-) group, which is irreversible (D'Autréaux and Toledano, 2007).

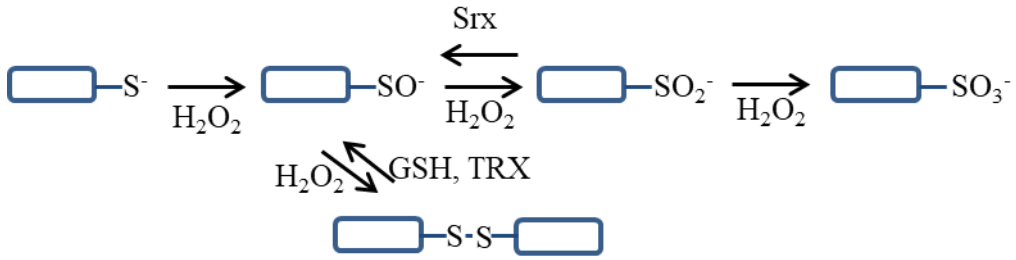

Figure 1.3 Cysteine thiol oxidation. H_2O_2 reacts with deprotonated cysteine thiols ($-S^-$) to produce a sulphenate group ($-SO^-$), and release H_2O. The sulphenate group is either resolved to form a disulphide bond, or can be further oxidised to sulphinate (SO_2^-) and sulphonate (SO_3^-) derivatives. Hyperoxidation to sulphinate and can be reversed by sulfiredoxin (Srx), whereas oxidation to sulphonate groups are irreversible in most proteins. Disulphide bonds can be reduced by the thioredoxin or glutathione systems.

1.2.2 H_2O_2 as a signalling molecule

Low concentrations of H_2O_2 have been shown to be important for a number of cellular processes, such as wound healing and cell migration (Suzuki and Mittler, 2012; van der Vliet and Janssen-Heininger, 2014). H_2O_2 reacts slowly with thiols, however it is able to oxidise specific cysteine residues due to differences in their local environment. For example, due to the pH of the cytosol (6.8-7.2), the majority of cysteine thiols are protonated, and unable to react with H_2O_2 (D'Autréaux and Toledano, 2007). However, cysteine thiols that exist in a local environment which lowers their p*K*a, allows them to become susceptible to oxidation (Morgan and Veal, 2007). This requirement provides a degree of specificity. Additionally, although H_2O_2 is able to diffuse through membranes and aquaporin channels, its enzymatic production and degradation allows for a degree of spatial regulation to be achieved (Forman *et al.*, 2010).

Protein tyrosine phosphatases (PTPs) have an active site motif, CX_5R, in which the cysteine residue exists as a thiolate at neutral pH (p*K*a 4.7-5.4) (Cho *et al.*, 2004). PTP's are therefore a target of oxidation by H_2O_2, which results in redox-dependent inactivation (Tonks, 2005). For example, PTP1B becomes oxidised to form a sulphonamide derivative following exposure to H_2O_2 (Salmeen *et al.*, 2003). In addition, Cdc25C, LMW-PTP and PTEN (phosphatase and tensin homolog) form disulphide bonds in response to H_2O_2 (Lee *et al.*, 2002; Cho *et al.*, 2004; Veal *et al.*, 2007). PTPs dephosphorylate Tyr residues resulting in the inactivation of MAPKs. Therefore, the inhibition of PTP activity by H_2O_2 results in an overall increase in ligand-stimulated Tyr phosphorylation, thereby facilitating signal transduction (Veal *et al.*, 2007).

The abundant glycolytic enzyme glyceraldehyde-3-phosphate dehydrogenase (GAPDH) is also highly reactive to H_2O_2 (Peralta *et al.*, 2015). GAPDH converts glyceraldehyde-3-phosphate (G3P) to 1,3-biphosphoglycerate in the glycolytic pathway (Nicholls *et al.*, 2011). In addition, GAPDH is involved in a number of cellular processes, such as; apoptosis, transcriptional regulation of gene expression and DNA repair (Nicholls *et al.*, 2011; Sirover, 2011). As a protective mechanism against irreversible oxidation, GAPDH undergoes reversible protein S-thiolation by glutathionylation in response to H_2O_2 (Grant *et al.*, 1999; Shenton *et al.*, 2002).

Whilst low levels of H_2O_2 have been shown to stimulate advantageous responses; in most cases, the target proteins/cysteine thiols that are regulated by H_2O_2 have not yet been

identified. A few of the best characterised examples of proteins whose activity is regulated by H_2O_2-induced oxidation of cysteine thiols will be discussed in more detail below.

1.2.3 Adaptive responses to H_2O_2

The adaptive mechanisms activated in response to intermediate levels of H_2O_2 allow the growth and survival of organisms in oxidative conditions. These mechanisms have been well characterised in bacteria and yeast cells, and are the best characterised examples of proteins regulated by cysteine oxidation.

Bacteria encounter a high range of environmental stresses, and have evolved a number of mechanisms in order to adapt. In *E. coli*, the OxyR TF binds to gene promoter regions, and upon oxidation of its redox-sensitive cysteines (Cys199 and Cys208) in response to 20 nM H_2O_2, undergoes a conformational change that activates the transcription of a number of genes important for the bacterial oxidative stress response (Tao *et al.*, 1989; Storz *et al.*, 1990; D'Autréaux and Toledano, 2007).

The H_2O_2 regulation of TFs in yeast is more intricate, requiring other proteins to promote the oxidation of the target TF. The fungal AP-1 (activating protein-1)-like TFs are heterodimer or homodimers of Jun, Fos, or activation transcription factor (ATF) basic region leucine zipper (bZIP) proteins, that bind to the DNA AP-1 binding site (Karin *et al.*, 1997; Toone and Jones, 1999). AP-1 TFs regulate different target genes and are involved in a number of cellular process, including proliferation, apoptosis and response to oxidative stress (Toone and Jones, 1999). In most lab strains of *S. cerevisiae*, H_2O_2 levels are sensed by the Gpx-like enzyme oxidant receptor peroxidase-1 (commonly referred to as Orp1 or Gpx3). The oxidation of the Orp1 catalytic cysteine (Cys36) by H_2O_2 is resolved to form an intermolecular disulphide bond with the bZIP TF Yap1 C-terminal Cys-rich domain (Cys598), with the aid of Yap1-binding protein (Ybp1) (Veal *et al.*, 2003; Bersweiler *et al.*, 2017). This disulphide bond is transposed to form two Yap1 intramolecular disulphides and a conformational change (Delaunay *et al.*, 2002). In the absence of oxidative stress, Yap1 shuttles between the cytosol and nucleus. The conformational change observed in the presence of H_2O_2, prevents the interaction of the nuclear export signal (NES) with the nuclear export protein exportin-1 (Crm1) (Kuge *et al.*, 2002). Therefore, Yap1 accumulates in the nucleus to promote the transcription of genes important for the oxidative stress response (D'Autréaux and Toledano, 2007). Yap1

has also been shown to be oxidised by Tsa1 (thiol-specific antioxidant), a peroxiredoxin, particularly in strains lacking Ybp1 (Veal *et al.*, 2003; Okazaki *et al.*, 2005).

The fission yeast *Schizosaccharomyces pombe*, have also evolved highly sophisticated methods to specifically adapt to particular levels of H_2O_2. *S. pombe* have 2 parallel H_2O_2-responsive pathways (figure 1.4). Exposure to low concentrations of H_2O_2 (0.07-0.2 mM) are sensed by thioredoxin peroxidase 1 (Tpx1), and lead to the oxidation and activation of the TF Pap1 (Chen *et al.*, 2007). Pap1 is usually exported from the nucleus by Crm1, however the oxidation of Pap1 causes the formation of an intramolecular disulphide bond, accompanied by a conformational change (Calvo *et al.*, 2013a). This conformational change blocks its NES causing Pap1 to accumulate in the nucleus. In addition, it promotes Pap1 interaction with Prr1, thereby enhancing Pap1 affinity for antioxidant promoters (Calvo *et al.*, 2012). The heterodimer is then able to interact with gene promoters, activating the transcription of a set of detoxification and repair genes (such as *tpx1, ctt1, srx1, trr1* and *trx1*), to allow for growth in H_2O_2 conditions (Veal *et al.*, 2014). As intracellular H_2O_2 concentrations increase (>1 mM), Tpx1 becomes hyperoxidised and Pap1 activation is inhibited (Bozonet *et al.*, 2005; Vivancos *et al.*, 2005). Instead, the Sty1 p38/JNK-related MAPK (mitogen-activated protein kinase) becomes increasingly phosphorylated (Quinn *et al.*, 2002). Sty1 phosphorylates Atf1 (activating transcription factor 1), inhibiting its ubiquitin-mediated degradation to improve the stability of the protein and mRNA (Lawrence *et al.*, 2007; Day and Veal, 2010). Atf1 binds the promoters of target genes and initiates transcription of distinct, and overlapping, sets of genes (such as *gpx1, gst3, ctt1* and *srx1*) to help combat oxidative damage (Veal *et al.*, 2014).

In the fungal pathogen *Candida albicans*, the AP1-like TF Cap1 is the major TF involved in the regulation of gene expression in response to oxidative stress (Wang *et al.*, 2006; Znaidi *et al.*, 2009). Similar to *S. cerevisiae*, the oxidation and activation of Cap1 in response to H_2O_2 is dependent on Gpx3 and Ybp1 (Patterson *et al.*, 2013).

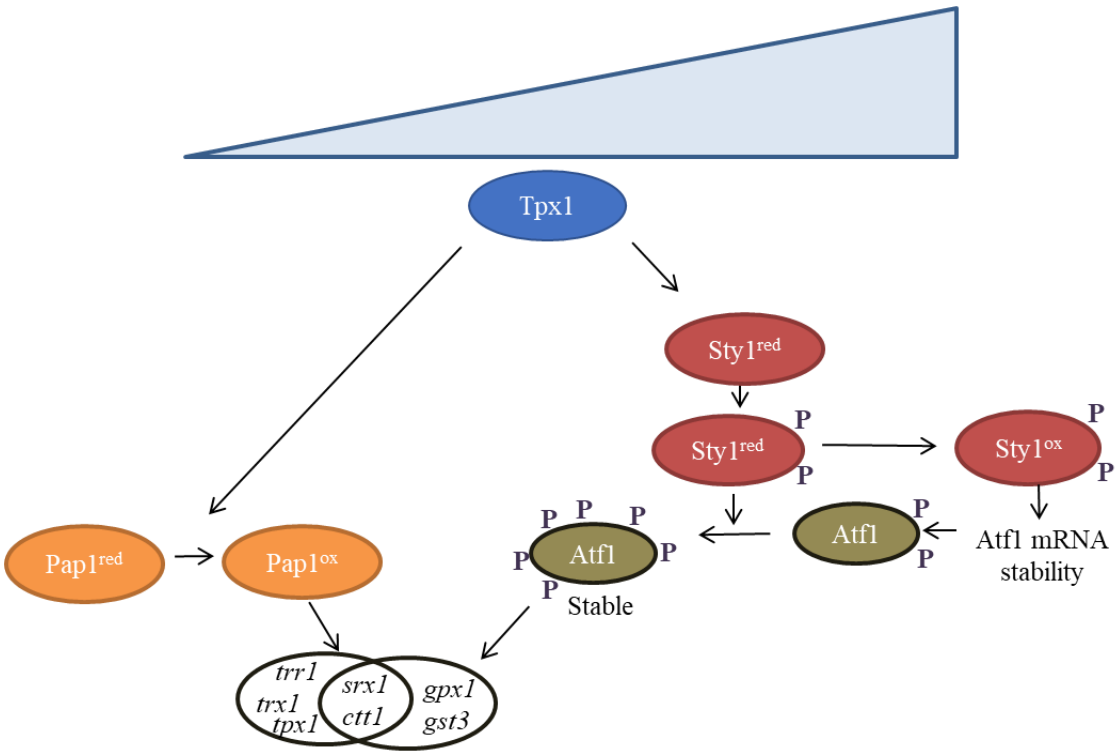

Figure 1.4 Adaptive responses to different concentrations of H_2O_2 in *S. pombe*. Levels of H_2O_2 are sensed by Tpx1. At low levels of intracellular H_2O_2, Pap1 becomes oxidised and accumulates in the nucleus to activate the transcription of a set of genes involved in the oxidative stress response (*trr1*, *trx1*, *tpx1*, *srx1* and *ctt1*). At higher intracellular H_2O_2 concentrations, Sty1 becomes phosphorylated. Sty1 phosphorylates Atf1 promoting its mRNA and protein stability. This leads to the increased transcription of distinct and overlapping set of genes important for cell survival (*gpx1*, *gst3*, *srx1* and *ctt1*).

In mammalian cells, the nuclear factor erythroid 2-related factor 2 (NRF2) bZIP TF is important for antioxidant response gene expression (Taguchi *et al.*, 2011). Under normal conditions, kelch-like ECH-associated protein 1 (KEAP1) binds NRF2 and an E3 ubiquitin ligase cullin 3 (CUL3), and this complex causes the ubiquitylation and proteasomal degradation of NRF2 (Kobayashi *et al.*, 2004; Furukawa and Xiong, 2005). However, in response to increasing levels of ROS KEAP1 redox-sensitive cysteines become oxidised, leading to a release of NRF2 from the complex. This allows NRF2 levels to increase and translocate to the nucleus to promote antioxidant gene expression (D'Autréaux and Toledano, 2007; Taguchi *et al.*, 2011; Holmström and Finkel, 2014).

1.2.4 Positive signalling at low H_2O_2 concentrations

In addition to the up-regulation of anti-oxidant gene expression, low levels of H_2O_2 are important for a number of cellular responses (Veal and Day, 2011; Finkel, 2011). For example, H_2O_2 gradients (100-200 µM) produced by injured epithelia act as a neutrophil chemoattractant to aid in wound response (Niethammer *et al.*, 2009; van der Vliet and Janssen-Heininger, 2014). In addition, by interacting with redox-sensitive targets, H_2O_2 regulates processes such as cell proliferation, apoptosis, energy metabolism and angiogenesis (Lennicke *et al.*, 2015). The main signalling pathways that are activated by oxidation and exert a pro-survival response are: the extracellular signal-regulated kinase (ERK), phosphoinositide 3-kinase (PI3K)/Akt and the nuclear factor (NF)-κB pathways (Finkel and Holbrook, 2000). Whereas, activation of c-Jun amino-terminal kinase (JNK), p38 mitogen-activated protein kinase (MAPK) and p53 are mainly linked to apoptosis (Finkel and Holbrook, 2000).

H_2O_2 also modulates the activity of the vascular endothelial growth factor receptor (VEGFR) 2, which regulates angiogenesis, cell proliferation, survival, migration and differentiation (Ushio-Fukai and Nakamura, 2008; Kaplan *et al.*, 2011). Another target for H_2O_2, is the epidermal growth factor (EGF) receptor; here oxidation of the active site Cys797 results in increased tyrosine kinase activity (Paulsen *et al.*, 2011; Sies, 2014). H_2O_2 also increases Akt activation, as well as the activation of MAPK pathways (Ushio-Fukai *et al.*, 1999; Truong and Carroll, 2013). For example, dimer formation of the mitogen-activated protein (MAP) kinase kinase kinase (MAPKKK) ASK1 is caused by exposure to H_2O_2, and is important for the ASK1-mediated induction of apoptosis (Machino *et al.*, 2003; Nomura *et al.*, 2013; Lennicke *et al.*, 2015). In addition, the AMP-

activated protein kinase (AMPK) has redox-sensitive cysteine residues (Cys130 and Cys174), which when oxidised inhibits its activity, thereby affecting energy metabolism (Shao *et al.*, 2014). The serine/threonine-protein kinase ATM also undergoes oxidation in the presence of H_2O_2, causing the activation of its activity. ATM is involved in regulation of the DNA repair process, as well as mitochondrial function and metabolic control (Sanli *et al.*, 2014; Guo *et al.*, 2010; Alexander *et al.*, 2010).

1.3 Role of 2-Cys Prx in H_2O_2 sensing and signalling

Peroxiredoxins are abundant antioxidant enzymes. In addition to detoxifying H_2O_2, they have a vital role in H_2O_2 sensing and signalling. Studies using mutant mice, yeast, worms and flies also indicate that Prx are important for maintaining genome stability, protecting against cancer and promoting longevity (Oláhová *et al.*, 2008; Huang *et al.*, 2003; Lee *et al.*, 2003; Neumann *et al.*, 2003). In response to H_2O_2, peroxiredoxins also display a chaperone function (Jang *et al.*, 2004), with the *S. cerevisiae* peroxiredoxin Tsa1 shown to protect against protein aggregation (Jang *et al.*, 2004; Weids and Grant, 2014). There are 3 proposed functions of peroxiredoxins in H_2O_2 signalling: to act as a barrier to increasing intracellular concentrations of H_2O_2, to act as a direct redox transducer in H_2O_2 signalling, and to promote the oxidation of thioredoxins.

1.3.1 The 3 classes of peroxiredoxins

There are 3 classes of peroxiredoxins: typical 2-Cys Prx, atypical 2-Cys Prx and 1-Cys Prx. In each class, the peroxidatic cysteine becomes oxidised by H_2O_2 to form a sulphenic acid group (Cys-SOH). In 2-Cys Prx, the peroxidatic cysteine sulphenic acid group reacts with a resolving cysteine in an adjacent Prx molecule (typical), in the same Prx (atypical), or in another protein, to form a disulphide bond (figure 1.5) (Choi HJ, 1998; Ellis and Poole, 1997). Prx dimers interact non-covalently to form decamer molecules (Harris *et al.*, 2001; Kitano *et al.*, 1999; Wood *et al.*, 2003b). In mammalian cells 6 isoforms of Prx are expressed with different subcellular localisations: four typical 2-Cys Prx (I-IV), an atypical 2-Cys Prx (V) and a 1-Cys Prx (VI). Prx I, II and VI demonstrate mainly cytosolic localisation, Prx III is localised to the mitochondria, and Prx IV is mostly detected in the ER. Finally, Prx V is localised to the cytosol, mitochondria and peroxisomes (Rhee *et al.*, 2012).

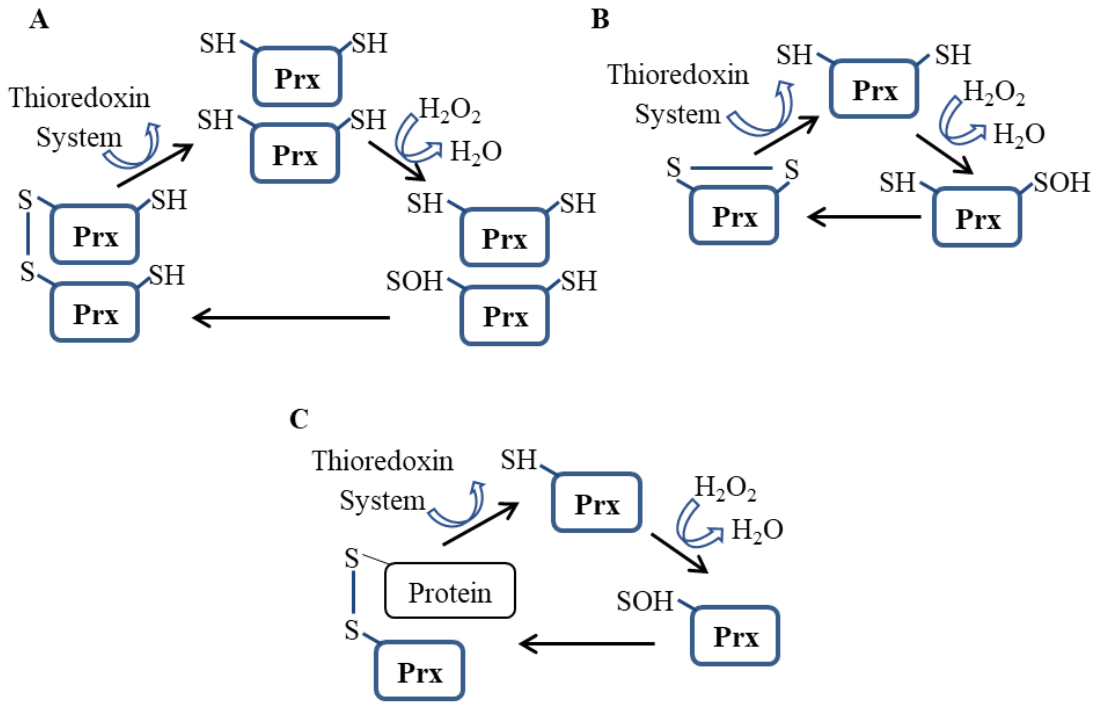

Figure 1.5 Mechanism of peroxiredoxins. [A] Typical 2-Cys Prx. The peroxidatic cysteine becomes oxidised by H_2O_2 to form a sulphenic acid group and H_2O. This resolves to form a disulphide bond with a resolving cysteine in an adjacent Prx molecule to form a homodimer structure. Oxidised Prx are reduced by the thioredoxin system. **[B] Atypical 2-Cys Prx.** Atypical Prx function as monomeric proteins; a disulphide bond is formed between the peroxidatic cysteine and resolving cysteine within the same Prx molecule. **[C] 1-Cys Prx.** 1-Cys Prx only have a peroxidatic cysteine. The resolving cysteine is supplied by a different protein.

1.3.2 Peroxiredoxins as antioxidants

Prx have a conserved arginine residue within their active site which reduces the pKa of the peroxidatic cysteine (Wood *et al.*, 2003b). This stabilises its thiolate form thus increasing its affinity for H_2O_2 making them efficient at reacting to low levels of H_2O_2 (D'Autréaux and Toledano, 2007). Typical 2-Cys Prx reduce H_2O_2 to H_2O, and the oxidised peroxidatic cysteine condenses with a resolving cysteine in another Prx to form a homodimer structure. Typical 2-Cys Prx also form redox-dependent large oligomeric structures which further increase the reactivity of the peroxidatic cysteine (Parsonage *et al.*, 2005).

1.3.3 Peroxiredoxins as chaperone proteins

Eukaryotic 2-Cys Prx contain GGLG and YF motifs which make them susceptible to hyperoxidation of the peroxidatic cysteine. This is due to structural features that slow disulphide formation (Wood *et al.*, 2003b). Disulphide bond formation requires a structural transition from a folded state to a locally unfolded state, whereas hyperoxidation occurs in the fully folded state (Nelson *et al.*, 2013). Reducing the rate of disulphide formation results in increased lifetime of the C_p-SOH intermediate, increasing the possibility of reacting with a second peroxide at high levels of H_2O_2 (Wood *et al.*, 2003a; Nelson *et al.*, 2013). This results in hyperoxidation to a sulphinic group (SO_2^-) and potentially further oxidation to a sulphonic group (SO_3^-). The sulfinylation of a peroxidatic cysteine can be reduced by sulfiredoxin (Srx1), whereas sulfonylation is irreversible (Woo *et al.*, 2003; Biteau *et al.*, 2003). Thus, the hyperoxidation of Prx converts it to a thioredoxin-resistant form, thereby inhibiting its peroxidase activity. Different Prx display different sensitivities to hyperoxidation; for example, mammalian mitochondrial Prx3 is more resistant than the cytoplasmic Prx1 and Prx2 (Cox *et al.*, 2009; Haynes *et al.*, 2013; Peskin *et al.*, 2013; Veal *et al.*, 2017).

The hyperoxidation of Prx is important for cell survival under acute stress conditions, and is proposed to have 3 roles (figure 1.6). Firstly, the inactivation of the peroxidase activity of the highly abundant and reactive Prx allows intracellular H_2O_2 levels to rise and to oxidise alternate redox-sensitive signalling proteins important for cell survival; also known as 'The Floodgate Model' (Wood *et al.*, 2003a). Secondly, the hyperoxidation of Prx to a thioredoxin-resistant form frees the cellular pool of reduced thioredoxin to reduce other substrates, e.g. methionine sulfoxide reductase (Mxr1) and other protein disulphides

that may form in response to high levels of H_2O_2 (Day *et al.*, 2012). Finally, the hyperoxidation of Prx promotes its chaperone and signalling activities. In response to heat or H_2O_2, Prx form oligomeric high molecular weight (HMW) structures similar to heat shock proteins (HSPs) (Schröder *et al.*, 2000; Jang *et al.*, 2004). Indeed, deletion of Tsa1 in *S. cerevisiae* cells results in reduced thermotolerance and increased aggregation of proteins (Jang *et al.*, 2004; Weids and Grant, 2014; Veal *et al.*, 2017). Additionally, in cells lacking Srx the H_2O_2-induced HMW structures remain for longer (Jang *et al.*, 2004). It has therefore been proposed that hyperoxidation of Prx promotes its chaperone activity (Jang *et al.*, 2004). Additionally, it has been shown that hyperoxidised Prx interact with Hsp70 and Hsp104 to promote the disaggregation of misfolded proteins (Hanzén *et al.*, 2016; Jang *et al.*, 2004). Interestingly, hyperoxidised Prx have a conserved role in circadian rhythms (Olmedo *et al.*, 2012; Cho *et al.*, 2014; Veal *et al.*, 2017). Recently, it has been discovered that peroxisomal acetyl-CoA oxidase (Pox1) converts light to H_2O_2 to be sensed by Tsa1, ultimately resulting in accumulation of the TF Msn2 in the nucleus (Bodvard *et al.*, 2017). Increases in hyperoxidised Prx have also been observed during ageing; for example, the increased hyperoxidation of Tsa1 during replicative ageing of yeast (Molin *et al.*, 2011; Nyström *et al.*, 2012; Veal *et al.*, 2017).

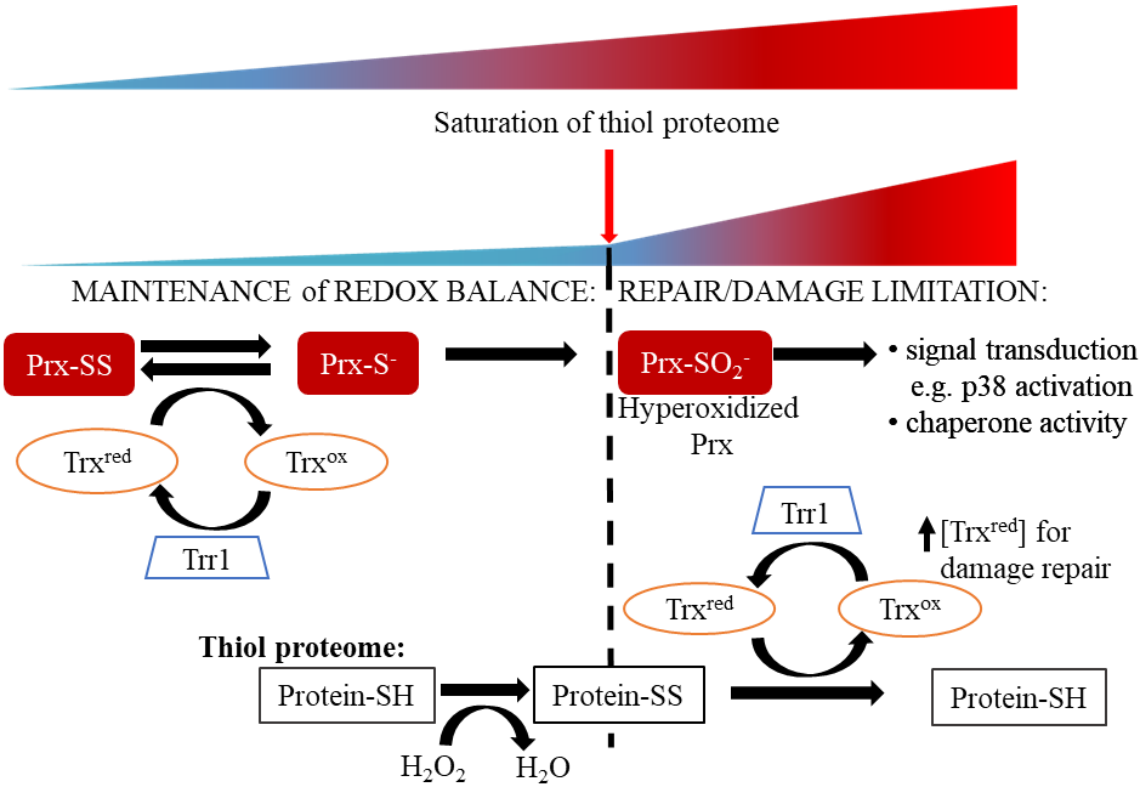

Figure 1.6 Proposed roles for Prx hyperoxidation: H_2O_2 signalling, thioredoxin activity and increased chaperone activity. The floodgate model hypothesises that hyperoxidation allows 2-Cys Prx to act as floodgates; buffering low levels of H_2O_2, but permitting the accumulation of higher levels of H_2O_2 in order to allow active H_2O_2 signalling. Alternatively, the hyperoxidation of Prx has also been demonstrated to be important for increasing chaperone activity, leading to the partial repair of the damage caused by oxidative stress. Finally, the floodgate mechanism of Prx hyperoxidation could be to allow thioredoxin the opportunity to reduce oxidised proteins, other than Prx. This is important as oxidation of protein thiols can alter protein structure leading to loss of function and protein damage.

1.3.4 Peroxiredoxins as signal transducers

In addition to the detoxification of H_2O_2, peroxiredoxins have peroxidase-independent functions in signal transduction. Peroxiredoxins have been proposed to promote H_2O_2 signal transduction by acting as direct redox transducers, where they directly oxidise target proteins via the formation of intermolecular disulphide bonds (figure 1.7) (Veal *et al.*, 2004; Jarvis *et al.*, 2012; Sobotta *et al.*, 2014).

As previously mentioned (section 1.2.3), in *S. cerevisiae* cells H_2O_2 is sensed by Gpx3 which directly oxidises the TF Yap1 via a redox-relay mechanism (Delaunay *et al.*, 2002). In *S. pombe*, Tpx1 forms mixed disulphides with Sty1, a p38/JNK-related MAPK signalling protein in response to a range of H_2O_2 concentrations, including those at which its thioredoxin peroxidase activity is inactivated by hyperoxidation of the peroxidatic cysteine (Veal *et al.*, 2004). Indeed, the resolving cysteine of Tpx1 is dispensable for the H_2O_2-dependent activation of Sty1, suggesting that the role of Tpx1 in activation of Sty1 is independent from its thioredoxin peroxidase activity.

In mammalian cells, the Prx, Prx1 (one of the mammalian orthologues of Tpx1) has been found to directly interact with ASK1 (apoptosis signal-regulating kinase) (Jarvis *et al.*, 2012). ASK1 is the eukaryotic MAPKKK (mitogen-activated protein kinase kinase kinase) which activates the p38 and JNK kinases in response to stress. A disulphide-exchange intermediate has also been observed between the mammalian Prx2 and the TF STAT3 (Sobotta *et al.*, 2014). Prx2 oxidises STAT3 resulting in the formation of disulphide-linked STAT3 oligomers which attenuate transcriptional activity (Sobotta *et al.*, 2014). Prdx1 has also been found to interact with PTEN, a protein with phosphatase activity, to inhibit tumorigenesis (Cao *et al.*, 2009). As well as the MAPK phosphatases MKP-1 and MKP-5 (Turner-Ivey *et al.*, 2013).

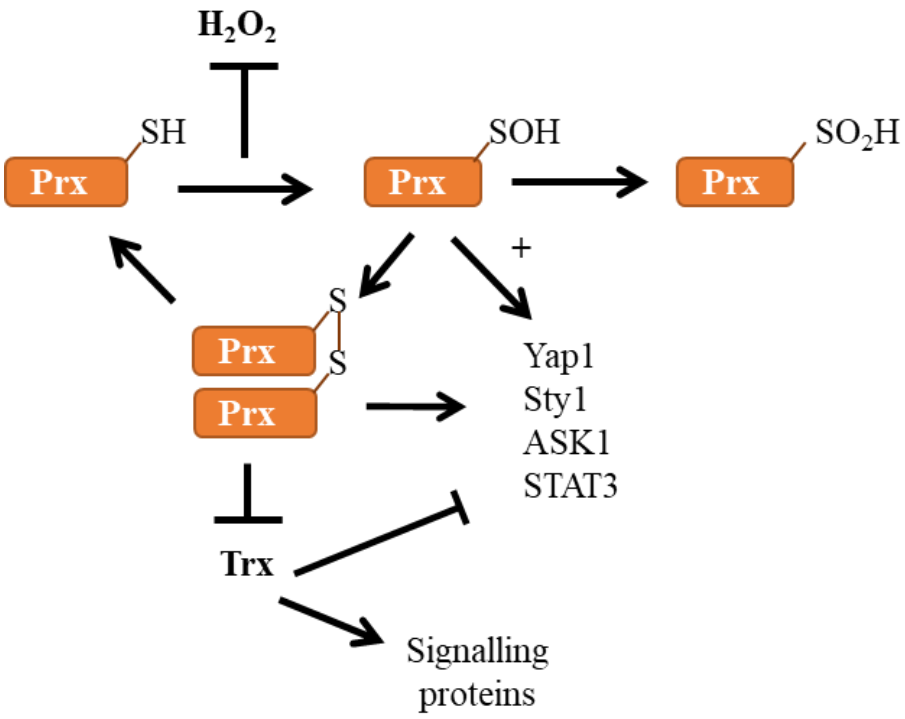

Figure 1.7 Peroxiredoxins as signal transducers. The peroxidatic cysteine of 2-Cys Prx reacts with H_2O_2 to form a sulphenate group, which resolves to form a disulphide with another 2-Cys Prx molecule. Oxidised Prx oxidise and activate the transcription factors Yap1 (*S. cerevisiae*), Sty1 (*S. pombe*), ASK1 and STAT3 (mammalian) leading to gene transcription. Reduced thioredoxins reduce oxidised peroxiredoxins thereby inactivating their signal transducing ability. In addition, thioredoxins reduce TFs thereby inhibiting further gene expression, and thioredoxins reduce downstream signalling proteins. It is therefore hypothesised that the promotion of thioredoxin oxidation may be another regulatory mechanism for signal transduction.

1.3.5 Peroxiredoxins promote the oxidation of thioredoxins

Another role for Prx, is to promote the oxidation of thioredoxin or thioredoxin-like proteins. For example, in *S. pombe* no Tpx1-Pap1 disulphide complex has been reported (Bozonet *et al.*, 2005; Vivancos *et al.*, 2005). It is the thioredoxin peroxidase activity of Tpx1 that is essential for the activation of the AP-1-like TF Pap1 in response to low H_2O_2 concentrations (figure 1.8) (Brown *et al.*, 2013). Exposure to low concentrations of H_2O_2 (0.07-0.2 mM) cause the oxidation of Tpx1, which promotes the oxidation and activation of Pap1 via the thioredoxin-like protein 1 (Txl1) (Bozonet *et al.*, 2005; Vivancos *et al.*, 2005; Brown *et al.*, 2013). Whereas Tpx1 is the main substrate of thioredoxin (Trx1), Txl1 is the main reductant of Pap1. Therefore, to sustain Pap1 oxidation at low levels of H_2O_2, the reduction of Pap1 by Txl1 must be inhibited. Tpx1 is therefore important to competitively inhibit the direct reduction of the oxidised form of Pap1 by Txl1 (Brown *et al.*, 2013). As expected, the peroxidase defective mutant *tpx1*^{C169S} *S. pombe* cells, in which the resolving cysteine is replaced by serine, display increased sensitivity to H_2O_2. Although *S. pombe* expressing *tpx1*^{C169S} retain the ability to promote H_2O_2-dependent Sty1 activation, they are unable to promote the oxidation of Pap1. Previous work in our lab has established that this is because the thioredoxin peroxidase activity of Tpx1 is essential to promote the oxidation of thioredoxin proteins. However, genetic loss of the *txl1* gene rescued the H_2O_2 sensitivity of *tpx1*^{C169S} indicating that the main role of the thioredoxin peroxidase activity of Tpx1 in H_2O_2 resistance is to promote Txl1 oxidation (Brown *et al.*, 2013). In addition, PrxIV promotes disulphide formation in the ER of mammalian cells, thereby promoting the oxidation of thioredoxin (Tavender and Bulleid, 2010).

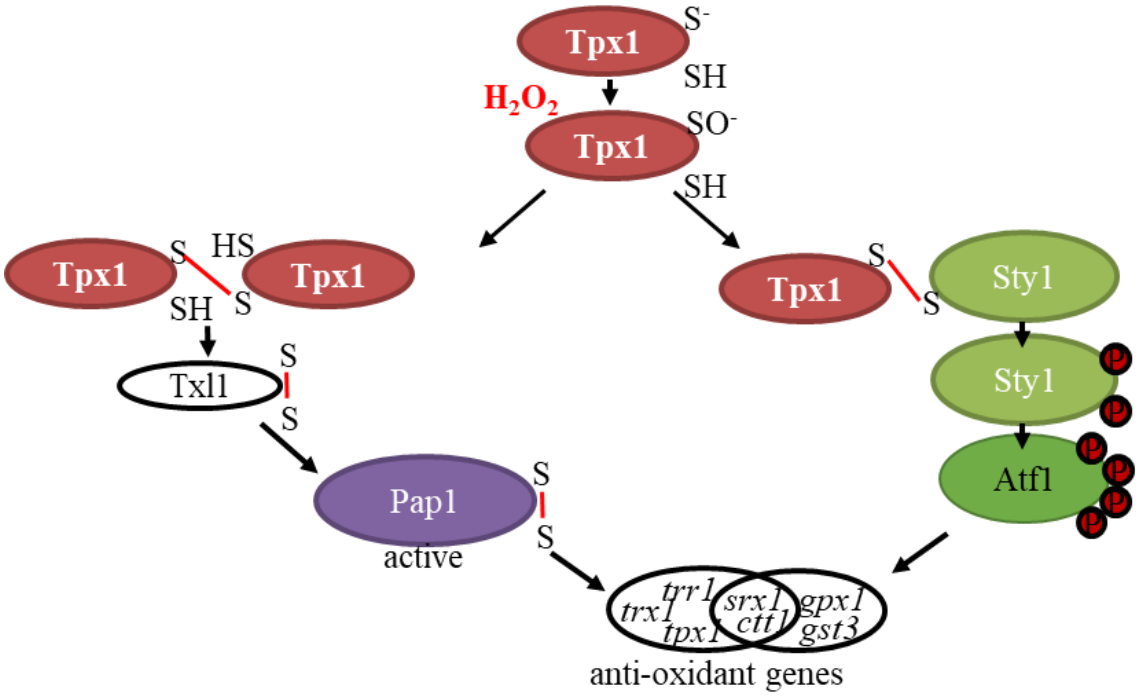

Figure 1.8 Tpx1 promotes the oxidation of Txl1. The 2-Cys Prx Tpx1 forms a direct disulphide with the Sty1 MAPK. This requires only the Tpx1 peroxidatic cysteine and leads to the phosphorylation and activation of TF Atf1. No Tpx1-Pap1 complex has been detected in *S. pombe*. The activation of the TF Pap1 requires both the Tpx1 peroxidatic and resolving cysteine, and relies on the promotion of the oxidation of thioredoxin-like protein 1 (Txl1).

1.4 Maintaining protein thiol oxidation in subcellular compartments

1.4.1 Maintaining protein thiol oxidation in the ER

The formation of disulphide bonds is an important factor of protein folding and function. Cells therefore have specialised compartments to promote the formation of disulphide bonds, such as the endoplasmic reticulum (ER). The ER maintains an oxidative environment and has specialised oxidoreductases in order to aid oxidative folding (Oka and Bulleid, 2013). Similar to the cytosol, the main redox buffer of the ER is glutathione. However, levels of oxidised glutathione are much higher due to the absence of glutathione reductases in the ER, resulting in a low GSH:GSSG ratio (1:1 to 3:1) (Margittai *et al.*, 2015; Østergaard *et al.*, 2004). In addition, oxidoreductases in the ER have a much lower reduction potential, compared to thioredoxin, meaning their mode of action is to exchange a disulphide with a substrate protein opposed to reducing an existing disulphide (Chambers *et al.*, 2010).

The protein disulphide isomerase (PDI) family catalyse the formation of disulphide bonds in the ER. PDI proteins contain a thioredoxin-like fold and the CXXC motif active site. They are able to catalyse thiol-disulphide exchange reactions by promoting disulphide bond formation, breaking disulphide bonds, and rearranging non-native disulphide bonds to native ones (Oka and Bulleid, 2013). Following disulphide bond formation PDI are re-oxidised by ER oxidoreductin 1 (Ero1). Ero1 is essential for PDI activity (Frand and Kaiser, 1998). Ero1 also has the CXXC motif and uses FAD as a cofactor to transfer electrons from PDI to O_2 (Tu and Weissman, 2002). Ero1 activity results in the formation of H_2O_2, therefore its activity is tightly regulated by a negative feedback loop (Gross *et al.*, 2006; Baker *et al.*, 2008).

2-Cys peroxiredoxins and glutathione peroxidases are also localised to the ER in order to detoxify H_2O_2. In mammalian cells, PrxIV is localised to the ER and couples the breakdown of H_2O_2 to disulphide bond formation in PDI (Tavender *et al.*, 2010) (Zito *et al.*, 2010). Additionally, GPx7 and GPx8 are ER-localised in mammalian cells. These proteins have direct roles in disulphide bond formation by interacting with Ero1, and have been shown to promote disulphide bond formation in substrates in the presence of PDI and H_2O_2 (Nguyen *et al.*, 2011).

1.4.2 Maintaining protein thiol oxidation in the mitochondria

Another subcellular compartment important for oxidative protein folding is the mitochondrial intermembrane space (IMS) (Sideris and Tokatlidis, 2010). The majority of mitochondrial proteins are synthesised by cytosolic ribosomes, and then transported in an unfolded state to the mitochondria by chaperone proteins, such as the *S. cerevisiae* Hsp70 and Hsp90 (Neupert and Herrmann, 2007). Upon reaching the mitochondria, the unfolded precursors are imported across the outer membrane (OM) via the TOM complex (Milenkovic *et al.*, 2007). Proteins are localised to specific mitochondrial compartments by targeting signals recognised by import machinery; for example, matrix-targeted proteins are imported across the inner mitochondrial membrane (IMM) by the Tim22 complex (Chatzi *et al.*, 2016; MacPherson and Tokatlidis, 2017).

Glutathione is able to freely diffuse between the cytosol and the mitochondrial IMS via Porin channels resulting in a reducing environment (Kojer *et al.*, 2012). The IMS therefore also contains oxidative folding machinery known as the Mia pathway (Banci *et al.*, 2009; Chacinska *et al.*, 2004). The oxidoreductase Mia40/Tim40 is bound to the IMM at its N-terminus and has a CPC active site motif (Chatzi *et al.*, 2013). Mia40 forms a mixed disulphide intermediate with the imported preprotein and its CX9C motif, and initiates protein folding (Banci *et al.*, 2009). The IMS protein is released fully folded, and this introduction of disulphide bonds traps the protein in the IMS (Banci *et al.*, 2010). Mia40 is recycled by a thiol-disulphide exchange reaction with the flavin adenine dinucleotide (FAD)-linked sulfhydryl oxidase Erv1. Finally, Erv1 is recycled by cytochrome c (Allen *et al.*, 2005; Lionaki *et al.*, 2010).

In addition to oxidative protein folding, mitochondria are major sources of ROS production. Therefore, as a protective mechanism many antioxidants are also localised to the mitochondria (Toledano *et al.*, 2013). The copper-zinc binding protein SOD1 is localised to the IMS of the mitochondria. The manganese-SOD2 enzyme is also localised in the matrix (Chatzi *et al.*, 2016). Additionally, a number of glutathione peroxidase, glutaredoxins and thioredoxins are localised to the mitochondria. For example, in *S. cerevisiae* Gpx1 is localised to the OM, and Gpx2 is localised on the matrix-side of the IM to protect against lipid peroxidation (Avery and Avery, 2001; Ukai *et al.*, 2011). Gpx3 is localised to the IMS and promotes Mia40-dependent oxidative folding (Vögtle *et al.*, 2012; Kritsiligkou *et al.*, 2017). Grx2 is localised to the IMS and the matrix (Porras *et al.*,

2006; Porras *et al.*, 2010). Trx3, Trr2 and Prx1 are also localised to the matrix (Pedrajas *et al.*, 1999; Pedrajas *et al.*, 2010). Trx1 and Trr1 are localised to the IMS (Chatzi *et al.*, 2016).

1.4.3 Maintaining protein thiol oxidation in the cytoplasm

The cytosol has a reducing environment. This is mainly due to the high abundance of the low-molecular weight redox buffer glutathione (GSH) (López-Mirabal and Winther, 2008). Under normal growth conditions the GSH:GSSG ratio is approximately 3000:1 (Østergaard *et al.*, 2004). The cytosolic proteins are also maintained in a reduced state by the thioredoxin and glutaredoxin systems, which utilise NADPH as the electron donor.

However, as a by-product of normal cellular metabolism, ROS are produced in subcellular compartments such as mitochondria, peroxisomes and ER, and reach the cytosol. In addition to the glutathione system there are a range of redox enzymes which are up-regulated following increases in H_2O_2 levels, and are equipped to remove ROS: catalase, SOD, glutathione peroxidases and peroxiredoxins (López-Mirabal and Winther, 2008).

1.5 Detection of intracellular levels of H_2O_2 *in vivo*

To gain a better understanding of H_2O_2 signalling, it is important to be able to monitor real-time intracellular H_2O_2 concentration changes *in vivo*. Original small molecular fluorescent probes recruited to visualise ROS in cells, such as 2',7'-dichlorofluorescin diacetate (DCFDA), have been widely used but frequently lack specificity to particular oxidants, and can promote further oxidation in cells (Guo *et al.*, 2014). The Pf3-Ac (acetylated peroxyflour-3), and other probes of the monoboronate family, have been commonly used to detect intracellular H_2O_2. For example, the Nuclear Peroxy Emerald 1 (NucPE1) probe has been used to detect differences in nuclear H_2O_2 levels in wild-type *C. elegans* (Dickinson *et al.*, 2011). Additionally, the Peroxy Orange 1 probe has been utilised to investigate H_2O_2 levels in *C. elegans* in which important ageing-related genes had been knocked down (Fu *et al.*, 2015).

The advantage of using these small fluorescent probes is that they will only react with H_2O_2 once activated by esterase inside the cell (Dickinson *et al.*, 2010). Additionally, the irreversibility of these probes means that they don't impact on thioredoxin or glutathione oxidation in the cell. However, disadvantages of these include prone to photo-bleaching

by visible light, and a lack ratio-metric properties (Lukyanov and Belousov, 2014). Researchers therefore cannot tell if levels of the probe are equal throughout all cells, and if a high reading equates to a high concentration of intracellular H_2O_2, or a high quantity of probe within the cell. In order to monitor real-time changes, efforts have shifted to the use of genetic fluorescent redox sensors, specifically HyPer for H_2O_2 (Belousov *et al.*, 2006). The main challenge in designing a tool to detect levels of H_2O_2 *in vivo* is the demonstration of appropriate levels of selectivity and specificity (Lukyanov and Belousov, 2014).

1.5.1 The use of HyPer in the detection of *in vivo* levels of H_2O_2

The HyPer sensor was synthesised by insertion of the circularly permutated yellow fluorescent protein (cpYFP) into an OxyR domain (the prokaryotic H_2O_2-sensing protein). HyPer has 2 excitation peaks at 420 nm and 500 nm, and an emission peak at 516 nm (Belousov *et al.*, 2006). It has a number of advantages: sensitivity to H_2O_2, reversible, ratio-metric read-out, a fast reaction rate constant, no mammalian interacting proteins, and can be targeted to sub-cellular compartments (Lukyanov and Belousov, 2014; Belousov *et al.*, 2006; Markvicheva *et al.*, 2011; Bilan *et al.*, 2013; Elsner *et al.*, 2011). However, it also has a number of disappointing attributes. Firstly, due to its midpoint potential of -185 mV, HyPer can only be used in reducing environments such as the cytosol (Lukyanov and Belousov, 2014; Belousov *et al.*, 2006). Secondly, the open barrel structure of HyPer causes a pH sensitivity; a shift of 0.2 pH units is sufficient to alter the mean ratio to the same degree as a full reduction or oxidation event (Lukyanov and Belousov, 2014; Roma *et al.*, 2012; Wang *et al.*, 2013). GFP fluoresce via their chromophore groups which contain a Tyr residue that switched between a protonated (neutral) or deprotonated (anionic) state (Lukyanov and Belousov, 2014). The open barrel structure of HyPer means that a change in pH can lead to chromophore protonation (Elsliger *et al.*, 1999). It is therefore recommended that the use of HyPer should be accompanied with use of the pH-sensitive SHyPer (HyPer-C119S) as a control (Lukyanov and Belousov, 2014). However, throughout the literature this is often not the case.

HyPer has been used as an *in vivo* H_2O_2 sensor in *C. elegans*. It has been used to report that H_2O_2 levels were high during development, undergo decline during adulthood, and increase again throughout ageing (Knoefler *et al.*, 2012). An alternate study also found

that H_2O_2 levels increase with age; and additionally, that this is delayed following dietary restriction (Back *et al.*, 2012).

The importance of careful interpretation and characterisation of reporters was recently exemplified by the use of circularly permutated yellow fluorescent protein (cpYFP) as a O_2^- sensor in *C. elegans*. This came under scrutiny when a paper described that 'mitoflashes' observed in early adulthood predicts lifespan (Shen *et al.*, 2014). A responding paper demonstrated that the changes in the cpYFP fluorescence observed, were due to fluctuations in pH, and not levels of superoxide (Schwarzländer *et al.*, 2014).

1.5.2 The use of roGFP in detection of glutathione redox potential and H_2O_2

Reduction-oxidation GFP (roGFP) sensors introduced redox-sensitive cysteines directly into the GFP. Oxidation of these cysteines results in the change of the chromophore protonation state, and a change in excitation band from 400 nm to 490 nm. The roGFP2 sensor contains cysteine residues at S147 and Q204, and the mutations C48S and S65T (Hanson *et al.*, 2004; Dooley *et al.*, 2004). Similar to HyPer, it has also been described as pH sensitive, however its ratio-metric readout is pH stable (Gutscher *et al.*, 2008). The use of a ratio-metric read-out is also preferable as it prevents other imaging artefacts, such as saturation, and allows the comparison between intracellular compartments (Lukyanov and Belousov, 2014).

The roGFP2 sensor has been manipulated to specifically detect H_2O_2, by fusion with Orp1 (Gpx3) (Gutscher *et al.*, 2009). Orp1 reacts with H_2O_2, and following oxidation Orp1 uses the roGFP2 as its reducing substrate, subsequently oxidising roGFP2 and causing a change in fluorescence. This was designed based on the mechanism of H_2O_2-induced activation of Yap1 by Orp1/Gpx3 as a method to increase sensitivity to H_2O_2 (Delaunay *et al.*, 2002).

The roGFP2 sensor has also been developed to detect glutathione redox potential in yeast and mammalian systems, by fusion with glutaredoxin (Morgan *et al.*, 2011). This method was conducted to investigate *in vivo* glutathione reductase and glutathione coupling. The Grx1-roGFP2 sensor was successfully used in *Drosophila*, to find that cytosolic glutathione redox homeostasis *in vivo* appears maintained with age, but mitochondrial E_{GSH} is more variable (Albrecht *et al.*, 2011). Another group also used roGFP to monitor glutathione in *C. elegans* and predicted that glutathione had a smaller effect as a cellular redox buffer than previously thought (Romero-Aristizabal *et al.*, 2014).

1.5.3 Improving the specificity of H_2O_2 sensor for *C. elegans*

When using the HyPer sensor in *C. elegans*, the lowest dose of extracellular H_2O_2 to be detected was 0.5 mM (Back *et al.*, 2012). It has been previously reported in the literature that HyPer is able to detect H_2O_2 concentrations as low as 5 µM (Belousov *et al.*, 2006). This difference in detection levels is predicted to be due to the cuticle of the *C. elegans*. The cuticle acts as a barrier to protect it from its environment (Back *et al.*, 2012). This is also echoed in other papers, where the concentrations of reactants exposed to *C. elegans* are much higher than used on the dissected tissue of *Drosophila* (Albrecht *et al.*, 2011; Romero-Aristizabal *et al.*, 2014).

It has been estimated that the lowest steady-state H_2O_2 levels in mammalian cells is around 1 nM, but can rise to as much as 500-700 nM (Ezeriņa *et al.*, 2014). It is vital that genetic sensors are sensitive enough to detect these ranges in order to elucidate the signalling properties of H_2O_2. The intracellular detection limit of the HyPer and roGFP2-Orp1 is only around 100 nM (Ezeriņa *et al.*, 2014). To address this, the fusion of roGFP2 to other substrates has been considered. The 2-cys peroxiredoxins are more sensitive to H_2O_2 than Orp1, and predicted to be able to detect very low nanomolar concentrations (Sobotta *et al.*, 2013; Low *et al.*, 2007). It has therefore been proposed that the fusion of roGFP2 to PRDX-2 could provide a highly sensitive and specific sensor for H_2O_2 (Ezeriņa *et al.*, 2014). Despite this, there are still limitations to consider when using genetic probes *in vivo*; such as how the probes affect the systems they are in, and only the use of a steady state read-out. For example, by providing oxidisable cysteines the HyPer and Orp1-roGFP2 tools have antioxidant activity and compete with signalling proteins and other peroxiredoxins for H_2O_2 (Lukyanov and Belousov, 2014).

1.6 Summary and Aims

1.6.1 *S. pombe* and *C. elegans* as models for investigating H_2O_2 signalling

The ease of genetic manipulation of the *S. pombe* and *C. elegans* organisms make these models highly suitable for studying H_2O_2 signalling. *S. pombe* have one 2-Cys Prx, Tpx1, which has already been successfully manipulated to elucidate mechanisms and beneficial adaptive responses to H_2O_2 (Veal *et al.*, 2014; Brown *et al.*, 2013). The *tpx1*Δ and the peroxidase defective $tpx1^{C169S}$ cells are sensitive to H_2O_2. Access to *S. pombe* gene deletion libraries has made high-throughput screening a quick and cost-effective method

to screen thousands of genes. Genetic screening techniques also remove the bias toward more abundant proteins, often encountered when using proteomic approaches.

Additionally, the low cost, short generation time, lifespan and sequenced genome, make the nematode worm *C. elegans* an attractive model for investigating the biology of ageing (Olsen *et al.*, 2006). The transparency of *C. elegans* also allows for the use of sophisticated *in vivo* imaging techniques. The use of *C. elegans* as a model for studying peroxiredoxins has already revealed many important insights. The *C. elegans* genome contains 2 typical 2-Cys Prx: a cytosolic PRDX-2 and the mitochondrial PRDX-3. PRDX-2 has been characterised to have tissue-specific roles; whereas intestinal PRDX-2 protects against both H_2O_2 and arsenite stress, the expression of PRDX-2 in other tissues limits resistance to arsenite, and inhibits expression of the phase II detoxification genes (Oláhová *et al.*, 2008). The *prdx-2* mutant worms possess multiple phenotypes: reduced peroxide resistance, developmental delay, reduced growth and lower fecundity, reduced lifespan, reduced insulin secretion and contain twice as much glutathione as N2 worms (Isermann *et al.*, 2004; Oláhová *et al.*, 2008; Oláhová and Veal, 2015).

1.6.2 Aims

Whilst high concentrations of H_2O_2 cause cellular damage that is observed in many diseases and in ageing, low levels of H_2O_2 can initiate positive signalling responses that are important for maintaining normal health and longevity. How organisms sense and use H_2O_2 to signal these positive responses is therefore of great medical interest. Nevertheless, identifying target proteins that mediate responses to low levels of H_2O_2 remains challenging, partly because proteomic approaches to identify H_2O_2 targets are biased towards abundant proteins, and also because they are unable to determine whether detected oxidation events are functional. Additionally, in order to study the different H_2O_2 responses it is important to be able to monitor *in vivo* changes in intracellular H_2O_2.

Detecting intracellular H_2O_2 levels *in vivo* has been problematic in the past due to limitations on the specificity and sensitivity of small molecular fluorescent probes. Research efforts have therefore shifted towards using genetic fluorescent redox sensors in order to monitor real-time changes in H_2O_2 concentrations. With this in mind, the first objective of this project was:

- to examine Prx-coupled roGFP2 as a new genetic *in vivo* H_2O_2 sensor in *C. elegans*, and to determine whether transgenic animals expressing N-roGFP2::*prdx-2* can be used to detect small changes in intracellular H_2O_2 levels.

The localisation of Prx to the mitochondria has been observed in a number of model organisms. In addition, mutant Prx display a number of mitochondrial defects; such as, the impaired ETC and altered mitochondria morphology of *tpx1*Δ cells (Latimer, Day, Brown and Veal, unpublished). The recent discovery that in *S. cerevisiae* cells, Gpx3 is localised to the mitochondrial IMS, and that here it has an important role in protein homeostasis and redox regulation revealed some interesting insights (Vögtle *et al.*, 2012; Kritsiligkou *et al.*, 2017). A pool of Pap1 and Sty1 has also previously been detected in the mitochondria of *S. pombe* cells (Di *et al.*, 2012; Latimer thesis, 2017). This led to the hypothesis that a pool of Tpx1 may also be present in the mitochondria of *S. pombe* cells, and may have an important role in mitochondrial function. Therefore, the second objective of this project was:

- to test whether a pool of Tpx1 is localised to the IMS, and whether this may be involved in supporting mitochondrial function and the activation of Pap1.

Finally, 2-Cys Prx have multiple roles in promoting H_2O_2 signal transduction; such as, acting as direct redox transducers, or by promoting the oxidation of thioredoxins. The peroxidase defective *tpx1*^{C169S} *S. pombe* cells are sensitive to H_2O_2 and unable to promote the oxidation of thioredoxin; H_2O_2 resistance however, is restored by the subsequent loss of *txl1*. With this in mind, the third objective of this project was a non-hypothesis driven approach to find new regulators of H_2O_2 signalling, by:

- using high-throughput genetic screening in peroxiredoxin mutant *S. pombe* in order to identify other thioredoxin-regulated proteins and downstream genes involved in mediating H_2O_2 signal transduction.

Chapter 2

Chapter 2. Materials and Methods

2.1 Fission yeast techniques

2.1.1 *S. pombe* strains and growth conditions

The *Schizosaccharomyces pombe* strains used in this study are listed in table 2.1. Cells were grown at 30 °C in either standard rich media YE5S (0.5 % (w/v) yeast extract, 3 % (w/v) glucose, 225 mg/l adenine, histidine, leucine, uracil and lysine hydrochloride, 2 % Difco Bacto Agar), or Edinburgh minimal media (EMM; 14.7 mM potassium hydrogen phthalate ($C_8H_5O_4K$), 15.5 mM di-sodium hydrogen orthophosphate (Na_2HPO_4), 93.5 mM ammonium chloride (NH_4Cl), 2 % (w/v) glucose, 20 ml/l salts (0.26 M magnesium chloride ($MgCl_2.6H_2O$), 4.99 mM calcium chloride ($CaCl_2.2H_2O$), 0.67 M potassium chloride (KCl) and 14.1 mM di-sodium sulphate (Na_2SO_4)), 1 ml/l vitamins (4.2 mM panthothenic acid, 81.2 mM nicotinic acid, 55.5 mM inositol and 40.8 µM biotin), 0.1 ml/l minerals (80.9 mM boric acid, 23.7 mM magnesium sulphate ($MnSO_4$), 13.9 mM zinc sulphate ($ZnSO_4.7H_2O$), 7.40 mM iron chloride ($FeCl_2.6H_2O$), 2.47 mM molybdic acid, 6.02 mM potassium iodide (KI), 1.6 mM copper sulphate ($CuSO_4.5H_2O$) and 47.6 mM citric acid), 2 % (w/v) Difco Bacto Agar). EMM was supplemented with required amino acids for selective growth, and when applicable; 15 µM thiamine was added to repress nmt promoter activity. *S. pombe* cultures were grown aerobically using an orbital shaker at 180 rpm until mid-log phase (OD_{595} = 0.3-0.5) and harvested by centrifugation at 3000 rpm for 1 min.

Strain	Genotype	Construction	Source
NT4	*h^+ ade6-M210 leu1-32 ura4-D18*	-	Laboratory stock
NT5	*h^- ade6-M210 leu1-32 ura4-D18*	-	Laboratory stock
SW61	*h^- ade6-M210 leu1-32*	-	S. Whitehall
Pot1	*h^- ade6-M210 leu1-32 ura4-D18 mat1_m-cyhS smt0 rpl42::cyh(R) (sP56Q) Nat::POT1::HpHMX*	-	P. Banks
Ura1	*h^- ade6-M210 leu1-32 ura4-D18 mat1_m-cyhS, smt0 rpl42::cyhR(sP56Q) ura1::NATMX*	-	P. Banks
Ura5	*h^- ade6-M210 leu1-3 ura4-D18 mat1_m-cyhS, smt0 rpl42::cyhR(sP56Q) ura5::NATMX*	-	P. Banks
JR42	*h^+ ade6 leu1-32 ura4-D18 tpx1::ura4$^+$ tpx1^{C169S}:LEU2*	-	(Brown *et al.*, 2013)
JR68	*h^+ ade6-M210 leu1-32 ura4-D18 tpx1::ura4$^+$ tpx1$^+$:LEU2*	-	(Brown *et al.*, 2013)
EV76	*h^- ade6 leu1-32 ura4-D18 txl1::kan^{mx4}*	-	(Brown *et al.*, 2013)
JB92	*h^+ ade6 leu1-32 ura4-D18 tpx1::ura4$^+$ tpx1^{C169S}:LEU2 txl1::kan^{mx4}*	-	(Brown *et al.*, 2013)
VXOO	*h^+ ade6-M210 leu1-32 ura4-D18 tpx1::ura4$^+$*	-	Laboratory stock
EV45	*h^+ ade6 leu1-32 ura4-D18 tpx1::ura4$^+$*	-	(Veal *et al.*, 2004)

JB99	*h⁻ ade6 leu1-32 ura4-D18 tpx1::ura4⁺ tpx1⁺:LEU2 txl1::kan^{mx4}*	-	J. Brown
WH10-14	*h⁺ ade6-M216 leu1-32 ura4-D18 grx1::kan^{r}*	-	(Chung *et al.*, 2004)
cox4rfp:hyg	*h⁺ ade6-M210 leu1-32 ura4-D18 his7-366 cox4rfp:kan*	Emily Holmes with kanamycin in 428 background	Kind gift Caroline Wilkinson
HL16	*h⁺ ade6-M210 leu1-32 ura4-D18 tim40egfp::ura4⁺*	-	H. Latimer
DRG21	*h90 ade6.210 leu1.32 ura4-D18 pka1-13Myc-kan^{MX6}*	-	(Gupta *et al.*, 2011a)
SP870	*h90 ade6.210 leu1.32 ura4-D18*	-	(Gupta *et al.*, 2011a)
KS84	*h⁻ ade6-704 leu1-32 ura4-D18 csn5::ura4*	-	(Mundt *et al.*, 2002)
AMC348	*h⁻ ade6-704 leu1-32 ura4-D18 csn1-cMyc:kan^{MX6}*	-	(Mundt *et al.*, 2002)
AMC350	*h⁻ ade6-704 leu1-32 ura4-D18 csn5-cMyc::kan^{MX6}*	-	(Mundt *et al.*, 2002)
ZU10	*h⁻ ade6-M210 leu1-32 ura4-D18 tpx1::ura4⁺ tpx1⁺:nat^{MX6}*	JR68 transformed with natMX6	This study
ZU11	*h⁻ ade6-M210 leu1-32 ura4-D18 tpx1::ura4⁺ tpx1^{C169S}:nat^{MX6}*	JR42 transformed with natMX6	This study
ZU12	*h⁻ ade6-M210 leu1-32 ura4-D18 tpx1::nat^{MX6}*	VXOO transformed with natMX6	This study

ZU13	*h? ade6-M210 leu1-32 ura4-D18 tpx1::ura4^{+} tpx1^{C169S}:nat^{MX6} cgi121::kan^{MX4}*	Isolate from SGA	This study
ZU14	*h^{+} ade6-M210 leu1-32 ura4-D18 tpx1::nat^{MX6}*	VXOO transformed with natMX6	This study
ZU16	*h? ade6-M210 leu1-32 ura4-D18 tpx1::ura4^{+} tpx1^{C169S}:nat^{MX6} spn4::kan^{MX4}*	Isolate from SGA	This study
ZU17	*h? ade6-M210 leu1-32 ura4-D18 tpx1::ura4^{+} tpx1^{C169S}:nat^{MX6} uds1::kan^{MX4}*	Isolate from SGA	This study
ZU18	*h? ade6-M210 leu1-32 ura4-D18 tpx1::ura4^{+} tpx1^{C169S}:nat^{MX6} SPBC83.19c::kan^{MX4}*	Isolate from SGA	This study
ZU19	*h? ade6-M210 leu1-32 ura4-D18 tpx1::ura4^{+} tpx1^{C169S}:nat^{MX6} SPAC11G7.01::kan^{MX4}*	Isolate from SGA	This study
ZU20	*h? ade6-M210 leu1-32 ura4-D18 tpx1::ura4^{+} tpx1^{C169S}:nat^{MX6} pus1:kan^{MX4}*	Isolate from SGA	This study
ZU21	*h? ade6-M210 leu1-32 ura4-D18 tpx1::ura4^{+} tpx1^{C169S}:nat^{MX6} cgi121::kan^{MX4}*	Isolate from SGA	This study
ZU22	*h? ade6-M210 leu1-32 ura4-D18 tpx1::ura4^{+} tpx1^{C169S}:nat^{MX6} cgi121::kan^{MX4}*	Isolate from SGA	This study

ZU23	*h? ade6-M210 leu1-32 ura4-D18 tpx1::ura4^{+} tpx1^{C169S}:nat^{MX6} cgi121::kan^{MX4}*	Isolate from SGA	This study
ZU24	*h? ade6-M210 leu1-32 ura4-D18 tpx1::ura4^{+} tpx1^{C169S}:nat^{MX6} cgi121::kan^{MX4}*	Isolate from SGA	This study
ZU25	*h? ade6-M210 leu1-32 ura4-D18 tpx1::ura4^{+}*	ZU11 x *cgi121*Δ (Bioneer)	This study
ZU26	*h? ade6-M210 leu1-32 ura4-D18 tpx1::ura4^{+} cgi121::kan^{MX4}*	ZU11 x *cgi121*Δ (Bioneer)	This study
ZU27	*h? ade6-M210 leu1-32 ura4-D18 tpx1::ura4^{+} tpx1^{C169S}:nat^{MX6} cgi121::kan^{MX4}*	ZU11 x *cgi121*Δ (Bioneer)	This study
ZU28	*h? ade6-M210 leu1-32 ura4-D18 tpx1::ura4^{+} tpx1^{C169S}:nat^{MX6}*	ZU11 x *cgi121*Δ (Bioneer)	This study
ZU29	*h? ade6-M210 leu1-32 ura4-D18 tpx1::ura4^{+} cgi121::kan^{MX4}*	ZU11 x ZU13	This study
ZU30	*h? ade6-M210 leu1-32 ura4-D18 tpx1::ura4^{+} tpx1^{C169S}:nat^{MX6}*	ZU11 x ZU13	This study
ZU31	*h? ade6-M210 leu1-32 ura4-D18 tpx1::ura4^{+} tpx1^{C169S}:nat^{MX6}*	ZU11 x ZU13	This study
ZU40	*h? ade6-M210 leu1-32 ura4-D18 tpx1::ura4^{+} tpx1^{C169S}:nat^{MX6} grx1::kan^{r}*	ZU11 x WH10-14	This study
ZU41	*h? ade6-M210 leu1-32 ura4-D18 tpx1::ura4^{+}*	ZU11 x WH10-14	This study
ZU42	*h? ade6-M210 leu1-32 ura4-D18 tpx1::ura4^{+}*	ZU11 x WH10-14	This study

ZU53	*h? ade6-M210 leu1-32 ura4-D18 tpx1::ura4^{+}*	ZU11 x WH10-14	This study
ZU54	*h? ade6-M210 leu1-32 ura4-D18 tpx1::ura4^{+} tpx1^{C169S}:nat^{MX6} grx1::kan^{r}*	ZU11 x WH10-14	This study
ZU55	*h? ade6-M210 leu1-32 ura4-D18 tpx1::ura4^{+} tpx1^{C169S}:nat^{MX6} grx1::kan^{r}*	ZU11 x WH10-14	This study
ZU56	*h? ade6-M210 leu1-32 ura4-D18 tpx1::ura4^{+}*	ZU11 x WH10-14	This study
ZU57	*h? ade6 leu1-32 ura4-D18 tpx1::nat^{MX6} csn5::ura4^{+}*	KS84 x ZU14	This study
ZU59	*h^{+} ade6 leu1-32 ura4-D18 tpx1::ura4^{+} tpx1^{C169S}:LEU2 txl1::kan^{mx4}*	EV76 x JR42	This study
ZU60	*h^{+} ade6 leu1-32 ura4-D18 tpx1::ura4^{+} tpx1^{C169S}:LEU2 txl1::kan^{mx4}*	EV76 x JR42	This study
ZU61	*h^{+} ade6 leu1-32 ura4-D18 tpx1::ura4^{+} tpx1^{C169S}:LEU2 txl1::kan^{mx4}*	EV76 x JR42	This study
ZU62	*h^{+} ade6 leu1-32 ura4-D18 tpx1::ura4^{+} tpx1^{C169S}:LEU2 txl1::kan^{mx4}*	EV76 x JR42	This study
ZU67	*h^{-} ade6-M210 leu1-32 ura4-D18 tpx1::nat^{MX6} ssm4::kan^{mx4}*	Isolate from SGA	This study
ZU68	*h^{-} ade6-M210 leu1-32 ura4-D18 tpx1::nat^{MX6} lys9::kan^{mx4}*	Isolate from SGA	This study

ZU69	*h⁻ ade6-M210 leu1-32 ura4-D18 tpx1::nat^{MX6} csn5::kan^{mx4}*	Isolate from SGA	This study
ZU70	*h⁻ ade6-M210 leu1-32 ura4-D18 tpx1::nat^{MX6} pka1::kan^{mx4}*	Isolate from SGA	This study
ZU72	*h⁻ ade6-M210 leu1-32 ura4-D18 tpx1::nat^{MX6} pka1::kan^{mx4}*	ZU12 x *pka1*Δ (Bioneer)	This study
ZU73	*h⁻ ade6-M210 leu1-32 ura4-D18 tpx1::nat^{MX6} pka1::kan^{mx4}*	ZU12 x *pka1*Δ (Bioneer)	This study
ZU74	*h⁻ ade6-M210 leu1-32 ura4-D18 tpx1::nat^{MX6} pka1::kan^{mx4}*	ZU12 x *pka1*Δ (Bioneer)	This study

Table 2.1 *S. pombe* strains used in this study

2.1.2 Yeast mating

Haploid *S. pombe* strains were mated by mixing growing cells of opposite mating types (h^+ and h^-) on EMM ½ G (EMM with NH_4Cl replaced with 5.91 mM sodium glutamate) agar plates. Strains were mixed with 10 µl sterile nH_2O and incubated at 25 °C for 72 h, or until tetrad formation (visible using a light microscope). Tetrads and spores were then separated from vegetative cells by manual dissection using a Singer micromanipulator, or spores selected using a random sporulation protocol.

2.1.3 Tetrad dissection

Following tetrad formation, a scraping of mated cells were resuspended in 100 µl H_2O, vortexed and 10 µl resuspension was dropped down a YE5S plate. The plate was dried at 37 °C before asci were isolated using a Singer micromanipulator and aligned in grid formation. Asci were dissected following ~3 h incubation at 37 °C, with each spore being separated in a line of four. Plates were incubated at 30 °C until visible colonies formed. Genotypes of the strains were determined by patching colonies onto the appropriate selection plates.

2.1.4 Random sporulation

A scraping of mated cells were resuspended in 100 µl 0.5 % (v/v) glusulase (PerkinElmer) and incubated overnight at 30 °C. Following this, 42.5 µl 100 % ethanol

(EtOH) was added and the mix was incubated at room temperature for 20 mins to kill vegetative cells. Cells were spread onto EMM agar plates supplemented with the appropriate amino acids, or YE5S plates supplemented with the appropriate antibiotics, and incubated at 30 °C until visible colonies formed. Genotypes of strains were determined by patching colonies onto the appropriate selection plates.

2.1.5 Yeast genomic DNA extraction

A scraping of cells were transferred to an microfuge tube containing 30 µl 0.2 % (w/v) SDS. Samples were vortexed for 15 s, boiled at 100 °C for 2 mins, and spun in a microcentrifuge at 13,000 rpm for 1 min. 1 µl of supernatant was used per PCR reaction.

2.1.6 Chemical transformation of DNA into *S. pombe*

Cells were inoculated from plate into 100 ml YE5S and incubated at 30 °C with agitation overnight. Cells were diluted to OD_{595} = 0.15 and further incubated until reached mid-log phase (OD_{595} = 0.4-0.5). Exponentially growing cells were pelleted by centrifugation at 2000 rpm for 3 mins, washed with 20 ml H_2O, resuspended in 500 µl H_2O and pooled into a microfuge tube. Cells were collected by centrifugation in a microcentrifuge at 2000 x rpm for 3 mins and washed in H_2O and spun again. Pellets were resuspended in 500 µl H_2O, pooled and spun in a microcentrifuge at 7000 rpm for 30 s. Pellets were washed in 1 x Lithium acetate/Tris-EDTA (1 x LiAc/TE) (10 mM Tris-HCl (pH 7.5), 1 mM EDTA (pH 8.0), 100 mM lithium acetate (pH 7.0)), spun once more and resuspended in 1 ml LiAc/TE. Cells were mixed with 2 µl salmon sperm DNA (10 mg/ml) (Invitrogen) and 1-2 µg transforming plasmid (Table 2.2) or PCR-generated DNA and incubated at room temperature for 10 mins. 260 µl polyethylene glycol/LiAc/TE (PEG/LiAc/TE) (40 % (v/v) PEG-4000, 10 mM Tris-HCl pH8, 1 mM EDTA pH8, 0.1 M lithium acetate pH7.5) was added and mixed gently. Samples were incubated at 30 °C with agitation for 1 h. 43 µl dimethyl sulphoxide (DMSO) was added and samples were heat shocked at 42 °C for 5 mins. Cells were collected by centrifugation in a microcentrifuge at 7000 rpm for 30 s. Cells were washed with 1 ml H_2O, pelleted again and resuspended in 200 µl H_2O. Transformed cells were selected either based on complementation of an auxotrophic marker (by plating onto EMM agar supplemented with appropriate amino acids), or on the basis of antibiotic resistance (by incubating in 1 ml YE5S at 30 °C overnight, before plating onto YE5S agar supplemented with 0.1 mg/ml clonNAT (clonNAT nourseothricin (HKI,jena)) (Goldstein and McCusker, 1999), and incubated at 30 °C for 4 – 5 days).

Plasmid	Source
pRep1	(Maundrell, 1993)
pRep1Tpx1	(Veal *et al.*, 2004)
pRep1Tpx1^{C169S}	(Veal *et al.*, 2004)
pRep1FlagTpx1	(Veal *et al.*, 2004)
pRep1FlagTpx1^{C169S}	(Veal *et al.*, 2004)
pRep1csn5	E. Veal unpublished
pRep41flagtxl1	(Brown *et al.*, 2013)
pRep41-GFPpap1	(Toone *et al.*, 1998)
pRS316	Laboratory stock
pRS316-up40-cyb2-Gpx3-myc	(Kritsiligkou *et al.*, 2017)
pFA6a-natMX6	Laboratory stock

Table 2.2 Plasmids used in this study.

2.1.7 Cell size analysis

Cell size was quantified using the CASY Cell Counter + Analyser System, Model TT (Schärfe system): 4 µl exponentially growing cells were added to 10 ml filter sterilised CASYton solution for measurement.

2.2 Phenotypic Tests

2.2.1 High-throughput genetic screening

High-throughput genetic screening was conducted by The High Throughput Screening Facility (HTSF) in the Faculty of Medical Sciences at Newcastle University.

2.2.1.1 Synthetic Genetic Array (SGA)

ZU10, ZU11 and ZU12 strains were systematically crossed with the *S. pombe* haploid non-essential deletion mutant library (3,400 strains, Geneticin deletion library (G418)) (Bioneer) (Kim *et al.*, 2010) to generate synthetic genetic arrays, using the BM3 colony pinning robot (S&P Robotics). The query strains (ZU10, ZU11, ZU12), and the *S. pombe*

haploid non-essential deletion mutant library were freshly pinned into a 768 format onto YE5S plates (0.5 % (w/v) yeast extract, 0.115 % (w/v) YE5S amino acid powder, 2 % (w/v) Difco Bacto agar, 3 % (w/v) dextrose) supplemented with either 0.1 mg/ml clonNAT, or 0.1 mg/ml G418 respectively, and incubated at 30 °C for 3 days. Strains were pinned onto the same EMM 1/2G agar plate (11 plates in total) and incubated at 25 °C for 3 days for sporulation. Vegetative cells were killed by incubating the plates at 42 °C for an additional 3 days. Spores were subsequently re-pinned onto YE5S agar and incubated at 30 °C for 4 days. To select for double mutants, cells were re-pinned onto YE5S containing 0.1 mg/ml clonNAT and incubated at 30 °C for 2 days, and finally pinned onto YE5S containing 0.1 mg/ml clonNAT and 0.1 mg/ml G418, and incubated at 30 °C for 2 days (figure 2.1).

2.2.1.2 SGA Analysis

Images of the final plate were taken using the spImager software. Cell density is quantified from the photographs using the image analysis tool Colonyzer. The SGA data was analysed using the R visualisation tool; fitness of the double mutant strains was represented as a 2D scatter plot. Fitness was ordered by genetic interaction score. Each Bioneer deletion strain is crossed with ZU10, ZU11 and ZU12 in quadruplet within each SGA screen, and each SGA was conducted at least twice. The entire *S. pombe* deletion library is spotted over 11 rectangular agar plates, and around the periphery of each plate the *mug134*Δ strain is spotted 76 times to act as a control for the increased space and nutrients around the edge of the plate.

2.2.1.3 Quantitative Fitness Analysis (QFA)

QFA analysis was undertaken on the double mutant strains generated from the $tpx1^{C169S}$ SGA using the Beckman Coulter Biomek FX robot (5 out of 11 plates). Cells were pinned to inoculate 200 µl liquid cultures (YE5S + 6.5µg/ml clonNAT + 6.5 µg/ml G418) in a 96 well plate and incubated at 30 °C until grown to saturation. Liquid cultures were diluted 10 x and incubated at 30 °C for another 16 h. Cells were then pinned in a 384 format onto YE5S agar containing 6.5 µg/ml clonNAT, 6.5 µg/ml G418 and either no stress, 250 µM tBOOH, 500 µM H_2O_2 or 750 µM H_2O_2, and incubated at 30 °C for 60 h (figure 2.1). The *tpx1*Δ SGA did not undergo QFA.

2.2.1.4 QFA Analysis

QFA plates were imaged at 15 different time points over 60 h (around once every 260 mins) using the spImager software. Cell density was quantified using the image analysis tool Colonyzer. The QFA R package was used for analysing the QFA data: sensitivity of the double mutant strains to the exposed stress is represented as an overall 2D scatter plot, additionally, growth curves of each individual strain were plotted. Fitness was ordered by genetic interaction score. To account for reproducibility strains were tested in quadruplicate within the QFA, and an average fitness score was calculated. This QFA was conducted once.

SGA

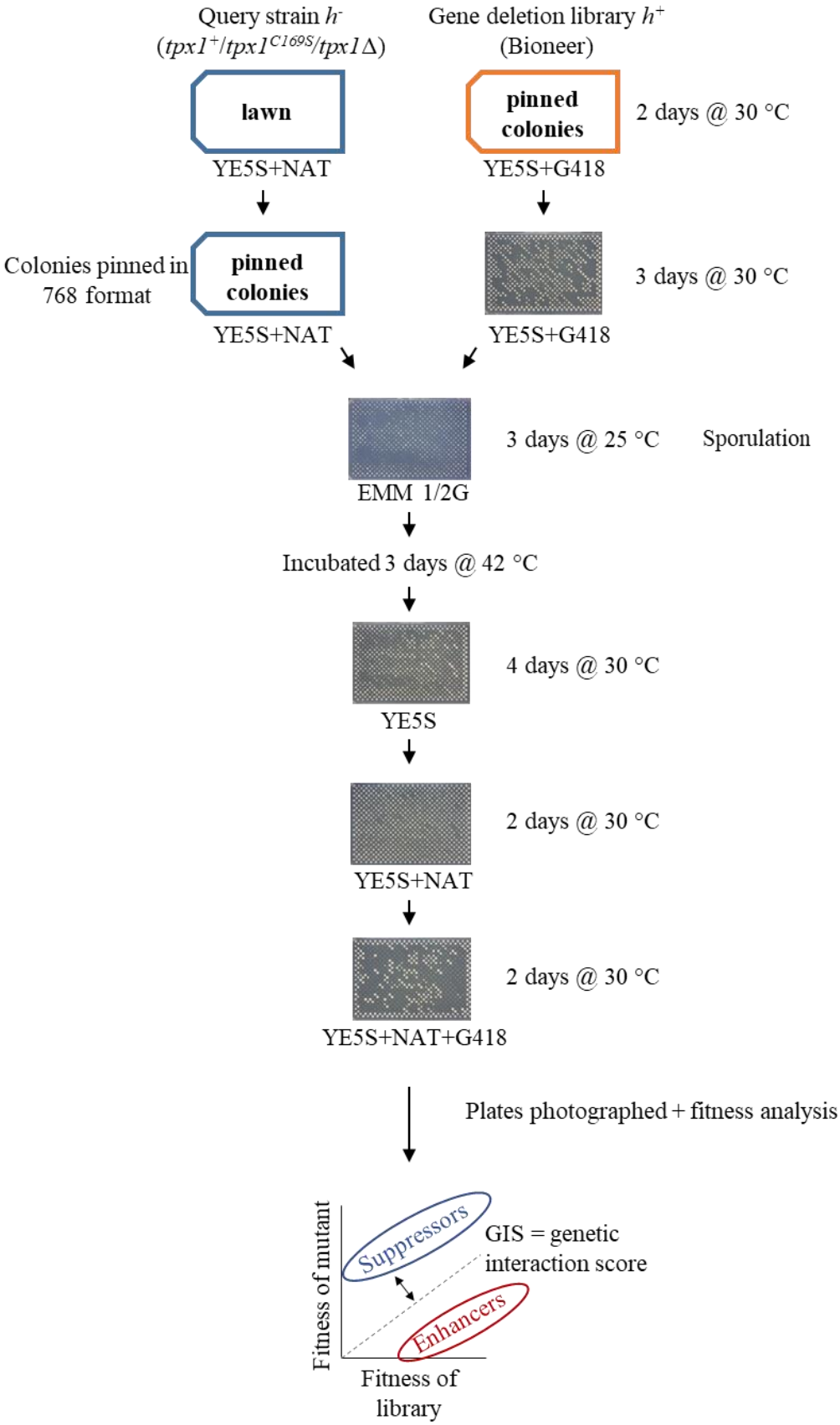
Query strain h⁻
(tpx1⁺/tpx1^C169S/tpx1Δ)
Gene deletion library h⁺
(Bioneer)
lawn
YE5S+NAT
pinned colonies
YE5S+G418
2 days @ 30 °C
Colonies pinned in 768 format
pinned colonies
YE5S+NAT
YE5S+G418
3 days @ 30 °C
EMM 1/2G
3 days @ 25 °C
Sporulation
Incubated 3 days @ 42 °C
YE5S
4 days @ 30 °C
YE5S+NAT
2 days @ 30 °C
YE5S+NAT+G418
2 days @ 30 °C
Plates photographed + fitness analysis
Fitness of mutant
Suppressors
Enhancers
GIS = genetic interaction score
Fitness of library

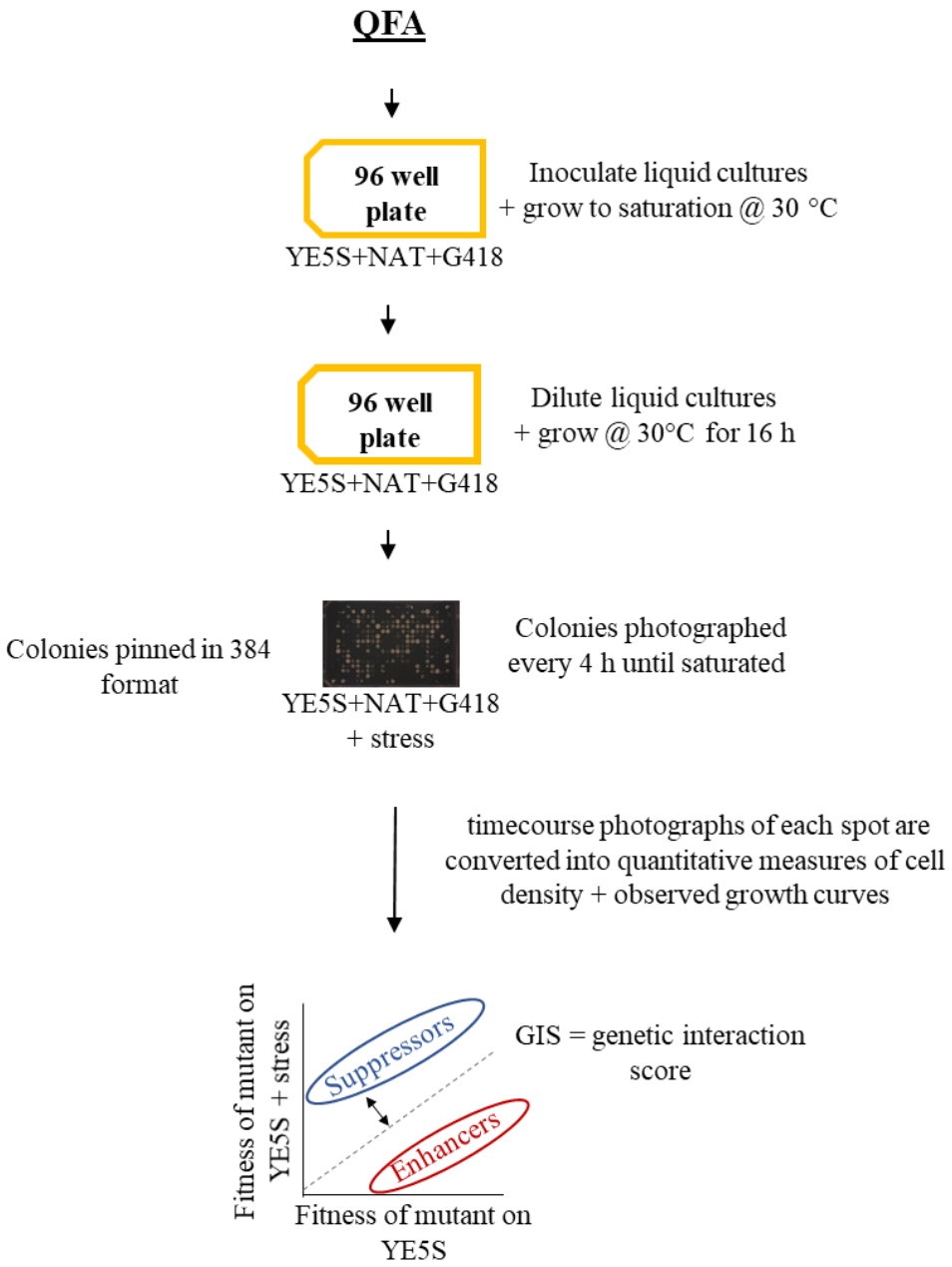

Figure 2.1 SGA and QFA Methodology. SGA: Using the BM3 colony pinning robot, query strains were systematically crossed with the *S. pombe* haploid non-essential deletion mutation library (Biooneer) and photographed to determine strain fitness compared with wild-type. **QFA:** Using the Beckman Coulter Biomek FX robot, the double mutant strains (SGA) were grown in liquid cultures and spotted onto agar plates containing different stress reagents. Cells were photographed over 60 h and their fitness with and without exposure to stress was measured. **Image analysis:** The genetic interaction score (GIS) was calculated by comparing mutant SGA strain fitness to wild-type strains fitness (SGA), or with and without exposure to stress (QFA).

2.2.2 Halo Tests

Cultures grown overnight at 30 °C in YE5S were diluted back to OD_{595} = 0.1 and further incubated at 30 °C with agitation until reaching an OD_{595} = 0.3 - 0.5. 15 µl 1.7 mM H_2O_2 or 15 µl 0.8 M tBOOH was pipetted onto a small circle of filter paper and placed in the centre of a dried YE5S plate. 30 µl of cells was then pipetted in a line towards the centre of the plate. Plates were dried on the bench and incubated at 30 °C for 2 days.

2.2.3 Spot Tests

Cells grown overnight at 30 °C in YE5S were diluted back to OD_{595} = 0.1 and further incubated at 30 °C with agitation until reaching an OD_{595} = 0.3 – 0.5. Exponentially growing cells (cells doubling every 2-3 h) were diluted back to the most dilute and serially diluted before spotting onto freshly prepared agar plates. To compare growth on different agar, cells were routinely spotted onto YE5S, EMM supplemented with the appropriate amino acids, and 3 % glycerol plates (0.5 % (w/v) yeast extract, 3 % (v/v) glycerol, supplemented with 225 mg/l adenine, histidine, leucine, uracil, lysine). To test stress sensitivities cells were also spotted onto YE5S agar plates containing varying concentrations of the oxidising reagents hydrogen peroxide (H_2O_2) (Sigma-Aldrich). Plates were incubated at 30 °C, or 37 °C, as indicated, for 2-4 days and imaged at 24 h intervals.

2.3 *C. elegans* Techniques

2.3.1 *C. elegans* strains

The *Caenorhabditis elegans* strains used in this study are listed in table 2.3.

Strain	Genotype	Source
N2	WT	Laboratory stock
EB277 (75-1)	*[N-roGFP2::prdx-2 rol-6]*	Nisha Hirani and Colin Dolphin
EB276 (76-2)	*[C-roGFP2::prdx-2 rol-6]*	Nisha Hirani and Colin Dolphin
EB278 (77-1)	*[C-roGFP2::prdx-3 rol-6]*	Nisha Hirani and Colin Dolphin
PS6192 (EB254)	*syIs268 [myo-3p::TOM20::mRFP] (50 µg/µl) + unc-119 (50 ng/µl)*	Kind gift of Amir Sapir
EB253	*prdx-2(gk169) syIs268 [myo-3p::TOM20::mRFP] (50 µg/µl) + unc-119 (50 ng/µl)*	VE1xPS6192 (Oláhová, unpublished)
CB5600 (EB255)	*him-8(e1489) IV. ccIs4251 [(pSAK2) myo-3p::GFP::LacZ::NLS + (pSAK4) myo-3p::mitochondrial GFP + dpy-20(+)] I*	CGC
EB260	*prdx-2(gk169) him-8(e1489) IV. ccIs4251 [(pSAK2) myo-3p::GFP::LacZ::NLS + (pSAK4) myo-3p::mitochondrial GFP + dpy-20(+)] I*	CB5600xVE1 (Oláhová, unpublished)

Table 2.3 *C. elegans* strains used in this study

2.3.2 Growth and maintenance of *C. elegans*

Strains were maintained on Nematode Growth Media-Lite (NGM-L) agar (2 % (w/v) NaCl (Sigma), 4 % (w/v) Bacto tryptone (BD), 4 % (w/v) Bacto agar (BD), 3 % (w/v) KH_2PO_4 (Biochemika) and 0.5 % (w/v) K_2HPO_4 (Biochemika)), supplemented with 8 nM cholesterol (Sigma-Aldrich). Plates were seeded with a thin lawn of *E. coli* OP50 culture in the centre of the plate, which had grown shaking overnight at 37 °C in LB broth liquid media supplemented with 100 µg streptomycin (Sigma-Aldrich). The *Escherichia coli* strain used in this study is listed in table 2.4. Seeded plates were dried at room

temperature for 48 h and were then stored at 4 °C. Approximately 5 adult animals were transferred to freshly seeded NGM-L plates with a platinum wire pick each week using a stereo microscope (Leica CLS 50x), and maintained at 15 °C. For the roGFP2 stocks, only animals that exhibit the rolling phenotype (*rol-6*) were picked for maintenance and experimentation.

Name	Phenotype	Source
OP50	Str^r	Laboratory stock

Table 2.4 *E. coli* strains used in this study

2.3.3 Treatment of *C. elegans* with exogenous reagents

When investigating the effect of exogenous reagents, the M9 containing 0.06 % levamisole was supplemented with a final concentration of 0, 0.2, 1 and 5 mM H_2O_2 (Sigma-Aldrich), or 50 mM diamide (Sigma-Aldrich), or 100 mM DTT (Sigma-Aldrich), or 20 mM N-Ethylmaleimide (NEM) (Sigma-Aldrich).

2.3.4 Starvation of *C. elegans*

For starvation experiments L4 larval stage were transferred to an unseeded NGM-L plate and incubated at 15 °C for 1, 4 or 8 hours.

2.3.5 Infection of *C. elegans* with *C. albicans*

C. elegans at L4 larval stage were incubated at 25 °C on unseeded NGM-L plates for 1 h, worms were then moved to Brain Heart Infusion (BHI, Scientific Laboratory Suppliers) agar plates seeded with wild-type *C. albicans* (JC747) or, NGM-L plates seeded with OP50 for 1 h or 24 h. The *Candida albicans* strain used in the study is listed in table 2.5.

Name	Genotype	Source
JC747	SN148 Clp30	(da Silva Dantas *et al.*, 2010)

Table 2.5 *C. albicans* strain used in this study

2.4 Molecular biology techniques

2.4.1 Polymerase chain reaction

2.4.1.1 PCR to confirm gene deletion strains

PCR for confirming gene deletion strains were performed using a DreamTaq kit (Thermo Fisher). 50 µl reaction mixes contained: 1 µl genomic DNA, 1 x buffer, 100 pmol forward primer (table 2.6), 100 pmol reverse primer, 200 µM dNTP (dATP, dCTP, dGTP, dTTP), 0.5 µl DreamTaq DNA polymerase. PCR was performed in a thermocycler using the programme: 94 °C for 2 min, 94 °C for 30 s, ~50 °C for 30s, 72 °C for 1-3 min (steps 2-4 cycled 44 times), 72 °C for 10 min.

2.4.1.2 PCR for sequencing

PCR for sequencing was performed using High Fidelity PCR system (NEB): 50 µl reaction mixes contained: 1 x HF buffer, 200 µM dNTPs, 1 µl forward primer (table 2.6), 1 µl reverse primer, 0.5 µl Phusion DNA polymerase, 1 µl genomic DNA. The following programme was used: 94 °C for 1 min 30 s, 94 °C for 30 s, ~50 °C for 30 s, 72 °C for 2 min (steps 2-4 cycled 44 times), 72 °C for 10 min.

2.4.1.3 PCR to confirm mating type

The mating type of *S. pombe* strains was confirmed by PCR using a 50 µl Simply Red (Thermo Fisher) reaction mix (5 µl buffer, 3 µl $MgCl_2$, 1 µl 10 mM dNTP, 0.5 µl enzyme, 38 µl H_2O, 0.5 µl MTI primer, 0.5 µl MP primer and 0.5 µl MM primer (table 2.6)), using the programme: 94 °C for 2 min, 94 °C for 20 s, 50 °C for 30 s, 72 °C for 2 min (steps 2-4 repeated for 35 cycles), 72 °C for 10 mins.

2.4.1.4 PCR amplification of natMX6 cassette

For generation of nourseothricin-resistant (NAT^r) *tpx1*$^+$ (ZU10) and *tpx1*^{C169S} (ZU11) strains, the natMX6 cassette (1246 bp) was amplified from pFA6a-natMX6 (3704 bp) using a 100 µl Phusion reaction mix (20 µl 5 x GC buffer, 6 µl $MgCl_2$, 1 µl LEUNATF primer, 1 µl LEUNATB primer (table 2.6), 2 µl 10 mM dNTPs, 1 µl Phusion enzyme, 1 µl plasmid template (pFA6a-natMX6), 5 µl DMSO and 63 µl nH_2O) (Biolabs) and the programme: 94 °C for 2 mins, 94 °C for 1 min, 50 °C for 1 min, 72 °C for 3 mins (steps 2-4 repeated for 30 cycles), 72 °C for 20 mins and paused at 4 °C (Goldstein and McCusker, 1999) was used. This same method was used for generation of the *tpx1*Δ (ZU12) strain, however primers: UraNatF and UraNatR (table 2.6) were used. Primers were designed so that the natMX6 cassette replaced the *leu2*$^+$ gene (ZU10, ZU11), or *ura4*$^+$ gene (ZU12) downstream of the *tpx1* locus.

2.4.1.5 Amplification of IMS targeting sequence

The *S. cerevisiae* cytochrome b2 inter-membrane space (IMS) targeting sequence (235 bp) was amplified from pRS316up40cytb2GPX3Myc (Kritsiligkou *et al.*, 2017) using primers (IMSFP, IMSRP) (Table 2.6) designed to introduce an NdeI restriction site flagging either side of the sequence. The High Fidelity PCR system (NEB) was used: 1 x buffer, 1 µl IMSFP, 1 µl IMSRP, 200 µM dNTPs, 1 µl Phusion DNA polymerase, 1 µl pRS316up40cytb2GPX3Myc, with the following programme: 94 °C for 2 min, 94 °C for 30 s, 45 °C for 30 s, 72 °C for 2 min, 94 °C for 30 s, 55 °C for 30 s, 72 °C for 2 min (steps 5-7 cycled 44 times), 72 °C for 10 min. The DNA in the PCR reaction was separated on a 0.7 % (w/v) agarose gel (2.4.3) and the IMS-target sequence (253 bp) excised and purified, as described previously (2.4.4).

2.4.2 Oligonucleotide primer sequences

Oligonucleotide sequences were synthesised by Sigma-Aldrich. Sequences are listed in table 2.6.

Primer	Oligonucleotide sequence 5'-3'	Source
MTI(738)	AGAAGAGAGAGTAGTTGAAG	Laboratory stock
MP(739)	ACGGTAGTCATCGGTCTTCC	Laboratory stock
MM(740)	TACGTTCAGTAGACGTAGTG	Laboratory stock
Uds1 F	GACCGATCATTGCAACGTGA	Sigma Aldrich
Uds1 R	CGATTCAATCTCCAACTGGT	Sigma Aldrich
Hsr1 F	GATAGGATCCCCCTTGCAAT	Sigma Aldrich
Hsr1 R	GCCTAAAGATAGCAAAGCAGG	Sigma Aldrich
Cgi121 F	GCTAAGTCAGTAGCTGGAGT	Sigma Aldrich
Cgi121 R	GAAGAATCCACACAACGTTCC	Sigma Aldrich
SPAC4G9.14 F	AACTATCGTCACCATCGG	Sigma Aldrich
SPAC4G9.14 R	TCGTAAGCCCGACTGAGTAA	Sigma Aldrich

Grx1 F	TACGTGCTCCACTGACGTAT	Sigma Aldrich
Grx1 R	GGAGTTGGGAACTCTGACTAATG	Sigma Aldrich
XbaTsaC	CCCAGTTTCTAGACTAGTGCTTGGA AAAGTACTTC	Laboratory stock
HindTsaN	CCCAGCTAAGCTTATGAGTTTGCAA ATCGGTAAAC	Laboratory stock
Kanmx4+840R	CTAGCGTCACCACTCATTGG	Laboratory stock
Sptsa.V6	GCGCATCGATTGGGTGGATGTGCGC	Laboratory stock
Tpx1FPZU	GCTCACTTGCTTACTTCATGC	Sigma Aldrich
Tpx1RPZU	AGCACATTAGCAGACGTC	Sigma Aldrich
LEUNATF	TCGACTACGTCGTTAAGGCCGTTTCT GACAGAGTAAAATTCTTGAGGGAAC TTTCACCATTATGGGAAATGGTTCA AGAAGGTATTGACTCGGATCCCCGG GTTAATTAA	Sigma Aldrich
LEUNATB	GGAGAACTTCTAGTATATCTACATA CCTAATATTATTGCCTTATTAAAAAT GGAATCCCAACAATTACATCAAAAT CCACATTCTCTTCAGAATTCGAGCTC GTTTAAAC	Sigma Aldrich
nmtend	GCAGCTTGAATGGGCTTCC	Laboratory stock
UraNatF	CAAATCCCACTGGCTATATGTATGC ATTTGTGTTAAAAAAGTTTGTATAG ATTATTTAATCTACTCAGCATTCTTT CTCTAAATAGGAATCGGATCCCCGG GTTAATTAA	Sigma Aldrich
UraNatR	ATTGACGAAACTTTTTGACATCTAAT TTATTCTGTTCCAACACCAATGTTTA	Sigma Aldrich

	TAACCAAGTTTTATCTTGTTTGTCTA CATGGTATTTTAGAATTCGAGCTCGT TTAAAC	
Spn4 FP	GCATACTTCCCAGCAATCTA	Sigma Aldrich
Spn4 RP	CCATTCTCAAGGCAATGAAAG	Sigma Aldrich
Pus1 FP	GGAAGGATTAGTCACGGGTT	Sigma Aldrich
Pus1 RP	GAGTGATTCCTTTTAGTGCC	Sigma Aldrich
SPAC11G7.01 FP	CCTGGTTCGTAACTTTAAGG	Sigma Aldrich
SPAC11G7.01 RP	CAACGCGATTACCAAATTG	Sigma Aldrich
Pap1 F	GCTACGGCGGTGTTTAGAA	Sigma Aldrich
Pap1 R	GCGTTGATTATATCACGAGG	Sigma Aldrich
IMS RP	CTCGATTCATATGATCCAGTTTCGGC TCGTT	Sigma Aldrich
IMS FP	CCCAGCTCATATGCTAAAATACAAA CCTTTACTAAAAA	Sigma Aldrich
T7	TAATACGACTCACTATAGGG	Laboratory stock
Pka1 FP 1	GATTACTGCTATTGTTGCGG	Sigma Aldrich
Pka1 FP 2	GAGTGAAAGGCTCAGTATTG	Sigma Aldrich
Pka1 RP 1	ACGTCACTTGCATTGCAC	Sigma Aldrich
Csn5 FP	ACAAGGGATTGGCGATTGTG	Sigma Aldrich
Csn5 RP	CTTTTTAAAGTGGTGTGTCATCG	Sigma Aldrich
Kan RP	ATCACGCTAACATTTGATTAAAATA G	Sigma Aldrich

Table 2.6 Oligonucleotide primers used in this study. Primers containing restriction enzyme sites are underlined.

2.4.3 Agarose gel electrophoresis

1 % (w/v) agarose gels prepared in 1 x TAE (40 mM Tris-acetate, 1 mM EDTA [pH 8.0]) with 0.02 % (v/v) ethidium bromide were used to separate DNA. Gels were imaged using a gel reader (Quantity One programme) or UV lamp.

2.4.4 DNA extraction

DNA bands were excised from agarose gel and extracted using a QIAquick gel extraction kit (QIAGEN). DNA was de-salted using MilliporeSigma DNA filter paper for 30 min at room temperature. DNA concentrations were measured using a nanodrop spectrophotometer (Labtech) at absorbance 260 nm.

2.4.5 DNA sequencing

DNA sequence analysis was performed by GATC BioTech (UK).

2.4.6 Bacterial growth conditions and transformations

E. coli were grown in Luria Broth (LB) (2 % (w/v) Bacto tryptone, 1 % (w/v) Bacto yeast extract, 1 % (w/v) NaCl [pH7.2]) supplemented with 0.1 mg/ml ampicillin (Sigma-Aldrich) overnight at 37 °C. For the formation of solid media, 2 % (w/v) Bacto agar was added.

For propagation of plasmids, competent *E. coli* with the genotype *e74^{-}(mcrA^{-}) Δ(mcrCB-hsdSMR-mrr)171 endA1 SupE44 thi-1 gyrA96 relA lac recB recJ shcJ umuC ::Tn5 (Kan^{r}) uvrC[F'proABlacI^{q}ZΔmisTn10(Tet^{r})]* (laboratory stock) were used. 100 µl competent cells were gently added to 1 µl plasmid DNA and incubated on ice for 30 mins. Cells were heat-shocked at 42 °C for 2 min in a water bath. 1 ml LB was added to the cells, which were gently mixed then incubated at 37 °C for 1 h. Cells were plated onto LB plates containing 0.1 mg/ml ampicillin (Sigma-Aldrich) and incubated at 37 °C overnight.

2.4.7 Plasmid DNA extraction

Plasmid DNA was isolated from a 5 ml overnight culture of *E. coli* cells using the GenElute Plasmid Miniprep kit (Sigma-Aldrich), following the manufacturer's protocol.

2.4.8 Cloning an IMS targeting sequence into pRep1Tpx1

2.4.8.1 Restriction endonuclease digestion, phosphatase treatment and DNA ligation reactions

The IMS-targeting sequence containing DNA and 3 µg pRep1Tpx1 were digested in 50 µl reactions with 1 x buffer D (Promega), 0.5 µl BSA (Promega) and 1 µl *Nde*I (Thermo Scientific) at 37 °C for 3 h. The *Nde*I -digested pRep1Tpx1 was then treated with alkaline phosphatase (1 µl alkaline phosphatase and 10 µl 10 x phosphatase buffer) (NEB) at 37 °C for 1 h then separated on a 0.7 % (w/v) agarose gel from which the digested band was excised, purified and de-salted, as described previously (2.4.4). The IMS fragment was cleaned up using a QIAquick nucleotide removal kit (QIAGEN) and de-salted for 30 mins at room temperature. Ligation reactions were set up in 20 µl volumes with a molar ratio of 1 vector (50 ng):5 insert fragment (1 x T4 ligase buffer, 50 ng digested pRep1Tpx1, 50 ng digested IMS fragment, 1 µl T4 ligase (Promega)) and incubated at 15 °C overnight (figure 2.2)

2.4.8.2 SURE competent cell transformation

For cloning, plasmid transformation was performed using SURE competent cells (200238, Agilent). 100 µl competent cells were gently mixed with 1.7 µl β-mercaptoethanol and incubated on ice for 10 min. The 20 µl ligation mix was then gently added to each tube and incubated on ice for a further 30 min. Cells were heat-pulsed at 42 °C in a water bath for 45 s, and incubated on ice for a further 2 min. 900 µl pre-heated (42 °C) LB media was added and samples were incubated at 37 °C for 1 h with shaking. Samples were plated onto an LB plates containing 0.1 mg/ml ampicillin (Sigma-Aldrich) and incubated at 37 °C overnight.

2.4.8.3 Checking transformation colonies

Colonies were grown in 5 ml LB+Amp at 37 °C overnight and plasmids extracted as described previously (2.4.7). 1 µg plasmid DNA was digested in 30 µl reactions with 1 x buffer H (Promega), 0.3 µl BSA (Promega), 1 µl Pst1 and 1 µl BamHI (Thermo Scientific) at 37 °C for 1 h. Digested plasmids were run on a 0.7 % (w/v) agarose gel and imaged using a gel reader (Quantity One programme) or UV lamp. To confirm fragment orientation the plasmids presenting expected fragment sizes were sequenced (2.4.5) (figure 2.2).

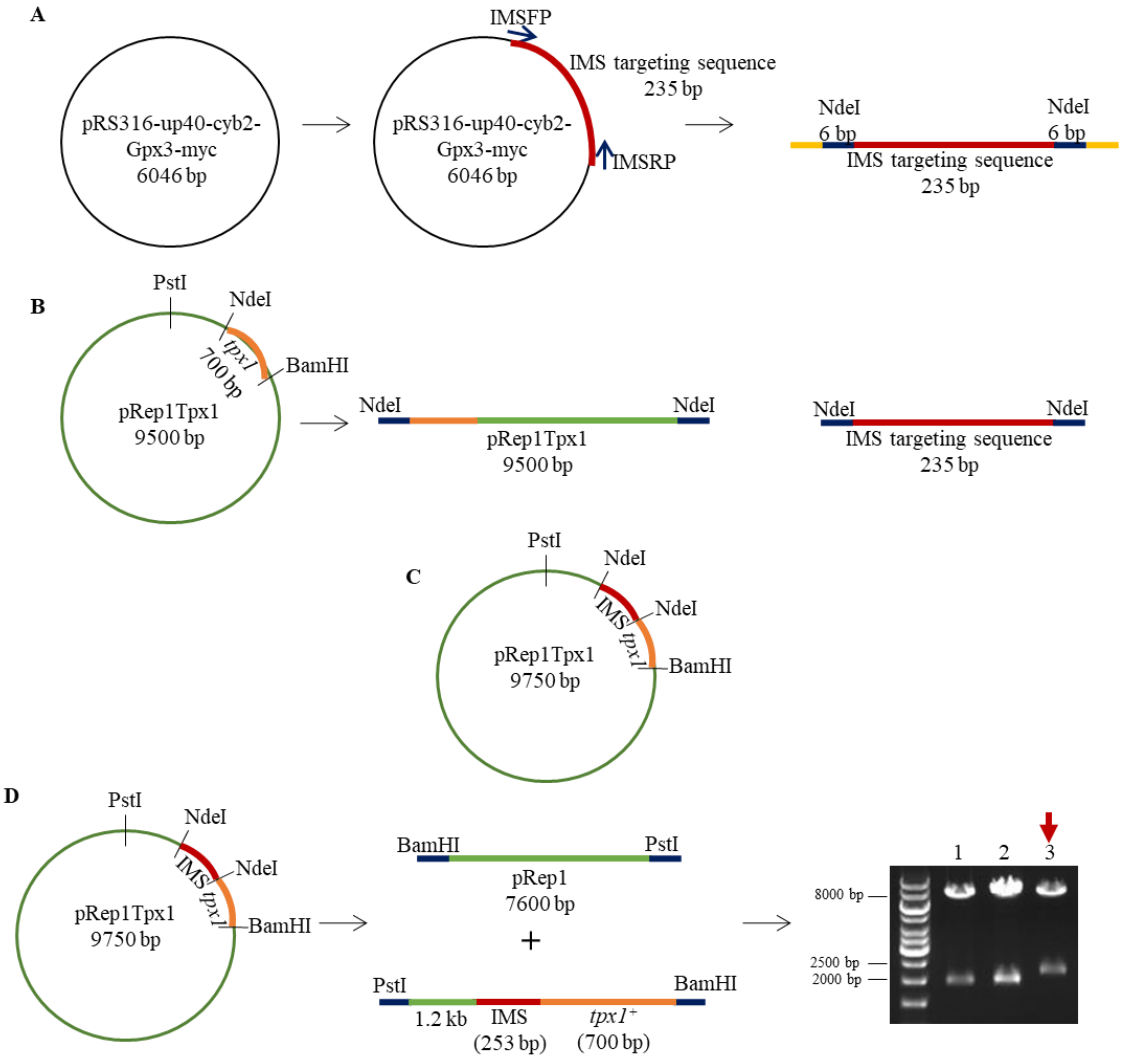

Figure 2.2 Cloning an IMS targeting sequence into pRep1Tpx1. [A] Amplification of IMS targeting sequence. The *S. cerevisiae* cytochrome b2 mitochondrial inner membrane space targeting sequence (235 bp) (red) was amplified from pRS316-up40-cyb2-Gpx3-myc (black) using primers IMSFP and IMSRP, designed to introduce NdeI restriction sites (blue) and flanking ends (yellow). **[B] NdeI digestion of pRep1Tpx1 and IMS fragment.** pRep1Tpx1 and the IMS fragment were digested with the NdeI enzyme (Thermo Scientific) at 37 °C for 3 h. The plasmid also underwent AP treatment to prevent re-ligation. **[C] Ligation of NdeI digested pRep1Tpx1 and IMS fragment.** Ligation reactions were set up with a vector:fragment 1:5 ratio and incubated at 15 °C overnight. **[D] BamHI and PstI digestion of generated plasmids.** To check the position and orientation of generated plasmids; plasmids were extracted from *E. coli* and digested with BamHI and PstI at 37 °C for 1 h. Digested plasmids were run on 0.7 % agarose gel and bands visualised using a gel reader. Plasmids exhibiting expected fragment sizes; 7.6 kb and 2.1 kb (as opposed to 1.8 kb) were sequenced, for example clone 3.

2.5 Protein Analysis

2.5.1 Examination of levels of Sty1 phosphorylation in *S. pombe*

Overnight cultures grown in 100 ml YE5S at 30 °C with agitation, were diluted to OD_{595} = 0.15 and further incubated until reached mid-log phase (OD_{595} = 0.4-0.5). Cells were treated with 6 mM H_2O_2 for 0, 10, 20 mins at 30 °C with agitation. 25 ml of exponentially growing cells were added to 25 ml ice and pelleted by centrifugation at 3000 x rpm for 1 min. Pellets were snap frozen in liquid nitrogen (N_2). Pellets were washed and resuspended in 200 µl ice-cold PLB (150 mM NaCl, 0.5 % (v/v) Nonidet P-40 (IGEPAL), 10 mM imidazole, 50 mM Tris-HCl pH 7.5) containing protease inhibitors (1 µg/ml p-leupeptin, 1 µg/ml pepstatin A, 1 % (v/v) aprotinin, 0.5 mg/ml phenylmethylsulfonyl fluoride (PMSF)) and phosphatase inhibitors (0.2 % (v/v) sodium vanadate (Na_3VO_4), 5 % (v/v) sodium fluoride (NaF)). Samples were then added to 750 µl of 0.5 mm ice cold glass beads (Biospec products) in a 1 ml ribolyser polypropylene tube (Greiner Bio-One) and cells were disrupted using a mini Beadbeater-16 (Biospec products); 15 s disruption, incubated on ice for 1 min and bead beaten again for 15 s. Tubes were pierced with a red hot needle, and cell lysate collected in an microfuge tube by centrifugation of 3000 rpm for 1 min. Cell lysate was clarified by centrifugation in a microcentrifuge at 13000 rpm for 10 mins at 4 °C. The supernatant was transferred to a fresh microcentrifuge tube. Protein concentrations were measured using the Coomassie blue reagent (Pierce) and absorbance at 595 nm. The remainder of the lysate was mixed with 2 x SDS loading buffer with β-mercaptoethanol (0.5 % (w/v) bromophenol blue, 10 % (w/v) SDS (Biochemika), 50 % (v/v) glycerol (BDH), 10 % (v/v) *β*-mercaptoethanol, 625 mM Tris-HCl pH 6.8). Samples were stored at -80 °C.

2.5.2 Preparation of whole cell lysates

2.5.2.1 Protein oxidation analysis using NEM and AMS

Overnight cultures grown at 30 °C with agitation, were diluted to OD_{595} = 0.15 and further incubated until reached mid-log phase (OD_{595} = 0.4-0.5). Exponentially growing cells (OD_{595} 0.5 = $1x10^7$ cells/ml) were treated with various concentrations of H_2O_2, or tBOOH, for different time periods, as stated in figure legends. Cells were added to an equal volume of 20 % (w/v) trichloroacetic acid (TCA). Cells were pelleted by centrifugation at 3000 rpm for 1 min and snap frozen in liquid N_2. Cell pellets were

thawed and resuspended in 200 µl 10 % (w/v) TCA and transferred to a ribolyser polypropylene tube (Greiner Bio-One). 750 µl of 0.5 mm glass beads (Biospec products) were added, and samples were bead beaten in a mini Beadbeater-16 (Biospec products) for 15 s, incubated on ice for 1 min and bead beaten again for 15 s. An additional 500 µl 10 % (w/v) TCA was added and precipitated protein samples were transferred to microfuge tubes by piercing the ribolyser polypropylene tube (Greiner Bio-One)tube with a red hot needle, and centrifugation at 2000 rpm for 1 min. Samples underwent centrifugation in a microcentrifuge at 13000 rpm for 10 mins at 4 °C. Followed by 3 cycles of acetone washes: resuspension in 200 µl acetone, vortex for 15 s, centrifugation in a microcentrifuge at 13000 x rpm for 1 min. Following the final acetone wash, samples were air dried at room temperature for 10 min. Pellets were resuspended in 20 µl TCA buffer (1 % (w/v) SDS, 1 mM EDTA, 100 mM Tris-HCl pH 8), supplemented with 25 mM AMS (4-acetamido-4'-maleimidylstilbene-2,2'-disulphonic acid), or 200 mM NEM (N-Ethylmaleimide)) and incubated at 25 °C for 30 min, followed by incubation at 37 °C for 5 min. Insoluble material was pelleted by centrifugation in a microcentrifuge at 13000 rpm for 3 mins and the supernatant was transferred to a fresh microfuge tube. Protein concentration of whole cell lysate was determined using a Pierce BSA protein assay kit (Thermo Scientific). Equal volumes of supernatant was mixed with 2 x SDS loading buffer without β-mercaptoethanol. Samples were stored at -80 °C.

2.5.2.2 Protein oxidation analysis of glutathionylated residues

Cultures were grown overnight at 30 °C with agitation, were diluted to OD_{595} = 0.15 and further incubated until reached mid-log phase (OD_{595} = 0.4-0.5). 50 ml cells were treated with 1 mM tBOOH for 10 mins at 30 °C. 2 ml cells were added to an equal volume of 20 % (w/v) TCA and pelleted by centrifugation at 3000 x rpm for 1 min, and snap frozen in liquid N_2. Samples were treated as described in 2.5.2.1, however following acetone washes, pellets were resuspended in 20 µl TCA buffer (1 % (w/v) SDS, 1 mM EDTA, 100 mM Tris-HCl pH 8) supplemented with 25 mM NEM and incubated at 25 °C for 20 mins. Samples underwent centrifugation in a microcentrifuge at 13000 x rpm for 3 min and supernatant was transferred to a fresh microfuge tube. An equal volume of 20 % (w/v) TCA was added and samples were incubated on ice for 30 min. Samples underwent centrifugation in a microcentrifuge at 13000 x rpm for 15 mins. 300 µl acetone was added, samples were vortexed and spun again in a microcentrifuge at 13000 rpm for 5 mins. Pellets were resuspended in TCA buffer supplemented with 50 mM DTT, vortexed

vigorously and incubated at 37 °C for 1 h. An equal volume of 20 % (w/v) TCA was added and samples were incubated on ice for 30 min. Samples then underwent centrifugation in a microcentrifuge at 13000 rpm for 15 min. Pellets were resuspended in 300 µl acetone, vortexed and underwent centrifugation in a microcentrifuge at 13000 rpm for 5 mins. Pellets were resuspended in 20 µl TCA buffer supplemented with 25 mM allyl methyl sulphide (AMS) and vortexed vigorously. Samples were incubated at 25 °C for 30 mins, followed by incubation at 37 °C for 5 min. Samples underwent centrifugation in a microcentrifuge at 13000 x rpm for 3 min and the supernatant was transferred to a fresh microfuge tube. Equal volumes of supernatant was mixed with 2 x SDS loading buffer without *β*-mercaptoethanol. Protein concentration was determined using a Pierce BSA protein assay kit (Thermo Scientific). Samples were stored at -80 °C.

2.5.2.3 Protein oxidation using IAA (Pap1 oxidation assay)

Overnight cultures grown at 30 °C with agitation, were diluted to OD_{595} = 0.15 and further incubated until reached mid-log phase (OD_{595} = 0.4-0.5). Exponentially growing cells were treated with various concentrations of H_2O_2 for different time periods and were added to an equal volume of 20 % (w/v) TCA. Cells were pelleted by centrifugation at 3000 x rpm for 1 min and snap frozen in liquid N_2. Samples were treated as described in 2.5.2.1, however following acetone washes, pellets were resuspended in 30 µl iodoacetamide (IAA) buffer (100 mM TrisHCl pH8, 1 % (w/v) SDS, 75 mM IAA) and incubated at 25 °C for 20 mins. Samples underwent centrifugation in a microcentrifuge at 13000 x rpm for 3 mins and supernatant was transferred to a fresh microfuge tube. Samples were treated with alkaline phosphate (AP) at 37 °C for 1 h. Equal volumes of supernatant were mixed with 2 x SDS loading buffer without *β*-mercaptoethanol. Protein concentration was determined using a Pierce BSA protein assay kit (Thermo Scientific). Samples were stored at -80 °C.

2.5.3 Mitochondrial Isolation and Subfractionation

Protocols adapted from Bonnefoy (Chiron *et al.*, 2007) and a mammalian cells method (Bruni *et al.*, 2013).

2.5.3.1 Isolation of *S. pombe* mitochondria

S. pombe were grown overnight in 500 ml YE5S at 30 °C to an OD_{595} = 1.0 in a 1 L flask. Cells were collected by centrifugation at 2000 g for 10 min at room temperature. Pellets

were washed with 100 ml dH_2O, collected by centrifugation at 4000 rpm and resuspended in 25 ml 10 mM ethylenediaminetetraacetic acid (EDTA). Cells were treated using a weight per volume ratio of 1:3 ml pre-warmed (37 °C) digestion buffer (1.2 M sorbitol, 10 mM sodium citrate, 0.2 mM EDTA, pH 5.8) supplemented with 0.3 % (v/v) β-mercaptoethanol (Sigma-Aldrich), 1 mg/ml zymolyase 100T (AMS Biotechnology) and 1 mg/ml from *Trichoderma harzianum* lytic enzymes (Sigma-Aldrich), and incubated at 37 °C for 30 mins, with agitation every 5 mins. Digestion was monitored by adding 1 µl 10 % (w/v) SDS to 9 µl cells, preparing slides and viewing lysed cells under a microscope. Cells were transferred to ice (4 °C) for at least 5 min to stop the digestion reaction. Cells were pelleted by centrifugation at 2000 g for 15 mins at 4 °C then resuspended in 4 ml homogenization buffer (HB) (0.6 M mannitol, 1 mM EGTA, 10 mM Tris-HCl pH7.4) supplemented with 0.1 % (w/v) BSA and 5 mM PMSF. Protoplasts were broken using 10 strokes of the glass homogenizer (2 ml at a time) and incubated on ice. A 'total' sample was obtained by adding 200 µl HB with 0.1 % (w/v) BSA and 5 mM PMSF to un-resuspended material from the previous step, centrifugation in a microcentrifuge at 2,500 g rpm for 3 min at 4 °C and resuspension in 100 µl lysis buffer. Following homogenization, samples underwent centrifugation at 2,500 g for 10 min at 4 °C. The supernatant was transferred to a pre-chilled microfuge tube. The pellet was resuspended in 1 ml HB with 0.1 % (w/v) BSA and 5 mM PMSF, transferred to the glass homogenizer, and underwent another 10 strokes of homogenization. Samples underwent centrifugation in a microcentrifuge at 2500 g for 10 min at 4 °C. The supernatant was pooled with the previous supernatant sample, and the pellet was resuspended in 800 µl HB with 0.1 % (w/v) BSA and 5 mM PMSF for a final round of homogenization. The pooled supernatants underwent centrifugation in a microcentrifuge at 12,000 g for 10 min at 4 °C, and the supernatant transferred to a fresh microfuge tube. The mitochondrial pellet was resuspended in 600 µl HB with 0.5 % (w/v) BSA. Both the supernatant sample and the resuspended mitochondrial pellet sample underwent centrifugation in a microcentrifuge at 12000 g for 5 mins at 4 °C. 1 ml was taken from the supernatant sample as the 'cytosolic' fraction. The mitochondrial pellet was resuspended in 100 µl HB. The protein concentration of fractions was measured using a Bradford assay. A fraction corresponding to 60 µg 'unshaved' mitochondrial material was retained at this point. To shave the mitochondria, 7.5 µg of proteinase K (Sigma-Aldrich) diluted 1:20 in 10 mM Tris-HCl pH 7.4 buffer, was added to 1.5 mg mitochondrial protein and incubated on ice for 30 mins. 5 mM PMSF was added, and the sample underwent centrifugation in a

microcentrifuge at 12,000 g for 5 mins at 4 °C. The shaved mitochondrial pellet was resuspended in 130 µl HB containing 0.5 % (w/v) BSA and 5 mM PMSF, centrifuged again, and resuspended in 150 µl HB. 60 µg shaved mitochondria was taken as a 'shaved mitochondrial' fraction. Samples were prepared using 4 x Laemmli sample buffer (BioRad). Gels were loaded equally, with 50 µg mitochondrial protein per gel. If not continuing to the mitochondrial subfractionation protocol, samples and raw material were snap frozen in liquid N_2 and stored at -80 °C.

2.5.3.2 Subfractionation of *S. pombe* mitochondria

The shaved mitochondrial material underwent centrifugation in a microcentrifuge at 11,000 g for 5 mins at 4 °C. The pellet was resuspended in 500 µl 10 mM Tris-HCl pH 7.4 and split into 2 microfuge tubes in a ratio of 1:3 (125 µl mitoplast: 375 µl shaved mitoplast fractions). 0.6 µg proteinase k was added to the 'shaved mitoplast' fraction. Both fractions were incubated on ice for 30 mins, and 5 mM PMSF added. An equal volume of 2 x HB was added to each sample, and samples underwent centrifugation in a microcentrifuge at 12000 g for 10 mins at 4 °C. Each pellet (shaved and unshaved) were resuspended in 400 µl HB containing 0.5 % (w/v) BSA, centrifuged in a microcentrifuge at 12,000 g for 5 min at 4 °C, and resuspended in HB. If preparing an 'inner membrane' fraction, 100 µl of sample resuspended in HB underwent centrifugation in a microcentrifuge at 12,000 g for 5 mins at 4 °C. The pellet was gently resuspended in 1 ml 100 mM Na_2CO_3 and incubated on ice for 30 mins. Sample underwent centrifugation at 100,000 g for 15 mins at 4 °C, and the pellet was resuspended in HB. Samples were prepared using 4 x sample buffer (Laemmli). Gels were loaded equally, and with 50 µg mitochondrial protein per gel. Samples and raw material were snap frozen in liquid N_2 and stored at -80 °C.

2.5.4 SDS-PAGE and Western blotting

Proteins were separated using sodium dodecyl sulfate-polyacrylamide gel electrophoresis (SDS-PAGE). Samples were loaded onto a 2 % stacking gel with an appropriate percentage resolving gel (UK, 1970) and ran at 200 V for approximately 1 h in 1 x SDS running buffer (19.2 mM glycine, 0.1 % SDS, 25 mM Tris-HCl pH 8).

Proteins were then transferred to a 0.45 µM nitrocellulose membrane (GE Healthcare) in 1 x transfer buffer (25 mM Tris-HCl pH 8.0, 19.2 mM glycine, 20 % (v/v) methanol) at 100 V for 1-3 h. The membrane was blocked using 10 % (w/v) BSA (Sigma) in 1 x TBST

(20 mM Tris-HCl pH 7.6, 137 mM NaCl, 0.1 % (v/v) Tween-20 (Sigma)), and when appropriate, with phosphatase inhibitors (5 % (v/v) NaF and 0.2 % (v/v) Na_3VO_4), for 30 min at room temperature. The membrane was incubated on a rocking platform with gentle agitation overnight at 4 °C, with a primary antibody diluted with TBST containing 5 % (w/v) BSA (and if appropriate, phosphatase inhibitors (5 % (v/v) NaF and 0.2 % (v/v) Na_3VO_4)). The antibodies used in this study are listed in Table 2.7. The membrane was washed 4 times with 1 x TBST for 5 min and incubated with the corresponding secondary antibody (Sigma-Aldrich) diluted 1:2000 in 5 % (w/v) BSA in 1 x TBST for 1 h at room temperature. The membrane was again washed 4 times with 1 x TBST for 5 min. The membrane was treated with enhanced chemiluminescence (GE healthcare) and developed using X-ray film (Fujifilm). For re-probing, membranes were treated with stripping buffer (62.5 mM Tris.HCl pH6.7, 2 % (w/v) SDS, 0.1 M β-mercaptoethanol) at 50 °C for 30 min with agitation. Following this, membranes were washed 4 times with 1 x TBST for 10 mins, blocked with 5 % (w/v) BSA for 30 min at room temperature, and re-probed with a fresh primary antibody overnight at 4 °C.

Antibody (species raised in)	**Source (Catalogue Number)**	**Dilution**
Primary		
Arg8 3-173 (rabbit)	(Steele *et al.*, 1996)	1:4000
Cyt c (mouse)	From Francesco Bruni, Newcastle University (Abcam, ab13575)	1:1000
GFP (rabbit)	Thermo Fisher Scientific (A6455)	1:1000
Hog1 (rabbit)	Santa Cruz Biotechnology (sc-9079)	1:1000
Myc (mouse)	Santa Cruz Biotechnology (C0907)	1:1000
Pap1 (rabbit)	From Nic Jones and Caroline Wilkinson, University of Manchester (custom-made by donors)	1:1000
p-p38 (rabbit)	Cell Signalling Technology (9211S)	1:1000
$SO_{2/3}$ (mouse)	(Tomalin *et al.*, 2016)	1:1000

Tomm20 (rabbit)	Santa Cruz Biotechnology (FL-145)	1:2000
Tpx1 (rabbit)	(Day *et al.*, 2012)	1:1000
Tubulin (mouse)	(Asakawa *et al.*, 2006)	1:1000
Secondary		
Anti-rabbit HRP-conjugated	Sigma-Aldrich (A6154)	1:2000
Anti-mouse HRP-conjugated	Sigma-Aldrich (A4416)	1:2000

Table 2.7 Antibodies used in this study

2.6 Microscopy

2.6.1 Fluorescence microscopy

2.6.1.1 *S. pombe* cell size, morphology and nuclei staining

1 ml of exponentially growing cells were pelleted by centrifugation at 7,000 x rpm for 30 s, and resuspended in 1 ml dH_2O. Cells were pelleted again, and resuspended in 30 µl dH_2O. 2 µl cells were spread onto Poly-L-lysine coated slides using a pipette tip, and left to dry. For nuclei (DNA) staining; 15 µl Vectashield mounting medium (containing 1.5 mg/ml DAPI (4'-6-diamidino-2-phenylindole) (Vector laboratories)) was also pipetted onto the slides. Slides were covered with a glass cover slip and sealed using nail varnish. DIC and DAPI (excitation at 450-490 nm wavelength) images of cells were captured using a Zeiss Axioscope fluorescence microscope with a 63 x oil immersion objective and Axiovision digital imaging software.

2.6.1.2 Examination of *C. elegans* by fluorescent microscopy

Microscope slides were made by pipetting a drop of molten 2.5 % (w/v) agarose between 2 slides to form a pad. Once set, worms were picked and transferred into 5 µl M9 (6 % (w/v) Na_2HPO_4 (BDH), 3 % (w/v) KH_2PO_4 (Biochemika), 5 % (w/v) NaCl (Sigma), 0.25 % (w/v) $MgSO_4$ (BDH)) containing 0.06 % (w/v) levimasole (Sigma-Aldrich) for immobilisation, and covered with a coverslip.

2.6.2 Confocal microscopy

Confocal microscopy was conducted in collaboration with the Newcastle University BioImaging Unit.

2.6.2.1 Imaging mitochondria and Pap1 in *S. pombe*

Exponentially growing cells expressing Cox4-RFP and Pap1-GFP were harvested by centrifugation at 3,000 x rpm for 2 min. Cells were washed in 1 ml phosphate-buffered saline (PBS), underwent centrifugation at 7,000 x rpm for 30 s and were resuspended in 100 µl PBS. Glass slides and coverslips were prepared by washing in 70 % (v/v) ethanol. 5 µl Poly-L-lysine was used to coat slides and air dried. 2 µl cells was added to the slides, as well as a drop of Prolong Diamond Antifade Mount (Thermo Fisher). Mounted cells were covered with a glass cover slip and sealed using nail varnish. GFP fluorescence, RFP fluorescence and DIC images of cells were captured using the Leica TCS SP2 UV AOBS confocal microscope with a 60 x oil immersion objective and digital imaging software. Images were prepared using ImageJ.

2.6.2.2 Imaging mitochondria in *C. elegans*

Slides were prepared as described in 2.6.1.2. L4 larval stage worms (EB254, EB253, EB255, EB260) were imaged using a Nikon A1R inverted confocal microscope, using a 20 x oil immersion lens, and the Elements software package. Resonant z-stack (0.12 µm/px), GFP fluorescence (488 nm, eGFP wavelength), RFP fluorescence (568 nm, TRITC wavelength) and TD images were captured. Images were exported using NIS-Elements Viewer (Nikon) and prepared using ImageJ.

2.6.2.3 Measurement of roGFP2 oxidation in *C. elegans*

Worms were imaged at L4 larval stage unless stated otherwise. Slides were prepared as described in 2.6.1.2, and worms were treated as described in 2.3.3-2.3.5. Images were captured using a Nikon A1R inverted confocal microscope, using a 20 x oil immersion lens, and the Elements software package. Levels of oxidised probe (roGFP2^{ox}) were captured at 407 nm, and levels of reduced probe (roGFP2^{red}) were captured at 488 nm, along with TD images. Resonant (~1.751 µm per slice) or Galvano (1 slice) images were obtained of the anterior intestinal cells depending on the experiment. Wild-type worms (N2) were imaged to remove background signal or autofluorescence. Thresholds were set using 5 mM H_2O_2 and 20 mM NEM to avoid signal saturation. The software NIS Elements Viewer and Volocity (PerkinElmer) were used to analyse the images obtained and create a ratio channel. A mean ratio (roGFP2^{ox}/roGFP2^{red}) of the left intestinal cell and the right intestinal cell were generated separately, and then averaged, to avoid

interference of the lumen. Two-tailed T-tests were performed to calculate p-values to check variance of results.

2.7 Experimental replication

All experiments were performed at least twice unless otherwise stated.

Chapter 3

Chapter 3. Validation of the N-roGFP2::*prdx-2* genetic *in vivo* H_2O_2 sensor to detect endogenous changes in intracellular H_2O_2

3.1 Introduction

To understand how endogenous H_2O_2 affects cell growth, migration and ageing, it is important to be able to monitor changes in H_2O_2 concentrations, in real-time, *in vivo*. The lowest steady state H_2O_2 level in mammalian cells is estimated to be around 1 nM, but can rise to 500-700 nM (Stone and Yang, 2006). To study endogenous signalling events, it is vital that sensors are specific and sensitive enough to detect these low levels. Small molecular fluorescent probes have been widely used but frequently lack specificity to H_2O_2 (Guo *et al.*, 2014). As described in section 1.1.4 and 1.5, the genetically encoded sensor HyPer has been used in *C. elegans* to detect H_2O_2 levels during development and ageing (Knoefler *et al.*, 2012; Back *et al.*, 2012). Additionally, fusion of roGFP2 to Orp1 (roGFP2-Orp1) has been used to detect H_2O_2 levels in cells and *Drosophila*; however, detection limit may only be around 100 nM H_2O_2 (Gutscher *et al.*, 2009; Albrecht *et al.*, 2011; Ezeriņa *et al.*, 2014). In addition, the original HyPer sensors are highly pH-sensitive (Lukyanov and Belousov, 2014).

The specificity and sensitivity of peroxiredoxins to react with nanomolar levels of H_2O_2 has been predicted to generate a highly sensitive and specific tool for H_2O_2 detection (Ezeriņa *et al.*, 2014). Indeed, the fusion of thiol peroxidases (for example Tsa2) with roGFP2 have recently been demonstrated to offer highly improved H_2O_2 sensitivity compared to previous genetic sensors (Roma *et al.*, 2017). We have tested whether the fusion of a roGFP2 sensor to the highly abundant and H_2O_2-sensitive peroxiredoxin 2 (PRDX-2), in *C. elegans*, is able to act as a genetic tool to detect very low, endogenous concentrations of H_2O_2 (figure 3.1, (Meyer and Dick, 2010)). The roGFP2::*prdx* fosmid constructs were generated by our collaborators via recombination of the roGFP2 domain to replace a RT-Cassette at the N- or C-terminus of PRDX-2, or the C-terminus of PRDX-3 (as described in (Hirani *et al.*, 2013)). Constructs were microinjected with the co-marker pRF4 into gravid N2s. The resulting rolling lines were analysed via single worm

lysis, and PCR, to confirm the presence of the roGFP2 insert (Hirani *et al.*, 2013). Here I have investigated whether these animals can be used as a genetic tool to detect *in vivo* changes in intracellular H_2O_2 levels, with the view to investigate whether there are differences between the levels of H_2O_2 in different cells or in response to different conditions.

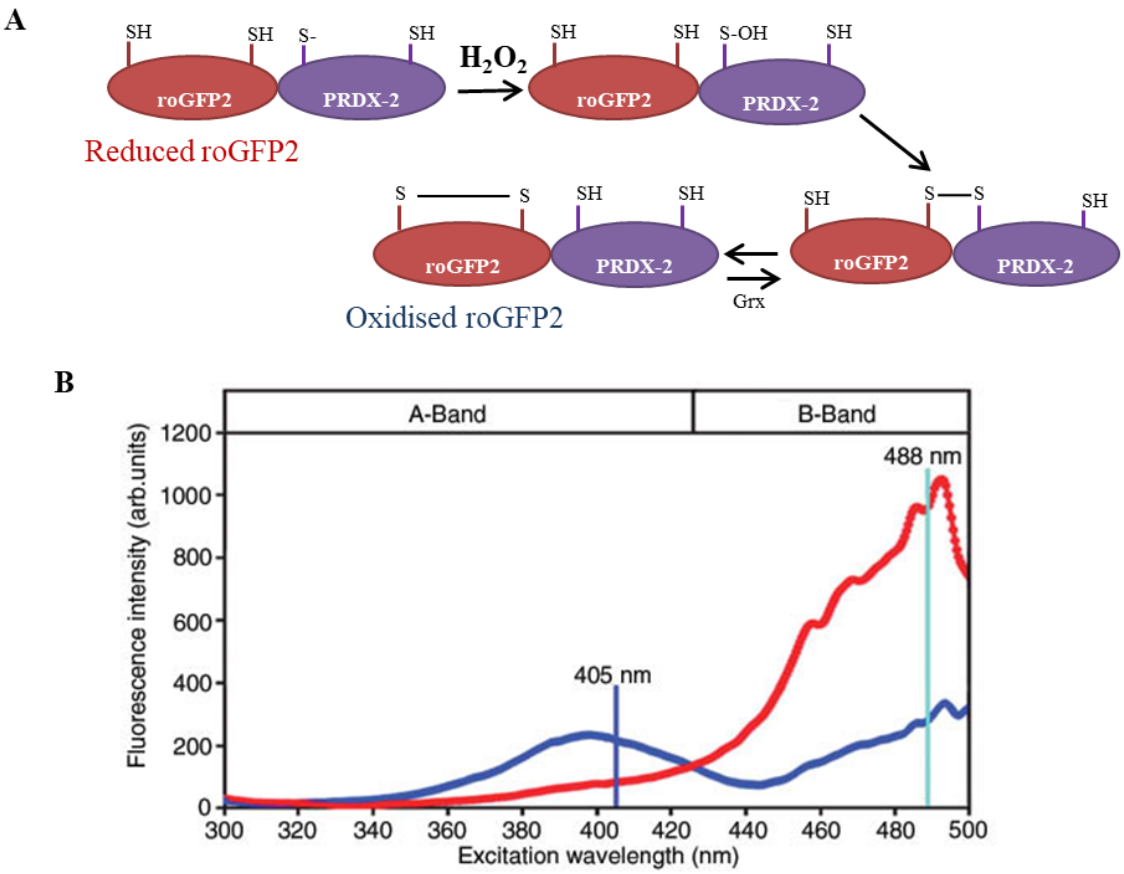

Figure 3.1 Mechanism of the N-roGFP2::*prdx-2* as a H_2O_2 sensor. [A] Structure and proposed mechanism of N-roGFP2::*prdx-2*. H_2O_2 oxidises the peroxidatic cysteine of PRDX-2 to form a sulphenic group, which resolves to form an intermolecular disulfide bond. PRDX-2 then uses roGFP2 as a reductant, subsequently oxidising the roGFP2 domain resulting in a shift in fluorescent intensity. **[B] Fluorescent intensities of roGFP2.** The reduced form of the sensor has peak fluorescence intensity at 488 nm, whereas the oxidised form is detected around 405 nm (Meyer and Dick, 2010)**.**

3.2 Results

3.2.1 N-roGFP2::*prdx-2* and C-roGFP2::*prdx-2* reporters are expressed in the cytosol, whereas the C-roGFP2::*prdx-3* reporter has mitochondrial expression

First, we examined the *in vivo* expression pattern of N-roGFP2::*prdx-2*, C-roGFP2::*prdx-2* and C-roGFP2::*prdx-3* reporters. L4-stage worms were picked for confocal microscopy, and z-stack images of GFP fluorescence were captured and compiled to generate detailed 3D images (figure 3.2).

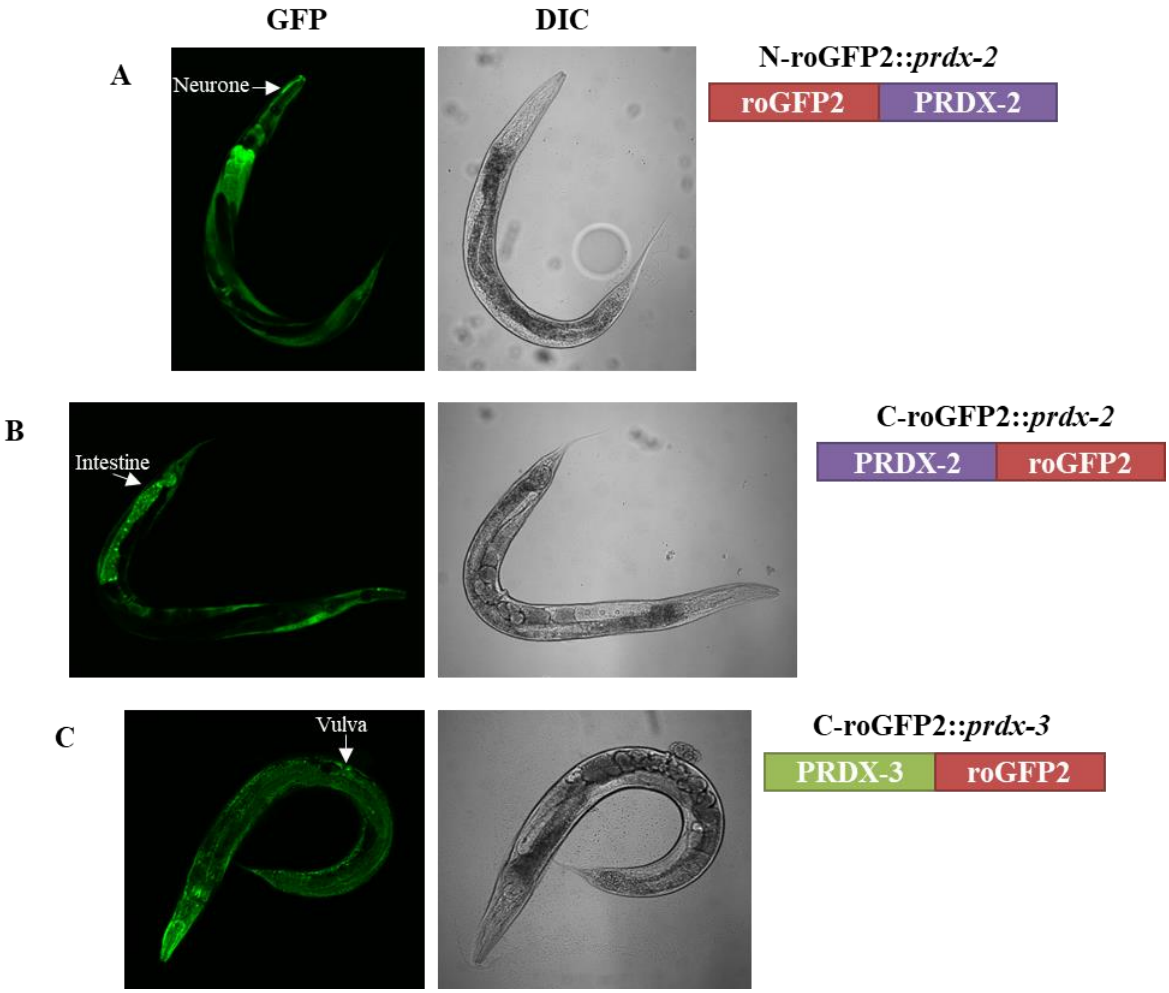

Figure 3.2 N-roGFP2::*prdx-2*, C-roGFP2::*prdx-2* and C-roGFP2::*prdx-3* reporters are expressed in multiple *C. elegans* tissues. Fluorescent and light imaging of L4 *C. elegans* expressing either the N-roGFP2::*prdx-2* [A], C-roGFP2::*prdx-2* [B], or the C-roGFP2::*prdx-3* [C] reporters. A representation of a 3D image obtained by resonant z-stack images of GFP fluorescence using confocal microscopy. Arrows indicate tissues with GFP expression.

Expression of the N-roGFP2::*prdx-2* and C-roGFP2::*prdx-2* reporters was detected in the cytosol of a range of tissues (figure 3.2A, 3.2B). This is consistent with previous reports that the *prdx-2* promoter driving the expression of each construct is active in the pharynx, nervous system, tail, reproductive system, intestine, vulva and muscle tissue of *C. elegans* (Hunt-Newbury *et al.*, 2007). As well as immunostaining technique that has detected endogenous PRDX-2 protein in the cytoplasm of these tissues (Oláhová *et al.*, 2008).

Expression of the C-roGFP2::*prdx-3* reporter was also detected in the pharynx, nervous system, vulva and intestine (figure 3.2C). However, PRDX-3::GFP appeared to be present in distinct punctate structures in contrast to the N-roGFP2::*prdx-2* or C-roGFP2::*prdx-2* reporters, consistent with the expected localisation of PRDX-3 in the mitochondrial matrix and the localisation of endogenous PRDX-3, revealed by immunostaining with specific antibodies (Oláhová PhD thesis).

Notably, the C-roGFP2::*prdx-2* reporter gave "blob"-like patterns in comparison to the N-roGFP2::*prdx-2* reporter (figure 3.2B). This expression pattern has been observed previously using PRDX-2::YFP (Hirani *et al.*, 2013). A similar result has also been recorded by another group who observed large "blob"-like patterns when inserting the GFP domain before the stop codon of a gene, compared to inserting the GFP domain after the start codon of the same gene (Craig *et al.*, 2013). In light of these issues with other C-terminal translational fusions of PRDX-2, we selected the N-roGFP2::*prdx-2* reporter for further experiments.

3.2.2 Maintenance at different temperatures did not affect the oxidation/reduction ratio of N-roGFP2::*prdx-2* in the anterior intestine

In order to examine whether the N-roGFP2::*prdx-2 C. elegans* could be used as a tool to detect *in vivo* levels of H_2O_2, a number of studies were conducted. Although GFP+PRDX-2 was expressed from the *prdx-2* promoter, and expressed in a range of tissues through-out the worm, we chose to begin to conduct our quantitative analysis on the 2 anterior intestinal cells. As the 2 anterior intestinal cells are large, easy to distinguish, and express robust inducible defences against rises in reactive oxygen species these made for viable candidates for testing (An and Blackwell, 2003).

First, we investigated whether the maintenance of the N-roGFP2::*prdx-2* worms at different temperatures would affect the ratio of oxidised-reduced probe ($roGFP2^{ox}$/$roGFP2^{red}$). Worms grow at a faster rate and have increased mitochondria, and

mitochondrial activity, at 25 °C (Labrousse *et al.*, 1999). We therefore hypothesised that this may cause a significant change in the levels of intracellular H_2O_2 that might be detected by the altered oxidation state of the N-roGFP2::*prdx-2* reporter. To test this, the N-roGFP2::*prdx-2* worms were maintained at 15 °C, 20 °C or 25 °C for several generations. The anterior intestinal cells of L4-stage worms were imaged at 407 nm (roGFP2^{ox}), and 488 nm (roGFP2^{red}), and a mean ratio of roGFP2^{ox}/roGFP2^{red} was calculated using Volocity analysis software (figure 3.3). No significant change in the roGFP2^{ox}/roGFP2^{red} ratio was detected between maintaining worms at 15 °C, 20 °C, or 25 °C. Nevertheless, all subsequent experiments were carried out with worms that had been maintained at 15 °C.

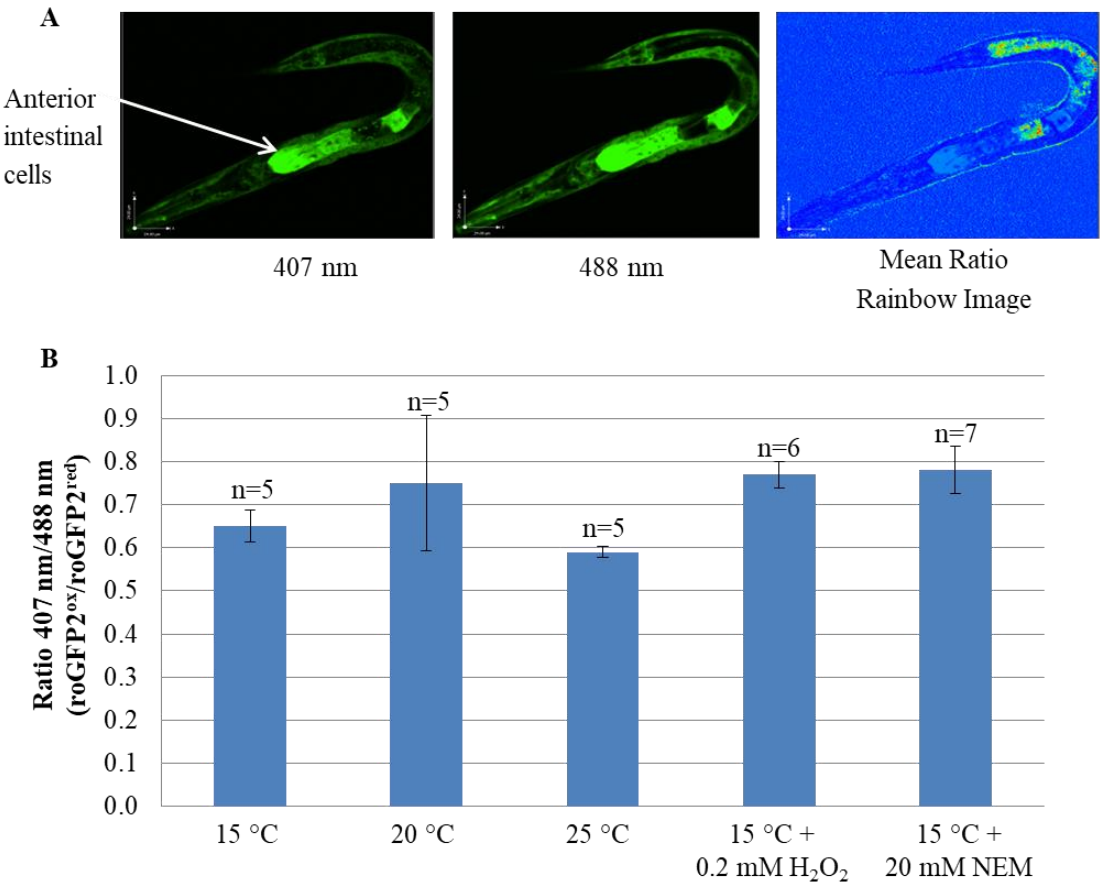

Figure 3.3 Effect of temperature, NEM and H_2O_2 treatment on the ratio of roGFP2^{ox}/roGFP2^{red} in anterior intestinal cells. [A] Images of worms taken at 407 nm and 488 nm were used to generate a Rainbow image reflecting the ratio of oxidised-to-reduced probe (roGFP2^{ox}/roGFP2^{red}) (red=highest and blue=lowest level of H_2O_2). [B] *C. elegans* expressing the N-roGFP2::*prdx-2* reporter were maintained at either 15 °C, 20 °C or 25 °C for multiple generations. Volocity software was used to generate a mean ratio of roGFP2^{ox}/roGFP2^{red} across the anterior intestinal cells.

To begin calibrating the reporter and providing a baseline for relative ratio measurement, we also examined whether treatment with 0.2 mM H_2O_2, or 20 mM NEM, which alkylates free thiols preventing disulphide formation, caused a change in the roGFP2^{ox}/roGFP2^{red} ratio. However, no significant change in roGFP2^{ox}/roGFP2^{red} ratio was observed between the 0.2 mM H_2O_2, or 20 mM NEM treatment groups, suggesting that neither treatment caused an alteration in the redox state of the PRDX-2+roGFP2 fusion.

3.2.3 The oxidation of N-roGFP2::*prdx-2* is specific for H_2O_2

It was important to establish mean ratio values for the complete reduction, and complete oxidation of the reporter, so that relative H_2O_2 levels could be more accurately assessed (Lukyanov and Belousov, 2014). To address this, and to determine whether the N-roGFP2::*prdx-2* reporter is specific for H_2O_2, worms were exposed to a selection of reagents in situ, immediately prior to examination by confocal microscopy (figure 3.4). These reagents and concentrations had previously been demonstrated to: cause the maximal oxidation (diamide), or maximal reduction (DTT) of thiols of a roGFP probe in *C. elegans* (Romero-Aristizabal *et al.*, 2014), or to block oxidation (NEM) of a roGFP::Orp1 probe in *Drosophila* (Albrecht *et al.*, 2011).

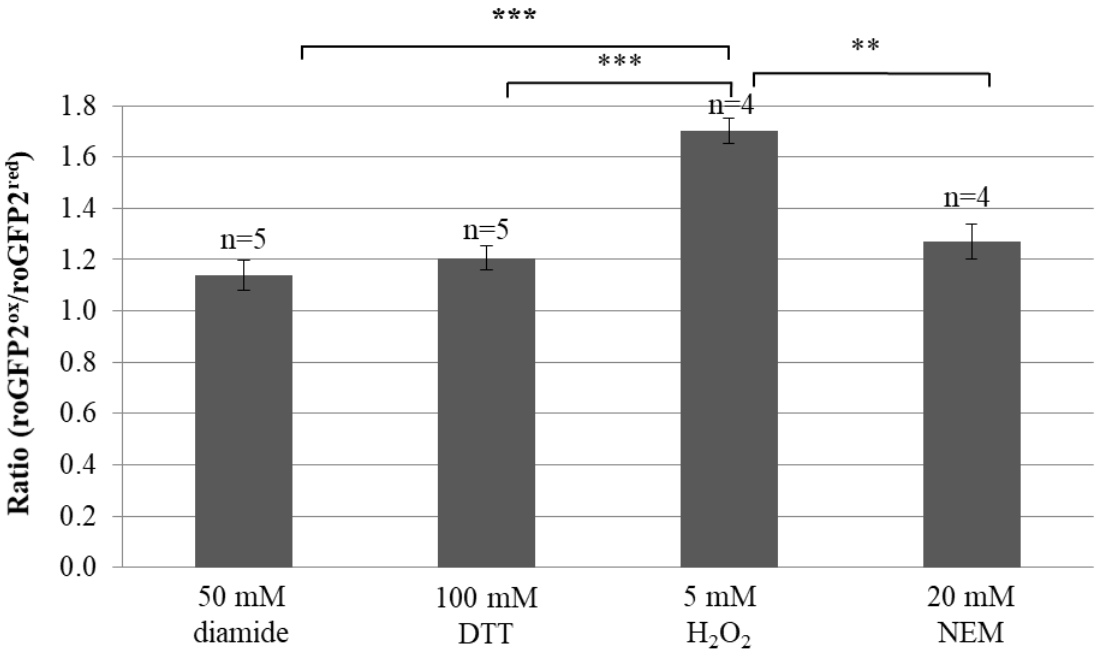

Figure 3.4 5 mM H_2O_2 significantly increased the ratio of roGFP2^{ox}/roGFP2^{red}, whereas treatment with diamide, or DTT did not alter the ratio of roGFP2^{ox}/roGFP2^{red} relative to NEM, (= p<0.01 (T-test)).**
Mean ratio of roGFP2^{ox}/roGFP2^{red} across the anterior intestinal cells following treatment with various oxidants (diamide, H_2O_2), a reductant (DTT), or an alkylating agent (NEM). Only treatment with 5 mM H_2O_2 significantly increased the roGFP2^{ox}/roGFP2^{red} ratio relative to 20 mM NEM (** = p<0.01 (T-test)), and relative to 50 mM diamide or 100 mM DTT (*** = p<0.001) (T-test)).

However, only treatment with 5 mM H_2O_2 caused a significant increase in the roGFP2^{ox}/roGFP2^{red} ratio, relative to treatment with 20 mM NEM ($p<0.01$). No significant change in roGFP2^{ox}/roGFP2^{red} ratio was observed following treatment with 50 mM diamide, or 100 mM DTT relative to NEM. This suggested that the N-roGFP2::PRDX-2 probe was specifically oxidised in response to H_2O_2. Therefore, 5 mM H_2O_2 and 20 mM NEM treatments, were incorporated in subsequent experiments as controls for a high oxidation ratio value, and a baseline ratio value, respectively.

3.2.4 Treatment with 1 or 5 mM extracellular H_2O_2 causes an increase in the oxidation/reduction ratio of N-roGFP2::*prdx-2* in the anterior intestine

To investigate the concentration of extracellular H_2O_2, required to produce a change in the roGFP2^{ox}/roGFP2^{red} ratio of anterior intestinal cells, worms were exposed to different concentrations of H_2O_2 ranging from 0.2 mM – 5 mM (figure 3.5). These concentrations were chosen as PRDX-2 has been reported to be oxidised to disulphide by only 0.2 mM H_2O_2, with hyperoxidised PRDX-2 not detected until 1 mM, and becoming fully hyperoxidised at 5 mM H_2O_2 (Oláhová *et al.*, 2008). Additionally, treatment with 0.2 mM or 1 mM H_2O_2 is sublethal to wild-type worms, however worms are killed following prolonged exposure to 5 mM (Oláhová *et al.*, 2008). No significant difference was observed in roGFP2^{ox}/roGFP2^{red} ratio in response to exposure to 0.2 mM H_2O_2, in comparison to NEM. This result was also observed previously (figure 3.3). However, treatment with 1 mM or 5mM extracellular H_2O_2 caused a significant increase in roGFP2^{ox}/roGFP2^{red} ratio relative to NEM ($p<0.05$). Notably, there was no significant increase in the oxidation of the sensor in animals exposed to 5 mM rather than 1 mM H_2O_2.

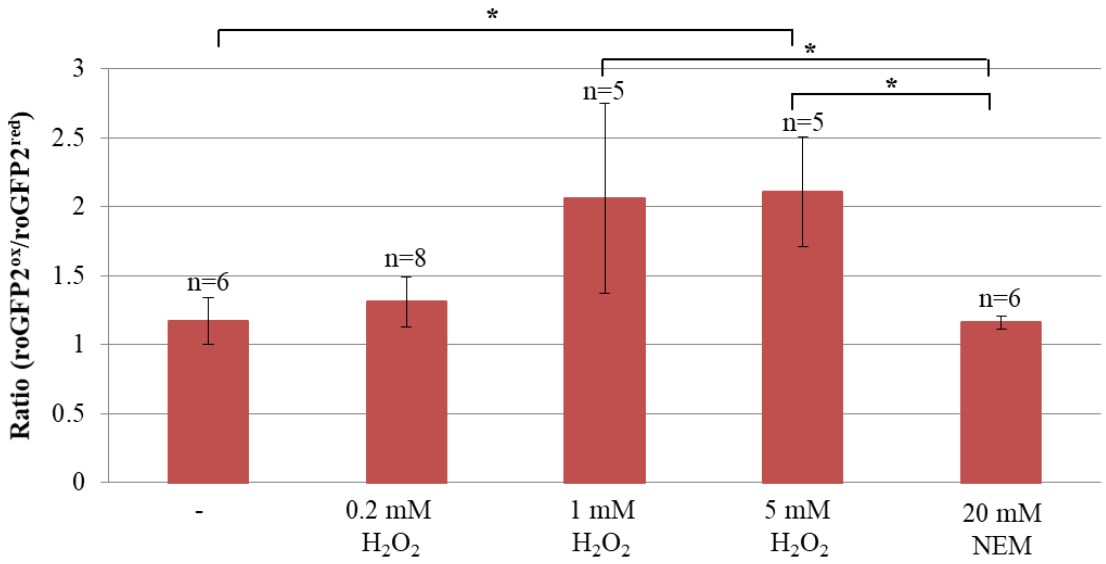

Figure 3.5 Exposure to 1 or 5 mM extracellular H_2O_2 was required to cause an increase in the ratio of roGFP2^{ox}/roGFP2^{red} in anterior intestinal cells, relative to NEM, (* = p<0.05 (T-test)). Mean ratio of roGFP2^{ox}/roGFP2^{red} across the anterior intestinal cells following treatment with a range of H_2O_2 concentrations, or 20 mM NEM. Only the treatment with 1 or 5 mM H_2O_2 gave a statistically significant change in the ratio of roGFP2^{ox}/roGFP2^{red} (* = p<0.05 (T-test)).

3.2.5 Starvation of *C. elegans* did not affect the oxidation/reduction ratio of N-roGFP2::*prdx-2* in the anterior intestine

C. elegans activate similar transcriptional responses to fasting and peroxide (Blackwell *et al.*, 2015; Goh *et al.*, 2018). For instance, work in our lab has shown that the transcriptional regulator NHR-49 activates a protective transcriptional response in response to either peroxide or fasting (Goh *et al.*, 2018). Moreover, ROS signals have been proposed to mediate some of the effects of dietary restriction on lifespan (Schmeisser *et al.*, 2013). We therefore tested whether increases in intracellular H_2O_2 could be detected in worms that were starved (without *E. coli*) for 1, 4 or 8 hours (figure 3.6). 4-8 h is long enough to activate *fmo-2* in response to fasting which is why these time periods were chosen (Goh *et al.*, 2018). However, no significant change in $roGFP2^{ox}$/$roGFP2^{red}$ ratio of anterior intestinal cells was detected following any starvation period. This suggests that fasting does not cause as substantial an increase in intestinal H_2O_2 as treatment of *C. elegans* with 1 mM extracellular H_2O_2.

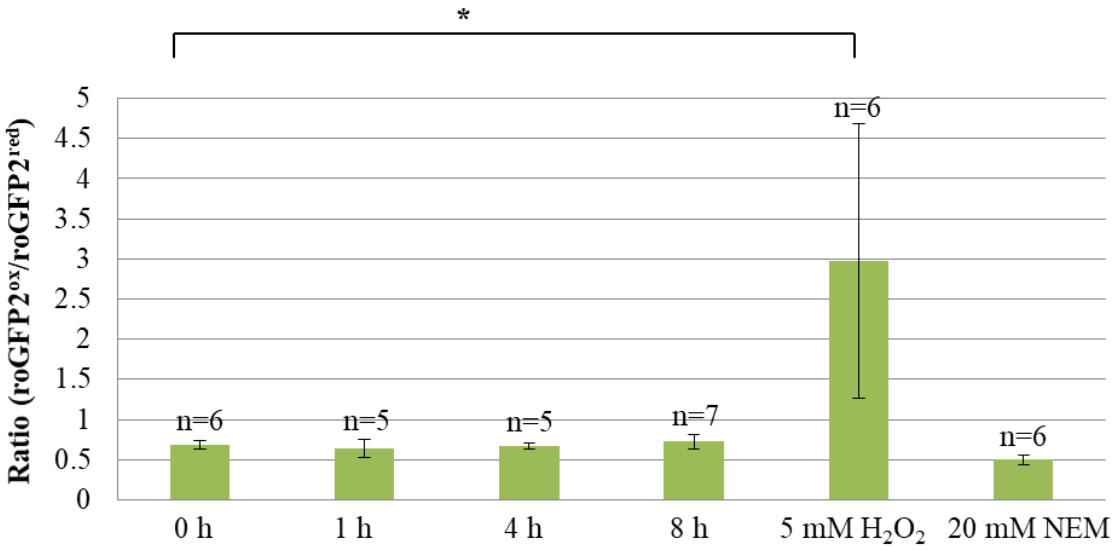

Figure 3.6 Fasting for up to 8 hours did not alter the ratio of roGFP2^{ox}/roGFP2^{red} in anterior intestinal cells. Worms were moved onto unseeded NGM-L plates for 1, 4 or 8 hours, and then picked for confocal microscopy analysis. No significant difference in the ratio of roGFP2^{ox}/roGFP2^{red} of anterior intestinal cells was observed following starvation up to 8 hours.

3.2.6 Consistent differences in the oxidation/reduction ratio of N-roGFP2::*prdx-2* could not be detected between larval stages

HyPer has previously been used in *C. elegans* to detect increases in intracellular H_2O_2 levels during larval development (Knoefler *et al.*, 2012). To determine whether we could observe obvious changes in intracellular H_2O_2 levels during development, worms of different larval stages (L2-L4) were imaged using confocal microscopy (figure 3.7). For this analysis, whole body images of the worms were taken at 407 nm and 488 nm, and roGFP2^{ox}/roGFP2^{red} ratio 'rainbow' images were generated using Volocity software. The roGFP2^{ox}/roGFP2^{red} ratio 'rainbow' images reveal a colour coded system; red pixels indicate high roGFP2^{ox}/roGFP2^{red} ratio values, and blue pixels represent the lowest. Individual images revealed differences in endogenous H_2O_2 levels between different tissues throughout the worm. The blue appearance of the anterior intestinal cells (indicating low levels of H_2O_2) was observed in all larval stages tested. From our qualitative analysis we could not identify consistent differences within or between groups of different larval stage worms.

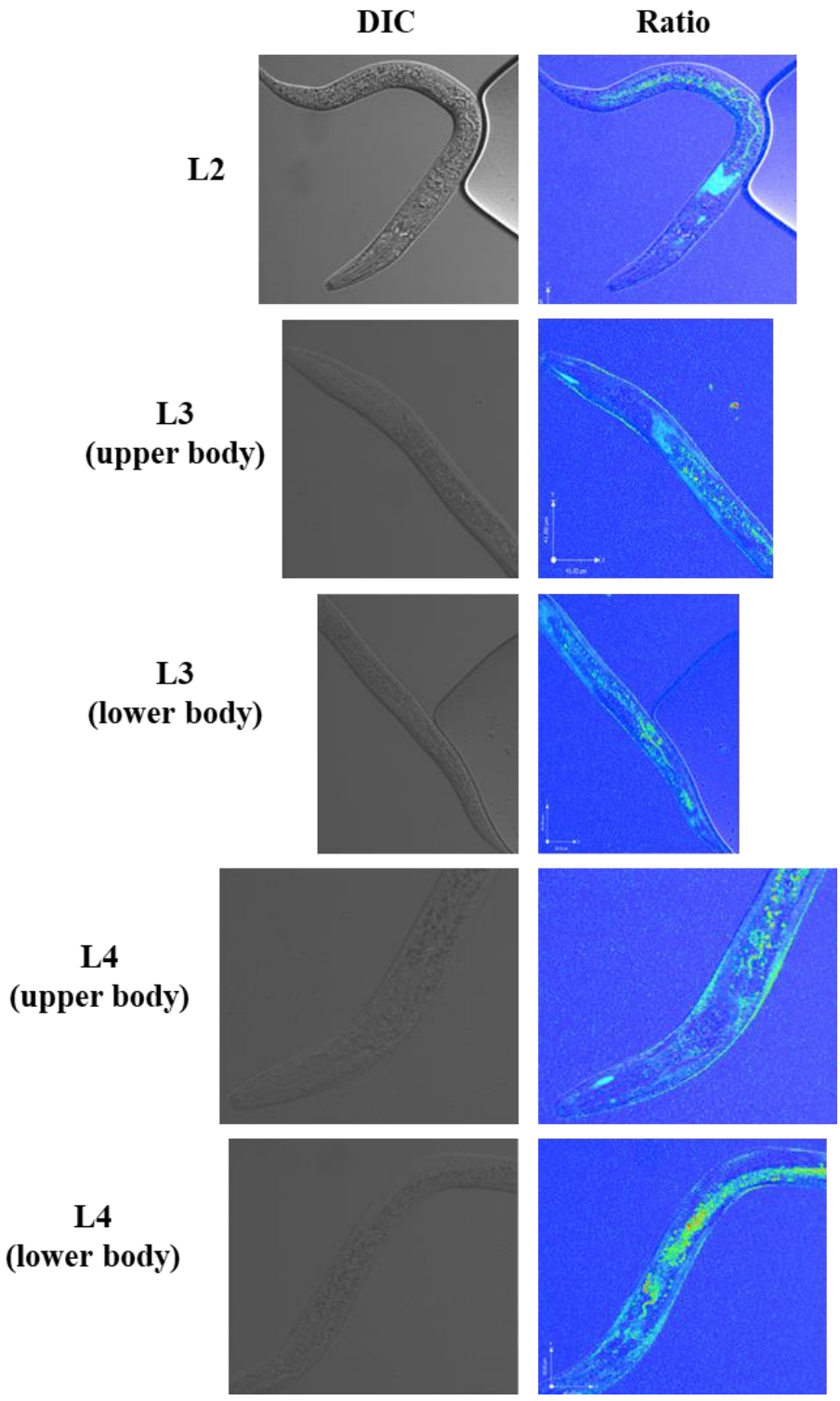

Figure 3.7 No consistent qualitative differences were observed between *C. elegans* expressing N-roGFP2::*prdx-2* at different larval stages (L2, L3, L4). *C. elegans* expressing the N-roGFP2::*prdx-2* reporter were maintained at 15 °C. L2, L3 or L4-stage worms were picked for confocal microscopy analysis. No consistent qualitative differences in intensity ($roGFP2^{ox}$/$roGFP2^{red}$ ratio) were observed between groups of worms at different larval stages.

3.2.7 Exposure to the fungal pathogen *C. albicans* causes an increase in the oxidation/reduction ratio of N-roGFP2::*prdx-2* in the anterior intestine

ROS have an important role in innate immunity (as described in section 1.2.4). In mammalian cells, the NOX and DUOX (dual oxidases) enzymes produce H_2O_2 which is used to kill pathogens (Bedard *et al.*, 2007). Although *C. elegans* lack dedicated immune cells (macrophages and neutrophils) it does share a primitive innate immune response which includes a DUOX enzyme that seems to be important in response to infection (Bedard *et al.*, 2007). *C. elegans* encode the DUOX enzyme BLI-3, which is required for normal cuticle formation (Thein *et al.*, 2009). Interestingly, *bli-3(im10)* mutant worms are more susceptible to infection by *Candida albicans* than wild-type worms; although it is possible that this increased susceptibility to infection of *bli-3(im10)* worms is due to defective cuticle formation (van der Hoeven *et al.*, 2015).

The infection of *C. elegans* with *Enterococcus faecalis* has been demonstrated (using an amplex red assay) to cause an increased production of H_2O_2 that is proposed to help defend against infection (Chávez *et al.*, 2007). To confirm this finding using a genetic H_2O_2 sensor, and to determine whether we could detect an increase in $roGFP2^{ox}/roGFP2^{red}$ ratio following infection with *C. albicans*, the N-roGFP2::*prdx-2* reporter worms were transferred to unseeded plates for 1 h to remove any contaminating *E. coli*, then transferred to plates seeded with either *E. coli* or *C. albicans* (figure 3.8). No significant increase in $roGFP2^{ox}/roGFP2^{red}$ ratio was observed between 1 h incubation with *E. coli* and 1 h incubation with *C. albicans*. However, notably a significant increase in $roGFP2^{ox}/roGFP2^{red}$ ratio was observed following 1 hour incubation with *C. albicans*, relative to 24 hour incubation with *E. coli* ($p<0.05$). Additionally, the $roGFP2^{ox}/roGFP2^{red}$ ratio was substantially increased following incubation with *C. albicans* for 24 hours (relative to 1 or 24 hour incubation with *E. coli* ($p<0.01$)). This data provides evidence that the infection of *C. elegans*, with the fungal pathogen *C. albicans*, results in an increase in H_2O_2 levels in anterior intestinal cells.

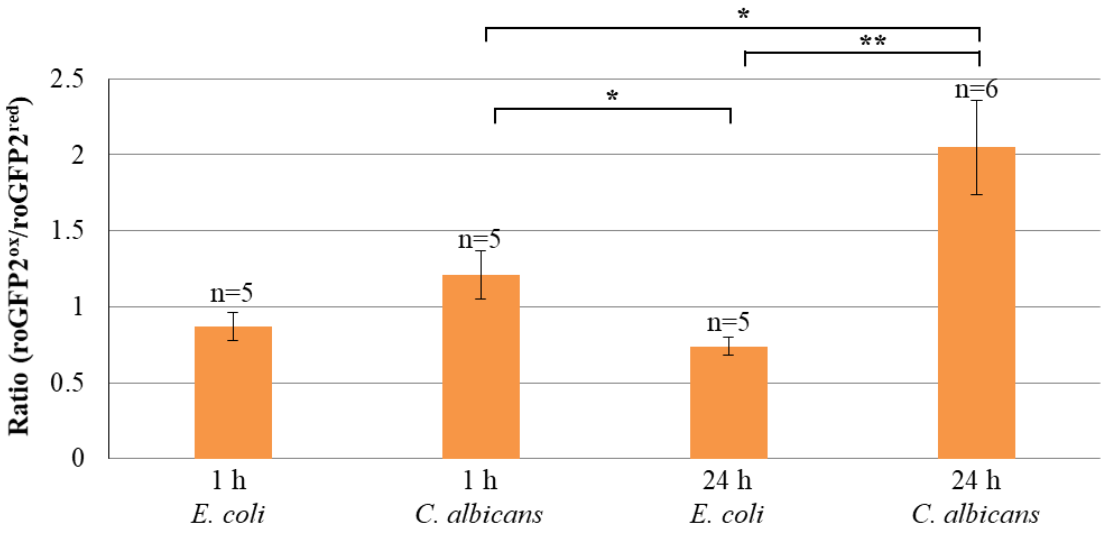

Figure 3.8 A substantial increase in the ratio of roGFP2^{ox}/roGFP2^{red} was detected in anterior intestinal cells following 24 h infection with the fungal pathogen *Candida albicans*, compared with *E. coli* (= p<0.01 (T-test)).** *C. elegans* expressing the N-roGFP2::*prdx-2* reporter were maintained at 25 °C. L3/L4-stage worms were moved onto unseeded NGM-L plates for 1 hour, and then moved onto either NGM-L agar seeded with *E. coli*, or BHI agar seeded with *C. albicans*, for 1 or 24 hours. L4-stage worms were then picked for confocal microscopy analysis. A significant increase in the ratio of roGFP2^{ox}/roGFP2^{red} was detected following 24 h infection with *C. albicans*, compared with *E. coli* (** = p<0.01 (T-test)). The increase in mean ratio from 1 h *C. albicans* infection to 24 h was also significant (* = p<0.05 (T-test)).

3.3 Discussion

In this chapter we investigated whether the N-roGFP2::*prdx-2* reporter is able to act as a genetic *in vivo* H_2O_2 sensor to detect endogenous changes in intracellular H_2O_2 levels. Our data suggests that N-roGFP2::*prdx-2* shows some specificity for H_2O_2, but is insufficiently sensitive to detect low levels of H_2O_2 or differences in endogenous levels between tissues. Preliminary testing revealed that the N-roGFP2::*prdx-2* reporter was expressed in the cytosol of a range of *C. elegans* tissues consistent with published PRDX-2::GFP expression and PRDX-2::YFP expression (Hunt-Newbury *et al.*, 2007; Hirani *et al.*, 2013). Additionally, we found that this expression is altered by fusion of roGFP2 to the C-terminus of *prdx-2*. Altered expression of proteins following fusion of a GFP domain to the C-terminus of a protein had been noted before and therefore use of C-terminal translational fusions of PRDX-2 was not conducted (Craig *et al.*, 2013).

Analysis of the 2 anterior intestinal cells only allowed us to generate mean ratio values for a specific structure of the worm. Each cell was analysed separately and a mean $roGFP2^{ox}/roGFP2^{red}$ ratio calculated to ensure that values from the intestinal lumen did not affect results. This, however, means that we did not collect mean $roGFP2^{ox}/roGFP2^{red}$ ratio values for other cell types in the worm. Additionally, analysis of intestinal cells could become problematic in studies of aged worms due to the accumulation of autofluorescence from lipofuscin (Clokey and Jacobson, 1986).

Advantages of using the *prdx-2* promoter include allowing us to express a sensitive H_2O_2 sensor in multiple cellular compartments, without the complication of saturation. Recently, genetic H_2O_2 sensors have been further developed to avoid interference with cells redox balance. For example, the Morgan lab have developed roGFP2-Tsa2ΔC_R in which the H_2O_2-sensing proteins resolving cysteine is removed (Roma *et al.*, 2017). Our sensor has not accounted for this. Additionally, we are unsure of to what extent PRDX-2 forming oligomeric structures in response to H_2O_2 impacts our results. This concern has been previously highlighted in the literature (Ezeriņa *et al.*, 2014).

As we could not detect any significant changes in H_2O_2 levels of the anterior intestine in response to changes in temperature, larval stage, or low extracellular H_2O_2 concentrations, we concluded that the N-roGFP2::*prdx-2* reporter was not sensitive enough to detect the low endogenous changes in H_2O_2 levels in response to these stimuli. However, our sample sizes were relatively small (n=~7), and it is possible that small

changes in H_2O_2 levels may have only been detected when examining a large group of worms; particularly as evidence for heterogeneity in clonal populations of *C. elegans* exists (Wu *et al.*, 2006). Larger sample sizes would be required to provide definitive results.

It can also be argued that the inability to detect a change in roGFP2^{ox}/roGFP2^{red} ratio following starvation for 8 hours is not surprising as the N-roGFP2::*prdx-2* reporter was unable to detect an increase in roGFP2^{ox}/roGFP2^{red} ratio following treatment with 0.2 mM extracellular H_2O_2. However, it could also indicate that fasting uses an alternate signal to activate NHR-49 opposed to peroxide. Previous experimentation revealed that 5-10 mM tBOOH induced similar activation of *fmo-2* as fasting (Goh *et al.*, 2018). Therefore, the apparent absence of a detectable increase in H_2O_2 in these 2 intestinal cells could be indicative of a separate mechanism being used to activate NHR-49 in response to fasting.

The yeast cells *C. albicans* are pathogenic to *C. elegans* and often used as a model for innate immunity (Pukkila-Worley *et al.*, 2011). Excitingly, we were able to detect large changes in roGFP2^{ox}/roGFP2^{red} ratio in response to infection. Due to the established inability of the N-roGFP2::*prdx-2* reporter to detect low changes in endogenous H_2O_2 levels, this result indicates a substantial increase in H_2O_2 levels in the anterior intestine following infection. However, to test whether the increase in intestinal H_2O_2 levels in response to *C. albicans* is robust, this experiment requires replication with a larger sample size, and with the appropriate controls (exposure to 5 mM H_2O_2 and 20 mM NEM). Additionally, it is unclear whether the increase in H_2O_2 is produced as a defence mechanism as part of the *C. elegans* host response, or as a mechanism of *C. albicans* to cause damage and invade host tissue. This could be determined by measuring the roGFP2^{ox}/roGFP2^{red} ratio following exposure of the worms to heat-killed *C. albicans*; which are avirulent.

We also established that the roGFP2^{ox}/roGFP2^{red} ratio of the N-roGFP2::*prdx-2* reporter is resistant to exposure to the oxidant diamide, and the reductant DTT, highlighting a specificity for high levels of H_2O_2. We determined that a significant increase in roGFP2^{ox}/roGFP2^{red} ratio is observed in L4-stage worms following exposure to 1 mM H_2O_2. It would be of great interest to determine in future work whether ageing affects the capacity of *C. elegans* to buffer against rises in intracellular H_2O_2. As the HyPer sensor

has been published to detect exogenous levels of 0.5 mM H_2O_2, we therefore cannot conclude that the N-roGFP2::*prdx-2* reporter is more sensitive than the HyPer sensor (Back *et al.*, 2012).

We also determined a potential limit of the roGFP2^{ox}/roGFP2^{red} ratio, as observed between exposure of 1 mM and 5 mM H_2O_2. We propose that this is due to PRDX-2 beginning to become hyperoxidised at 1 mM H_2O_2, and therefore inhibiting further coupled oxidation of the sensor as H_2O_2 concentration increases. PRDX-2 has been detected to undergo hyperoxidation in response to 1 mM H_2O_2, and to become fully hyperoxidised in response to 5 mM H_2O_2 (Oláhová *et al.*, 2008). To confirm whether N-roGFP2::*prdx-2* is or isn't hyperoxidised with similar sensitivity to endogenous PRDX-2, a western blot of N-roGFP2::*prdx-2* worms exposed to 0.2, 1 or 5 mM H_2O_2 and blotting for PRDX-2^{SOOH} should be conducted.

To conclude, the N-roGFP2::*prdx-2 in vivo* H_2O_2 sensor shows some specificity for H_2O_2, but was unable to detect small changes in intracellular H_2O_2 in response to stimuli such as changes in temperature, larval stages and starvation, or differences in endogenous levels between tissues. However, the N-roGFP2::*prdx-2* reporter is a reliable method to detect large changes in intracellular H_2O_2 levels, following events such exposure to extracellular H_2O_2, or infection.

Chapter 4

Chapter 4. Investigating the role of cytosolic family 2-Cys Prx in mitochondrial function

4.1 Introduction

The mitochondrial sub-compartments, the IMS and the matrix, have a reducing environment (as discussed in section 1.4) (Kaludercic *et al.*, 2014). However, thiols are highly susceptible to oxidation due to the high level of ROS produced as a by-product of the mitochondrial respiratory chain (Go and Jones, 2008; Murphy, 2009). In addition, the majority of mitochondrial proteins are synthesised by cytosolic ribosomes and imported in an unfolded state into the mitochondrial sub-compartments. Once in the IMS for example, oxidative protein folding occurs via the Mia pathway further contributing to H_2O_2 production (Banci *et al.*, 2009). Oxidative stress affects mitochondrial activity, such as protein import by arresting the ADP/ATP carrier (AAC) of the Tim22 pathway (Curran SP, 2004). Therefore, maintenance of ROS homeostasis is extremely important and mitochondria possess their own antioxidant enzymes, such as SOD, Gpx and Prx (as discussed in section 1.4) (Toledano *et al.*, 2013). Interestingly, most eukaryotes have a mitochondrial matrix-targeted 2-Cys Prx that is targeted to the matrix, whereas *S. pombe* express a single 2-Cys Prx gene encoding a Prx, Tpx1, that does not include a matrix-targeting sequence, and which immunostaining suggests is predominantly cytoplasmic (Day *et al.*, 2012).

Previous studies of mutant yeast and worms lacking, Tpx1 (*S. pombe*) or the cytosolic 2-Cys Prx PRDX-2 (*C. elegans*), have revealed a number of phenotypes. These include an increased sensitivity to H_2O_2 of *tpx1*Δ, and therefore a role for Tpx1 in transcriptional responses to H_2O_2 (Veal *et al.*, 2004). As well as both Tpx1 and PRDX-2 being important for stress-induced activation of p38-related MAPK (Veal *et al.*, 2004; Oláhová *et al.*, 2008; Latimer and Veal, 2016). Tpx1 is also required for H_2O_2-induced activation of the TF Pap1 (as described in 1.2.3) (Bozonet *et al.*, 2005; Vivancos *et al.*, 2005). In addition, unpublished work by the Veal lab has revealed that *S. pombe tpx1*Δ cells have an impaired electron transport chain, as well as altered mitochondria morphology (Latimer, Day, Brown and Veal, unpublished). Notably, *prdx-2(gk169)* mutant *C. elegans*, lacking

the single orthologue of mammalian Prx1 and 2, PRDX-2, also have evidence of a mitochondrial defect, with a reduced electrochemical gradient across the inner mitochondrial membrane, and fragmented mitochondrial network (Oláhová and Veal, unpublished). Although it is possible that deletion of a cytosolic Prx might indirectly cause mitochondrial defects, the discovery that a pool of Sty1 (Di *et al.*, 2012) and a significant portion of Pap1 (Latimer thesis, 2017), that are both activated by Tpx1, are co-purified with mitochondria led to the hypothesis that a pool of Tpx1 might be present in the mitochondria, and important for mitochondrial function.

In parallel, the discovery that a pool of the thioredoxin peroxidase, Gpx3 is present in the mitochondrial IMS (Vögtle *et al.*, 2012; Kritsiligkou *et al.*, 2017) of *S. cerevisiae* raised the possibility that activation of Yap1 and Pap1 might involve a mitochondrial pool of the sensor peroxidases, GPx3 and Tpx1. Moreover, *gpx3*Δ mutant *S. cerevisiae* also have mitochondrial defects, including aberrant mitochondrial morphology, lower inner membrane potential, and defective protein import capacity which are rescued by expression of a Gpx3 targeted to the IMS by fusion to the IMS-targeting sequence of cytb2 (Kritsiligkou *et al.*, 2017).

The aim of this chapter was to investigate further the basis for the mitochondrial defects of *tpx1*Δ mutant *S. pombe* and *prdx-2(gk169)* mutant *C. elegans,* and to test the hypothesis that a pool of mitochondrially targeted Tpx1 might be important for Tpx1's H_2O_2-signalling functions.

4.2 Results

4.2.1 *tpx1*Δ mutant *S. pombe* and *prdx-2(gk169)* mutant *C. elegans* have mitochondrial defects

4.2.1.1 *prdx-2(gk169) C. elegans* have fragmented mitochondria compared with wild-type *C. elegans*

To determine whether loss of PRDX-2 affects mitochondrial morphology, wild-type (WT) and *prdx-2(gk169)* L4 stage larvae, expressing a matrix-targeted GFP (mtGFP) (EB225 and EB260 respectively), or an RFP-tagged TOMM-20 (EB254 and EB253 respectively) were analysed by confocal microscopy (as described in 2.6.2.2).

Wild type *C. elegans* displayed complex mitochondrial networks (figure 4.1A and 4.1B). However, the mitochondrial networks in *prdx-2(gk169)* mutant worms were fragmented

(figure 4.1C and 4.1D). This data provides clearer evidence of fragmented mitochondria in peroxiredoxin mutant worms, supporting the additional unpublished work of the Veal lab, which also identified disrupted mitochondrial morphology in *prdx-2(gk169)* worms by fluorescence microscopy, as well as reduced electrochemical gradient across the mitochondrial inner membrane.

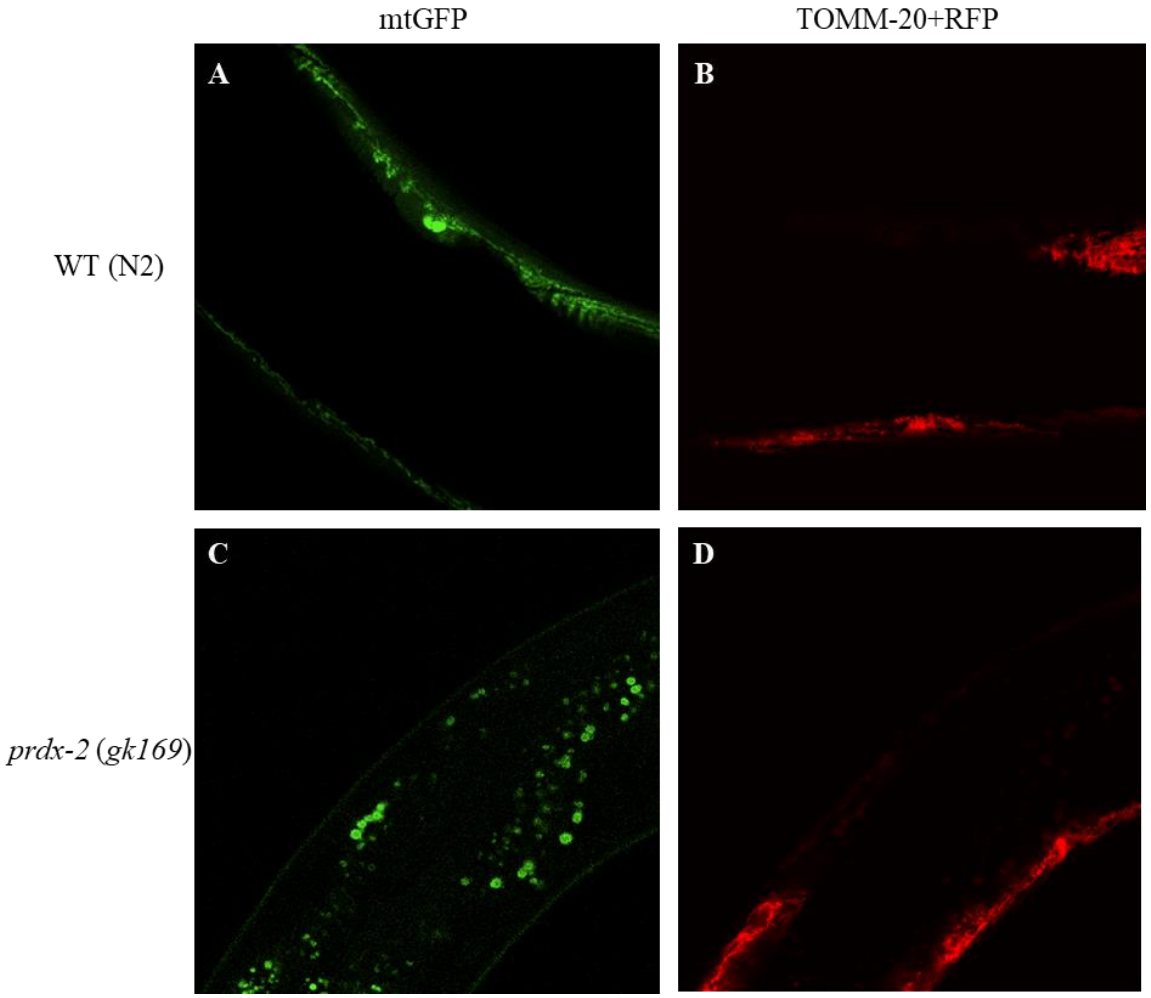

Figure 4.1 The effect of loss of PRDX-2 on mitochondrial morphology compared with wild-type *C. elegans*. Comparison of wild-type and *prdx-2(gk169)* mutant L4 larval stage *C. elegans* that had been maintained at 15 °C expressing [A and C] mitochondrial matrix-targeted GFP expressed from the myo-3 promoter (mtGFP) (EB255 and EB260), or [B and D] a mitochondrial outer membrane protein (TOMM-20) tagged with RFP (TOMM-20+RFP) (EB254 and EB253) by confocal microscopy at 488 nm (mtGFP) and 568 nm (TOMM-20+RFP).

4.2.1.2 *tpx1*Δ mutant *S. pombe* have reduced growth on non-fermentable carbon source

To test whether the altered mitochondrial morphology of *tpx1*Δ mutant cells might also correlate with a reduced mitochondrial activity, we compared the growth of *tpx1*Δ and *tpx1*$^+$ cells on media containing glucose as a carbon source (YE5S), or glycerol (3 % glycerol) as a carbon source. Cells are unable to utilise glycerol to generate energy by fermentation. Therefore, on plates containing glycerol in place of glucose, cells rely on their mitochondrial activity to generate the energy required for growth (Matsuzawa *et al.*, 2010). As previously reported, the growth of *tpx1*Δ cells on YE5S is impaired in comparison to wild-type *tpx1*$^+$ cells (figure 4.2) (Jara *et al.*, 2007; Paulo *et al.*, 2014). However, this growth defect was exacerbated on plates containing glycerol instead of glucose, consistent with Tpx1 being required for mitochondrial activity.

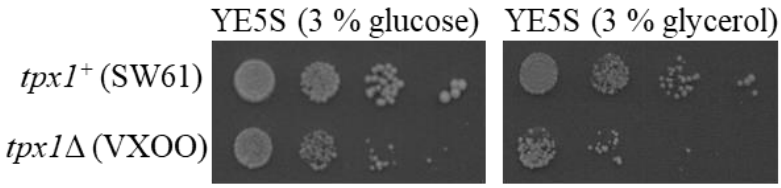

Figure 4.2 Growth of wild-type and *tpx1*Δ mutant on fermentable and non-fermentable carbon sources. Growth of serially diluted, exponentially growing *tpx1*$^+$ (SW61) and *tpx1*Δ (VXOO). Cells spotted onto rich media supplemented with 3 % glucose (YE5S) and media supplemented with 3 % glycerol (3 % glycerol). Imaged after 3 days (YE5S) and 13 days (3 % glycerol).

4.2.2 Pap1 is localised to the mitochondria and this localisation is dependent on the presence of Tpx1 in *S. pombe*

4.2.2.1 Tpx1 and Pap1 are localised to *S. pombe* mitochondrial intermembrane space

In order to investigate the location of the mitochondrial pool of Tpx1, or Pap1, previously detected (Latimer thesis, 2017) a mitochondrial isolation and sub-fractionation protocol was optimised from established *S. cerevisiae*, or mammalian cell, mitochondrial sub-fractionation protocols (as described in 2.5.3). Mitochondria were isolated from cells expressing GFP-tagged Tim40 and then treated with proteinase k in order to shave any cytoplasmic proteins that stuck to the outer edge of the mitochondrial outer membrane (OM). As expected, Tpx1 was detected in the 'total' cell extract. Although the majority of Tpx1 was also detected in the cytosolic fraction, as observed previously (Latimer thesis, 2017) a faint band corresponding to Tpx1 was also detected in the mitochondrial fraction. This pool of mitochondrial Tpx1 was enriched in the shaved mitochondrial fraction, further indicative of mitochondrial localisation (figure 4.3, first panel). Pap1 was also detected in the 'total' cell extract. Interestingly, only a faint band of Pap1 was detected in the cytosolic fraction, but, consistent with previous findings (Latimer thesis, 2017), a lower molecular weight band for Pap1 was detected in the mitochondrial, and shaved mitochondrial fractions (figure 4.3, second panel).

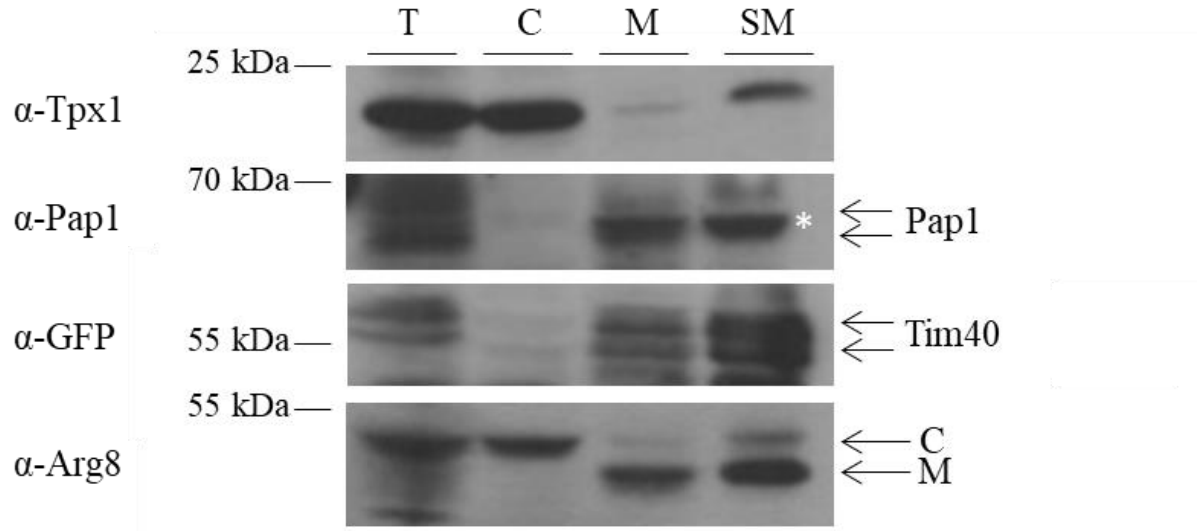

Figure 4.3 Tpx1 and Pap1 co-purify with mitochondria.
Western blot analysis with anti-Tpx1, anti-GFP, anti-Pap1 and anti-Arg8 antibodies, of fractionated cell lysate from *S. pombe* cells expressing GFP-tagged Tim40 (HL16) (T = total cell lysate, C = cytosolic fraction, M = mitochondrial fraction, SM = shaved mitochondria). The α-Arg8 antibody recognises the *S. pombe* mitochondrial protein Arg1 (M), but also cross-reacts with an unknown cytosolic protein (C) of a different molecular weight. Arrow heads indicate specific protein bands. * indicates non-specific band.

The mitochondrial inner membrane protein Tim40 was detected in the 'total' cell extract, in the mitochondrial fraction, and in the shaved mitochondrial fractions (figure 4.3, third panel). The absence of Tim40+GFP from the cytosolic fraction suggests that the isolation of mitochondria was effective. This conclusion was also supported by the detection of only the higher molecular weight anti-Arg8 cross-reactive protein (C) in the cytosolic fraction, whereas the lower molecular weight (M) Arg8 (the mitochondrial protein Arg1) was, as expected, confined to the mitochondrial fractions (figure 4.3, fourth panel) (Dujeancourt *et al.*, 2013; Kühl *et al.*, 2011). Nevertheless, a very low amount of the anti-Arg8 cross-reactive cytosolic protein (C) was detected in the mitochondrial fractions. This contamination of cytosolic proteins appears to be higher in the 'shaved mitochondria' fraction (SM) than in the mitochondrial fraction (M). It therefore remains possible that the detection of Tpx1 in the mitochondrial fractions could be due to some contamination of mitochondrial fractions with cytosolic proteins. Moreover, it was possible that, rather than representing a mitochondrial pool, Tpx1 co-purified with mitochondria was found on the outer surface of the outer membrane.

Therefore, to investigate this further, the extraction was repeated to determine whether Tpx1 and/or Pap1 were detected in internal mitochondrial compartments. In addition, the protocol was expanded to include additional mitochondrial sub-fractionation steps, in order to determine in which mitochondrial compartment Tpx1 or Pap1 may be present. In this sub-fractionation experiment, and the following isolation experiments, it is important to note that the 'total' cell extract was taken after nucleic proteins had been removed and will now be referred to as 'nuclear-free cell lysate'.

As previously observed (figure 4.3), Tpx1 was predominantly detected in the cytosolic fraction (figure 4.4, first panel). Tpx1 was also detected in the shaved mitochondrial fraction, indicative of a pool of Tpx1 that is protected from the proteinase K by crossing the OM into the mitochondria. Interestingly, this band is lost following mitoplasting (from which the OM was removed by treatment with 10 mM Tris-HCl). No band for Tpx1 is detected in the mitoplast fraction, shaved mitoplast fraction, or the inner membrane fraction. The reduction in protein levels following the mitoplasting step is indicative of the loss of a mitochondrial intermembrane space protein.

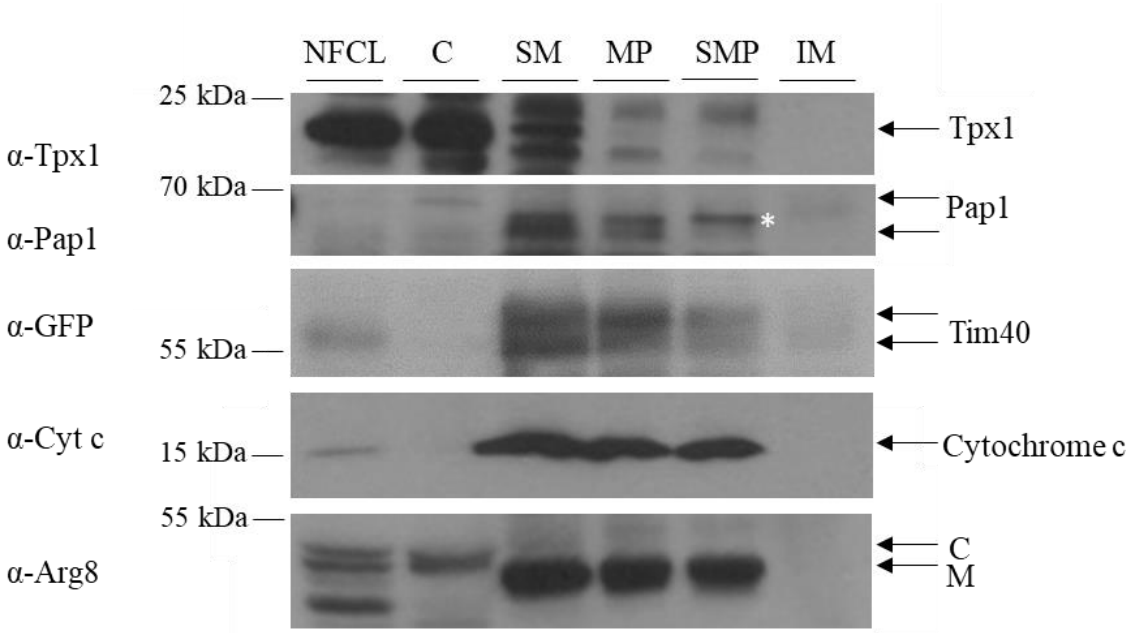

Figure 4.4 Tpx1 and Pap1 are present in the mitochondrial intermembrane space. Western blot analysis, with anti-Tpx1, anti-Pap1, anti-GFP, anti-Cytochrome c and anti-Arg8 antibodies, of sub-fractionated cell lysate from *S. pombe* cells expressing GFP-tagged Tim40 (HL16) (NFCL = nuclear free cell lysate, C = cytosolic fraction, SM = shaved mitochondria, MP = mitoplast, SMP = shaved mitoplast, IM = inner membrane). Anti-Arg8 detects the *S. pombe* mitochondrial protein Arg1 (M), and cross-reacts with a higher molecular weight unknown cytosolic protein (C). Arrow heads indicate specific protein bands. * indicates non-specific band.

In this experiment Pap1 was not detected in the nuclear free cell lysate (figure 4.4, second panel), likely due to the removal of the nucleic proteins in the sample. A low level of Pap1 was detected in the cytosolic fraction; it is noteworthy that when blotting for Pap1, the cytosolic Pap1 consistently appears to have a higher molecular weight than the mitochondrial Pap1. This is consistent with previous research in which *pap1Δ* cells are loaded alongside wild-type *S. pombe* cells (Latimer thesis, 2017). Additionally, both bands shift in size when Pap1-pk is blotted. As seen previously (figure 4.3), Pap1 was detected in the shaved mitochondrial fraction (figure 4.4, second panel). Slightly less Pap1 is detected following the mitoplasting step (from which the OM was removed by treatment with 10 mM Tris-HCl). Detection of Pap1 was lost following protease-treatment (shaving) of the mitoplast which is expected to degrade IMS proteins, and no Pap1 was detected in the mitochondrial inner membrane fraction. This banding pattern is indicative of an IMS-targeted protein. The detection of Pap1 in the mitoplast fraction, that is then lost following protease treatment, is likely due to Pap1 sticking to the outside of the IM.

Tim40GFP (a mitochondrial inner membrane protein) was detected in the nuclear free cell lysate (figure 4.4, third panel). The Tim40 band is also detected in the shaved mitochondrial fraction, the mitoplast fraction, the shaved mitoplast fraction, and the inner membrane fraction. No Tim40 was detected in the cytosolic fraction; indicating no cross-contamination of the mitochondrial proteins with the cytosol. Additionally, the detection of only the higher molecular weight anti-Arg8 cross-reactive protein (C) in the cytosolic fraction, as well as only the lower molecular weight (M) Arg8 (the mitochondrial protein Arg1) band in the mitochondrial and mitoplast fractions (figure 4.4, fifth panel) also indicates a clean separation of cellular fractions.

As a control we examined the distribution of Cytochrome-c, a highly conserved protein, which is localised exclusively in the IMS (Kühlbrandt, 2015) (figure 4.4, fourth panel). As expected, consistent with its IMS-localisation, Cytochrome-c was detected in the nuclear free cell lysate, Cytochrome-c was not detected in the cytosolic fraction, but was, instead, enriched in the shaved mitochondria fraction. Cytochrome-c was also detected in the mitoplast and shaved mitoplast fractions. Despite its IMS localisation, Cytochrome-c is anchored to the mitochondrial inner membrane (Ott *et al.*, 2002). It is therefore possible that Cytochrome c is protected from loss during mitoplast shaving.

4.2.2.2 Pap1 requires Tpx1 for mitochondrial localisation

The increased H_2O_2 sensitivity of *S. pombe tpx1*Δ cells appears to be largely due to an inability to oxidise the transcription factor Pap1 (Bozonet *et al.*, 2005; Vivancos *et al.*, 2005). The detection of Tpx1 and Pap1 in the IMS led to the hypothesis that IMS localisation of both proteins might be vital for Pap1 oxidation and activation. To test the hypothesis that one of Tpx1's roles in the oxidation of Pap1 might be to promote the localisation of Pap1 to the IMS we examined the effect of loss of Tpx1 on Pap1 localisation.

To determine whether the presence of Tpx1 is required for the mitochondrial localisation of Pap1; mitochondrial isolations of cells lacking Tpx1 (*tpx1*Δ), and of cells wild-type for Tpx1, but expressing pk-tagged Pap1 (Pap1-pk) were conducted. Blotting for pk-tagged Pap1 results in a size shift due to the pk-tag; this allowed for clearer distinction between detection of Pap1 and non-specific bands.

As seen previously (figure 4.3, figure 4.4), cells wild-type for Tpx1 detected Tpx1 in the nuclear free cell lysate and cytosolic fraction, and a smaller pool of Tpx1 in the mitochondrial fraction (figure 4.5, first panel). Whilst Pap1 was detected in the cytosolic fractions of both *tpx1*Δ and Pap1-pk strains, levels of Pap1 in the cytosolic fraction of the *tpx1*Δ strain appear increased (figure 4.5, second panel). Interestingly, Pap1 is detected in the mitochondrial fraction of the Pap1-pk strain, but is lost in the *tpx1*Δ mitochondrial fraction. Perhaps the lack of Pap1 mitochondrial localisation is the reason for the increased levels of cytosolic Pap1 in the *tpx1*Δ strain.

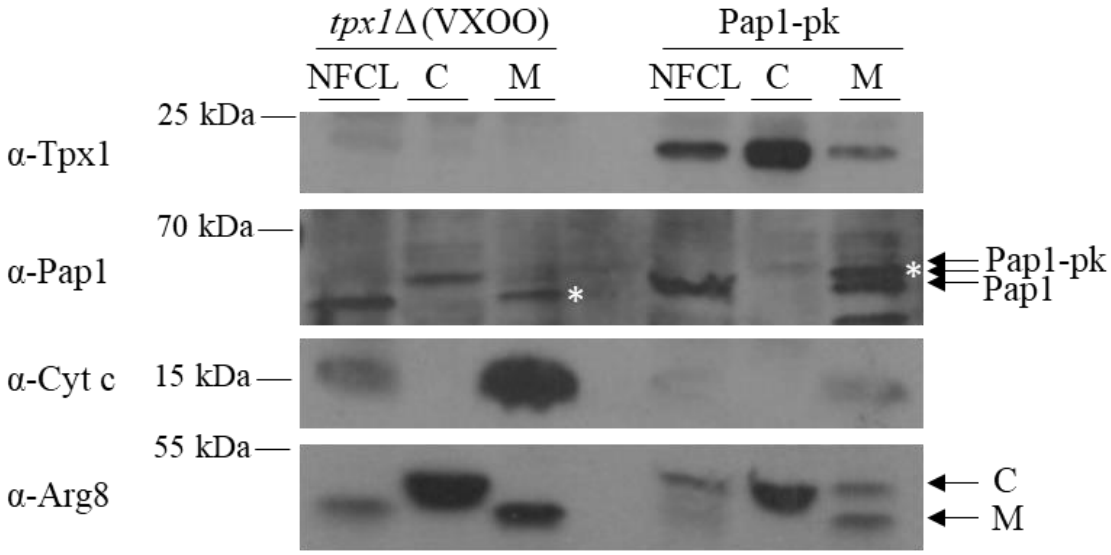

Figure 4.5 Pap1 requires Tpx1 for mitochondrial localisation. Western blot analysis with anti-Tpx1, anti-Pap1, anti-Cytochrome c and anti-Arg8 antibodies of fractionated cell lysate from *S. pombe* cells lacking Tpx1 (*tpx1*Δ (VXOO)), or expressing pk-tagged Pap1 (Pap1-pk) (NFCL = nuclear free cell lysate, C = cytosolic fraction, M = mitochondrial fraction). Anti-Arg8 detects the *S. pombe* mitochondrial protein Arg1 (M), and cross-reacts with a higher molecular weight cytosolic protein (C). Arrow heads indicate specific protein bands. * indicates non-specific band. Experiment conducted once.

In both strains, the blotting for Cytochrome-c revealed no contamination of the cytosolic fraction with mitochondrial proteins. However levels of cytochrome c appear higher in *tpx1*Δ cells. It is important to note that the *tpx1*Δ and *pap1-pk* strains are not isogenic. 50 µg mitochondrial material is loaded onto each gel so this difference in results is unlikely due to unequal loading. It is unclear however whether this result is real or due to inefficient transferring. Finally, the detection of only the higher molecular weight anti-Arg8 cross-reactive protein (C) in the cytosolic fraction, as well as only the lower molecular weight (M) Arg8 (the mitochondrial protein Arg1) band in the mitochondrial fraction of *tpx1*Δ also indicates a clean separation of cellular fractions (figure 4.5, fourth panel). However, in the mitochondrial fraction of the Pap1-pk strain a small amount of contamination of cytosolic proteins (C) is observed.

4.2.2.3 The Tpx1 resolving cysteine (169) is not required for Tpx1 or Pap1 localisation to the mitochondria

As Tpx1 appears to be required for Pap1 import into the mitochondria we wanted to investigate whether specifically the Tpx1 resolving cysteine (169) is necessary for Pap1 interaction with mitochondrial protein import machinery. The *tpx1*^{C169S} mutant is unable to support the activating oxidation and nuclear localisation of Pap1 as it is unable to promote the oxidation of Txl1 (as described in 1.3.5) (Brown *et al.*, 2013). However, *tpx1*^{C169S} is able to promote the formation of non-native disulphide forms. Mitochondrial isolation experiments were performed on *S. pombe* cells expressing wild-type *tpx1*$^{+}$, or on cells expressing Tpx1 with a mutated resolving cysteine, *tpx1*^{C169S} cells.

As previously (figures 4.3, 4.4 and 4.5), a small portion of both wild type Tpx1 and Tpx1^{C169S} was detected in the mitochondrial fraction (figure 4.6, first panel). *tpx1*^{C169S} cells appear to have a lower level of Tpx1^{C169S} in the nuclear free cell lysate than wild-type cells. However, have a larger pool of Tpx1^{C169S} localised to the mitochondria. As seen previously (also observed in figure 4.4), Pap1 is not detected in the nuclear free cell lysate for *tpx1*$^{+}$ or *tpx1*^{C169S} cells, but is detected in the cytosolic fractions of both strains (figure 4.6, second panel). Excitingly, Pap1 is detected in the mitochondrial fraction of both *tpx1*$^{+}$ and *tpx1*^{C169S} cells.

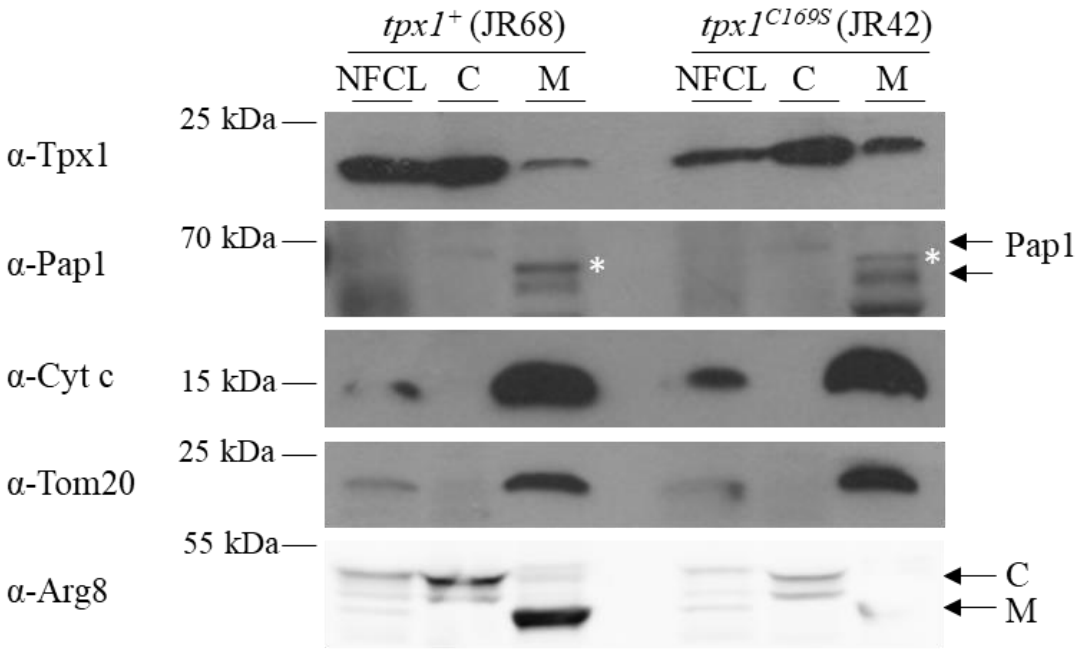

Figure 4.6 Effect of substitution of resolving cysteine of Tpx1 on the mitochondrial pools of Tpx1 and Pap1. Western blot analysis of fractionated cell lysate from *S. pombe* cells wild-type for Tpx1 (*tpx1*$^{+}$ (JR68)), or expressing the Tpx1 trapping mutant (*tpx1*^{C169S} (JR42)) with anti-Tpx1, anti-Pap1, anti-Cytochrome c, anti-Tomm20 and anti-Arg8 antibodies (NFCL = nuclear free cell lysate, C = cytosolic fraction, M = mitochondrial fraction). Anti-Arg8 detects the *S. pombe* mitochondrial protein Arg1 (M), and cross-reacts with a higher molecular weight cytosolic protein (C). Arrow heads indicate specific protein bands. * indicates non-specific band. Experiment conducted once.

In both the *tpx1*$^{+}$ and the *tpx1*^{C169S} strains, the mitochondrial proteins Cytochrome-c and Tom20 were detected in the nuclear free cell lysate and in the mitochondrial cell fractions as expected (figure 4.6, third and fourth panels). The lack of both proteins in the cytosolic fractions revealed that there is no detectable contamination of the cytosolic fraction with mitochondrial proteins. In addition, detection of the higher molecular weight anti-Arg8 cross-reactive protein (C) in the cytosolic fraction, as well as only the lower molecular weight (M) Arg8 (the mitochondrial protein Arg1) band in the mitochondrial fraction also indicates a clean separation of cellular fractions.

In both the Cytochrome-c and Tom20 panels (figure 4.6, third and fourth panels), banding appears more intense in the *tpx1*^{C169S} mitochondrial fraction, compared to the *tpx1*$^{+}$ mitochondrial fraction. Due to this observation, it is possible that a higher concentration of proteins were loaded in the *tpx1*^{C169S} mitochondrial sample. This could therefore explain the increase in the mitochondrial levels of Tpx1^{C169S} and Pap1 observed in the *tpx1*^{C169S} strain.

4.2.3 From confocal microscopy analysis it is unclear whether Pap1 is localised to the mitochondria and whether this localisation is dependent on the presence of Tpx1

To investigate the localisation of Pap1 further, we investigated the localisation of a Pap1-GFP fusion, ectopically expressed in *wildtype* or *tpx1*Δ cells expressing an RFP-tagged form of the mitochondrial protein Cox4 using confocal microscopy.

As expected, the distribution of Cox4RFP was consistent with its presence in complex mitochondrial networks (Matsuyama *et al.*, 2006) (figure 4.7A, middle panels). As, Pap1GFP was expressed from a multicopy plasmid, levels of GFP-tagged Pap1 expression varied between cells but in general when the signals from the 2 fluorescent channels were merged (figure 4.7A, right panels), most GFP and RFP fluorescence was apparently present in distinct cell locations. However, a few cells, particularly those with lower levels of Pap1GFP expression appear yellow in colour suggesting co-localisation of Pap1 with Cox4.

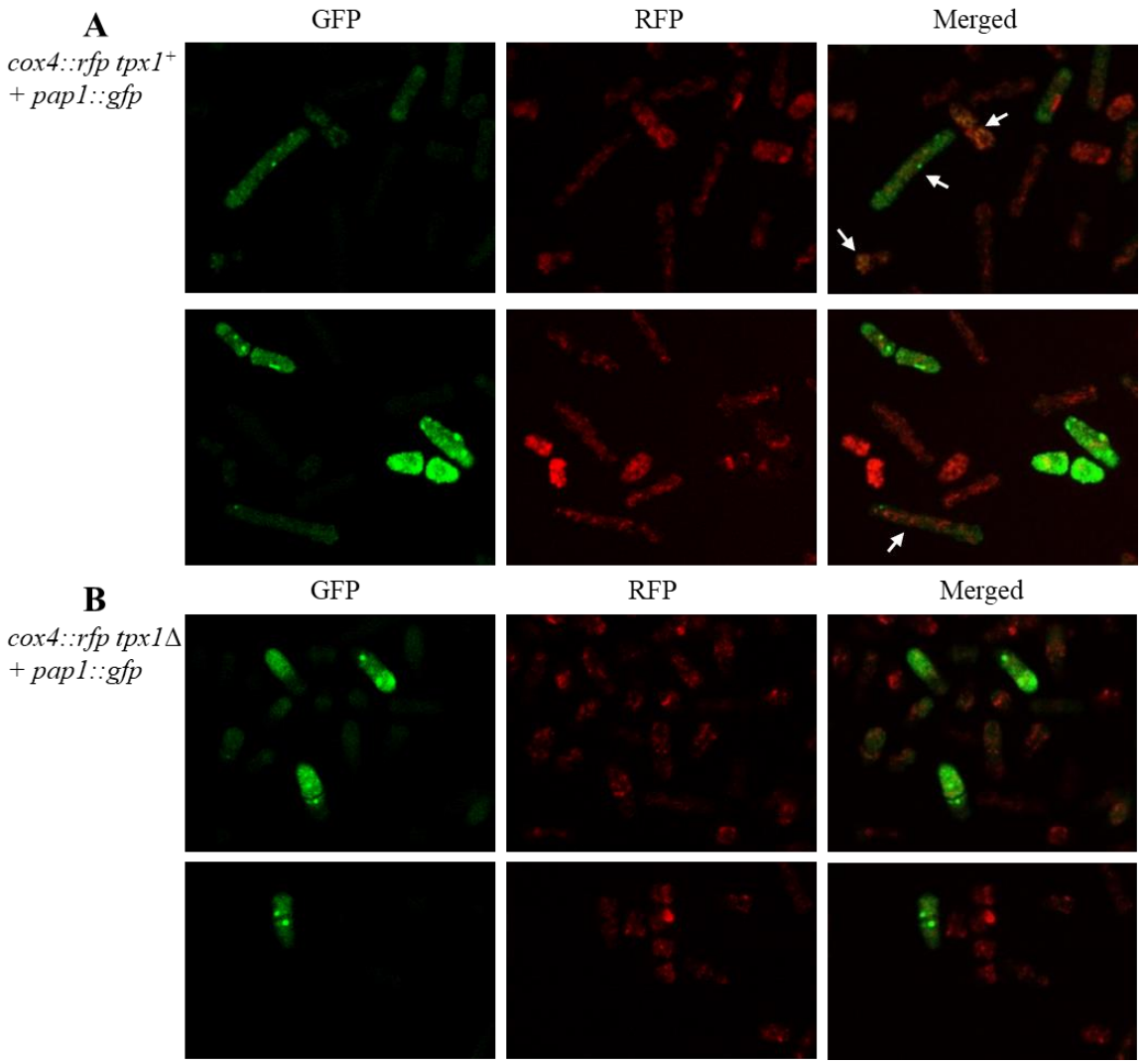

Figure 4.7 Confocal microscopy analysis of wild type and *tpx1*Δ *S. pombe* expressing RFP-tagged Cox4 and GFP-tagged Pap1. Examination of the localisation of Pap1 in exponentially growing *S. pombe* cells either wild-type for Tpx1 (*tpx1*$^{+}$) [A], or lacking Tpx1 (*tpx1*Δ) [B] expressing RFP-tagged Cox4 and transformed with pRep41Pap1GFP. White arrows indicate co-localisation of Tpx1 and Pap1.

Examination of the distribution of Cox4RFP in *tpx1*Δ cells suggested that mitochondria were more fragmented in *tpx1*Δ cells (figure 4.7B, middle panels). As in the *tpx1*$^+$ cells, Pap1GFP was found diffuse across the cell, with Pap1GFP levels more concentrated in certain areas (figure 4.7B, left panels). The absence of yellow, colocalization of the RFP and GFP signals, suggests that there was no Pap1GFP present in the mitochondria of any of *tpx1*Δ cells (figure 4.7B, right panels). However, given that co-localisation of both proteins was only observed in a small subset of *tpx1*$^+$ cells, it is unclear whether this reflects an essential requirement for Tpx1 in mitochondrial localisation of a pool of Pap1.

4.2.4 Targeting Tpx1 to the mitochondrial intermembrane space can rescue the growth, and H_2O_2 resistance of *tpx1*Δ mutant *S. pombe* cells

4.2.4.1 Targeting a low level of Tpx1 to the mitochondrial intermembrane space can rescue the growth of *tpx1*Δ mutant *S. pombe* cells on minimal media

In *S. cerevisiae*, targeting Gpx3 to the mitochondrial IMS by fusion of an 18 amino acid IMS-targeting sequence present in the cytB2 protein, rescued the morphology and function of the mitochondria of the *gpx3*Δ cells, indicating that the IMS-based Gpx3 is important for normal mitochondrial function (Kritsiligkou *et al.*, 2017). In order to test whether the IMS-based Tpx1 pool might be important for mitochondrial function or cell responses to H_2O_2, we investigated whether targeting a peroxiredoxin to the mitochondria could rescue the cell growth defect or H_2O_2 resistance of *tpx1*Δ cells. Although there have been no investigations of IMS-targeting sequences in *S. pombe*, studies in yeast and human cells indicate that the processes involved in IMS-targeting are highly conserved (Vögtle *et al.*, 2009). Therefore, we generated a plasmid expressing, from the thiamine-repressible nmt1 promoter, one (pRep1cytb2IMS+Tpx1) or two (pRep12xcytb2IMS+Tpx1) copies of the IMS targeting sequence from the *S. cerevisiae* cytb2 protein fused to the N-terminal end of Tpx1 (as described in 2.4.8). Plasmids were expressed in *S. pombe tpx1*$^+$ and *tpx1*Δ cells and maintained with or without the presence of thiamine to control the expression levels of Tpx1 and cytb2Tpx1.

Although, as expected, the overexpression of Tpx1 (pRep1Tpx1) did not affect the growth of *tpx1*$^+$ cells, the growth of *tpx1*$^+$ cells expressing Tpx1 with one IMS targeting sequence (pRep1cytb2IMS+Tpx1) was greatly reduced with fewer viable colonies than expected given the OD-based spotting of equal numbers of cells compared with the vector control. However, this reduction in growth was not observed in *tpx1*$^+$ cells expressing

Tpx1 with two IMS-targeting sequences (pRep12xcytb2IMS+Tpx1). Moreover, these colonies were smaller indicating a cell cycle defect. As expected, the *tpx1*Δ cells transformed with the empty vector (pRep1) had a severe growth defect when compared with the growth of *tpx1*$^{+}$ cells transformed with the same vector (pRep1) (figure 4.8, top panel). The growth defect of *tpx1*Δ cells was rescued by ectopic expression of Tpx1 (pRep1Tpx1), as expected, but was not improved by either of the constructs expressing Tpx1 fused to the cytb2 IMS-targeting sequence (pRep1cytb2IMS+Tpx1 or pRep12xcytb2IMS+Tpx1).

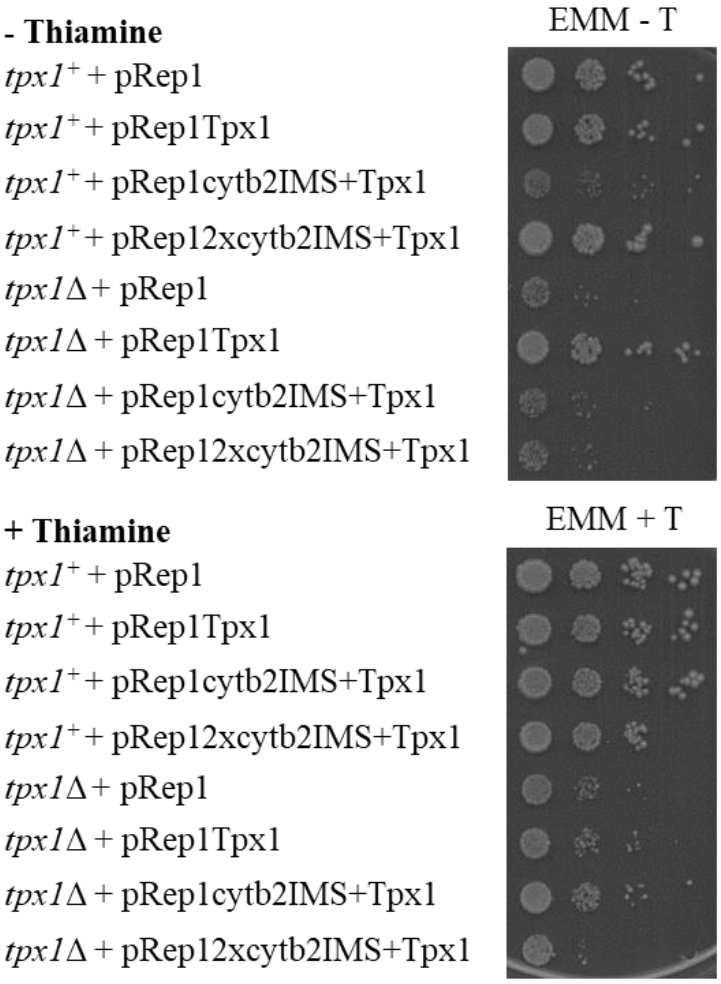

Figure 4.8 The effect of expression of wild-type and IMS-targeted Tpx1 on the growth of wild-type and *tpx1*Δ mutant *S. pombe*. Examination of the growth of exponentially growing *S. pombe tpx1*$^+$ (NT4) or *tpx1*Δ (EV45) cells transformed with the expression vector pRep1, pRep1Tpx1, pRep1cytb2IMS+Tpx1 or pRep12xcytb2IMS+Tpx1. Plates were incubated at 30 °C and the images presented were scanned after 6 days. Cells were transformed, maintained and spotted as indicated on plates containing thiamine (+T).

As high levels of cytb2Tpx2 appear to be toxic to cells we sought to reduce the expression of cytb2Tpx1 by observing growth in the presence of thiamine; which represses the nmt promoter under which Tpx1 or cytb2Tpx1 are expressed. As observed previously, the growth of *tpx1*$^{+}$ cells expressing the empty vector (pRep1), or overexpressing Tpx1 (pRep1Tpx1) exhibit normal growth on minimal media (figure 4.8, lower panel). This was unaffected by targeting Tpx1 to the IMS with one IMS targeting sequence (pRep1cytb2IMS+Tpx1). However, targeting Tpx1 to the IMS with two IMS targeting sequences (pRep12xcytb2IMS+Tpx1) slightly reduced growth on minimal media. For *tpx1*Δ cells, a growth defect is observed in cells expressing the empty vector (pRep1), as expected (figure 4.8, lower panel). The growth defect was not rescued by the overexpression of Tpx1 (pRep1Tpx1). Interestingly, growth of *tpx1*Δ cells was improved by targeting Tpx1 to the IMS with one IMS targeting sequence (pRep1cytb2IMS+Tpx1). However, targeting Tpx1 to the IMS with two IMS targeting sequences (pRep12xcytb2IMS+Tpx1) resulted in a growth defect.

From these observations it seems that although targeting a high level of Tpx1 to the IMS may be toxic to cells, our data is consistent with low levels of IMS-targeted Tpx1 restoring growth.

4.2.4.2 Targeting Tpx1 to the mitochondrial intermembrane space can rescue the H_2O_2 resistance of *tpx1*Δ mutant *S. pombe* cells

Tpx1 mutant cells are sensitive to H_2O_2 due to signalling defects including impaired H_2O_2-induced activation of Pap1 and Sty1 (Veal *et al.*, 2004; Bozonet *et al.*, 2005). In order to investigate whether targeting Tpx1 to the mitochondria could rescue the H_2O_2 resistance of *tpx1*Δ cells, cells were also spotted onto minimal media agar supplemented with a range of H_2O_2 concentrations. The ability of low levels of IMS-targeted Tpx1 to improve the growth of *tpx1*Δ cells was confirmed (figure 4.9).

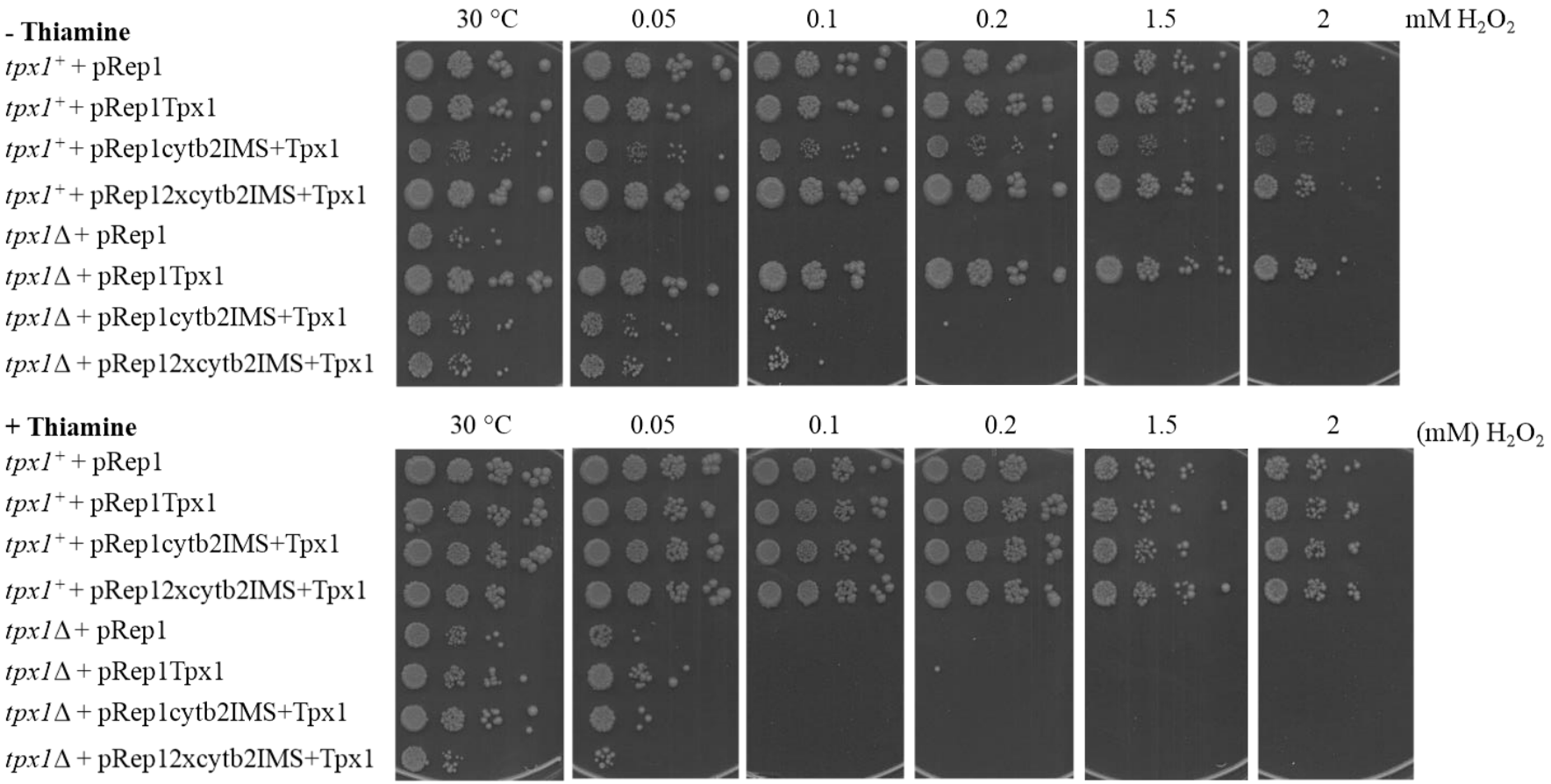

Figure 4.9 Targeting Tpx1 to the mitochondria increased H_2O_2 resistance of *tpx1*Δ cells. Examination of the H_2O_2 resistance of exponentially growing *S. pombe tpx1*$^+$ (NT4) or *tpx1*Δ (EV45) cells transformed with the expression vector pRep1, pRep1Tpx1, pRep1cytb2IMS+Tpx1 or pRep12xcytb2IMS+Tpx1. Plates were incubated at 30 °C and the images presented were scanned after 10 days. Cells were transformed, maintained and spotted with or without 15 µM thiamine.

tpx1$^+$ cells expressing Tpx1 targeted to the IMS using one IMS targeting sequence (pRep1cytb2IMS+Tpx1) displayed increased sensitivity to H_2O_2. As expected, the growth of *tpx1*Δ cells expressing the empty vector (pRep1) was severely inhibited at the lowest concentration of H_2O_2 compared to *tpx1*$^+$ cells (figure 4.9, top panel). Additionally, the H_2O_2 resistance of *tpx1*Δ cells was rescued to wild-type *tpx1*$^+$ levels following the overexpression of Tpx1 (pRep1Tpx1). Excitingly, the growth of *tpx1*Δ cells expressing Tpx1 targeted to the IMS (Rep1cytb2IMS+Tpx1 or pRep12xcytb2IMS+Tpx1) displayed increased H_2O_2 resistance up to 0.1 mM H_2O_2, when compared with *tpx1*Δ cells transformed with the empty vector (pRep1).

In the presence of thiamine, the growth and H_2O_2 resistance of *tpx1*$^+$ cells is unaffected by the overexpression of Tpx1, or the targeting of Tpx1 to the IMS (figure 4.9, bottom panel). The *tpx1*Δ cells transformed with the empty vector (pRep1) were sensitive to the lowest concentration of H_2O_2, as seen previously. The H_2O_2 resistance of *tpx1*Δ cells was not rescued by the overexpression of Tpx1 (pRep1Tpx1). Targeting Tpx1 to the IMS (pRep1cytb2IMS+Tpx1 or pRep12xcytb2IMS+Tpx1) in *tpx1*Δ cells no longer improved H_2O_2 resistance compared with cells transformed with the empty vector (pRep1). This result indicates that targeting Tpx1 to the IMS using an 18 amino acid IMS-targeting sequence is able to slightly improve the H_2O_2 resistance of *tpx1*Δ cells.

4.2.4.3 The targeting of *S. cerevisiae* Gpx3 to the mitochondrial intermembrane space does not rescue the growth of *tpx1*Δ mutant *S. pombe* cells

We also investigated whether targeting Gpx3, which supports Yap1 activation in *S. cerevisiae* (Delaunay et al., 2002), to the IMS of *S. pombe* cells (the *S. pombe* homologue of Gpx3 is Gpx1) would affect growth of *tpx1*Δ cells. We examined the growth and H_2O_2 resistance of *tpx1*$^+$ and *tpx1*Δ cells transformed with the *S. cerevisiae* empty vector pRS316, or a plasmid engineered to express Gpx3 with an IMS targeting sequence (pRS316up40cytb2GPX3Myc).

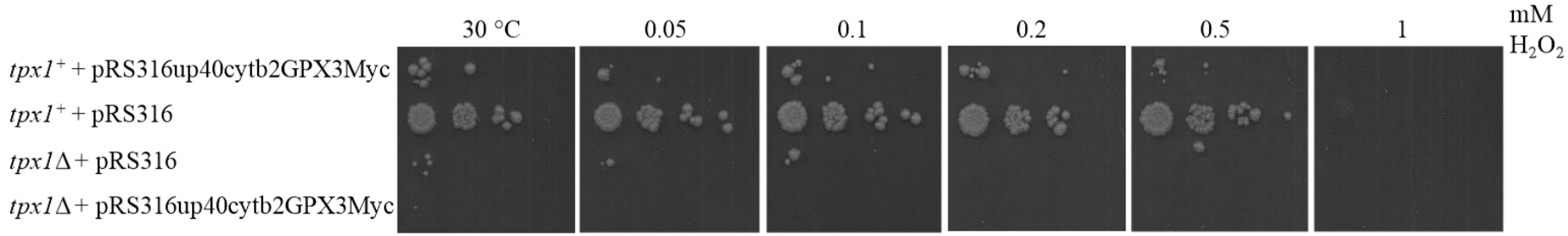

Figure 4.10 Spot test analysis of the growth and H_2O_2 resistance of *tpx1*$^+$ or *tpx1*Δ cells with and without targeting *S. cerevisiae* Gpx3 to the mitochondria. Examination of the growth and H_2O_2 resistance of *S. pombe tpx1*$^+$ (NT4) or *tpx1*Δ (EV45) cells transformed with the *S. cerevisiae* empty vector pRS316, or with the expression vector pRS316-up40-cytb2-GPX3Myc. Plates were incubated at 30 °C and the images presented were scanned after 9 days. Experiment conducted once.

Targeting a pool of Gpx3 to the IMS (pRS316up40cytb2GPX3Myc) in *tpx1*$^{+}$ cells resulted in fewer viable cells compared to *tpx1*$^{+}$ cells transformed with the empty vector (pRS316) (figure 4.10). As expected, the growth of *tpx1*Δ cells was impaired in comparison with *tpx1*$^{+}$. The growth of *tpx1*Δ cells containing pRS316up40cytb2GPX3Myc appeared to be reduced still further than vector control cells, indicating that the growth defect may be exacerbated by expressing Gpx3 with an IMS targeting sequence. Therefore, it appears that the targeting Gpx3 to the mitochondrial IMS is toxic to *S. pombe*, regardless of the presence of Tpx1 (figure 4.10). Moreover, targeting Gpx3 to the mitochondrial intermembrane space did not increase the H_2O_2 resistance of *tpx1*Δ *S. pombe* cells.

4.3 Discussion

In this chapter, I have provided further evidence of the mitochondrial defects previously observed in peroxiredoxin mutant *tpx1*Δ *S. pombe* and *prdx-2(gk169) C. elegans*. In addition, I have confirmed the presence of a mitochondrial pool of the peroxiredoxin Tpx1, and established that this pool appears to be sub-localised to the IMS. Although my mitochondrial fractionation data also supports the IMS localisation of Pap1, and suggest that this may require Tpx1, this would require further confirmation given the presence of multiple Pap1 bands on westerns and the absence of clear co-localisation of Pap1GFP and a mitochondrial protein, Cox4RFP, when examined by confocal microscopy. However, intriguingly, my data suggests that the targeting of a low level of Tpx1 to the IMS of *tpx1*Δ *S. pombe* cells may cause a slight increase in the H_2O_2 resistance of these cells, which could indicate that IMS-targeted expression of Tpx1 is able to restore H_2O_2-induced Pap1 activation to these cells.

The clear reduction in growth of *S. pombe tpx1*Δ cells on a non-fermentable carbon source is indicative of defects in mitochondrial respiratory activity. This data, in conjunction with the unpublished work revealing an impaired mitochondrial electron transport chain, and disrupted mitochondrial morphology in *tpx1*Δ *S. pombe* cells (Latimer thesis, 2017), provides evidence for an important role of Tpx1 in *S. pombe* mitochondrial function. This, in combination with the images obtained of fragmented mitochondria in peroxiredoxin mutant *S. pombe* and *C. elegans* by confocal microscopy, and the reduction in electrochemical gradient across the *C. elegans* mitochondrial inner membrane (previous unpublished work of the Veal lab), supports the theory that these

presumed cytosolic peroxiredoxins are required for normal mitochondrial function. This is not the first example of cytosolic peroxiredoxins found to have a role in cellular sub-compartments. For example, Gpx3 has a role in redox homeostasis and oxidative protein folding in the IMS in *S. cerevisiae* (Kritsiligkou *et al.*, 2017).

Excitingly, our sub-fractionation data revealed the IMS localisation of Tpx1. This finding is similar to the detection of Gpx3 in the IMS of *S. cerevisiae* cells (Vögtle *et al.*, 2012; Kritsiligkou *et al.*, 2017). Due to the presence of oxidative protein folding machinery, and the high levels of ROS produced by the ETC, a H_2O_2 detoxification system is required in the IMS (Daithankar *et al.*, 2012). In *S. cerevisiae*, Gpx3 is targeted to the IMS by an IMS-targeting sequence and has a vital role in redox regulation of this sub-compartment (Kritsiligkou *et al.*, 2017). In addition to acting as an antioxidant, Gpx3 interacts with the Mia40 oxidative protein folding machinery as an oxidoreductase. *gpx3*Δ cells display reduced mitochondrial matrix import and mitochondrial morphological defects similar to the *S. pombe tpx1*Δ (Kritsiligkou *et al.*, 2017). We therefore propose a similar role for Tpx1 in maintaining redox homeostasis of the IMS compartment.

In addition, our analysis of the cellular localisation of Pap1 revealed low cytosolic protein levels, and instead defined a pool of Pap1 in the mitochondria of wild-type cells. Mitochondrial sub-fractionation experiments further revealed the likely localisation of Pap1 to the IMS. We speculate that the reason for the reduction in mobility observed in the bands for mitochondrial Pap1, compared with cytosolic Pap1, could be due to the cleavage of an IMS targeting sequence, and therefore a reduction in molecular weight. Additionally, we speculate that localisation to the IMS facilitates the oxidation and activation of Pap1.

Analysis of the localisation Pap1 in *tpx1*Δ cells, whilst requiring confirmation, revealed that the mitochondrial localisation of Pap1 may be dependent on the presence of Tpx1. Levels of Pap1 were reduced in the mitochondria of *tpx1*Δ cells, and accompanied by an increase in cytosolic Pap1. Additionally, the confocal microscopy analysis suggested a possible co-localisation with mitochondria in some *tpx1*$^+$ cells, which was lost in *tpx1*Δ cells. These findings however require further investigation for confirmation. Repetition of the mitochondrial isolations and confocal microscopy analysis is necessary. Analysis of Pap1 localisation in in *tpx1*$^+$ or *tpx1*Δ cells by immunostaining has previously been published (Bozonet *et al.*, 2005; Brown *et al.*, 2013; Calvo *et al.*, 2013b). Results reflect

that Pap1 is unable to translocate to the nucleus in response to H_2O_2 in *tpx1*Δ cells. If the localisation of Pap1 to the IMS is required for its activation and oxidation, and this IMS localisation is inhibited by the deletion of Tpx1, this model fits with the published data.

To test our hypothesis that the localisation of Tpx1 and Pap1 to the IMS facilitates the oxidation and activation of Pap1, we tested the growth and H_2O_2 resistance of *tpx1*$^+$ and *tpx1*Δ cells expressing IMS-targeted Tpx1. The growth of *tpx1*Δ cells was only improved in cells expressing one copy of the IMS targeting sequence in the presence of thiamine. Contrastingly, the H_2O_2 resistance of *tpx1*Δ cells was slightly improved in all cells targeting Tpx1 to the mitochondria in the absence of thiamine. This potentially indicates that a very low level of mitochondrial Tpx1 may improve the growth of *tpx1*Δ cells, whereas a high level of mitochondrial Tpx1 is required to increase H_2O_2 resistance. This however requires extensive further study. For instance, although the reduced growth and H_2O_2 resistance of cells expressing the IMS-targeted Tpx1 suggests that Tpx1 localisation or function has been affected by addition of the cytb2 IMS-targeting sequence, mitochondrial sub-fractionation of these strains is required to confirm that Tpx1 was successfully targeted into the IMS. Mitochondrial sub-fractionation is also required to determine whether in strains expressing 1 cytb2 IMS-targeting sequence, or 2 cytb2 IMS-targeting sequences, all Tpx1 is targeted to the IMS, and therefore rescued cell growth or H_2O_2 resistance is not due to a small pool of cytoplasmic Tpx1. Importantly, it would also be necessary to examine the localisation and H_2O_2-induced oxidation of Pap1 in these cells before any conclusions as to whether this IMS-targeted form was able to support H_2O_2-induced activation of Pap1. Similarly, future investigations should examine whether mitochondrial phenotypes, such as; electron transport chain function, mitochondrial morphology are rescued by expression of cytb2-Tpx1.

Targeting Gpx3 to the IMS in *gpx3*Δ *S. cerevisiae* cells rescues mitochondrial import defects and mitochondrial morphology (Kritsiligkou *et al.*, 2017). The overexpression of Gpx1, the *S. pombe* homologue of Gpx3, increases the H_2O_2 resistance of *S. pombe* (Vivancos *et al.*, 2004). However, here, like Tpx1, the targeting of *S. cerevisiae* Gpx3 to the IMS was toxic to wild-type and *tpx1*Δ *S. pombe* cells. Mitochondrial sub-fractionation of these strains is required to confirm that Gpx3 was successfully expressed and targeted into the IMS. Additionally, it is important to test whether the overexpression of wild-type Gpx3 improves the growth or H_2O_2 resistance of *tpx1*Δ.

Based on the data presented, we propose that pools of Tpx1 and Pap1 are present in the IMS. We propose that the compartmentalisation of Tpx1 and Pap1 to the IMS may facilitate the oxidation and activation of Pap1, but this would require further investigation. We speculate that the role of Tpx1 in the mitochondrial intermembrane space may be similar to the role of Gpx3 in *S. cerevisiae*; that Tpx1 may act here maintain redox homeostasis.

Chapter 5

Chapter 5. High through-put genetic screening of *tpx1* mutants revealed new candidate H_2O_2 regulated proteins

5.1 Introduction

How organisms sense and use low levels of H_2O_2 to signal positive responses, such as; cell growth, division and migration, is of great medical interest. However, identifying target proteins that respond to H_2O_2 has so far been challenging; partly because proteomic approaches to identify H_2O_2 targets are biased towards abundant proteins, and also because they are unable to determine whether oxidation events are functional. The quantitative redox proteomic technique oxidative isotope-coded affinity tags (OxICAT) has been used in a number of model organisms to identify abundant H_2O_2 regulated proteins (Baker *et al.*, 2015; Leichert *et al.*, 2008; Brandes *et al.*, 2011; Menger *et al.*, 2015; Kumsta *et al.*, 2011). In addition, two-hybrid analysis has also been used as a method to identify novel thioredoxin targets (Brodegger *et al.*, 2004; Vignols *et al.*, 2005). As well as mechanism-based proteomic screens that use resolving cysteine mutants to identify redox targets (Nakao *et al.*, 2015). In this chapter we have aimed to take a high throughput genetic approach to identify new targets of H_2O_2/thioredoxin, that may not have been detected by proteomic methods, based on the discovery that the thioredoxin peroxidase activity of the single 2-Cys Prx, Tpx1, plays an important role as an H_2O_2-dependent inhibitor of thioredoxin family proteins (Brown *et al.*, 2013).

Tpx1 is essential for transcriptional responses to H_2O_2 (as discussed in section 1.2.3) and has multiple roles in promoting H_2O_2 signal transduction (as discussed in sections 1.3.4 and 1.3.5). In cells exposed to H_2O_2, Tpx1 disulphides are the major substrate for thioredoxin. We have demonstrated that, under these circumstances, as thioredoxin reductase activity is limiting, the thioredoxin peroxidase activity of Tpx1 results in both thioredoxin family members, Trx1 and the thioredoxin-like protein 1, Txl1, becoming completely oxidised (Day *et al.*, 2012; Brown *et al.*, 2013). Txl1 is the main reductant of Pap1, therefore, the Tpx1-dependent oxidation of Txl1, promotes sustained oxidation of Pap1 to its active form. The discovery that deletion of the *txl1* gene however, rescues the H_2O_2 resistance and Pap1 oxidation of the $tpx1^{C169S}$ demonstrates that the main, essential

role of the thioredoxin peroxidase activity of Tpx1 in H_2O_2 resistance is to promote Txl1 oxidation (Brown *et al.*, 2013). Hence, we proposed that if the failure to oxidise thioredoxin, that regulates the activity of many proteins (section 1.3.5), contributes to the sensitivity of *tpx1*Δ and *tpx1*^{C169S} mutant cells to peroxides, then loss of Trx or Trx-target genes might increase the H_2O_2 resistance of these cells. Accordingly, in this chapter we tested whether a high through-put genetic screening approach in *tpx1*^{C169S} or *tpx1*Δ backgrounds could be used to identify other thioredoxin-regulated proteins and/or downstream genes that are important for cell growth and/or in H_2O_2 signalling and stress conditions.

The *S. pombe* genome-wide deletion mutant library (Bioneer) has previously been used in many studies, such as to screen for: global fitness profiling (Han *et al.*, 2010), genes involved in cadmium tolerance (Kennedy *et al.*, 2008) and genes required for caffeine tolerance (Calvo *et al.*, 2009). The library has also undergone quantitative fitness analysis (QFA) to identify suppressors and enhancers of telomere defects (Narayanan *et al.*, 2015). In this chapter, we set out to generate synthetic genetic arrays (SGA) combining *tpx1* mutant alleles (*tpx1*$^{+}$, *tpx1*^{C169S} *and tpx1*Δ) with this deletion library. The goal of this study was to examine and compare the fitness of these SGA, using QFA, on plates containing peroxide, with the aim of identifying genes encoding proteins that are regulated by/mediate responses to these stress conditions.

5.2 Results

5.2.1 SGA analysis of the peroxidase defective *tpx1*^{C169S} *S. pombe* identified 31 genes important for growth in *tpx1*^{C169S}

5.2.1.1 Construction of nourseothricin-resistant *tpx1*$^{+}$, *tpx1*^{C169S} and *tpx1*Δ strains

To allow for antibiotic selection following high through-put genetic screening, nourseothricin-resistant (NAT^{r}) *tpx1*$^{+}$, *tpx1*^{C169S} and *tpx1*Δ strains were generated. The natMX6 cassette, was amplified from the pFA6-natMX6 plasmid with appropriate flanking sequences, and transformed into cells expressing *tpx1*$^{+}$ (JR68), *tpx1*^{C169S} (JR42) or *tpx1*Δ (VXOO) (figure 5.1). To test whether the natMX6 cassette had recombined in the targeted locus, nourseothricin-resistant colonies were screened by patching onto EMM plates lacking leucine (*tpx1*$^{+}$, *tpx1*^{C169S}), or lacking uracil (*tpx1*Δ), supplementation. This enabled the identification of colonies unable to synthesise leucine/uracil, and

therefore indicated homologous recombination of the natMX6 cassette with the *LEU2*, or *ura4*$^{+}$, gene. Spores tested from 7 *tpx1*^{C169S} tetrads, and 10 *tpx1*$^{+}$ tetrads, confirmed that all spores exhibiting nourseothricin-resistance (NAT^{r}) were also Leu^{-} (data not shown).

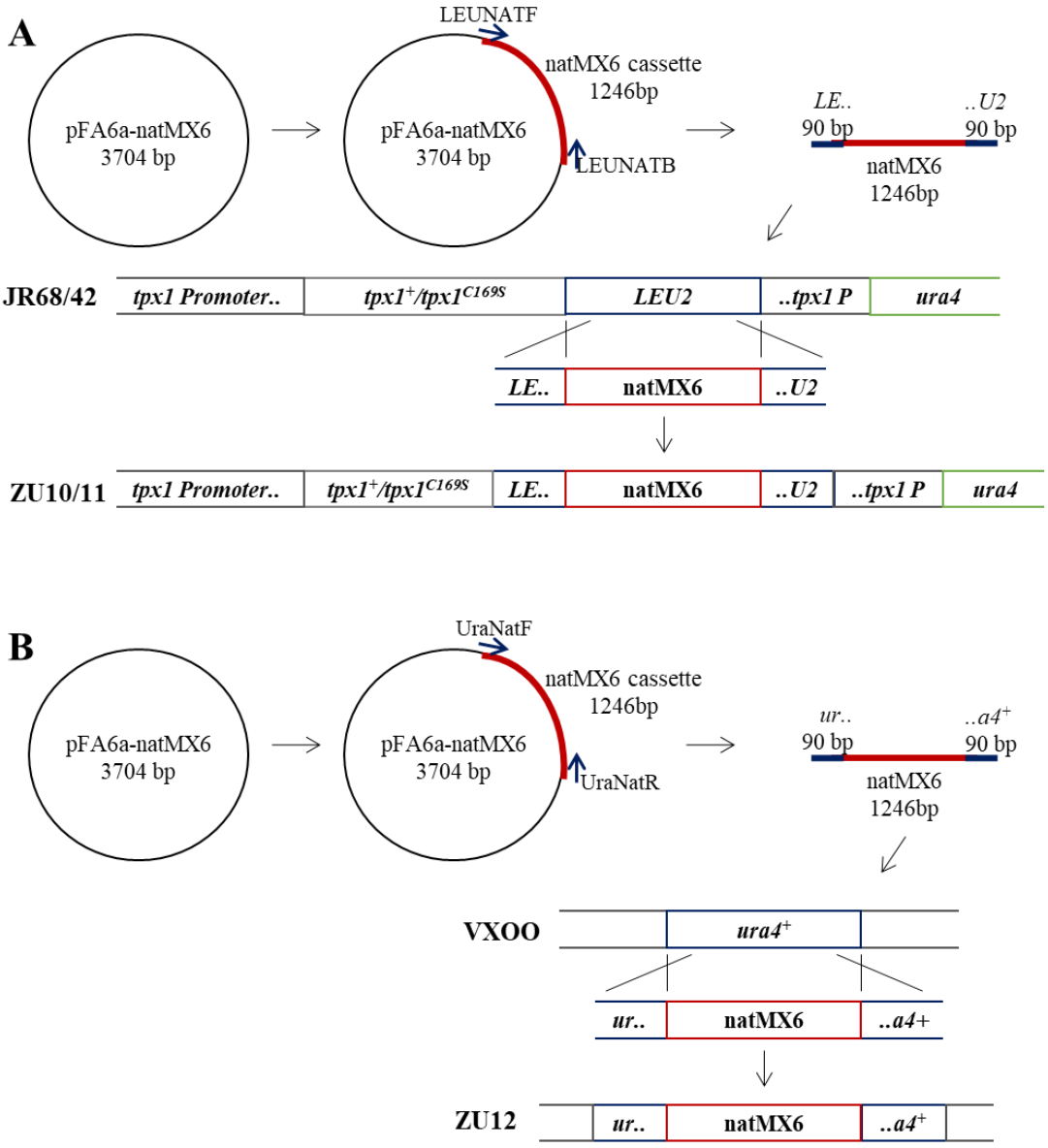

Figure 5.1 Construction of nourseothricin-resistant *tpx1*$^{+}$ (ZU10), *tpx1*^{C169S} (ZU11) [A] and *tpx1*Δ (ZU12) [B] strains. The natMX6 cassette was amplified from the pFA6a-natMX6 plasmid by PCR. Primers were designed to direct the natMX6 cassette to recombine out the LEU2 marker (ZU10, ZU11) [A], or the *ura4* marker (ZU12) [B] downstream of *tpx1* locus. The *tpx1*$^{+}$ (JR68), *tpx1*^{C169S} (JR42), *tpx1*Δ (VXOO) starting strains were transformed with the natMX6 cassette and cells were plated onto YE5S + clonNAT plates for selection. Nat-resistant colonies were also screened for *leu2*$^{-}$/*ura4*$^{-}$ phenotype where appropriate.

5.2.1.2 Nourseothricin-resistance is closely linked to the *tpx1*^{C169S} mutation

To test for the rate of recombination of the NAT marker and the C169S mutation the NAT^r *tpx1*$^+$ (ZU10) and *tpx1*^{C169S} (ZU11) strains were backcrossed with their corresponding starting strains, *tpx1*$^+$ (JR68) or *tpx1*^{C169S} (JR42) respectively, and following dissection spores were patched onto onto rich media containing 0.1 mg/ml clonNAT, and minimal media supplemented with histidine and adenine to confirm Leu$^-$ genotype.

To test that the natMX6 cassette was closely linked to *tpx1*, and that loss of the C169S mutation by recombination with the wild-type allele during meiosis did not occur frequently enough to be an issue during screening; the NAT^r *tpx1*^{C169S} strain (ZU11) was backcrossed with a *tpx1*$^+$ strain (NT4). Following random sporulation, the NAT^r spores were patched onto rich media with and without 1 mM H_2O_2 to test for a H_2O_2-sensitive phenotype. All 112 of the NAT^r colonies tested were unable to grow in the presence of 1 mM H_2O_2; indicative that the *tpx1*^{C169S} mutation had not recombined with the *tpx1*$^+$ from the NT4 strain (figure 5.2).

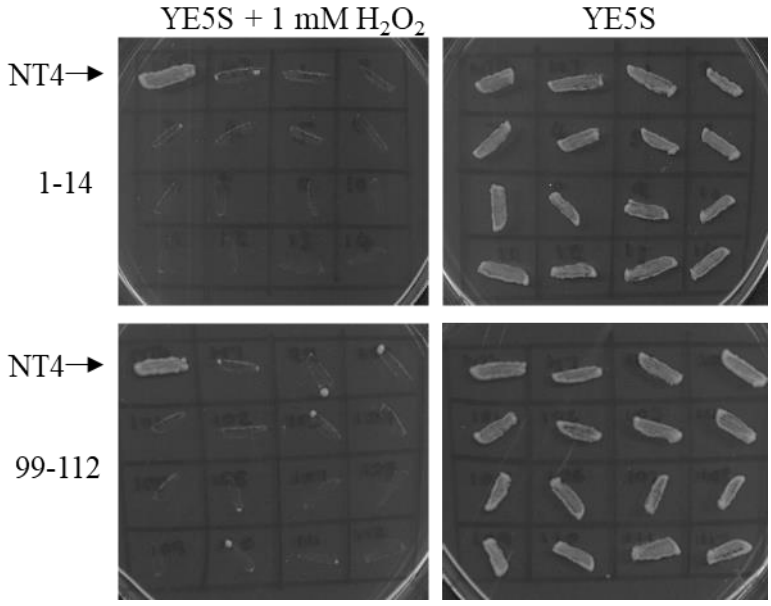

Figure 5.2 The nourseothricin-resistant phenotype is closely linked to sensitivity to H_2O_2. The NAT^r spores generated by crossing *tpx1*^{C169S} (ZU11) with *tpx1*$^+$ (NT4), were patched onto YE5S agar with and without 1 mM H_2O_2 for growth analysis.

5.2.1.3 Replacing the *leu2* gene with a natMX6 cassette had no effect on the growth or H_2O_2 sensitivity of *tpx1*$^+$ and *tpx1*^{C169S} strains

To confirm that replacing the *leu2* gene with a natMX6 cassette had no effect on growth, or H_2O_2 sensitivity, and importantly, to determine the most effective H_2O_2 concentration to use in the screen to identify mutations that increase the resistance of *tpx1*^{C169S}, spot tests were conducted on the starting *tpx1*$^+$ (JR68) and *tpx1*^{C169S} (JR42) strains as well as the generated NAT^r *tpx1*$^+$ (ZU10) and *tpx1*^{C169S} (ZU11) strains (figure 5.3). A *tpx1*Δ (VXOO) strain and *tpx1*^{C169S}*txl1*Δ (JB92) were also spotted for comparison. As expected, the *tpx1*Δ (VXOO) strain had reduced growth on YE5S, compared to *tpx1*$^+$ and *tpx1*^{C169S} strains, and was extremely sensitive to the lowest dose (0.25 mM) of H_2O_2. The two *tpx1*$^+$ strains (JR68 and ZU10) exhibited similar growth on control plates and similar sensitivity to H_2O_2. The two *tpx1*^{C169S} strains (JR42 and ZU11) also exhibited similar growth on control plates and sensitivity to H_2O_2. Together these results indicated that replacing a *leu2* marker with a natMX6 cassette did not affect the growth, or H_2O_2 sensitivity. Moreover, consistent with previous results, at the highest dose of H_2O_2, the growth of the *tpx1*^{C169S}*txl1*Δ (JB92) was more severely inhibited than strains expressing wild-type Tpx1, these cells were not sensitive to the low concentrations of H_2O_2 that inhibited the growth of the *tpx1*^{C169S} strain, (Brown *et al.*, 2013) and (Brown and Veal, unpublished).

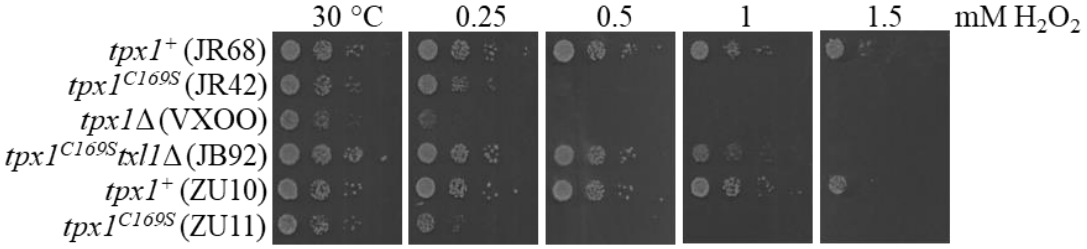

Figure 5.3 Replacing the *leu2* gene with a natMX6 cassette did not have a significant effect on the growth or H_2O_2 sensitivity of *tpx1*$^+$ and *tpx1*^{C169S} strains. Analysis of exponentially growing *tpx1*$^+$ (JR68), *tpx1*^{C169S} (JR42), *tpx1*Δ (VXOO), *tpx1*^{C169S}*txl1*Δ (JB92), and the nourseothricin-resistant *tpx1*$^+$ (ZU10) and *tpx1*^{C169S} (ZU11) strains pinned on YE5S agar containing the indicated concentrations of H_2O_2.

5.2.1.4 SGA analysis identified 31 candidate genes important for growth when the Tpx1 peroxidase activity is removed

To allow for genome-wide mapping of synthetic genetic interactions, the *tpx1*$^{+}$ (ZU10) and *tpx1*^{C169S} (ZU11) strains were systematically crossed (in the High Throughput screening facility (HTSF) at Newcastle University) with 3,400 non-essential gene deletion strains (Bioneer) to generate synthetic genetic arrays (section 2.2.1.1, figure 2.1). To identify genes important for growth in the peroxidase defective *tpx1*^{C169S}, photographs of the final plates were taken using spImager software, and cell density was calculated using the image analysis tool Colonyzer (section 2.2.1.2). The fitness of each of the generated strains on YE5S was compared with the fitness of the deletion gene with *tpx1*$^{+}$ to generate a genetic interaction score (GIS). GIS represents the distance of the hit from the line of best fit; with the highest GIS scores indicating the greatest effect of the presence of the *tpx1*^{C169S} mutant allele on growth. Each gene deletion strain was repeated in quadruplicate within a SGA screen, and from this a mean GIS was generated. This SGA was conducted on 2 separate occasions, and results presented here represent a mean of all 8 repeats. Of the genes presenting the highest negative GIS (gene mutants which have negatively affected the growth of cells expressing *tpx1*^{C169S}), the 100 genes with the highest negative GIS were taken from the first SGA repeat (figure 5.4), and the 100 genes with the highest negative GIS were taken from the second SGA repeat (figure 5.5), and compared to compile a list of 31 genes that presented with the lowest GIS in all 8 repeats (table 5.1).

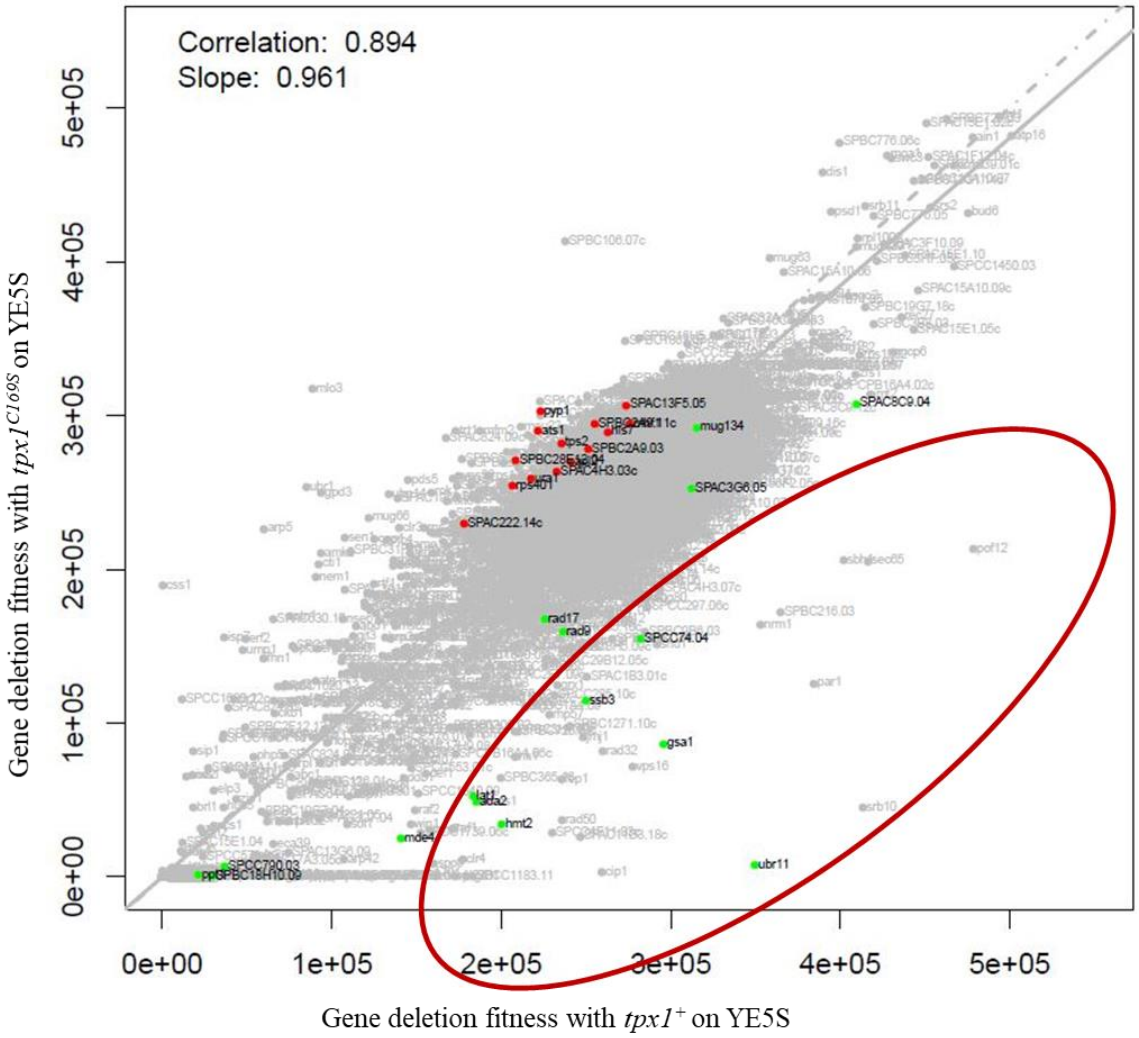

Figure 5.4 Fitness of the Bioneer deletion library crossed with *tpx1*$^{+}$ (x-axis) plotted against the fitness of the Bioneer deletion library crossed with *tpx1*^{C169S} mutation (y-axis) from SGA replicate 1. The red circle represents gene mutants which have negatively affected the growth of cells expressing *tpx1*^{C169S} (candidate hits with the highest negative GIS).

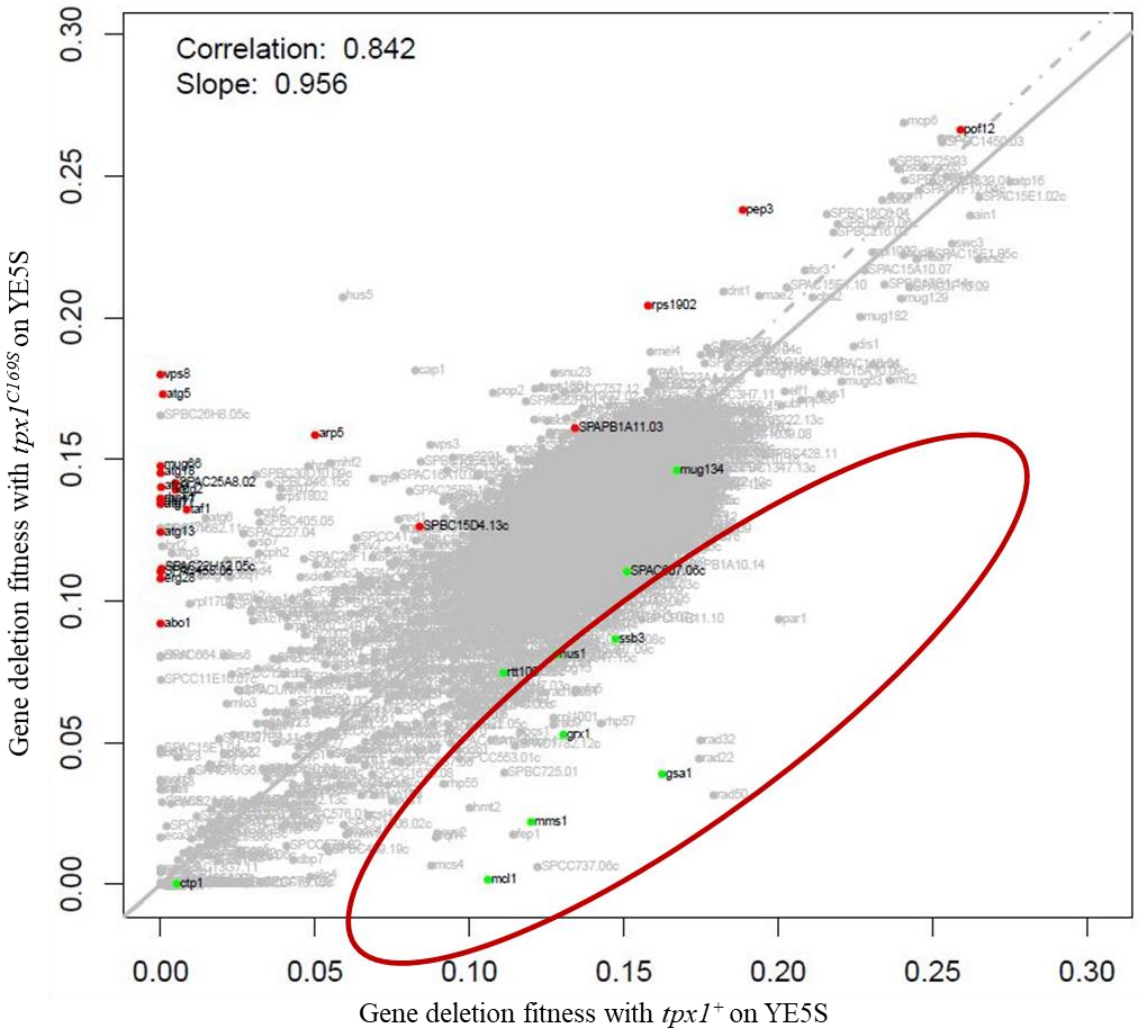

Figure 5.5 Fitness of the Bioneer deletion library crossed with *tpx1*$^{+}$ (x-axis) plotted against the fitness of the Bioneer deletion library crossed with *tpx1*^{C169S} mutation (y-axis) from SGA replicate 2. The red circle represents gene mutants which have negatively affected the growth of cells expressing *tpx1*^{C169S} (candidate hits with the highest negative GIS).

Position	Gene name	Gene Description
5.5	*gsa1*	glutathione synthetase large and small subunit
6	*par1*	protein phosphatase PP2A regulatory subunit B-56
6	*rad50*	DNA repair protein
10	*mre11*	nuclease
14	*fep1*	iron-sensing transcription factor
16.5	*mcs4*	response regulator
17	*hmt2*	sulfide-quinone oxidoreductase
19	*mms1*	E3 ubiquitin ligase complex subunit
27.5	*rad57*	RecA family ATPase
28	*rad1*	checkpoint clamp complex protein
29.5	*ssb3*	DNA replication factor A subunit
32	*tom7*	mitochondrial TOM complex subunit
32.5	*maa1*	mitochondrial aspartate aminotransferase
34	*grx1*	glutaredoxin
40	*SPCC4F11.03c*	*Schizosaccharomyces* specific protein
42	*ada2*	SAGA complex subunit
45.5	*nde1*	mitochondrial NADH dehydrogenase
45.5	*rdl2*	mitochondrial thiosulfate sulfurtransferase
47.5	*ctt1*	catalase
50	*imt2*	mannosyltransferase
50.5	*mde4*	microtubule-site clamp monopolin complex subunit
50.5	*mph1*	dual specificity protein kinase
50.5	*SPBC1271.10c*	transmembrane transporter
54	*lat1*	dihydrolipoamide S-acetyltransferase E2
58	*SPAC1782.12c*	DUF423 protein
63	*SPCC297.06c*	conserved fungal protein
64	*dbl2*	meiotic chromosome segregation protein
64.5	*ddb1*	damaged DNA binding protein
74	*rad54*	DNA-dependent ATPase
75	*kgd1*	2-oxoglutarate dehydrogenase
79.5	*adn1*	adhesion defective protein

Table 5.1 Gene names and descriptions for the 31 candidate genes with the highest negative GIS from 2 independent *tpx1*^{C169S} SGA screens. Candidate genes that had the highest negative GIS (that were detected in the bottom 100 hits), in both replicate screen 1 and replicate screen 2, were compiled. Candidate genes have been ordered by their average GIS position; with hits that possess the same average GIS position ordered alphabetically. Genes highlighted in green indicate that the *S. cerevisiae* orthologue has previously been identified as synthetic lethal with *tsa1*Δ.

Promisingly, of these 31 genes, orthologues of 6 genes (*rad50, mre11, mms1, rad57, rad1* and *ada2*) had previously been reported to have negative genetic interactions with *TSA1* encoding one of the two Tpx1 orthologues in *S. cerevisiae* (Huang and Kolodner, 2005; Molin *et al.*, 2011; Hanzén *et al.*, 2016; Pan *et al.*, 2006). The gene deletion with, consistently, the greatest negative effect on the growth of $tpx1^{C169S}$ was glutathione synthetase (*gsa1*). However, a number of other genes with functions linked to oxidative stress responses were identified, including the response regulator *mcs4* that is required for activity of the Sty1 MAPK, a glutaredoxin, *grx1*, and the catalase, *ctt1*. Several genes encoding mitochondrial proteins were also found to be important for growth specifically in the $tpx1^{C169S}$ background: *tom7*, *maa1*, *nde1* and *rdl2*.

5.2.2 QFA analysis of the peroxidase defective $tpx1^{C169S}$ *S. pombe*

5.2.2.1 Cells required a 16 h dilution period to reach exponential growth phase

In order to identify gene deletions that affected the stress sensitivity of the $tpx1^{C169S}$ strain, we first had to optimise the conditions for QFA. Preliminary analysis revealed that the HTSF standard dilution time of 6 h was too short for our *S. pombe* SGA strains to reach exponential growth phase in liquid culture, resulting in too few cells being spotted. Based on the growth curves generated, following either a 16 h or 24 h dilution period, indicated that most cells had reached exponential growth phase by 16 h and that this allowed sufficient cells to be spotted to result in full spot growth that was reduced by exposure to concentrations of H_2O_2 that had been previously established as inhibiting the growth of $tpx1^{C169S}$ cells, but not control strains (figure 5.6).

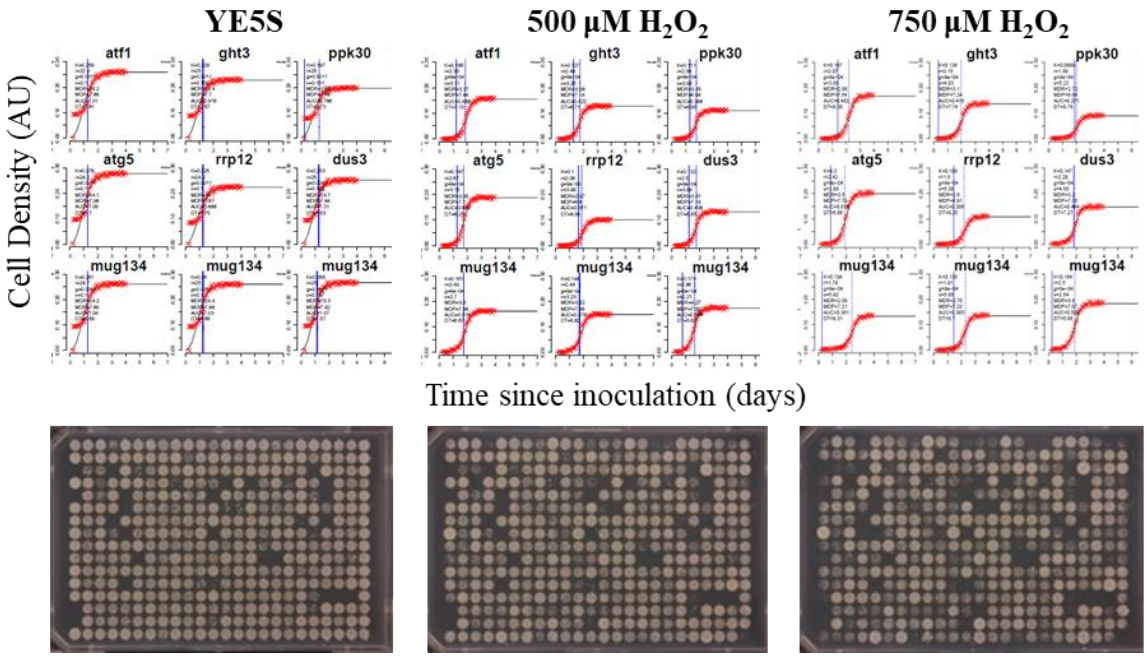

Figure 5.6 Growth curves and corresponding spot tests of 7 *S. pombe* single deletion strains from library plate 1 (Bioneer) generated following a 16 h dilution period in liquid culture in a test run. Liquid culture was inoculated with strains and incubated at 30 °C with shaking overnight. Once cultures reached saturation, strains were diluted 10 x and incubated at 30 °C for either 16 h (pictured) or 24 h (not included), and spotted onto agar containing different stressors. Plates were imaged over time and growth curves calculated.

5.2.2.2 The conditions of 500 µM H_2O_2, 750 µM H_2O_2 and 250 µM tBOOH were chosen for the detection of sensitivity suppressors

To determine the most suitable concentrations of stress reagents, a test screen of the growth of the ZU10 and ZU11 crossed with SGA plate 1 (the 308 fittest strains in the non-essential gene deletion library) was carried out on YE5S plates containing: 250 µM tBOOH, 500 µM tBOOH, 250 µM H_2O_2, 500 µM H_2O_2 and 750 µM H_2O_2. Based on the fitness graphs generated (figure 5.7), the 500 µM H_2O_2, 750 µM H_2O_2 and 250 µM tBOOH conditions were chosen as most appropriate. This was based on their limited toxicity to *tpx1*$^{+}$ cells, which allowed the most sensitive detection of suppressors of the *tpx1*^{C169S} sensitivity phenotypes as a large 'cloud' of hits with few outliers. Including the oxidative stressor tBOOH in the analysis allowed for distinction between signalling pathways that do or do not activate Sty1 (Chen *et al.*, 2007).

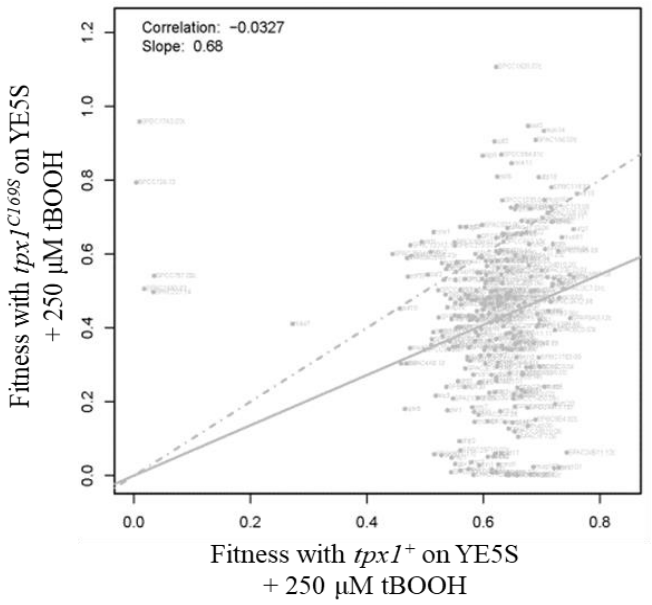
Correlation: −0.0327
Slope: 0.68
Fitness with $tpx1^{C169S}$ on YE5S + 250 µM tBOOH
Fitness with $tpx1^{+}$ on YE5S + 250 µM tBOOH

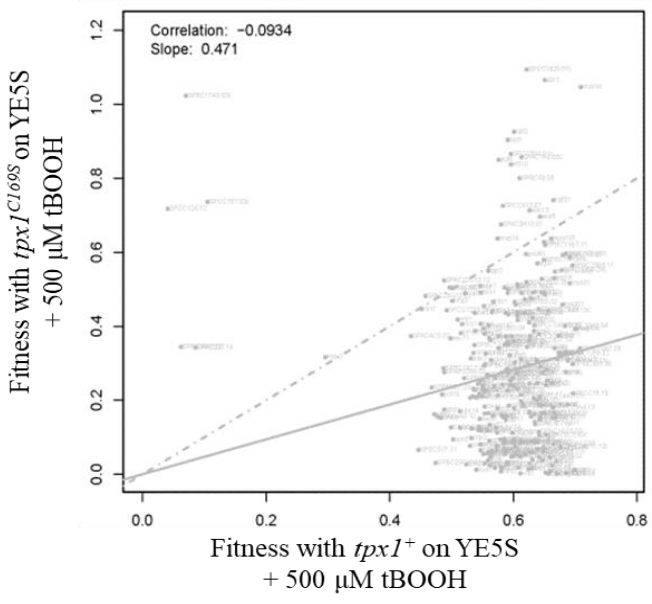
Correlation: −0.0934
Slope: 0.471
Fitness with $tpx1^{C169S}$ on YE5S + 500 µM tBOOH
Fitness with $tpx1^{+}$ on YE5S + 500 µM tBOOH

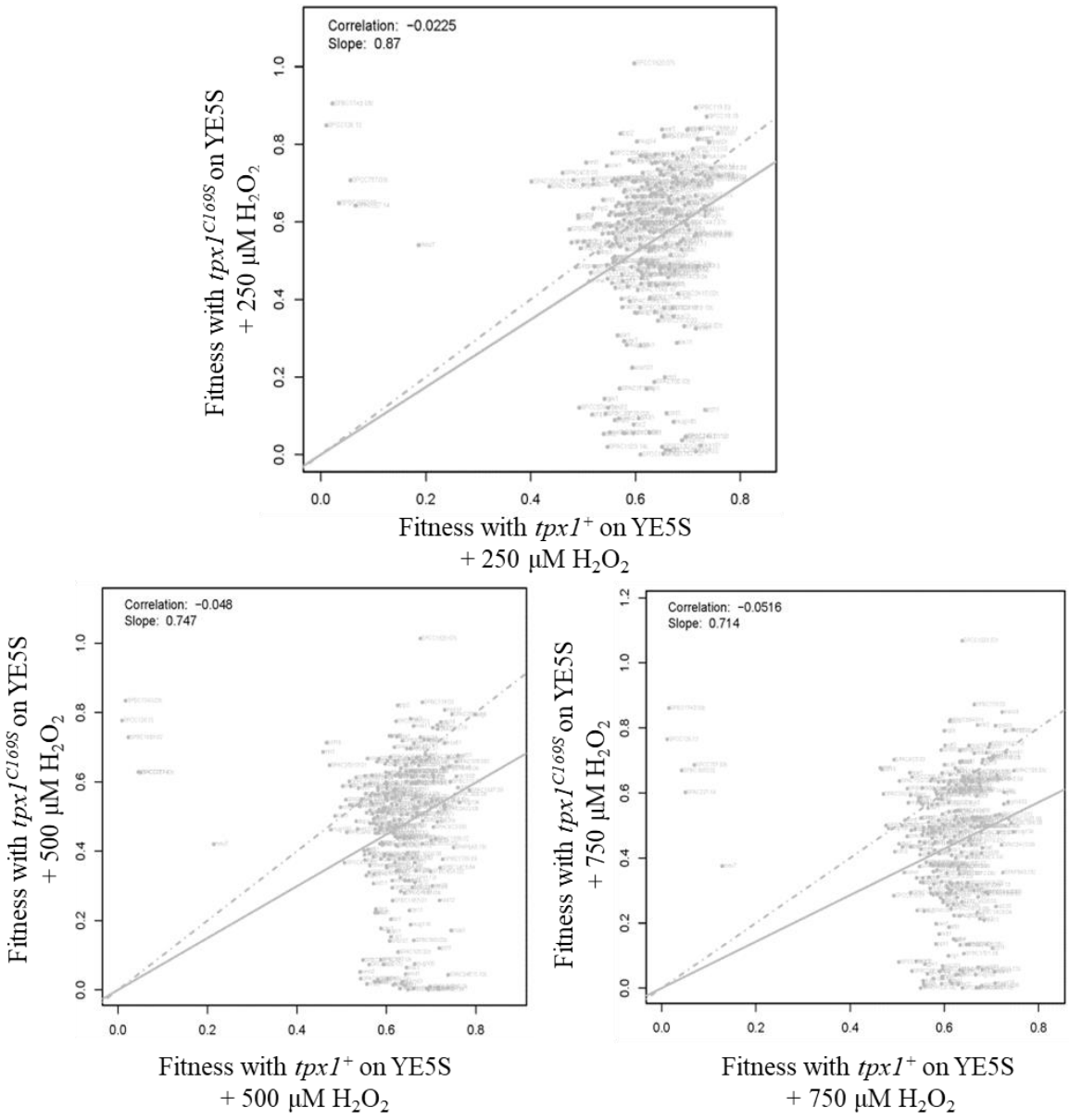

Figure 5.7 Fitness graphs generated from the *tpx1*^{C169S} QFA test screen using 250 µM H_2O_2, 500 µM H_2O_2, 750 µM H_2O_2, 500 µM tBOOH and 750 µM tBOOH stress conditions. The *tpx1*$^{+}$ and *tpx1*^{C169S} SGA's were spotted onto YE5S agar containing different concentrations of oxidative (H_2O_2 or tBOOH) stress. Plates were imaged and GIS calculated.

5.2.2.3 QFA identified 26 gene mutants as putative suppressors of the *tpx1*^{C169S} H_2O_2 sensitivity phenotype

For QFA, library plates 1-5 of the *tpx1*^{C169S} SGA (fittest library strains) were grown in liquid media, and spotted onto agar with and without stress (e.g. H_2O_2) (section 2.2.1.3, figure 2.1). The growth curves, and graphs generated from the QFA revealed the fitness of the *tpx1*^{C169S} SGA with and without exposure to stress (figure 5.8) (section 2.2.1.4).

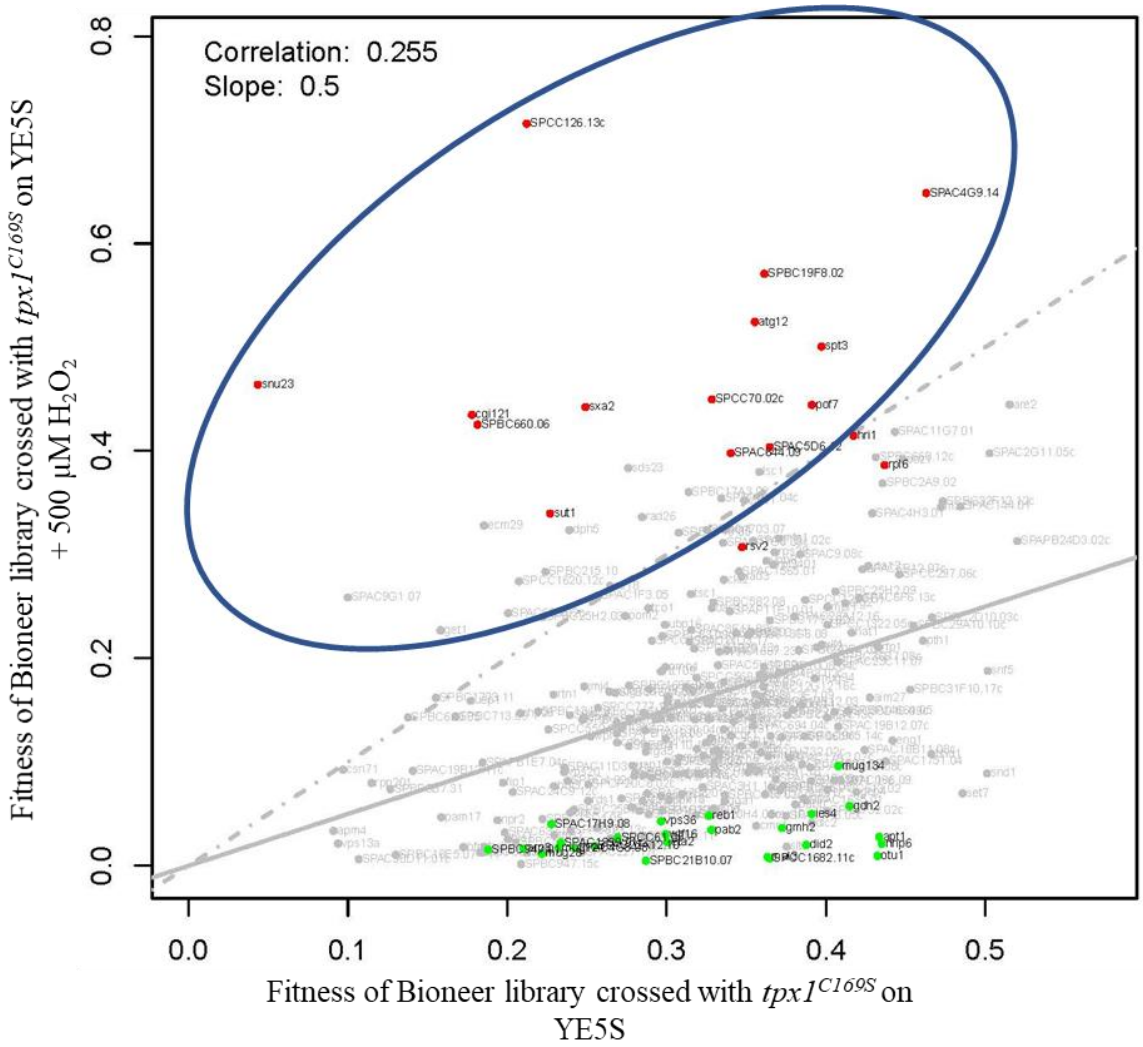

Figure 5.8 Example QFA graph: comparison of the fitness of 384 strains (library plate 5) of the *tpx1*^{C169S} SGA in the presence or absence of 500 µM H_2O_2. The *tpx1*^{C169S} SGA was cultured in media and spotted onto agar with (y-axis) or without (x-axis) H_2O_2. Enhancers or suppressors of the H_2O_2 sensitivity of *tpx1*^{C169S} were identified using the GIS (the distance from the line of best fit; with the plots furthest from the line of best fit having the highest GIS). The blue circle represents suppressors of *tpx1*^{C169S} stress sensitivity (that have the highest positive GIS (red points)). Enhancers of *tpx1*^{C169S} stress sensitivity have the highest negative GIS (green points).

The QFA data generated was analysed for each stress condition (250 µM tBOOH, 500 µM H_2O_2 and 750 µM H_2O_2 (plus an additional 100 µM H_2O_2 for plate 5 only)), with 2 comparisons (the *tpx1*^{C169S} SGA with stress against the *tpx1*^{C169S} SGA without stress, as well as the *tpx1*$^{+}$ SGA with stress against the *tpx1*^{C169S} SGA with stress). For this section, the top 10 % of strains (~30) with the highest positive mean GIS were picked from each library plate, for each comparison, and analysed to determine if each candidate gene was a hit when treated with just H_2O_2, or also with the other stressor (tBOOH).

In order to validate that suppressors of H_2O_2 sensitivity represent genes that are important for the H_2O_2 sensitivity of *tpx1*^{C169S} cells, a list of 155 strains with the highest positive GIS was compiled for further testing. These 155 double mutant strains were all fitter than the starting strain *tpx1*^{C169S} in the presence of H_2O_2. Perplexingly, *grx1*, which was previously identified as exhibiting a synthetic sick interaction with *tpx1*^{C169S}, was one of the candidate genes identified as increasing H_2O_2 resistance, possibly an indication of reversion of the C169S mutation to wild-type. Given the high throughput nature of the screening it was important to confirm that these strains were more resistant to H_2O_2. Thus, of these 155 strains, 91 were re-tested by halo test. Halo test analysis was chosen over spot test analysis to minimise the effect of differences in growth rate. For example, the testing of 4 of the 91 strains (*tpx1*^{C169S}*grx1*Δ, *tpx1*^{C169S}*slx4*Δ, *tpx1*^{C169S}*ybt1*Δ and *tpx1*^{C169S}*ubp11*Δ) revealed that two strains (*tpx1*^{C169S}*grx1*Δ and *tpx1*^{C169S}*slx4*Δ) displayed restored H_2O_2 resistance to wild-type *tpx1*$^{+}$ levels (ZU10), one strain (*tpx1*^{C169S}*ybt1*Δ) displayed similar H_2O_2 resistance to the starting strain *tpx1*^{C169S} (ZU11), and one strain (*tpx1*^{C169S}*ubp11*Δ*)* displayed increased H_2O_2 sensitivity when compared with the starting strain *tpx1*^{C169S} (ZU11) (figure 5.9). This revealed variability in H_2O_2 resistance between candidate genes identified by the QFA analysis.

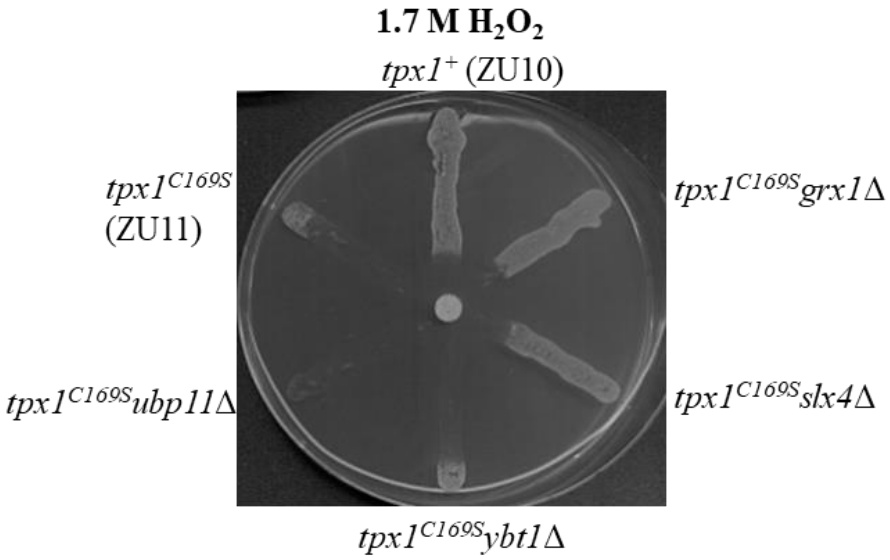

Figure 5.9 Example halo test: SGA generated strains with increased and reduced resistance to H_2O_2 compared with the *tpx1*^{C169S} (ZU11) starting strain. Strains generated by the *tpx1*^{C169S} SGA, as well as the query strains *tpx1*$^+$ (ZU10) and *tpx1*^{C169S} (ZU11), were pipetted in a line towards filter paper soaked in 1.7 M H_2O_2. Plates were incubated at 30 °C and photographed.

Overall, of the 91 double mutant strains tested by halo test, 26 displayed increased resistance to H_2O_2 compared with the *tpx1*^{C169S} starting strain (ZU11) (table 5.2). Of these 26 strains, 17 also displayed increased resistance to tBOOH (highlighted in red). As each gene mutant was independently crossed with the test strain 4 times, generating 4 isolates with the same genotype, it was possible that some of the lack of reproducibility (29 %), could reflect variability between the 4 isolates. For instance, as mean GIS was used in analysis, it is possible that the single strain tested by halo test was the 1 isolate, out of 4 isolates, that didn't have an increased stress resistance phenotype. For example, all 4 isolates of *tpx1*^{C169S}*uds1*Δ from the QFA were tested by halo test: results revealed that 2 of the 4 isolates displayed H_2O_2 resistance restored to wild-type *tpx1*$^+$ levels.

Gene ID crossed with *tpx1*^{C169S}	Gene Name	Gene Description	No. of isolates with increased stress resistance compared with *tpx1*^{C169S}	
			H_2O_2	tBOOH
SPAC13G6.07c	*rps601*	40S ribosomal protein S6	1/1	1/1
SPAC9G1.11c	*spn4*	mitotic septin	1/1	1/1
SPAC11E3.04c	*ubc13*	ubiquitin conjugating enzyme E2	1/1	0/1
SPAC1687.22c	*puf3*	RNA-binding protein	2/2	1/2
SPAC3H1.11	*hsr1*	transcription factor	1/1	1/1
SPAC4G9.14	*sym1*	mitochondrial Mpv17/PMP22 family protein 2	1/1	0/1
SPAC22F3.11c	*snu23*	U4/U6 x U5 tri-snRNP complex subunit	1/1	1/1
SPAC688.06c	*slx4*	structure-specific endonuclease subunit	1/1	0/1
SPAC4F10.20	*grx1*	glutaredoxin	2/2	2/2
SPAC1296.03c	*sxa2*	serine carboxypeptidase	1/1	1/1
SPAC11G7.01	*SPAC11G7.01*	*S. pombe* specific protein	1/1	1/1
SPBC16G5.03	*mrz1*	ubiquitin-protein ligase E3	1/1	1/1
SPBC27.04	*uds1*	septation protein	2/4	0/4
SPBC83.19c	*SPBC83.19c*	*S. pombe* specific protein	1/1	1/1
SPBC19F8.02	*nud3*	nuclear distribution protein NUDC homolog	1/1	0/1
SPBC29A10.05	*exo1*	exonuclease I	1/1	0/1
SPBC776.02c	*dis2*	serine/threonine protein phosphatase PP1 subfamily	1/1	0/1
SPBC691.01	*pfa5*	vacuolar membrane palmitoyltransferase	1/1	1/1
SPCC1393.03	*rps1501*	40S ribosomal protein S15	1/1	1/1
SPCC1620.08	*lsc2*	succinate-CoA ligase beta subunit	1/1	0/1
SPCC126.13c	*sap18*	histone deacetylase complex subunit	1/1	1/1
SPCC24B10.12	*cgi121*	EKC/KEOPS complex subunit	4/4	4/4
SPCC126.03	*pus1*	tRNA pseudouridine synthase	1/1	0/1
SPCC576.14	*dph5*	diphthine synthase	1/1	1/1
SPCC737.06c	*gcs2*	glutamate-cysteine ligase regulatory subunit	1/1	1/1
SPCC576.01c	*xan1*	alpha ketoglutarate dependent xanthine dioxygenase	1/1	1/1

Table 5.2 The 26 SGA strains that displayed higher H_2O_2 resistance by halo test, compared with the *tpx1*^{C169S} (ZU11) starting strain. Of all the SGA-generated strains manually tested by halo test 26 strains exhibited an increase in H_2O_2 resistance phenotype compared with *tpx1*^{C169S}. Strains highlighted in red had both H_2O_2 and tBOOH resistance restored to wild-type *tpx1*$^{+}$ levels. Strains highlighted in black had similar H_2O_2 resistance to wild-type *tpx1*$^{+}$, but were still as sensitive to tBOOH as *tpx1*^{C169S}. Each strain is scored for the number of different isolates tested, and of these number of isolates that displayed increased stress resistance.

5.2.2.4 Reconstruction of 7 of these strains revealed that the suppression of H_2O_2 stress sensitivity was not caused by the candidate gene

As the populations of 'double mutant' strains generated by the screen are not clonal it was important to confirm the 26 candidate genes as suppressor's. The single gene deletion was manually re-crossed with the *tpx1*^{C169S} (ZU11), and the H_2O_2 resistance of each strain from the generated tetrads tested. To decide which of the 26 strains would be crossed manually, strains were sorted in order of standard error; so that the gene mutations which between all 4 isolates had given the most consistent rescue phenotype were investigated first. Seven of the candidate strains (*cgi121*Δ, *SPAC4G9.14*Δ, *SPBC16G5.03*Δ, *uds1*Δ, *rps601*Δ, *hsr1*Δ and *ubc13*Δ) were manually re-crossed with the starting strain *tpx1*^{C169S} (ZU11), and underwent tetrad dissection followed by halo test and spot test analysis. Before crossing, strains were checked by PCR to ensure they had the correct gene deletion. However, all 7 of the double mutant strains generated from these crosses were no more H_2O_2 resistant than the parent *tpx1*^{C169S} strain, even when multiple double mutants were analysed (figure 5.10 and data not shown). These data suggests that the increased stress resistance observed in the *tpx1*^{C169S}*uds1*Δ isolate 2 and isolate 4 strains and the *tpx1*^{C169S}*hsr1*Δ strain (table 5.2, figure 5.10) was not due to the deletion of *uds1 or hsr1*.

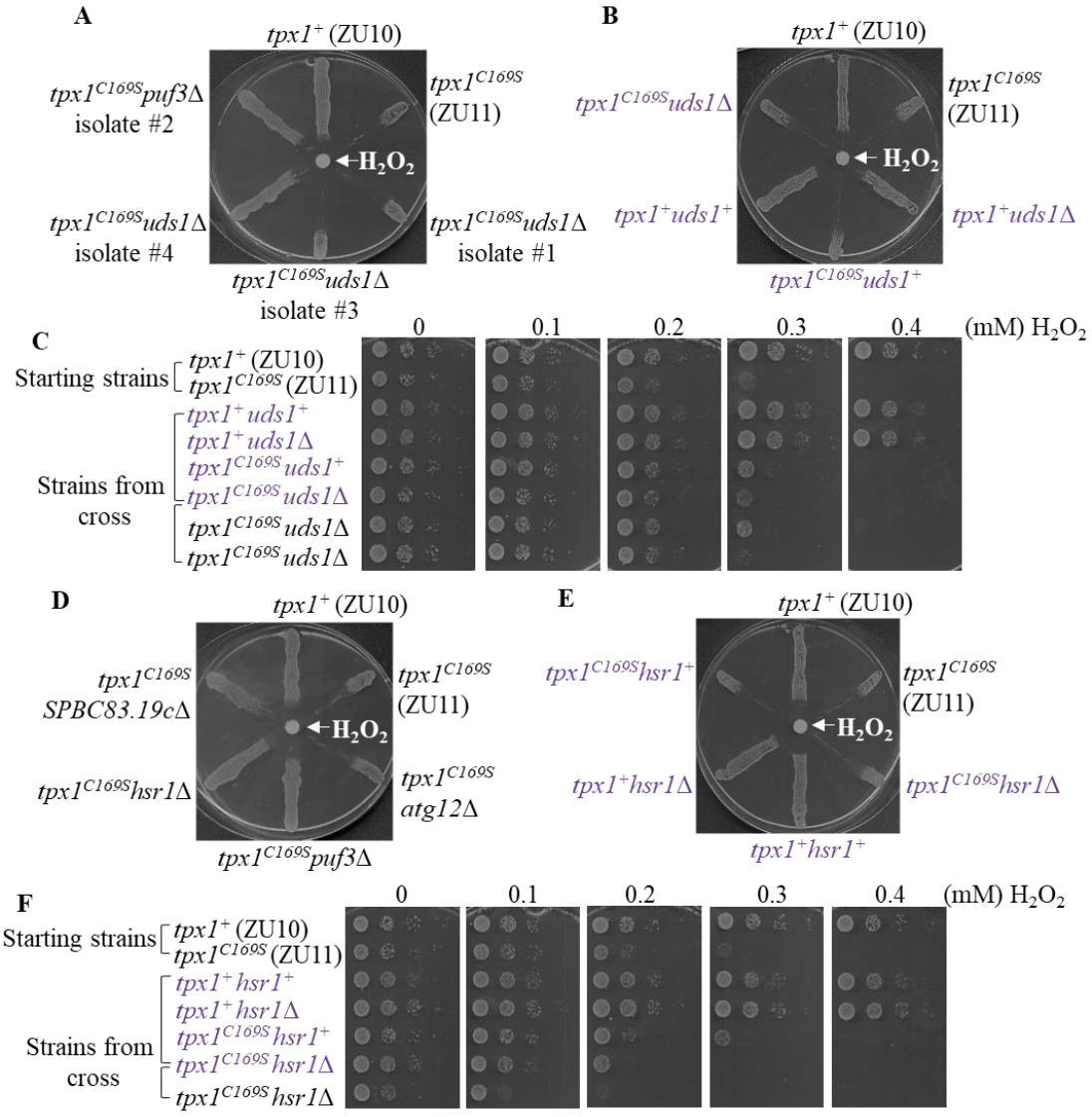

Figure 5.10 Halo test analysis of SGA-generated strains [A and D], as well as halo test and spot test analysis of isogenic strains (in purple) generated from manually re-crossing *tpx1*^{C169S} with *uds1*Δ [B and C], or *hsr1*Δ [E and F]. SGA isolates were screened by halo test to investigate H_2O_2 sensitivity [A and D]. Strains that displayed increased H_2O_2 resistance in comparison to *tpx1*^{C169S} (ZU11) were manually re-crossed, for example *uds1*Δ (Bioneer) with *tpx1*^{C169S} (ZU11), and *hsr1*Δ (Bioneer) with *tpx1*^{C169S} (ZU11). The H_2O_2 sensitivities of the tetrads generated (in purple), and additional double mutants, were tested by halo test and spot test [B, C, E and F].

Finally, the strongest candidate gene mutant; that increased the H_2O_2 resistance of all 4 isolates from the QFA, by halo test (figure 5.11A) and spot test (figure 5.11B), was investigated. As with the other strains, when halo tests were performed on isogenic strains generated by manually crossing *tpx1*^{C169S} and *cgi121*Δ, the resulting *tpx1*^{C169S}*cgi121*Δ mutant strain was even more sensitive to H_2O_2 than the *tpx1*^{C169S} single mutant (ZU11 and the isogenic *tpx1*^{C169S}*cgi121*$^{+}$) (figure 5.11C). Disappointingly, this again indicated that the increased stress resistance of the *tpx1*^{C169S}*cgi121*Δ mutants isolated by the screen was not due to the loss of *cgi121*.

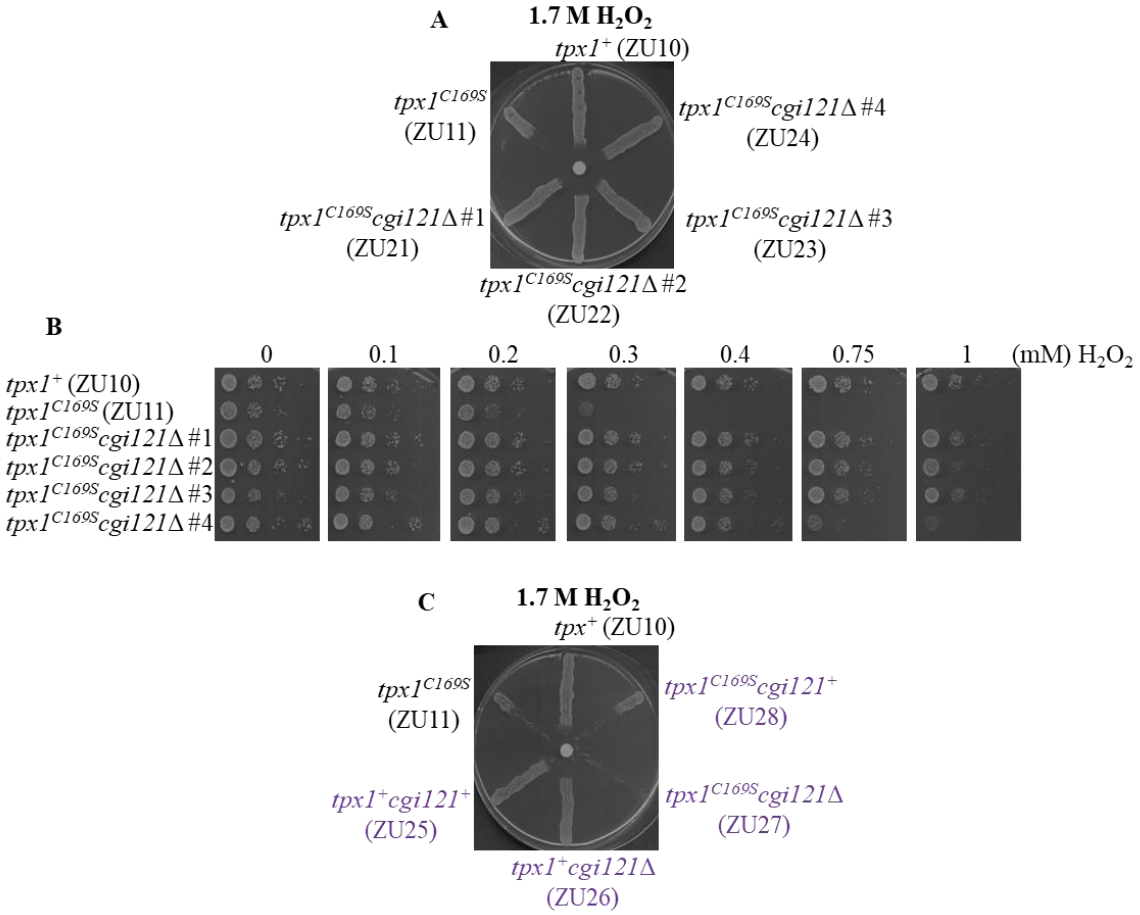

Figure 5.11 Halo test and spot test analysis of all 4 isolates of SGA-generated *tpx1^{C169S}cgi121*Δ [A and B], as well as a halo test performed on isogenic strains (in purple) generated from re-crossing *cgi121*Δ (Bioneer) with *tpx1^{C169S}* (ZU11) [C]. Halo test [A] and spot test [B] analysis of the H_2O_2 sensitivity of the 4 isolates of *tpx1^{C169S}cgi121*Δ (ZU21, ZU22, ZU23 and ZU24) generated from the SGA, compared with the starting strains *tpx1^{+}* (ZU10) and *tpx1^{C169S}* (ZU11). Halo test analysis of the H_2O_2 sensitivity of the tetrad (ZU25, ZU26, ZU27 and ZU28) generated from re-crossing *tpx1^{C169S}* (ZU11) and *cgi121*Δ (Bioneer) [C].

5.2.2.5 Increased resistance of 3 isolates of *tpx1^{C169S}cgi121Δ* was caused by the loss of the C169S point mutation in *tpx1^{+}*

Although our initial analysis had suggested that the rate of loss of the *tpx1^{C169S}* by recombination with the wild-type allele during meiosis was extremely low (figure 5.2); nevertheless, one possible explanation for the increased H_2O_2 resistance of some of the isolates in the screen was that the C169S mutation was no longer present in these isolates. Hence, to test whether the 4 isolates of *tpx1^{C169S}cgi121*Δ still contained *tpx1^{C169S}*, we attempted to amplify the *tpx1* ORF for sequencing using primers specific for the 5' end of the *tpx1* ORF and to the nmt terminator sequence present in the engineered *tpx1^{+}* and *tpx1^{C169S}* strains (P1 (Sptsa.V6), P2 (nmtend), respectively) (figure 5.12) (Day *et al.*, 2012). However, amplification of the *tpx1* gene using the nmtend reverse primer only generated a product in the *tpx1^{C169S}cgi121*Δ isolate 4, suggesting that the nmt terminator had been lost by recombination. Indeed, subsequent amplification of *tpx1* (using primers P1 (Sptsa.V6) and P3 (XbaTsaC)), and sequencing, revealed that, although they were NAT^{R}, *tpx1^{C169S}cgi121*Δ isolates 1-3 were wild-type for *tpx1*, providing an explanation for their increased H_2O_2 resistance. However, sequencing confirmed that isolate number 4 had retained the C169S point mutation in *tpx1*. Interestingly, this difference between these isolates was consistent with the spot test results (figure 5.11B), in which isolates 1-3 had restored H_2O_2 resistance to wild-type *tpx1^{+}* (ZU10) levels, whereas isolate 4 displayed only partial increased H_2O_2 resistance compared to wild-type *tpx1^{+}* levels.

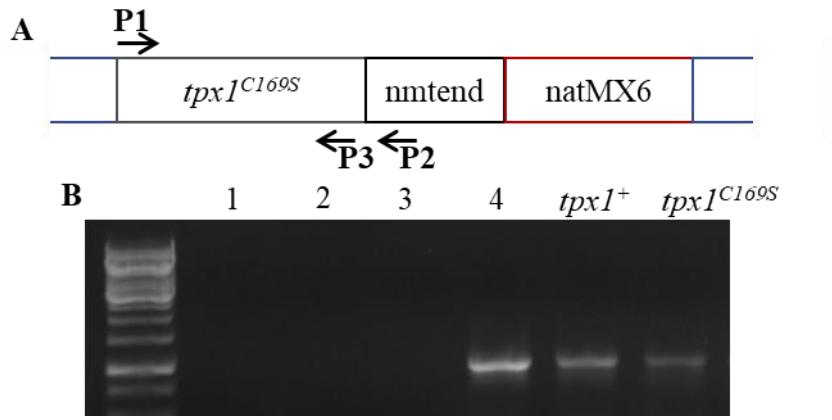

Figure 5.12 Amplification of *tpx1* by PCR using a primer directed to an nmtend sequence as an indication of genotype. [A] Structure of the *tpx1*^{C169S} (ZU11) strain. To generate the C169S point mutation in *tpx1*, a plasmid expressing an 'nmtend' sequence was used. To PCR up *tpx1;* a forward primer directed to the start of the *tpx1* gene (P1), as well as a reverse primer complementary to the 'nmtend' sequence (P2), was used. For subsequent sequencing, primers P1 and P3 were used. **[B] PCR products from the amplification of *tpx1* in the 4 *tpx1*^{C169S}*cgi121*Δ isolates (ZU21, ZU22, ZU23 and ZU24) using primers P1 and P3.** A PCR product was only generated with *tpx1*^{C169S}*cgi121*Δ isolate 4 (ZU24), and the two starting strains *tpx1*$^{+}$ (ZU10) and *tpx1*^{C169S} (ZU11).

Nevertheless, these data raised the possibility that the increased H_2O_2 resistance of many of the isolates was due to the loss of the *tpx1*^{C169S} mutation. To test whether the 26 strains (table 5.2) that displayed increased H_2O_2 resistance via halo test had also undergone recombination to express wild-type *tpx1*$^{+}$, *tpx1* was amplified using the P1 and P2 primers. Of the 26 strains tested by PCR, 14 generated a product suggesting they had retained the C169S mutation: *tpx1*^{C169S}*rps601*Δ, *tpx1*^{C169S}*rps1501*Δ, *tpx1*^{C169S}*spn4*Δ, *tpx1*^{C169S}*uds1*Δ, *tpx1*^{C169S}*puf3*Δ, *tpx1*^{C169S}*hsr1*Δ, *tpx1*^{C169S}*SPBC83.19c*Δ, *tpx1*^{C169S}*sap18*Δ, *tpx1*^{C169S}*grx1*Δ, *tpx1*^{C169S}*pus1*Δ, *tpx1*^{C169S}*dis1*Δ, *tpx1*^{C169S}*dph5*Δ, *tpx1*^{C169S}*SPAC11G7.01*Δ and *tpx1*^{C169S}*pfa5*Δ (although this requires confirmation by sequencing or western blot analysis). However, P1 and P2 primers failed to generate a product with the other 12 (of the 26) strains suggesting that the *tpx1*^{C169S} allele may have undergone a recombination event during meiosis with the wild-type *tpx1*$^{+}$ allele in the library strain.

Additionally, the locus of the 7 candidate genes from chromosome 3 were assessed to consider whether these genes were closely linked to *tpx1* and therefore likely to recombine with wild-type *tpx1*$^{+}$ during meiosis (position 2.085 Mb): *rps1501* (798 kb),

lsc2 (2.159 Mb), *sap18* (2.14 Mb), *cgi121* (921 kb), *pus1* (2.12 Mb), *dph5* (2.103 Mb) and *gcs2* (1.895 Mb). Five genes were positioned close to the *tpx1* locus: *lsc2*, *sap18*, *pus1*, *dph5* and *gcs2*. Two of which (*lsc2* and *gcs2*) seemed to have undergone recombination with the wild-type $tpx1^{+}$ with the data generated from PCR test so far.

5.2.2.6 Estimating the rate of loss of the $tpx1^{C169S}$ mutation

To investigate the reversion rate of the C169S point mutation to wild-type $tpx1^{+}$ further, the null mutations spotted around the periphery of each QFA plate were analysed. Increased space/nutrients for growth, affects the growth of spots at the periphery of the plate. Therefore, each peripheral spot on the library plates includes the same gene mutation, *mug134*Δ, so that interactions of test strains with other genes are only analysed in central positions. If there was a high rate of reversion/recombination of the $tpx1^{C169S}$ allele then we would expect that this should be detected by increased H_2O_2 resistance amongst some of these isolates. Hence photographic images generated during the QFA, were analysed to determine how many of the 76 $tpx1^{C169S}$*mug134*Δ isolates had increased H_2O_2 resistance (table 5.3).

Plate no.	Reversion Rate (%)
1	23
2	13
3	5
4	1.7
5	1.7

Table 5.3 Estimation of the potential 'reversion rate' of $tpx1^{C169S}$*mug134*Δ strains to wild-type $tpx1^{+}$. The possible rate of loss of $tpx1^{C169S}$ (reversion rate) was estimated from the number of the 76 $tpx1^{C169S}$*mug134*Δ spots with increased H_2O_2 resistance.

This suggested that loss of H_2O_2 sensitivity, presumably the result of recombination/loss of *tpx1*^{C169S} could have occurred at a detectably high frequency, particularly in library plate 1 (23 %). The reversion rate dropped with the fitness of each library plate (plate 1 represents the fittest in the gene deletion library, with plate 5 representing the least fittest gene deletions tested by QFA). This result suggested that it would be difficult to distinguish a strain where the *tpx1*^{C169S} allele was lost and wild-type *tpx1*$^{+}$ restored, from one where the detected gene had affected rescue of H_2O_2 resistance.

5.2.2.7 Median QFA revealed an additional 15 candidate genes as suppressors of the H_2O_2 sensitivity of *tpx1*^{C169S}

In order to account for variability between repeats, QFA data was re-analysed using the median of the 4 GIS (instead of the mean). The median analysis exhibited a large overlap of candidate genes with the mean analysis. However, this also revealed an additional 15 candidate genes predicted to have increased stress resistance in comparison to *tpx1*^{C169S} (ZU11) (table 5.4). Included in this list were 4 transmembrane transporters (*SPCC576.17c*, *gms2*, *ght2* and *sut1*) and a vacuolar transmembrane chaperone complex subunit, *vtc4*.

Gene Name	Description
snf22	ATP-dependent DNA helicase
lys3	saccharopine dehydrogenase
SPCC576.17c	pyridoxamine/pyridoxine/pyridoxal transmembrane transporter
gms2	UDP-galactose transmembrane transporter
mus81	Holliday junction resolvase subunit
arg11	N-acetyl-gamma-glutamyl-phosphate reductase/acetylglutamate kinase
arg4	arginine specific carbamoyl-phosphate synthase
naa30	NatC N-acetyltransferase complex catalytic subunit
mbx2	MADS-box transcription factor
ght2	hexose transmembrane transporter
vtc4	vacuolar transmembrane chaperone complex subunit
SPAC644.09	alanine racemase
SPBC2A9.02	NAD dependent epimerase/dehydratase family protein
sut1	alpha-glucoside transmembrane transporter
egt2	ergothioneine biosynthesis protein

Table 5.4 Median suppressor analysis of the *tpx1^{C169S}* QFA generated an additional 15 candidate genes predicted to contribute (upon deletion) to the H_2O_2 sensitivity of the *tpx1^{C169S}* (ZU11). The *tpx1^{C169S}* QFA data was analysed using the median GIS score to order candidate gene hits.

5.2.2.8 Reconstruction of the *tpx1^{C169S}arg4*Δ strain revealed the suppression of *tpx1^{C169S}* H_2O_2 sensitivity was not due to the deletion of *arg4*

Six of the 15 additional strains from the median analysis (*arg4*Δ, *arg11*Δ, *ght2*Δ, *gms2*Δ, *SPAC644.09*Δ and *lys3*Δ) were re-crossed manually with *tpx1^{C169S}* (ZU11), and spot tests were conducted to test H_2O_2 sensitivity. However, none of the 6 double mutant strains were more H_2O_2 resistant than the *tpx1^{C169S}* (ZU11 or isogenic strain) so the basis of the isolates increased H_2O_2 resistance, was undetermined, but not due to loss of the associated gene (figure 5.13).

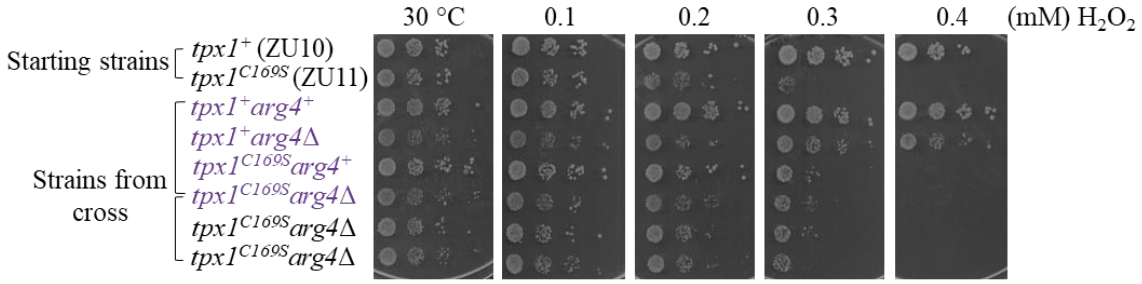

Figure 5.13 Spot test analysis performed on isogenic strains (tetrad in purple) generated from manually crossing *tpx1*^{C169S} (ZU11) with *arg4*Δ (Bioneer) with and without H_2O_2. Exponentially growing isogenic strains, and starting strains (*tpx1*$^{+}$ (ZU10) and *tpx1*^{C169S} (ZU11)) were spotted onto agar with and without H_2O_2.

5.2.2.9 H_2O_2 resistance of the *tpx1*^{C169S}*cgi121*Δ isolate 4 strain does not follow the deletion of *cgi121*

Next, we investigated the basis of the increased H_2O_2 resistance phenotype of the *tpx1*^{C169S}*cgi121*Δ isolate 4, in which the C169S mutation was retained (section 5.2.2.5). First, the *tpx1*^{C169S}*cgi121*Δ isolate 4 strain (ZU24) was back-crossed with *tpx1*^{C169S} (ZU11), to test whether the increased H_2O_2 resistance was linked to the *cgi121* marker. The strains generated were patched onto different selection plates to test for genotype and H_2O_2 resistance (table 5.5). This revealed that the H_2O_2 resistance phenotype did not follow the kan^{R} marker of the *cgi121*Δ (spore B4 (ZU30)).

Genotype			Growth on selective media			
Tetrad	Spore	Genotype	-URA	+Kan	+Nat	+H_2O_2
B	3	*tpx1*$^{+}$*cgi121*Δ	✗	✓	✗	✓
	4	***tpx1***^{C169S}***cgi121***$^{+}$	✓	✗	✓	✓
	5	*tpx1*^{C169S}*cgi121*$^{+}$	✓	✗	✓	✗
A	6	*tpx1*^{C169S}*cgi121*Δ	✓	✓	✓	✓
	7	*tpx1*^{C169S}*cgi121*Δ	✗	✓	✓	✗
	9	*tpx1*$^{+}$*cgi121*$^{+}$	✗	✗	✗	✓

Table 5.5 Growth analysis of spores from backcrossing the *tpx1*^{C169S}*cgi121*Δ isolate 4 (ZU24) with *tpx1*^{C169S} (ZU11). Following the mating of *tpx1*^{C169S}*cgi121*Δ isolate 4 (ZU24) with *tpx1*^{C169S} (ZU11), spores were separated by manual dissection, and patched onto agar selection plates (EMM+HAL, YE5S + 1 mg/ml G418, YE5S + 1 mg/ml clonNAT and YE5S + 1 mM H_2O_2). The growth of each spore on different selection plates was recorded (✓ = growth, ✗ = no growth). The spore B4 (ZU30) demonstrates that the H_2O_2 resistance phenotype does not follow the deletion of *cgi121*. The fourth spore in each tetrad did not give rise to a colony.

Indeed, the backcrossed *tpx1*^{C169S}*cgi121*$^{+}$ (ZU30) strain had a similar H_2O_2 resistance to the *tpx1*^{C169S}*cgi121*Δ isolate 4 strain (ZU24) (figure 5.14). Excitingly, this indicates that the H_2O_2 resistance is due to an additional unidentified mutation in this strain. This also explains why no increase in stress resistance was observed when *cgi121*Δ and *tpx1*^{C169S} were re-crossed manually (figure 5.11).

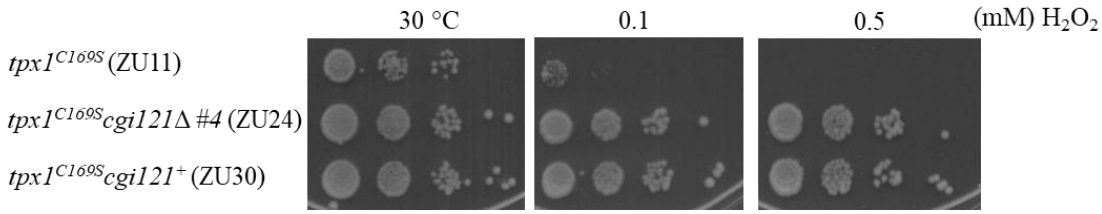

Figure 5.14 Analysis of the H_2O_2 resistance of the *tpx1^{C169S}cgi121^{+}* (ZU30) strain. Growth of serially diluted exponentially growing *tpx1^{C169S}* (ZU11), *tpx1^{C169S}cgi121*Δ #4 (ZU24) and *tpx1^{C169S}cgi121^{+}* (ZU30) cells spotted onto YE5S plates containing the indicated concentrations of H_2O_2.

Previous work established that loss of *txl1*, a thioredoxin-like protein, rescues the H_2O_2 resistance of *tpx1^{C169S}* to wild-type levels (Brown *et al.*, 2013). Hence, to test whether the increased resistance might be due to loss of *txl1* , the *txl1* open reading frame in *tpx1^{C169S}cgi121*Δ isolate 4 (ZU24) was sequenced. No mutations were found in the *txl1* ORF, however this does not rule out mutations in the promoter which prevents *txl1* expression.

5.2.2.10 Pap1 oxidation in response to 0.2 mM H_2O_2 is restored in the *tpx1^{C169S}cgi121^{+}* strain

In *tpx1^{C169S}* mutant cells the activation of Pap1, that is required for adaptation to H_2O_2, is prevented. Hence, we tested whether the increased H_2O_2 resistance of the H_2O_2-resistant *tpx1^{C169S}* strain (*tpx1^{C169S}cgi121^{+}* (ZU30)) reflected restoration of Pap1 activation. In unstressed cells, Tpx1 is in monomeric form and Pap1 is reduced (figure 5.15). We can infer that the thioredoxin reductase (*trr1)* in *tpx1^{C169S}cgi121^{+}* is also not mutated (and still functional), as Pap1 is not constitutively oxidised in this strain.

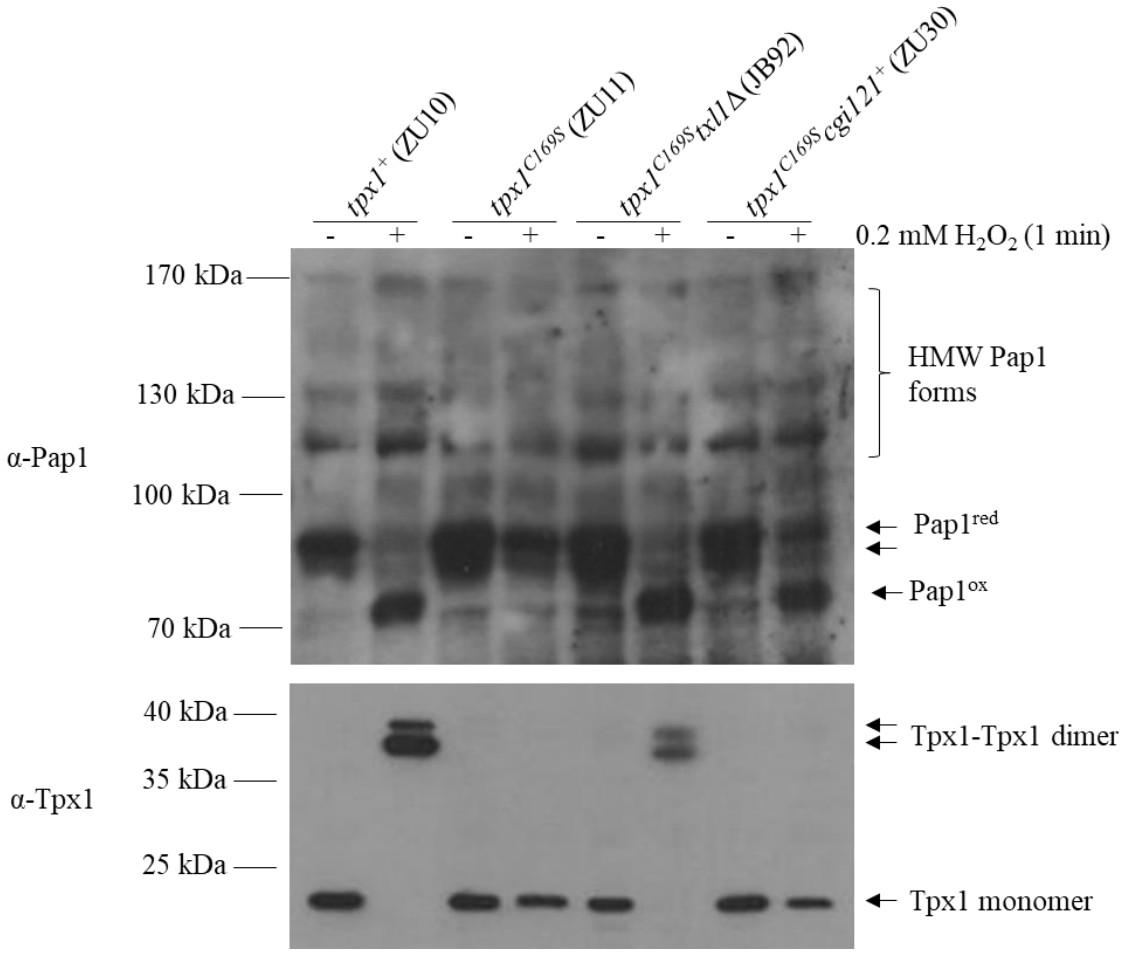

Figure 5.15 Analysis of Tpx1 and Pap1 oxidation in the *tpx1^{C169S}cgi121^{+}* (ZU30) strain. Oxidation state of Pap1 and Tpx1 in *tpx1^{+}* (ZU10), *tpx1^{C169S}* (ZU11), *tpx1^{C169S}txl1*Δ (JB92) and *tpx1^{C169S}cgi121^{+}* (ZU30) cells, analysed by western blot using anti-Tpx1 and anti-Pap1 antibodies before and after 1 min exposure to 0.2 mM H_2O_2.

As expected, following treatment with 0.2 mM H_2O_2 for 1 minute, Pap1 oxidation and the formation of Tpx1-Tpx1 dimers were detected in the *tpx1*$^{+}$ (ZU10) strain, and not in the *tpx1*^{C169S} (ZU11) strain (Brown *et al.*, 2013). In the *tpx1*^{C169S}*cgi121*$^{+}$ strain, although the absence of Tpx1-Tpx1 disulphides indicates that actively cycling Tpx1 is absent, Pap1 was oxidised to its active form. This suggests that the thioredoxin peroxidase activity of Tpx1 is dispensable for Pap1 activation in these cells, despite the apparent presence of Txl1.

As expected, H_2O_2-induced Pap1 oxidation was also restored in the *tpx1*^{C169S}*txl1*Δ (JB92) strain. However, we were surprised to detect H_2O_2-induced formation of Tpx1-Tpx1 disulphides, this suggested that the *tpx1*^{C169S} mutation might have reverted to generate a wild-type *tpx1*$^{+}$. Hence, the *tpx1*^{C169S}*txl1*Δ strain was re-constructed by manually re-crossing *tpx1*^{C169S} (JR42) and *txl1*Δ (EV76), and plating out spores isolated by random sporulation (section 2.1.4). The H_2O_2 resistance and oxidation of Pap1 was assessed in several of the resulting strains (figure 5.16). As expected, the *tpx1*$^{+}$ strains tested (JR68 and EV76) displayed wild-type levels of H_2O_2 resistance at low levels of H_2O_2 (up to 0.3 mM); although, as previously observed (Brown and Veal, unpublished), EV76 was more sensitive than JR68 at 1 mM H_2O_2. The growth of *tpx1*^{C169S} (JR42) was inhibited by 0.1 mM H_2O_2, and the newly constructed *tpx1*^{C169S}*txl1*Δ (ZU59, ZU60, ZU61, ZU62) strains showed similar sensitivity to H_2O_2 (figure 5.16A); suggesting that loss of *txl1* did not restore the H_2O_2 resistance of a *tpx1*^{C169S} mutant to wild-type *tpx1*$^{+}$ levels. Moreover, Pap1 oxidation was not restored following exposure to 0.2 mM H_2O_2 for 1 min (figure 5.16B), in contrast to the previous work with the original *tpx1*^{C169S}*txl1*Δ strain (JB92) (Brown *et al.*, 2013). Thus, these data raised the possibility that, like the *tpx1*^{C169S}*cgi121*Δ *#4* (ZU24) isolate identified by our screen, the restoration of Pap1 oxidation and increased H_2O_2 resistance in the original *tpx1*^{C169S}*txl1*Δ strain (JB92) was not associated with loss of the deleted gene.

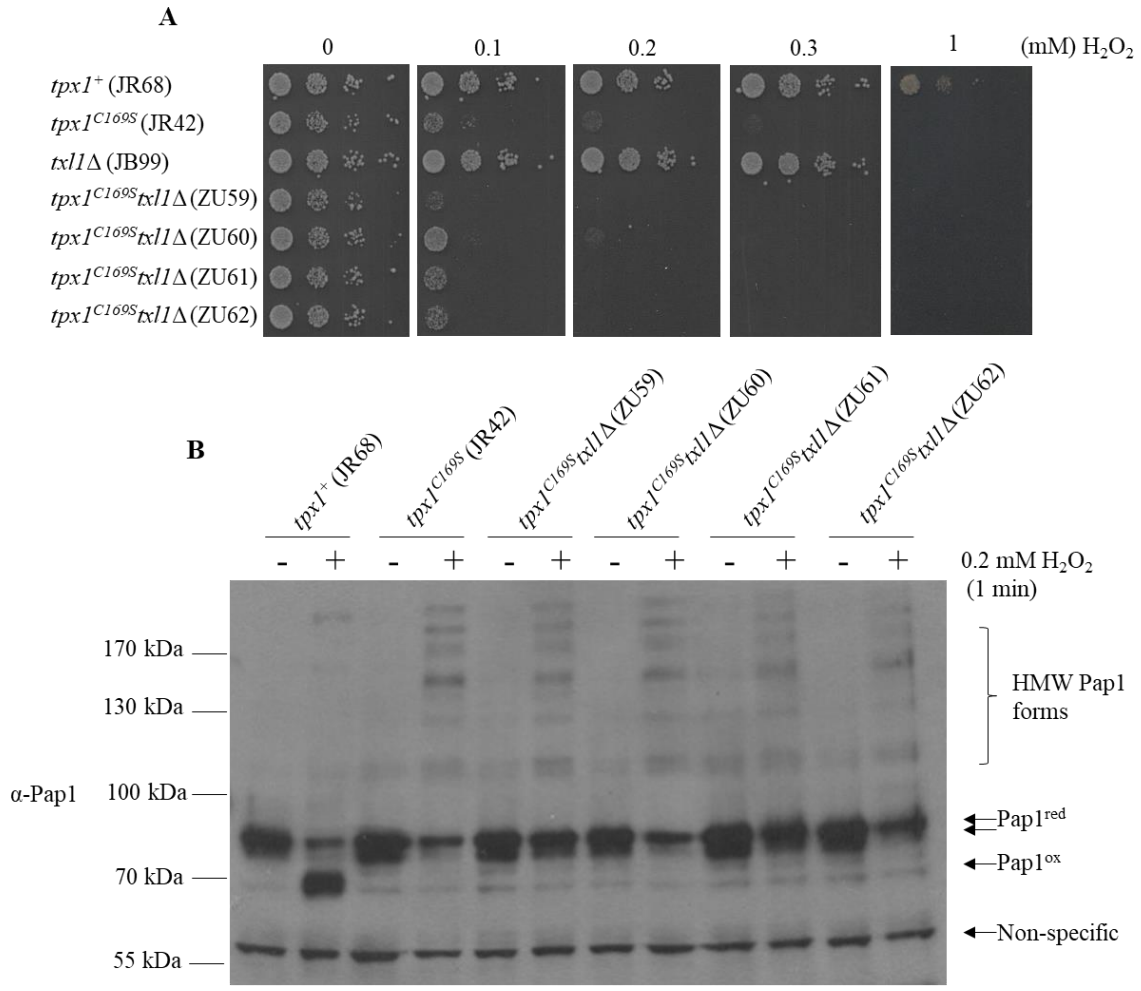

Figure 5.16 Effect of loss of Txl1 on the [A] H_2O_2 resistance and [B] H_2O_2-induced oxidation of Pap1 in tpx1^{C169S} mutant cells. [A] Growth of serially diluted exponentially growing *tpx1*$^{+}$ (JR68), *tpx1*^{C169S} (JR42), *txl1*Δ (JB99) and *tpx1*^{C169S}*txl1*Δ (ZU59, ZU60, ZU61, ZU62) cells spotted onto plates containing the indicated concentrations of H_2O_2. [B] Oxidation state of Pap1 in *tpx1*$^{+}$ (JR68), *tpx1*^{C169S} (JR42) and *tpx1*^{C169S}*txl1*Δ (ZU59, ZU60, ZU61, ZU62) cells, analysed by western blot using anti-Pap1 antibodies before and after 1 min exposure to 0.2 mM H_2O_2.

However, the presence of wild-type Tpx1 in the revived JB92 strain, which was confirmed by sequencing, made it impossible to use this strain to identify the cause of the restored Pap1 activation we had previously observed. Moreover, when the oxidation state of Pap1 and Tpx1 were re-examined in *tpx1*^{C169S}*cgi121*$^{+}$ (ZU30) and *tpx1*^{C169S}*txl1*Δ (JB92) Tpx1-Tpx1 disulphides were detected in both strains following exposure to 0.2 mM H_2O_2 (figure 5.17). These data suggested that *tpx1*^{C169S} may also have spontaneously reverted to wildtype *tpx1*$^{+}$ in the *tpx1*^{C169S}*cgi121*$^{+}$ (ZU30).

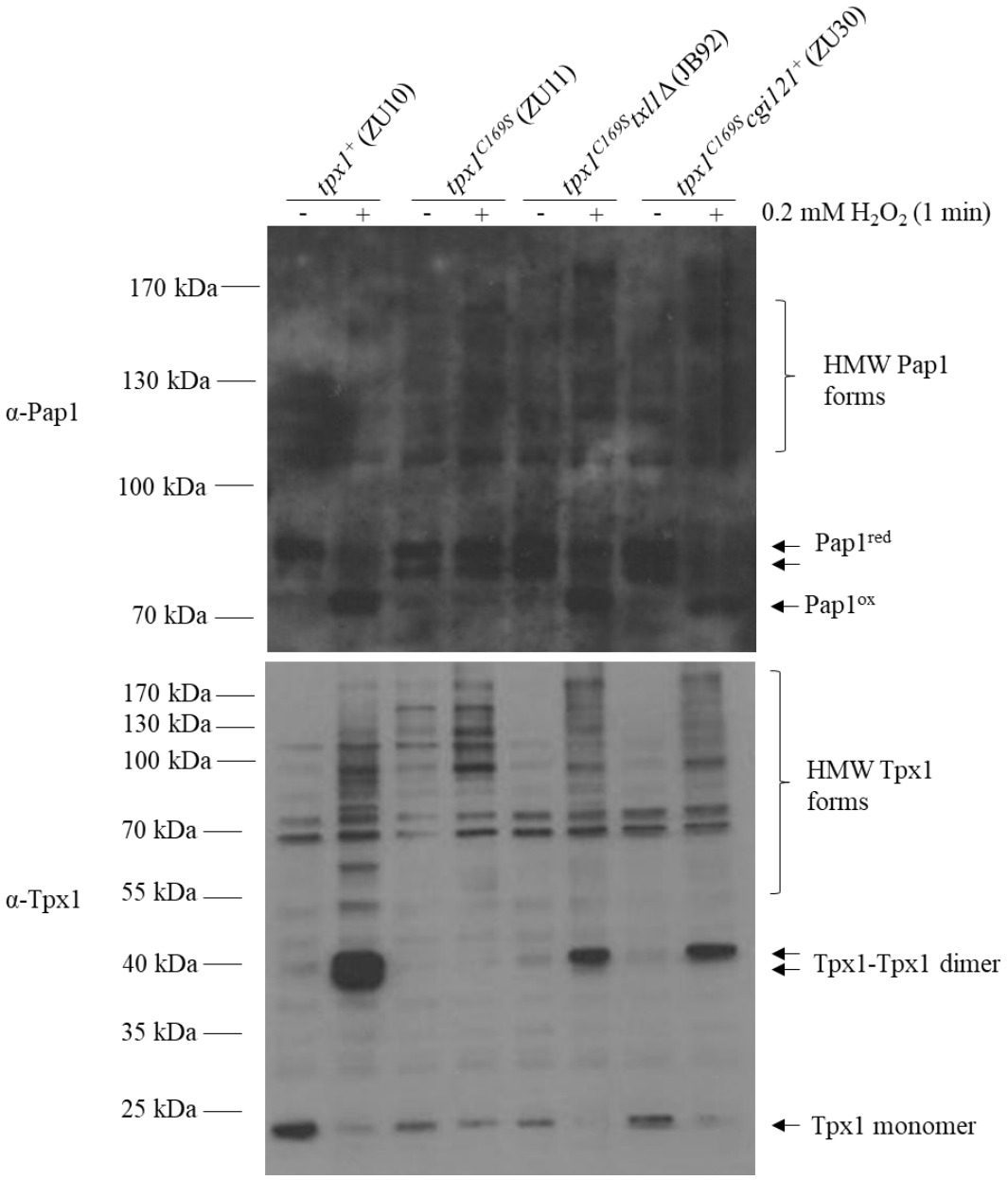

Figure 5.17 Analysis of the oxidation of Tpx1 and Pap1 in the *tpx1^{C169S}cgi121^{+}* (ZU30) strain. Oxidation state of Pap1 and Tpx1 in *tpx1^{+}* (ZU10), *tpx1^{C169S}* (ZU11), *tpx1^{C169S}txl1*Δ (JB92) and *tpx1^{C169S}cgi121^{+}* (ZU30) cells, analysed by western blot using anti-Tpx1 and anti-Pap1 antibodies before and after 1 min exposure to 0.2 mM H_2O_2.

5.2.2.11 Identification of *tpx1*^{C169S}-containing strains with increased H_2O_2 resistance despite absence of H_2O_2-inducible Pap1 oxidation

4 of the 14 H_2O_2-resistant screen isolates that generated a PCR product with the nmtend primer (section 5.2.2.5) indicating that the 3' end of the *tpx1*^{C169S} had not been lost by recombination, were revealed, by sequencing, to bear a wild-type *tpx1*$^{+}$ (*tpx1*^{C169S}*puf3*Δ, *tpx1*^{C169S}*grx1*Δ, *tpx1*^{C169S}*pfa5*Δ and *tpx1*^{C169S}*dis1*Δ). This revealed that screening with the nmtend primer was not a reliable way to screen for the presence of the *tpx1*^{C169S} allele. Moreover, this suggested that spontaneous reversion might be responsible for the increased resistance of many of the strains isolated by the screen. Indeed, when the oxidation state of Tpx1 was examined in the other 10 H_2O_2-resistant isolates 5 (*tpx1*^{C169S}*rps601*Δ, *tpx1*^{C169S}*rps1501*Δ, *tpx1*^{C169S}*hsr1*Δ, *tpx1*^{C169S}*SPCC126.13c*Δ and *tpx1*^{C169S}*dph5*Δ) were found to form Tpx1-Tpx1 dimers in response to 0.2 mM H_2O_2 (figure 5.18). As expected, this reversion to wild-type *tpx1*$^{+}$ was accompanied by restoration of H_2O_2-inducible Pap1 oxidation. However, the 5 remaining strains (*tpx1*^{C169S}*spn4*Δ, *tpx1*^{C169S}*uds1*Δ, *tpx1*^{C169S}*SPBC83.19c*Δ, *tpx1*^{C169S}*SPAC11G7.01*Δ and *tpx1*^{C169S}*pus1*Δ) were unable to form Tpx1-Tpx1 dimers following H_2O_2 exposure, indicating that strains had retained the *tpx1*^{C169S} mutation (figure 5.18). Intriguingly, this suggested that the H_2O_2 resistance of these 5 *tpx1*^{C169S} mutant strains was increased compared with *tpx1*^{C169S} even in the absence of Pap1 oxidation.

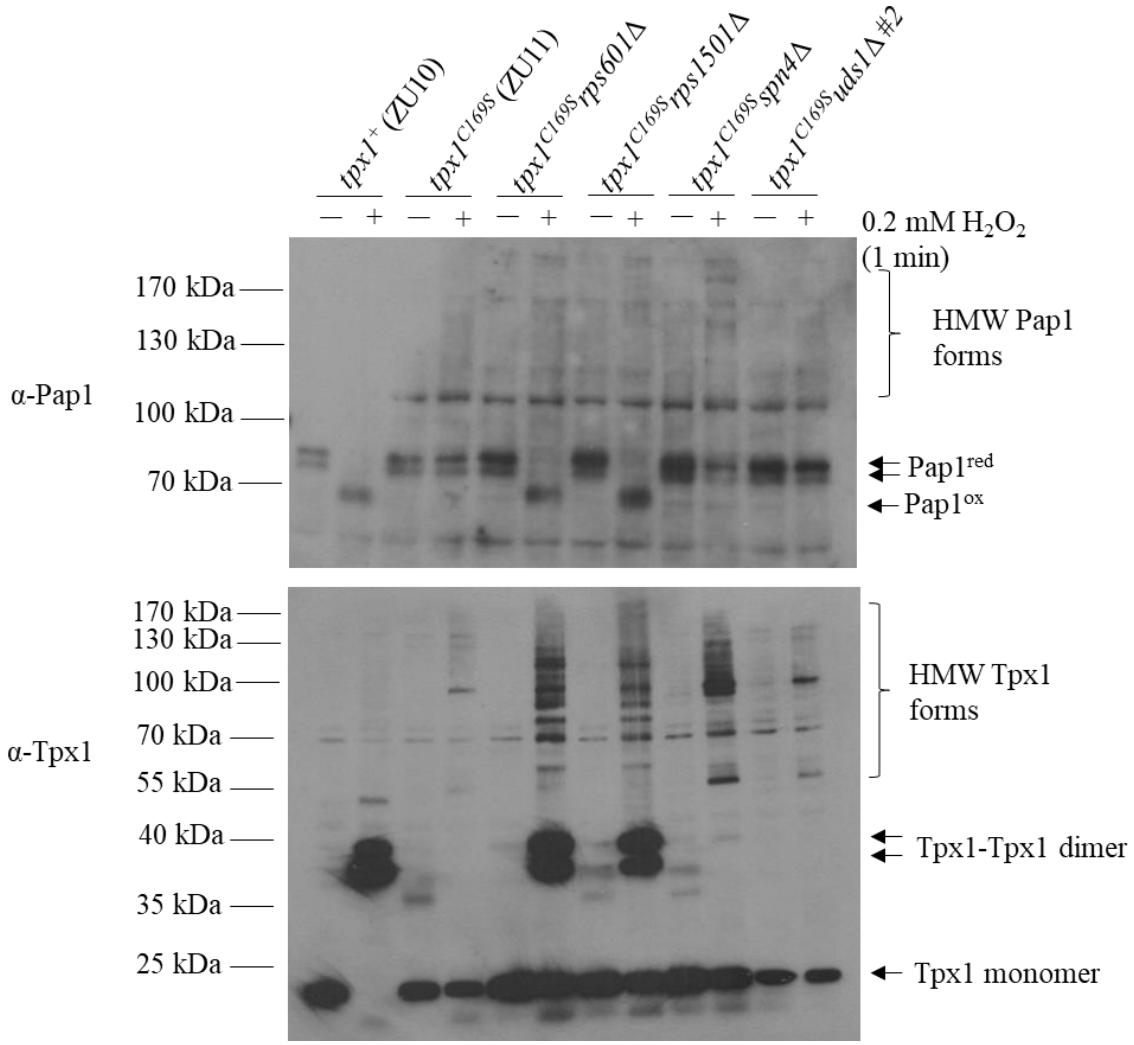
tpx1+ (ZU10)
tpx1C169S (ZU11)
tpx1C169Srps601Δ
tpx1C169Srps1501Δ
tpx1C169Sspn4Δ
tpx1C169Suds1Δ#2
— + — + — + — + — + — +
0.2 mM H2O2
(1 min)
α-Pap1
170 kDa
130 kDa
100 kDa
70 kDa
HMW Pap1
forms
Pap1red
Pap1ox
α-Tpx1
170 kDa
130 kDa
100 kDa
70 kDa
55 kDa
40 kDa
35 kDa
25 kDa
HMW Tpx1
forms
Tpx1-Tpx1 dimer
Tpx1 monomer

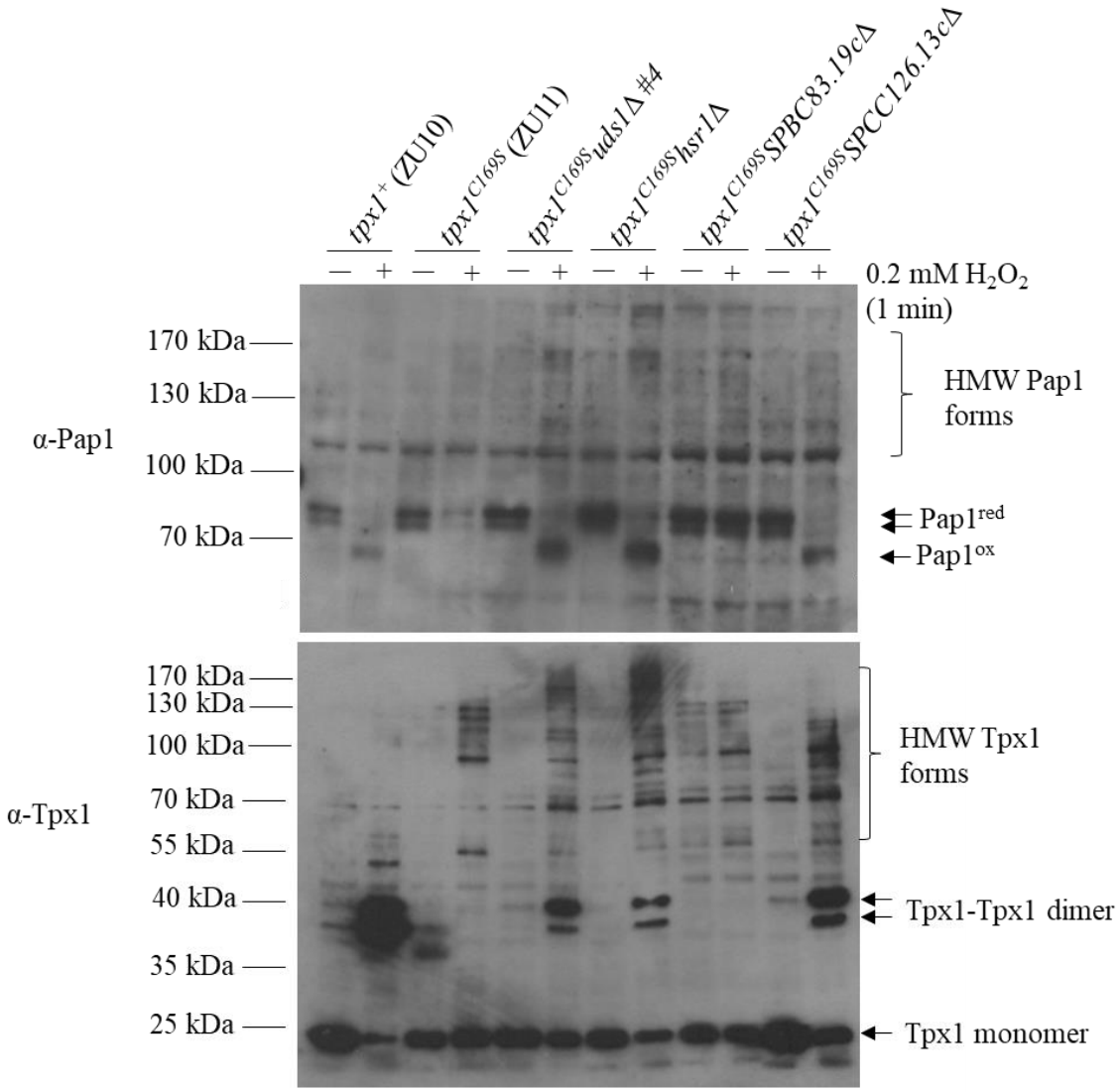
tpx1+ (ZU10)
tpx1C169S (ZU11)
tpx1C169Suds1Δ #4
tpx1C169Shsr1Δ
tpx1C169SSPBC83.19cΔ
tpx1C169SSPCC126.13cΔ
— + — + — + — + — + — +
0.2 mM H2O2
(1 min)
α-Pap1
170 kDa
130 kDa
100 kDa
70 kDa
HMW Pap1
forms
Pap1red
Pap1ox
α-Tpx1
170 kDa
130 kDa
100 kDa
70 kDa
55 kDa
40 kDa
35 kDa
25 kDa
HMW Tpx1
forms
Tpx1-Tpx1 dimer
Tpx1 monomer

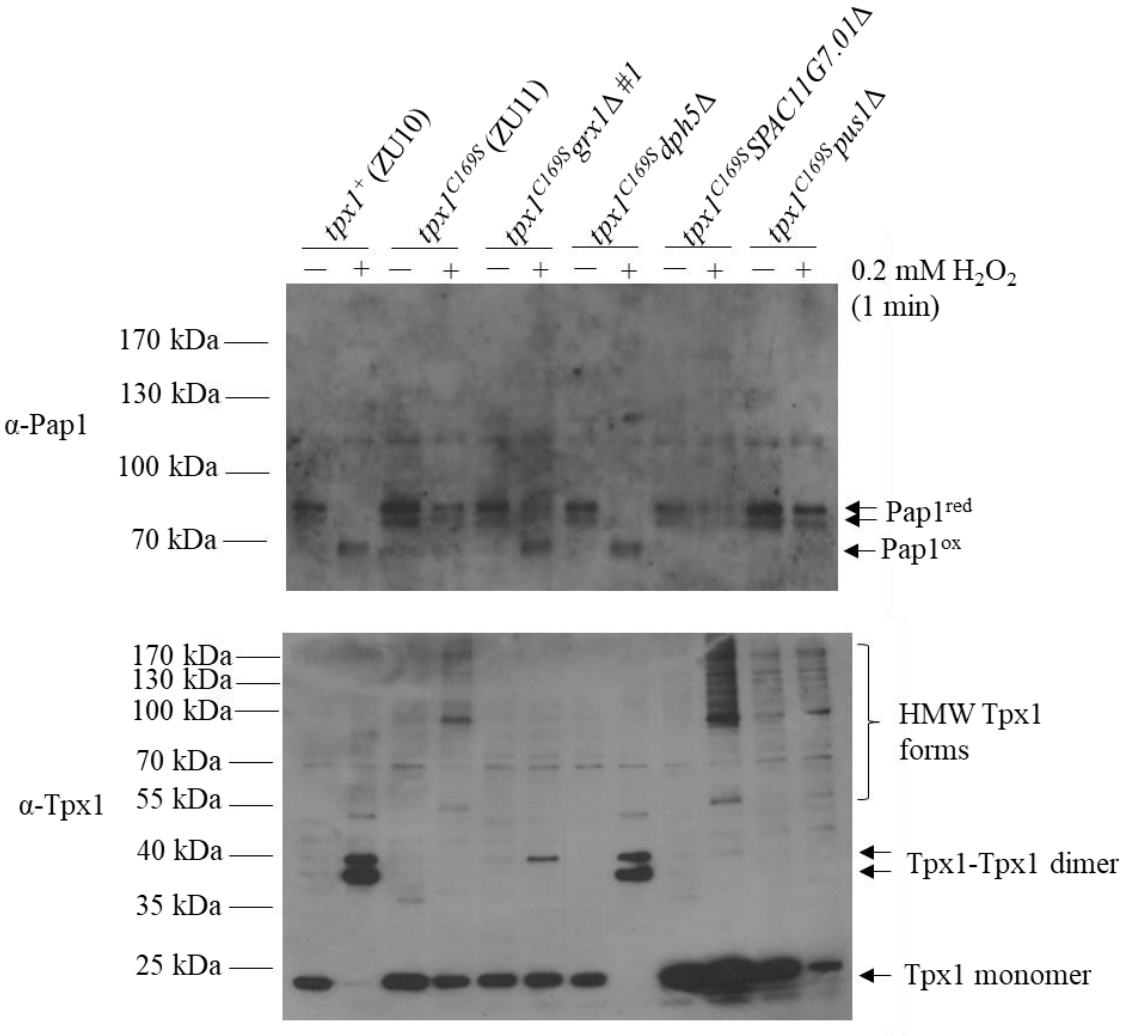

Figure 5.18 Analysis of the oxidation of Pap1 and Tpx1 in H_2O_2-resistant isolates identified by screen. Oxidation state of Pap1 and Tpx1 in *tpx1*$^{+}$ (ZU10), *tpx1*^{C169S} (ZU11), and the following H_2O_2-resistant isolates identified by the screen: *tpx1*^{C169S}*rps601*Δ, *tpx1*^{C169S}*rps1501*Δ, *tpx1*^{C169S}*spn4*Δ, *tpx1*^{C169S}*uds1*Δ #2, *tpx1*^{C169S}*uds1*Δ #4, *tpx1*^{C169S}*hsr1*Δ, *tpx1*^{C169S}*SPBC83.19c*Δ, *tpx1*^{C169S}*SPCC126.13*Δ, *tpx1*^{C169S}*grx1*Δ #1, *tpx1*^{C169S}*dph5*Δ, *tpx1*^{C169S}*SPAC11G7.01*Δ, *tpx1*^{C169S}*pus1*Δ. Cells were analysed by western blot using anti-Tpx1 and anti-Pap1 antibodies before and after 1 min exposure to 0.2 mM H_2O_2.

To investigate this further, the H_2O_2-resistance of these 5 strains (*tpx1*^{C169S}*spn4*Δ, *tpx1*^{C169S}*uds1*Δ, *tpx1*^{C169S}*SPBC83.19c*Δ, *tpx1*^{C169S}*SPAC11G7.01*Δ and *tpx1*^{C169S}*pus1*Δ) were re-examined by spot test (figure 5.19A). Although the *tpx1*^{C169S}*uds1*Δ, *tpx1*^{C169S}*SPBC83.19c*Δ isolates appeared to be have a similar H_2O_2 sensitivity to the parent *tpx1*^{C169S} strain, this analysis confirmed that 3 strains (*tpx1*^{C169S}*spn4*Δ, *tpx1*^{C169S}*SPAC11G7.01*Δ and *tpx1*^{C169S}*pus1*Δ) were more H_2O_2 resistant than *tpx1*^{C169S} (ZU11).

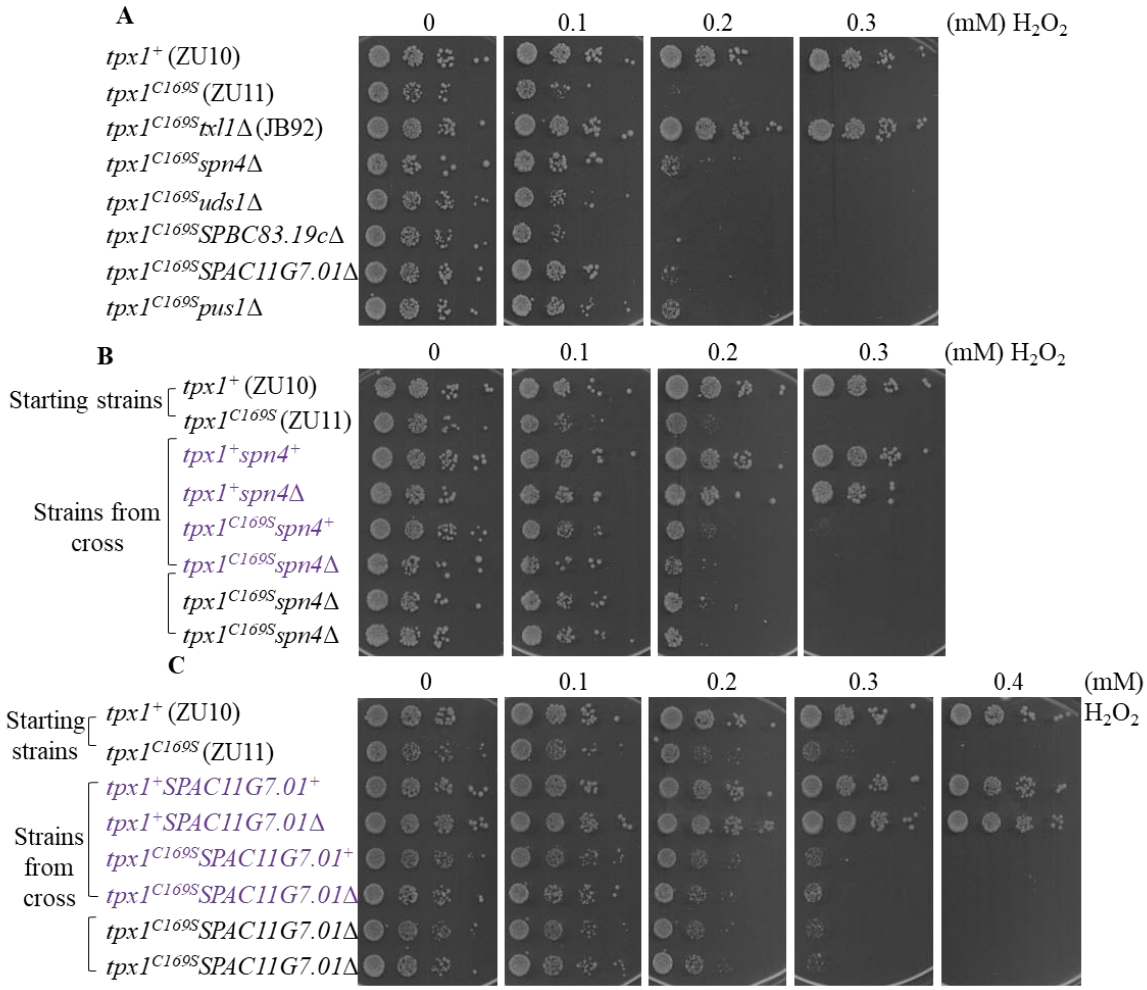

Figure 5.19 Spot test analysis on the H_2O_2 resistant strains that retained the C169S mutation. [A] Spot test analysis of the 5 strains predicted to have increased H_2O_2 resistance and retained the C169S mutation. Growth of serially diluted exponentially growing *tpx1*$^{+}$ (ZU10), *tpx1*^{C169S} (ZU11), *txp1*^{C169S}*txl1*Δ (JB92), and the following isolates from the screen: *tpx1*^{C169S}*spn4*Δ, *tpx1*^{C169S}*uds1*Δ, *tpx1*^{C169S}*SPBC83.19c*Δ, *tpx1*^{C169S}*SPAC11G7.01*Δ and *tpx1*^{C169S}*pus1*Δ spotted onto plates containing the indicated concentrations of H_2O_2. **[B] Spot test analysis of isogenic strains from re-crossing *tpx1*^{C169S} (ZU11) and *spn4*Δ (Bioneer).** Growth of serially diluted exponentially growing *tpx1*$^{+}$ (ZU10), *tpx1*^{C169S} (ZU11), and strains generated from manually re-crossing *tpx1*^{C169S} and *spn4*Δ (tetrad in purple) spotted onto plates containing the indicated concentrations of H_2O_2. **[C] Spot test analysis of isogenic strains from re-crossing *tpx1*^{C169S} (ZU11) and *SPAC11G7.01*Δ (Bioneer).** Growth of serially diluted exponentially growing *tpx1*$^{+}$ (ZU10), *tpx1*^{C169S} (ZU11), and strains generated from manually re-crossing *tpx1*^{C169S} and *SPAC11G7.01*Δ (tetrad in purple) spotted onto plates containing the indicated concentrations of H_2O_2.

Next, we set out to determine whether deletion of *spn4*, *SPAC11G7.01* or *pus1* was responsible for this increased H_2O_2 resistance. As there are likely to be some errors in the positioning of gene mutants in the library, we first confirmed by PCR (primers: Spn4 FP, Spn4 RP, SPAC11G7.01 FP, SPAC11G7.01 RP, Pus1 FP and Pus1 RP) that these genes were the ones that were deleted in these isolates. Strains *tpx1*^{C169S} (ZU11) and *spn4*Δ or *SPAC11G7.01*Δ (Bioneer) were manually re-crossed. However, the double mutants generated were not more H_2O_2 resistant than the *tpx1*^{C169S} (figure 5.19B and C). This suggests that the increased H_2O_2 resistance of the *tpx1*^{C169S}*spn4*Δ and *tpx1*^{C169S}*SPAC11G7.01*Δ isolated in the screen, is due to an unidentified background mutation, rather than the loss of the candidate gene. These strains were retained for future analysis but, to circumvent the problems with recombination/loss of the point mutation in *tpx1*, an SGA screen using a *tpx1*Δ strain was also carried out.

5.2.3 SGA analysis of *tpx1*Δ identified candidate H_2O_2 regulated proteins

5.2.3.1 Replacing *ura4*$^+$ with a nat(MX6) cassette has no effect on growth of *tpx1*Δ strain

To undergo SGA analysis, a nourseothricin-resistant (NAT^r) *tpx1*Δ strain was generated (figure 5.1B). Spot tests were conducted on the starting *tpx1*Δ (VXOO), the generated NAT^r *tpx1*Δ (ZU12), as well as a *tpx1*$^+$ (SW61) strain (figure 5.20). This revealed that the 2 *tpx1*Δ strains had similar growth on YE5S at 30 °C, indicating that recombining out the *ura4* gene with a natMX6 cassette had no effect on the growth of cells. As expected, both *tpx1*Δ strains grew more slowly than the *tpx1*$^+$ strain, suggesting that, as well as genes essential for growth in a *tpx1*Δ, an SGA screen might also identify gene deletions that improved growth.

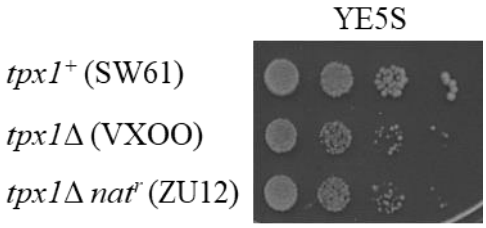

Figure 5.20 Spot test analysis of the growth of *tpx1*Δ (VXOO) and nourseothricin-resistant *tpx1*Δ (ZU12). Exponentially growing cells *tpx1*$^{+}$ (SW61), *tpx1*Δ (VXOO) and *tpx1*Δ (ZU12) were spotted onto YE5S agar to investigate growth.

5.2.3.2 SGA analysis of *tpx1*Δ identified candidate genes important for the growth of *tpx1*Δ

To identify genes important for growth in a *tpx1*Δ, high through-put genetic screening was conducted by the HTSF at Newcastle University. The *tpx1*Δ (ZU12) was systematically crossed with approximately 3,400 non-essential gene deletion strains (Bioneer) to generate a synthetic genetic array, to allow genome-wide mapping of synthetic genetic interactions (section 2.2.1.1, figure 2.1). Photographs of the final plates were taken using spImager software, and cell density was calculated using the image analysis tool Colonyzer (section 2.2.1.2). The fitness of the generated strains on YE5S were ordered by genetic interaction score (GIS). The SGA was repeated twice, and results were compared to a range of wild-type controls previously conducted by the HTSF: *ura1*, *ura5*, *pot1*, ZU10.

To identify genetic interactions which enhanced the growth defect of *tpx1*Δ, the bottom 55 candidate genes (the 55 genes with the highest negative GIS) were taken from comparing the *tpx1*Δ SGA against the *ura1* SGA (figure 5.21), and comparing the *tpx1*Δ SGA with the *ura5* SGA, for both *tpx1*Δ SGA repeats (essentially 8 repeats in which each candidate is screened in quadruplet per screen). From this analysis, there were 21 candidate genes which came out in all 4 comparisons (table 5.6). Interestingly, when comparing the list of enhancers of the growth defect for *tpx1*Δ (table 5.6), with the list of enhancers of the growth defect for *tpx1*^{C169S} (table 5.1), there was only one candidate gene which came out of both analyses: *ctt1* (catalase). This suggests that different genes may be more important for growth in the *tpx1*^{C169S} than in a *tpx1*Δ mutant.

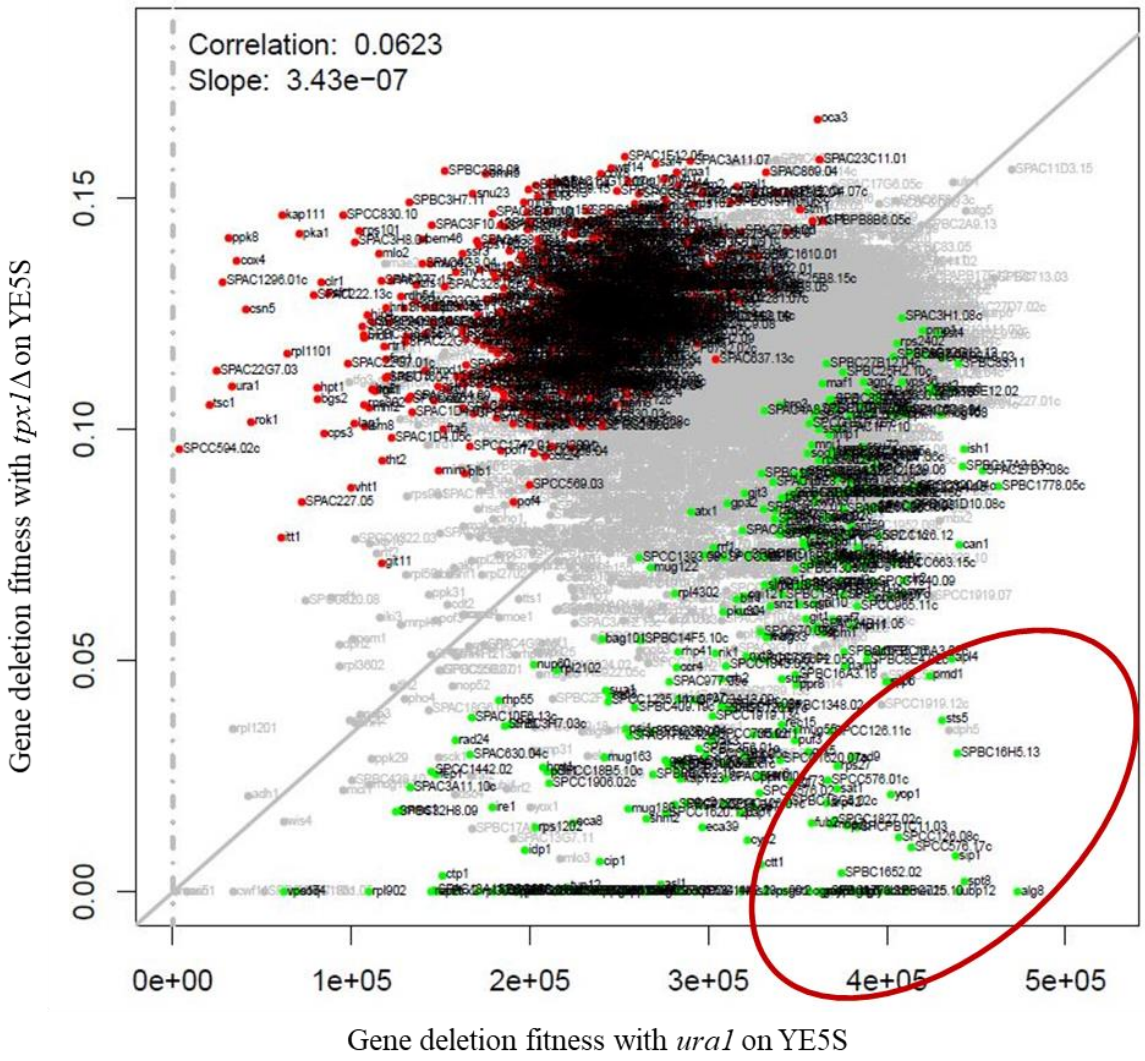

Figure 5.21 Fitness of the Bioneer deletion library crossed with the first *tpx1*Δ SGA (y-axis), compared to the fitness of the Bioneer deletion library crossed with the *tpx1*$^{+}$ wild-type strain *ura1* (x-axis). The red circle represents gene mutants which have enhanced the growth defect of *tpx1*Δ (hits with the highest negative GIS).

Average GIS Position	Gene Name	Gene Description:
2.75	alg8	glucosyltransferase
5.25	spt8	SAGA complex subunit
7.75	png1	ING family homolog
9.75	ubc6	ubiquitin conjugating enzyme E2
11.75	sip1	Pof6 interacting protein Sip1, predicted AP-1 accessory protein
12	ubp12	CSN-associated deubiquitinating enzyme
12.5	gly1	threonine aldolase
12.75	alg5	dolichyl-phosphate beta-glucosyltransferase
14.75	meu15	Schizosaccharomyces pombe specific protein
17.5	SPBC1652.02	APC amino acid transmembrane transporter
18.25	gst2	glutathione S-transferase
20.25	ogm1	protein O-mannosyltransferase
20.75	pcy1	cholinephosphate cytidylyltransferase
24.75	SPBC1773.12	transcription factor, zf-fungal binuclear cluster type
28.25	SPCC126.08c	lectin family glycoprotein receptor
30.25	arp42	SWI/SNF and RSC complex subunit
33.75	ctt1	catalase
34	pub1	HECT-type ubiquitin-protein ligase E3
41.75	spf1	Set1C PHD Finger protein
42.25	coq5	C-methyltransferase
43.75	svf1	Svf1 family protein

Table 5.6 Gene names and descriptions for the 21 candidate genes that enhance the *tpx1*Δ growth defect (highest negative GIS). The list of candidate genes that had the highest negative GIS (that were detected in the bottom 55 hits) in both *tpx1*Δ SGA replicates, with both the *ura1* and *ura5* wild-type *tpx1*$^{+}$ comparisons. Candidate genes have been ordered by their average GIS position. The gene highlighted in red, *ctt1*, is the only hit to also come out as a synthetic sick interaction with both the *tpx1*^{C169S} SGA replicates.

Moreover, when comparing the synthetic sick interactions from table 5.6, with orthologues from *tsa1*Δ screens conducted in *S. cerevisiae* (Huang and Kolodner, 2005; Molin *et al.*, 2011; Hanzén *et al.*, 2016; Pan *et al.*, 2006), only one gene, *URE2* (YNL229C), that is related in sequence, if not function, to GST2, was recorded as having a synthetic sick interaction in a *tsa1*Δ (Molin *et al.*, 2011). Surprisingly, this revealed much less overlap with *S. cerevisiae tsa1*Δ screens than with the synthetic sick hits from the $tpx1^{C169S}$ SGA analyses.

5.2.3.3 SGA analysis of *tpx1*Δ identified candidate genes that suppressed the growth defect of *tpx1*Δ

Next, we examined the data to determine if we could identify candidate suppressors of the growth defect of *tpx1*Δ, or candidates for mutants that are rescued by the loss of *tpx1*. The SGA analysis was conducted on cells pinned from solid media, rather than exponentially growing in liquid media, as in figure 5.8 and in QFA, likely making the difference between the growth of the *tpx1*Δ mutant and wild-type strains less pronounced. Nevertheless, we noted that, when the fitness of the first or second *tpx1*Δ SGA was compared to the control *ura1* library (figure 5.22) (figure 5.23), although most strains had a similar fitness in both backgrounds, similar outliers, with a positive GIS score were observed. Accordingly, 9 candidate genes, came out in the top 1 % (32 strains) with the highest positive GIS, in at least two comparisons (with *ura1*, *ura5*, *pot1* or ZU10), or in more than one of the SGA repeats, were short-listed for further testing (table 5.7). The strain in which loss of *tpx1* had the greatest effect on growth was *lys9*Δ; an average GIS position of 221 in $tpx1^{+}$ SGA, compared to 3067 in *tpx1*Δ SGA. These 9 candidate genes were short-listed for verification, as well as *txl1* as this had previously been reported to rescue the H_2O_2 resistance of $tpx1^{C169S}$ (Brown *et al.*, 2013).

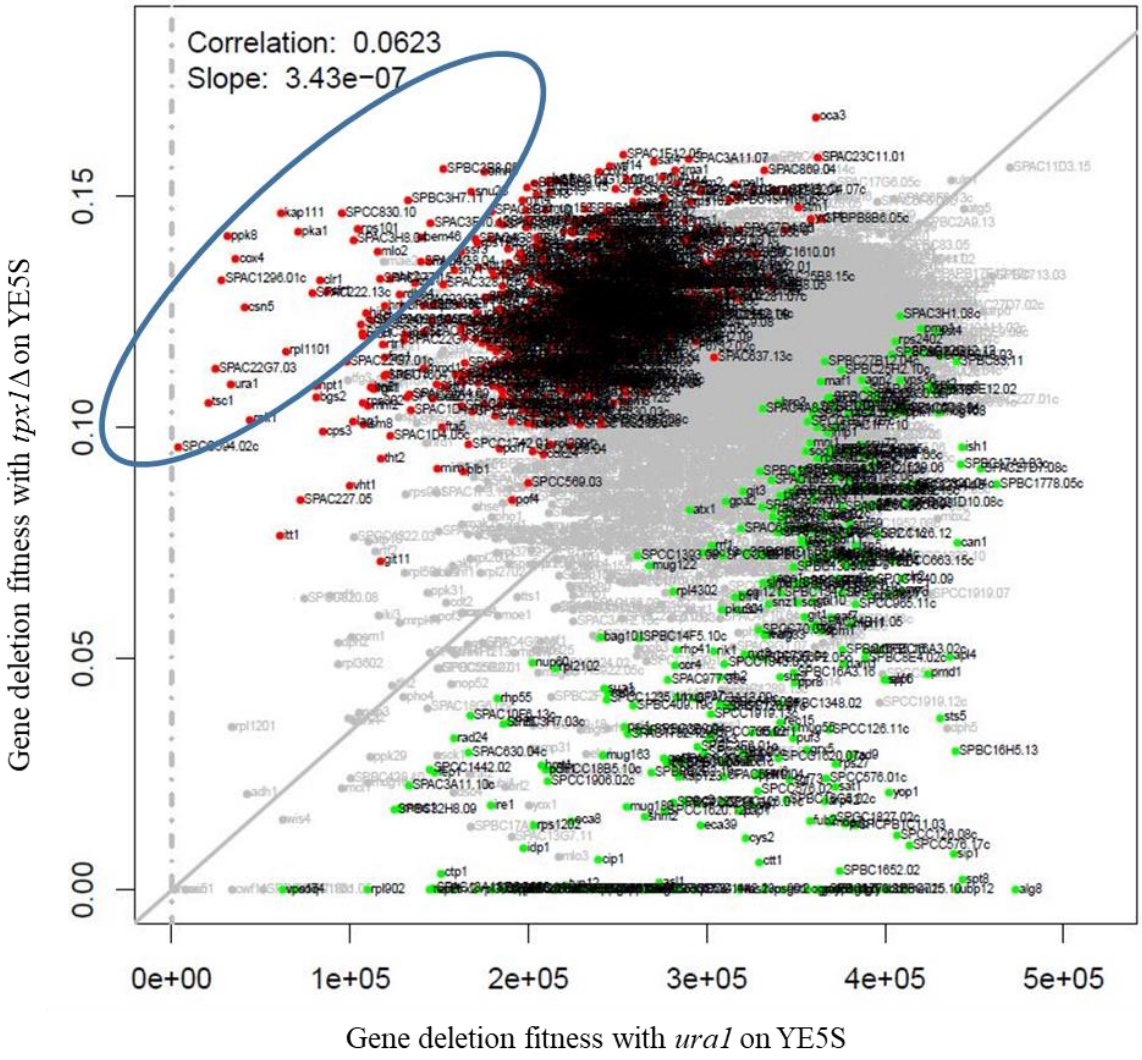

Figure 5.22 Fitness of the Bioneer deletion library crossed with the first *tpx1*Δ SGA (y-axis), compared to the fitness of the Bioneer deletion library crossed with the *tpx1*$^{+}$ wild-type strain *ura1* (x-axis). The blue circle represents gene mutants which have suppressed the growth defect of cells expressing *tpx1*Δ (hits with the highest positive GIS).

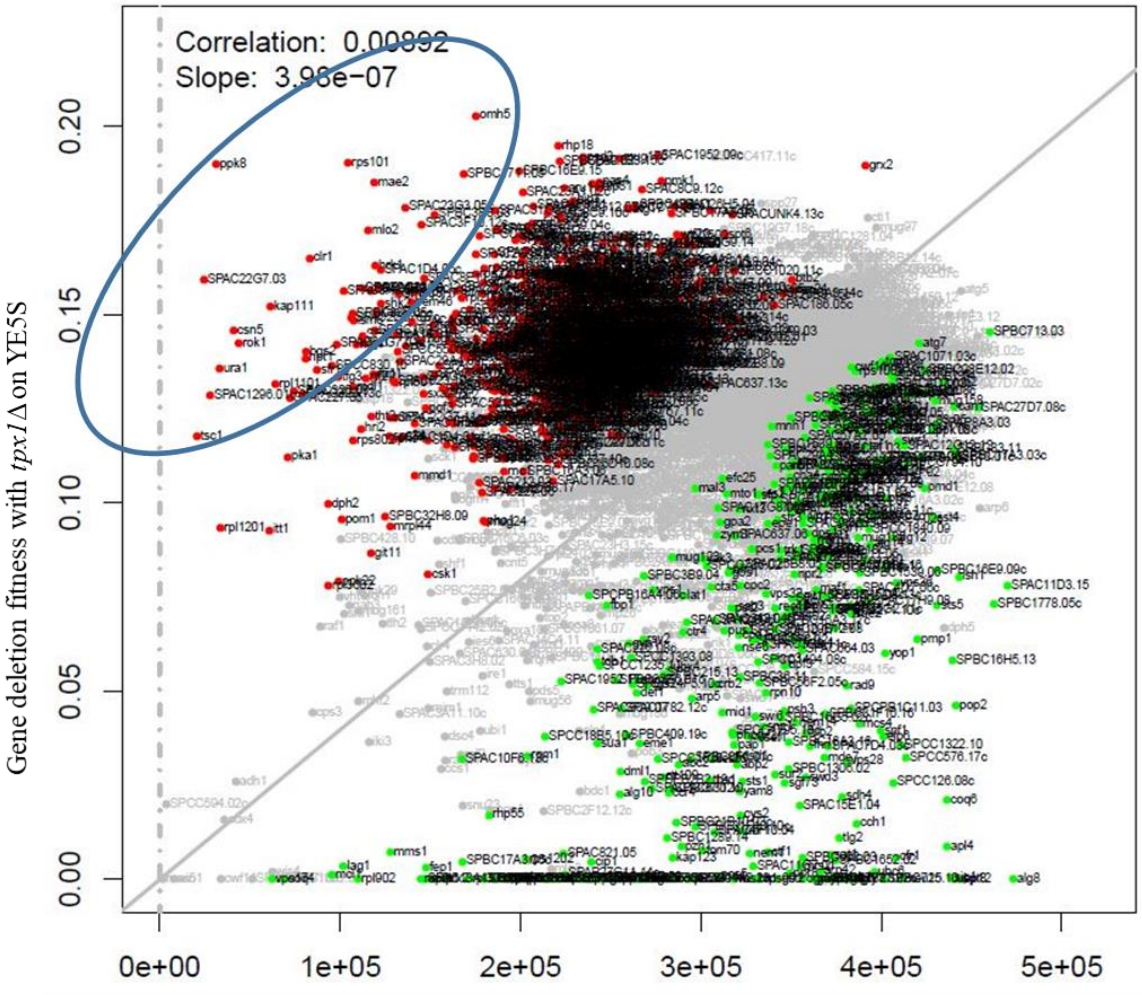

Figure 5.23 Fitness of the Bioneer deletion library crossed with the second *tpx1*Δ SGA (y-axis), compared to the fitness of the Bioneer deletion library crossed with the *tpx1*$^{+}$ wild-type strain *ura1* (x-axis). The blue circle represents gene mutants which have suppressed the growth defect of cells expressing *tpx1*Δ (hits with the highest positive GIS).

Gene Name	Human orthologue	Gene Description	Average SGA position with *tpx1*$^{+}$	Average SGA position with *tpx1*^{C169S}	Average SGA position with *tpx1*Δ
csn5	COPS5	COP9/signalosome complex subunit	1121	2517	3074
lys9	AASS	Saccharopine dehydrogenase	221	1539	3067
mlo2	UBR7	Ubiquitin protein ligase E3 component human N-recognin 7 homolog	308	561.5	3068
pmk1	MAPK7	MAP kinase	138	2236.5	2687
oca3	EMC2	TPR repeat protein	1101	1846.5	2031
pka1	PRKACG	cAMP-dependent protein kinase catalytic subunit	2434	459.5	3025.5
ssm4	CLIP2	Dynactin microtubule-binding subunit, p150-Glued	1865	2806.5	1144
aly1	-	Arrestin related	2527	2610	2487.5
SPAC1952.09c	-	Acetyl-CoA hydrolase	2269	2673.5	2895.5

Table 5.7 Gene names and descriptions of the 9 candidate genes which consistently suppressed the growth defect of *tpx1*Δ. The list of candidate genes which generated a high positive GIS in either *tpx1*Δ SGA repeat 1 and 2, or with more than wild-type *tpx1*$^{+}$ strain. The average GIS position of the gene from the *tpx1*Δ SGA is reported alongside the average GIS position with *tpx1*$^{+}$ and *tpx1*^{C169S}.

5.2.3.4 Ten of the double mutants generated from *tpx1*Δ SGA analyses suppressed the growth defect and H_2O_2 sensitivity of *tpx1*Δ

When spot test analysis was performed to assess the growth and H_2O_2 sensitivity of each of the SGA-generated strains bearing a candidate suppressing mutation (*csn5, lys9, mlo2, pmk1, oca3, pka1, ssm4, aly1, SPAC1952.09c or txl1*) (figure 5.24), the growth of all 10 strains was similar to wildtype. Moreover, although all 10 strains were inhibited by lower doses of H_2O_2 than the wildtype strain, their H_2O_2 resistance of these strains was much greater than that of the *tpx1*Δ strain.

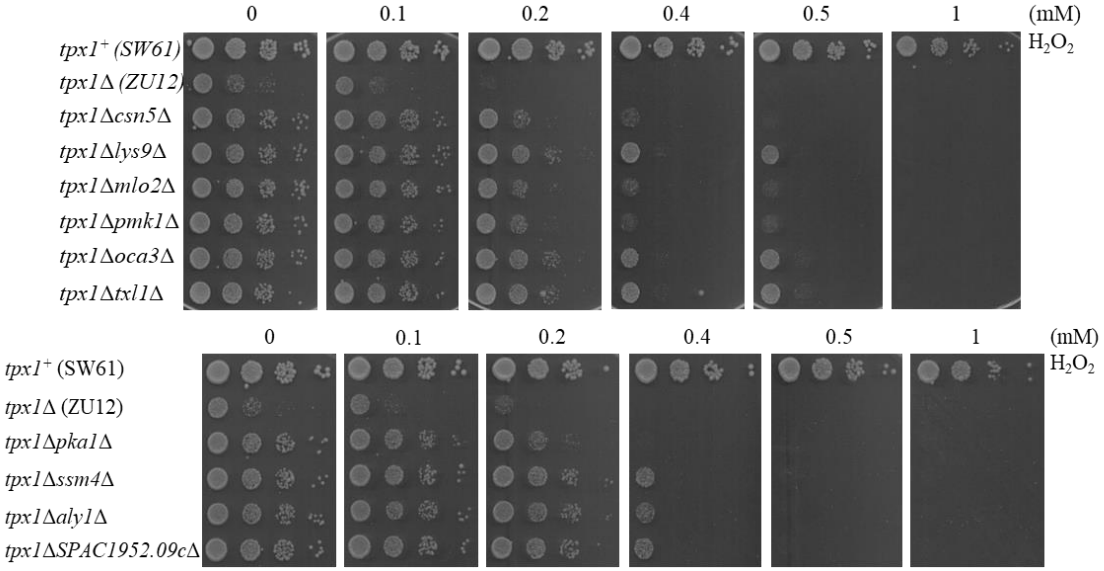

Figure 5.24 Spot test analysis of the 9 strains identified from the *tpx1*Δ SGA suppressor analysis. Growth of serially diluted exponentially growing *tpx1*$^+$ (ZU10), *tpx1*Δ (ZU12), and the following isolates from the screen: *tpx1*Δ*csn5*Δ, *tpx1*Δ*lys9*Δ, *tpx1*Δ*mlo2*Δ, *tpx1*Δ*pmk1*Δ, *tpx1*Δ*oca3*Δ, *tpx1*Δ*txl1*Δ, *tpx1*Δ*pka1*Δ, *tpx1*Δ*ssm4*Δ, *tpx1*Δ*aly1*Δ, *tpx1*Δ*SPAC1952.09c*Δ spotted onto plates containing the indicated concentrations of H_2O_2.

5.2.3.5 Deletion of five of the candidate genes suppressed the growth defect, and H_2O_2 sensitivity, of *tpx1*Δ when manually re-crossed

To validate the improvement of growth and H_2O_2 resistance, 7 of the candidate strains (*csn5*Δ, *lys9*Δ, *mlo2*Δ, *pmk1*Δ, *oca3*Δ, *pka1*Δ and *ssm4*Δ) were manually re-crossed with *tpx1*Δ (ZU12), and random spores generated (section 2.1.4). The double mutants generated were spotted onto different agar to compare growth with the Bioneer single mutant (e.g. *pmk1*Δ), and with the *tpx1*Δ (ZU12) starting strain (figure 5.25). Also spotted was a "*tpx1*Δ"; a NAT^r (but kanamycin-sensitive) colony formed from a mating and random sporulation protocol. Unexpectedly, this strain demonstrated growth similar to wild-type $tpx1^+$ strain. We therefore speculated that this strain may have recombined to express $tpx1^+$, but retain the nat(MX6) cassette.

Five (*tpx1*Δ*pmk1*Δ, *tpx1*Δ*pka1*Δ, *tpx1*Δ*ssm4*Δ, *tpx1*Δ*lys9*Δ and *tpx1*Δ*csn5*Δ) of the 7 re-crossed strains demonstrated improved growth on YE5S and EMM compared with *tpx1*Δ (ZU12). Strains were also spotted onto 3 % glycerol agar where 3 of the strains (*tpx1*Δ*ssm4*Δ, *tpx1*Δ*lys9*Δ and *tpx1*Δ*csn5*Δ) had improved growth compared with *tpx1*Δ (ZU12). This indicated that deletion of *ssm4*, *lys9* and *csn5* may have improved mitochondrial respiration of *tpx1*Δ.

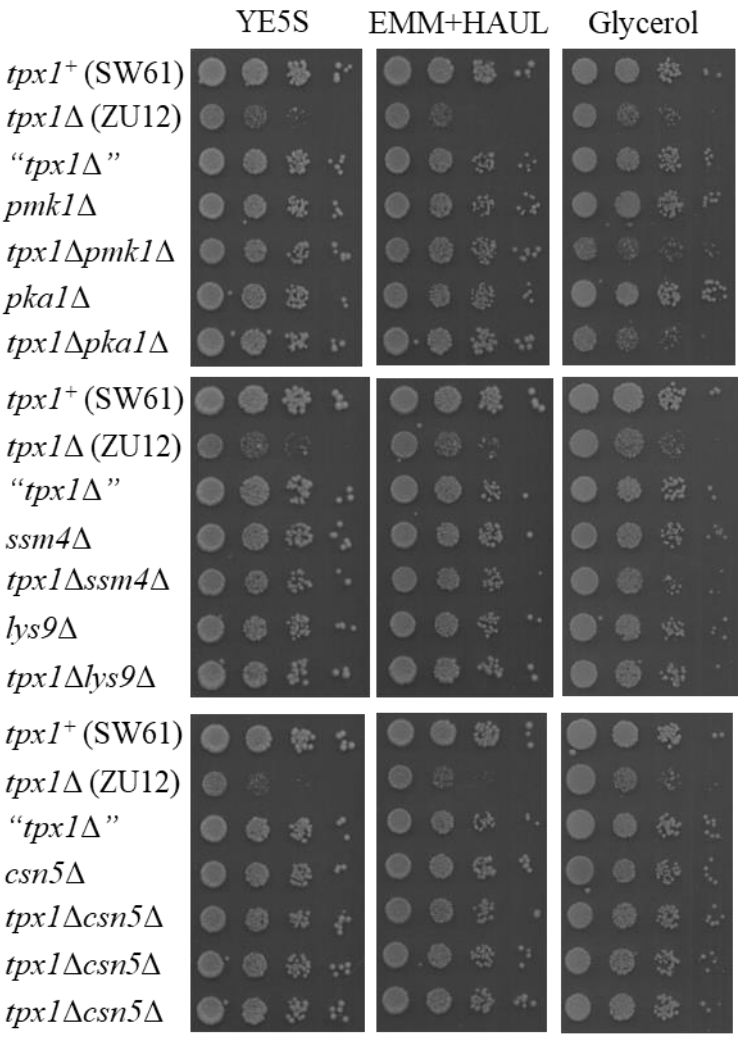

Figure 5.25 Spot test analysis of the 5 re-crossed suppressor strains to compare growth. The Bioneer single mutant strains (e.g. *pmk1*Δ) were re-crossed with the *tpx1*Δ (ZU12) to generate double mutant strains (e.g. *tpx1*Δ*pmk1*Δ). Serially diluted exponentially growing *tpx1*$^{+}$ (SW61), *tpx1*Δ (ZU12), "*tpx1*Δ", *pmk1*Δ, *tpx1*Δ*pmk1*Δ, *pka1*Δ, *tpx1*Δ*pka1*Δ, *ssm4*Δ, *tpx1*Δ*ssm4*Δ, *lys9*Δ, *tpx1*Δ*lys9*Δ, *csn5*Δ, *tpx1*Δ*csn5*Δ were spotted onto YE5S, EMM and 3 % glycerol plates.

Strains were also spotted onto YE5S agar containing a range of concentrations of H_2O_2 (figure 5.26). This revealed that *tpx1*Δ*ssm4*Δ, *tpx1*Δ*lys9*Δ and *tpx1*Δ*csn5*Δ had restored H_2O_2 resistance to wild-type H_2O_2 levels (up to 1 mM). The *tpx1*Δ*pmk1*Δ strain had increased H_2O_2 resistance compared to *tpx1*Δ, however started to become sensitive at around 1 mM, a concentration that was too low to inhibit the growth of *pmk1*Δ cells. Similar observations were made for the *tpx1*Δ*pka1*Δ strain although the single mutant *pka1*Δ strain was also more sensitive at 1 mM H_2O_2 than wild-type *S. pombe*.

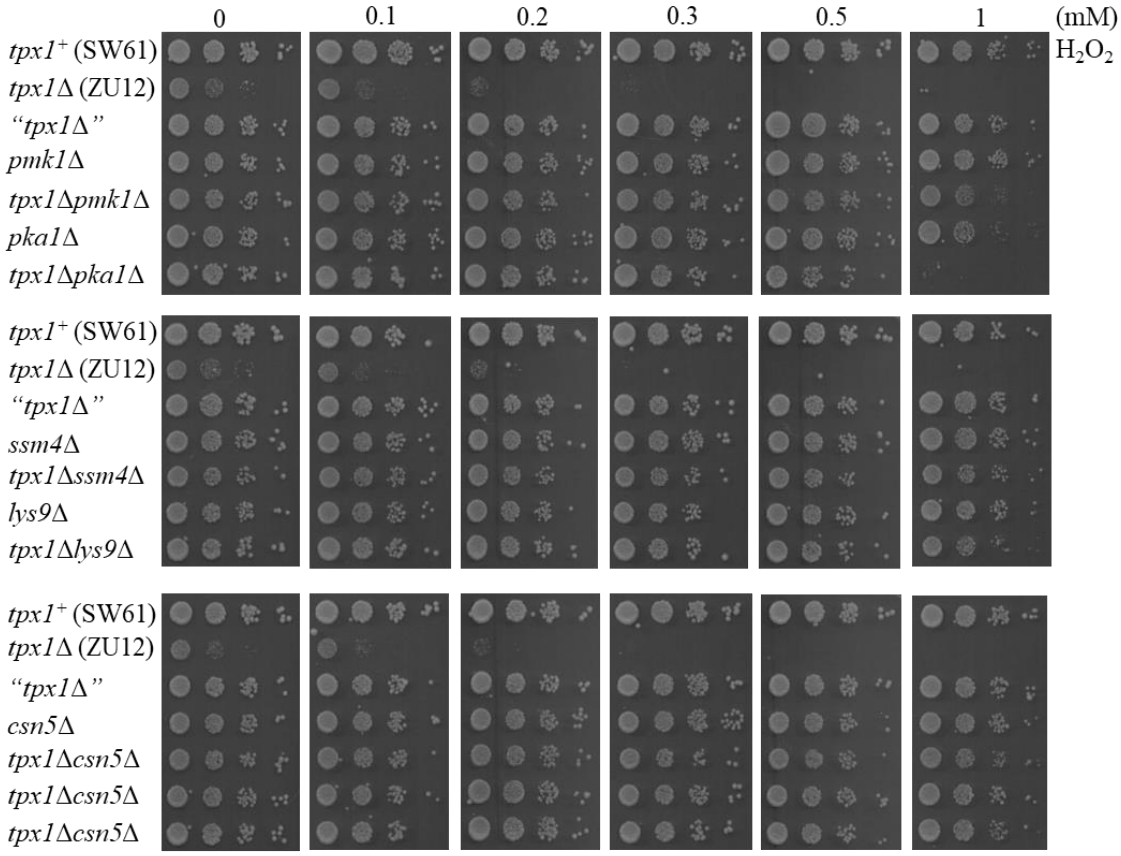

Figure 5.26 Spot test analysis of the 5 re-crossed suppressor strains to compare H_2O_2 resistance. The Bioneer single mutant strains (e.g. *pmk1*Δ) were re-crossed with the *tpx1*Δ (ZU12) to generate double mutant strains (e.g. *tpx1*Δ*pmk1*Δ). Serially diluted exponentially growing *tpx1*$^+$ (SW61), *tpx1*Δ (ZU12), "*tpx1*Δ", *pmk1*Δ, *tpx1*Δ*pmk1*Δ, *pka1*Δ, *tpx1*Δ*pka1*Δ, *ssm4*Δ, *tpx1*Δ*ssm4*Δ, *lys9*Δ, *tpx1*Δ*lys9*Δ, *csn5*Δ, *tpx1*Δ*csn5*Δ were spotted onto YE5S plates containing the indicated concentrations of H_2O_2.

5.2.4 Investigating whether Pka1 is regulated by H_2O_2/Tpx1

The *pka1* candidate gene was chosen for further work, as the partial rescue in resistance of *tpx1*Δ*pka1*Δ to 1 mM H_2O_2, indicated that this improvement in growth in the presence of H_2O_2 was not due to a recombination event to gain a *tpx1*$^+$. *pka1* encodes the single cAMP-dependent protein kinase catalytic subunit. Moreover, previous work identified that Pka1 co-immunopurified with Tpx1 dependent on the presence of the peroxidatic cysteine in Tpx1 (Latimer thesis, 2017). This raised the possibility that Tpx1 might form disulphide complexes with Pka1.

5.2.4.1 Investigating the genetic interaction of *tpx1* and *pka1*

The *tpx1*Δ (ZU12) strain was re-crossed with *pka1*Δ (Bioneer). 26 of the tetrads generated were manually dissected, and the spores that formed were patched onto selection plates to determine genotype (table 5.8). Spores that did not form a visible colony were viewed under a microscope and the number of cell divisions, or ungerminated spores, recorded. From this analysis it was revealed that only 43 % of spores formed visible colonies. Indeed, the lab has previously encountered difficulty in crossing the *tpx1*Δ strain. The frequency of double mutants generated (*tpx1*Δ*pka1*Δ) was 27.6 %. Of the 52 spores expected to be *tpx1*Δ, only 9 grew (17.3 %): 8 were *tpx1*Δ*pka1*Δ and 1 was *tpx1*Δ*pka1*$^+$. This data indicated that deleting *pka1* in a *tpx1*Δ improved cell viability. Indeed, deletion of *pka1* has previously been reported increase mating efficiency, increase sporulation frequency and increase viability in stationary phase (Kim *et al.*, 2014; Fujita and Yamamoto, 1998; Maeda *et al.*, 1994; Gupta et al., 2011a).

	Genotype of spores:			
Tetrad no.	1	2	3	4
1	2 cells	4 cells	*tpx1⁺pka1Δ*	*tpx1⁺pka1⁺*
2	4 cells	-	*tpx1⁺pka1⁺*	*tpx1⁺pka1Δ*
3	4 cells	*tpx1Δpka1Δ*	4 cells	*tpx1⁺pka1⁺*
4	*tpx1⁺pka1⁺*	4 cells	-	-
5	-	*tpx1⁺pka1Δ*	-	-
6	*tpx1Δpka1Δ*	*tpx1⁺pka1⁺*	*tpx1⁺pka1⁺*	-
7	*tpx1⁺pka1⁺*	-	6 cells	*tpx1Δpka1Δ*
8	*tpx1⁺pka1Δ*	4 cells	-	*tpx1⁺pka1⁺*
9	*tpx1⁺pka1⁺*	*tpx1⁺pka1⁺*	-	-
10	*tpx1⁺pka1Δ*	*tpx1⁺pka1⁺*	8 cells	*tpx1Δpka1Δ*
11	*tpx1⁺pka1⁺*	-	-	-
12	*tpx1⁺pka1Δ*	-	-	-
13	4 cells	*tpx1⁺pka1Δ*	-	-
14	*tpx1⁺pka1⁺*	-	-	-
15	*tpx1⁺pka1⁺*	-	*tpx1⁺pka1⁺*	-
16	*tpx1⁺pka1Δ*	*tpx1⁺pka1⁺*	*tpx1Δpka1Δ*	5 cells
17	*tpx1Δpka1Δ*	8 cells	*tpx1⁺pka1Δ*	*tpx1⁺pka1⁺*
18	6 cells	*tpx1⁺pka1Δ*	-	5 cells
19	*tpx1⁺pka1⁺*	-	-	-
20	4 cells	*tpx1⁺pka1⁺*	*tpx1⁺pka1Δ*	*tpx1Δpka1Δ*
21	-	*tpx1⁺pka1⁺*	2 cells	*tpx1Δpka1Δ*
22	*tpx1⁺pka1Δ*	5 cells	-	4 cells
23	-	3 cells	*tpx1⁺pka1Δ*	8 cells
24	*tpx1⁺pka1Δ*	-	-	-
25	*tpx1Δpka1⁺*	-	-	-
26	*tpx1⁺pka1Δ*	2 cells	4 cells	*tpx1⁺pka1⁺*

Table 5.8 Genotype analysis of 26 tetrads generated from re-crossing *tpx1*Δ (ZU12) with *pka1*Δ (Bioneer). Following dissection, spores that formed colonies were patched onto selection plates to determine genotype: wild-type *tpx1⁺pka1⁺* in green, single mutants *tpx1⁺pka1*Δ in orange, *tpx1*Δ*pka1⁺* in red and double mutants *tpx1*Δ*pka1*Δ in yellow. Spores which didn't grow to colony sizes were viewed under a microscope and cells which had stopped dividing were counted. The '-' indicates an ungerminated spore.

To assess whether the *tpx1*Δ*pka1*Δ strains had improved growth compared to *tpx1*Δ; 3 of the *tpx1*Δ*pka1*Δ mutants generated (ZU72, ZU73, ZU74) were assessed by conducting growth curves and spot tests onto different agar plates (figure 5.27). The three *tpx1*Δ*pka1*Δ strains grew at a similar rate, and had the slowest growth in liquid culture compared with all other strains (figure 5.27A). The two *tpx1*Δ strains (ZU12 and the isogenic *tpx1*Δ*pka1*$^{+}$) had a similar growth rate to each other, and slightly improved growth compared to *tpx1*Δ*pka1*Δ. As expected, the 3 strains expressing wild-type *tpx1*$^{+}$ grew the fastest in 6 h (ZU10, isogenic *tpx1*$^{+}$*pka1*$^{+}$ and isogenic *tpx1*$^{+}$*pka1*Δ). When spotted onto different agar (figure 5.27B), the 3 *tpx1*$^{+}$ strains still exhibited high growth rate on all media, with the *tpx1*Δ (ZU12) and *tpx1*Δ*pka1*$^{+}$ strains showing restricted growth on YE5S, EMM and glycerol in comparison. Unexpectedly, the 3 *tpx1*Δ*pka1*Δ strains did not share the same phenotype. Two of the *tpx1*Δ*pka1*Δ strains (ZU72, ZU74) had restricted growth on YE5S, EMM and glycerol, more so than the *tpx1*Δ strains. However, one of the *tpx1*Δ*pka1*Δ strains (ZU73) had improved growth, almost to wild-type *tpx1*$^{+}$ levels on all agar.

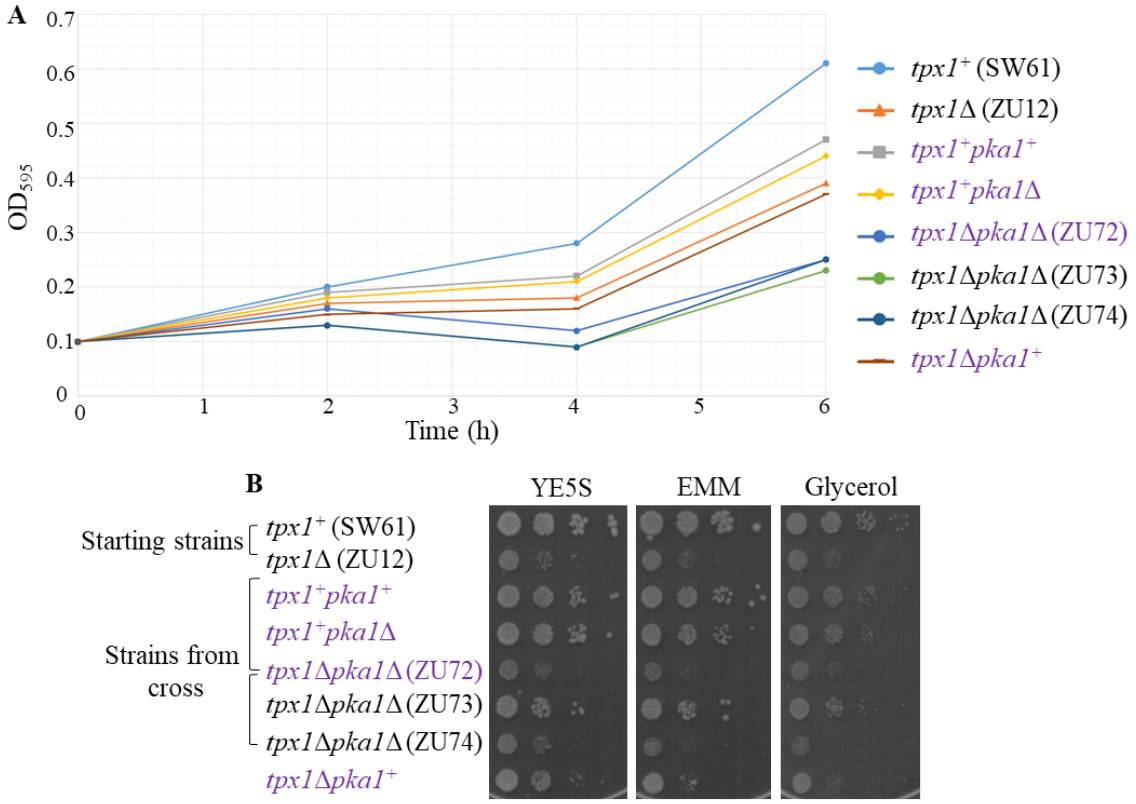

Figure 5.27 Growth curve [A] and spot test [B] analysis of isogenic strains (tetrad in purple) generated from manually crossing *tpx1*Δ (ZU12) with *pka1*Δ. [A] Growth curve analysis of isogenic strains *tpx1*$^{+}$*pka1*$^{+}$, *tpx1*$^{+}$*pka1*Δ, *tpx1*Δ*pka1*$^{+}$ and multiple *tpx1*Δ*pka1*Δ (ZU72, ZU73, ZU74), and starting strains *tpx1*$^{+}$ (SW61) and *tpx1*Δ (ZU12). Overnight YE5S cultures were diluted to OD_{595} = 0.1, and cells were incubated at 30 °C with agitation; the OD_{595} was measured every 2 h for 6 h. [B] Spot test analysis of isogenic strains and starting strains on different agar. Exponentially growing cells were spotted onto YE5S, EMM or 3 % glycerol agar plates to assess growth. The figure shown is of the YE5S plate scanned after incubation at 30 °C 72 h, and the EMM and glycerol plates scanned after 120 h.

A similar finding was observed when spotting strains onto agar containing different concentrations of H_2O_2 (figure 5.28A). Strains expressing wild-type *tpx1*$^+$ had unrestricted growth up to 1 mM H_2O_2, whereas the growth of the two single mutant *tpx1*Δ strains (ZU12 and isogenic *tpx1*Δ*pka1*$^+$) was inhibited in the presence of 0.1 mM H_2O_2. Two of the *tpx1*Δ*pka1*Δ strains (ZU72 and ZU74) exhibited similar sensitivity to H_2O_2 as the two single mutant *tpx1*Δ strains. However, the *tpx1*Δ*pka1*Δ (ZU73) strain displayed partial rescue of H_2O_2 resistance up to 0.5 mM H_2O_2.

To investigate further, all 8 of the *tpx1*Δ*pka1*Δ strains generated were patched onto rich agar with and without 1 mM H_2O_2 (figure 5.28B). Only 1 of the 8 strains grew in the presence of 1 mM H_2O_2; ZU73 – the same strain that displayed partially rescued H_2O_2 resistance by spot test. As 7 of the *tpx1*Δ*pka1*Δ strains displayed sensitivity to H_2O_2 similar to the *tpx1*Δ strains it seems probable that the ZU73 strain may have acquired another, unidentified, mutation that is responsible for its increased H_2O_2 resistance, rather than loss of *pka1*. From this we conclude that, although loss of *pka1* increases the ability of *tpx1* mutant spores to germinate and form a colony, loss of *pka1* does not rescue the growth or H_2O_2-sensivity of *tpx1*Δ mutant.

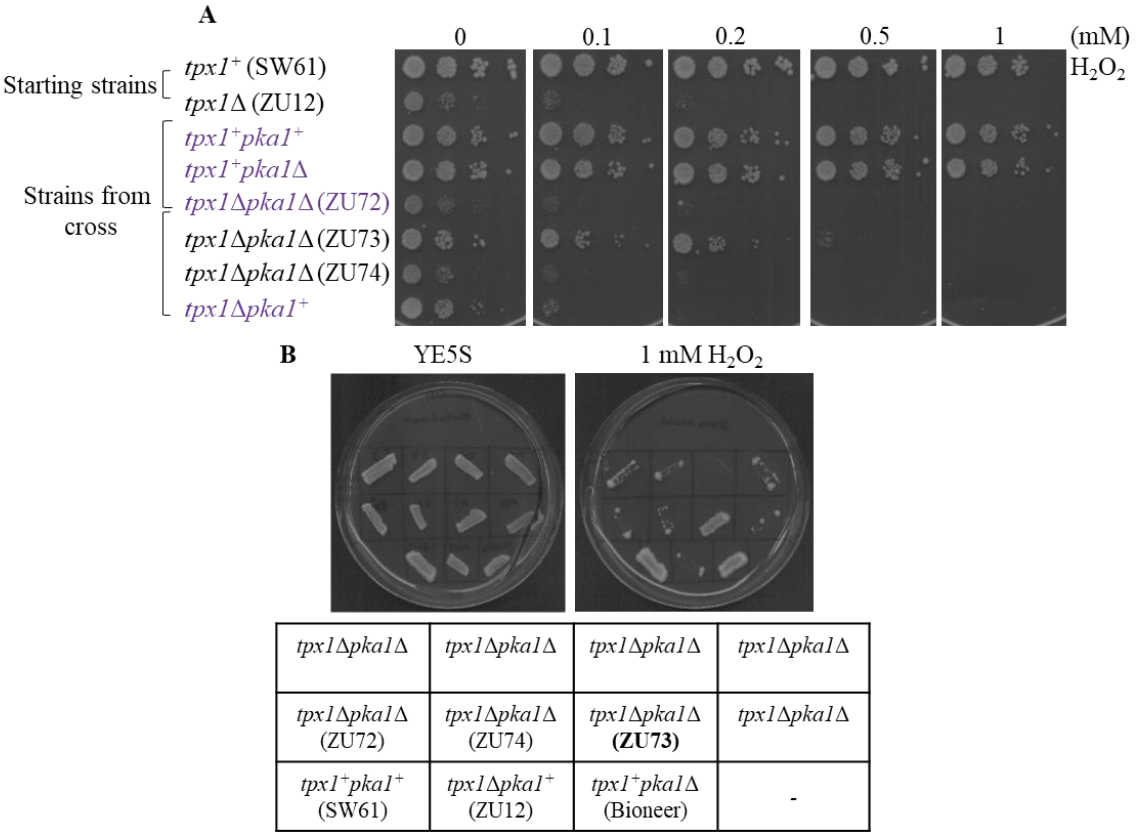

*tpx1*Δ*pka1*Δ	*tpx1*Δ*pka1*Δ	*tpx1*Δ*pka1*Δ	*tpx1*Δ*pka1*Δ
*tpx1*Δ*pka1*Δ (ZU72)	*tpx1*Δ*pka1*Δ (ZU74)	*tpx1*Δ*pka1*Δ **(ZU73)**	*tpx1*Δ*pka1*Δ
tpx1$^+$*pka1*$^+$ (SW61)	*tpx1*Δ*pka1*$^+$ (ZU12)	*tpx1*$^+$*pka1*Δ (Bioneer)	-

Figure 5.28 Analysis of H_2O_2 resistance of isogenic strains generated from manually crossing *tpx1*Δ (ZU12) with *pka1*Δ (Bioneer). [A] Spot test analysis of isogenic strains, and starting strains, in the presence of different concentrations of H_2O_2. Exponentially growing isogenic strains (tetrad in purple) *tpx1*$^+$*pka1*$^+$, *tpx1*$^+$*pka1*Δ, *tpx1*Δ*pka1*$^+$ and multiple *tpx1*Δ*pka1*Δ (ZU72, ZU73, ZU74) strains, and the starting strains *tpx1*$^+$ (SW61) and *tpx1*Δ (ZU12) were spotted onto YE5S containing the indicated concentrations of H_2O_2, and were scanned after 72 h at 30 °C. **[B] Patch test analysis of all 8 *tpx1*Δ*pka1*Δ strains to determine typical resistance to 1 mM H_2O_2.** All 8 *tpx1*Δ*pka1*Δ strains (including ZU72, ZU73 and ZU74) generated from the cross of *tpx1*Δ (ZU12) with *pka1*Δ (Bioneer), were patched onto YE5S plates with or without 1mM H_2O_2 to assess the differences in H_2O_2 resistance between strains.

5.2.4.2 Investigating whether Pka1 undergoes oxidation in response to 0.2 mM H_2O_2, and whether this is via interaction with Tpx1

As Pka1 had a genetic interaction with Tpx1, and had previously been identified as a potential $Tpx1^{C169S}$ interacting protein (Latimer thesis, 2017), we set out to investigate whether Pka1 underwent oxidation in response H_2O_2. Cells expressing Myc-tagged Pka1 were treated with 0.2 mM H_2O_2 and assessed by western blot (figure 5.29). A band corresponding to Myc-tagged Pka1 (that was not present in the $Pka1^+$ lanes) was observed ~90 kDa (figure 5.29A). This band exhibited a shift in mobility following treatment with AMS. AMS reacts with reduced protein thiols resulting in protein-AMS adducts which increases the mass by ~0.5 kDa (Rudyk and Eaton, 2014). Pka1 expresses 7 cysteine residues, therefore a shift in mobility of ~3.5 kDa may be expected. Interestingly, levels of Myc-tagged Pka1 appear reduced following exposure to 0.2 mM H_2O_2. A longer exposure of the western blot reveals high molecular weight (HMW) complexes that are not present in the Pka^+ lanes (figure 5.29B). This reveals Myc-tagged Pka1 undergoing modification, or forming complexes with other proteins and may explain the differences in levels of Myc-tagged Pka1 observed ~90 kDa.

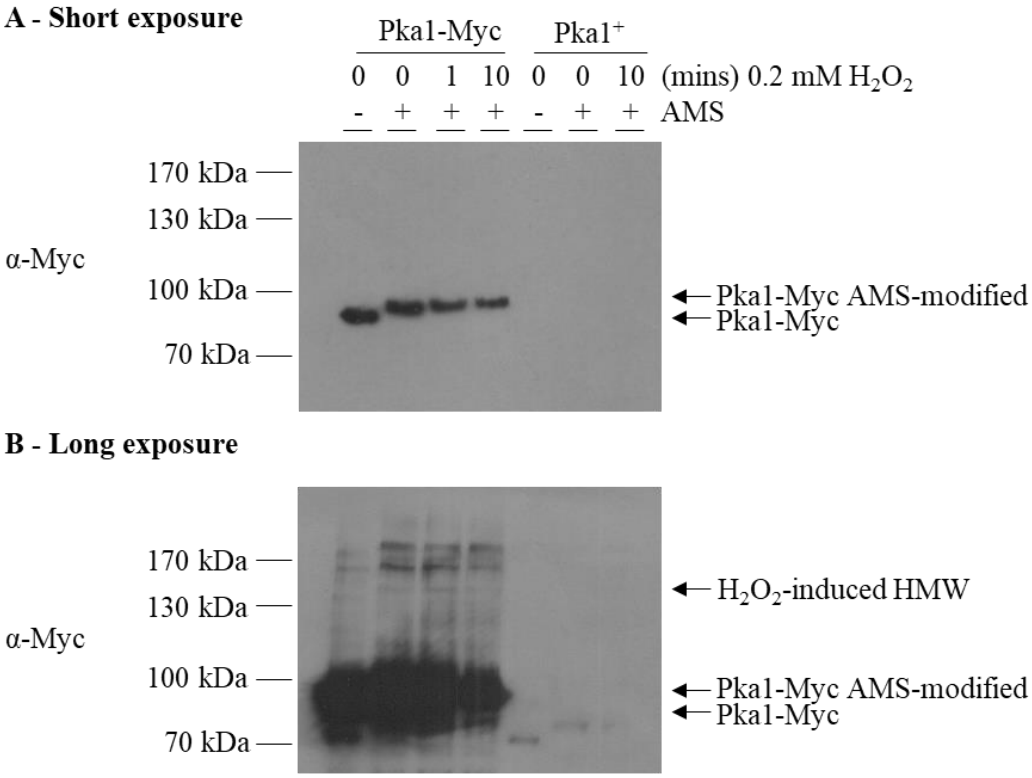

Figure 5.29 H_2O_2 does not affect the mobility of Myc-tagged Pka1. Western blot analysis ([A] short exposure, [B] long exposure) of Pka1-Myc (DRG21) or Pka1$^+$ (SP870) isolated from cells before or after exposure to 0.2 mM H_2O_2 and treated with AMS, as indicated. Anti-Myc antibody was used to detect Myc-tagged Pka1.

Next, we investigated whether the formation of the HMW bands of Pka1 in response to 0.2 mM H_2O_2, were affected by the overexpression of Tpx1, or $Tpx1^{C169S}$ (as indicated by previous mass spectrometry analysis (Latimer thesis, 2017). Myc-tagged Pka1 cells were transformed with expression vectors Rep1, Rep1Tpx1 or $Rep1Tpx1^{C169S}$, treated with 0.2 mM H_2O_2 and assessed by western blot (figure 5.30). A low level of HMW bands ~170 kDa were observed in cells expressing endogenous levels of Pka1 and Tpx1 (Pka1-Myc + Rep1), as observed previously (figure 5.29). The overexpression of Tpx1 (Pka1-Myc + Rep1Tpx1) revealed clear HMW H_2O_2-induced complexes (~130 kDa and ~170 kDa). These HMW H_2O_2-induced bands were observed more intensely and at a higher frequency in cells overexpressing the trapping mutant $Tpx1^{C169S}$ (Pka1-Myc + $Rep1Tpx1^{C169S}$) in response to 0.2 mM H_2O_2 for 1 min, and were more intense following incubation for 10 mins. All high molecular weight bands disappeared with the addition of β-mercaptoethanol; which reduces disulphide bonds.

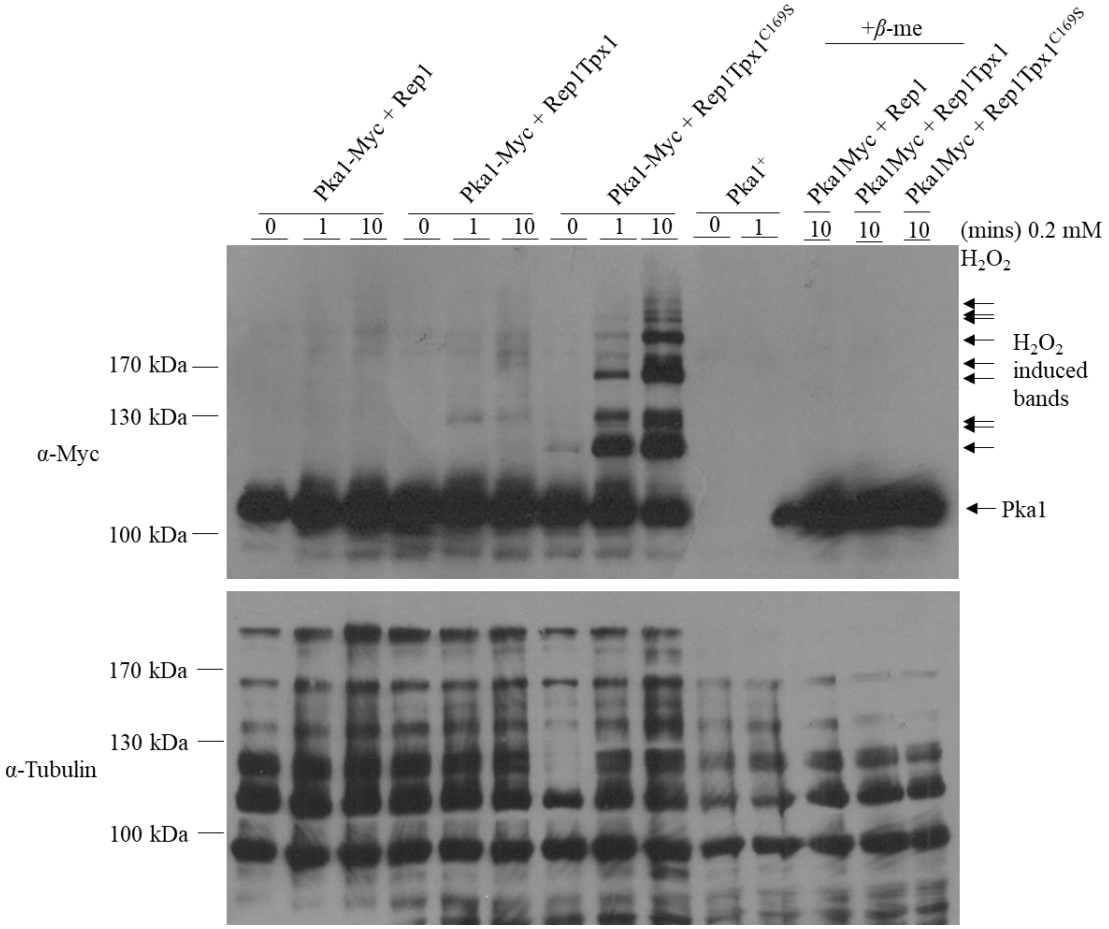

Figure 5.30 Overexpression of Tpx1, or the trapping mutant Tpx1^{C169S}, promoted H_2O_2 induced oxidation of Pka1. Western blot analysis of Pka1 (SP870), or Myc-tagged Pka1 (DRG21) expressing Rep1, Rep1Tpx1 or Rep1Tpx1^{C169S} isolated from cells following treatment with 0.2 mM H_2O_2 for 0, 1 or 10 mins. Anti-Myc and anti-Tubulin antibodies were used. Myc-tagged Pka1 samples were run with or without β-mercaptoethanol.

To investigate whether any of the Pka1 HMW complexes contain Tpx1; cells expressing Myc-tagged Pka1 were also transformed with the expression vector Rep1FlagTpx1^{C169S}. Cells were treated with H_2O_2 and analysed by western blot as previously (figure 5.31). Excitingly, when comparing the multiple H_2O_2-induced HMW bands observed in cells overexpressing the mutant Tpx1^{C169S}, with cells overexpressing the flag-epitope tagged Tpx1^{C169S}, a shift in mobility was observed. This change in mobility was consistent with the expected increase in MW likely to result from the presence of the Flag-epitope in the oxidised Pka1 forms that were detected. This result therefore provides evidence of a direct protein-protein interaction of at least Pka1 and Tpx1. This interaction occurred more frequently at the longer incubation time (10 mins) with H_2O_2. The larger high molecular weight complexes (≥ 170 kDa) could contain multiple Tpx1 proteins, or additional unidentified protein complexes.

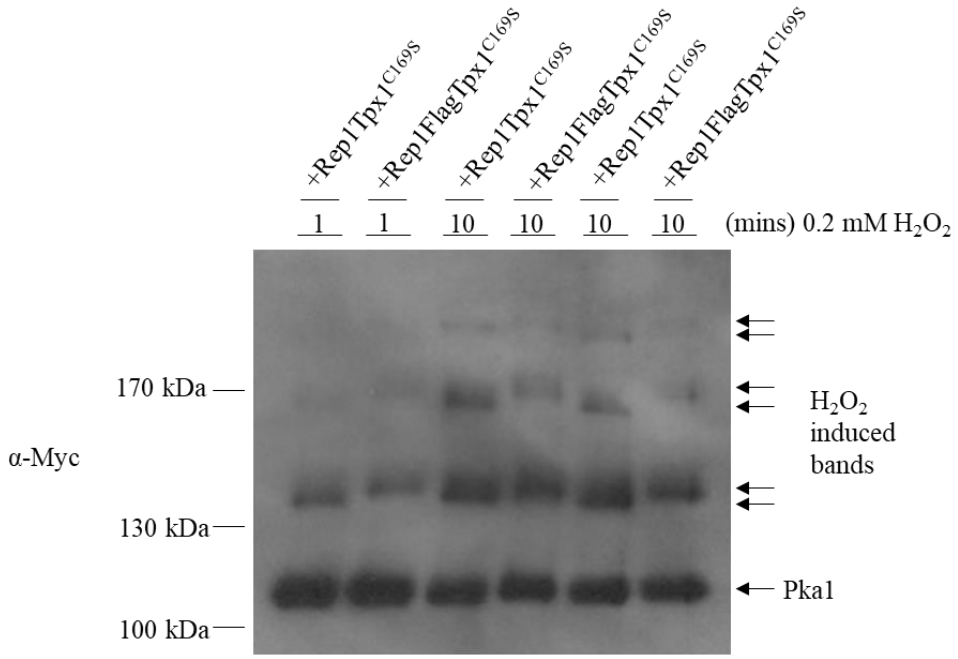

Figure 5.31 Pka1 forms a mixed disulphide with Tpx1 in response to 0.2 mM H_2O_2. Western blot analysis of Myc-tagged Pka1 (DRG21) expressing Rep1Tpx1^{C169S} or Rep1FlagTpx1^{C169S}, isolated from cells following treatment with 0.2 mM H_2O_2 for 1 or 10 mins. Anti-Myc antibody was used to detect Myc-tagged Pka1.

5.2.5 Investigating whether Csn5 is regulated by H_2O_2/Tpx1

When re-crossing and testing candidate genes identified by SGA analysis as suppressors of the *tpx1*Δ growth defect (section 5.2.3.5); three separate *tpx1*Δ*csn5*Δ strains had shown a consistent improvement in growth and H_2O_2 resistance compared to *tpx1*Δ (figure 5.25 and 5.26). Csn5 was therefore chosen as the second candidate gene to undergo further investigation. Csn5 is a COP9/signalosome complex protease subunit.

5.2.5.1 Investigating the genetic interaction of *csn5* and *tpx1*

To investigate whether deleting *csn5* affected the growth of a *tpx1*Δ*;* an independently generated (using a different strain background) *csn5*Δ (KS84) was crossed with *tpx1*Δ (VXOO), and underwent tetrad dissection to generate *tpx1*Δ*csn5*Δ (ZU57). The growth of the generated *tpx1*Δ*csn5*Δ was monitored in liquid for 5 h (figure 5.32A). The *tpx1*Δ*csn5*Δ exhibited faster growth in liquid than the *tpx1*Δ, almost to wild-type *tpx1*$^+$ growth. However, this would need repeating to a longer time point for confirmation.

The *tpx1*Δ*csn5*Δ strain was also spotted onto YE5S, EMM or glycerol agar alongside *tpx1*$^+$, *tpx1Δ* and *csn5*Δ strains (figure 5.32B). The glycerol agar differs to YE5S in that it is a non-fermentable carbon source and poor growth is indicative of a mitochondrial defect. When spotted onto YE5S or EMM agar, *tpx1*Δ*csn5*Δ had slightly improved growth compared to the *tpx1*Δ (ZU12). However, growth of the *tpx1*Δ*csn5*Δ was severely reduced on glycerol agar compared to *tpx1*Δ. This would indicate that deletion of *csn5* in a *tpx1*Δ worsens the already apparent mitochondrial defects experienced by the *tpx1*Δ strain (Latimer, Day, Brown and Veal, unpublished).

Exponentially growing cells were also spotted onto YE5S containing different concentrations of H_2O_2 in order to investigate H_2O_2 resistance (figure 5.32C). Excitingly, the *tpx1*Δ*csn5*Δ (ZU57) showed a partial increase in H_2O_2 resistance up to 0.1 mM H_2O_2, when compared to the *tpx1*Δ. From this we conclude that loss of *csn5* slightly rescued the growth and H_2O_2 resistance of *tpx1*Δ mutant.

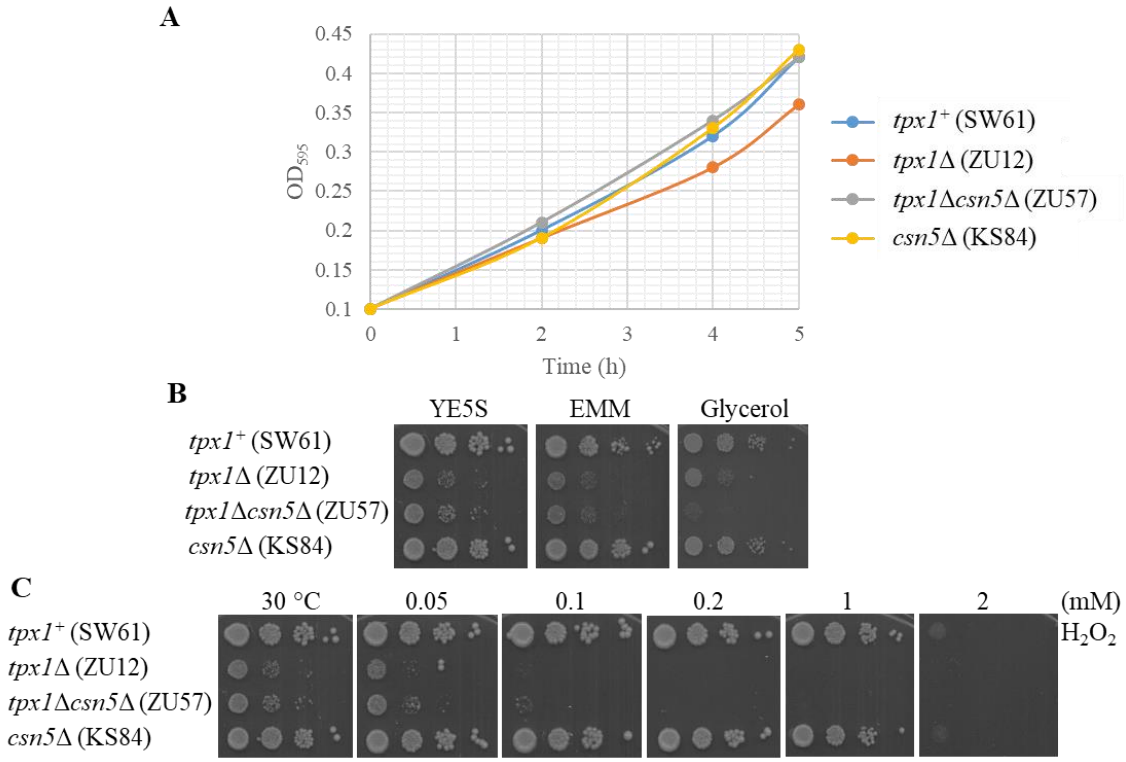

Figure 5.32 Growth curve [A] and spot test [B and C] analysis of strains revealed that deleting *csn5* in a *tpx1*Δ may slightly improve growth and H_2O_2 resistance. [A] Growth curve analysis of *tpx1*$^+$ (SW61), *tpx1*Δ (ZU12), *tpx1*Δ*csn5*Δ (ZU57) and *csn5*Δ (KS84) strains at 30 °C in YE5S for 5 h. Overnight YE5S cultures were diluted to OD_{595} = 0.1, and cells were incubated at 30 °C with agitation. [B] Exponentially growing *tpx1*$^+$ (SW61), *tpx1*Δ (ZU12), *tpx1*Δ*csn5*Δ (ZU57) and *csn5*Δ (KS84) cells were spotted onto YE5S, EMM or 3 % glycerol agar plates to assess growth. The YE5S plate was scanned after 3 days, the EMM and glycerol plates were scanned after 5 days. [C] Serially diluted exponentially growing *tpx1*$^+$ (SW61), *tpx1*Δ (ZU12), *tpx1*Δ*csn5*Δ (ZU57) and *csn5*Δ (KS84) cells were spotted onto YE5S containing the indicated concentrations of H_2O_2. Plates were scanned after 72 h incubation at 30 °C.

5.2.5.2 Investigating whether Csn5 undergoes oxidation in response to 0.2 mM H_2O_2, and whether this is via interaction with Tpx1

To investigate whether we could detect oxidised forms of Csn5 endogenously, or in response to H_2O_2; exponentially growing cells expressing Myc-tagged Csn5 were treated with 0.2 mM H_2O_2 and assessed by western blot (figure 5.33). A band corresponding to Myc-tagged Csn5 (that was not present in $Csn5^+$ lanes) was observed ~70 kDa. Csn5 expresses 5 cysteine residue; this band therefore exhibited a shift in mobility following AMS treatment. A number of HMW bands were detected, however, the majority were also present in the $Csn5^+$ lanes indicating that they were non-specific for Myc-tagged Csn5. Excitingly however, a HMW H_2O_2 induced band was detected ~150 kDa in only Myc-tagged Csn5 following exposure to 0.2 mM H_2O_2 for 1 min. This high molecular weight complex occurred at greater frequency following 10 mins exposure to 0.2 mM H_2O_2.

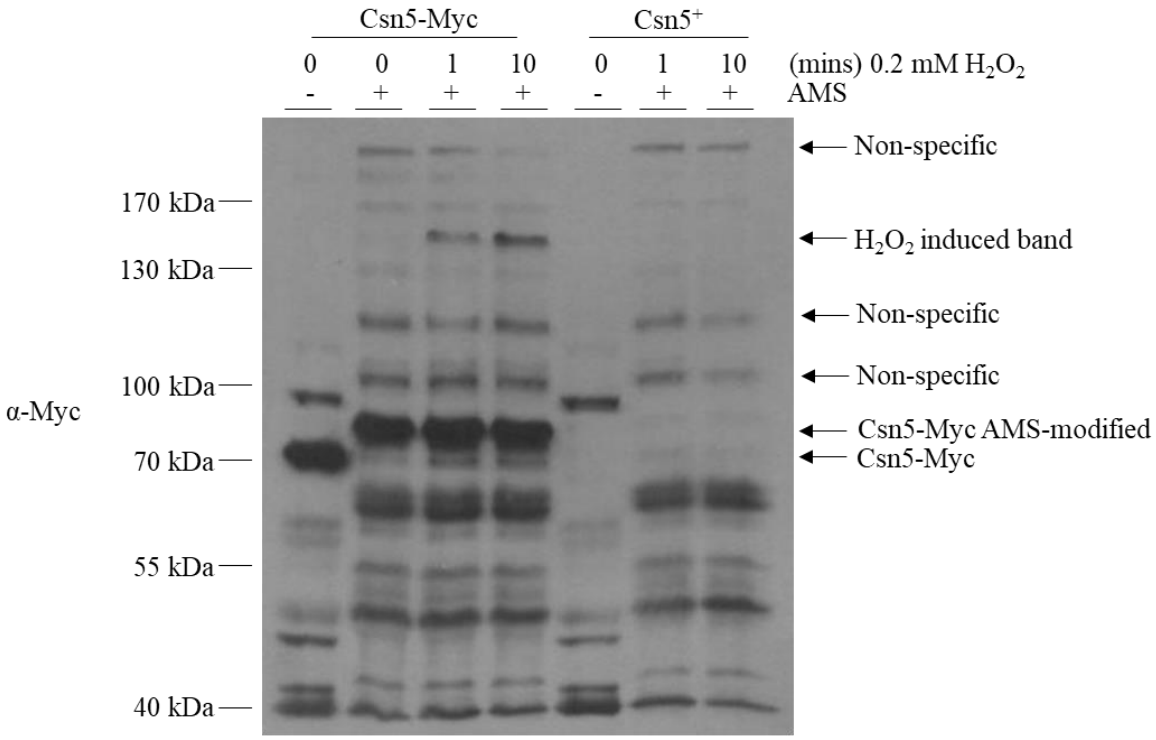

Figure 5.33 High molecular weight oxidised forms of endogenous Csn5 were detected following exposure to 0.2 mM H_2O_2. Western blot analysis of Myc-tagged Csn5 (AMC350) or $Csn5^+$ (NT4) isolated from cells before or after exposure to 0.2 mM H_2O_2 for 0, 1, or 10 mins, and treated with AMS as indicated. Anti-Myc antibody was used to detect Myc-tagged Csn5.

To investigate whether the formation of the H_2O_2-induced HMW band of Csn5 was affected by the overexpression of Tpx1, or Tpx1^{C169S}; Myc-tagged Csn5 cells were transformed with expression vectors Rep1, Rep1Tpx1 or Rep1Tpx1^{C169S}, treated with 0.2 mM H_2O_2 and assessed by western blot (figure 5.34). As observed previously (figure 5.33), a HMW H_2O_2-induced band was observed ~150 kDa in cells expressing endogenous levels of Tpx1 (Csn5-Myc + Rep1) following exposure to 0.2 mM H_2O_2 for 1 min. This HMW complex occurred more frequently following treatment with 0.2 mM H_2O_2 for 10 mins. This H_2O_2-induced band was also observed in cells overexpressing Tpx1 (Csn5-Myc + Rep1Tpx1) following exposure to 0.2 mM H_2O_2 for 1 min, and with greater frequency following 10 mins. When overexpressing the trapping mutant Tpx1^{C169S} (Csn5-Myc + Rep1Tpx1^{C169S}) multiple HMW H_2O_2-induced bands were observed following 1 min and 10 min exposure to 0.2 mM H_2O_2. These bands were not visible without H_2O_2 treatment, and disappeared following the addition of β-mercaptoethanol; which reduces disulphide bonds.

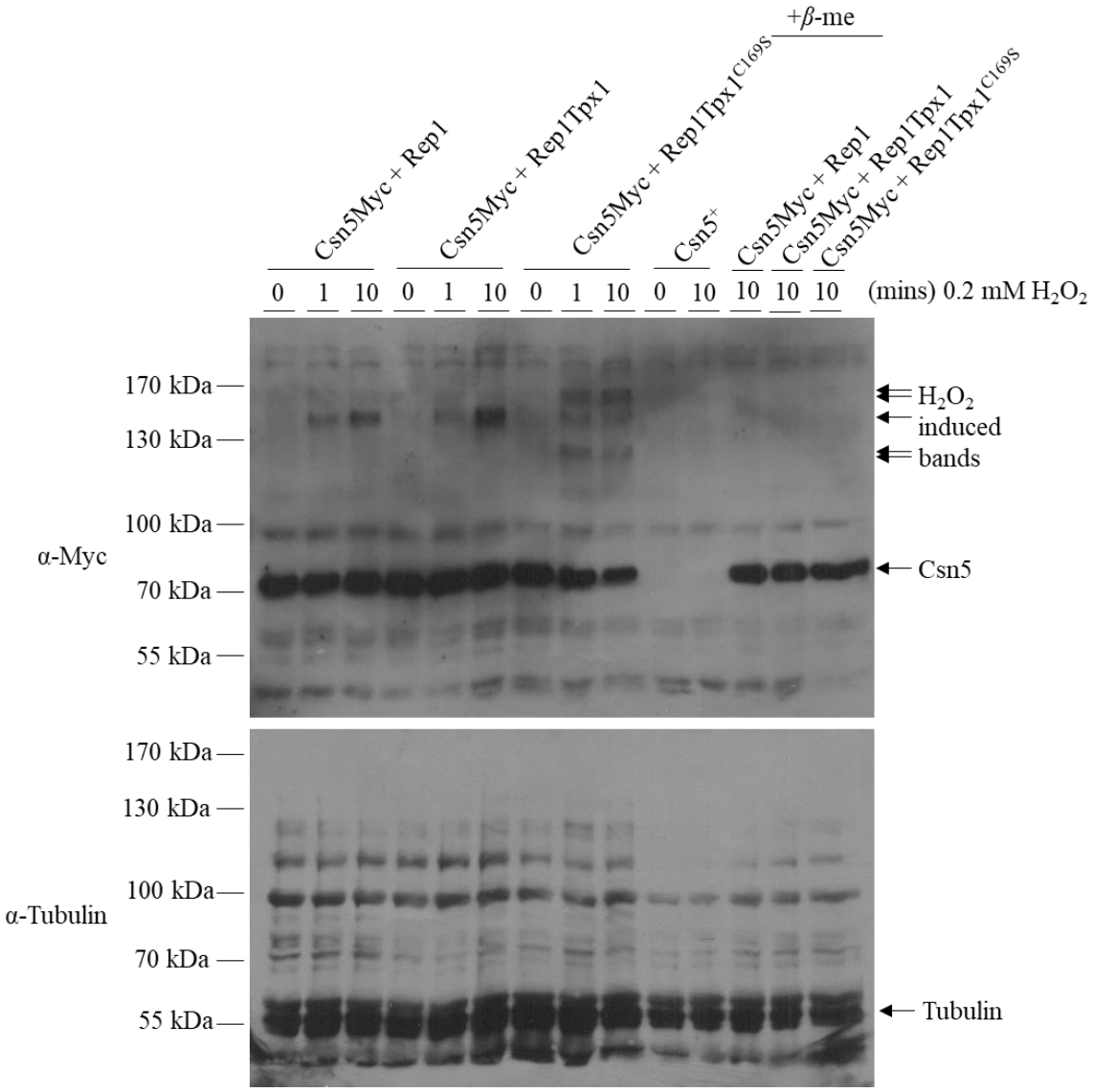

Figure 5.34 Overexpression of Tpx1, or the trapping mutant Tpx1^{C169S}, promoted H_2O_2 induced oxidation of Csn5. Western blot analysis of Csn5 (NT4), or Myc-tagged Csn5 (AMC350) expressing Rep1, Rep1Tpx1 or Rep1Tpx1^{C169S} isolated from cells following treatment with 0.2 mM H_2O_2 for 0, 1 or 10 mins. Anti-Myc and anti-Tubulin antibodies were used. Myc-tagged Csn5 samples were run with or without β-mercaptoethanol.

To establish whether any of the Csn5 HMW H_2O_2 induced complexes contained Tpx1; cells expressing Myc-tagged Csn5 were also transformed with the expression vector Rep1FlagTpx1 or Rep1FlagTpx1^{C169S}. Cells were treated with H_2O_2 and analysed by western blot (figure 5.35). Excitingly, when comparing the ~120 kDa or ~150 kDa H_2O_2-induced band observed in cells overexpressing the mutant Tpx1^{C169S}, with cells overexpressing the flag-epitope tagged Tpx1^{C169S}, a shift in mobility was observed. This change in mobility was consistent with the expected increase in MW likely to result from the presence of the Flag-epitope in the oxidised Csn5 forms that were detected. This result therefore provides evidence of a direct protein-protein interaction of at least Csn5 and Tpx1. It is not clear from this blot whether the other high molecular weight H_2O_2 induced bands observed in the trapping mutant in the previous blot (~170 kDa) exhibit a shift in mobility with the addition of a flag-tag. These larger HMW complexes ($\geq$ 170 kDa) could contain multiple Tpx1 proteins, or additional unidentified proteins.

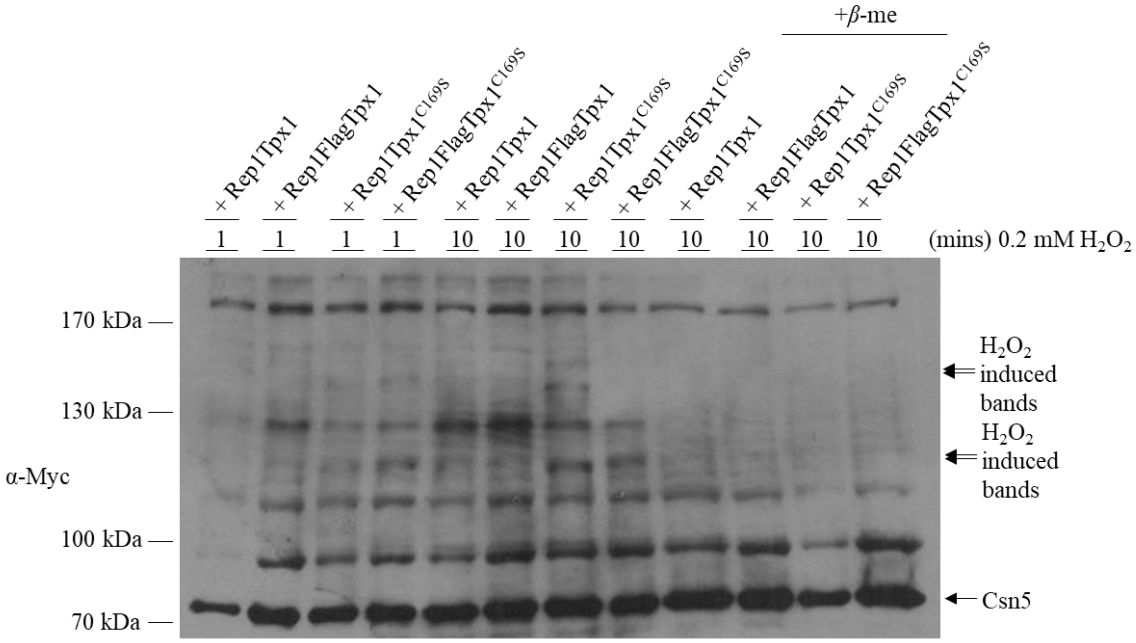

Figure 5.35 Csn5 forms a mixed disulphide with Tpx1 in response to 0.2 mM H_2O_2. Western blot analysis of cells expressing Myc-tagged Csn5 (AMC350) expressing Rep1Tpx1, Rep1FlagTpx1, Rep1Tpx1^{C169S} or Rep1FlagTpx1^{C169S}, isolated from cells following treatment with 0.2 mM H_2O_2 for 1 or 10 mins. Anti-Myc antibody was used to detect Myc-tagged Csn5.

S. pombe have 5 Csn (COP9/signalosome complex protease subunit) proteins: *csn1, csn2, csn3, cns4* and *csn5*. It is reported that cells have ~3000 copies of Csn5 per cell. In contrast, levels of Csn3 and Csn4 are non-detectable, whereas cells have 1547 copies of Csn2, and 834 copies of Csn1 (Marguerat *et al.*, 2012). In order to investigate whether other subunits of the COP9/signalosome complex (in addition to Csn5) are oxidised in response to H_2O_2; cells expressing Myc-tagged Csn1 were also transformed with expression vectors Rep1Tpx1 and Rep1Tpx1^{C169S}, treated with 0.2 mM H_2O_2, and assessed by western blot (figure 5.36). Myc-tagged Csn1 was detected ~100 kDa. No H_2O_2 induced HMW bands were detected following exposure to 0.2 mM H_2O_2 for 1 or 10 mins. Therefore Csn5 may be the only subunit of the COP9/signalosome complex protease that undergoes oxidation by Tpx1 in response to H_2O_2 to exert an effect on cell growth and H_2O_2 resistance.

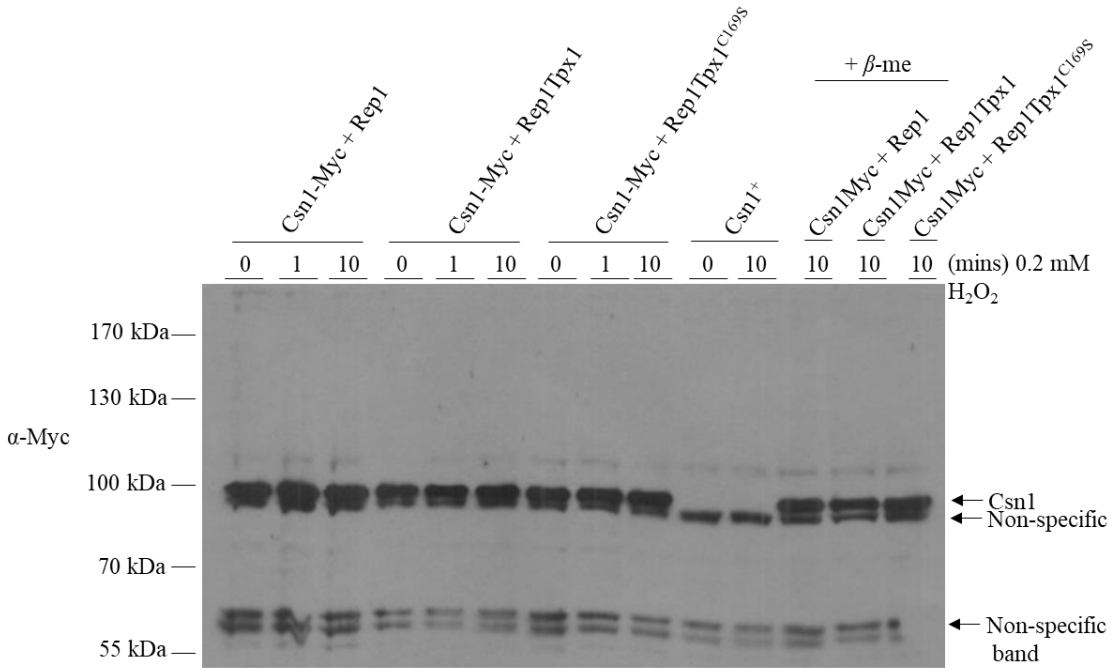

Figure 5.36 H_2O_2 induced oxidation of Csn1 was not detected with endogenous levels of Tpx1, or with overexpression of Tpx1 or the trapping mutant Tpx1^{C169S}. Western blot analysis of Csn1 (NT4), or Myc-tagged Csn1 (AMC348) expressing Rep1, Rep1Tpx1 or Rep1Tpx1^{C169S}, isolated from cells following treatment with 0.2 mM H_2O_2 for 0, 1 or 10 mins. Anti-Myc antibody was used to detect Myc-tagged Csn1. Myc-tagged Csn1 samples were run with or without β-mercaptoethanol.

5.3 Discussion

The aim of this chapter was to use high through-put genetic screening to identify new candidate H_2O_2 regulated proteins. From SGA work using the mutant *tpx1*^{C169S}, we have provided preliminary evidence of 31 candidate non-essential *S. pombe* genes that are important for growth in the absence of thioredoxin peroxidase activity. Excitingly, orthologues of six of these candidate genes (*rad50, mre11, mms1, rad57, rad1* and *ada2*) also exhibit a synthetic sick interaction with the peroxiredoxin mutant *tsa1Δ* in *S. cerevisiae* indicative of a conserved function across species. Interestingly, these candidate genes were not identified by the *tpx1*Δ SGA as important for the growth of a *tpx1*Δ. The *tpx1*^{C169S} cells exhibit normal growth, but exhibit sensitivity to H_2O_2 due to removal of their thioredoxin peroxidase activity, and therefore their ability to oxidise and activate the TF Pap1. Tpx1^{C169S} does retain some Tpx1 signalling functions however; such as regulation of H_2O_2-induced Sty1 activation, or formation of disulphide bonds with other proteins. Whereas, *tpx1*Δ cells lack all Tpx1 activity and exhibit an obvious growth defect in addition to their H_2O_2 sensitivity. The distinction between the SGA-generated candidate genes for *tpx1*^{C169S} and *tpx1*Δ indicate that some candidate genes may be important specifically in the presence of Tpx1^{C169S}, or the absence of any Tpx1 activity. Additionally, this finding indicates that the *S. cerevisiae tsa1*Δ more closely resembles a *S. pombe* strain lacking only the Tpx1 thioredoxin peroxidase activity (*tpx1*^{C169S}), than a *tpx1*Δ; although this may be because *S. cerevisiae* also express *tsa2*, so a *tsa1*Δ still retains *tsa2* activity.

The use of QFA in order to identify suppressors of the *tpx1*^{C169S} H_2O_2 sensitivity phenotype revealed a high rate of reversion of the C169S point mutation to wild-type *tpx1*$^{+}$ (~23 % for library plate 1), as well as a strong selection pressure for unidentified mutations. In spite of this, work from the QFA of *tpx1*^{C169S} identified a spontaneously generated allele in the *tpx1*^{C169S}*cgi121*$^{+}$ (ZU30) strain that restored H_2O_2 resistance and Pap1 oxidation in cells lacking the thioredoxin activity of Tpx1. Additionally, QFA of *tpx1*^{C169S} also identified 3 other double mutant strains (*tpx1*^{C169S}*spn4Δ,* *tpx1*^{C169S}*SPAC11G7.01Δ* and *tpx1*^{C169S}*pus1Δ*) with an unidentified mutation which exhibited partial rescue of H_2O_2 resistance, despite the absence of H_2O_2-induced oxidation of Pap1. These 3 strains require extensive further testing. The restoration of H_2O_2 resistance without the oxidation of Pap1 could reveal alternate mechanisms for protecting against exposure to H_2O_2. Alternatively, it is possible that Pap1 may be

constitutively nuclear in these cells, similar to a *trr1*Δ or *hba1*Δ (Calvo *et al.*, 2012). The localisation of Pap1 in *tpx1*^{C169S}*spn4Δ, tpx1*^{C169S}*SPAC11G7.01Δ* and *tpx1*^{C169S}*pus1Δ* cells can be easily investigated using fluorescent microscopy techniques, or cellular fractionation and western blotting.

Surprisingly, we found that the loss of *txl1* in a *tpx1*^{C169S} did not restore H_2O_2 resistance, or Pap1 oxidation, to wild-type *tpx1*$^{+}$ levels as previously published (Brown *et al.*, 2013). Sequencing revealed that the rescue in H_2O_2 resistance and Pap1 oxidation observed in the JB92 strain (*tpx1*^{C169S}*txl1*Δ) was due to the reversion of the C169S mutation to wild-type *tpx1*$^{+}$. Perplexingly, this event was also observed in the ZU30 (*tpx1*^{C169S}*cgi121*$^{+}$) strain. Subsequent blotting for Tpx1 revealed a reversion from monomeric Tpx1, despite the presence of 0.2 mM H_2O_2, to dimer Tpx1-Tpx1 formation, over time. This finding indicates that the *tpx1*^{C169S} is too unstable to undergo high throughput genetic screening with the Bioneer library. And, unfortunately, that the initial discovery that the loss of *txl1* in a *tpx1*^{C169S} restores H_2O_2 resistance and Pap1 oxidation may have been due to a reversion to *tpx1*$^{+}$. Our findings have also indicated that the Bioneer background has an unidentified mutation that increases resistance to H_2O_2. In order to identify this mutation the SGA-generated strains could be back-crossed and undergo full genome sequencing.

From investigation into the growth of *tpx1*Δ; SGA analysis provided evidence for 21 candidate genes which were identified as consistently important for the growth of *tpx1*Δ. Only one of which (catalase) was also identified from the *tpx1*^{C169S} SGA, as well as required for growth in *prdx-2(gk169)* mutant *C. elegans* (Crook-McMahon *et al.*, 2014). This revealed a conserved role for catalase as important in Prx mutants. Analysis for suppressors of the growth defect of *tpx1*Δ successfully identified at least 2 proteins (Pka1 and Csn5) that are oxidised by H_2O_2, and interact with Tpx1. This result validates the use of high throughput genetic screening as a reliable method to identify H_2O_2 regulated proteins. Hence, future work should include evaluation of the remaining 3 candidate genes (*pmk1*, *ssm4* and *lys9*), that upon deletion showed evidence of rescuing the growth, and H_2O_2 resistance, of *tpx1*Δ when manually re-crossed. This future work should include analysis of strains: viability, growth and H_2O_2 resistance; as well as, western blot analysis to determine protein oxidation following treatment of H_2O_2, and the impact of overexpressing Tpx1, or FlagTpx1.

Our discovery that Pka1, a cAMP-dependent protein kinase, is oxidised in response to 0.2 mM H_2O_2, and forms a direct protein-protein interaction with Tpx1, is extremely exciting. Whilst we were able to verify that deleting *pka1* in a *tpx1*Δ improved cell viability, an improvement of cell growth, in liquid, or on solid agar, could not be replicated and therefore we were unable to confirm the results of the SGA analysis.

PKA is a highly conserved serine or threonine kinase, and is a heterotetramer formed by 2 regulatory and 2 catalytic subunits (Taylor *et al.*, 1990). The cAMP/PKA pathway is the major glucose-sensing pathway that regulates sexual differentiation in *S. pombe* (Gupta *et al.*, 2011b). Excitingly, many aspects of the PKA pathway are conserved in mammalian cells (Hoffman, 2005). Glucose is detected by the G protein-coupled receptor, Git3, and transferred to a heterotrimeric guanine nucleotide-binding protein (Gpa2, Git5 and Git11) (Hoffman, 2005; Cohen *et al.*, 2014). The activation of Gpa2 leads to activation of adenylate cyclase (Cyr1) to generate cAMP from ATP (Kawamukai *et al.*, 1991; Gupta *et al.*, 2011b). Increase in intracellular cAMP positively regulates Pka1 activity (Hoffman, 2005). cAMP binds the regulatory subunits and leads to the release of the catalytic subunits. PKA is activated by phosphorylation of the catalytic subunit and in high glucose environments, PKA localises to the nucleus. In low glucose environments PKA is localised to the cytoplasm (Tudisca *et al.*, 2010; Gupta *et al.*, 2011b), and glucose starvation leads to sexual development and gluconeogenesis via the activation of Pmk1 (Cohen *et al.*, 2014).

The PKA pathway also has important roles in the regulation of stress responses. In *S. cerevisiae*, PKA inhibits the nuclear import of TF Msn2 and Msn4 by phosphorylation of their nuclear localisation signal (NLS) (Gorner *et al.*, 1998; Gorner *et al.*, 2002; Smets *et al.*, 2010). Msn2 and Msn4 activate the transcription of stress response element (STRE)-controlled genes (Martinez-Pastor *et al.*, 1996; Schmitt and McEntee, 1996). STRE genes protect against many different types of stress, including oxidative, osmotic and heat (Smith *et al.*, 1998; Gash *et al.*, 2000; Hasan *et al.*, 2002, Smets *et al.*, 2010). Thereby, activation of the PKA pathway downregulates cellular stress resistance (Smith *et al.*, 1998; Thevelein *et al.*, 2000).

Decreased activity in the PKA pathway has also been linked to caloric restriction (CR)-induced life span extension (along with decreased activation of the TOR pathway, and IGF-1 signalling) (Enns *et al.*, 2009; Lin *et al.*, 2000; Molin *et al.*, 2011; Kaeberlein,

2010). In *S. cerevisiae*, CR has been found to induce H_2O_2 resistance mediated by reduction of cAMP-PKA activity. This is dependent on Tsa1 (Molin *et al.*, 2011). The translation-initiation-factor-2 (eIF2) kinase, Gcn2, relieves cAMP-PKA-dependent inhibition of Srx1 translation, which subsequently reduces hyperoxidised Tsa1 restoring it's peroxidase activity (Molin *et al.*, 2011).

Additionally, another interesting study in *S. cerevisiae* has also revealed a role for PKA in light-sensing (Bodvard *et al.*, 2017). Light signal is converted to H_2O_2 by peroxisomal oxidase (Pox1); this is sensed by Tsa1, and transduced to cytosolic thioredoxins. Oxidised thioredoxins inhibit PKA-dependent phosphorylation by inhibiting the nuclear retention of PKA catalytic subunits (Bodvard *et al.*, 2017). This proposed mechanism fits with our findings: if an important role of Tpx1 is to inhibit the activity of Pka1 via the oxidation of thioredoxins, then it makes sense that deletion of Tpx1 would remove this inhibition of Pka1 activity leading to a number of deleterious phenotypes, however subsequent deletion of Pka1 would rescue these phenotypes. This is very exciting, and suggests that Prx may have a conserved role in regulating Pka1. However, our identification of Tpx1-Pka1 disulphides suggests that Tpx1 may inhibit Pka1 directly, not just by promoting the oxidation of thioredoxin. This finding is analogous with Tpx1 having 2 roles in oxidation of Pap1 (figure 5.37) (Calvo *et al.*, 2013b; Brown *et al.*, 2013).

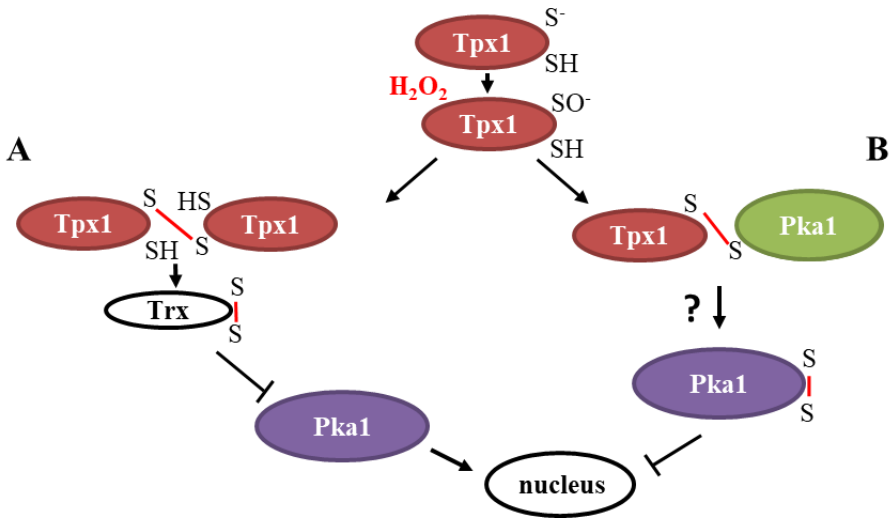

Figure 5.37 Predicted model of the regulation of Pka1 by Tpx1. Tpx1 becomes oxidised in response to H2O2. [A] Tpx1 is reduced by thioredoxins, and oxidised thioredoxins inhibit PKA-dependent phosphorylation by inhibiting the nuclear retention of PKA catalytic subunits, thereby allowing TFs to accumulate in the nucleus. [B] An intermolecular disulphide is formed between Tpx1 and Pka1 in response to H2O2. This may resolve to form an intramolecular disulphide within Pka1, thus inhibiting its activity.

The *S. pombe* Pka1 has 7 cysteines; however, multiple sequence alignment revealed that despite Pka1 being conserved across multiple species, only one cysteine residue is conserved in the catalytic subunits from *S. pombe* to human (figure 5.38). This cysteine was not conserved in the *S. cerevisiae* regulatory subunit BCY1 (Barraza *et al.*, 2017). This is interesting as it is the *bcy1*Δ that was investigated by the Molin group (Bodvard *et al.*, 2017). The detection of Tpx1-Pka1 disulphides in *S. pombe* may indicate that *S. pombe* regulates PKA activity differently to *S. cerevisiae*.


NP_012231.1 ----------MVSSLPKESQAELQLFQNEINAANPSDFL---QFSANYFNKRLEQQRA 45
NP_002721.1 ---------- 0
NP_595159.1 MDTTAVASKGSTNVGSSTDT-LSTSASLHPSMNAGSVNEYSEQQRHGTNSFNGKPSVHDS 59
NP_015121.1 ---------- 0
NP_012371.2 ---------- 0
NP_012755.1 ---------- 0
NP_012231.1 F-----LKAREPEFKAKNIVLFPEPEESFSRPQSAQSQSRSRSSVMFKSPFVNEDPHSNV 100
NP_002721.1 ---------- 0
NP_595159.1 VGSDASVSNGHNNH--NESSLWTS---GIPKALEEATKSKKPDSLVSTSTSGCASAHSVG 114
NP_015121.1 ----------ME 2
NP_012371.2 ----------MSTEEQNGGGQKSL- 14
NP_012755.1 ----------MYVDPMNNNEIRKLS 15
NP_012231.1 FKSGFNLDPHEQDT--HQQA--QEEQQHTREKTSTPPLPMHFNAQRRTSVSG-------- 148
NP_002721.1 ----------MG-NAAAAKKGSEQESV-- 16
NP_595159.1 YQNIDNLIPSPLPESASRSSSQSSHQRH--SRDGRGELGSEHG-ERRSAMDGLRDRHI-R 170
NP_015121.1 FVA---ERAQPVGQ----TIQQQNVNTY-----GQGVLQPHHD------LQQRQQ----- 39
NP_012371.2 --------DDRQGE----ESQKGETSERETTATESGNESKSVE------KEGGETQEKPK 56
NP_012755.1 ITAKTETTPDNVGQ----DIPVNAHSVHE-----ECSSNTPVE------INGRNSGKLKE 60
NP_012231.1 --------ETLQPNNFDDWTP---DHYKEKSEQQLQRLEKSIRNNFLFNKLDSDSKRLVI 197
NP_002721.1 ----KEFLAKAKEDFLKKWESPAQNTAHLDQFERIKTLGTGSFGRVMLVKHKETGNHYAM 72
NP_595159.1 KVRVSQLLDLQRRRI-RPADHTTKDRYGIQDFNFLQTLGTGSFGRVHLVQSNHNRLYYAI 229
NP_015121.1 QQQQRQHQQLLTSQL-PQKSLVSKGKYTLHDFQIMRTLGTGSFGRVHLVRSVHNGRYYAI 98
NP_012371.2 QPHVTYYNEEQYKQF-IAQARVTSGKYSLQDFQILRTLGTGSFGRVHLIRSRHNGRYYAM 115
NP_012755.1 E---ASAGICLVKKP-MLQYRDTSGKYSLSDFQILRTLGTGSFGRVHLIRSNHNGRFYAL 116
NP_012231.1 NCLEEKSVPKGATIIKQGDQGDYF-------YVVEKGTVDFYVNDNKVN-SSGPGSSFGE 249
NP_002721.1 KILDKQKVVKLKQIEHTLNEKRILQAVNFPFLVKLEFSFKDNSNLYMVMEYVPGGEMFSH 132
NP_595159.1 KVLEKKKIVDMKQIEHTCDERYILSRVQHPFITILWGTFQDAKNLFMVMDFAEGGELFSL 289
NP_015121.1 KVLKKQQVVKMKQVEHTNDERRMLKLVEHPFLIRMWGTFQDARNIFMVMDYIEGGELFSL 158
NP_012371.2 KVLKKEIVVRLKQVEHTNDERLMLSIVTHPFIIRMWGTFQDAQQIFMIMDYIEGGELFSL 175
NP_012755.1 KTLKKHTIVKLKQVEHTNDERRMLSIVSHPFIIRMWGTFQDSQQVFMVMDYIEGGELFSL 176
NP_012231.1 LALM--YNSPRAATVVATSDCLLWALDRLTFRKILLGSSFKKRLMYDDLLKSMPVLKSLT 307
NP_002721.1 LRRIGRFSEPH-ARFYAAQIVL--TFE---------- 156
NP_595159.1 LRKCHRFPEKV-AKFYAAEVIL--ALD---------- 313
NP_015121.1 LRKSQRFPNPV-AKFYAAEVIL--ALE---------- 182
NP_012371.2 LRKSQRFPNPV-AKFYAAEVCL--ALE---------- 199
NP_012755.1 LRKSQRFPNPV-AKFYAAEVCL--ALE---------- 200
NP_012231.1 TYDRAKLADALDTKIYQPGETIIREGDQGENFYLIEYGAVDVSKKG---------- 353
NP_002721.1 ----------YLHSLDLIYRDLKPENLLIDQQGYIQVTDFGFAKRVKGR-TWTLC 200
NP_595159.1 ----------YLHHNQIVYRDLKPENLLLDRFGHLKIVDFGFAKRVSTSNCCTLC 358
NP_015121.1 ----------YLHAHNIIYRDLKPENILLDRNGHIKITDFGFAKEVQTV-TWTLC 226
NP_012371.2 ----------YLHSKDIIYRDLKPENILLDKNGHIKITDFGFAKYVPDV-TYTLC 243
NP_012755.1 ----------YLHSKDIIYRDLKPENILLDKNGHIKITDFGFAKYVPDV-TYTLC 244

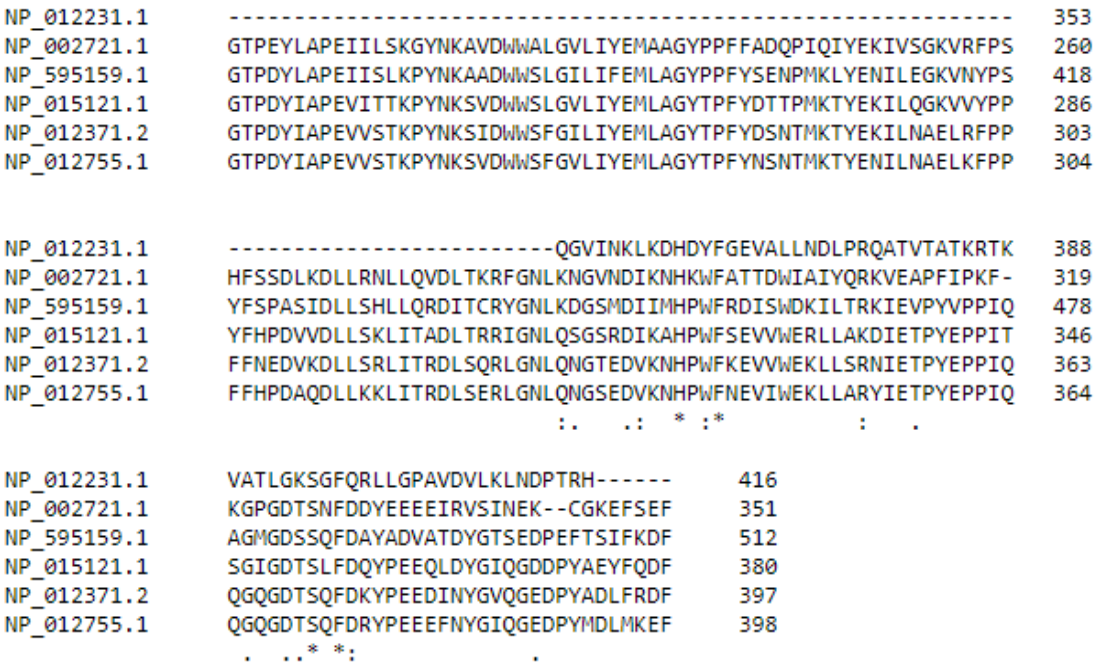

Figure 5.38 Multiple sequence alignment of the orthologues of cAMP-dependent protein kinase: Pka1 (*S. pombe*), TPK1, TPK2, TPK3 and BCY1 (*S. cerevisiae*) and PRKACA (human). The amino acid sequences retrieved from the NCBI protein database (NCBI, ncbi.nlm.nih.gov) (accession numbers NP_002721.1 for human PRKACA, NP_595159.1 for *S. pombe* Pka1, NP_012371.2 for *S. cerevisiae* TPK1, NP_015121.1 for *S. cerevisiae* TPK2, NP_012755.1 for *S. cerevisiae* TPK3 and NP_012231.1 for *S. cerevisiae* BCY1) were aligned using the Clustal Omega programme. An asterisk (*) indicates positions with a fully conserved residue, a colon (:) indicates conservation between groups with strongly similar properties, a period (.) indicates conservation between groups of weakly similar properties. Arrow indicates one cysteine residue conserved in the cAMP-dependent protein kinase catalytic subunits between 3 species.

Future work in *S. pombe*, such as site-directed mutagenesis, is required to determine whether Pka1 activity is regulated by Prx/H_2O_2. *S. pombe* is a more suitable model to study the activity of Pka1 than *S. cerevisiae*, as there are 4 Pka1 homologues in *S. cerevisiae* with some functional redundancy. The previous associations of Pka1 with life span extension makes this an extremely exciting discovery. As reduced lifespan is one of the phenotypes of the *tpx1*Δ, it would be exciting to investigate whether the deletion of *pka1* in these cells rescues this short lifespan phenotype. This data would reveal whether the inability to regulate Pka1 may be why the *tpx1*Δ is short lived, and also does not undergo an increase in lifespan in response to CR.

We also revealed that deleting *csn5* improved the growth and H_2O_2 resistance of *tpx1*Δ. Additionally, we discovered that oxidation of endogenous Csn5 (but not Csn1) was easily detected following exposure to 0.2 mM H_2O_2, and was enhanced with the overexpression of Tpx1 forms. Excitingly, some of the high molecular weight H_2O_2 induced bands provided evidence of a direct protein-protein interaction with Tpx1. *S. pombe* have 5 Csn (COP9/signalosome complex subunits) proteins. Our data suggests that specifically subunit 5 (Csn5) is forming disulphide with Tpx1. Interestingly, Csn5 is much more abundant than some of the other CSN subunits raising the possibility that it has other CSN-dependent activities that are regulated by H_2O_2/Tpx1. The CSN complex is highly conserved from yeast to human (Kato and Yoneda-Kato, 2009). The *S. cerevisiae* orthologue of Csn5, RRI1 (Vilella *et al.*, 2009), is the catalytic subunit of the CSN complex (Licursi *et al.*, 2013). Additionally, Csn5 also has a human orthologue, COPS5; however, in humans the CSN complex consists of 8 sub-units (Chamovitz *et al.*, 1996; Deng *et al.*, 2000).

The CSN complex, is a multi-subunit complex that controls protein turnover (Merlet *et al.*, 2009). CSN regulates protein degradation in 3 ways: regulation of the cullin-RING-E3 ligases by deneddylation (removal of the ubiquitin-like modifier NEDD8 from Cullin-Ring ubiquitin ligases), regulation of COP1, and regulation of deubiquitination (Kato and Yoneda-Kato, 2009). The subunit Csn5 contains a specific MPN domain, known as the Jab1/Mpn domain metalloenzyme (JAMM,) and is responsible for neddylation (Cope *et al.*, 2002).

In addition to its role as regulator of the proteasome system, CSN has also been found to be involved in many other cellular and developmental processes (Licursi *et al.*, 2013; Wei *et al.*, 2008). In mammalian cells, CSN5 was identified as Jab1 (Jun-activation-domain-binding protein 1), and was discovered to interact with various intracellular regulators, such as; Cdk inhibitor p27, the leucocyte antigen receptor and the tumour suppressor p53 (Tomoda *et al.*, 1999; Bech-Otschir *et al.*, 2001; Zhang *et al.*, 2007; Kato and Yoneda-Kato, 2009). Jab1/CSN5 has therefore been found to have important roles in checkpoint control, signal transduction, development and the cell cycle (Kato and Yoneda-Kato, 2009; Wei and Deng, 2003), and therefore has emerged as an important player in the development of cancer (Pan *et al.*, 2014; Lee *et al.*, 2011; Richardson and Zundel, 2005; Wang *et al.*, 2016). Jab1/CSN5 inhibition has therefore been proposed as a novel therapeutic strategy against cancer (Pan *et al.*, 2014). Depletion of Jab1/CSN5 has been

shown to inhibit proliferation and induce apoptosis in NPC, and breast cancer cells (Pan *et al.*, 2012; Ming-Chuan *et al.*, 2007).

CSN-deficient animals are short-lived, possibly due to the deleterious effects of constitutively high levels of phase 2 detoxification (Oláhová *et al.*, 2008; Wakabayashi *et al.*, 2003; Tullet *et al.*, 2008; Crook-McMahon *et al.*, 2014). Indeed, in *C. elegans*, Csn2 and Csn5 were found to suppress basal phase 2 gene expression under normal growth conditions (Wang *et al.*, 2010), but was required for stress-induced increases in *gcs*-1 expression (Crook-McMahon *et al.*, 2014). Furthermore, the *prdx*-2(*gk169*) mutant has high phase 2 gene expression, and the RNAi screen conducted revealed that *csn-5* RNAi reduced this expression back to wild-type levels (Crook-McMahon *et al.*, 2014). This therefore suggested that *csn-5* RNAi recues some phenotypes of the *prdx-2(gk169)* mutant, and therefore that increased CSN5 activity may be responsible for some of *prdx-2(gk169)* mutant phenotypes, which is consistent with our *S. pombe* screen.

The *S. pombe* Csn5 has 5 cysteines; however, multiple sequence alignment revealed that despite Csn5 being conserved across multiple species, only two cysteine residues are conserved from *S. pombe* to human (figure 5.39).

Figure 5.39 Multiple sequence alignment of the orthologues of COP9 signalosome complex protease subunit 5: Csn5 (*S. pombe*), RRI1 (*S. cerevisiae*) and COPS5 (human). The amino acid sequences retrieved from the NCBI protein database (NCBI, ncbi.nlm.nih.gov) (accession numbers NP_006828.2 for human COPS5, NP_593131.1 for *S. pombe* Csn5 and NP_010065.2 for *S. cerevisiae* RRI1) were aligned using the ClustalW2 programme. An asterisk (*) indicates positions with a fully conserved residue, a colon (:) indicates conservation between groups with strongly similar properties, a period (.) indicates conservation between groups of weakly similar properties. Arrows indicate two cysteine residues conserved between all 3 species.

Future work in *S. pombe*, such as an assay for CSN function, is required to determine whether Csn5 activity is regulated by Prx/H_2O_2. The existence of a human orthologue of Csn5, and its established role in multiple cellular processes, and human disease, make this an extremely exciting discovery. Finally, the discovery that Pka1 and Csn5 are oxidised in response to H_2O_2 reveals that our high throughput genetic screening approach to identify H_2O_2/thioredoxin regulated proteins was a success.

Chapter 6

Chapter 6. *Grx1* is important for the growth and signalling of *tpx1^{C169S}*

6.1 Introduction

Results from the high through-put genetic screening of *tpx1* mutants (discussed in Chapter 5) revealed a number of glutathione-related genes as important for growth in *tpx1^{C169S}* cells. The SGA analysis of *tpx1^{C169S}* identified that *gsa1*, a glutathione synthase, consistently gave the highest negative GIS when assessing candidate genes important for growth. In addition, *grx1*, a glutaredoxin, was also identified as consistently having a synthetic sick genetic interaction with the *tpx1^{C169S}* mutation (averaging as the candidate gene with the 14th highest negative GIS) (table 5.1).

Glutathione is an important tri-peptide involved in a number of cellular processes, such as maintaining intracellular redox potential, and the regulation of cell redox-dependent signalling (as discussed in section 1.1.2.6) (Mieyal *et al.*, 2008; Kalinina *et al.*, 2014). Additionally, GSH has multiple roles in iron metabolism (Lushchak, 2012). For example, the depletion of GSH impairs iron-sulphur cluster maturation, and negatively affects cytosolic iron delivery (Sipos *et al.*, 2002; Muhlenhoff *et al.*, 2010; Kumar *et al.*, 2011). Interestingly, our SGA analysis revealed that whilst *gsa1* and *grx1* were essential for growth in *tpx1^{C169S}* cells, they apparently were not essential in cells lacking Tpx1 (*tpx1*Δ). This suggests that GSH might have an important role specifically in *tpx1^{C169S}* cells; which lack the thioredoxin peroxidase activity of Tpx1 but retain some signalling functions, rather than the deletion mutant that lacks all Tpx1 activity.

Glutaredoxins catalyse the deglutathionylation of protein thiols, and in turn are recycled by GSH. Glutaredoxins also reduce protein disulphide bonds, and under reduced GSH/GSSG ratio cell conditions are able to catalyse the S-glutathionylation of proteins (Kalinina *et al.*, 2014). Grx are important for the recycling of RNR in dNTP synthesis, reduction of ascorbate, and metal homeostasis (Boronat *et al.*, 2017; Foyer and Noctor, 2011; Jozefczak *et al.*, 2012). The apparent importance of *grx1* in *tpx1^{C169S}* cells, as opposed to *tpx1*Δ cells, was of great interest to us. This potential relationship between the role of glutaredoxin, Grx1, and Tpx1^{C169S} was explored further.

6.2 Results

6.2.1 Deletion of *grx1* in a *tpx1^{C169S}* reduces cell viability, growth, and affects cell morphology

6.2.1.1 Deletion of *grx1* in a *tpx1^{C169S}* is synthetic lethal

To confirm *grx1* as having a synthetic lethal genetic interaction with the *tpx1^{C169S}* mutation; a *grx1*Δ strain (WH10-14) (of a different background to the Bioneer library) was PCR checked, and manually crossed with a *tpx1^{C169S}* (ZU11) strain. Ten tetrads were dissected, and the spores that formed colonies were patched onto different selection plates to determine genotype. The spores wild-type for *tpx1^{+}* (*tpx1^{+}grx1^{+}*, *tpx1^{+}grx1*Δ) exhibited high viability at 91.7% and 100% respectively (table 6.1). The presence of the *tpx1^{C169S}* point mutation reduced spore viability from 91.7% to 77.8% (*tpx1^{C169S}grx1^{+}*). However, only 27.3% of *tpx1^{C169S}grx1*Δ cells gave rise to colonies, confirming that *grx1* was more important in cells lacking the resolving cysteine of Tpx1.

Genotype	Viability (%)
tpx1^{+}grx1^{+}	91.7
*tpx1^{+}grx1*Δ	100
tpx1^{C169S}grx1^{+}	77.8
*tpx1^{C169S}grx1*Δ	27.3

Table 6.1 Analysis of the ability to form a colony and genotype of 10 dissected tetrads from a cross between *tpx1^{C169S}* and *grx1*Δ. The *tpx1^{C169S}* (ZU11) strain was crossed with the *grx1*Δ (WH10-14). Following dissection of 10 tetrads, spores that formed colonies were patched onto selection plates for genotype analysis.

6.2.1.2 The *tpx1^{C169S}grx1*Δ has morphological defects compared to *tpx1^{+}*, *tpx1^{C169S}* and *grx1*Δ cells

To investigate whether deleting *grx1* affected the morphology of cells; exponentially growing cells were examined by fluorescence microscopy (section 2.6.1.1). From qualitative analysis, deleting *grx1* in a *tpx1^{+}* strain appeared to reduce cell length (comparisons between *tpx1^{+}grx1^{+}* and *tpx1^{+}grx1*Δ strains) (figure 6.1). Whereas, the introduction of a C169S mutation in a *grx1^{+}* strain increased cell width (comparisons between *tpx1^{+}grx1^{+}* and *tpx1^{C169S}grx1^{+}* strains). The combination of the two mutations, in a *tpx1^{C169S}grx1*Δ strain, revealed obvious changes in cell morphology compared to all starting strains. These dramatic differences in morphology were most obviously characterised by an increase in frequency of multi-nucleated cells, which were substantially larger in length than wild-type *S. pombe* cells. These multi-nucleated cells were accompanied by much smaller cells, some of which were almost circular. Together these images suggested that growth controls were impaired in the *tpx1^{C169S}grx1*Δ strains.

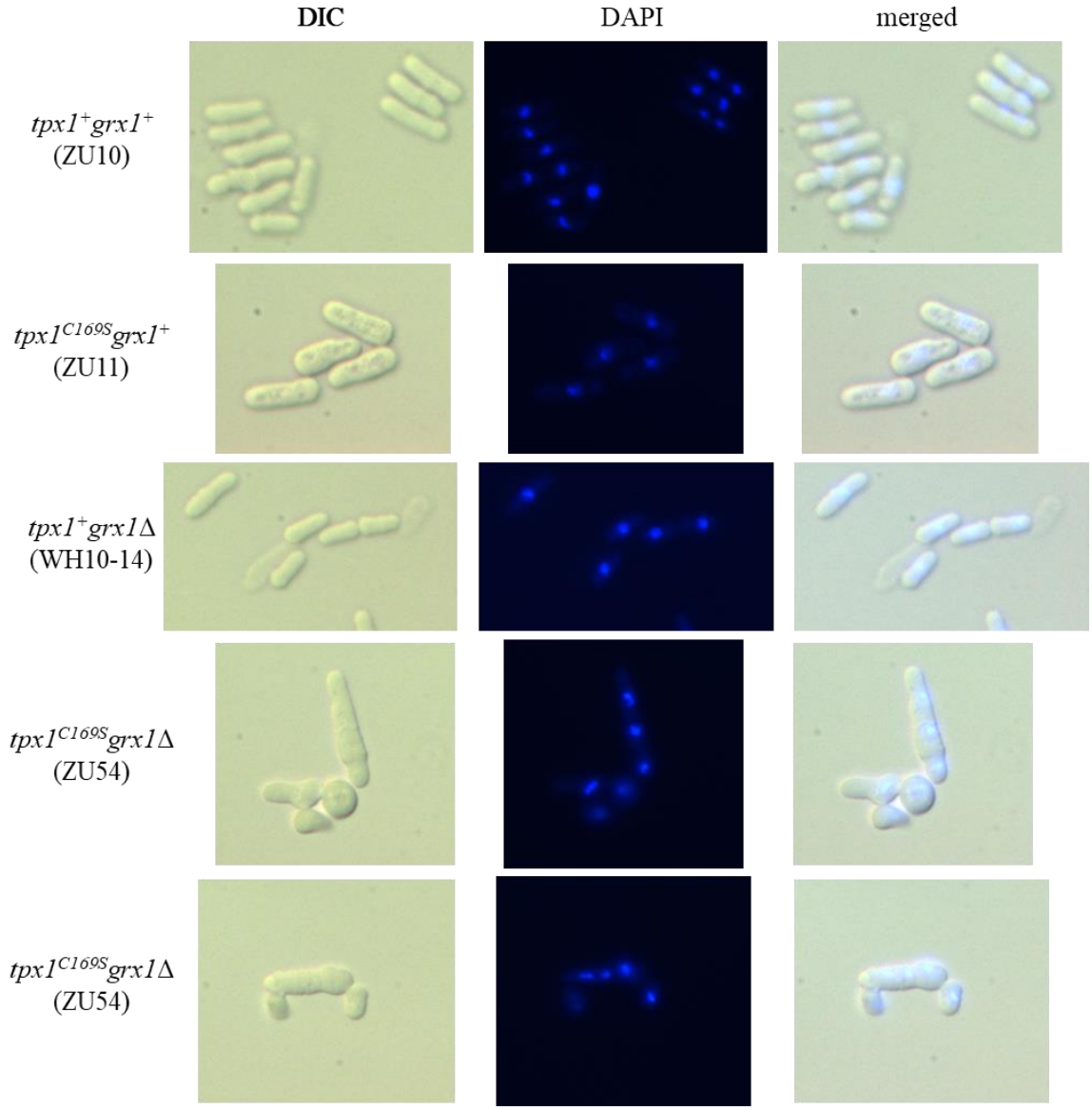

Figure 6.1 Morphology of *tpx1*$^{+}$, *tpx1*^{C169S}, *grx1*Δ and *tpx1*^{C169S}*grx1*Δ cells. Exponentially growing *tpx1*$^{+}$ (ZU10), *tpx1*^{C169S} (ZU11), *grx1*Δ (WH10-14) and *tpx1*^{C169S}*grx1*Δ (ZU54) cells were collected and spread onto Poly-lysine coated slides. Nuclei were stained using Vectashield mounting medium and the DIC, DAPI and merged images were collected using a Zeiss Axioscope fluorescence microscope.

6.2.1.3 The *tpx1^{C169S}grx1*Δ has reduced growth compared to *tpx1^{C169S}* and *grx1*Δ

To assess whether the deletion of *grx1* in a *tpx1^{C169S}* strain also reduced the rate of cell growth; *tpx1^{C169S}grx1Δ* strains generated from the cross were grown to exponential phase and spotted onto rich agar with the following control strains for comparison: *tpx1^{+}*, *tpx1^{C169S}*, *grx1*Δ and *tpx1*Δ (figure 6.2). As expected, the *tpx1^{+}* strains, as well as the *tpx1^{C169S}* strain, exhibited normal growth on YE5S after 48 and 72 h incubation at 30 °C. The growth of the *tpx1^{C169S}grx1*Δ strains was consistently reduced in all 3 strains, compared to the *tpx1^{C169S}*. However, the deletion of *grx1* in a *tpx1^{C169S}* did not reduce cell growth to the same extent as a *tpx1*Δ.

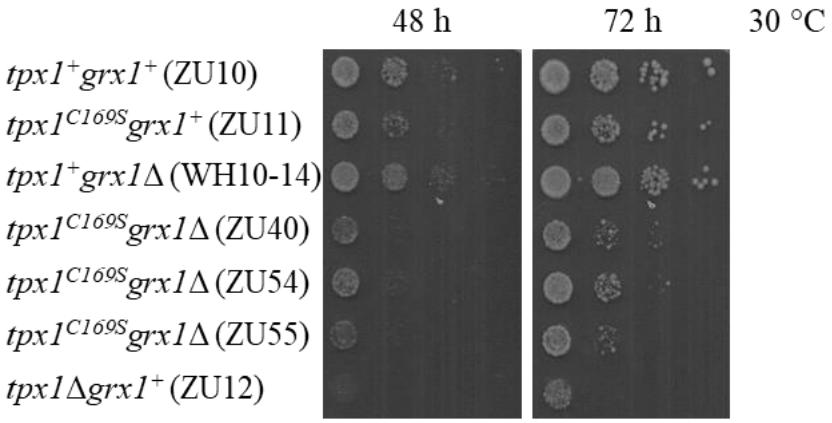

Figure 6.2 Loss of *grx1* reduced the viability of *tpx1^{C169S}* strain. Exponentially growing *tpx1^{+}* (ZU10), *tpx1^{C169S}* (ZU11), *grx1*Δ (WH10-14), *tpx1^{C169S}grx1*Δ (ZU40, ZU54, ZU55) and *tpx1*Δ (ZU12) strains were spotted onto YE5S agar. Plates were incubated at 30 °C and scanned after 48 and 72 hours.

6.2.2 Deletion of *grx1* affects the signalling of *tpx1^{C169S}*

6.2.2.1 Deleting *grx1* in a *tpx1^{C169S}* strain removes the ability of Pap1 and Tpx1 to form high molecular weight complexes

Although Tpx1^{C169S} lacks some Tpx1 activity, it retains some Tpx1 signalling functions; such as, regulation of H_2O_2-induced Sty1 activation, support of the partial oxidation of Pap1 to inactive non-native disulphides, and the formation of disulphides with other proteins, such as Pka1 and Csn5 (as discussed in Chapter 5) (Veal *et al.*, 2004). As the deletion of *grx1* revealed a synthetic lethal genetic interaction with *tpx1^{C169S}*, we investigated whether the deletion of *grx1* affected the signalling abilities of a *tpx1^{C169S}* strain. Firstly, the oxidation status of Tpx1 and Pap1 in *tpx1^{C169S}grx1*Δ cells, in response to 0.2 mM H_2O_2 for 1 min, was investigated. As expected, cells wild-type for *tpx1^{+}* (*tpx1^{+}grx1^{+}* and *tpx1^{+}grx1*Δ) formed Tpx1-Tpx1 dimer complexes in response to H_2O_2, as well as oxidised forms of Pap1 (Pap1^{ox}) (figure 6.3A) (Brown *et al.*, 2013). In addition, a very high molecular weight Pap1-containing band (>170 kDa) was also observed in response to 0.2 mM H_2O_2.

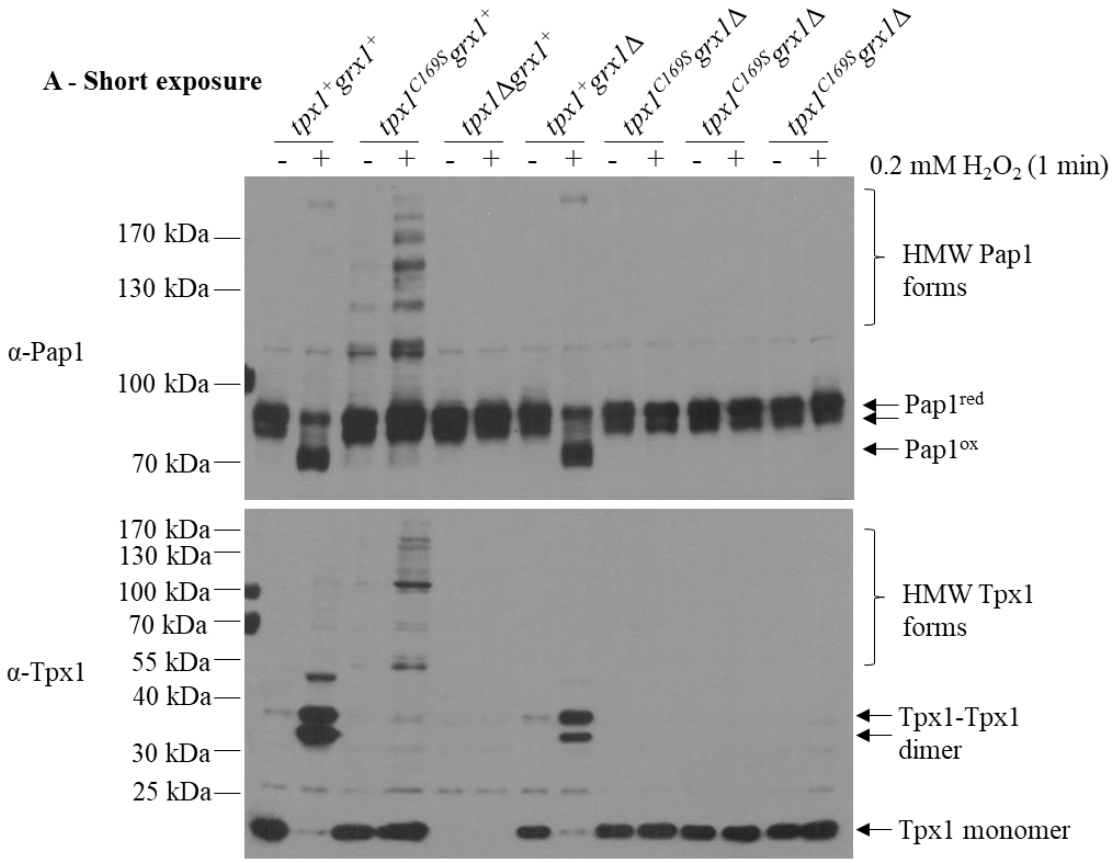
A - Short exposure
tpx1+grx1+
tpx1C169Sgrx1+
tpx1Δgrx1+
tpx1+grx1Δ
tpx1C169Sgrx1Δ
tpx1C169Sgrx1Δ
tpx1C169Sgrx1Δ
- + - + - + - + - + - + - +
0.2 mM H2O2 (1 min)
170 kDa
130 kDa
100 kDa
70 kDa
α-Pap1
HMW Pap1 forms
Pap1red
Pap1ox
170 kDa
130 kDa
100 kDa
70 kDa
55 kDa
40 kDa
30 kDa
25 kDa
α-Tpx1
HMW Tpx1 forms
Tpx1-Tpx1 dimer
Tpx1 monomer

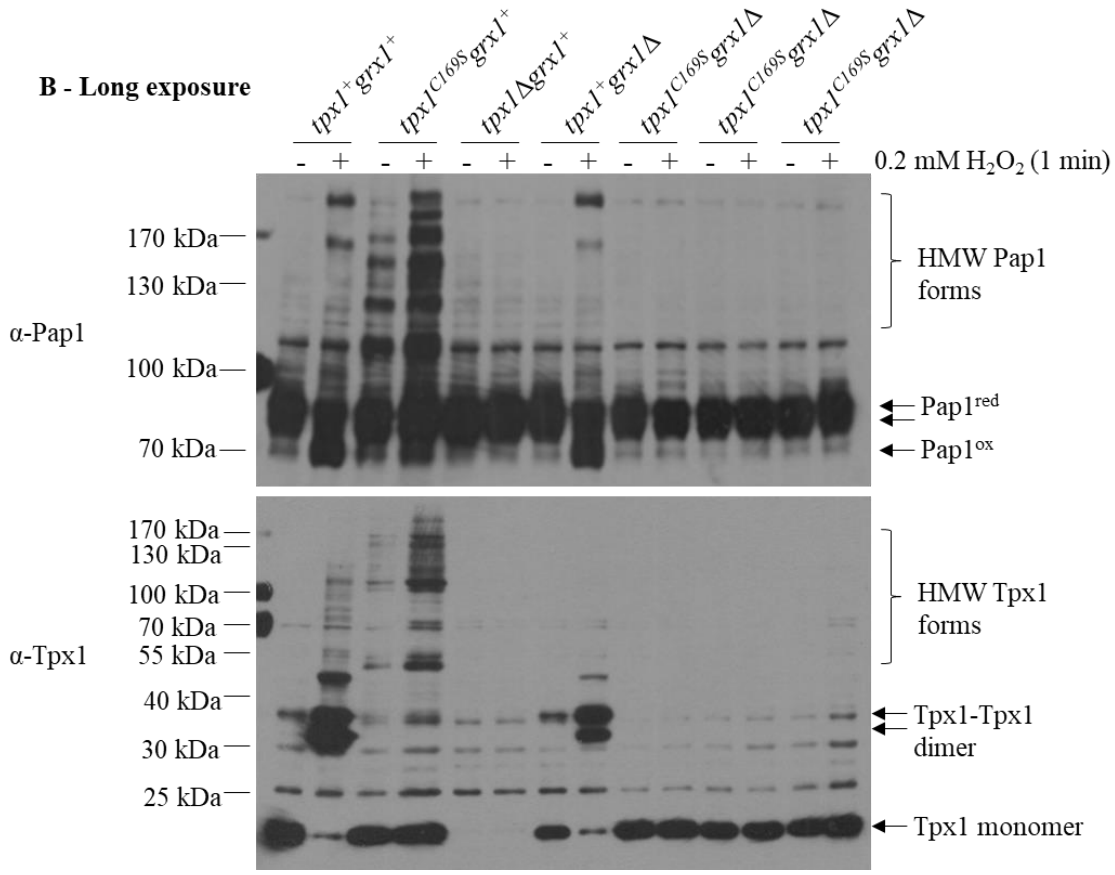

Figure 6.3 A short exposure [A] and long exposure [B] of the western blot analysis of Pap1 and Tpx1 oxidation in *tpx1*^{C169S}*grx1*Δ strains in response to 0.2 mM H_2O_2. Western blot analysis of Pap1 and Tpx1 isolated from *tpx1*$^{+}$ (ZU10), *tpx1*^{C169S} (ZU11), *tpx1*Δ (ZU12), *grx1*Δ (WH10-14) and *tpx1*^{C169S}*grx1*Δ (ZU40, ZU54, ZU55) cells following treatment with 0.2 mM H_2O_2 for 1 min. Anti-Pap1 and anti-Tpx1 antibodies were used to detect Pap1 and Tpx1 respectively.

As published, in the trapping mutant *tpx1*^{C169S}*grx1*$^{+}$, Tpx1 is unable to form Tpx1-Tpx1 dimers, or oxidise Pap1 to its active nuclear-localised form, in response to 0.2 mM H_2O_2 for 1 min (Brown *et al.*, 2013). Additionally, when blotting for Tpx1, exposure to H_2O_2 does reveal a ladder of high molecular weight bands indicative of Tpx1^{C169S} forming disulphide bonds with other unidentified proteins or protein complexes. This ladder of high molecular weight bands is also observed when blotting for Pap1, revealing the presence of Pap1 in multiple protein complexes as well (Brown *et al.*, 2013). These high molecular weight ladders are *tpx1*^{C169S}-dependent, and were lost in the *tpx1*Δ strain.

However, the Tpx1 and Pap1 blots for the *tpx1*^{C169S}*grx1*Δ strains were identical to the *tpx1*Δ strain, rather than the *tpx1*^{C169S} strain (*tpx1*^{C169S}*grx1*$^{+}$), even following a longer exposure (figure 6.3B). This suggested that loss of *grx1* removes the ability of Pap1 and Tpx1 to form high molecular weight complexes in a *tpx1*^{C169S} mutant strain. We propose that *grx1* is required for the H_2O_2-reactivity of *tpx1*^{C169S}, and hence its ability to promote the formation of Pap1-disulphide bonded forms.

6.2.2.2 The *tpx1*^{C169S}*grx1*Δ strain is resistant to tBOOH-induced hyperoxidation of the Tpx1 peroxidatic cysteine

To test this hypothesis, we examined the sensitivity of Tpx1^{C169S} to hyperoxidation of its peroxidatic cysteine by high concentrations of tBOOH. In response to high concentrations of peroxides (e.g. H_2O_2, tBOOH), as in other eukaryotic Prx, the peroxidatic cysteine of Tpx1 undergoes hyperoxidation to thioredoxin-resistant sulphinic and sulphonic derivatives (Day *et al.*, 2012; Veal *et al.*, 2017). With the use of an antibody raised to a peptide containing the $SO_{2/3}$ (sulphinate or sulphonate)-derivative of the peroxidatic cysteine of Prx, this modification can be visualised by western blotting (Tomalin *et al.*, 2016; Veal *et al.*, 2017). For example, in cells expressing wild-type *tpx1*$^{+}$ (*tpx1*$^{+}$*grx1*$^{+}$ and *tpx1*$^{+}$*grx1*Δ), a band corresponding to hyperoxidised Tpx1, is observed following 10 mins exposure of cells to 1 mM tBOOH (figure 6.4). As expected, this band was also present in the *tpx1*^{C169S}*grx1*$^{+}$ strain following tBOOH treatment, but absent from the *tpx1*Δ strain. However, no hyperoxidation of Tpx1^{C169S} was detected in multiple, independently generated, *tpx1*^{C169S}*grx1*Δ strains. This strongly supported our hypothesis that, in the absence of *grx1*, the Tpx1^{C169S} peroxidatic cysteine is insensitive to oxidation.

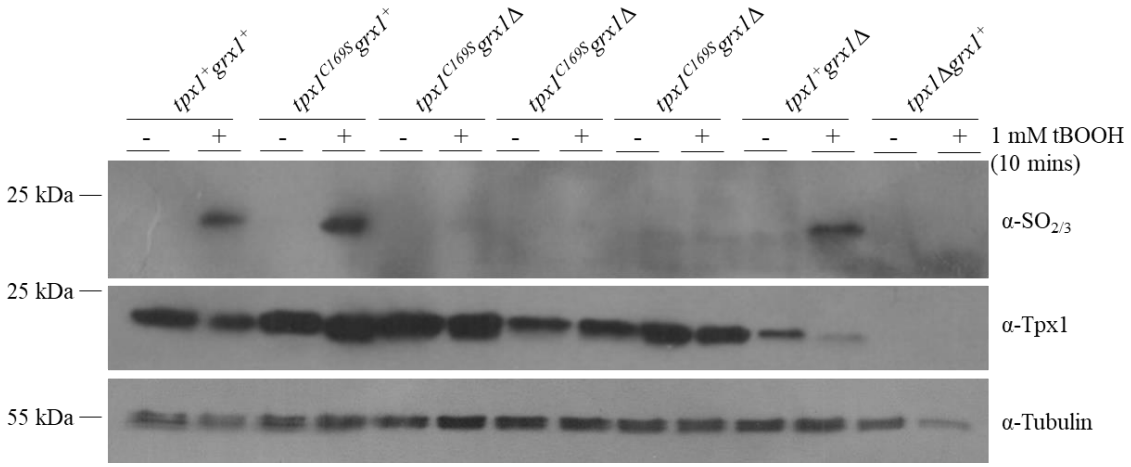

Figure 6.4 Western blot analysis of Tpx1 and hyperoxidised Tpx1 in *tpx1^{C169S}grx1*Δ strains in response to 1 mM tBOOH. Western blot analysis of Tpx1, Tpx1-$SO_{2/3}$ and Tubulin isolated from *tpx1*$^{+}$ (ZU10), *tpx1^{C169S}* (ZU11), *tpx1^{C169S}grx1*Δ (ZU40, ZU54, ZU55), *grx1*Δ (WH10-14) and *tpx1*Δ (ZU12) cells following treatment with 1 mM tBOOH for 10 mins. Anti-$SO_{2/3}$ (hyperoxidised Tpx1), anti-Tpx1 and anti-Tubulin antibodies were used.

6.2.2.3 Detection of a glutathionylated residue by SDS-PAGE separation

Based on the observations that, unlike the *tpx1*^{C169S}, the *tpx1*^{C169S}*grx1*Δ strains: aren't able to form a ladder of high molecular weight complexes in response to low H_2O_2 concentrations, and don't undergo Tpx1 hyperoxidation in response to high tBOOH levels, we proposed that the peroxidatic cysteine of Tpx1 may be glutathionylated. Indeed, Prx2 has been shown to be able to function as a glutathione peroxidase (Peskin *et al.*, 2016). The presence of this glutathionylation modification would therefore block hyperoxidation events, and the formation of direct disulphides with other protein/protein complexes. This hypothesis fits with the current data as following the deletion of *grx1*, the Tpx1 peroxidatic cysteine would remain glutathionylated and therefore would be resistant to subsequent oxidation modifications.

In order to test whether the single remaining cysteine C47 is glutathionylated; *tpx1*^{C169S} , *tpx1*^{C169S}*grx1*Δ and *tpx1*Δ cells were treated with 1 mM tBOOH and collected. Samples underwent multiple TCA protein extractions with treatments of: NEM, with or without DTT, and resuspension with AMS (figure 6.5A). This protocol was designed in order to allow us to determine whether a glutathionylated residue was present or not, due to observed changes in protein mobility with different treatments. Initial treatment with NEM would block a free thiol thereby preventing further modification. However, a glutathionylated residue would avoid modification by NEM, and would undergo reduction by treatment with DTT, and subsequently bind AMS. AMS binding causes a change in protein size and therefore a reduction in protein mobility of ~0.3 kDa. Therefore, if a glutathionylated residue is present, a size difference of ~0.3 kDa should be observed when comparing samples with and without DTT treatment. Whereas, if no glutathionylation occurs no change in protein size should be observed. Samples were loaded onto 2 separate long gels: one set were run in the presence of β-mercaptoethanol (figure 6.5C), and one set without (figure 6.5B).

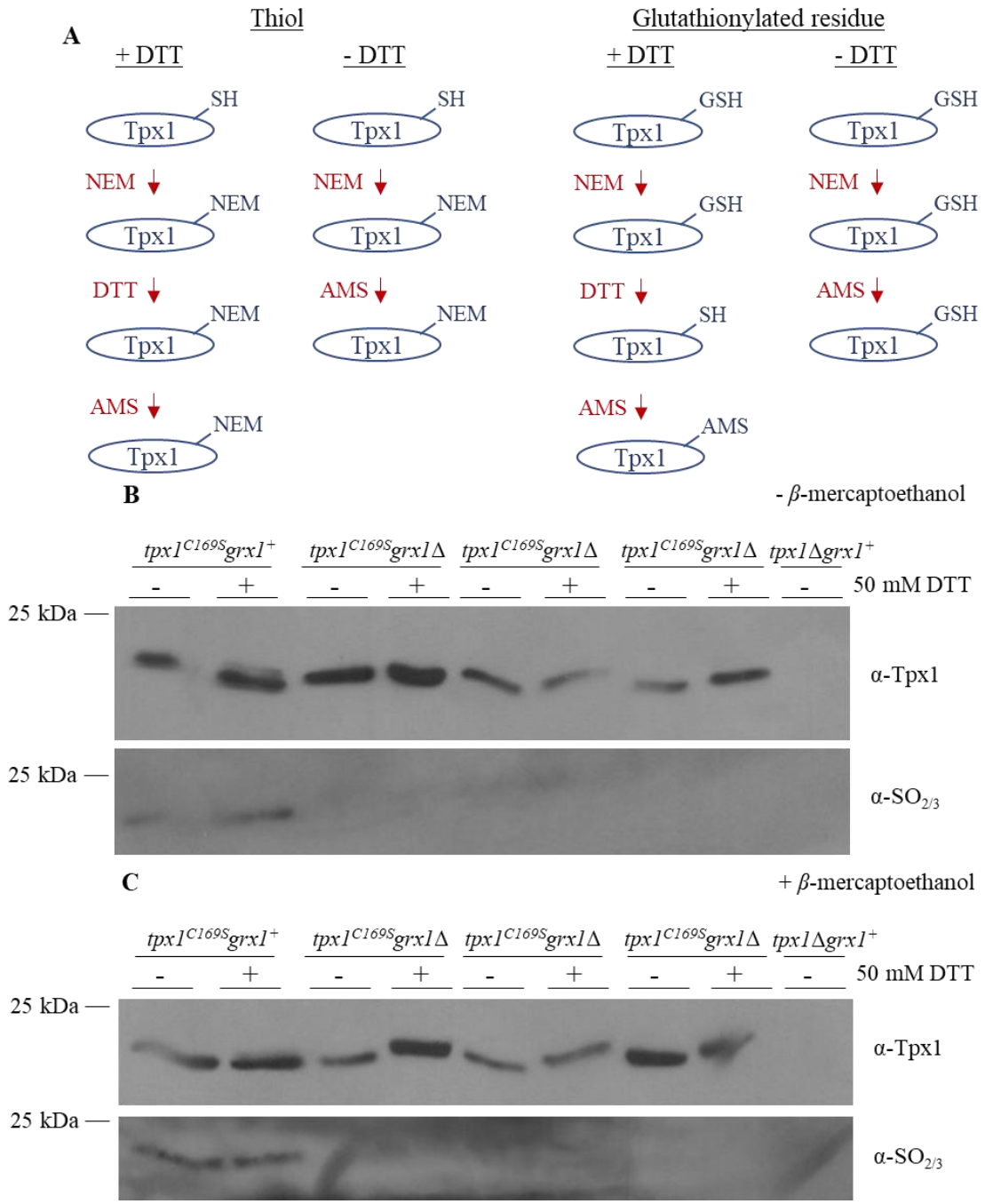

Figure 6.5 Detection of a glutathionylated residue by SDS-PAGE separation. **[A]** Method flowchart. Cells were collected, and following rounds of TCA protein extractions, pellets were resuspended with 25 mM NEM, then with or without 50 mM DTT, and finally with 25 mM AMS. [B and C] Western blot analysis of Tpx1 and Tpx1-$SO_{2/3}$ isolated from *tpx1*^{C169S} (ZU11), *tpx1*^{C169S}*grx1*Δ (ZU40, ZU54, ZU55) and *tpx1*Δ (ZU12) cells following treatment with 1 mM tBOOH for 10 mins. Samples were mixed with loading buffer without *β*-mercaptoethanol **[B]**, or with *β*-mercaptoethanol **[C]**. Samples were separated on a long-gel by SDS-PAGE and analysed by western blotting using anti-Tpx1 and anti-$SO_{2/3}$ (hyperoxidised Tpx1) antibodies. A shift in mobility is detected indicative of a glutathionylated reside (0.3 kDa).

The treatment of a *tpx1*^{C169S}*grx1*$^{+}$ strain with 1 mM tBOOH for 10 mins, resulted in the hyperoxidation of the Tpx1 peroxidatic cysteine detected by the anti-$SO_{2/3}$ antibody (figure 6.5B and C). As seen previously (figure 6.4), the hyperoxidation of the Tpx1 peroxidatic cysteine is lost in *tpx1*^{C169S}*grx1*Δ strains in response to 1 mM tBOOH (figure 6.5B and C).

When blotting for Tpx1 in the *tpx1*^{C169S}*grx1*$^{+}$ strain, 2 bands were detected following treatment with DTT, whereas one band was detected in samples that omitted DTT treatment (figure 6.5B). Interestingly, the higher molecular weight band is lost in samples prepared with loading dye containing *β*-mercaptoethanol (figure 6.5C), as opposed to without (figure 6.5B). This provided supporting evidence towards the hypothesis that in *tpx1*^{C169S}*grx1*$^{+}$ cells, Tpx1^{C169S} exists in a mixed population of glutathionylated Tpx1, and non-glutathionylated Tpx1. For example, in samples that did not undergo reduction by DTT treatment: glutathionylated thiols would not undergo AMS modification, and the non-glutathionylated thiols would be blocked by the NEM treatment and therefore would also not undergo AMS modification (figure 6.5A). However, following DTT treatment, glutathionylated cells would be reduced and allow AMS binding (and a subsequent reduction in mobility of ~0.3 kDa), whereas non-glutathionylated thiols would have bound DTT-resistant NEM, and not undergone AMS modification; resulting in the detection of 2 bands of different molecular weight.

In comparison, in the *tpx1*^{C169S}*grx1*Δ strains, only one band is detected for Tpx1 in each sample, with (figure 6.5B) or without (figure 6.5C) *β*-mercaptoethanol. Excitingly, across all strains the preparation of samples with the reductant DTT, resulted in a slight reduction of mobility of bands. This indicates that the DTT treatment has reduced a glutathionylated residue allowing for AMS binding, as opposed to the presence of a DTT-resistant NEM-bound thiol. The slight reduction in mobility is representative of an AMS modification (~0.3 kDa).

6.2.2.4 Deleting *grx1* removes *tpx1*^{C169S} ability to support H_2O_2-dependent activation of the Sty1 MAPK

At high concentrations of H_2O_2, an important role of Tpx1 is to promote the activation of Sty1 (Veal *et al.*, 2004). In cells wild-type for *tpx1*$^{+}$, Sty1 phosphorylation can be observed using a pp38 antibody in response to 6 mM H_2O_2 for 10 mins (figure 6.6A) (Veal *et al.*, 2004). Interestingly, in the trapping mutant *tpx1*^{C169S}*grx1*$^{+}$, levels of Sty1

phosphorylation were increased following H_2O_2 treatment. This result is supported by additional unpublished work in the Veal lab. The increase in Sty1 phosphorylation was also observed in the *tpx1*Δ*grx1*$^{+}$ strain; and could be due to the fact that following the loss of Tpx1 activity, Sty1 activation becomes much more important for cell survival at high H_2O_2 concentrations. In the three *tpx1*^{C169S}*grx1*Δ strains, Sty1 phosphorylation is considerably reduced in comparison to the *tpx1*$^{+}$, *tpx1*^{C169S} and *tpx1*Δ strains. This result indicated that deleting *grx1* removed *tpx1*^{C169S} ability to support H_2O_2-dependent activation of Sty1 MAPK. An additional interesting result from this figure, is that Sty1 phosphorylation appears highest in the *tpx1*$^{+}$*grx1*Δ strain.

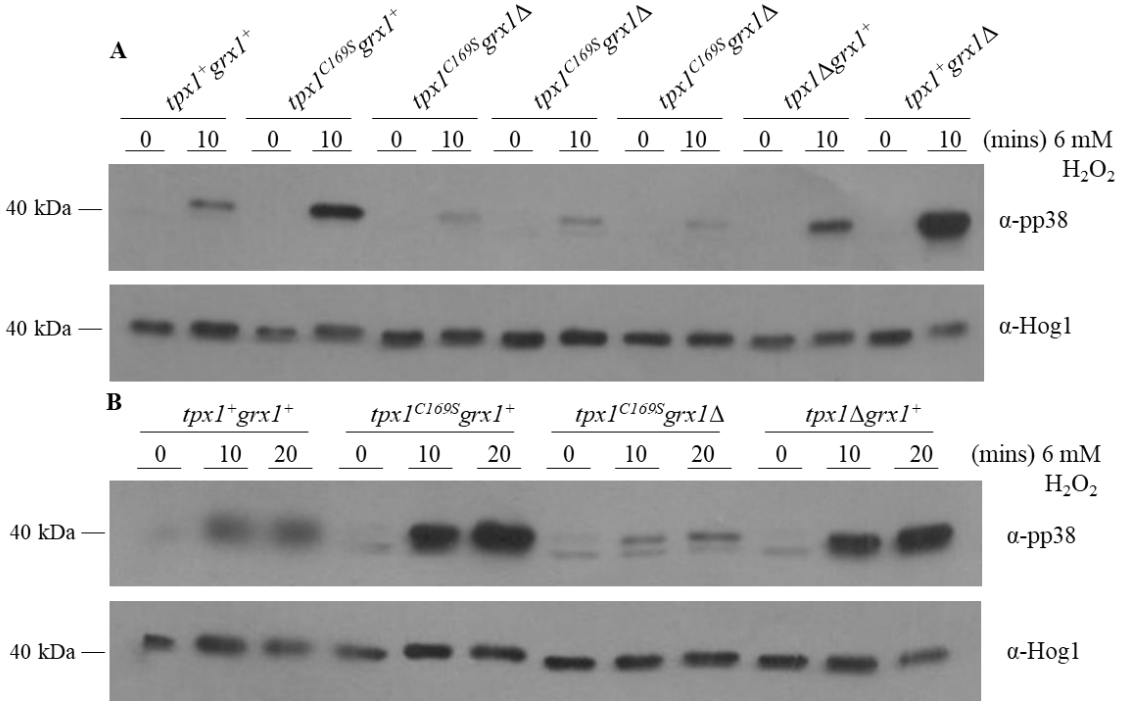

Figure 6.6 Western blot analysis of Sty1 phosphorylation in *tpx1^{C169S}grx1*Δ strains compared with *tpx1*$^{+}$ or *tpx1^{C169S}* in response to 6 mM H_2O_2. Western blot analysis of Sty1 phosphorylation and Sty1 isolated from *tpx1*$^{+}$ (ZU10), *tpx1^{C169S}* (ZU11), *tpx1^{C169S}grx1*Δ (ZU40, ZU54, ZU55), *tpx1*Δ (ZU12) and *grx1*Δ (WH10-14) cells following treatment with 6 mM H_2O_2 for 0 or 10 mins **[A]**, or from *tpx1*$^{+}$ (ZU10), *tpx1^{C169S}* (ZU11), *tpx1^{C169S}grx1*Δ (ZU40) and *tpx1*Δ (ZU12) cells following treatment with 6 mM H_2O_2 for 0, 10 or 20 mins **[B]**. Sty1 phosphorylation levels were detected using an anti-pp38 antibody, and Sty1 protein levels were analysed using an anti-Hog antibody.

Further evidence that Sty1 phosphorylation is reduced in the *tpx1*^{C169S}*grx1*Δ strain, compared with *tpx1*$^{+}$ or *tpx1*^{C169S}, in response to 6 mM H_2O_2 is provided using a time course experiment (figure 6.6B). From this result it is clear that the *tpx1*^{C169S}*grx1*$^{+}$ and *tpx1*Δ*grx1*$^{+}$ strains have increased Sty1 phosphorylation in response to 6 mM H_2O_2 for 10 to 20 mins, compared with the wild-type *tpx1*$^{+}$*grx1*$^{+}$ strain. It is also clear that deleting *grx1* in a *tpx1*^{C169S} strain (*tpx1*^{C169S}*grx1*Δ) drastically reduced Sty1 phosphorylation, even lower than wild-type *tpx1*$^{+}$*grx1*$^{+}$ levels, despite Sty1 protein levels remaining constant (α-Hog1).

6.3 Discussion

Work conducted in the previous chapter identified a number of glutathione-related genes as being important for growth in cells where the thioredoxin peroxidase activity of Tpx1 is lost (*tpx1*^{C169S}). In a different strain background, we have verified that the deletion of *grx1* in a *tpx1*^{C169S} reduces cell viability and growth compared to *tpx1*$^{+}$ or *tpx1*^{C169S} cells. Interestingly, cell growth inhibition in *tpx1*^{C169S}*grx1*Δ cells is not as severe as in *tpx1*Δ cells, suggesting that some Tpx1 non-signalling properties may still be functional to promote growth (for example chaperone activity (as discussed in section 1.3.3)). We also provide qualitative data for the severe morphological defects observed in *tpx1*^{C169S}*grx1*Δ cells in contrast to *tpx1*$^{+}$ or *tpx1*^{C169S} cells, which are indicative of severe cell cycle defects.

Most excitingly, we provide extensive evidence that the deletion of *grx1* in *tpx1*^{C169S} removes important Tpx1 signalling functions in response to a range of oxidative stressors. In response to a low concentration of H_2O_2, the *tpx1*^{C169S}*grx1*Δ cells are unable to form high molecular weight complexes with Tpx1 or Pap1, acting instead like a *tpx1*Δ strain. We therefore propose that *grx1* is required for the H_2O_2-reactivity of a *tpx1*^{C169S}, and hence its ability to promote the formation of Pap1-disulphide bonds.

In response to a high concentration of tBOOH, the *tpx1*^{C169S}*grx1*Δ strains did not undergo hyperoxidation of the Tpx1 peroxidatic cysteine; thus further supporting the hypothesis that, in the absence of *grx1*, the Tpx1^{C169S} peroxidatic cysteine is insensitive to oxidation. Following on, analysis of *tpx1*^{C169S}*grx1*$^{+}$ cells provided supporting evidence towards the hypothesis that Tpx1^{C169S} exists in a mixed population of glutathionylated Tpx1, and non-glutathionylated Tpx1. We therefore conclude that the reason for the loss of Tpx1 signalling functions in a *tpx1*^{C169S}*grx1*Δ is due to the constitutive glutathionylation of the

Tpx1 peroxidatic cysteine. The separation by SDS-PAGE of samples treated with or without DTT provides evidence of a shift in mobility ~0.3 kDa; indicative of the presence of a glutathionylated modification. We argue that this glutathionylation modification blocks Tpx1 from undergoing subsequent oxidation modifications, therefore preventing direct protein-protein disulphides, as well as hyperoxidation. In support of this, the mammalian peroxiredoxin 2 (Prx2) has also been observed to undergo glutathionylation, which was in turn reduced by glutaredoxin 1 (Grx1) (Peskin *et al.*, 2016).

Finally, in response to a high concentration of H_2O_2, Sty1 phosphorylation is almost completely diminished in *tpx1*^{C169S}*grx1*Δ compared to *tpx1*$^{+}$, or *tpx1*^{C169S}*grx1*$^{+}$ strains. This result indicated that the deletion of *grx1* removed *tpx1*^{C169S} ability to support H_2O_2-dependent activation of Sty1 MAPK, and further supported our hypothesis that a redox-active peroxidatic cysteine is important for Tpx1's signalling roles. To conclude, we provide evidence that the glutathione peroxidase activity of Tpx1 might be important for regulating some of Tpx1's signalling activities; for example, in promoting the oxidation of Pap1, and activation of Sty1. Based on our discovery, it will also be interesting to determine whether Tpx1^{C169S} is able to support the regulation of Pka1 and Csn5, and whether Grx1 is required for this activity.

Chapter 7

Chapter 7. Final Discussion

Whilst high concentrations of H_2O_2 cause the cellular damage observed in many diseases and ageing, low levels have been shown to be important for normal health and longevity. How organisms sense H_2O_2, and use it to signal positive responses is therefore of great interest. The research outlined in this thesis has provided new targets and tools, as well as mechanistic insight, into the role of H_2O_2 and Prx in response to peroxide. The results are summarised, and future perspectives are discussed below.

7.1 Summarising key findings from this study

To understand how endogenous H_2O_2 affects cell growth, migration and ageing, it is important to be able to monitor changes in H_2O_2 concentrations, in real-time, *in vivo*. However, to study endogenous signalling events, it is vital that sensors are specific and sensitive enough to detect these low H_2O_2 levels. To circumvent issues that arise from using small molecular fluorescent probes, we tested whether the fusion of a roGFP2 sensor to the highly abundant and H_2O_2-sensitive PRDX-2, in *C. elegans*, is able to act as a genetic tool to detect very low, endogenous concentrations of intracellular H_2O_2. Whilst our data suggests that the N-roGFP2::*prdx-2* sensor shows some specificity for H_2O_2, it was insufficiently sensitive to detect low levels of H_2O_2 in response to stimuli such as changes in temperature, larval stages and starvation, or differences in endogenous levels between tissues. Therefore, for the investigation of low levels of H_2O_2, other more sensitive detectors would be appropriate, as well as able to undergo targeting to specific organelles or cell types.

Following the discovery that mutant yeast and worms lacking cytosolic 2-Cys Prx display a number of mitochondrial defects, and that a pool of Pap1 and Sty1 had previously been co-purified with *S. pombe* mitochondria; the second aim of the project was to test whether a pool of Tpx1 is localised to the IMS, and whether this may be involved in supporting mitochondrial function and the activation of Pap1. This hypothesis also reflects the discovery that a pool of Gpx3 is present in the mitochondrial IMS of *S. cerevisiae* cells, and that IMS-based Gpx3 is important for normal mitochondrial function (Vögtle *et al.*, 2012; Kritsiligkou *et al.*, 2017). Indeed, we provide further evidence for mitochondrial

defects in *tpx1*Δ mutant *S. pombe*, and *prdx-2*(*gk169*) mutant *C. elegans*, and identify the presence of a pool of Tpx1 in the mitochondrial IMS. Additionally, we present evidence suggesting the IMS localisation of Pap1, and that a direct role of Tpx1 in the IMS may contribute to the function of Tpx1 in H_2O_2 resistance, and H_2O_2-induced activation of Pap1, however this requires further study.

Finally, the third aim of this project was to use high throughput genetic screening in Prx mutant *S. pombe* in order to identify new targets of H_2O_2, that may not have been detected by proteomic methods. From SGA analysis of *tpx1*^{C169S} we identify 31 candidate non-essential genes that are important for growth in the absence of thioredoxin peroxidase activity. Interestingly, these hits exhibit more overlap with synthetic sick interactions of *S. cerevisiae tsa1*Δ, than with *S. pombe tpx1*Δ. The distinction between the SGA-generated candidate genes for *tpx1*^{C169S} and *tpx1*Δ indicate that some candidate genes may be important specifically in the presence of Tpx1^{C169S}, or the absence of any Tpx1 activity. Additionally, we provide further proof that catalase is required for growth of Prx mutants; as catalase gave a consistently high negative GIS in *tpx1*^{C169S} and *tpx1*Δ *S. pombe*, and was previously identified as required for growth in *prdx-2(gk169) C. elegans* (Crook-McMahon *et al.*, 2014).

From QFA analysis, we found that the *tpx1*^{C169S} is too unstable to undergo high throughput genetic screening with the Bioneer library. Additionally, we predict that the Bioneer background has an unidentified mutation that increases resistance to H_2O_2. We are unaware if other authors have encountered a similar problem using the Bioneer library. Surprisingly, we found that the loss of *txl1* in a *tpx1*^{C169S} did not restore H_2O_2 resistance, or Pap1 oxidation, to wild-type *tpx1*$^{+}$ levels as previously published (Brown *et al.*, 2013). Sequencing revealed that the rescue in H_2O_2 resistance and Pap1 oxidation observed in the JB92 strain (*tpx1*^{C169S}*txl1*Δ) was due to the reversion of the C169S mutation to wild-type *tpx1*$^{+}$.

The SGA analysis for suppressors of *tpx1*Δ growth defect identified 5 candidate genes where loss of function partially suppressed the growth defects associated with loss of *tpx1*. At least 2 of these proteins (the single *S. pombe* cAMP-dependent protein kinase, Pka1, and the COP9/signalosome complex protease subunit, Csn5) were confirmed to undergo oxidation, through the formation of direct protein-protein disulphide complexes with Tpx1 in response to 0.2 mM H_2O_2. Indeed, the loss of *pka1* in a *tpx1*Δ improved cell

viability. We therefore validate the high throughput genetic screening approach as a method to identify new candidate H_2O_2 regulated proteins.

Pka1 is highly conserved, and the PKA pathway has been linked to CR-induced lifespan extension and light-sensing (Molin *et al.*, 2011). Indeed, Pka1 activity has previously been identified as being regulated by oxidised thioredoxins in *S. cerevisiae* (Bodvard *et al.*, 2017). This is very exciting, and suggests that Prx may have a conserved role in regulating Pka1. However, our identification of Tpx1-Pka1 disulphides suggests that Tpx1 may inhibit Pka1 directly, not just by promoting the oxidation of thioredoxin. This finding is analogous with Tpx1 having 2 roles in oxidation of Pap1 (Calvo *et al.*, 2013b; Brown *et al.*, 2013).

Additionally, we confirmed that loss of *csn5* improved the growth and H_2O_2 resistance of *tpx1*Δ. The CSN complex is also highly conserved, and our data suggests that specifically subunit 5 is forming the disulphide with Tpx1. Indeed, Csn5 RNAi had also been previously discovered to recue some phenotypes of the *prdx-2(gk169)* mutant in *C. elegans*, which is consistent with the results of our *S. pombe* screen (Crook-McMahon *et al.*, 2014).

Finally, our high throughput genetic screening also identified that the glutaredoxin, *grx1*, was important for growth in *tpx1*^{C169S} cells. Further investigation revealed that the deletion of *grx1* in *tpx1*^{C169S} removes important Tpx1 signalling functions in response to a range of oxidative stressors, including the H_2O_2-dependent activation of Sty1 MAPK. This suggested that Tpx1^{C169S} is constitutively glutathionylated in the absence of Grx1, and supported the hypothesis that a redox-active peroxidatic cysteine is important for Tpx1's signalling roles, as well as raising the possibility that Tpx1^{C169S} may function as a glutathione peroxidase. Indeed, the mammalian Prx2 has also been observed to undergo glutathionylation, which was in turn reduced by Grx1 (Peskin *et al.*, 2016).

7.2 Future perspectives

Excitingly, testing of the N-roGFP2::*prdx-2* sensor in *C. elegans* revealed a substantial increase in H_2O_2 in anterior intestinal cells in response to infection with the fungal pathogen *C. albicans*. However, it was unclear whether the increase in H_2O_2 was produced as a defence mechanism as part of the *C. elegans* host response, or as a mechanism of *C. albicans* to cause damage and invade host tissue. This requires further

investigation incorporating avirulent heat-killed *C. albicans* to determine the role for H_2O_2 in infection. Additionally, we were unable to detect an increase in H_2O_2 in anterior intestinal cells following starvation for up to 8 hours; this could suggest an alternate signal is required to activate NHR-49 opposed to peroxide.

Our mitochondrial fractionation data suggested the IMS-localisation of Pap1, and that this may require Tpx1. Additionally, data suggested that the targeting of a low level of Tpx1 to the IMS of *tpx1*Δ *S. pombe* cells may cause a slight increase in the H_2O_2 resistance of these cells, which could indicate that IMS-targeted expression of Tpx1 is able to restore H_2O_2-induced Pap1 activation to these cells. This, however, requires extensive further research. The dependence of Pap1 IMS-localisation on the presence of Tpx1 requires confirmation via repetition of mitochondrial isolations and confocal microscopy analysis. It is also important to examine the H_2O_2-induced oxidation state of Pap1 in cells targeting Tpx1 to the IMS. Similarly, future investigations should examine whether mitochondrial phenotypes, such as; electron transport chain function, or mitochondrial morphology, are rescued by the expression of cytb2-Tpx1. This will help elucidate whether the localisation of Pap1 to the IMS is required for its activation and oxidation.

Our high throughput genetic screening also detected unidentified mutations in 4 strains from the $tpx1^{C169S}$ QFA (which rescued H_2O_2 resistance despite retaining the C169S mutation): 3 of which rescued H_2O_2 resistance, despite the absence of H_2O_2-induced Pap1 oxidation, and 1 of which restored H_2O_2 resistance as well as Pap1 oxidation. To investigate the possibility that the Bioneer background has an unidentified mutation that increases resistance to H_2O_2, and in order to identify the mutation in the SGA-generated strains, isolates could be back-crossed and undergo full genome sequencing.

Additionally, as the Pka1 and Csn5 hits from the *tpx1*Δ SGA were confirmed as undergoing oxidation in response to H_2O_2, and forming direct disulphides with Tpx1, the 3 additional candidate genes (*pmk1*, *ssm4* and *lys9*) should be investigated. Future evaluation should include analysis of strains viability, growth and H_2O_2 resistance; as well as, western blot analysis to determine protein oxidation following treatment of H_2O_2, and the impact of overexpressing Tpx1, or FlagTpx1.

Pka1 and Csn5 themselves require further research. As reduced lifespan is one of the phenotypes of the *tpx1*Δ, it would be exciting to investigate whether the deletion of *pka1* in these cells rescues this short lifespan phenotype. This data would reveal whether the

inability to regulate Pka1 may be why the *tpx1*Δ is short lived, and does not undergo an increase in lifespan in response to CR. Additionally, site-directed mutagenesis and an assay for CSN function is required to determine whether Csn5 activity is regulated by Prx/H_2O_2.

Finally, we provided evidence that the glutathione peroxidase activity of Tpx1 might be important for regulating some of Tpx1's signalling activities; for example, in promoting the oxidation of Pap1, and activation of Sty1. Based on our discovery, it will also be interesting to determine whether $Tpx1^{C169S}$ is able to support the regulation of Pka1 and Csn5, and whether Grx1 is required for this activity.

7.3 Concluding remarks

Low levels of H_2O_2 have been shown to be important for normal health and longevity. However, the detection of endogenous levels of H_2O_2 *in vivo*, and the identification of H_2O_2-regulated proteins has had many challenges in the redox field. In this study we have validated the use of high throughput genetic screening in the identification of new candidate H_2O_2-regulated proteins. Excitingly, this has led to a vast number of exciting avenues for future research.

Bibliography

ALBRECHT, SIMONE C., BARATA, ANA G., GROßHANS, J., TELEMAN, AURELIO A. & DICK, TOBIAS P. 2011. In Vivo Mapping of Hydrogen Peroxide and Oxidized Glutathione Reveals Chemical and Regional Specificity of Redox Homeostasis. *Cell Metabolism,* 14**,** 819-829.

ALEXANDER, A., CAI, S.-L., KIM, J., NANEZ, A., SAHIN, M., MACLEAN, K. H., INOKI, K., GUAN, K.-L., SHEN, J., PERSON, M. D., KUSEWITT, D., MILLS, G. B., KASTAN, M. B. & WALKER, C. L. 2010. ATM signals to TSC2 in the cytoplasm to regulate mTORC1 in response to ROS. *Proceedings of the National Academy of Sciences of the United States of America,* 107**,** 4153-4158.

ALLEN, S., BALABANIDOU, V., SIDERIS, D. P., LISOWSKY, T. & TOKATLIDIS, K. 2005. Erv1 Mediates the Mia40-dependent Protein Import Pathway and Provides a Functional Link to the Respiratory Chain by Shuttling Electrons to Cytochrome c. *Journal of Molecular Biology,* 353**,** 937-944.

AN, J. H. & BLACKWELL, T. K. 2003. SKN-1 links C. elegans mesendodermal specification to a conserved oxidative stress response. *Genes & Development,* 17**,** 1882-1893.

ANDZIAK, B. & BUFFENSTEIN, R. 2006. Disparate patterns of age-related changes in lipid peroxidation in long-lived naked mole-rats and shorter-lived mice. *Aging Cell,* 5**,** 525-532.

ASAKAWA, K., KUME, K., KANAI, M., GOSHIMA, T., MIYAHARA, K., DHUT, S., TEE, W. W., HIRATA, D. & TODA, T. 2006. The V260I Mutation in Fission Yeast α-Tubulin Atb2 Affects Microtubule Dynamics and EB1-Mal3 Localization and Activates the Bub1 Branch of the Spindle Checkpoint. *Molecular Biology of the Cell,* 17**,** 1421-1435.

AVERY, A. M. & AVERY, S. V. 2001. Saccharomyces cerevisiae Expresses Three Phospholipid Hydroperoxide Glutathione Peroxidases. *Journal of Biological Chemistry,* 276**,** 33730-33735.

BACK, P., DE VOS, W. H., DEPUYDT, G. G., MATTHIJSSENS, F., VANFLETEREN, J. R. & BRAECKMAN, B. P. 2012. Exploring real-time in vivo redox biology of developing and aging Caenorhabditis elegans. *Free Radical Biology and Medicine,* 52**,** 850-859.

BAKER, K. M., CHAKRAVARTHI, S., LANGTON, K. P., SHEPPARD, A. M., LU, H. & BULLEID, N. J. 2008. Low reduction potential of Ero1α regulatory disulphides ensures tight control of substrate oxidation. *The EMBO Journal,* 27**,** 2988-2997.

BAKER, M. A., WEINBERG, A., HETHERINGTON, L., VILLAVERDE, A. I. S. B. & VELKOV, T. 2015. Analysis of Protein Thiol Changes Occurring During Rat Sperm Epididymal Maturation1. *Biology of Reproduction,* 92**,** 11, 1-10-11, 1-10.

BANCI, L., BERTINI, I., CEFARO, C., CENACCHI, L., CIOFI-BAFFONI, S., FELLI, I. C., GALLO, A., GONNELLI, L., LUCHINAT, E., SIDERIS, D. & TOKATLIDIS, K. 2010. Molecular chaperone function of Mia40 triggers consecutive induced folding steps of the substrate in mitochondrial protein import. *Proceedings of the National Academy of Sciences of the United States of America,* 107**,** 20190-20195.

BANCI, L., BERTINI, I., CEFARO, C., CIOFI-BAFFONI, S., GALLO, A., MARTINELLI, M., SIDERIS, D. P., KATRAKILI, N. & TOKATLIDIS, K. 2009. MIA40 is an oxidoreductase that catalyzes oxidative protein folding in mitochondria. *Nature Structural &Amp; Molecular Biology,* 16**,** 198.

BARRAZA, C. E., SOLARI, C. A., MARCOVICH, I., KERSHAW, C., GALELLO, F., ROSSI, S., ASHE, M. P. & PORTELA, P. 2017. The role of PKA in the translational response to heat stress in Saccharomyces cerevisiae. *PLOS ONE,* 12**,** e0185416.

BECH-OTSCHIR, D., KRAFT, R., HUANG, X., HENKLEIN, P., KAPELARI, B., POLLMANN, C. & DUBIEL, W. 2001. COP9 signalosome-specific phosphorylation targets p53 to degradation by the ubiquitin system. *The EMBO Journal,* 20**,** 1630-1639.

BEDARD, K., LARDY, B. & KRAUSE, K.-H. 2007. NOX family NADPH oxidases: Not just in mammals. *Biochimie,* 89**,** 1107-1112.

BELOUSOV, V. V., FRADKOV, A. F., LUKYANOV, K. A., STAROVEROV, D. B., SHAKHBAZOV, K. S., TERSKIKH, A. V. & LUKYANOV, S. 2006. Genetically encoded fluorescent indicator for intracellular hydrogen peroxide. *Nature Methods,* 3**,** 281.

BERSWEILER, A., D'AUTRÉAUX, B., MAZON, H., KRIZNIK, A., BELLI, G., DELAUNAY-MOISAN, A., TOLEDANO, M. B. & RAHUEL-CLERMONT, S. 2017. A scaffold protein that chaperones a cysteine-sulfenic acid in H2O2 signaling. *Nature Chemical Biology,* 13**,** 909.

BILAN, D. S., PASE, L., JOOSEN, L., GOROKHOVATSKY, A. Y., ERMAKOVA, Y. G., GADELLA, T. W. J., GRABHER, C., SCHULTZ, C., LUKYANOV, S. & BELOUSOV, V. V. 2013. HyPer-3: A Genetically Encoded H2O2 Probe with Improved Performance for Ratiometric and Fluorescence Lifetime Imaging. *ACS Chemical Biology,* 8**,** 535-542.

BITEAU, B., LABARRE, J. & TOLEDANO, M. B. 2003. ATP-dependent reduction of cysteine–sulphinic acid by S. cerevisiae sulphiredoxin. *Nature,* 425**,** 980.

BLACKWELL, T.K., STEINBAUGH, M.J., HOURIHAN, J.M., EWALD, C.Y. & ISIK, M. 2015. SKN-1/Nrf stress responses, and aging in Caenorhabditis elegans. *Free radical biology and medicine,* 88:290-301.

BODVARD, K., PEETERS, K., ROGER, F., ROMANOV, N., IGBARIA, A., WELKENHUYSEN, N., PALAIS, G., REITER, W., TOLEDANO, M. B., KÄLL, M. & MOLIN, M. 2017. Light-sensing via hydrogen peroxide and a peroxiredoxin. *Nature Communications,* 8**,** 14791.

BOKOV, A., CHAUDHURI, A. & RICHARDSON, A. 2004. The role of oxidative damage and stress in aging. *Mechanisms of Ageing and Development,* 125**,** 811-826.

BORONAT, S., DOMÈNECH, A., CARMONA, M., GARCÍA-SANTAMARINA, S., BAÑÓ, M. C., AYTÉ, J. & HIDALGO, E. 2017. Lack of a peroxiredoxin suppresses the lethality of cells devoid of electron donors by channelling electrons to oxidized ribonucleotide reductase. *PLoS Genetics,* 13**,** e1006858.

BOZONET, S. M., FINDLAY, V. J., DAY, A. M., CAMERON, J., VEAL, E. A. & MORGAN, B. A. 2005. Oxidation of a Eukaryotic 2-Cys Peroxiredoxin Is a Molecular Switch Controlling the Transcriptional Response to Increasing Levels of Hydrogen Peroxide. *Journal of Biological Chemistry,* 280**,** 23319-23327.

BRAND, M. D. 2010. The sites and topology of mitochondrial superoxide production. *Experimental gerontology,* 45**,** 466-472.

BRANDES, N., REICHMANN, D., TIENSON, H., LEICHERT, L. I. & JAKOB, U. 2011. Using Quantitative Redox Proteomics to Dissect the Yeast Redoxome. *Journal of Biological Chemistry,* 286**,** 41893-41903.

BRIGELIUS-FLOHÉ, R. & MAIORINO, M. 2013. Glutathione peroxidases. *Biochimica et Biophysica Acta (BBA) - General Subjects,* 1830**,** 3289-3303.

BRODEGGER, T., STOCKMANN, A., OBERSTRAß, J., NELLEN, W. & FOLLMANN, H. 2004. Novel thioredoxin targets in Dictyostelium discoideum identified by two-hybrid analysis: interactions of thioredoxin with elongation factor 1α and yeast alcohol dehydrogenase. *Biological Chemistry,* 385(12):1185-92.

BROWN, JONATHON D., DAY, ALISON M., TAYLOR, SARAH R., TOMALIN, LEWIS E., MORGAN, BRIAN A. & VEAL, ELIZABETH A. 2013. A Peroxiredoxin Promotes H2O2 Signaling and Oxidative Stress Resistance by Oxidizing a Thioredoxin Family Protein. *Cell Reports,* 5**,** 1425-1435.

BRUNI, F., GRAMEGNA, P., OLIVEIRA, J. M. A., LIGHTOWLERS, R. N. & CHRZANOWSKA-LIGHTOWLERS, Z. M. A. 2013. REXO2 Is an Oligoribonuclease Active in Human Mitochondria. *PLOS ONE,* 8**,** e64670.

CALVO, I. A., AYTÉ, J. & HIDALGO, E. 2013a. Reversible thiol oxidation in the H2O2-dependent activation of the transcription factor Pap1. *Journal of Cell Science,* 126**,** 2279-2284.

CALVO, ISABEL A., BORONAT, S., DOMÈNECH, A., GARCÍA-SANTAMARINA, S., AYTÉ, J. & HIDALGO, E. 2013b. Dissection of a Redox Relay: H2O2-Dependent Activation of the Transcription Factor Pap1 through the Peroxidatic Tpx1-Thioredoxin Cycle. *Cell Reports,* 5**,** 1413-1424.

CALVO, I. A., GABRIELLI, N., IGLESIAS-BAENA, I., GARCÍA-SANTAMARINA, S., HOE, K.-L., KIM, D. U., SANSÓ, M., ZUIN, A., PÉREZ, P., AYTÉ, J. & HIDALGO, E. 2009. Genome-Wide Screen of Genes Required for Caffeine Tolerance in Fission Yeast. *PLoS ONE,* 4**,** e6619.

CALVO, I. A., GARCÍA, P., AYTÉ, J. & HIDALGO, E. 2012. The transcription factors Pap1 and Prr1 collaborate to activate antioxidant, but not drug tolerance, genes in response to H(2)O(2). *Nucleic Acids Research,* 40**,** 4816-4824.

CAO, J., SCHULTE, J., KNIGHT, A., LESLIE, N. R., ZAGOZDZON, A., BRONSON, R., MANEVICH, Y., BEESON, C. & NEUMANN, C. A. 2009. Prdx1 inhibits tumorigenesis via regulating PTEN/AKT activity. *The EMBO Journal,* 28**,** 1505-1517.

CHACINSKA, A., PFANNSCHMIDT, S., WIEDEMANN, N., KOZJAK, V., SANJUÁN SZKLARZ, L. K., SCHULZE-SPECKING, A., TRUSCOTT, K. N., GUIARD, B., MEISINGER, C. & PFANNER, N. 2004. Essential role of Mia40 in import and assembly of mitochondrial intermembrane space proteins. *The EMBO Journal,* 23**,** 3735-3746.

CHAE, H. Z., KANG, S. W. & RHEE, S. G. 1999. Isoforms of mammalian peroxiredoxin that reduce peroxides in presence of thioredoxin. *Methods in Enzymology.* Academic Press. 300:219-26.

CHAMBERS, J. E., TAVENDER, T. J., OKA, O. B. V., WARWOOD, S., KNIGHT, D. & BULLEID, N. J. 2010. The Reduction Potential of the Active Site Disulfides of Human Protein Disulfide Isomerase Limits Oxidation of the Enzyme by Ero1α. *The Journal of Biological Chemistry,* 285**,** 29200-29207.

CHAMOVITZ, D. A., WEI, N., OSTERLUND, M. T., VON ARNIM, A. G., STAUB, J. M., MATSUI, M. & DENG, X.-W. 1996. The COP9 Complex, a Novel Multisubunit Nuclear Regulator Involved in Light Control of a Plant Developmental Switch. *Cell,* 86**,** 115-121.

CHATZI, A., MANGANAS, P. & TOKATLIDIS, K. 2016. Oxidative folding in the mitochondrial intermembrane space: A regulated process important for cell physiology and disease. *Biochimica et Biophysica Acta,* 1863**,** 1298-1306.

CHATZI, A., SIDERIS, D. P., KATRAKILI, N., POZIDIS, C. & TOKATLIDIS, K. 2013. Biogenesis of yeast Mia40 – uncoupling folding from import and atypical recognition features. *The FEBS Journal,* 280**,** 4960-4969.

CHÁVEZ, V., MOHRI-SHIOMI, A., MAADANI, A., VEGA, L. A. & GARSIN, D. A. 2007. Oxidative Stress Enzymes Are Required for DAF-16-Mediated Immunity Due to Generation of Reactive Oxygen Species by Caenorhabditis elegans. *Genetics,* 176**,** 1567-1577.

CHELIKANI, P., FITA, I. & LOEWEN, P. C. 2004. Diversity of structures and properties among catalases. *Cellular and Molecular Life Sciences CMLS,* 61**,** 192-208.

CHEN, D., WILKINSON, C. R. M., WATT, S., PENKETT, C. J., TOONE, W. M., JONES, N., BÄHLER, J. & WEISSMAN, J. 2007. Multiple Pathways Differentially Regulate Global Oxidative Stress Responses in Fission Yeast. *Molecular Biology of the Cell,* 19**,** 308-317.

CHIRON, S., GAISNE, M., GUILLOU, E., BELENGUER, P., CLARK-WALKER, G. D. & BONNEFOY, N. 2007. Studying Mitochondria in an Attractive Model: Schizosaccharomyces pombe. *In:* LEISTER, D. & HERRMANN, J. M. (eds.) *Mitochondria: Practical Protocols.* Totowa, NJ: Humana Press.

CHO, C.-S., YOON, H. J., KIM, J. Y., WOO, H. A. & RHEE, S. G. 2014. Circadian rhythm of hyperoxidized peroxiredoxin II is determined by hemoglobin autoxidation and the 20S proteasome in red blood cells. *Proceedings of the National Academy of Sciences of the United States of America,* 111**,** 12043-12048.

CHO, S.-H., LEE, C.-H., AHN, Y., KIM, H., KIM, H., AHN, C.-Y., YANG, K.-S. & LEE, S.-R. 2004. Redox regulation of PTEN and protein tyrosine phosphatases in H2O2-mediated cell signaling. *FEBS Letters,* 560**,** 7-13.

CHOI HJ, K. S., YANG CH, RHEE SG, RYU SE 1998. Crystal structure of a novel human peroxidase enzyme at 2.0 A resolution. *Nature structional biology,* 5**,** 400-6.

CHUNG, W.-H., KIM, K.-D., CHO, Y.-J. & ROE, J.-H. 2004. Differential expression and role of two dithiol glutaredoxins Grx1 and Grx2 in Schizosaccharomyces pombe. *Biochemical and Biophysical Research Communications,* 321**,** 922-929.

CLOKEY, G. V. & JACOBSON, L. A. 1986. The autofluorescent "lipofuscin granules" in the intestinal cells of Caenorhabditis elegans are secondary lysosomes. *Mechanisms of Ageing and Development,* 35**,** 79-94.

COHEN, A., KUPIEC, M. & WEISMAN, R. 2014. Glucose Activates TORC2-Gad8 Protein via Positive Regulation of the cAMP/cAMP-dependent Protein Kinase A (PKA) Pathway and Negative Regulation of the Pmk1 Protein-Mitogen-activated Protein Kinase Pathway. *The Journal of Biological Chemistry,* 289**,** 21727-21737.

COPE, G. A., SUH, G. S. B., ARAVIND, L., SCHWARZ, S. E., ZIPURSKY, S. L., KOONIN, E. V. & DESHAIES, R. J. 2002. Role of Predicted Metalloprotease Motif of Jab1/Csn5 in Cleavage of Nedd8 from Cul1. *Science,* 298**,** 608-611.

COX, A. G., PEARSON, A. G., PULLAR, J. M., JÖNSSON, T. J., LOWTHER, W. T., WINTERBOURN, C. C. & HAMPTON, M. B. 2009. Mitochondrial peroxiredoxin 3 is more resilient to hyperoxidation than cytoplasmic peroxiredoxins. *The Biochemical journal,* 421**,** 51-58.

CRAIG, H. L., WIRTZ, J., BAMPS, S., DOLPHIN, C. T. & HOPE, I. A. 2013. The significance of alternative transcripts for Caenorhabditis elegans transcription factor genes, based on expression pattern analysis. *BMC Genomics,* 14**,** 249-249.

CROOK-MCMAHON, H. M., OLÁHOVÁ, M., BUTTON, E. L., WINTER, J. J. & VEAL, E. A. 2014. Genome-wide screening identifies new genes required for stress-induced phase 2 detoxification gene expression in animals. *BMC Biology,* 12**,** 64.

CURRAN SP, L. D., LEVERICH EP, HWANG DK, BEVERLY KN, KOEHLER CM 2004. The role of Hot13p and redox chemistry in the mitochondrial TIM22 import pathway. *The Journal of Biological Chemistry,* 279**,** 43744-51.

D'AUTRÉAUX, B. & TOLEDANO, M. B. 2007. ROS as signalling molecules: mechanisms that generate specificity in ROS homeostasis. *Nature Reviews Molecular Cell Biology,* 8**,** 813.

DA SILVA DANTAS, A., PATTERSON, M. J., SMITH, D. A., MACCALLUM, D. M., ERWIG, L. P., MORGAN, B. A. & QUINN, J. 2010. Thioredoxin regulates multiple hydrogen peroxide-induced signaling pathways in Candida albicans. *Molecular and cellular biology,* 30**,** 4550-4563.

DAITHANKAR, V. N., WANG, W., TRUJILLO, J. R. & THORPE, C. 2012. Flavin-linked Erv-family sulfhydryl oxidases release superoxide anion during catalytic turnover. *Biochemistry,* 51**,** 265-272.

DAY, ALISON M., BROWN, JONATHON D., TAYLOR, SARAH R., RAND, JONATHAN D., MORGAN, BRIAN A. & VEAL, ELIZABETH A. 2012. Inactivation of a Peroxiredoxin by Hydrogen Peroxide Is Critical for Thioredoxin-Mediated Repair of Oxidized Proteins and Cell Survival. *Molecular Cell,* 45**,** 398-408.

DAY, A. M. & VEAL, E. A. 2010. Hydrogen Peroxide-sensitive Cysteines in the Sty1 MAPK Regulate the Transcriptional Response to Oxidative Stress. *The Journal of Biological Chemistry,* 285**,** 7505-7516.

DELAUNAY, A., PFLIEGER, D., BARRAULT, M.-B., VINH, J. & TOLEDANO, M. B. 2002. A Thiol Peroxidase Is an H2O2 Receptor and Redox-Transducer in Gene Activation. *Cell,* 111**,** 471-481.

DENG, X.-W., DUBIEL, W., WEI, N., HOFMANN, K., MUNDT, K., COLICELLI, J., KATO, J.-Y., NAUMANN, M., SEGAL, D., SEEGER, M., GLICKMAN, M., CHAMOVITZ, D. A. & CARR, A.

2000. Unified nomenclature for the COP9 signalosome and its subunits: an essential regulator of development. *Trends in Genetics,* 16**,** 202-203.

DI, Y., HOLMES, E. J., BUTT, A., DAWSON, K., MIRONOV, A., KOTIADIS, V. N., GOURLAY, C. W., JONES, N. & WILKINSON, C. R. M. 2012. H(2)O(2) stress-specific regulation of S. pombe MAPK Sty1 by mitochondrial protein phosphatase Ptc4. *The EMBO Journal,* 31**,** 563-575.

DICKINSON, B. C., HUYNH, C. & CHANG, C. J. 2010. A Palette of Fluorescent Probes with Varying Emission Colors for Imaging Hydrogen Peroxide Signaling in Living Cells. *Journal of the American Chemical Society,* 132**,** 5906-5915.

DICKINSON, B. C., TANG, Y., CHANG, Z. & CHANG, C. J. 2011. Development of a Nuclear-Localized Fluorescent Probe for Hydrogen Peroxide and Applications to the Study of Sirtuin-Mediated Oxidative Stress Responses in vivo. *Chemistry & biology,* 18**,** 943-948.

DOOLEY, C. T., DORE, T. M., HANSON, G. T., JACKSON, W. C., REMINGTON, S. J. & TSIEN, R. Y. 2004. Imaging Dynamic Redox Changes in Mammalian Cells with Green Fluorescent Protein Indicators. *Journal of Biological Chemistry,* 279**,** 22284-22293.

DU, Y., ZHANG, H., LU, J. & HOLMGREN, A. 2012. Glutathione and Glutaredoxin Act as a Backup of Human Thioredoxin Reductase 1 to Reduce Thioredoxin 1 Preventing Cell Death by Aurothioglucose. *The Journal of Biological Chemistry,* 287**,** 38210-38219.

DUJEANCOURT, L., RICHTER, R., CHRZANOWSKA-LIGHTOWLERS, Z.M., BONNEFOY, N. & HERBERT, C.J. 2013. Interactions between peptidyl tRNA hydrolase homologs and the ribosomal release factor Mrf1 in S. pombe mitochondria. *Mitochondrion,* 13:871-880.

EKLUND, H., GLEASON, F. K. & HOLMGREN, A. 1991. Structural and functional relations among thioredoxins of different species. *Proteins: Structure, Function, and Bioinformatics,* 11**,** 13-28.

ELCHURI, S., OBERLEY, T. D., QI, W., EISENSTEIN, R. S., JACKSON ROBERTS, L., VAN REMMEN, H., EPSTEIN, C. J. & HUANG, T.-T. 2004. CuZnSOD deficiency leads to persistent and widespread oxidative damage and hepatocarcinogenesis later in life. *Oncogene,* 24**,** 367.

ELLIS, H. R. & POOLE, L. B. 1997. Roles for the Two Cysteine Residues of AhpC in Catalysis of Peroxide Reduction by Alkyl Hydroperoxide Reductase from Salmonella typhimurium. *Biochemistry,* 36**,** 13349-13356.

ELSLIGER, M.-A., WACHTER, R. M., HANSON, G. T., KALLIO, K. & REMINGTON, S. J. 1999. Structural and Spectral Response of Green Fluorescent Protein Variants to Changes in pH. *Biochemistry,* 38**,** 5296-5301.

ELSNER, M., GEHRMANN, W. & LENZEN, S. 2011. Peroxisome-Generated Hydrogen Peroxide as Important Mediator of Lipotoxicity in Insulin-Producing Cells. *Diabetes,* 60**,** 200-208.

ENNS, L. C., MORTON, J. F., TREUTING, P. R., EMOND, M. J., WOLF, N. S., MCKNIGHT, G. S., RABINOVITCH, P. S. & LADIGES, W. C. 2009. Disruption of Protein Kinase A in Mice Enhances Healthy Aging. *PLOS ONE,* 4**,** e5963.

EVANS, P. & HALLIWELL, B. 2001. Micronutrients: oxidant/antioxidant status. *British Journal of Nutrition,* 85**,** S67-S74.

EZERIŅA, D., MORGAN, B. & DICK, T. P. 2014. Imaging dynamic redox processes with genetically encoded probes. *Journal of Molecular and Cellular Cardiology,* 73**,** 43-49.

FINKEL, T. 2011. Signal transduction by reactive oxygen species. *The Journal of Cell Biology,* 194**,** 7-15.

FINKEL, T. & HOLBROOK, N. J. 2000. Oxidants, oxidative stress and the biology of ageing. *Nature,* 408**,** 239.

FORMAN, H. J., MAIORINO, M. & URSINI, F. 2010. Signaling Functions of Reactive Oxygen Species. *Biochemistry,* 49**,** 835-842.

FOYER, C.H. & NOCTOR, G. 2011. Ascorbate and Glutathione: The Heart of the Redox Hub. *Plant Physiology,* 155(1):2-18.

FRAND, A. R. & KAISER, C. A. 1998. The ERO1 Gene of Yeast Is Required for Oxidation of Protein Dithiols in the Endoplasmic Reticulum. *Molecular Cell,* 1**,** 161-170.

FRIDOVICH, I. 1995. Superoxide Radical and Superoxide Dismutases. *Annual Review of Biochemistry,* 64**,** 97-112.

FU, X., TANG, Y., DICKINSON, B. C., CHANG, C. J. & CHANG, Z. 2015. An oxidative fluctuation hypothesis of aging generated by imaging H2O2 levels in live Caenorhabditis elegans with altered lifespans. *Biochemical and Biophysical Research Communications,* 458**,** 896-900.

FUJITA, M. & YAMAMOTO, M. 1998. S. pombe sck2+, a second homologue of S. cerevisiae SCH9 in fission yeast, encodes a putative protein kinase closely related to PKA in function. *Current genetics,* 33**,** 248-254.

FURUKAWA, M. & XIONG, Y. 2005. BTB Protein Keap1 Targets Antioxidant Transcription Factor Nrf2 for Ubiquitination by the Cullin 3-Roc1 Ligase. *Molecular and Cellular Biology,* 25**,** 162-171.

GASCH, A.P., SPELLMAN, P.T., KAO, C.M., CARMEL-HAREL, O., EISEN, M.B., STORZ, G., BOTSTEIN, D & BROWN, P.O. 2000. Genomic expression programs in the response of yeast cells to environmental changes. *Molecular Biology of the Cell,* 11(12):4241-4257.

GILL, S. S. & TUTEJA, N. 2010. Reactive oxygen species and antioxidant machinery in abiotic stress tolerance in crop plants. *Plant Physiology and Biochemistry,* 48**,** 909-930.

GIUSTARINI, D., DALLE-DONNE, I., TSIKAS, D. & ROSSI, R. 2009. Oxidative stress and human diseases: Origin, link, measurement, mechanisms, and biomarkers. *Critical Reviews in Clinical Laboratory Sciences,* 46**,** 241-281.

GO, Y.-M. & JONES, D. P. 2008. Redox compartmentalization in eukaryotic cells. *Biochimica et biophysica acta,* 1780**,** 1273-1290.

GOH, G. Y. S., WINTER, J. J., BHANSHALI, F., DOERING, K. R. S., LAI, R., LEE, K., VEAL, E. A. & TAUBERT, S. 2018. NHR-49/HNF4 integrates regulation of fatty acid metabolism with a protective transcriptional response to oxidative stress and fasting. *Aging Cell,* 17**,** e12743.

GOLDSTEIN, A. L. & MCCUSKER, J. H. 1999. Three new dominant drug resistance cassettes for gene disruption in Saccharomyces cerevisiae. *Yeast,* 15**,** 1541-1553.

GÖRNER, W., DURCHSCHLAG, E., MARTINEZ-PASTOR, M.T., ESTRUCH, F., AMMERER, G., HAMILTON, B., RUIS, H. & SCHÜLLER, C. 1998. Nuclear localization of the C2H2 zinc finger protein Msn2p is regulated by stress and protein kinase A activity. *Genes & Development,* 12(4):586-597.

GÖRNER, W., DURCHSCHLAG, E., WOLF, J., BROWN, E.L., AMMERER, G., RUIS, H. & SCHÜLLER, C. 2002. Acute glucose starvation activates the nuclear localization signal of a stress-specific yeast transcription factor. *EMBO Journal,* 21:135-144.

GÓTH, L., RASS, P. & PÁY, A. 2004. Catalase enzyme mutations and their association with diseases. *Molecular Diagnosis,* 8**,** 141-149.

GRANT, C. M., QUINN, K. A. & DAWES, I. W. 1999. Differential Protein S-Thiolation of Glyceraldehyde-3-Phosphate Dehydrogenase Isoenzymes Influences Sensitivity to Oxidative Stress. *Molecular and Cellular Biology,* 19**,** 2650-2656.

GROSS, E., SEVIER, C. S., HELDMAN, N., VITU, E., BENTZUR, M., KAISER, C. A., THORPE, C. & FASS, D. 2006. Generating disulfides enzymatically: Reaction products and electron acceptors of the endoplasmic reticulum thiol oxidase Ero1p. *Proceedings of the National Academy of Sciences of the United States of America,* 103**,** 299-304.

GUO, H., ALEYASIN, H., DICKINSON, B. C., HASKEW-LAYTON, R. E. & RATAN, R. R. 2014. Recent advances in hydrogen peroxide imaging for biological applications. *Cell & Bioscience,* 4**,** 64.

GUO, Z., KOZLOV, S., LAVIN, M. F., PERSON, M. D. & PAULL, T. T. 2010. ATM Activation by Oxidative Stress. *Science,* 330**,** 517-521.

GUPTA, D. R., PAUL, S. K., OOWATARI, Y., MATSUO, Y. & KAWAMUKAI, M. 2011a. Complex Formation, Phosphorylation, and Localization of Protein Kinase A of

Schizosaccharomyces pombe upon Glucose Starvation. *Bioscience, Biotechnology, and Biochemistry,* 75**,** 1456-1465.
GUPTA, D. R., PAUL, S. K., OOWATARI, Y., MATSUO, Y. & KAWAMUKAI, M. 2011b. Multistep regulation of protein kinase A in its localization, phosphorylation and binding with a regulatory subunit in fission yeast. *Current Genetics,* 57**,** 353.
GUTSCHER, M., PAULEAU, A.-L., MARTY, L., BRACH, T., WABNITZ, G. H., SAMSTAG, Y., MEYER, A. J. & DICK, T. P. 2008. Real-time imaging of the intracellular glutathione redox potential. *Nature Methods,* 5**,** 553.
GUTSCHER, M., SOBOTTA, M. C., WABNITZ, G. H., BALLIKAYA, S., MEYER, A. J., SAMSTAG, Y. & DICK, T. P. 2009. Proximity-based Protein Thiol Oxidation by H2O2-scavenging Peroxidases. *The Journal of Biological Chemistry,* 284**,** 31532-31540.
HALLIWELL, B. A. G., J.M.C 2007. Free radicals in biology and medicine. *Oxford: Clarendon,* 4.
HALLIWELL, B. A. G., J.M.C. 1999. Free Radicals in Biology and Medicine. *Oxford University Press, Oxford***,** 1-25.
HAN, T. X., XU, X.-Y., ZHANG, M.-J., PENG, X. & DU, L.-L. 2010. Global fitness profiling of fission yeast deletion strains by barcode sequencing. *Genome Biology,* 11**,** R60-R60.
HANSCHMANN, E.-M., GODOY, J. R., BERNDT, C., HUDEMANN, C. & LILLIG, C. H. 2013. Thioredoxins, Glutaredoxins, and Peroxiredoxins—Molecular Mechanisms and Health Significance: from Cofactors to Antioxidants to Redox Signaling. *Antioxidants & Redox Signaling,* 19**,** 1539-1605.
HANSON, G. T., AGGELER, R., OGLESBEE, D., CANNON, M., CAPALDI, R. A., TSIEN, R. Y. & REMINGTON, S. J. 2004. Investigating Mitochondrial Redox Potential with Redox-sensitive Green Fluorescent Protein Indicators. *Journal of Biological Chemistry,* 279**,** 13044-13053.
HANZÉN, S., VIELFORT, K., YANG, J., ROGER, F., ANDERSSON, V., ZAMARBIDE-FORÉS, S., ANDERSSON, R., MALM, L., PALAIS, G., BITEAU, B., LIU, B., TOLEDANO, MICHEL B., MOLIN, M. & NYSTRÖM, T. 2016. Lifespan Control by Redox-Dependent Recruitment of Chaperones to Misfolded Proteins. *Cell,* 166**,** 140-151.
HARMAN, D. 1956. Aging: a theory based on free radical and radiation chemistry. *J. Gerontol,* 11**,** 298-300.
HARMAN, D. 1972. The biologic clock: the mitochondria? *Journal of the American Geriatrics Society,* 4, 145-7.
HARRIS, J. R., SCHRÖDER, E., ISUPOV, M. N., SCHEFFLER, D., KRISTENSEN, P., LITTLECHILD, J. A., VAGIN, A. A. & MEISSNER, U. 2001. Comparison of the decameric structure of peroxiredoxin-II by transmission electron microscopy and X-ray crystallography. *Biochimica et Biophysica Acta (BBA) - Protein Structure and Molecular Enzymology,* 1547**,** 221-234.
HASAN, R., LEROY, C., ISNARD, A.D., LABARRE, J., BOY-MARCOTTE, E. & TOLEDANO, M.B. 2002. The control of the yeast H2O2 response by the Msn2/4 transcription factors. *Molecular Microbiology,* 45(1):233-41.
HAYNES, A. C., QIAN, J., REISZ, J. A., FURDUI, C. M. & LOWTHER, W. T. 2013. Molecular Basis for the Resistance of Human Mitochondrial 2-Cys Peroxiredoxin 3 to Hyperoxidation. *The Journal of Biological Chemistry,* 288**,** 29714-29723.
HERRERO, E., ROS, J., BELLÍ, G. & CABISCOL, E. 2008. Redox control and oxidative stress in yeast cells. *Biochimica et Biophysica Acta (BBA) - General Subjects,* 1780**,** 1217-1235.
HIRANI, N., WESTENBERG, M., GAMI, M. S., DAVIS, P., HOPE, I. A. & DOLPHIN, C. T. 2013. A simplified counter-selection recombineering protocol for creating fluorescent protein reporter constructs directly from C. elegans fosmid genomic clones. *BMC Biotechnology,* 13**,** 1-1.
HOFFMAN, C. S. 2005. Glucose sensing via the protein kinase A pathway in Schizosaccharomyces pombe. *Biochemical Society transactions,* 33**,** 257-260.

HOLMSTRÖM, K. M. & FINKEL, T. 2014. Cellular mechanisms and physiological consequences of redox-dependent signalling. *Nature Reviews Molecular Cell Biology,* 15**,** 411.

HUANG, M.-E. & KOLODNER, R. D. 2005. A Biological Network in Saccharomyces cerevisiae Prevents the Deleterious Effects of Endogenous Oxidative DNA Damage. *Molecular Cell,* 17**,** 709-720.

HUANG, M.-E., RIO, A.-G., NICOLAS, A. & KOLODNER, R. D. 2003. A genomewide screen in Saccharomyces cerevisiae for genes that suppress the accumulation of mutations. *Proceedings of the National Academy of Sciences of the United States of America,* 100**,** 11529-11534.

HUNT-NEWBURY, R., VIVEIROS, R., JOHNSEN, R., MAH, A., ANASTAS, D., FANG, L., HALFNIGHT, E., LEE, D., LIN, J., LORCH, A., MCKAY, S., OKADA, H. M., PAN, J., SCHULZ, A. K., TU, D., WONG, K., ZHAO, Z., ALEXEYENKO, A., BURGLIN, T., SONNHAMMER, E., SCHNABEL, R., JONES, S. J., MARRA, M. A., BAILLIE, D. L. & MOERMAN, D. G. 2007. High-Throughput In Vivo Analysis of Gene Expression in Caenorhabditis elegans. *PLoS Biology,* 5**,** e237.

IGHODARO, O. M. & AKINLOYE, O. A. 2017. First line defence antioxidants-superoxide dismutase (SOD), catalase (CAT) and glutathione peroxidase (GPX): Their fundamental role in the entire antioxidant defence grid. *Alexandria Journal of Medicine*, 54(4):287-93.

IMLAY, J. A. 2003. Pathways of Oxidative Damage. *Annual Review of Microbiology,* 57**,** 395-418.

ISERMANN, K., LIEBAU, E., ROEDER, T. & BRUCHHAUS, I. 2004. A Peroxiredoxin Specifically Expressed in Two Types of Pharyngeal Neurons is Required for Normal Growth and Egg Production in Caenorhabditis elegans. *Journal of Molecular Biology,* 338**,** 745-755.

JANG, H. H., LEE, K. O., CHI, Y. H., JUNG, B. G., PARK, S. K., PARK, J. H., LEE, J. R., LEE, S. S., MOON, J. C., YUN, J. W., CHOI, Y. O., KIM, W. Y., KANG, J. S., CHEONG, G.-W., YUN, D.-J., RHEE, S. G., CHO, M. J. & LEE, S. Y. 2004. Two Enzymes in One. *Cell,* 117**,** 625-635.

JARA, M., VIVANCOS, A. P., CALVO, I. A., MOLDÓN, A., SANSÓ, M. & HIDALGO, E. 2007. The Peroxiredoxin Tpx1 Is Essential as a H(2)O(2) Scavenger during Aerobic Growth in Fission Yeast. *Molecular Biology of the Cell,* 18**,** 2288-2295.

JARVIS, R. M., HUGHES, S. M. & LEDGERWOOD, E. C. 2012. Peroxiredoxin 1 functions as a signal peroxidase to receive, transduce, and transmit peroxide signals in mammalian cells. *Free Radical Biology and Medicine,* 53**,** 1522-1530.

JOZEFCZAK, M., REMANS, T., VANGRONSVELD, J. & CUYPERS, A. 2012. Glutathione is a key player in metal-induced oxidative stress defenses. *International Journal of Molecular Sciences,* 13:3145-3175.

KAEBERLEIN, M. 2010. Lessons on longevity from budding yeast. *Nature,* 464**,** 513-519.

KALININA, E. V., CHERNOV, N. N. & NOVICHKOVA, M. D. 2014. Role of glutathione, glutathione transferase, and glutaredoxin in regulation of redox-dependent processes. *Biochemistry (Moscow),* 79**,** 1562-1583.

KALUDERCIC, N., DESHWAL, S. & DI LISA, F. 2014. Reactive oxygen species and redox compartmentalization. *Frontiers in Physiology,* 5**,** 285.

KAPLAN, N., URAO, N., FURUTA, E., KIM, S.-J., RAZVI, M., NAKAMURA, Y., MCKINNEY, R. D., POOLE, L. B., FUKAI, T. & USHIO-FUKAI, M. 2011. Localized Cysteine Sulfenic Acid Formation by Vascular Endothelial Growth Factor: Role in Endothelial Cell Migration and Angiogenesis. *Free radical research,* 45**,** 1124-1135.

KARIN, M., LIU, Z.-G. & ZANDI, E. 1997. AP-1 function and regulation. *Current Opinion in Cell Biology,* 9**,** 240-246.

KATO, J. Y. & YONEDA-KATO, N. 2009. Mammalian COP9 signalosome. *Genes to Cells,* 14**,** 1209-1225.

KAWAMUKAI, M., FERGUSON, K., WIGLER, M. & YOUNG, D. 1991. Genetic and biochemical analysis of the adenylyl cyclase of Schizosaccharomyces pombe. *Cell Regulation,* 2**,** 155-164.

KENNEDY, P. J., VASHISHT, A. A., HOE, K.-L., KIM, D.-U., PARK, H.-O., HAYLES, J. & RUSSELL, P. 2008. A Genome-Wide Screen of Genes Involved in Cadmium Tolerance in Schizosaccharomyces pombe. *Toxicological Sciences,* 106**,** 124-139.

KIM, D.-U., HAYLES, J., KIM, D., WOOD, V., PARK, H.-O., WON, M., YOO, H.-S., DUHIG, T., NAM, M., PALMER, G., HAN, S., JEFFERY, L., BAEK, S.-T., LEE, H., SHIM, Y. S., LEE, M., KIM, L., HEO, K.-S., NOH, E. J., LEE, A.-R., JANG, Y.-J., CHUNG, K.-S., CHOI, S.-J., PARK, J.-Y., PARK, Y., KIM, H. M., PARK, S.-K., PARK, H.-J., KANG, E.-J., KIM, H. B., KANG, H.-S., PARK, H.-M., KIM, K., SONG, K., SONG, K. B., NURSE, P. & HOE, K.-L. 2010. Analysis of a genome-wide set of gene deletions in the fission yeast Schizosaccharomyces pombe. *Nature biotechnology,* 28**,** 617-623.

KIM, J.-Y., KIM, E.-J., LOPEZ-MAURY, L., BÄHLER, J. & ROE, J.-H. 2014. A metabolic strategy to enhance long-term survival by Phx1 through stationary phase-specific pyruvate decarboxylases in fission yeast. *Aging (Albany NY),* 6**,** 587-601.

KITANO, K., NIIMURA, Y., NISHIYAMA, Y. & MIKI, K. 1999. Stimulation of peroxidase Activity by Decamerization Related to Ionic Strength: ApPC Protein from Amphibacillus xylanus. *The Journal of Biochemistry,* 126**,** 313-319.

KNOEFLER, D., THAMSEN, M., KONICZEK, M., NIEMUTH, N. J., DIEDERICH, A.-K. & JAKOB, U. 2012. Quantitative In Vivo Redox Sensors Uncover Oxidative Stress as an Early Event in Life. *Molecular cell,* 47**,** 767-776.

KOBAYASHI, A., KANG, M.-I., OKAWA, H., OHTSUJI, M., ZENKE, Y., CHIBA, T., IGARASHI, K. & YAMAMOTO, M. 2004. Oxidative Stress Sensor Keap1 Functions as an Adaptor for Cul3-Based E3 Ligase To Regulate Proteasomal Degradation of Nrf2. *Molecular and Cellular Biology,* 24**,** 7130-7139.

KOJER, K., BIEN, M., GANGEL, H., MORGAN, B., DICK, T. P. & RIEMER, J. 2012. Glutathione redox potential in the mitochondrial intermembrane space is linked to the cytosol and impacts the Mia40 redox state. *The EMBO Journal,* 31**,** 3169-3182.

KRITSILIGKOU, P., CHATZI, A., CHARALAMPOUS, G., MIRONOV, A., GRANT, C. M. & TOKATLIDIS, K. 2017. Unconventional Targeting of a Thiol Peroxidase to the Mitochondrial Intermembrane Space Facilitates Oxidative Protein Folding. *Cell Reports,* 18**,** 2729-2741.

KUGE, S., TODA, T., IIZUKA, N. & NOMOTO, A. 2002. Crm1 (XpoI) dependent nuclear export of the budding yeast transcription factor yAP-1 is sensitive to oxidative stress. *Genes to Cells,* 3**,** 521-532.

KÜHL, I., DUJEANCOURT, L., GAISNE, M., HERBERT, C.J. & BONNEFOY, N. 2011. A genome wide study in fission yeast reveals nine PPR proteins that regulate mitochondrial gene expression. *Nucleic Acids Research,* 39(18):8029-8041.

KÜHLBRANDT, W. 2015. Structure and function of mitochondrial membrane protein complexes. *BMC Biology,* 13**,** 89.

KUMAR, C., IGBARIA, A., D'AUTREAUX, B., PLANSON, A.G., JUNOT, C., GODAT, E., BACHHAWAT, A.K., DELAUNAY-MOISAN, A & TOLEDANO, M.B. 2011. Glutathione revisited: a vital function in iron metabolism and ancillary role in thiol-redox control. *The EMBO journal,* 30(10):2044-56.

KUMSTA, C., THAMSEN, M. & JAKOB, U. 2011. Effects of Oxidative Stress on Behavior, Physiology, and the Redox Thiol Proteome of Caenorhabditis elegans. *Antioxidants & Redox Signaling,* 14**,** 1023-1037.

LABROUSSE, A. M., ZAPPATERRA, M. D., RUBE, D. A. & VAN DER BLIEK, A. M. 1999. C. elegans Dynamin-Related Protein DRP-1 Controls Severing of the Mitochondrial Outer Membrane. *Molecular Cell,* 4**,** 815-826.

LARSEN, P. L. 1993. Aging and resistance to oxidative damage in Caenorhabditis elegans. *Proceedings of the National Academy of Sciences of the United States of America,* 90**,** 8905-8909.

LATIMER, H. R. & VEAL, E. A. 2016. Peroxiredoxins in Regulation of MAPK Signalling Pathways; Sensors and Barriers to Signal Transduction. *Molecules and Cells,* 39**,** 40-45.
LAURENT TC, M. E., REICHARD P 1964. Enzymatic synthesis of deoxyribonucleotides. IV. Isolation and characterization of thioredoxin, the hydrogen donor from Escherichia Coli B. *The Journal of Biological Chemistry,* 239**,** 3436-44.
LAWRENCE, C. L., MAEKAWA, H., WORTHINGTON, J. L., REITER, W., WILKINSON, C. R. M. & JONES, N. 2007. Regulation of Schizosaccharomyces pombe Atf1 Protein Levels by Sty1-mediated Phosphorylation and Heterodimerization with Pcr1. *Journal of Biological Chemistry,* 282**,** 5160-5170.
LEE, M.-H., ZHAO, R., PHAN, L. & YEUNG, S.-C. J. 2011. Roles of COP9 signalosome in cancer. *Cell Cycle,* 10**,** 3057-3066.
LEE, S.-R., YANG, K.-S., KWON, J., LEE, C., JEONG, W. & RHEE, S. G. 2002. Reversible Inactivation of the Tumor Suppressor PTEN by H2O2. *Journal of Biological Chemistry,* 277**,** 20336-20342.
LEE, T.-H., KIM, S.-U., YU, S.-L., KIM, S. H., PARK, D. S., MOON, H.-B., DHO, S. H., KWON, K.-S., KWON, H. J., HAN, Y.-H., JEONG, S., KANG, S. W., SHIN, H.-S., LEE, K.-K., RHEE, S. G. & YU, D.-Y. 2003. Peroxiredoxin II is essential for sustaining life span of erythrocytes in mice. *Blood,* 101**,** 5033-5038.
LEICHERT, L. I., GEHRKE, F., GUDISEVA, H. V., BLACKWELL, T., ILBERT, M., WALKER, A. K., STRAHLER, J. R., ANDREWS, P. C. & JAKOB, U. 2008. Quantifying changes in the thiol redox proteome upon oxidative stress in vivo. *Proceedings of the National Academy of Sciences of the United States of America,* 105**,** 8197-8202.
LENNICKE, C., RAHN, J., LICHTENFELS, R., WESSJOHANN, L. A. & SELIGER, B. 2015. Hydrogen peroxide – production, fate and role in redox signaling of tumor cells. *Cell Communication and Signaling : CCS,* 13**,** 39.
LICURSI, V., SALVI, C., DE CESARE, V., RINALDI, T., MATTEI, B., FABBRI, C., SERINO, G., BRAMASOLE, L., ZIMBLER, J. Z., PICK, E., BARNES, B. M., BARD, M. & NEGRI, R. 2013. The COP9 signalosome is involved in the regulation of lipid metabolism and of transition metals uptake in Saccharomyces cerevisiae. *The FEBS Journal,* 281**,** 175-190.
LIN, S.-J., DEFOSSEZ, P.-A. & GUARENTE, L. 2000. Requirement of NAD and SIR2 for Life-Span Extension by Calorie Restriction in Saccharomyces cerevisiae. *Science,* 289**,** 2126.
LIONAKI, E., AIVALIOTIS, M., POZIDIS, C. & TOKATLIDIS, K. 2010. The N-terminal Shuttle Domain of Erv1 Determines the Affinity for Mia40 and Mediates Electron Transfer to the Catalytic Erv1 Core in Yeast Mitochondria. *Antioxidants & Redox Signaling,* 13**,** 1327-1339.
LIU, X., JIANG, N., HUGHES, B., BIGRAS, E., SHOUBRIDGE, E. & HEKIMI, S. 2005. Evolutionary conservation of the clk-1-dependent mechanism of longevity: loss of mclk1 increases cellular fitness and lifespan in mice. *Genes & Development,* 19**,** 2424-2434.
LÓPEZ-MIRABAL, H. R. & WINTHER, J. R. 2008. Redox characteristics of the eukaryotic cytosol. *Biochimica et Biophysica Acta (BBA) - Molecular Cell Research,* 1783**,** 629-640.
LOW, F. M., HAMPTON, M. B., PESKIN, A. V. & WINTERBOURN, C. C. 2007. Peroxiredoxin 2 functions as a noncatalytic scavenger of low-level hydrogen peroxide in the erythrocyte. *Blood,* 109**,** 2611-2617.
LU, J. & HOLMGREN, A. 2014. The thioredoxin antioxidant system. *Free Radical Biology and Medicine,* 66**,** 75-87.
LUKYANOV, K. A. & BELOUSOV, V. V. 2014. Genetically encoded fluorescent redox sensors. *Biochimica et Biophysica Acta (BBA) - General Subjects,* 1840**,** 745-756.
LUSHCHAK, V. I. 2012. Glutathione Homeostasis and Functions: Potential Targets for Medical Interventions. *Journal of Amino Acids,* 2012**,** 26.
MACHINO, T., HASHIMOTO, S., MARUOKA, S., GON, Y., HAYASHI, S., MIZUMURA, K., NISHITOH, H., ICHIJO, H. & HORIE, T. 2003. Apoptosis signal-regulating kinase 1-mediated signaling

pathway regulates hydrogen peroxide-induced apoptosis in human pulmonary vascular endothelial cells. *Critical Care Medicine,* 31**,** 2776-2781.
MACPHERSON, L. & TOKATLIDIS, K. 2017. Protein trafficking in the mitochondrial intermembrane space: mechanisms and links to human disease. *Biochemical Journal,* 474**,** 2533-2545.
MAEDA, T., WATANABE, Y., KUNITOMO, H. & YAMAMOTO, M. 1994. Cloning of the pka1 gene encoding the catalytic subunit of the cAMP-dependent protein kinase in Schizosaccharomyces pombe. *Journal of Biological Chemistry,* 269**,** 9632-7.
MARGITTAI, É., ENYEDI, B., CSALA, M., GEISZT, M. & BÁNHEGYI, G. 2015. Composition of the redox environment of the endoplasmic reticulum and sources of hydrogen peroxide. *Free Radical Biology and Medicine,* 83**,** 331-340.
MARGUERAT, S., SCHMIDT, A., CODLIN, S., CHEN, W., AEBERSOLD, R. & BÄHLER, J. 2012. Quantitative Analysis of Fission Yeast Transcriptomes and Proteomes in Proliferating and Quiescent Cells. *Cell,* 151**,** 671-683.
MARINHO, H. S., REAL, C., CYRNE, L., SOARES, H. & ANTUNES, F. 2014. Hydrogen peroxide sensing, signaling and regulation of transcription factors. *Redox Biology,* 2**,** 535-562.
MARKVICHEVA, K. N., BILAN, D. S., MISHINA, N. M., GOROKHOVATSKY, A. Y., VINOKUROV, L. M., LUKYANOV, S. & BELOUSOV, V. V. 2011. A genetically encoded sensor for H2O2 with expanded dynamic range. *Bioorganic & Medicinal Chemistry,* 19**,** 1079-1084.
MARTINEZ-PASTOR, M.T., MARCHLER, G., SCHULLER, C., MARCHLER-BAUER, A., RUIS, H. & ESTRUCH, F. 1996. The *Saccharomyces cerevisiae* zinc finger proteins Msn2p and Msn4p are required for transcriptional induction through the stress response element (STRE). *The EMBO Journal,* 15:2227-2235.
MATSUYAMA, A., ARAI, R., YASHIRODA, Y., SHIRAI, A., KAMATA, A., SEKIDO, S., KOBAYASHI, Y., HASHIMOTO, A., HAMAMOTO, M., HIRAOKA, Y., HORINOUCHI, S. & YOSHIDA, M. 2006. ORFeome cloning and global analysis of protein localization in the fission yeast Schizosaccharomyces pombe. *Nature Biotechnology,* 24**,** 841.
MATSUZAWA, T., OHASHI, T., HOSOMI, A., TANAKA, N., TOHDA, H. & TAKEGAWA, K. 2010. The gld1 + gene encoding glycerol dehydrogenase is required for glycerol metabolism in Schizosaccharomyces pombe. *Applied Microbiology and Biotechnology,* 87**,** 715-727.
MATTSON, M. P. 2008. Hormesis Defined. *Ageing research reviews,* 7**,** 1-7.
MAUNDRELL, K. 1993. Thiamine-repressible expression vectors pREP and pRIP for fission yeast. *Gene,* 123**,** 127-130.
MENGER, KATJA E., JAMES, ANDREW M., COCHEMÉ, HELENA M., HARBOUR, M. E., CHOUCHANI, EDWARD T., DING, S., FEARNLEY, IAN M., PARTRIDGE, L. & MURPHY, MICHAEL P. 2015. Fasting, but Not Aging, Dramatically Alters the Redox Status of Cysteine Residues on Proteins in Drosophila melanogaster. *Cell Reports,* 11**,** 1856-1865.
MERLET, J., BURGER, J., GOMES, J. E. & PINTARD, L. 2009. Regulation of cullin-RING E3 ubiquitin-ligases by neddylation and dimerization. *Cellular and Molecular Life Sciences,* 66**,** 1924-1938.
MEYER, A. J. & DICK, T. P. 2010. Fluorescent Protein-Based Redox Probes. *Antioxidants & Redox Signaling,* 13**,** 621-650.
MIEYAL, J. J., GALLOGLY, M. M., QANUNGO, S., SABENS, E. A. & SHELTON, M. D. 2008. Molecular Mechanisms and Clinical Implications of Reversible Protein S-Glutathionylation. *Antioxidants & Redox Signaling,* 10**,** 1941-1988.
MILENKOVIC, D., MÜLLER, J., STOJANOVSKI, D., PFANNER, N. & CHACINSKA, A. 2007. Diverse mechanisms and machineries for import of mitochondrial proteins. *Biological Chemistry,* 388(9):891-7.
MING-CHUAN, H., HUI-CHIU, C. & WEN-CHUN, H. 2007. HER-2/neu transcriptionally activates Jab1 expression via the AKT/β-catenin pathway in breast cancer cells. *Endocrine-Related Cancer Endocr Relat Cancer,* 14**,** 655-667.

MOLIN, M., YANG, J., HANZÉN, S., TOLEDANO, MICHEL B., LABARRE, J. & NYSTRÖM, T. 2011. Life Span Extension and H2O2 Resistance Elicited by Caloric Restriction Require the Peroxiredoxin Tsa1 in Saccharomyces cerevisiae. *Molecular Cell,* 43**,** 823-833.

MORGAN, B., SOBOTTA, M. C. & DICK, T. P. 2011. Measuring EGSH and H2O2 with roGFP2-based redox probes. *Free Radical Biology and Medicine,* 51**,** 1943-1951.

MORGAN, B. A. & VEAL, E. A. 2007. Functions of Typical 2-Cys Peroxiredoxins in Yeast. *Sub-cellular Biochemistry,* 44, 253-265.

MÜHLENHOFF, U., MOLIK, S., GODOY, J.R., UZARSKA, M.A., RICHTER, N., SEUBERT, A., ZHANG, Y., STUBBE, J., PIERREL, F., HERRERO, E., LILLIG, C.H. & LILL, R. 2010. Cytosolic monothiol glutaredoxins function in intracellular iron sensing and trafficking via their bound iron-sulfur cluster. *Cell metabolism,* 12(4):373-385.

MUNDT, K. E., LIU, C. & CARR, A. M. 2002. Deletion Mutants in COP9/Signalosome Subunits in Fission Yeast Schizosaccharomyces pombe Display Distinct Phenotypes. *Molecular Biology of the Cell,* 13**,** 493-502.

MURPHY, MICHAEL P. 2009. How mitochondria produce reactive oxygen species. *Biochemical Journal,* 417**,** 1-13.

NAKAO, L. S., EVERLEY, R. A., MARINO, S. M., LO, S. M., DE SOUZA, L. E., GYGI, S. P. & GLADYSHEV, V. N. 2015. Mechanism-based Proteomic Screening Identifies Targets of Thioredoxin-like Proteins. *The Journal of Biological Chemistry,* 290**,** 5685-5695.

NARAYANAN, S., DUBARRY, M., LAWLESS, C., BANKS, A. P., WILKINSON, D. J., WHITEHALL, S. K. & LYDALL, D. 2015. Quantitative Fitness Analysis Identifies exo1Δ and Other Suppressors or Enhancers of Telomere Defects in Schizosaccharomyces pombe. *PLoS ONE,* 10**,** e0132240.

NELSON, K. J., PARSONAGE, D., KARPLUS, P. A. & POOLE, L. B. 2013. Evaluating peroxiredoxin sensitivity towards inactivation by peroxide substrates. *Methods in enzymology,* 527**,** 10.1016/B978-0-12-405882-8.00002-7.

NEUMANN, C. A., KRAUSE, D. S., CARMAN, C. V., DAS, S., DUBEY, D. P., ABRAHAM, J. L., BRONSON, R. T., FUJIWARA, Y., ORKIN, S. H. & VAN ETTEN, R. A. 2003. Essential role for the peroxiredoxin Prdx1 in erythrocyte antioxidant defence and tumour suppression. *Nature,* 424**,** 561.

NEUPERT, W. & HERRMANN, J. M. 2007. Translocation of Proteins into Mitochondria. *Annual Review of Biochemistry,* 76**,** 723-749.

NGUYEN, V. D., SAARANEN, M. J., KARALA, A.-R., LAPPI, A.-K., WANG, L., RAYKHEL, I. B., ALANEN, H. I., SALO, K. E. H., WANG, C.-C. & RUDDOCK, L. W. 2011. Two Endoplasmic Reticulum PDI Peroxidases Increase the Efficiency of the Use of Peroxide during Disulfide Bond Formation. *Journal of Molecular Biology,* 406**,** 503-515.

NICHOLLS, C., LI, H. & LIU, J.-P. 2011. GAPDH: A common enzyme with uncommon functions. *Clinical and Experimental Pharmacology and Physiology,* 39**,** 674-679.

NIETHAMMER, P., GRABHER, C., LOOK, A. T. & MITCHISON, T. J. 2009. A tissue-scale gradient of hydrogen peroxide mediates rapid wound detection in zebrafish. *Nature,* 459**,** 996-999.

NOMURA, K., LEE, M., BANKS, C., LEE, G. & MORRIS, B. J. 2013. An ASK1-p38 signalling pathway mediates hydrogen peroxide-induced toxicity in NG108-15 neuronal cells. *Neuroscience Letters,* 549**,** 163-167.

NYSTRÖM, T., YANG, J. & MOLIN, M. 2012. Peroxiredoxins, gerontogenes linking aging to genome instability and cancer. *Genes & Development,* 26**,** 2001-2008.

OKA, O. B. V. & BULLEID, N. J. 2013. Forming disulfides in the endoplasmic reticulum. *Biochimica et Biophysica Acta (BBA) - Molecular Cell Research,* 1833**,** 2425-2429.

OKAZAKI, S., NAGANUMA, A. & KUGE, S. 2005. Peroxiredoxin-Mediated Redox Regulation of the Nuclear Localization of Yap1, a Transcription Factor in Budding Yeast. *Antioxidants & Redox Signaling,* 7**,** 327-334.

OLÁHOVÁ, M., TAYLOR, S. R., KHAZAIPOUL, S., WANG, J., MORGAN, B. A., MATSUMOTO, K., BLACKWELL, T. K. & VEAL, E. A. 2008. A redox-sensitive peroxiredoxin that is important for longevity has tissue- and stress-specific roles in stress resistance. *Proceedings of the National Academy of Sciences of the United States of America,* 105**,** 19839-19844.

OLÁHOVÁ, M. & VEAL, E. A. 2015. A peroxiredoxin, PRDX-2, is required for insulin secretion and insulin/IIS-dependent regulation of stress resistance and longevity. *Aging Cell,* 14**,** 558-568.

OLIVER CN, A. B., MOERMAN EJ, GOLDSTEIN S, STADTMAN ER 1987. Age-related changes in oxidized proteins. *The Journal of Biological Chemistry,* 262**,** 5488-91.

OLMEDO, M., O'NEILL, J. S., EDGAR, R. S., VALEKUNJA, U. K., REDDY, A. B. & MERROW, M. 2012. Circadian regulation of olfaction and an evolutionarily conserved, nontranscriptional marker in Caenorhabditis elegans. *Proceedings of the National Academy of Sciences of the United States of America,* 109**,** 20479-20484.

OLSEN, A., VANTIPALLI, M.C. & LITHGOW, G.J. 2006. Using Caenorhabditis elegans as a model for aging and age-related diseases. *Annals of the New York Academy of Sciences,* 1067:120-8.

ØSTERGAARD, H., TACHIBANA, C. & WINTHER, J. R. 2004. Monitoring disulfide bond formation in the eukaryotic cytosol. *The Journal of Cell Biology,* 166**,** 337-345.

OTT, M., ROBERTSON, J. D., GOGVADZE, V., ZHIVOTOVSKY, B. & ORRENIUS, S. 2002. Cytochrome c release from mitochondria proceeds by a two-step process. *Proceedings of the National Academy of Sciences of the United States of America,* 99**,** 1259-1263.

OWUSU-ANSAH, E., SONG, W. & PERRIMON, N. 2013. Muscle mitohormesis promotes longevity via systemic repression of insulin signaling. *Cell,* 155(3):699-712.

PAN, J. L. & BARDWELL, J. C. A. 2006. The origami of thioredoxin-like folds. *Protein Science : A Publication of the Protein Society,* 15**,** 2217-2227.

PAN, X., YE, P., YUAN, D. S., WANG, X., BADER, J. S. & BOEKE, J. D. 2006. A DNA Integrity Network in the Yeast Saccharomyces cerevisiae. *Cell,* 124**,** 1069-1081.

PAN, Y., YANG, H. & CLARET, F. X. 2014. Emerging roles of Jab1/CSN5 in DNA damage response, DNA repair, and cancer. *Cancer Biology & Therapy,* 15**,** 256-262.

PAN, Y., ZHANG, Q., TIAN, L., WANG, X., FAN, X., ZHANG, H., CLARET, F. X. & YANG, H. 2012. Jab1/CSN5 negatively regulates p27 and plays a role in the pathogenesis of nasopharyngeal carcinoma. *Cancer research,* 72**,** 1890-1900.

PARKES, T.L., ELIA, A.J., DICKINSON, D., HILLIKER, A.J., PHILIPS, J.P. & BOULIANNE, G.L. 1998. Extension of Drosophila lifespan by overexpression of human SOD1 in motorneurons. *Nature Genetics,* 2:171-4.

PARSONAGE, D., YOUNGBLOOD, D. S., SARMA, G. N., WOOD, Z. A., KARPLUS, P. A. & POOLE, L. B. 2005. Analysis of the Link between Enzymatic Activity and Oligomeric State in AhpC, a Bacterial Peroxiredoxin. *Biochemistry,* 44**,** 10.1021/bi050448i.

PATTERSON, M. J., MCKENZIE, C. G., SMITH, D. A., DA SILVA DANTAS, A., SHERSTON, S., VEAL, E. A., MORGAN, B. A., MACCALLUM, D. M., ERWIG, L.-P. & QUINN, J. 2013. Ybp1 and Gpx3 Signaling in Candida albicans Govern Hydrogen Peroxide-Induced Oxidation of the Cap1 Transcription Factor and Macrophage Escape. *Antioxidants & Redox Signaling,* 19**,** 2244-2260.

PAULO, E., GARCÍA-SANTAMARINA, S., CALVO, I. A., CARMONA, M., BORONAT, S., DOMÈNECH, A., AYTÉ, J. & HIDALGO, E. 2014. A genetic approach to study H2O2 scavenging in fission yeast – distinct roles of peroxiredoxin and catalase. *Molecular Microbiology,* 92**,** 246-257.

PAULSEN, C. E., TRUONG, T. H., GARCIA, F. J., HOMANN, A., GUPTA, V., LEONARD, S. E. & CARROLL, K. S. 2011. Peroxide-dependent sulfenylation of the EGFR catalytic site enhances kinase activity. *Nature Chemical Biology,* 8**,** 57.

PEDRAJAS, J. R., KOSMIDOU, E., MIRANDA-VIZUETE, A., GUSTAFSSON, J.-Å., WRIGHT, A. P. H. & SPYROU, G. 1999. Identification and Functional Characterization of a Novel Mitochondrial Thioredoxin System in Saccharomyces cerevisiae. *Journal of Biological Chemistry,* 274**,** 6366-6373.

PEDRAJAS, J. R., PADILLA, C. A., MCDONAGH, B. & BÁRCENA, J. A. 2010. Glutaredoxin Participates in the Reduction of Peroxides by the Mitochondrial 1-CYS Peroxiredoxin in Saccharomyces cerevisiae. *Antioxidants & Redox Signaling,* 13**,** 249-258.

PERALTA, D., BRONOWSKA, A. K., MORGAN, B., DÓKA, É., VAN LAER, K., NAGY, P., GRÄTER, F. & DICK, T. P. 2015. A proton relay enhances H2O2 sensitivity of GAPDH to facilitate metabolic adaptation. *Nature Chemical Biology,* 11**,** 156.

PESKIN, A. V., DICKERHOF, N., POYNTON, R. A., PATON, L. N., PACE, P. E., HAMPTON, M. B. & WINTERBOURN, C. C. 2013. Hyperoxidation of Peroxiredoxins 2 and 3: RATE CONSTANTS FOR THE REACTIONS OF THE SULFENIC ACID OF THE PEROXIDATIC CYSTEINE. *The Journal of Biological Chemistry,* 288**,** 14170-14177.

PESKIN, A. V., PACE, P. E., BEHRING, J. B., PATON, L. N., SOETHOUDT, M., BACHSCHMID, M. M. & WINTERBOURN, C. C. 2016. Glutathionylation of the Active Site Cysteines of Peroxiredoxin 2 and Recycling by Glutaredoxin. *The Journal of Biological Chemistry,* 291**,** 3053-3062.

PORRAS, P., MCDONAGH, B., PEDRAJAS, J. R., BÁRCENA, J. A. & PADILLA, C. A. 2010. Structure and function of yeast glutaredoxin 2 depend on postranslational processing and are related to subcellular distribution. *Biochimica et Biophysica Acta (BBA) - Proteins and Proteomics,* 1804**,** 839-845.

PORRAS, P., PADILLA, C. A., KRAYL, M., VOOS, W. & BÁRCENA, J. A. 2006. One Single In-frame AUG Codon Is Responsible for a Diversity of Subcellular Localizations of Glutaredoxin 2 in Saccharomyces cerevisiae. *Journal of Biological Chemistry,* 281**,** 16551-16562.

PUKKILA-WORLEY, R., AUSUBEL, F. M. & MYLONAKIS, E. 2011. Candida albicans Infection of Caenorhabditis elegans Induces Antifungal Immune Defenses. *PLoS Pathogens,* 7**,** e1002074.

QUINN, J., FINDLAY, V. J., DAWSON, K., MILLAR, J. B. A., JONES, N., MORGAN, B. A. & TOONE, W. M. 2002. Distinct Regulatory Proteins Control the Graded Transcriptional Response to Increasing H2O2 Levels in Fission Yeast Schizosaccharomyces pombe. *Molecular Biology of the Cell,* 13**,** 805-816.

RHEE, S. G., WOO, H. A., KIL, I. S. & BAE, S. H. 2012. Peroxiredoxin Functions as a Peroxidase and a Regulator and Sensor of Local Peroxides. *The Journal of Biological Chemistry,* 287**,** 4403-4410.

RICHARDSON, K. S. & ZUNDEL, W. 2005. The Emerging Role of the COP9 Signalosome in Cancer. *Molecular cancer research : MCR,* 3**,** 645-653.

RISTOW, M. & ZARSE, K. 2010. How increased oxidative stress promotes longevity and metabolic health: The concept of mitochondrial hormesis (mitohormesis). *Experimental Gerontology,* 45**,** 410-418.

ROMA, L. P., DEPONTE, M., RIEMER, J. & MORGAN, B. 2017. Mechanisms and Applications of Redox-Sensitive Green Fluorescent Protein-Based Hydrogen Peroxide Probes. *Antioxidants & Redox Signaling,* 29**,** 552-568.

ROMA, LETICIA P., DUPREZ, J., TAKAHASHI, HILTON K., GILON, P., WIEDERKEHR, A. & JONAS, J.-C. 2012. Dynamic measurements of mitochondrial hydrogen peroxide concentration and glutathione redox state in rat pancreatic β-cells using ratiometric fluorescent proteins: confounding effects of pH with HyPer but not roGFP1. *Biochemical Journal,* 441**,** 971-978.

ROMERO-ARISTIZABAL, C., MARKS, D. S., FONTANA, W. & APFELD, J. 2014. Regulated spatial organization and sensitivity of cytosolic protein oxidation in Caenorhabditis elegans. *Nature communications,* 5**,** 5020-5020.

RUDYK, O. & EATON, P. 2014. Biochemical methods for monitoring protein thiol redox states in biological systems. *Redox Biology,* 2**,** 803-813.

SALMEEN, A., ANDERSEN, J. N., MYERS, M. P., MENG, T.-C., HINKS, J. A., TONKS, N. K. & BARFORD, D. 2003. Redox regulation of protein tyrosine phosphatase 1B involves a sulphenyl-amide intermediate. *Nature,* 423**,** 769.

SANLI, T., STEINBERG, G. R., SINGH, G. & TSAKIRIDIS, T. 2014. AMP-activated protein kinase (AMPK) beyond metabolism: A novel genomic stress sensor participating in the DNA damage response pathway. *Cancer Biology & Therapy,* 15**,** 156-169.

SANZ, A. 2016. Mitochondrial reactive oxygen species: Do they extend or shorten animal lifespan? *Biochimica et Biophysica Acta (BBA) - Bioenergetics,* 1857**,** 1116-1126.

SCHMEISSER, S., PRIEBE, S., GROTH, M., MONAJEMBASHI, S., HEMMERICH, P., GUTHKE, R., PLATZER, M. & RISTOW, M. 2013. Neuronal ROS signaling rather than AMPK/sirtuin-mediated energy sensing links dietary restriction to lifespan extension. *Molecular Metabolism,* 2**,** 92-102.

SCHMITT, A.P. & MCENTEE, K. 1996. Msn2p, a zinc finger DNA binding protein, is the transcriptional activator of the multistress response in *Saccharomyces cerevisiae*. *Proceedings of the National Academy of Science of the United States of America,* 93(12):5777-82.

SCHRÖDER, E., LITTLECHIL*, J. A., LEBEDEV, A. A., ERRINGTON, N., VAGIN, A. A. & ISUPOV, M. N. 2000. Crystal structure of decameric 2-Cys peroxiredoxin from human erythrocytes at 1.7Å resolution. *Structure,* 8**,** 605-615.

SCHWARZLÄNDER, M., WAGNER, S., ERMAKOVA, Y. G., BELOUSOV, V. V., RADI, R., BECKMAN, J. S., BUETTNER, G. R., DEMAUREX, N., DUCHEN, M. R., FORMAN, H. J., FRICKER, M. D., GEMS, D., HALESTRAP, A. P., HALLIWELL, B., JAKOB, U., JOHNSTON, I. G., JONES, N. S., LOGAN, D. C., MORGAN, B., MÜLLER, F. L., NICHOLLS, D. G., REMINGTON, S. J., SCHUMACKER, P. T., WINTERBOURN, C. C., SWEETLOVE, L. J., MEYER, A. J., DICK, T. P. & MURPHY, M. P. 2014. The 'mitoflash' probe cpYFP does not respond to superoxide. *Nature,* 514**,** E12-E14.

SHAO, D., OKA, S.-I., LIU, T., ZHAI, P., AGO, T., SCIARRETTA, S., LI, H. & SADOSHIMA, J. 2014. A Redox-Dependent Mechanism for Regulation of AMPK Activation by Thioredoxin1 during Energy Starvation. *Cell Metabolism,* 19**,** 232-245.

SHEN, E.-Z., SONG, C.-Q., LIN, Y., ZHANG, W.-H., SU, P.-F., LIU, W.-Y., ZHANG, P., XU, J., LIN, N., ZHAN, C., WANG, X., SHYR, Y., CHENG, H. & DONG, M.-Q. 2014. Mitoflash frequency in early adulthood predicts lifespan in Caenorhabditis elegans. *Nature,* 508**,** 128.

SHENTON, D., PERRONE, G., QUINN, K. A., DAWES, I. W. & GRANT, C. M. 2002. Regulation of Protein S-Thiolation by Glutaredoxin 5 in the Yeast Saccharomyces cerevisiae. *Journal of Biological Chemistry,* 277**,** 16853-16859.

SIDERIS, D. P. & TOKATLIDIS, K. 2010. Oxidative Protein Folding in the Mitochondrial Intermembrane Space. *Antioxidants & Redox Signaling,* 13**,** 1189-1204.

SIES, H. 2014. Role of Metabolic H2O2 Generation: REDOX SIGNALING AND OXIDATIVE STRESS. *Journal of Biological Chemistry,* 289**,** 8735-8741.

SIPOS, K., LANGE, H., FEKETE, Z., ULLMANN, P., LILL, R. & KISPAL, G. 2002. Maturation of cytosolic iron-sulfur proteins requires glutathione. *The journal of biological chemistry,* 277(30):26944-9.

SIROVER, M. A. 2011. On the functional diversity of glyceraldehyde-3-phosphate dehydrogenase: Biochemical mechanisms and regulatory control. *Biochimica et Biophysica Acta (BBA) - General Subjects,* 1810**,** 741-751.

SMETS, B., GHILLEBERT, R., SNIJDER, P. D., BINDA, M., SWINNEN, E., VIRGILIO, C.D. & WINDERICKS, J. 2010. Life in the midst of scarcity: adaptations to nutrient availability in *Saccharomyces cerevisiae*. *Current Genetics,* 56(1):1-32.

SMITH, C. D., CARNEY, J. M., STARKE-REED, P. E., OLIVER, C. N., STADTMAN, E. R., FLOYD, R. A. & MARKESBERY, W. R. 1991. Excess brain protein oxidation and enzyme dysfunction in normal aging and in Alzheimer disease. *Proceedings of the National Academy of Sciences of the United States of America,* 88**,** 10540-10543.

SMITH, A., WARD, M.P. & GARRETT, S. 1998. Yeast PKA represses Msn2p/Msn4p-dependent gene expression to regulate growth, stress response and glycogen accumulation. *The EMBO Journal,* 17(13):3556-3564.

SOBOTTA, M. C., BARATA, A. G., SCHMIDT, U., MUELLER, S., MILLONIG, G. & DICK, T. P. 2013. Exposing cells to H2O2: A quantitative comparison between continuous low-dose and one-time high-dose treatments. *Free Radical Biology and Medicine,* 60**,** 325-335.

SOBOTTA, M. C., LIOU, W., STÖCKER, S., TALWAR, D., OEHLER, M., RUPPERT, T., SCHARF, A. N. D. & DICK, T. P. 2014. Peroxiredoxin-2 and STAT3 form a redox relay for H2O2 signaling. *Nature Chemical Biology,* 11**,** 64.

SOHAL, R. S. 1988. Effect of hydrogen peroxide administration on life span, superoxide dismutase, catalase, and glutathione in the adult housefly, Musca domestica. *Experimental Gerontology,* 3:211-6.

STEELE, D. F., BUTLER, C. A. & FOX, T. D. 1996. Expression of a recoded nuclear gene inserted into yeast mitochondrial DNA is limited by mRNA-specific translational activation. *Proceedings of the National Academy of Sciences of the United States of America,* 93**,** 5253-5257.

STEFANATOS, R., SRIRAM, A., KIVIRANTA, E., MOHAN, A., AYALA, V., JACOBS, H.T., PAMPLONA, R. & SANZ, A. 2012. dj-1β regulates oxidative stress, insulin-like signaling and development in Drosophila melanogaster. *Cell cycle,* 20:3876-87.

STONE, J. R. & YANG, S. 2006. Hydrogen Peroxide: A Signaling Messenger. *Antioxidants & Redox Signaling,* 8**,** 243-270.

STORZ, G., TARTAGLIA, L. & AMES, B. 1990. Transcriptional regulator of oxidative stress-inducible genes: direct activation by oxidation. *Science,* 248**,** 189-194.

SUN, J., FOLK, D., BRADLEY, T.J. & TOWER, J. 2002. Induced overexpression of mitochondrial Mn-superoxide dismutase extends the life span of adult Drosophila melanogaster. *Genetics,* 2:661-72.

SUZUKI, N. & MITTLER, R. 2012. Reactive oxygen species-dependent wound responses in animals and plants. *Free Radical Biology and Medicine,* 53**,** 2269-2276.

TAGUCHI, K., MOTOHASHI, H. & YAMAMOTO, M. 2011. Molecular mechanisms of the Keap1–Nrf2 pathway in stress response and cancer evolution. *Genes to Cells,* 16**,** 123-140.

TAN, S.-X., GREETHAM, D., RAETH, S., GRANT, C. M., DAWES, I. W. & PERRONE, G. G. 2010. The Thioredoxin-Thioredoxin Reductase System Can Function in Vivo as an Alternative System to Reduce Oxidized Glutathione in Saccharomyces cerevisiae. *The Journal of Biological Chemistry,* 285**,** 6118-6126.

TAO, K., MAKINO, K., YONEI, S., NAKATA, A. & SHINAGAWA, H. 1989. Molecular cloning and nucleotide sequencing of oxyR, the positive regulatory gene of a regulon for an adaptive response to oxidative stress in Escherichia coli: Homologies between OxyR protein and a family of bacterial activator proteins. *Molecular and General Genetics MGG,* 218**,** 371-376.

TAVENDER, T. J. & BULLEID, N. J. 2010. Peroxiredoxin IV protects cells from oxidative stress by removing H(2)O(2) produced during disulphide formation. *Journal of Cell Science,* 123**,** 2672-2679.

TAVENDER, T. J., SPRINGATE, J. J. & BULLEID, N. J. 2010. Recycling of peroxiredoxin IV provides a novel pathway for disulphide formation in the endoplasmic reticulum. *The EMBO Journal,* 29**,** 4185-4197.

TAYLOR, S. S., BUECHLER, J. A. & YONEMOTO, W. 1990. cAMP-Dependent Protein Kinase: Framework for a Diverse Family of Regulatory Enzymes. *Annual Review of Biochemistry,* 59**,** 971-1005.

THEIN, M. C., WINTER, A. D., STEPEK, G., MCCORMACK, G., STAPLETON, G., JOHNSTONE, I. L. & PAGE, A. P. 2009. Combined Extracellular Matrix Cross-linking Activity of the Peroxidase MLT-7 and the Dual Oxidase BLI-3 Is Critical for Post-embryonic Viability in Caenorhabditis elegans. *The Journal of Biological Chemistry,* 284**,** 17549-17563.

THEVELEIN, J.M., CAUWENBERG, L., COLOMBO, S., DE WINDE, J.H., DONATION, M., DUMORTIER, F., KRAAKMAN, L., LEMAIRE, K., MA, P., NAUWELAERS, D., ROLLAND, F., TEUNISSEN, A., VAN DIJCK, P., VERSELE, M., WERA, S. & WINDERICKX, J. 2000. Nutrient-induced signal transduction through the protein kinase A pathway and its role in the control of metabolism, stress resistance, and growth in yeast. *Enzyme and microbial technology,* 26:819-825.

TOLEDANO, M. B., DELAUNAY-MOISAN, A., OUTTEN, C. E. & IGBARIA, A. 2013. Functions and Cellular Compartmentation of the Thioredoxin and Glutathione Pathways in Yeast. *Antioxidants & Redox Signaling,* 18**,** 1699-1711.

TOMALIN, L. E., DAY, A. M., UNDERWOOD, Z. E., SMITH, G. R., DALLE PEZZE, P., RALLIS, C., PATEL, W., DICKINSON, B. C., BÄHLER, J., BREWER, T. F., CHANG, C. J.-L., SHANLEY, D. P. & VEAL, E. A. 2016. Increasing extracellular H2O2 produces a bi-phasic response in intracellular H2O2, with peroxiredoxin hyperoxidation only triggered once the cellular H2O2-buffering capacity is overwhelmed. *Free Radical Biology & Medicine,* 95**,** 333-348.

TOMODA, K., KUBOTA, Y. & KATO, J.-Y. 1999. Degradation of the cyclin-dependent-kinase inhibitor p27Kip1 is instigated by Jab1. *Nature,* 398**,** 160.

TONKS, N. K. 2005. Redox Redux: Revisiting PTPs and the Control of Cell Signaling. *Cell,* 121**,** 667-670.

TOONE, W. M. & JONES, N. 1999. AP-1 transcription factors in yeast. *Current Opinion in Genetics & Development,* 9**,** 55-61.

TOONE, W. M., KUGE, S., SAMUELS, M., MORGAN, B. A., TODA, T. & JONES, N. 1998. Regulation of the fission yeast transcription factor Pap1 by oxidative stress: requirement for the nuclear export factor Crm1 (Exportin) and the stress-activated MAP kinase Sty1/Spc1. *Genes & Development,* 12**,** 1453-1463.

TRUONG, T. H. & CARROLL, K. S. 2013. Redox regulation of protein kinases. *Critical reviews in biochemistry and molecular biology,* 48**,** 332-356.

TU, B. P. & WEISSMAN, J. S. 2002. The FAD- and O2-Dependent Reaction Cycle of Ero1-Mediated Oxidative Protein Folding in the Endoplasmic Reticulum. *Molecular Cell,* 10**,** 983-994.

TUDISCA, V., RECOUVREUX, V., MORENO, S., BOY-MARCOTTE, E., JACQUET, M. & PORTELA, P. 2010. Differential localization to cytoplasm, nucleus or P-bodies of yeast PKA subunits under different growth conditions. *European Journal of Cell Biology,* 89**,** 339-348.

TULLET, J. M. A., HERTWECK, M., AN, J. H., BAKER, J., HWANG, J. Y., LIU, S., OLIVEIRA, R. P., BAUMEISTER, R. & BLACKWELL, T. K. 2008. Direct Inhibition of the Longevity-Promoting Factor SKN-1 by Insulin-like Signaling in C. elegans. *Cell,* 132**,** 1025-1038.

TURNER-IVEY, B., MANEVICH, Y., SCHULTE, J., KISTNER-GRIFFIN, E., JEZIERSKA-DRUTEL, A., LIU, Y. & NEUMANN, C. A. 2013. Role for Prdx1 as a specific sensor in redox-regulated senescence in breast cancer. *Oncogene,* 32**,** 5302-5314.

UK, L. 1970. Cleavage of structural proteins during the assembly of the head of bacteriophage T4. *Nature,* 227**,** 680-5.

UKAI, Y., KISHIMOTO, T., OHDATE, T., IZAWA, S. & INOUE, Y. 2011. Glutathione peroxidase 2 in Saccharomyces cerevisiae is distributed in mitochondria and involved in sporulation. *Biochemical and Biophysical Research Communications,* 411**,** 580-585.

USHIO-FUKAI, M., ALEXANDER, R. W., AKERS, M., YIN, Q., FUJIO, Y., WALSH, K. & GRIENDLING, K. K. 1999. Reactive Oxygen Species Mediate the Activation of Akt/Protein Kinase B by

Angiotensin II in Vascular Smooth Muscle Cells. *Journal of Biological Chemistry,* 274**,** 22699-22704.
USHIO-FUKAI, M. & NAKAMURA, Y. 2008. Reactive Oxygen Species and Angiogenesis: NADPH Oxidase as Target for Cancer Therapy. *Cancer letters,* 266**,** 37-52.
VAN DER HOEVEN, R., CRUZ, M. R., CHÁVEZ, V. & GARSIN, D. A. 2015. Localization of the Dual Oxidase BLI-3 and Characterization of Its NADPH Oxidase Domain during Infection of Caenorhabditis elegans. *PLoS ONE,* 10**,** e0124091.
VAN DER VLIET, A. & JANSSEN-HEININGER, Y. M. W. 2014. Hydrogen peroxide as a damage signal in tissue injury and inflammation: Murderer, mediator, or messenger? *Journal of cellular biochemistry,* 115**,** 427-435.
VAN RAAMSDONK, J. M. & HEKIMI, S. 2009. Deletion of the Mitochondrial Superoxide Dismutase sod-2 Extends Lifespan in Caenorhabditis elegans. *PLoS Genetics,* 5**,** e1000361.
VEAL, E. & DAY, A. 2011. Hydrogen Peroxide as a Signaling Molecule. *Antioxidants & Redox Signaling,* 15**,** 147-151.
VEAL, E. A., DAY, A. M. & MORGAN, B. A. 2007. Hydrogen Peroxide Sensing and Signaling. *Molecular Cell,* 26**,** 1-14.
VEAL, E. A., FINDLAY, V. J., DAY, A. M., BOZONET, S. M., EVANS, J. M., QUINN, J. & MORGAN, B. A. 2004. A 2-Cys Peroxiredoxin Regulates Peroxide-Induced Oxidation and Activation of a Stress-Activated MAP Kinase. *Molecular Cell,* 15**,** 129-139.
VEAL, E. A., ROSS, S. J., MALAKASI, P., PEACOCK, E. & MORGAN, B. A. 2003. Ybp1 Is Required for the Hydrogen Peroxide-induced Oxidation of the Yap1 Transcription Factor. *Journal of Biological Chemistry,* 278**,** 30896-30904.
VEAL, ELIZABETH A., TOMALIN, LEWIS E., MORGAN, BRIAN A. & DAY, ALISON M. 2014. The fission yeast Schizosaccharomyces pombe as a model to understand how peroxiredoxins influence cell responses to hydrogen peroxide. *Biochemical Society Transactions,* 42**,** 909-916.
VEAL, E. A., UNDERWOOD, Z. E., TOMALIN, L. E., MORGAN, B. A. & PILLAY, C. S. 2017. Hyperoxidation of Peroxiredoxins: Gain or Loss of Function? *Antioxidants & Redox Signaling,* 28**,** 574-590.
VIGNOLS, F., BRÉHÉLIN, C., SURDIN-KERJAN, Y., THOMAS, D. & MEYER, Y. 2005. A yeast two-hybrid knockout strain to explore thioredoxin-interacting proteins in vivo. *Proceedings of the National Academy of Sciences of the United States of America,* 102**,** 16729-16734.
VILELLA, A. J., SEVERIN, J., URETA-VIDAL, A., HENG, L., DURBIN, R. & BIRNEY, E. 2009. EnsemblCompara GeneTrees: Complete, duplication-aware phylogenetic trees in vertebrates. *Genome Research,* 19**,** 327-335.
VIVANCOS, A. P., CASTILLO, E. A., BITEAU, B., NICOT, C., AYTÉ, J., TOLEDANO, M. B. & HIDALGO, E. 2005. A cysteine-sulfinic acid in peroxiredoxin regulates H2O2-sensing by the antioxidant Pap1 pathway. *Proceedings of the National Academy of Sciences of the United States of America,* 102**,** 8875-8880.
VIVANCOS, A. P., CASTILLO, E. A., JONES, N., AYTÉ, J. & HIDALGO, E. 2004. Activation of the redox sensor Pap1 by hydrogen peroxide requires modulation of the intracellular oxidant concentration. *Molecular Microbiology,* 52**,** 1427-1435.
VÖGTLE, F. N., BURKHART, J. M., RAO, S., GERBETH, C., HINRICHS, J., MARTINOU, J.-C., CHACINSKA, A., SICKMANN, A., ZAHEDI, R. P. & MEISINGER, C. 2012. Intermembrane Space Proteome of Yeast Mitochondria. *Molecular & Cellular Proteomics : MCP,* 11**,** 1840-1852.
VÖGTLE, F. N., WORTELKAMP, S., ZAHEDI, R. P., BECKER, D., LEIDHOLD, C., GEVAERT, K., KELLERMANN, J., VOOS, W., SICKMANN, A., PFANNER, N. & MEISINGER, C. 2009. Global Analysis of the Mitochondrial N-Proteome Identifies a Processing Peptidase Critical for Protein Stability. *Cell,* 139**,** 428-439.

WAKABAYASHI, N., ITOH, K., WAKABAYASHI, J., MOTOHASHI, H., NODA, S., TAKAHASHI, S., IMAKADO, S., KOTSUJI, T., OTSUKA, F., ROOP, D. R., HARADA, T., ENGEL, J. D. & YAMAMOTO, M. 2003. Keap1-null mutation leads to postnatal lethality due to constitutive Nrf2 activation. *Nature Genetics,* 35**,** 238.

WANG, J., ROBIDA-STUBBS, S., TULLET, J. M. A., RUAL, J.-F., VIDAL, M. & BLACKWELL, T. K. 2010. RNAi Screening Implicates a SKN-1–Dependent Transcriptional Response in Stress Resistance and Longevity Deriving from Translation Inhibition. *PLOS Genetics,* 6**,** e1001048.

WANG, L., ZHENG, J.-N. & PEI, D.-S. 2016. The emerging roles of Jab1/CSN5 in cancer. *Medical Oncology,* 33**,** 90.

WANG, X., FANG, H., HUANG, Z., SHANG, W., HOU, T., CHENG, A. & CHENG, H. 2013. Imaging ROS signaling in cells and animals. *Journal of Molecular Medicine (Berlin, Germany),* 91**,** 917-927.

WANG, Y., CAO, Y.-Y., JIA, X.-M., CAO, Y.-B., GAO, P.-H., FU, X.-P., YING, K., CHEN, W.-S. & JIANG, Y.-Y. 2006. Cap1p is involved in multiple pathways of oxidative stress response in Candida albicans. *Free Radical Biology and Medicine,* 40**,** 1201-1209.

WEI, N. & DENG, X. W. 2003. The COP9 Signalosome. *Annual Review of Cell and Developmental Biology,* 19**,** 261-286.

WEI, N., SERINO, G. & DENG, X.-W. 2008. The COP9 signalosome: more than a protease. *Trends in Biochemical Sciences,* 33**,** 592-600.

WEIDS, A. J. & GRANT, C. M. 2014. The yeast peroxiredoxin Tsa1 protects against protein-aggregate-induced oxidative stress. *Journal of Cell Science,* 127**,** 1327-1335.

WOO, H. A., CHAE, H. Z., HWANG, S. C., YANG, K.-S., KANG, S. W., KIM , K. & RHEE, S. G. 2003. Reversing the Inactivation of Peroxiredoxins Caused by Cysteine Sulfinic Acid Formation. *Science,* 300**,** 653-656.

WOOD, Z. A., POOLE, L. B. & KARPLUS, P. A. 2003a. Peroxiredoxin Evolution and the Regulation of Hydrogen Peroxide Signaling. *Science,* 300**,** 650-653.

WOOD, Z. A., SCHRÖDER, E., ROBIN HARRIS, J. & POOLE, L. B. 2003b. Structure, mechanism and regulation of peroxiredoxins. *Trends in Biochemical Sciences,* 28**,** 32-40.

WU, D., REA, S. L., YASHIN, A. I. & JOHNSON, T. E. 2006. Visualizing hidden heterogeneity in isogenic populations of C. elegans. *Experimental Gerontology,* 41**,** 261-270.

YANG, W. & HEKIMI, S. 2010. A Mitochondrial Superoxide Signal Triggers Increased Longevity in Caenorhabditis elegans. *PLoS Biology,* 8**,** e1000556.

ZHANG, X.-C., CHEN, J., SU, C.-H., YANG, H.-Y. & LEE, M.-H. 2007. Roles for CSN5 in control of p53/MDM2 activities. *Journal of Cellular Biochemistry,* 103**,** 1219-1230.

ZHENG, H., LAPOINTE, J. & HEKIMI, S. 2010. Lifelong protection from global cerebral ischemia and reperfusion in long-lived Mclk1+/− mutants. *Experimental Neurology,* 223**,** 557-565.

ZITO, E., MELO, E. P., YANG, Y., WAHLANDER, Å., NEUBERT, T. A. & RON, D. 2010. Oxidative protein folding by an endoplasmic reticulum localized peroxiredoxin. *Molecular cell,* 40**,** 787-797.

ZNAIDI, S., BARKER, K. S., WEBER, S., ALARCO, A.-M., LIU, T. T., BOUCHER, G., ROGERS, P. D. & RAYMOND, M. 2009. Identification of the Candida albicans Cap1p Regulon. *Eukaryotic Cell,* 8**,** 806-820.

Communications

ANTIOXIDANTS & REDOX SIGNALING
Volume 28, Number 7, 2018

DOI: 10.1089/ars.2017.7214

Discoveries

FORUM REVIEW ARTICLE

Hyperoxidation of Peroxiredoxins: Gain or Loss of Function?

Elizabeth A. Veal,[1,2] Zoe E. Underwood,[1,2] Lewis E. Tomalin,[1,2]
Brian A. Morgan,[1] and Ché S. Pillay[3]

Abstract

Significance: In 2003, structural studies revealed that eukaryotic 2-Cys peroxiredoxins (Prx) have evolved to be sensitive to inactivation of their thioredoxin peroxidase activity by hyperoxidation (sulfinylation) of their peroxide-reacting catalytic cysteine. This was accompanied by the unexpected discovery, that the sulfinylation of this cysteine was reversible *in vivo* and the identification of a new enzyme, sulfiredoxin, that had apparently co-evolved specifically to reduce hyperoxidized 2-Cys Prx, restoring their peroxidase activity. Together, these findings have provided the impetus for multiple studies investigating the purpose of this reversible, Prx hyperoxidation.

Recent Advances: It has been suggested that inhibition of the thioredoxin peroxidase activity by hyperoxidation can both promote and inhibit peroxide signal transduction, depending on the context. Prx hyperoxidation has also been proposed to protect cells against reactive oxygen species (ROS)-induced damage, by preserving reduced thioredoxin and/or by increasing non-peroxidase chaperone or signaling activities of Prx.

Critical Issues: Here, we will review the evidence in support of each of these proposed functions, in view of the *in vivo* contexts in which Prx hyperoxidation occurs, and the role of sulfiredoxin. Thus, we will attempt to explain the basis for seemingly contradictory roles for Prx hyperoxidation in redox signaling.

Future Directions: We provide a rationale, based on modeling and experimental studies, for why Prx hyperoxidation should be considered a suitable, early biomarker for damaging levels of ROS. We discuss the implications that this has for the role of Prx in aging and the detection of hyperoxidized Prx as a conserved feature of circadian rhythms. *Antioxid. Redox Signal.* 28, 574–590.

Keywords: 2-Cys peroxiredoxin, signaling, chaperone, sulfiredoxin, circadian rhythm, thioredoxin, aging

Introduction

BIOINFORMATIC ANALYSIS HAS identified six families of peroxiredoxins, which all contain a highly peroxide-reactive cysteine. Four of these families are found in eukaryotes, with animal representatives limited to the Prx1–4 (typical 2-Cys Prx), Prx5 (atypical 2-Cys Prx), and Prx6 (1-Cys Prx) groups (73, 99). After initial oxidation of the cysteine-thiol to cysteine-sulfenyl, further oxidation is usually prevented by formation of a disulfide bond with a resolving cysteine that may be present in the same peptide, an interacting partner protein or glutathione. Recycling of the reduced peroxiredoxin then involves the transfer of electrons from NADPH or NADH *via* an oxidoreductase, such as thioredoxin (Trx). This redox coupling effectively allows the ''catalytic'' reduction of peroxides. However, if disulfide formation does not occur before the cysteine-sulfenyl encounters another peroxide molecule, then it will become ''hyperoxidized'' to a cysteine-sulfinyl (SO_2^-), which cannot be reduced by thioredoxin or by many other thiol reductants (Fig. 1). In the case of most prokaryotic peroxiredoxins, and all Prx5 and Prx6 family members, the formation of the disulfide with the resolving thiol occurs rapidly, such that hyperoxidation is not usually observed unless the peroxiredoxin is exposed to very high mM levels of

[1]Institute for Cell and Molecular Biosciences, Newcastle University, Newcastle upon Tyne, United Kingdom.
[2]Newcastle University Institute for Ageing, Newcastle University, Newcastle upon Tyne, United Kingdom.
[3]School of Life Sciences, University of KwaZulu-Natal, Pietermartizburg, South Africa.

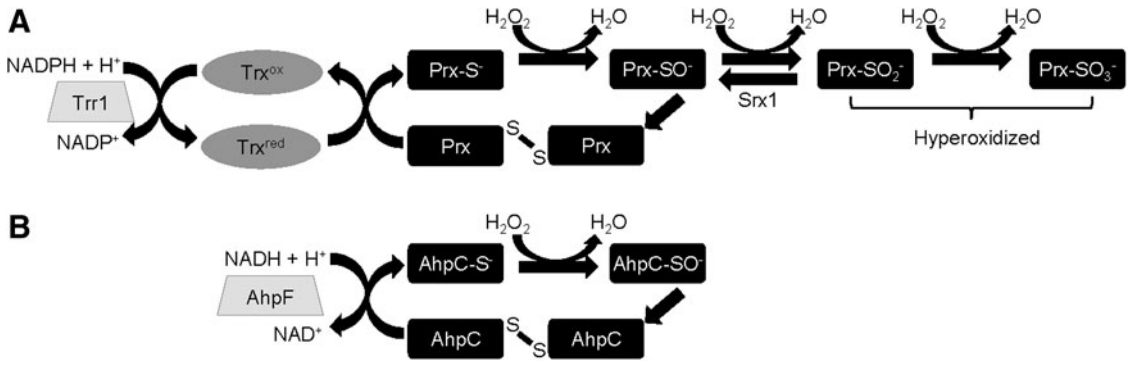

FIG. 1. Redox reactions of typical 2-Cys Prx in (A) eukaryotes and (B) bacteria in response to H_2O_2. H_2O_2 oxidizes the peroxidatic cysteine of 2-Cys Prx (Prx and AhpC) to form a sulfenic acid ($-SO^-$) derivative, which can be resolved by forming an intermolecular disulfide bond with an adjacent Prx molecule, or undergo further oxidation to sulfinic ($-SO_2^-$) and sulfonic ($-SO_3^-$) derivatives. The sulfinylated peroxidatic cysteine ($-SO_2^-$) can be reduced by sulfiredoxin (Srx1), and sulfonylation is irreversible. Prx disulfides are reduced by **(A)** thioredoxin or **(B)** flavoprotein disulfide reductase (AhpF) to complete the catalytic cycle. Thioredoxin is reduced and recycled by thioredoxin reductase (Trr) by using electrons from NADPH, whereas the thioredoxin-like domain of bacterial AhpF is reduced by a second dithiol center, within the thioredoxin reductase-like module of AhpF, by using electrons from NADH.

peroxides. Therefore, based on the high peroxide reactivity of the peroxidatic cysteine, it has been generally assumed that the main function of Prx, including the highly abundant 2-Cys Prx, is to protect cells against oxidative damage by catalytically removing peroxides. Indeed, the inability of bacterial and yeast mutants lacking 2-Cys Prx to grow under oxidative stress conditions is consistent with this view. However, the observation that eukaryotic typical 2-Cys Prx(Prx1-4) forms disulfides with their resolving cysteine relatively slowly, rendering them at least 50× more susceptible to hyperoxidation than their bacterial counterparts (98), has inevitably raised questions as to the value of the peroxidase activity of hyperoxidation-sensitive Prx in protecting against peroxide-induced oxidative damage. For instance, if, as their abundance and the oxidative stress sensitivity of Prx mutants suggests, 2-Cys Prx are an important reactive oxygen species (ROS) defense, then what selective advantage could there be in evolving to be sensitive to inactivation of their thioredoxin peroxidase activity by peroxide? Here, we will review studies over the past 15 years that have done much to define how and why these 2-Cys Prx become hyperoxidized and thus provide more than one answer to this intriguing question.

What Makes Some Prx More Sensitive to Sulfinylation of the Peroxidatic Cysteine?

Although typical 2-Cys Prxs are practically ubiquitously expressed, seminal studies by Wood *et al.* (2003) revealed that 2-Cys Prx that are sensitive to hyperoxidation share GGLG and YF motifs, which are not present in their prokaryotic peroxide-resistant counterparts (Fig. 2). By impeding the unfolding of the Prx to its locally unfolded state, these GGLG and YF motifs serve to delay the formation of the disulfide between the sulfenylated peroxidatic cysteine and the resolving cysteine, thus greatly increasing the probability that the sulfenylated cysteine will encounter a second peroxide molecule and become further oxidized to the sulfinylated form (Fig. 1). Subsequent work has identified that some eukaryotic 2-Cys Prx are more sensitive to hyperoxidation than others. For example, the peroxidatic cysteine of the mitochondrial 2-Cys Prx, Prx3, is more resistant to hyperoxidation than its cytoplasmic counterparts, Prx1 and Prx2, due to its higher rate of disulfide formation (23, 32, 70).

Other factors have also been shown to influence the sensitivity of Prx to hyperoxidation. Although the minimal catalytic unit of 2-Cys Prx is dimeric, under physiological conditions these dimers are cooperatively associated into oligomeric complexes, usually decamers, in which the reactivity of the peroxidatic cysteine (and thus the thioredoxin peroxidase activity) is increased, apart from the susceptibility to hyperoxidation (3, 67, 78). The rate of reduction of Prx disulfides also influences the extent to which Prx will become hyperoxidized *in vivo*. For instance, the lack of thioredoxin reductase activity in the endoplasmic reticulum (ER) limits the recycling of Prx4 disulfide dimers to the thiol state and thus the rate at which Prx4 can become hyperoxidized (15). The presence of other peroxide-removing activities has also been shown to protect Prx from hyperoxidation both *in vitro* and *in vivo* (21, 70, 84). Thus, the extent to which any 2-Cys Prx becomes hyperoxidized *in vivo* (Table 1) depends on a number of things, including the local concentration of peroxide and rate at which the sulfenylated form is able to locally unfold to allow disulfide formation, but also the concentrations of 2-Cys Prx and availability of thioredoxin.

How Is Hyperoxidation of Prx Reversed?

Although glutathione/glutaredoxins and thioredoxins can reduce oxidized cysteine derivatives, such as sulfenic, sulfenylamide, and disulfides, cysteine sulfinylation is resistant to reduction by any of these enzymes/redox couples. Consequently, cysteine sulfinylation has generally been considered irreversible. However, Woo *et al.* made the remarkable discovery that the hyperoxidation of the peroxide-reacting cysteine in human Prx1 to the sulfinylated derivative was slowly reversed *in vivo*, actively regenerating the thioredoxin peroxidase active form (94). At the same time, the enzyme responsible for reducing hyperoxidized 2-Cys Prx in yeast was identified as a 13 kDa H_2O_2-induced protein of previously unknown function and thus named ''sulfiredoxin'' (8).

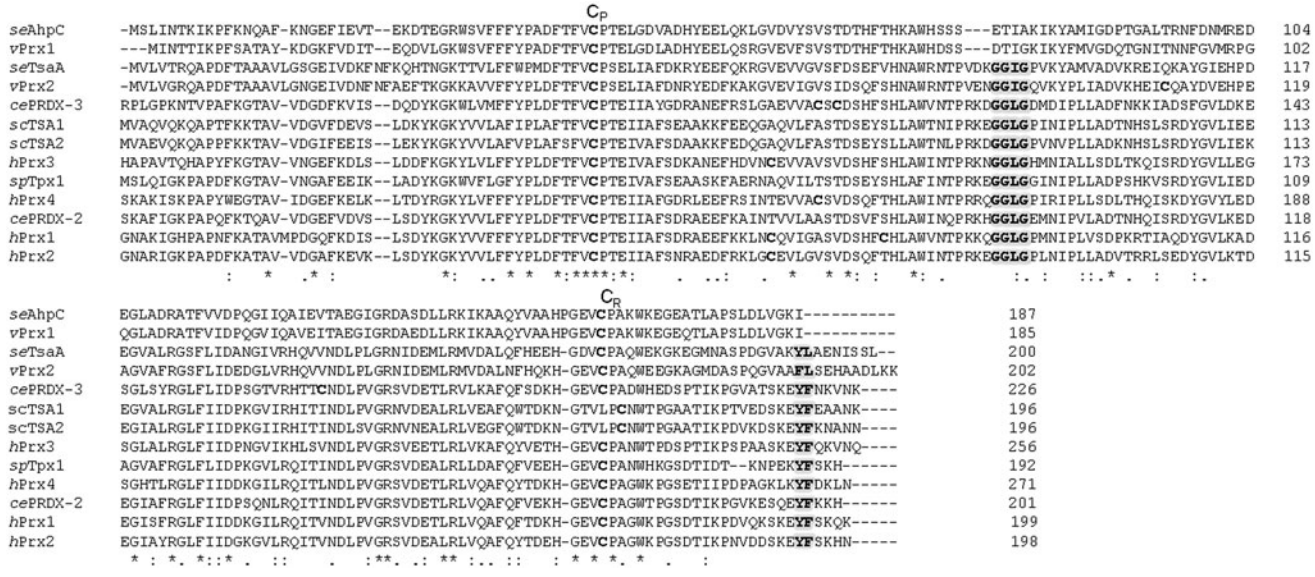

FIG. 2. Alignment of 2-Cys Prxs from *Salmonella enterica* (*se*AhpC and *se*TsaA), *Vibrio vulnificus* (*v*Prx1 and *v*Prx2), *Caenorhabditis elegans* (*ce*PRDX-2 and *ce*PRDX-3), *Saccharomyces cerevisiae* (*sc*TSA1 and *sc*TSA2), human (*h*Prx1, *h*Prx2, *h*Prx3, and *h*Prx4), and *Schizosaccharomyces pombe* (*sp*Tpx1). The amino acid sequences retrieved from the NCBI protein database (NCBI, ncbi.nlm.nih.gov) (accession numbers AAL19559 for *se*AhpC, AAL19356 for *se*TsaA, ADV88988 for *v*Prx1, ADV87477 for *v*Prx2, CTQ86475.1 for *ce*PRDX-2, CAA83619.1 for *ce*PRDX-3, KZV08815.1 for *sc*TSA1, KZV12693.1 for *sc*TSA2, NP_001189360.1 for hPrx1, NP_005800.3 for hPrx2, AAH59169.1 for hPrx3, NP_006397.1 for hPrx4, and CAA21182.1 for *sp*Tpx1) were aligned by using the Clustal Omega programme. Peroxidatic and resolving cysteines are indicated (C_p) and (C_R), respectively. The motifs, GG(L/I)G and YF/FL, considered specific for hyperoxidation-sensitive Prx (98) are *highlighted* (*bold text*/*gray*). Conserved amino acids are indicated: ''*'' indicates identity, '':'' indicates similar, and ''.'' indicates some similarity.

Significantly, homologues of sulfiredoxin were found to be encoded in the genomes of almost all the eukaryotes and prokaryotes where hyperoxidation-sensitive Prx are present, suggesting that this mechanism for reduction of hyperoxidized Prx is conserved (69). Although sulfiredoxin-mediated reduction of cysteine sulfinate still appears to be limited to the sulfinylated peroxidatic cysteine of 2-Cys Prx (95), human sulfiredoxin has also been shown to deglutathionylate actin and PTP1B (29) and denitrosylate the peroxidatic cysteine of Prx2 (81), raising the possibility that these activities also contribute to its *in vivo* function. Interestingly, sulfiredoxin shares some homology with bacterial ParB, a DNA-binding protein that is required for chromosomal partitioning, from which it appears to have evolved (4). However, importantly, the catalytic cysteine 99 that is essential for all known enzymatic activities of sulfiredoxin is not present in ParB.

Shortly after the discovery of sulfiredoxin, it was proposed that a second eukaryotic protein, sestrin, also catalyzed the reduction of hyperoxidized Prx (13). This function was proposed, in part, based on homology between sestrin and mycobacterial AhpD, an enzyme that reduces alkyl hydroperoxides and also disulfides in the Prx AhpC. However, subsequent studies have been unable to detect any *in vitro* or *in vivo* activity of sestrin in reducing hyperoxidized Prx (93). This is even the case in the nematode worm *Caenorhabditis elegans*, which lacks a sulfiredoxin encoding gene but expresses a sestrin homologue (61, 83). Further, other roles for sestrin have been identified that suggest that the lower levels of hyperoxidized Prx in cells in which sestrin is overexpressed may be due to indirect effects on the expression of sulfiredoxin and even other ROS-metabolizing enzymes [reviewed in Ho *et al.* (35)].

In contrast to sestrin, there is substantial evidence that sulfiredoxin is important for the reduction of hyperoxidized 2-Cys Prx under stress conditions in diverse phyla, including cyanobacteria (10), plants (75, 76), mammals (17), and the divergent yeasts *Saccharomyces cerevisiae* and *Schizosaccharomyces pombe* (8, 11, 88). Interestingly, the levels of sulfiredoxin mRNA have been found to be undetectably low in many organisms under normal growth conditions (11, 76, 88). Indeed, consistent with sulfiredoxin's functions being restricted to stress conditions, the phenotypes associated with loss of sulfiredoxin in mice, yeast, and plants have generally been found to relate to stress or toxin-induced conditions where its expression is induced (8, 11, 41, 43, 72, 76, 88, 91, 100). Moreover, although Prx are found in multiple cell compartments, organisms generally express a single sulfiredoxin gene, encoding proteins that have been shown to be largely confined to the cytoplasm in mammalian cells (57) or chloroplast in plants (76). These findings have raised questions as to whether reduction of hyperoxidized Prx has any significant role under normal physiological conditions, particularly in cell compartments that lack sulfiredoxin. Indeed, the absence of sulfiredoxin, or any evidence that hyperoxidized Prx become reduced, in *C. elegans* suggests that reducing hyperoxidized Prx is not of major importance, even in organisms where the Prx is sensitive to hyperoxidation (61, 83). However, in evolutionarily divergent yeast and in mammalian cells, sulfiredoxin gene expression is rapidly induced in response to various stress conditions. Moreover,

Table 1. A Comparison of the Findings of *In Vivo* Studies Investigating the Sensitivity of Prx to Hyperoxidation

		Source of ROS/% Prx hyperoxidized			
Species/cells	*2-Cys Prx*	*Exogenous treatment (bolus) required to increase hyperoxidation*	*Physiological/ other*	*Detection method (antibody)*	*References*
Bacteria					
Vibrio vulnificus	vPrx1	1000 μM H_2O_2 (5 min)/≤1%	—	Non-reducing western (αPrx1, αPrx2, $\alpha PrxSO_{2/3}$)	(2)
	vPrx2	30 μM H_2O_2 (5 min)/ ≥80%			
Anabaena	NP_488681	50 μM H_2O_2 (15 min)/ ~ 100%	Light (800 μE m^{-2} s^{-1})/ ~ 100%	2D PAGE, non-reducing western (αPrx [rice], αPrx [*Synechocystis*])	(68)
Synechocystis	NP_442066	1000 μM H_2O_2 (15 min)/≤50%			
Eukaryotes					
Saccharomyces cerevisiae	Tsa1	500 μM H_2O_2 (2 min)/≥50%		2D PAGE, Redox western (AMS) (αTsa1-Myc)	(8)
	Tsa1	400 μM H_2O_2 (20 min)/≥50%	Replicative aging/ ~ 20%	2D PAGE (αTsa1-Myc)	(53)
Schizosaccharomyces pombe	Tpx1	200 μM H_2O_2 (5 min)/≤10%	—	Redox western (AMS) (Tpx1-pk or Tpx1-HA), 2D PAGE	(11, 88)
		1000 μM H_2O_2 (5 min)/≥50%			
		1000 μM H_2O_2 (10 min)/ ~ 100%	—	Redox western (AMS) (αTpx1)	(27)
		200 μM H_2O_2 (30 s)/ ~ 5%		Redox western (AMS) (αTpx1)	(84)
Caenorhabditis elegans	PRDX-2	1000 μM H_2O_2 (5 min)/≤10%	—	Redox western (AMS) (αPRDX-2)	(61)
		5000 μM H_2O_2 (5 min)/ ~ 50%			
Mouse	Prdx3	ACTH injection (1 h)/ ~ 30%	Adrenal gland/ 10%–20%	$\alpha PrxSO_{2/3}$ compared with recombinant hyperoxidized Prdx3	(43)
	Prdx2		Hemoglobin autoxidation/ ~ 1%	$\alpha PrxSO_{2/3}$ compared with a Prx2 standard analyzed by 2D PAGE	(18)
Rat					
Hearts	Prdx1	100 μM H_2O_2 (5 min)/≤10%	—	Non-reducing western (maleimide) (αPrdx1, αPrdx2, αPrdx3, $\alpha PrxSO_{2/3}$)	(77)
	Prdx2	100 μM H_2O_2 (5 min)/≤10%			
Ovarian tissue	Prdx3		High-fat diet/8% maternal undernutrition/ 12%	Non-reducing western (αPrx3)	(7)
Preovulatory follicles	Prdx2	Gonadotropin (eCG/ hCG) treatment (2 h)/ ~ 28%	~ 15%	2D PAGE (αPrdx2)	(65)
Human					
HT1080 cells	Prx2	100 μM H_2O_2 (10 min)/ ~ 81%	~ 2%	1D IEF (αPrx2, αPrx3, αPrx4)	(15)
	Prx3	100 μM H_2O_2 (10 min)/ ~ 30%	~ 10%		
	Prx4	1000 μM H_2O_2 (10 min)/ ~ 27%	~ 15%		

(*continued*)

Table 1. (Continued)

Species/cells	2-Cys Prx	Source of ROS/% Prx hyperoxidized: Exogenous treatment (bolus) required to increase hyperoxidation	Source of ROS/% Prx hyperoxidized: Physiological/ other	Detection method (antibody)	References
Jurkat (T lymphoma) cells	Prx1	20 μM H_2O_2 (10 min)/~48%	UVB (5 min) ≤10%	Non-reducing western (αPrx1, αPrx2, αPrx3)	(23)
	Prx2	20 μM H_2O_2 (10 min)/~80%	UVB (5 min) ≤10%		
	Prx3	40 μM H_2O_2 (10 min) ~5%	—		
Confluent human articular chondrocytes	Prx2	25 μM menadione (60 min)	Age of donor/ ≤20%	Non-reducing western (IAM) (α$PrxSO_{2/3}$, αPrx2 and αPrx3)	(21)
	Prx3	25 μM menadione (5 min)	Age of donor/≤5%		

Examples of studies investigating the extent of hyperoxidation of Prx in response to physiological changes and exogenous sources of reactive oxygen species. The minimum level of stress and earliest time point at which Prx hyperoxidation was detected are indicated, together with the extent of hyperoxidation and the methodology by which this was estimated.

1D, one-dimensional; 2D, two-dimensional; ACTH, adrencorticotrophic hormone; eCG, equine chorionic gonadotropin; hCG, human chorionic gonadotropin; IAM, iodoacetamide; IEF, isoelectric focusing; PAGE, polyacrylamide gel electrophoresis; ROS, reactive oxygen species; UVB, ultraviolet B.

sulfiredoxin is also imported into the mitochondria under stress conditions where it is important for reducing hyperoxidized Prx3 (44, 57). Nevertheless, although it is widely accepted that sulfiredoxin is important for the reduction of hyperoxidized Prx, it is notable that transcriptional, post-transcriptional, and post-translational mechanisms are present to ensure that, under optimal growth conditions, sulfiredoxin levels are kept very low and restricted to specific compartments (8, 11, 41, 44, 53). Indeed, the evolved sensitivity of eukaryotic 2-Cys Prx to hyperoxidation of the peroxidatic cysteine, and the tightly regulated expression and localization of sulfiredoxin, provides strong circumstantial evidence to suggest there are advantages to be gained from hyperoxidation of 2-Cys Prx in response to rises in intracellular H_2O_2 levels. In the remainder of this review, we will explore the various possible advantages that Prx hyperoxidation has been proposed to confer and the evidence in support of each hypothesis.

Loss of Function: Advantages of Inhibiting Thioredoxin Peroxidase Activity

The co-evolution of sensitivity to hyperoxidation with the utilization of H_2O_2 as a signaling molecule led to the original proposal of "The Floodgate Model" (98). In this model, it was suggested that the abundance and reactivity of 2-Cys Prx with H_2O_2 meant that they presented a significant barrier to the utilization of H_2O_2 as a signaling molecule. Accordingly, it was proposed that, for H_2O_2 to encounter and react with a cysteine on a "signaling" protein, it was important to first overcome this Prx barrier. By inactivating the thioredoxin peroxidase activity, Prx hyperoxidation would thus allow H_2O_2 to accumulate and react with target H_2O_2-sensitive signaling proteins (Fig. 3A). The Floodgate model has certainly provided a plausible explanation for why Prx might have evolved to be sensitive to hyperoxidation, potentially solving the conundrum as to how H_2O_2-regulated target signaling proteins ever become oxidized in the presence of more abundant and more reactive 2-Cys Prx. In support of the principle underlying this hypothesis, phosphorylation has been shown to reduce the thioredoxin peroxidase activity of mammalian Prx1 and thus promote H_2O_2-dependent signaling in response to growth factors (16, 19, 97). However, there is no evidence that 2-Cys Prx become hyperoxidized to any significant extent by H_2O_2 generated in response to growth factors or most other physiological stimuli (19, 25, 97) (Table 1). Moreover, although Prx hyperoxidation has now been detected in many biological situations (Tables 1 and 2), there remain few examples demonstrating that Prx hyperoxidation is important for downstream increases in signaling. Perhaps the best evidence to date in support of the Floodgate model has come from studies that have detected increased hyperoxidation of mitochondrial Prx3 in the adrenal cortex in response to adrenocorticotrophic hormone (ACTH). This Prx3 hyperoxidation is caused by increased levels of mitochondrial H_2O_2 generated by cytochrome P450s during corticosteroid production. Importantly, ACTH-induced Prx3 hyperoxidation has been shown to be required for the associated increase in cytoplasmic activation of the p38 mitogen activated protein kinase (MAPK) (Fig. 3A) (43). However, the activation of p38 MAPK has been shown to require cytosolic Prx (22, 87) and involve the formation of disulfides between Prx1 and the mitogen activated protein kinase kinase kinase (MAPKKK) Ask1 (40). Thus, the hyperoxidation of Prx3 detected by Kil *et al.* may actually serve to increase the H_2O_2 available to oxidize another Prx, Prx1, rather than, as suggested by the Floodgate model, a less peroxide-reactive signaling protein. Moreover, despite the attention that this model has received, there is still remarkably little evidence that inactivation of the thioredoxin peroxidase activity of 2-Cys Prx by hyperoxidation is responsible for *in vivo* increases in H_2O_2. For example, even in the case of the significant ACTH-induced increases in Prx3 hyperoxidation, described earlier, it is unclear as to whether the extent to which Prx3 becomes hyperoxidized (<30%) would limit the removal of mitochondrial H_2O_2 sufficiently to cause an increase in cytoplasmic H_2O_2 (43).

Certainly the levels and duration of H_2O_2 exposure required to hyperoxidize the bulk of 2-Cys Prx activity seem to

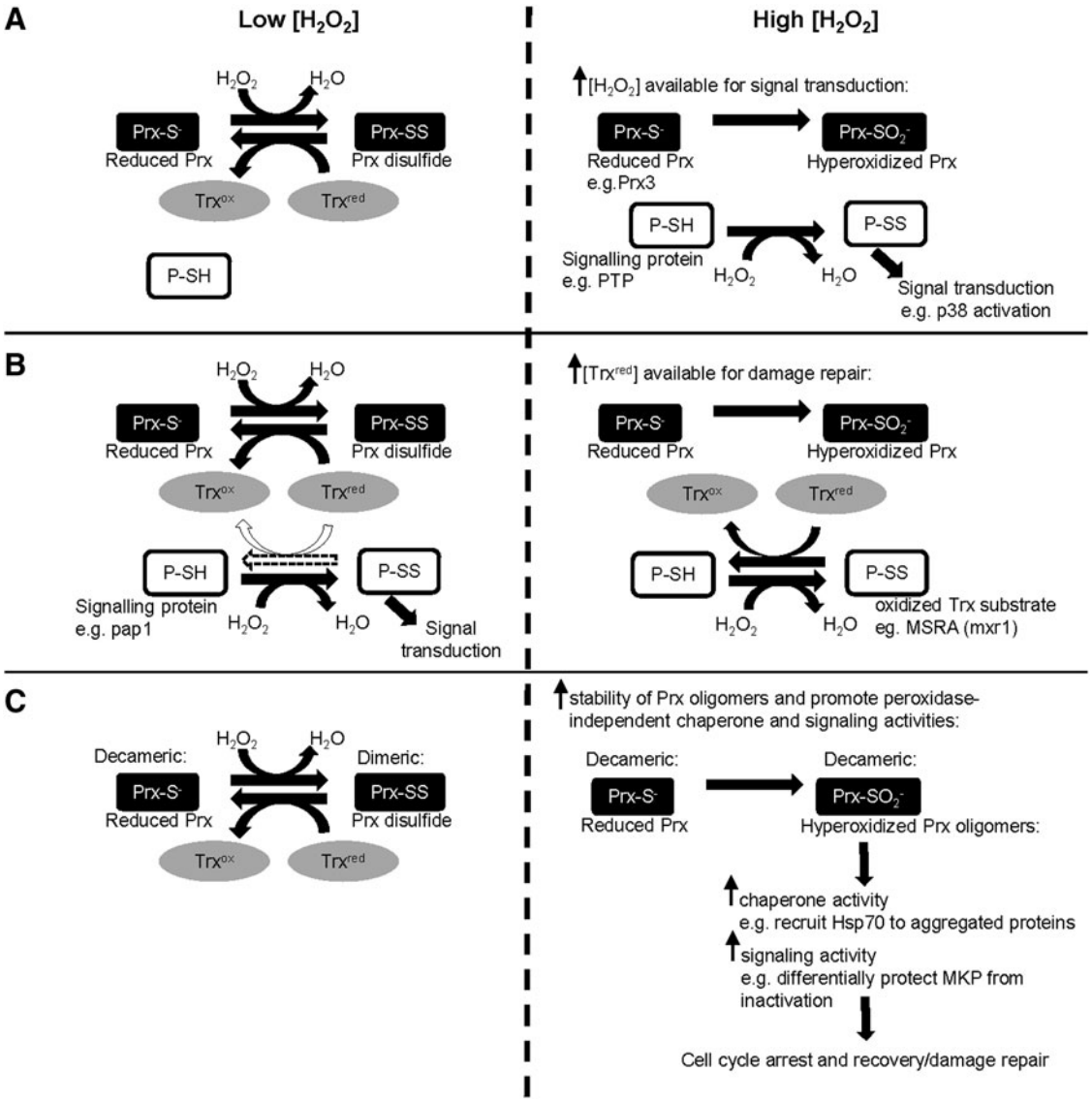

FIG. 3. Hyperoxidation of Prx has been proposed to (A) allow H_2O_2 signaling, (B) preserve thioredoxin activity by inhibiting their thioredoxin peroxidase activity, and (C) to promote alternative chaperone and signaling activities. **(A)** 2-Cys Prx are proposed to act as floodgates; buffering low levels of H_2O_2 and thus inhibiting the oxidation of signaling proteins (*e.g.*, PTP) with hyperoxidation, permitting the accumulation of H_2O_2 that activates H_2O_2 signal transduction (98). In support of this model, circadian increases in the hyperoxidation of mitochondrial Prx3 are important for the cytoplasmic activation of p38 in the adrenal cortex (43, 44). **(B)** In response to low levels of H_2O_2, the thioredoxin peroxidase activity of 2-Cys Prx promotes H_2O_2 signal transduction by competitively inhibiting the reduction of signaling proteins, for example, the AP-1-like transcription factor Pap1, by thioredoxin family proteins. Hyperoxidation of Prx to thioredoxin-resistant forms inhibits Pap1 activation (11, 88), but it is proposed to increase the availability of thioredoxin to reduce other oxidized proteins. In support of this, hyperoxidation of Prx is important for maintenance of thioredoxin and MSRA activity and survival of cells under acute stress conditions (27). **(C)** Hyperoxidation of Prx has also been demonstrated to increase the stability of Prx oligomers, thus enhancing signaling and chaperone activities that help repair oxidative stress-induced damage. For example, sulfinylated Prx interact with Hsp70, Hsp104, and misfolded protein aggregates, promoting the disaggregation of misfolded proteins (31, 38) and hyperoxidized Prx oligomers have been proposed to inhibit cell cycle progression (71) and senescence by differentially regulating the activity of specific phosphatases (MKP) to alter signal transduction under oxidative stress conditions (86). MKP, mitogen-activated kinase phosphatase; MSRA, methionine sulfoxide reductase A; PTP, protein tyrosine phosphatase.

be far in excess of that produced in response to growth factors or other endogenous ''non-stressful'' H_2O_2-generating events (Table 1). It is possible that the inactivation of the thioredoxin peroxidase activity of 2-Cys Prx leads to local increases in H_2O_2 available for signaling, as proposed for growth factor-induced Prx phosphorylation and for ACTH-induced increases in p38 activity (19, 43, 97). However, it remains challenging to detect such proposed local increases, and even more difficult to determine whether any increases in H_2O_2 are actually caused by, rather than the cause of, Prx

Table 2. Physiological Situations in Which Hyperoxidized Prx Have Been Detected but the Fraction of the Prx That Is Hyperoxidized Is Not Determined

Species/cells	*2-Cys-Prx*	*Physiological condition*	*Detection Method*	*Reference*
Bacteria				
Synechococcus elongatus	Prx	Circadian time (0–64 h) Peak intensity every 24 h	Non-reducing western ($\alpha PrxSO_{2/3}$)	(28)
Archaea				
Halobacterium salinarum	Prx	Circadian time (0–68 h) Peak intensity every 12 h	Non-reducing western ($\alpha PrxSO_{2/3}$)	(28)
Plants				
Ostreococcus tauri	Prx	Constant darkness (0–96 h) Peak intensity every 12 h	Non-reducing western ($\alpha PrxSO_{2/3}$)	(60)
Arabidopsis thaliana	Prx	Diurnal pattern (0–47 h) (16 h light, 8 h dark, 24 h light) Peak intensity continuous light	Non-reducing western (α-2-Cys Prx (rice), $\alpha PrxSO_{2/3}$)	(75)
Animals				
C. elegans (N2)	PRDX-2	Temperature cycle (16 h 13°C, 8 h 16°C) Peak intensity every 20 h	Non-reducing western ($\alpha PrxSO_{2/3}$)	(63)
Drosophila melanogaster	Prx	Circadian time (0–48 h) Peak intensity at 4–8 and 20–24 h	Non-reducing western ($\alpha PrxSO_{2/3}$)	(28)
Mice				
Erythrocytes	Prx2	Circadian time (0–48 h) Peak intensity every 24 h	($\alpha PrxSO_{2/3}$)	(18)
Adrenal gland, brown adipose, and heart cytosolic and mito fractions	Prx1/2, Prx3	12/12 h dark/light cycle Peak intensity every 24 h	($\alpha PrxSO_{2/3}$)	(44)
Adrenal gland homogenates	Prx3	Peak intensity every 24 h	($\alpha PrxSO_{2/3}$)	(43)
Liver	Prx1	Circadian time (0–21 h) Peak intensity at 0–12 h	Non-reducing western ($\alpha PrxSO_{2/3}$)	(28)
Rat				
Carotid artery	Prx1/2, Prx3	Balloon injury (0–7 days) Peak intensity 1–5 days	($\alpha PrxSO_{2/3}$)	(42)
Mongolian gerbil				
Hippocampal homogenates	Prx	Aged (1–24 months) Peak intensity 1–3, 18–24 months	($\alpha PrxSO_{2/3}$)	(102)
Hippocampal CA1 region	Prx	Forebrain ischemia (5 min) Peak intensity 5 days later	($\alpha PrxSO_{2/3}$)	(36)
Human				
PBMC	PRDX	Before, during, and 30 min post exercise Peak intensity during high exercise	Reducing western ($\alpha PrxSO_{2/3}$, α-β-actin*)	(89)
PBMC	PRDX	Asthma patients	Reducing western ($\alpha PrxSO_{2/3}$)	(46)
Erythrocytes	Prx1/2, Prx3	Constant darkness (0–60 h) Peak intensity every 12 h	Non-reducing western ($\alpha PrxSO_{2/3}$)	(59)
Cartilage	Prx	Increased during aging and in osteoarthritis	($\alpha PrxSO_{2/3}$) immunostaining	(21)

Examples of the physiological situations in which increases in hyperoxidized Prx have been detected, indicating the point at which peak levels of hyperoxidized Prx were detected and the method of detection. Immunoblots using anti-$PrxSO_{2/3}$ antibodies (96) to detect hyperoxidized Prx were normalized to levels of the indicated Prx, using appropriate anti-Prx antibodies, unless otherwise indicated (*).
PBMC, proliferating blood monocytes.

hyperoxidation. Moreover, recent *in silico* investigations have suggested that even localized increases in H_2O_2 are unlikely to be sufficient to promote rapid oxidation of signaling proteins, such as protein tyrosine phosphatase (PTP) (85). Indeed, there is increasing evidence that, rather than acting as barriers, Prx play direct, positive roles in promoting the H_2O_2-induced oxidation of, at least some, signaling proteins [for a review, see Netto and Antunes (55)]. For instance, in the fission yeast *S. pombe*, increases in exogenous H_2O_2 that are sufficient to cause H_2O_2-induced hyperoxidation of the 2-Cys Prx Tpx1

actually prevent the H_2O_2-induced oxidation and activation of the AP-1-like transcription factor Pap1, in complete contradiction to the predictions of the Floodgate model (11, 88).

Indeed, our further work in *S. pombe* has suggested an alternative advantage of inhibiting the thioredoxin peroxidase activity of Prx. Similar to the premise of the Floodgate model, we also proposed that the high abundance and H_2O_2 reactivity of 2-Cys Prx means that there are conditions under which loss of the thioredoxin peroxidase activity by hyperoxidation of Prx is important. However, in contrast to Wood *et al.*'s proposal that loss of Prx activity increases the H_2O_2 available for signaling functions, our work suggests that hyperoxidation is important to limit the oxidation of thioredoxin, the other substrate of Prx activity, thus increasing the amount of reduced thioredoxin available to reduce other oxidized proteins under stress conditions (Fig. 3B) (27). This alternative hypothesis arose, in part, from our observation that the sensitivity of 2-Cys Prx to hyperoxidation had coevolved in organisms in which Prx disulfides, generated during the catalytic reduction of peroxides, were reduced by thioredoxin, rather than by a dedicated Prx reductase, AhpF (Fig. 1). Thioredoxin is a relatively broad specificity oxidoreductase that not only is an essential cofactor for many enzymes that involve a redox step in their catalytic mechanism but also functions to reduce disulfides in signaling proteins, such as PTPs, the Ask1 MAPKKK or yeast AP-1-like transcription factors, and oxidatively ''damaged'' proteins under oxidative stress conditions [for reviews, see Refs. (30, 50)]. Accordingly, as demonstrated in *S. pombe*, when thioredoxin reductase activity is limiting, the consequence of coupling the peroxidase activity of the single 2-Cys Prx, Tpx1, to thioredoxin is that, in cells exposed to H_2O_2, Prx disulfides can dramatically deplete the amount of reduced thioredoxin available to reduce other substrates and repair oxidative protein damage (27). Indeed, we have shown that this ability of Tpx1 disulfides to drive thioredoxin oxidation, and thus inhibit the reduction of other oxidized proteins, is vital for stable H_2O_2-induced oxidation of the Pap1 transcription factor, which in its oxidized form activates a stress-protective gene expression program (12). These findings suggest that the coupling of Prx to thioredoxin may have evolved to provide a means for low levels of H_2O_2 to promote thioredoxin oxidation, and thus regulate the activity of downstream thioredoxin/thioredoxin family substrate proteins (Fig. 3B).

As Prx acquired this new H_2O_2-signaling function, as H_2O_2-dependent regulators of thioredoxin activity, we speculated that this may have generated the selection pressure for increased sensitivity to hyperoxidation; to uncouple Prx activity from thioredoxin under acute stress conditions and thus divert thioredoxin toward repair pathways (Fig. 3B). Indeed, we demonstrated that both thioredoxin and the thioredoxin-dependent repair enzyme, methionine sulfoxide reductase A (Mxr1), were inhibited under oxidative stress conditions in *S. pombe* cells expressing a hyperoxidation-resistant Tpx1 mutant ($Tpx1^{1\text{-}181}$) (27). Notably, although new gene expression is inhibited, preventing cells from adapting by increasing the expression of ROS defense proteins, both wild-type and Δ*tpx1* mutant yeast are able to recover after prolonged exposure to very high (25 m*M*) concentrations of H_2O_2 (27). However, ectopic expression of sulfiredoxin under these acute stress conditions, where it is not usually expressed, maintains the levels of Tpx1 disulfides, increasing the inhibition of thioredoxin and resulting in a Tpx1-dependent loss of cell viability (27). Thus, we demonstrated that hyperoxidation of Tpx1 is important for cell survival under acute stress conditions. This suggests that inactivation of the thioredoxin peroxidase activity of Tpx1 is vital to allow thioredoxin-dependent maintenance of essential activities when ROS levels inhibit new gene expression/protein synthesis.

Moreover, our data suggest that the inactivation of Tpx1 by hyperoxidation also protects *S. pombe* from damage at lower, sub-lethal concentrations. Notably, thioredoxin is not only important for repairing oxidative protein damage, and supporting the activity of methionine sulfoxide reductase, but also required for ribonucleotide reductase, which is important for DNA synthesis and repair. Indeed, consistent with the prolonged inhibition of thioredoxin in cells expressing hyperoxidation-resistant $Tpx1^{1\text{-}181}$ (27), the cell division cycle of these cells is de-regulated, and nuclear damage increased, when these cells are exposed to non-lethal levels of H_2O_2 at which Tpx1 is usually hyperoxidized [Brown, Morgan, and Veal, unpublished observations and Day *et al.* (27)].

Apart from revealing that inactivation of the thioredoxin peroxidase activity of Prx is important to repair damage and allow cell survival under acute stress conditions, these yeast studies suggest that the coupling of Prx to thioredoxins may have evolved as a key mechanism to allow H_2O_2 signaling. For instance, we have subsequently demonstrated that the thioredoxin peroxidase activity of Tpx1 is required for the H_2O_2-induced oxidation of the Pap1 transcription factor and oxidative stress resistance, not because it is required to remove peroxides, but because it promotes the H_2O_2-induced oxidation of the thioredoxin-like protein, Txl1 that reduces Pap1 (12). Accordingly, in cells expressing a thioredoxin peroxidase-defective Tpx1 mutant, $Tpx1^{C169S}$, the thioredoxin-like protein Txl1 is not oxidized in response to H_2O_2, Pap1 oxidation is inhibited, and cells are unable to mount Pap1-dependent transcriptional responses (12). Although the effect of Prx hyperoxidation on thioredoxin activity has yet to be investigated in other systems, Prx have been shown to act as important Trx regulators in plants and budding yeast, where they promote thioredoxin oxidation in response to light-stimulated increases in H_2O_2 (9, 26). Moreover, the observation that the facultative anaerobe, *Vibrio vulnificus*, possesses both a thioredoxin-coupled, hyperoxidation-sensitive 2-Cys Prx and a stress-induced, AhpF-coupled 2-Cys Prx suggests that 2-Cys Prx may also have evolved distinct functions in response to different levels of H_2O_2 in *Vibrio* and other prokaryotes (*Enterobacter* sp., *Pseudomonas* sp., *Pseudoalteromonas* sp., *Salmonella* sp., *Shewanella* sp.) where both robust and hyperoxidation-sensitive 2-Cys Prx are present (2, 33) (Fig. 2).

Thus, we propose that the coupling of thioredoxin to the reduction of 2-Cys Prx may have evolved originally in some bacteria as an effective means to regulate the host of cellular thioredoxin-dependent enzymatic and signaling activities in response to rises in H_2O_2. However, inevitably with this advantage came the risk that, under acute stress conditions, the continuous formation of Prx disulfides could lead to prolonged thioredoxin oxidation, preventing maintenance of vital cellular activities and repair of oxidatively damaged proteins or DNA. Moreover, if thioredoxin reductase activity is not limiting then, unchecked, the thioredoxin peroxidase

activity of Prx could potentially deplete NADPH and, consequently, inhibit the glutathione system too. Thus, given the importance of NADPH, thioredoxin, and glutathione for survival under oxidative stress conditions, this connection of the peroxidase activity of 2-Cys Prx to the thioredoxin system would be predicted to generate a strong selective pressure to de-couple thioredoxin from Prx reduction in cells exposed to high levels of oxidants.

Gain of Function: Increased Non-Peroxidase Activities of Hyperoxidized Prx

Both the models discussed earlier consider advantages of Prx hyperoxidation in terms of ''loss of function'' of the thioredoxin peroxidase activity, either to allow H_2O_2 signaling or to preserve thioredoxin in times of acute stress (Fig. 3). In addition to these proposals, Prx have been shown to be multifunctional proteins, with a chaperone activity that protects against protein aggregation (18, 34). Accordingly, although hyperoxidation inhibits the thioredoxin peroxidase activity of Prx, it has been proposed that it increases other chaperone and signaling activities of Prx that protect against oxidative damage (Fig. 3C). Here, we will review the evidence that although hyperoxidation inactivates the thioredoxin peroxidase activity of Prx, it may lead to a ''gain of function'' in other activities.

Chaperone Activity

The identification that 2-Cys Prx also have a chaperone function came from studies in the budding yeast *S. cerevisiae*. Investigations into the reduced thermotolerance of *S. cerevisiae* lacking the predominant 2-Cys Prx, Tsa1, lead to the discovery that 2-Cys Prx can protect against thermal aggregation of proteins *in vitro* and *in vivo* independent from their peroxidase activity by acting as molecular chaperones (38). This chaperone activity is promoted by heat or H_2O_2-induced formation of higher order Prx complexes (38, 82). Although the chaperone activity of Prx does not appear to require either of the cysteines that are essential for thioredoxin peroxidase activity, the reversible, H_2O_2-induced formation of higher order Prx complexes does require the peroxide-reacting cysteine, as well as the cycling activity of thioredoxin. Moreover, in cells lacking sulfiredoxin, these H_2O_2-induced higher molecular weight forms with increased chaperone activity persist for longer (38). Together, these findings suggest that hyperoxidized Prx more readily participates in higher molecular weight forms with increased chaperone activity. Thus, it has been proposed that, although hyperoxidation inactivates the peroxidase activity of Prx, it promotes this chaperone activity, reducing protein aggregation and, consequently, promotes the survival of cells exposed to thermal stress (38). Moreover, further oxidation of the peroxide-reacting cysteine to a sulfonyl derivative has been shown to further increase the chaperone activity of Tsa1 (48).

In vitro assays suggest that chaperone activity is likely to be a general feature of 2-Cys Prx, for example shared by human Prx1 and Prx2 (37, 54), and Prx from plants (45), protozoa (82), and bacteria (20). Other studies have also identified that other post-translational modifications (37), mutations, and changes in pH that promote formation of higher molecular weight oligomeric forms of Prx also increase this chaperone activity (20, 37). However, given that hyperoxidation is not essential for this chaperone activity (82), yet completely inhibits the thioredoxin peroxidase activity, it seems unlikely that increased chaperone activity alone could provide enough selective pressure to drive the evolution of peroxide-sensitive Prx. Indeed, it is possible that some of the *in vivo* protection against thermal protein aggregation associated with Prx hyperoxidation could also be due to increased availability of thioredoxin to reduce oxidized proteins (27). Recently, further light was cast on this issue by the discovery that hyperoxidation of *S. cerevisiae* Tsa1 is important for the *in vivo* recruitment of ATP-dependent chaperones (heat shock proteins) to aggregates that form under oxidative stress conditions (31). This suggests that hyperoxidized Prx can also facilitate the action of heat shock proteins (*e.g.*, Hsp70) in actively removing or refolding damaged proteins. Accordingly, this may provide an important advantage under oxidative stress conditions (31) (Fig. 4).

Other Activities for Hyperoxidized Prx

Prx hyperoxidation has also been proposed to increase or promote other peroxidase-independent signaling activities. In many cases, this is also proposed to be due to an increase in the stability of oligomeric forms. For instance, hyperoxidation of human Prx2 has been shown to result in the formation of filamentous oligomers. Interestingly, the presence of these forms is associated with cell cycle arrest (71). Although it is currently unclear how these structural changes serve to regulate cell responses, the potential for altering the interaction partners of Prx has been revealed by more recent studies. For example, in contrast with the predictions of the Floodgate model, and with the increased p38 activation associated with hyperoxidation of Prx3 (43) (Fig. 3A), hyperoxidation of human Prx1 increases its association with the phosphatase mitogen-activated kinase phosphatase (MKP)-5, thus preventing ROS-induced inactivation of MKP-5 and maintaining low p38MAPKα activity (86). By stabilizing the decameric form, hyperoxidation has also been shown to promote the non-covalent interaction of human Prx2 with a thioredoxin-like protein, Erp46 (64). Intriguingly, this latter study is consistent with the view that hyperoxidation may also serve to regulate the activity of thioredoxin/PDI-like proteins, which could also lead to downstream effects on protein folding/homeostasis or signaling under oxidative stress conditions.

Although Prx hyperoxidation leads to a loss of peroxidase activity, the recent identification that at least some eukaryotic Prx, including human Prdx1, also have catalase activity ($2\ H_2O_2 \rightarrow 2H_2O + O_2$), even when exposed to concentrations of H_2O_2 at which they are usually hyperoxidized, suggests that hyperoxidized Prx may retain some catalytic peroxide-removing activity (80, 101). Although the functional significance of this catalase activity has yet to be established, the dependence of this catalase activity on Fe^{3+} and a conserved GVL motif found in the majority of hyperoxidation-sensitive Prx (Fig. 2) raises the intriguing possibility that these Prx may have a bifunctional activity profile; with thioredoxin-dependent peroxidase and signaling activities at low H_2O_2 concentrations and catalase and chaperone/other signaling activities that are retained, or gained, at higher H_2O_2 concentrations.

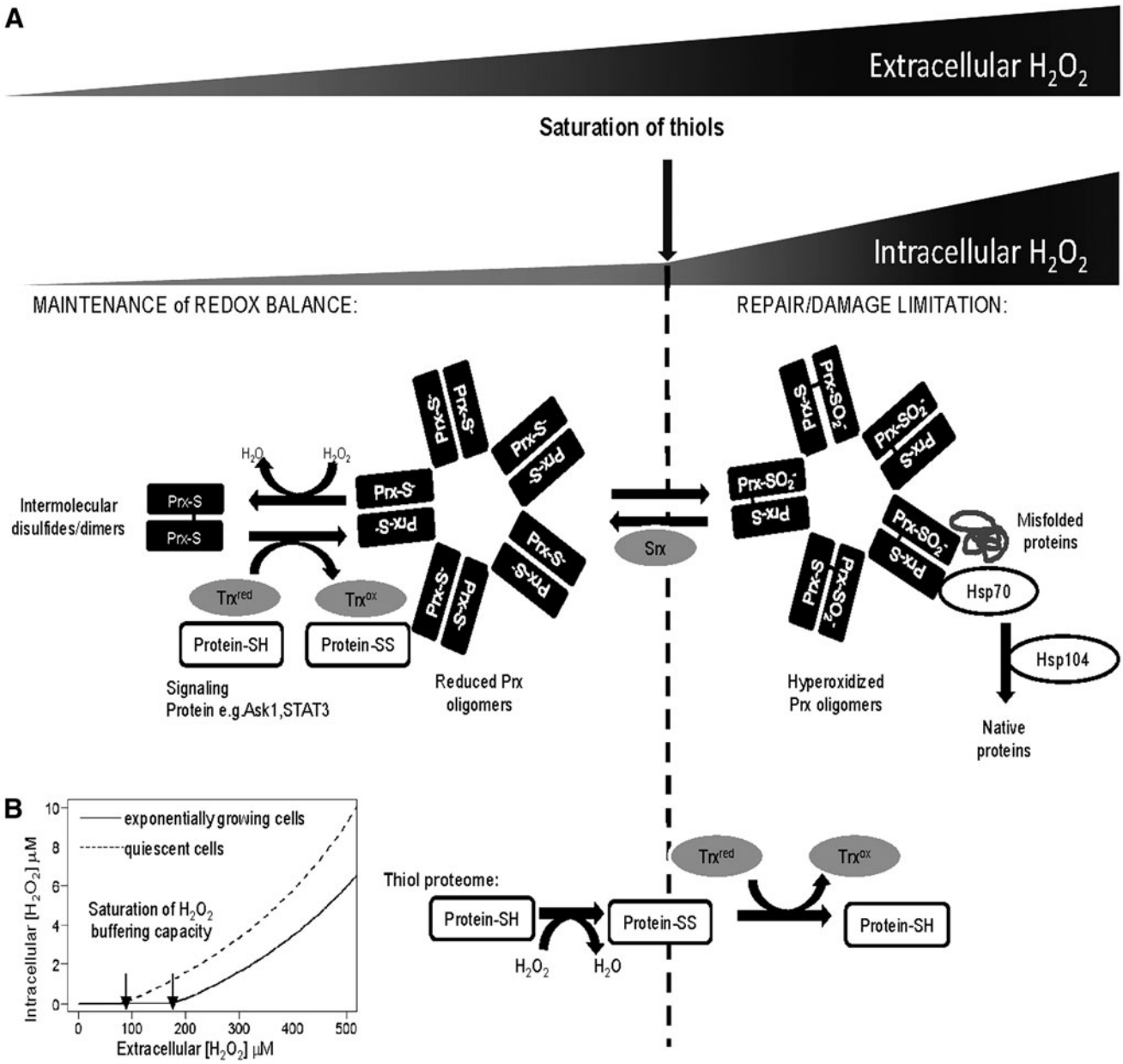

FIG. 4. Models depicting the bi-phasic intracellular response to external rises in H_2O_2 and the role of Prx hyperoxidation. Cells are able to buffer the intracellular environment against external rises in H_2O_2 (84). **(A)** Low levels of H_2O_2: Endogenous H_2O_2 react with the peroxidatic cysteine of Prx present in reduced decamers, in which it is highly sensitive to oxidation. During the catalytic cycle of Prx, disulfide bond formation promotes dissociation from the decamer. Prx disulfides promote H_2O_2 signal transduction by (i) promoting the oxidation and (ii) inhibiting the reduction of H_2O_2-signaling proteins, for example, the MAPKKK, Ask1, or transcription factors Pap1 and STAT3, by thioredoxin. If the extracellular H_2O_2 concentration exceeds the H_2O_2-buffering capacity of cellular thiols, intracellular levels of H_2O_2 rise. This rise in H_2O_2 causes the peroxidatic cysteines in Prx decamers to become hyperoxidized to sulfinylated derivatives that are resistant to reduction by thioredoxin. Hyperoxidation stabilizes oligomeric forms and promotes the interaction of Prx with misfolded proteins, generating aggregates to which it recruits heat shock proteins that actively promote refolding. At low H_2O_2, Trx reduces oxidized Prx disulfides. As H_2O_2 concentrations increase above the H_2O_2-buffering capacity, increased hyperoxidation of Prx means that more Trx is free to reduce oxidized proteins and act as a cofactor to other thioredoxin-dependent enzymes, such as MSRA and RNR, that are important for repair of oxidatively damaged proteins and DNA, respectively. **(B)** Effect of cell state/aging on the bi-phasic response to H_2O_2; our modeling predicts that lower levels of H_2O_2 are required to saturate the H_2O_2-buffering capacity of quiescent *S. pombe*, compared with cells that are exponentially growing. This is consistent with other work suggesting that aged cells are more sensitive to Prx hyperoxidation (21, 53) and suggests that Prx hyperoxidation may, therefore, play a more prominent role in protecting aging cells against damage. MAPKKK, mitogen-activated protein kinase kinase kinase; RNR, ribonucleotide reductase.

When Does Prx Hyperoxidation Occur *In Vivo* and to What Extent?

Detecting Prx hyperoxidation

In assessing the relative contributions of each of the proposed functions for Prx hyperoxidation *in vivo*, it is important to understand the circumstances under which Prx become hyperoxidized. The generation of antibodies that are specific to the hyperoxidized, sulfinylated or sulfonylated, forms of Prx ($\alpha PrxSO_{2/3}$) has provided an important tool for detection of hyperoxidized Prx, circumventing the need for electrophoretic or mass spectrometric methods to distinguish hyperoxidized from reduced Prx monomers (48, 96). This has led to a dramatic increase over recent years in the number of conditions under which Prx hyperoxidation has been detected (Table 2). In most cases, comparisons with the signal from an antibody that detects all Prx redox states is used as a control to ensure that changes in the level of hyperoxidized Prx are not due to changes in total Prx levels. These studies have provided important information as to the circumstances under which there is a detectable increase in hyperoxidized Prx. However, use of $\alpha PrxSO_{2/3}$ antibodies alone to detect Prx hyperoxidation does have some limitations. Most importantly, this approach gives no indication of the extent to which Prx are hyperoxidized, preventing any assessment of whether a tiny fraction or the vast majority of peroxide-reacting Prx cysteines are hyperoxidized. Moreover, although sulfonylation is unlikely to occur to any significant extent in physiological conditions, the $\alpha PrxSO_{2/3}$ antibodies, most frequently used, recognize both sulfinylated Prx, which is a substrate for sulfiredoxin, and sulfonylated Prx, which is not. Further, although the sequence identity of the sulfinylated peptide against which they are raised means these antibodies are effective at detecting hyperoxidation of 2-Cys Prx from a broad range of species, this also prevents them from distinguishing between different hyperoxidized 2-Cys Prx in the same sample, unless the Prx are sufficiently different in size to allow electrophoretic separation from other Prx, for example, Prx3 (Fig. 2). To examine whether specific Prx are hyperoxidized, and whether this hyperoxidized Prx represents a significant proportion of the total Prx, it is necessary to separate hyperoxidized Prx from other redox forms, before immunoblotting and analysis with antibodies to Prx that are not specific to a particular redox state. This separation can be effected in a number of ways; for example, by covalent modification of the reduced cysteines in protein samples with agents that allow electrophoretic separation of reduced and hyperoxidized Prx forms based on differences in mobility, for example, AMS, or by using isoelectric focusing gels that allow separation on the basis of charge differences (8, 14, 24, 90). Notably, the sensitivity of the peroxidatic thiol to oxidation means that, unless care is taken to prevent oxidation occurring *in vitro* during protein extraction, the relative amounts of reduced and disulfide-bonded Prx will not reflect the *in vivo* distribution (24). However, using these methods, it is possible to quantitatively determine the extent to which a specific Prx become hyperoxidized (14, 24, 27, 84) (Table 1). Nevertheless, although there are now a vast number of studies reporting *in vivo* hyperoxidation of Prx, in few cases has the percentage of Prx that remains in its catalytically active form also been determined (Tables 1 and 2). This is important for assessing the effect of hyperoxidation. For instance, even if hyperoxidized Prx is detected, if this only represents a tiny fraction of the total Prx, then it is unlikely that this will have a significant downstream, general effect on either H_2O_2 levels or the availability of reduced thioredoxin. It is possible that localized Prx hyperoxidation might have a localized effect on levels of H_2O_2 or reduced thioredoxin, particularly if there are physical constraints on the diffusion of H_2O_2 from the site at which it is generated *in vivo* [as discussed by Heppner *et al.* (34)]. However, if the bulk of the Prx remains in active cycling forms, we speculate that it is perhaps more likely that any biological effect of hyperoxidation is due to an increase in a Prx's chaperone or signaling activities (Fig. 3C).

Is Prx hyperoxidation a cause or consequence of oxidative stress?

In addition to providing invaluable insight into the structure and redox biochemistry of Prx, *in vitro* studies have demonstrated that some eukaryotic Prx are intrinsically more sensitive to hyperoxidation than others (23, 70). However, it is impossible for *in vitro* studies to simulate the complex cellular environment. The potential influence of other cell components on the sensitivity of Prx to hyperoxidation is illustrated by an *in vitro* study from the Winterbourn lab that demonstrated that the presence of other peroxide-removing enzymes, such as catalase, protects Prx against hyperoxidation (70). Indeed, the *in vitro* and *in vivo* sensitivity of Prx to hyperoxidation can be quite different. For instance, although Prx4 is as intrinsically sensitive to hyperoxidation as Prx2 *in vitro*, the absence of an efficient ER recycling system for Prx4 disulfides means that much less Prx4 becomes hyperoxidized *in vivo*, even in cells exposed to very high (10 m*M*) concentrations of H_2O_2 (15) (Table 1). Similarly, Prx2 has been shown to be less susceptible to extensive hyperoxidation in cells where thioredoxin activity is limiting (49). Therefore, to understand the physiological causes of Prx hyperoxidation, it is important to take into account the relative *in vivo* levels of Prx, thioredoxin, and other peroxide-metabolizing systems.

Over recent years, computational models, incorporating both reaction rate parameters, determined from biochemical studies of purified proteins, and *in vivo* considerations, such as cell H_2O_2 permeability and the relative concentrations of different enzymes, have started to be utilized to address how cells respond to oxidants (1, 6, 84, 85). In our recent study, we took this approach to investigate how the *in vivo* environment affects the oxidation state of Prx. Taking advantage of the presence of a single *S. pombe* Prx, Tpx1, the availability of quantitative proteomic data for the concentration of each *S. pombe* protein (52), and established redox Western blotting methods (27), we obtained quantitative time course data for the distribution of Tpx1 between different oxidation states in cells exposed to different concentrations of H_2O_2. Using these data, we were able to construct a mathematical model representing the redox reactions of Tpx1 that was able to simulate the *in vivo* data (84). We learned a number of things from this model. Notably, rather than a linear increase in the amount of Tpx1 that became hyperoxidized in response to exogenous H_2O_2, we discovered that Tpx1 was protected from hyperoxidation by an *in vivo* peroxide-removing activity, such that Tpx1 hyperoxidation was only detected when this activity was overcome and intracellular H_2O_2 concentrations began to increase (Fig. 4). Notably, this observation

that intracellular H_2O_2 levels undergo a biphasic response to increasing doses of extracellular H_2O_2 was also found to be true for a human kidney cell line (HEK293) (84). Moreover, although the amount of exogenous H_2O_2 required to breach the cellular peroxide-buffering capacity was much lower, nevertheless, as in *S. pombe*, hyperoxidation of Prx was only detected in kidney cells once the intracellular H_2O_2 concentrations began to rise more rapidly. Indeed, a perusal of the literature suggests that Prx hyperoxidation is also correlated with increases in intracellular H_2O_2 in other cells (Table 1). Of course, as Prx are very efficient at removing H_2O_2, it might be expected that inactivation of Prx by hyperoxidation would be correlated with a rise in intracellular H_2O_2. However, we were able to show that there was no change in the threshold extracellular H_2O_2 bolus required to cause intracellular H_2O_2 concentrations to rise in cells expressing a hyperoxidation-resistant Tpx1 mutant (84). Moreover, loss of Tpx1, the single glutathione peroxidase, Gpx1, or catalase did not affect the bi-phasic response of *S. pombe*. This suggests that none of these peroxidases makes a significant contribution to the cell's ability to buffer the internal environment against an external bolus of H_2O_2. In contrast, thioredoxin was found to be critical for this bi-phasic response. It is likely that other reductants, such as glutathione and methionine, also contribute to the cellular H_2O_2-buffering capacity, but a key role for thioredoxin is consistent with findings from a model constructed by the Kemp group that suggested that the thiol proteome makes an important contribution to the H_2O_2-buffering capacity of the cell (1). Although relatively limited protein thiol oxidation has generally been observed in mammalian cells treated with sufficient H_2O_2 to cause some Prx hyperoxidation (5), to our knowledge, the effect/s of sustained Prx activity in these circumstances on thioredoxin activity and the thiol proteome have not been investigated. Therefore, it remains possible that rapid thioredoxin-mediated reduction of protein disulfides, enhanced by diversion of thioredoxin from Prx toward other substrates, plays a widespread role in protecting proteins against sustained oxidation (Fig. 4). In any case, regardless of the nature of the H_2O_2-removing activity, our data imply that Prx hyperoxidation only occurs *in vivo* once this peroxide-buffering capacity is saturated and the intracellular H_2O_2 levels start to rise more rapidly (Fig. 4).

Intriguingly, our model and *in vivo* data also suggest that the main route by which Prx become hyperoxidized involves the sulfenylation of both peroxidatic cysteines in a Prx dimer, before formation of the disulfide bond between the Prx partners. The remaining sulfenylated peroxidatic cysteine in the disulfide-bonded dimer subsequently becomes sulfinylated by reacting with a second H_2O_2 molecule. Although other routes may also contribute, this reaction sequence is consistent with the detection of hyperoxidized disulfides before hyperoxidized monomer (27, 39, 84). Moreover, it also fits with our finding that hyperoxidized Prx were only detected once the cellular H_2O_2-buffering capacity was breached, as the chances of a second sulfenylation event taking place before disulfide formation would be greatly increased once intracellular H_2O_2 levels began to increase more substantially (84).

The finding that the trigger for Prx hyperoxidation is a rise in H_2O_2 after saturation of cellular H_2O_2-buffering capacity has important implications for the various situations in which hyperoxidized Prx are detected *in vivo*. For example, this implies that increases in Prx hyperoxidation, detected as a conserved feature of many circadian rhythms (Table 2 and references within), are preceded by an increase in the levels of H_2O_2 above the cell's H_2O_2-buffering capacity. Moreover, our data raise the intriguing possibility that differences between the intrinsic sensitivity of different Prx to hyperoxidation in different organisms or organelles may reflect the H_2O_2-buffering capacity of the specific Prx's *in vivo* environment.

Implications for the physiological roles of Prx

As discussed earlier, the simple view that, like their more robust bacterial counterparts, the main function of eukaryotic 2-Cys Prx is to remove H_2O_2 has been challenged by a number of discoveries. These include the increasing evidence that these 2-Cys Prx are multifunctional proteins, with chaperone and signaling activities that do not require their thioredoxin peroxidase activity, but that are increased by post-translational modifications, including hyperoxidation. In addition to peroxidase-independent functions of Prx, in their thioredoxin peroxidase-active form, Prx have been shown to actively promote redox signaling, both by acting as peroxide transducers to initiate the oxidation of redox-regulated proteins (40, 79) and by promoting the oxidation of thioredoxin family proteins (12) [for a review, see Netto and Antunes (55); Fig. 3B]. Both these functions are inhibited by Prx hyperoxidation, along with any ROS-detoxifying function of the thioredoxin peroxidase activity.

Based on these findings, it is possible that the increased ROS levels, oxidative damage, and/or activation of stress-activated signaling pathways frequently observed in cells lacking Prx could partly reflect loss of one or more of Prx's other activities, rather than rises in H_2O_2 directly caused by loss of the thioredoxin peroxidase activity. Indeed, as our studies suggest, although Prx may provide an effective means to reduce the low levels of peroxides generated by normal metabolism, in organisms where they are coupled with thioredoxin, this peroxidase activity is not well suited to deal with an increase in H_2O_2 above these levels, particularly when thioredoxin reductase activity is limiting (12, 84). Hence, we propose that Prx hyperoxidation should be viewed as a consequence rather than a cause of the associated rises in ROS. This is in accordance with others that have proposed that hyperoxidized Prx are a suitable early biomarker for oxidative stress (74).

Increases in hyperoxidized Prx have now been detected in response to many stimuli and, most intriguingly, as a conserved feature of many circadian rhythms (Table 2). In most of these studies, the anti-Prx$SO_{2/3}$ signal is normalized to the signal from an antibody that detects both reduced and hyperoxidized forms of the Prx in question (Table 2). Although, as discussed earlier, this is sufficient to demonstrate that the changes in hyperoxidized Prx do not reflect changes in total Prx levels, there remain few studies in which the % of Prx that is hyperoxidized has been accurately determined. Filling this gap will be important if we are to discern whether the main function of hyperoxidation in a given situation is to limit either the removal of H_2O_2 and/or oxidation of thioredoxin, which would most likely require the bulk of Prx to become hyperoxidized, or as a post-translational modification promoting the formation of stable oligomeric forms and interactions with signaling or chaperone/misfolded proteins. For

example, formation of a small or localized amount of hyperoxidized Prx, such as has been frequently observed (Table 1), may be unlikely to impact rates of peroxide removal or thioredoxin oxidation, but they might be sufficient to promote alternative chaperone or signaling functions (Figs. 3C and 4). Indeed, although Prx have been demonstrated to have localized ROS-protective activities, in some cases these do not require the resolving cysteine, which is essential for thioredoxin peroxidase activity. Hence, it seems likely that, in at least some cases, chaperone or signaling activities of Prx are responsible for protecting against rises in ROS (12, 51, 92).

Role of Prx hyperoxidation in aging

Increases in hyperoxidized Prx (Tsa1) have been detected during the replicative aging of budding yeast (53) (Table 1) that recent work suggests are important to protect against the aggregation of proteins (31). Accordingly, this raises the possibility that it is this increased chaperone function that may be responsible for the lower ROS levels and extended replicative lifespan of cells expressing sulfiredoxin, rather than the increased thioredoxin peroxidase activity of Tsa1 (53). This raises the possibility that hyperoxidized Prx may also contribute to the pro-longevity function of Prx in other models of aging (58).

We have used our modeling approach to examine how chronological aging might be predicted to affect the sensitivity of the *S. pombe* Prx, Tpx1, to hyperoxidation. Quiescent cells are an established model of chronological aging, with the chronological lifespan determined as the length of time quiescent cells retain the capacity to re-enter the cell cycle and divide. *S. pombe* cells undergo extensive changes in gene expression as they enter quiescence that promote their survival in stressful conditions (52). When our model is repopulated with the concentrations of proteins found in quiescent cells, it predicts that the H_2O_2-buffering capacity of quiescent *S. pombe* is much lower than that of exponentially growing cells (Fig. 4B). Although these predictions require experimental confirmation, this would be expected to increase the sensitivity of Tpx1 to hyperoxidation, consistent with the possibility that Prx hyperoxidation might also have a protective life-extending role in aging *S. pombe*. This fits with the observation that Prx2 is more susceptible to hyperoxidation in chondrocytes from older human subjects (21). However, it remains to be determined whether a chaperone activity for hyperoxidized Prx is important for the pro-longevity functions of Prx in animal models (47, 56, 61, 62). Although hyperoxidized PRDX-2 has been shown to extend *C. elegans* survival of a thermal stress (61), increases in hyperoxidized Prx are not detected during *C. elegans* aging, despite the lack of any sulfiredoxin activity (83). Notably, all somatic cells in adult *C. elegans* are post-mitotic, so together these studies raise the possibility that hyperoxidized Prx may be specifically important for maintaining the replicative capacity of aging mitotic cells (53).

Conclusions and Future Directions

Although, as discussed, the thioredoxin peroxidase activity of Prx may be more important for maintaining redox homeostasis and promoting ROS signal transduction than directly counteracting damaging rises in ROS, Prx, undoubtedly, play central roles in protective ROS responses. It is, therefore, not surprising that deregulation of their activity should have been linked to many diseases and aging [for reviews, see Refs. (58, 66)]. It is currently difficult to discern whether ROS-protective effects of Prx are due to removal of H_2O_2, positive H_2O_2-signaling functions, chaperone activity, or a combination of all three. Accordingly, a full understanding of how the different activities of Prx contribute to cellular defenses against rises in ROS will require a better spatial resolution of (i) where ROS levels increase, (ii) where hyperoxidized Prx are detected, (iii) correlation with the localized distribution of Prx between dimers and decamers, and (iv) the availability of thioredoxin/thioredoxin reductase and sulfiredoxin. We predict that new methods to measure intracellular changes in H_2O_2 or NADPH *in vivo* and mathematical models, incorporating *in vitro* kinetic analysis of the association and disassociation of Prx oligomers, and interactions with thioredoxin, sulfiredoxin, and other partner proteins, will together provide valuable tools toward a more complete understanding of how cells initiate appropriate responses to different levels of ROS and the key role/s that Prx play in these responses.

Acknowledgments

The authors thank the reviewers and many other colleagues in the peroxiredoxin field for their insightful comments and helpful discussions that have informed this article. Z.E.U. and L.E.T. were funded by the BBSRC (BB/F015895/1, BB/F016980/1, BB/F023065/1). Discussions between E.A.V. and C.S.P. were facilitated by an NRF Travel grant. They are grateful to the many contributors in this field whose work has informed this review and apologize to any person whose work they may have inadvertently overlooked.

References

1. Adimora NJ, Jones DP, and Kemp ML. A model of redox kinetics implicates the thiol proteome in cellular hydrogen peroxide responses. *Antioxid Redox Signal* 13: 731–743, 2010.
2. Bang YJ, Oh MH, and Choi SH. Distinct characteristics of two 2-Cys peroxiredoxins of *Vibrio vulnificus* suggesting differential roles in detoxifying oxidative stress. *J Biol Chem* 287: 42516–42524, 2012.
3. Barranco-Medina S, Kakorin S, Lazaro JJ, and Dietz KJ. Thermodynamics of the dimer-decamer transition of reduced human and plant 2-cys peroxiredoxin. *Biochemistry* 47: 7196–7204, 2008.
4. Basu MK and Koonin EV. Evolution of eukaryotic cysteine sulfinic acid reductase, sulfiredoxin (Srx), from bacterial chromosome partitioning protein ParB. *Cell Cycle* 4: 947–952, 2005.
5. Baty JW, Hampton MB, and Winterbourn CC. Proteomic detection of hydrogen peroxide-sensitive thiol proteins in Jurkat cells. *Biochem J* 389: 785–795, 2005.
6. Benfeitas R, Selvaggio G, Antunes F, Coelho PM, and Salvador A. Hydrogen peroxide metabolism and sensing in human erythrocytes: a validated kinetic model and reappraisal of the role of peroxiredoxin II. *Free Radic Biol Med* 74: 35–49, 2014.
7. Bernal AB, Vickers MH, Hampton MB, Poynton RA, and Sloboda DM. Maternal undernutrition significantly impacts ovarian follicle number and increases ovarian oxidative stress in adult rat offspring. *PLoS One* 5: e15558, 2010.

8. Biteau B, Labarre J, and Toledano MB. ATP-dependent reduction of cysteine-sulphinic acid by *S. cerevisiae* sulphiredoxin. *Nature* 425: 980–984, 2003.
9. Bodvard K, Peeters K, Roger F, Romanov N, Igbaria A, Welkenhuysen N, Palais G, Reiter W, Toledano MB, Kall M, and Molin M. Light-sensing via hydrogen peroxide and a peroxiredoxin. *Nat Commun* 8: 14791, 2017.
10. Boileau C, Eme L, Brochier-Armanet C, Janicki A, Zhang CC, and Latifi A. A eukaryotic-like sulfiredoxin involved in oxidative stress responses and in the reduction of the sulfinic form of 2-Cys peroxiredoxin in the cyanobacterium Anabaena PCC 7120. *New Phytol* 191: 1108–1118, 2011.
11. Bozonet SM, Findlay VJ, Day AM, Cameron J, Veal EA, and Morgan BA. Oxidation of a eukaryotic 2-Cys peroxiredoxin is a molecular switch controlling the transcriptional response to increasing levels of hydrogen peroxide. *J Biol Chem* 280: 23319–23327, 2005.
12. Brown JD, Day AM, Taylor SR, Tomalin LE, Morgan BA, and Veal EA. A peroxiredoxin promotes H_2O_2 signaling and oxidative stress resistance by oxidizing a thioredoxin family protein. *Cell Rep* 5: 1425–1435, 2013.
13. Budanov AV, Sablina AA, Feinstein E, Koonin EV, and Chumakov PM. Regeneration of peroxiredoxins by p53-regulated sestrins, homologs of bacterial AhpD. *Science* 304: 596–600, 2004.
14. Cao Z and Bulleid NJ. Detecting peroxiredoxin hyperoxidation by one-dimensional isoelectric focusing. *Biophys Rep* 1: 14–17, 2015.
15. Cao Z, Subramaniam S, and Bulleid NJ. Lack of an efficient endoplasmic reticulum-localized recycling system protects peroxiredoxin IV from hyperoxidation. *J Biol Chem* 289: 5490–5498, 2014.
16. Chang TS, Jeong W, Choi SY, Yu S, Kang SW, and Rhee SG. Regulation of peroxiredoxin I activity by Cdc2-mediated phosphorylation. *J Biol Chem* 277: 25370–25376, 2002.
17. Chang TS, Jeong W, Woo HA, Lee SM, Park S, and Rhee SG. Characterization of mammalian sulfiredoxin and its reactivation of hyperoxidized peroxiredoxin through reduction of cysteine sulfinic acid in the active site to cysteine. *J Biol Chem* 279: 50994–51001, 2004.
18. Cho CS, Yoon HJ, Kim JY, Woo HA, and Rhee SG. Circadian rhythm of hyperoxidized peroxiredoxin II is determined by hemoglobin autoxidation and the 20S proteasome in red blood cells. *Proc Natl Acad Sci U S A* 111: 12043–12048, 2014.
19. Choi MH, Lee IK, Kim GW, Kim BU, Han YH, Yu DY, Park HS, Kim KY, Lee JS, Choi C, Bae YS, Lee BI, Rhee SG, and Kang SW. Regulation of PDGF signalling and vascular remodelling by peroxiredoxin II. *Nature* 435: 347–353, 2005.
20. Chuang MH, Wu MS, Lo WL, Lin JT, Wong CH, and Chiou SH. The antioxidant protein alkylhydroperoxide reductase of *Helicobacter pylori* switches from a peroxide reductase to a molecular chaperone function. *Proc Natl Acad Sci U S A* 103: 2552–2557, 2006.
21. Collins JA, Wood ST, Nelson KJ, Rowe MA, Carlson CS, Chubinskaya S, Poole LB, Furdui CM, and Loeser RF. Oxidative stress promotes peroxiredoxin hyperoxidation and attenuates pro-survival signaling in aging chondrocytes. *J Biol Chem* 291: 6641–6654, 2016.
22. Conway JP and Kinter M. Dual role of peroxiredoxin I in macrophage-derived foam cells. *J Biol Chem* 281: 27991–28001, 2006.
23. Cox AG, Pearson AG, Pullar JM, Jonsson TJ, Lowther WT, Winterbourn CC, and Hampton MB. Mitochondrial peroxiredoxin 3 is more resilient to hyperoxidation than cytoplasmic peroxiredoxins. *Biochem J* 421: 51–58, 2009.
24. Cox AG, Winterbourn CC, and Hampton MB. Measuring the redox state of cellular peroxiredoxins by immunoblotting. *Methods Enzymol* 474: 51–66, 2010.
25. Cuddihy SL, Winterbourn CC, and Hampton MB. Assessment of redox changes to hydrogen peroxide-sensitive proteins during EGF signaling. *Antioxid Redox Signal* 15: 167–174, 2011.
26. Dangoor I, Peled-Zehavi H, Wittenberg G, and Danon A. A chloroplast light-regulated oxidative sensor for moderate light intensity in Arabidopsis. *Plant Cell* 24: 1894–1906, 2012.
27. Day AM, Brown JD, Taylor SR, Rand JD, Morgan BA, and Veal EA. Inactivation of a peroxiredoxin by hydrogen peroxide is critical for thioredoxin-mediated repair of oxidized proteins and cell survival. *Mol Cell* 45: 398–408, 2012.
28. Edgar RS, Green EW, Zhao Y, van Ooijen G, Olmedo M, Qin X, Xu Y, Pan M, Valekunja UK, Feeney KA, Maywood ES, Hastings MH, Baliga NS, Merrow M, Millar AJ, Johnson CH, Kyriacou CP, O'Neill JS, and Reddy AB. Peroxiredoxins are conserved markers of circadian rhythms. *Nature* 485: 459–464, 2012.
29. Findlay VJ, Townsend DM, Morris TE, Fraser JP, He L, and Tew KD. A novel role for human sulfiredoxin in the reversal of glutathionylation. *Cancer Res* 66: 6800–6806, 2006.
30. Hanschmann EM, Godoy JR, Berndt C, Hudemann C, and Lillig CH. Thioredoxins, glutaredoxins, and peroxiredoxins-molecular mechanisms and health significance: from cofactors to antioxidants to redox signaling. *Antioxid Redox Signal* 19: 1539–1605, 2013.
31. Hanzen S, Vielfort K, Yang J, Roger F, Andersson V, Zamarbide-Fores S, Andersson R, Malm L, Palais G, Biteau B, Liu B, Toledano MB, Molin M, and Nystrom T. Lifespan control by redox-dependent recruitment of chaperones to misfolded proteins. *Cell* 166: 140–151, 2016.
32. Haynes AC, Qian J, Reisz JA, Furdui CM, and Lowther WT. Molecular basis for the resistance of human mitochondrial 2-Cys peroxiredoxin 3 to hyperoxidation. *J Biol Chem* 288: 29714–29723, 2013.
33. Hebrard M, Viala JP, Meresse S, Barras F, and Aussel L. Redundant hydrogen peroxide scavengers contribute to Salmonella virulence and oxidative stress resistance. *J Bacteriol* 191: 4605–4614, 2009.
34. Heppner DE, Janssen-Heininger YM, and van der Vliet A. The role of sulfenic acids in cellular redox signaling: reconciling chemical kinetics and molecular detection strategies. *Arch Biochem Biophys* 616: 40–46, 2017.
35. Ho A, Cho CS, Namkoong S, Cho US, and Lee JH. Biochemical basis of sestrin physiological activities. *Trends Biochem Sci* 41: 621–632, 2016.
36. Hwang IK, Yoo KY, Kim DW, Choi JH, Lee IS, and Won MH. Hyperoxidized peroxiredoxins and glyceraldehyde-3-phosphate dehydrogenase immunoreactivity and protein

levels are changed in the gerbil hippocampal CA1 region after transient forebrain ischemia. *Neurochem Res* 32: 1530–1538, 2007.
37. Jang HH, Kim SY, Park SK, Jeon HS, Lee YM, Jung JH, Lee SY, Chae HB, Jung YJ, Lee KO, Lim CO, Chung WS, Bahk JD, Yun DJ, and Cho MJ. Phosphorylation and concomitant structural changes in human 2-Cys peroxiredoxin isotype I differentially regulate its peroxidase and molecular chaperone functions. *FEBS Lett* 580: 351–355, 2006.
38. Jang HH, Lee KO, Chi YH, Jung BG, Park SK, Park JH, Lee JR, Lee SS, Moon JC, Yun JW, Choi YO, Kim WY, Kang JS, Cheong GW, Yun DJ, Rhee SG, Cho MJ, and Lee SY. Two enzymes in one; two yeast peroxiredoxins display oxidative stress-dependent switching from a peroxidase to a molecular chaperone function. *Cell* 117: 625–635, 2004.
39. Jara M, Vivancos AP, Calvo IA, Moldon A, Sanso M, and Hidalgo E. The peroxiredoxin Tpx1 is essential as a H2O2 scavenger during aerobic growth in fission yeast. *Mol Biol Cell* 18: 2288–2295, 2007.
40. Jarvis RM, Hughes SM, and Ledgerwood EC. Peroxiredoxin 1 functions as a signal peroxidase to receive, transduce, and transmit peroxide signals in mammalian cells. *Free Radic Biol Med* 53: 1522–1530, 2012.
41. Jeong W, Bae SH, Toledano MB, and Rhee SG. Role of sulfiredoxin as a regulator of peroxiredoxin function and regulation of its expression. *Free Radic Biol Med* 53: 447–456, 2012.
42. Kang DH, Lee DJ, Kim J, Lee JY, Kim HW, Kwon K, Taylor WR, Jo H, and Kang SW. Vascular injury involves the overoxidation of peroxiredoxin type II and is recovered by the peroxiredoxin activity mimetic that induces reendothelialization. *Circulation* 128: 834–844, 2013.
43. Kil IS, Lee SK, Ryu KW, Woo HA, Hu MC, Bae SH, and Rhee SG. Feedback control of adrenal steroidogenesis via H_2O_2-dependent, reversible inactivation of peroxiredoxin III in mitochondria. *Mol Cell* 46: 584–594, 2012.
44. Kil IS, Ryu KW, Lee SK, Kim JY, Chu SY, Kim JH, Park S, and Rhee SG. Circadian oscillation of sulfiredoxin in the mitochondria. *Mol Cell* 59: 651–663, 2015.
45. Konig J, Galliardt H, Jutte P, Schaper S, Dittmann L, and Dietz KJ. The conformational bases for the two functionalities of 2-cysteine peroxiredoxins as peroxidase and chaperone. *J Exp Bot* 64: 3483–3497, 2013.
46. Kwon HS, Bae YJ, Moon KA, Lee YS, Lee T, Lee KY, Kim TB, Park CS, Moon HB, and Cho YS. Hyperoxidized peroxiredoxins in peripheral blood mononuclear cells of asthma patients is associated with asthma severity. *Life Sci* 90: 502–508, 2012.
47. Lee KS, Iijima-Ando K, Iijima K, Lee WJ, Lee JH, Yu K, and Lee DS. JNK/FOXO-mediated neuronal expression of fly homologue of peroxiredoxin II reduces oxidative stress and extends life span. *J Biol Chem* 284: 29454–29461, 2009.
48. Lim JC, Choi HI, Park YS, Nam HW, Woo HA, Kwon KS, Kim YS, Rhee SG, Kim K, and Chae HZ. Irreversible oxidation of the active-site cysteine of peroxiredoxin to cysteine sulfonic acid for enhanced molecular chaperone activity. *J Biol Chem* 283: 28873–28880, 2008.
49. Low FM, Hampton MB, Peskin AV, and Winterbourn CC. Peroxiredoxin 2 functions as a noncatalytic scavenger of low-level hydrogen peroxide in the erythrocyte. *Blood* 109: 2611–2617, 2007.
50. Lu J and Holmgren A. The thioredoxin antioxidant system. *Free Radic Biol Med* 66: 75–87, 2014.
51. MacDiarmid CW, Taggart J, Kerdsomboon K, Kubisiak M, Panascharoen S, Schelble K, and Eide DJ. Peroxiredoxin chaperone activity is critical for protein homeostasis in zinc-deficient yeast. *J Biol Chem* 288: 31313–31327, 2013.
52. Marguerat S, Schmidt A, Codlin S, Chen W, Aebersold R, and Bahler J. Quantitative analysis of fission yeast transcriptomes and proteomes in proliferating and quiescent cells. *Cell* 151: 671–683, 2012.
53. Molin M, Yang J, Hanzen S, Toledano MB, Labarre J, and Nystrom T. Life span extension and H_2O_2 resistance elicited by caloric restriction require the peroxiredoxin Tsa1 in *Saccharomyces cerevisiae*. *Mol Cell* 43: 823–833, 2011.
54. Moon JC, Hah YS, Kim WY, Jung BG, Jang HH, Lee JR, Kim SY, Lee YM, Jeon MG, Kim CW, Cho MJ, and Lee SY. Oxidative stress-dependent structural and functional switching of a human 2-Cys peroxiredoxin isotype II that enhances HeLa cell resistance to H_2O_2-induced cell death. *J Biol Chem* 280: 28775–28784, 2005.
55. Netto LE and Antunes F. The roles of peroxiredoxin and thioredoxin in hydrogen peroxide sensing and in signal transduction. *Mol Cells* 39: 65–71, 2016.
56. Neumann CA, Krause DS, Carman CV, Das S, Dubey DP, Abraham JL, Bronson RT, Fujiwara Y, Orkin SH, and Van Etten RA. Essential role for the peroxiredoxin Prdx1 in erythrocyte antioxidant defence and tumour suppression. *Nature* 424: 561–565, 2003.
57. Noh YH, Baek JY, Jeong W, Rhee SG, and Chang TS. Sulfiredoxin translocation into mitochondria plays a crucial role in reducing hyperoxidized peroxiredoxin III. *J Biol Chem* 284: 8470–8477, 2009.
58. Nystrom T, Yang J, and Molin M. Peroxiredoxins, gerontogenes linking aging to genome instability and cancer. *Genes Dev* 26: 2001–2008, 2012.
59. O'Neill JS and Reddy AB. Circadian clocks in human red blood cells. *Nature* 469: 498–503, 2011.
60. O'Neill JS, van Ooijen G, Dixon LE, Troein C, Corellou F, Bouget FY, Reddy AB, and Millar AJ. Circadian rhythms persist without transcription in a eukaryote. *Nature* 469: 554–558, 2011.
61. Olahova M, Taylor SR, Khazaipoul S, Wang J, Morgan BA, Matsumoto K, Blackwell TK, and Veal EA. A redox-sensitive peroxiredoxin that is important for longevity has tissue- and stress-specific roles in stress resistance. *Proc Natl Acad Sci U S A* 105: 19839–19844, 2008.
62. Olahova M and Veal EA. A peroxiredoxin, PRDX-2, is required for insulin secretion and insulin/IIS-dependent regulation of stress resistance and longevity. *Aging Cell* 14: 558–568, 2015.
63. Olmedo M, O'Neill JS, Edgar RS, Valekunja UK, Reddy AB, and Merrow M. Circadian regulation of olfaction and an evolutionarily conserved, nontranscriptional marker in *Caenorhabditis elegans*. *Proc Natl Acad Sci U S A* 109: 20479–20484, 2012.
64. Pace PE, Peskin AV, Han MH, Hampton MB, and Winterbourn CC. Hyperoxidized peroxiredoxin 2 interacts with the protein disulfide- isomerase ERp46. *Biochem J* 453: 475–485, 2013.
65. Park JI, Jeon HJ, Jung NK, Jang YJ, Kim JS, Seo YW, Jeong M, Chae HZ, and Chun SY. Periovulatory expression of hydrogen peroxide-induced sulfiredoxin and

peroxiredoxin 2 in the rat ovary: gonadotropin regulation and potential modification. *Endocrinology* 153: 5512–5521, 2012.
66. Park MH, Jo M, Kim YR, Lee CK, and Hong JT. Roles of peroxiredoxins in cancer, neurodegenerative diseases and inflammatory diseases. *Pharmacol Ther* 163: 1–23, 2016.
67. Parsonage D, Youngblood DS, Sarma GN, Wood ZA, Karplus PA, and Poole LB. Analysis of the link between enzymatic activity and oligomeric state in AhpC, a bacterial peroxiredoxin. *Biochemistry* 44: 10583–10592, 2005.
68. Pascual MB, Mata-Cabana A, Florencio FJ, Lindahl M, and Cejudo FJ. Overoxidation of 2-Cys peroxiredoxin in prokaryotes: cyanobacterial 2-Cys peroxiredoxins sensitive to oxidative stress. *J Biol Chem* 285: 34485–34492, 2010.
69. Perkins A, Poole LB, and Karplus PA. Tuning of peroxiredoxin catalysis for various physiological roles. *Biochemistry* 53: 7693–7705, 2014.
70. Peskin AV, Dickerhof N, Poynton RA, Paton LN, Pace PE, Hampton MB, and Winterbourn CC. Hyperoxidation of peroxiredoxins 2 and 3: rate constants for the reactions of the sulfenic acid of the peroxidatic cysteine. *J Biol Chem* 288: 14170–14177, 2013.
71. Phalen TJ, Weirather K, Deming PB, Anathy V, Howe AK, van der Vliet A, Jonsson TJ, Poole LB, and Heintz NH. Oxidation state governs structural transitions in peroxiredoxin II that correlate with cell cycle arrest and recovery. *J Cell Biol* 175: 779–789, 2006.
72. Planson AG, Palais G, Abbas K, Gerard M, Couvelard L, Delaunay A, Baulande S, Drapier JC, and Toledano MB. Sulfiredoxin protects mice from lipopolysaccharide-induced endotoxic shock. *Antioxid Redox Signal* 14: 2071–2080, 2011.
73. Poole LB and Nelson KJ. Distribution and features of the six classes of peroxiredoxins. *Mol Cells* 39: 53–59, 2016.
74. Poynton RA and Hampton MB. Peroxiredoxins as biomarkers of oxidative stress. *Biochim Biophys Acta* 1840: 906–912, 2014.
75. Puerto-Galan L, Perez-Ruiz JM, Guinea M, and Cejudo FJ. The contribution of NADPH thioredoxin reductase C (NTRC) and sulfiredoxin to 2-Cys peroxiredoxin overoxidation in Arabidopsis thaliana chloroplasts. *J Exp Bot* 66: 2957–2966, 2015.
76. Rey P, Becuwe N, Barrault MB, Rumeau D, Havaux M, Biteau B, and Toledano MB. The *Arabidopsis thaliana* sulfiredoxin is a plastidic cysteine-sulfinic acid reductase involved in the photooxidative stress response. *Plant J* 49: 505–514, 2007.
77. Schroder E, Brennan JP, and Eaton P. Cardiac peroxiredoxins undergo complex modifications during cardiac oxidant stress. *Am J Physiol Heart Circ Physiol* 295: H425–H433, 2008.
78. Seidel T, Seefeldt B, Sauer M, and Dietz KJ. In vivo analysis of the 2-Cys peroxiredoxin oligomeric state by two-step FRET. *J Biotechnol* 149: 272–279, 2010.
79. Sobotta MC, Liou W, Stocker S, Talwar D, Oehler M, Ruppert T, Scharf AN, and Dick TP. Peroxiredoxin-2 and STAT3 form a redox relay for H_2O_2 signaling. *Nat Chem Biol* 11: 64–70, 2015.
80. Sun CC, Dong WR, Shao T, Li JY, Zhao J, Nie L, Xiang LX, Zhu G, and Shao JZ. Peroxiredoxin 1 (Prx1) is a dual-function enzyme by possessing Cys-independent catalase-like activity. *Biochem J* 474: 1373–1394, 2017.
81. Sunico CR and Moreno-Lopez B. Evidence for endothelial nitric oxide as a negative regulator of Schwann cell dedifferentiation after peripheral nerve injury. *Neurosci Lett* 471: 119–124, 2010.
82. Teixeira F, Castro H, Cruz T, Tse E, Koldewey P, Southworth DR, Tomas AM, and Jakob U. Mitochondrial peroxiredoxin functions as crucial chaperone reservoir in *Leishmania infantum*. *Proc Natl Acad Sci U S A* 112: E616–E624, 2015.
83. Thamsen M, Kumsta C, Li F, and Jakob U. Is overoxidation of peroxiredoxin physiologically significant? *Antioxid Redox Signal* 14: 725–730, 2011.
84. Tomalin LE, Day AM, Underwood ZE, Smith GR, Pezze PD, Rallis C, Patel W, Dickinson BC, Bahler J, Brewer TF, Chang CJ, Shanley DP, and Veal EA. Increasing extracellular HO produces a bi-phasic response in intracellular H_2O_2, with peroxiredoxin hyperoxidation only triggered once the cellular H_2O_2-buffering capacity is overwhelmed. *Free Radic Biol Med* 95, 333–348, 2016.
85. Travasso RDM, Sampaio Dos Aidos F, Bayani A, Abranches P, and Salvador A. Localized redox relays as a privileged mode of cytoplasmic hydrogen peroxide signaling. *Redox Biol* 12: 233–245, 2017.
86. Turner-Ivey B, Manevich Y, Schulte J, Kistner-Griffin E, Jezierska-Drutel A, Liu Y, and Neumann CA. Role for Prdx1 as a specific sensor in redox-regulated senescence in breast cancer. *Oncogene* 32: 5302–5314, 2013.
87. Veal EA, Findlay VJ, Day AM, Bozonet SM, Evans JM, Quinn J, and Morgan BA. A 2-Cys peroxiredoxin regulates peroxide-induced oxidation and activation of a stress-activated MAP kinase. *Mol Cell* 15: 129–139, 2004.
88. Vivancos AP, Castillo EA, Biteau B, Nicot C, Ayte J, Toledano MB, and Hidalgo E. A cysteine-sulfinic acid in peroxiredoxin regulates H_2O_2-sensing by the antioxidant Pap1 pathway. *Proc Natl Acad Sci U S A* 102: 8875–8880, 2005.
89. Wadley AJ, Chen YW, Bennett SJ, Lip GY, Turner JE, Fisher JP, and Aldred S. Monitoring changes in thioredoxin and over-oxidised peroxiredoxin in response to exercise in humans. *Free Radic Res* 49: 290–298, 2015.
90. Wagner E, Luche S, Penna L, Chevallet M, Van Dorsselaer A, Leize-Wagner E, and Rabilloud T. A method for detection of overoxidation of cysteines: peroxiredoxins are oxidized in vivo at the active-site cysteine during oxidative stress. *Biochem J* 366: 777–785, 2002.
91. Wei Q, Jiang H, Baker A, Dodge LK, Gerard M, Young MR, Toledano MB, and Colburn NH. Loss of sulfiredoxin renders mice resistant to azoxymethane/dextran sulfate sodium-induced colon carcinogenesis. *Carcinogenesis* 34: 1403–1410, 2013.
92. Weids AJ and Grant CM. The yeast peroxiredoxin Tsa1 protects against protein-aggregate-induced oxidative stress. *J Cell Sci* 127: 1327–1335, 2014.
93. Woo HA, Bae SH, Park S, and Rhee SG. Sestrin 2 is not a reductase for cysteine sulfinic acid of peroxiredoxins. *Antioxid Redox Signal* 11: 739–745, 2009.
94. Woo HA, Chae HZ, Hwang SC, Yang KS, Kang SW, Kim K, and Rhee SG. Reversing the inactivation of peroxiredoxins caused by cysteine sulfinic acid formation. *Science* 300: 653–656, 2003.

95. Woo HA, Jeong W, Chang TS, Park KJ, Park SJ, Yang JS, and Rhee SG. Reduction of cysteine sulfinic acid by sulfiredoxin is specific to 2-cys peroxiredoxins. *J Biol Chem* 280: 3125–3128, 2005.
96. Woo HA, Kang SW, Kim HK, Yang KS, Chae HZ, and Rhee SG. Reversible oxidation of the active site cysteine of peroxiredoxins to cysteine sulfinic acid. Immunoblot detection with antibodies specific for the hyperoxidized cysteine-containing sequence. *J Biol Chem* 278: 47361–47364, 2003.
97. Woo HA, Yim SH, Shin DH, Kang D, Yu DY, and Rhee SG. Inactivation of peroxiredoxin I by phosphorylation allows localized H_2O_2 accumulation for cell signaling. *Cell* 140: 517–528, 2010.
98. Wood ZA, Poole LB, and Karplus PA. Peroxiredoxin evolution and the regulation of hydrogen peroxide signaling. *Science* 300: 650–653, 2003.
99. Wood ZA, Schroder E, Robin Harris J, and Poole LB. Structure, mechanism and regulation of peroxiredoxins. *Trends Biochem Sci* 28: 32–40, 2003.
100. Wu L, Jiang H, Chawsheen HA, Mishra M, Young MR, Gerard M, Toledano MB, Colburn NH, and Wei Q. Tumor promoter-induced sulfiredoxin is required for mouse skin tumorigenesis. *Carcinogenesis* 35: 1177–1184, 2014.
101. Yang KS, Kang SW, Woo HA, Hwang SC, Chae HZ, Kim K, and Rhee SG. Inactivation of human peroxiredoxin I during catalysis as the result of the oxidation of the catalytic site cysteine to cysteine-sulfinic acid. *J Biol Chem* 277: 38029–38036, 2002.
102. Yoo KY, Park OK, Yu J, Yan B, Li H, Lee CH, Choi JH, Kim DW, Hwang IK, and Won MH. Expression and changes of hyperoxidized peroxiredoxins in non-pyramidal and polymorphic cells in the gerbil hippocampus during normal aging. *Cell Mol Neurobiol* 29: 413–421, 2009.

Address correspondence to:
Dr. Elizabeth A. Veal
Institute for Cell and Molecular Biosciences
Newcastle University
Framlington Place
Newcastle upon Tyne
NE2 4HH
United Kingdom

E-mail: e.a.veal@ncl.ac.uk

Date of first submission to ARS Central, June 28, 2017; date of acceptance, July 29, 2017.

Abbreviations Used

ACTH = adrencorticotrophic hormone
AMS = 4-acetamido-4′-maleimidylstilbene-2,2′-disulfonic acid
ER = endoplasmic reticulum
H_2O_2 = hydrogen peroxide
MAPK = mitogen-activated protein kinase
MAPKKK = mitogen-activated protein kinase kinase kinase
MKP = mitogen-activated kinase phosphatase
NADH = reduced nicotinamide adenine dinucleotide
NADPH = reduced nicotinamide adenine dinucleotide phosphate
Prx = 2-Cys peroxiredoxins
PTP = protein tyrosine phosphatase
ROS = reactive oxygen species
SO_2^- = sulfinyl
SO_3^- = sulfonyl
Trx = thioredoxin

Free Radical Biology and Medicine 95 (2016) 333–348

Contents lists available at ScienceDirect

Free Radical Biology and Medicine

journal homepage: www.elsevier.com/locate/freeradbiomed

Original Contribution

Increasing extracellular H_2O_2 produces a bi-phasic response in intracellular H_2O_2, with peroxiredoxin hyperoxidation only triggered once the cellular H_2O_2-buffering capacity is overwhelmed

Lewis Elwood Tomalin [a], Alison Michelle Day [a], Zoe Elizabeth Underwood [a], Graham Robert Smith [b], Piero Dalle Pezze [a], Charalampos Rallis [c,1], Waseema Patel [a], Bryan Craig Dickinson [d], Jürg Bähler [c], Thomas Francis Brewer [e], Christopher Joh-Leung Chang [e], Daryl Pierson Shanley [a,*], Elizabeth Ann Veal [a,*]

[a] Institute for Cell and Molecular Biosciences, Newcastle University, Framlington Place, Newcastle upon Tyne NE2 4HH, UK
[b] Bioinformatics Support Unit, Newcastle University, Framlington Place, Newcastle upon Tyne NE2 4HH, UK
[c] University College London, Department of Genetics, Evolution & Environment and Institute of Healthy Ageing, Gower Street – Darwin Building, London WC1E 6BT, UK
[d] Department of Chemistry, The University of Chicago, Chicago, IL 60637, USA
[e] Howard Hughes Medical Institute and Departments of Chemistry and Molecular and Cell Biology, University of California, Berkeley, Berkeley, CA 94720, USA

ARTICLE INFO

Article history:
Received 14 August 2015
Received in revised form
25 February 2016
Accepted 29 February 2016
Available online 2 March 2016

Keywords:
Peroxiredoxin
Hydrogen peroxide
Thiol
Computational model
Signaling
Oxidation
Thioredoxin

ABSTRACT

Reactive oxygen species, such as H_2O_2, can damage cells but also promote fundamental processes, including growth, differentiation and migration. The mechanisms allowing cells to differentially respond to toxic or signaling H_2O_2 levels are poorly defined. Here we reveal that increasing external H_2O_2 produces a bi-phasic response in intracellular H_2O_2. Peroxiredoxins (Prx) are abundant peroxidases which protect against genome instability, ageing and cancer. We have developed a dynamic model simulating in vivo changes in Prx oxidation. Remarkably, we show that the thioredoxin peroxidase activity of Prx does not provide any significant protection against external rises in H_2O_2. Instead, our model and experimental data are consistent with low levels of extracellular H_2O_2 being efficiently buffered by other thioredoxin-dependent activities, including H_2O_2-reactive cysteines in the thiol-proteome. We show that when extracellular H_2O_2 levels overwhelm this buffering capacity, the consequent rise in intracellular H_2O_2 triggers hyperoxidation of Prx to thioredoxin-resistant, peroxidase-inactive form/s. Accordingly, Prx hyperoxidation signals that H_2O_2 defenses are breached, diverting thioredoxin to repair damage.

1. Introduction

Reactive oxygen species (ROS) generated by the partial reduction of oxygen during aerobic metabolism, immune cell attack or following exposure to radiation can cause lethal levels of cell damage. Hence, there is a strong driving force to evolve and maintain ROS-protective mechanisms. Nevertheless, altered redox homeostasis and increased oxidative cell damage are associated with the development of many common diseases, including cancer, diabetes, cardiovascular and neurodegenerative diseases. However, there is increasing evidence that low levels of ROS can also have beneficial effects; acting as signaling molecules to regulate diverse biological processes (for a review see [1]). Hence, there is considerable interest in understanding how cells optimize ROS defenses to provide adequate protection without compromising ROS-signaling functions. Here we have developed and used a mathematical model as a tool to understand what governs how cells respond to increases in hydrogen peroxide (H_2O_2).

Peroxiredoxins (Prx) are amongst the most prevalent enzymes involved in responses to H_2O_2. Prx are ubiquitous and highly expressed peroxidases which utilize reversibly oxidized cysteine

Abbreviations: Prx, peroxiredoxins; Trx, thioredoxin; Txl1, thioredoxin-like protein 1; Gpx1, glutathione peroxidase 1; AMS, 4-acetamido-4′-((iodoacetyl)amino) stilbene-2,2′-disulfonic acid; NEM, N-ethylmaleimide; ROS, reactive oxygen species; H_2O_2, hydrogen peroxide; CysP, peroxidatic cysteine; CysR, resolving cysteine; Pr-SS, protein disulfides; Pr-SH, protein thiols; DMEM, Dulbecco's Modified Eagles Medium; EMM, Edinburgh minimal media; TCA, trichloroacetic acid; DPBS, Dulbecco's phosphate-buffered saline; HRP, horse radish peroxidase; PF3, acetylated peroxyfluorescein 3; AIC, Akaike Information Criterion

* Corresponding authors.
E-mail addresses: daryl.shanley@ncl.ac.uk (D.P. Shanley), e.a.veal@ncl.ac.uk (E.A. Veal).
[1] Current Address: School of Health, Sport and Biosciences, University of East London, London E15 4LZ, UK.

http://dx.doi.org/10.1016/j.freeradbiomed.2016.02.035

residues to reduce peroxides (for a review see [2]) (Fig. 1A). Intriguingly, peroxiredoxins appear to have dual roles in cancer, acting as tumor suppressors but with increased Prx expression also associated with poor prognosis tumors and increased metastasis. Prx have also been shown to promote longevity in yeast, worms, flies and mammals (for a review see [3]). There is therefore great interest in understanding how Prx influence cell responses to H_2O_2.

The catalytic mechanism of the typical 2-Cys Prx subfamily involves the initial reaction of an active, peroxidatic cysteine (Cys_P) with peroxide to form a cysteine-sulfenic acid (SOH) (Fig. 1A). The sulfenylated peroxidatic cysteine then forms a disulfide with a second, resolving cysteine (Cys_R) in an adjacent Prx molecule. In eukaryotes, these Prx disulfides are reduced by the thioredoxin system. However, the sulfenylated peroxidatic cysteines of thioredoxin-coupled Prx are highly susceptible to further 'hyperoxidation' to thioredoxin-resistant sulfinic-derivatives, thus inactivating their thioredoxin peroxidase activity [4] (Fig. 1A). In contrast, bacterial 2-Cys Prx, such as the *E. coli* peroxiredoxin AhpC, are much less sensitive to hyperoxidation [5]. Conserved YF and GG(L/V/I)G amino acid motifs found in all hyperoxidation-sensitive Prx are responsible for this sensitivity [5]. The evolution of these conserved amino acid motifs suggests that Prx hyperoxidation confers a selective advantage in eukaryotes. Indeed, as described below, several possible functions have been proposed for hyperoxidation of Prx.

In eukaryotes, in which Prx are sensitive to inactivation, H_2O_2 is generated and utilized as a signaling molecule [2]. Thus it has been proposed that the thioredoxin peroxidase activity of Prx might act as a barrier to this signaling, and that inactivation of Prx might be important to allow H_2O_2 to regulate target proteins [5]. Although, Prx are not hyperoxidized in response to the low levels of H_2O_2 generated in response to growth factors [6], oscillations in the amount of hyperoxidized Prx have been associated with circadian rhythms across a wide range of species (for a review see [7]). Moreover, oscillations in the hyperoxidation of the mouse mitochondrial Prx, Prx3, have been shown to be important for circadian oscillations in p38 activation and adrenal steroid synthesis [8]. Nevertheless, it remains unclear whether the hyperoxidation of Prx in any of these contexts serves to increase the levels of H_2O_2 available for signaling. Moreover, work in the fission yeast *Schizosaccharomyces pombe* has shown that, rather than acting as a barrier, the thioredoxin peroxidase activity of the single *S. pombe* peroxiredoxin, Tpx1, is actually required for the H_2O_2-induced activation of the AP-1-like transcription factor Pap1 [9–11]. We have shown that the role of the thioredoxin peroxidase activity of Tpx1 in H_2O_2-induced Pap1 activation is to competitively inhibit the reduction of the active, oxidized form of Pap1 by the thioredoxin-like protein, Txl1 [11]. Accordingly, hyperoxidation of Tpx1 to a thioredoxin-resistant form prevents the H_2O_2-induced activation of Pap1 by increasing the availability of reduced Txl1 [11]. Based on these studies, it has been proposed that hyperoxidation

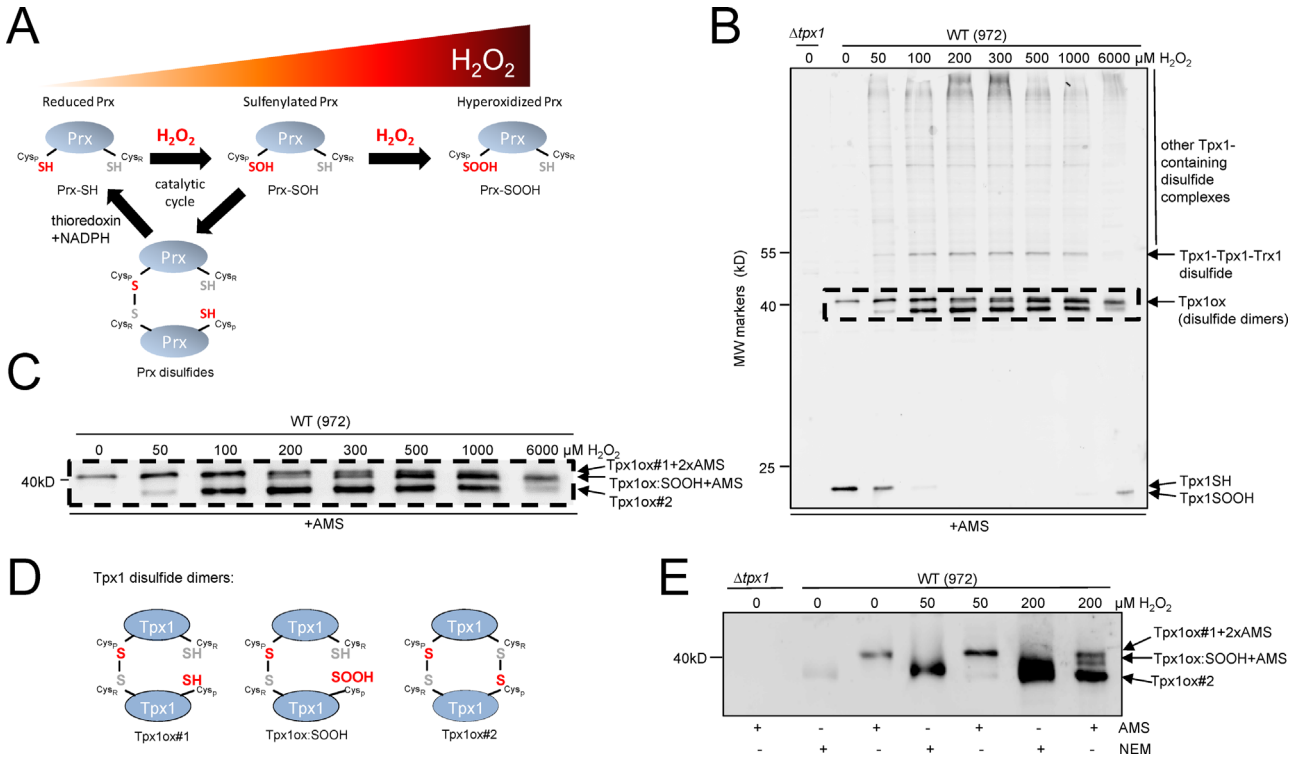

Fig. 1. The Prx, Tpx1, undergoes oxidation to multiple redox states following exposure to different concentrations of H_2O_2: (A) the thioredoxin peroxidase activity of Prx, such as Tpx1, involves the reversible oxidation of catalytic cysteines but is inactivated by hyperoxidation of the peroxidatic cysteine at high concentrations of H_2O_2. The catalytic breakdown of H_2O_2 by 2-Cys peroxiredoxins (Prx) involves the reaction of the peroxidatic cysteine (Cys_P) with H_2O_2. In the catalytic cycle the sulfenylated cysteine is stabilized by forming a disulfide with the resolving cysteine (Cys_R) in a neighboring Prx molecule. These Prx disulfides are reduced by the thioredoxin system using electrons from NADPH. In eukaryotes Prx disulfide formation is slow, rendering the sulfenylated Prx, Prx-SOH, susceptible to further oxidation to a sulfinylated, 'hyperoxidized' form (Prx-SOOH) that cannot be reduced by thioredoxin. This hyperoxidation is favored at higher concentrations of H_2O_2 inactivating the thioredoxin peroxidase activity of the Prx. Western blot analysis (anti-Tpx1 antibodies) of (B) and (C) AMS-treated protein extracts from wild-type (972) and Δ*tpx1* mutant (VX00) cells treated, as indicated, for 20 s with 0–6 mM H_2O_2 reveals that Tpx1 undergoes oxidation to a number of redox states following exposure to H_2O_2. The absence of bands in Δ*tpx1* mutant (VX00) cells indicates that all the bands detected in wild-type cells represent Tpx1 or Tpx1-containing complexes. (C) A magnified image of the ~40 kDa region outlined by the dotted line in (B) shows that 3 different Tpx1-containing disulfide dimers (Tpx1ox) are detected following treatment with concentrations ≥ 200 μM. (D) Different Tpx1ox forms are depicted which were separated in (E) on the basis of the reduced mobility associated with modification of free cysteine thiols by AMS (0.6 kDa) compared with NEM (0.1 kDa). (E) disulfide dimers (Tpx1ox) in duplicate samples extracted from wild-type or Δ*tpx1* mutant (VX00) cells before or following treatment for 20 s with the indicated concentration of H_2O_2 then reacted with AMS or NEM. As in (B), only low levels of Tpx1ox (disulfides) are detected in untreated cells or cells treated with 50 μM. See also Table S1 and Fig. S1.

of Tpx1 to a thioredoxin-resistant form is important to increase the pool of reduced thioredoxin available to repair oxidatively damaged proteins and support the activity of other enzymes, such as the methionine sulfoxide reductase, Mxr1 [12]. Consistent with this hypothesis, hyperoxidation of Tpx1 and the *C. elegans* peroxiredoxin PRDX-2 are important for cell survival under acute stress conditions [12,13]. Hyperoxidation of Prx has also been proposed to have other roles, for example, protecting cells against protein aggregation by promoting the ability of Prx to act as a chaperone [14]. However, it is still unclear under what conditions extensive Prx hyperoxidation occurs *in vivo* and when and where this might be important.

Although all eukaryotic Prx are inherently sensitive to hyperoxidation, other factors affect this sensitivity. For example, *in vitro* studies revealed that human cytosolic Prx1 is much more sensitive to hyperoxidation than the mitochondrial Prx, Prx3 [15]. This increased sensitivity reflects a 10-fold slower rate of Prx1 disulfide formation that increases the risk of further oxidation of the sulfenylated peroxidatic cysteine [16,17]. In addition to the intrinsic biochemical properties of the Prx itself, the *in vivo* sensitivity of Prx to hyperoxidation is also influenced by the local environment. For example, although *in vitro* the ER-localized Prx, Prx4, has a similar sensitivity to hyperoxidation to Prx1, a negligible proportion of Prx4 becomes hyperoxidized to its sulfinic form *in vivo*. This is due to the low abundance of disulfide reductases in the ER which causes Prx4 disulfides to accumulate instead [18]. As well as the availability of disulfide reductases, the extent to which Prx become hyperoxidized *in vivo* will also be influenced by other aspects of its local environment, such as local H_2O_2 concentration, compartmental volumes and competition with other peroxidases. Here we have developed a computational model incorporating both the biochemical properties and *in vivo* environment as a tool to investigate when Prx become hyperoxidized and the effect of hyperoxidation on cell responses to H_2O_2. Notably, our model predicts that cell's contain a Prx-independent H_2O_2-removing activity that becomes saturated following exposure to specific concentrations of extracellular H_2O_2. This results in a bi-phasic response to increased levels of ectopic H_2O_2 with Prx hyperoxidation only occurring once this H_2O_2–removing activity is saturated and intracellular H_2O_2 levels start to rise more rapidly. Importantly, we have experimentally confirmed these predictions in both yeast and human cells. As we discuss, our study provides new mechanistic insight into how Prx hyperoxidation and regulation of thioredoxin activity allow cells to implement appropriate responses to the different levels of H_2O_2 encountered *in vivo*.

2. Results

2.1. Quantitative analysis of how the in vivo oxidation of the Prx, Tpx1, changes in response to different concentrations of H_2O_2

To facilitate the generation of a mathematical model capable of simulating *in vivo* changes in Prx oxidation, we first obtained quantitative data for the *in vivo* oxidation of the single *S. pombe* peroxiredoxin Tpx1 following exposure of cells for 20 s to a range of H_2O_2 concentrations (0–6 mM) (Fig. 1 and Table S1). Western blot analysis of AMS-treated proteins using anti-Tpx1 antibodies detected multiple Tpx1-containing bands, as confirmed by the absence of these bands in Δ*tpx1* mutant cells (Fig. 1B). These included bands with mobilities of ~20 kDa and ~40 kDa consistent with representing reduced Tpx1 monomers (Tpx1SH) and Tpx1 disulfide dimers respectively. Under normal growth conditions the reduced monomeric band (Tpx1SH) was prevalent (Fig. 1B and Table S1). However, following treatment with H_2O_2, the levels of Tpx1SH decreased with the concomitant increased formation of disulfide dimers and higher molecular weight bands (> 40 kDa), which likely include mixed disulfides with other proteins (Fig. 1B and data not shown). The sensitivity of all of these bands to reduction by beta-mercaptoethanol to 20 kDa forms (Fig. S1A) indicating that each represents a different disulfide-bonded form of Tpx1.

Although difficult to resolve, as expected, a magnified image revealed three distinct bands with mobilities consistent with Tpx1 disulfide homodimers (40 kDa) (Fig. 1C). The differences in the mobility of these three Tpx1 dimer bands was consistent with each representing a different redox state, as observed previously for Tpx1 and human Prx [15,16,19] (Fig. 1D). Indeed, in samples treated with NEM, which alkylates reduced cysteines producing a minimal increase in MW (0.1 kDa), a single Tpx1-containing band was detected at ~40 kDa (Fig. 1E). This confirms that the differences in the mobility of the 3 bands in AMS-treated samples reflect the different numbers of cysteine residues available to react with AMS, which increases the MW by 0.6 kDa per reduced cysteine. The single Tpx1 disulfide dimer band detected under normal conditions was significantly retarded by AMS. This is consistent with this band representing Tpx1–Tpx1 dimers containing a single disulfide bond between one peroxidatic (Cys_P) and one resolving cysteine (Cys_R) with the other cysteines reduced and AMS-reactive (Tpx1ox#1) (Fig. 1D and E). In cells treated with 200 μM H_2O_2 two additional Tpx1 disulfide bands were detected in the AMS-treated samples. The similar mobility of the lowest of these bands in NEM and AMS-treated samples suggests that it lacks any reduced cysteine thiols to react with NEM or AMS, consistent with it representing Tpx1 disulfide dimer containing two disulfide bonds (Tpx1ox#2) (Fig. 1D and E). The third band detected after treatment with 200 μM H_2O_2 (Tpx1ox:SOOH+AMS) had an intermediate mobility. This was consistent with the binding of a single AMS molecule to a single reduced cysteine thiol, as would be expected for Tpx1 disulfide dimers containing a single disulfide bond and a hyperoxidized Cys_P (Tpx1ox:SOOH) with the remaining Cys_R available to react with AMS (Fig. 1D and E). This form has also been detected using anti-PrxSO3 antibodies specific to the sulfinylated/sulfonylated peroxidatic cysteine [12]. Thus we confirmed that the three distinct Tpx1 disulfide dimers we detected represented redox states previously described for *S. pombe* and human peroxiredoxins [15,16,19]. In addition to the bands at 40 kDa, a band at 55 kDa was also detected (Figs. 1B, 2A, B and S1) that represents a Tpx1 dimer in a disulfide complex with Trx1 (Fig. S1B), a reaction intermediate in the reduction of Tpx1ox#2 by Trx1. Changes in the relative intensities of the various Tpx1 forms in cells treated with different H_2O_2 concentrations indicated that, as expected, Tpx1ox#1, Tpx1ox#2 and Tpx1ox:SOOH become the most prominent forms at the lowest, mid and high H_2O_2 concentrations respectively (Fig. 1 and Table S1).

2.2. Quantitative analysis of in vivo changes in the oxidation of Tpx1 with time following exposure to H_2O_2

To allow development of a dynamic model, we obtained kinetic data; determining how the relative abundance of different Tpx1 redox forms changed with time (≤ 600 s) following treatment with 100 μM or 200 μM H_2O_2. This time-course was selected to represent the initial H_2O_2 response, before H_2O_2-induced increases in mRNA levels [20,21] have had any significant effect on total Tpx1 protein levels, or the levels of other proteins which might impact on Tpx1 oxidation [9,10,22] (Fig. 2 and data not shown). Tpx1ox#1 and Tpx1ox#2 were detected following treatment with 100 μM H_2O_2, but the relative levels of these forms did not change with time (Fig. 2A). Importantly, there was negligible formation of Tpx1ox:SOOH during the 100 μM time course (Table S1), as was confirmed using antibodies specific to hyperoxidized Tpx1 (Fig.

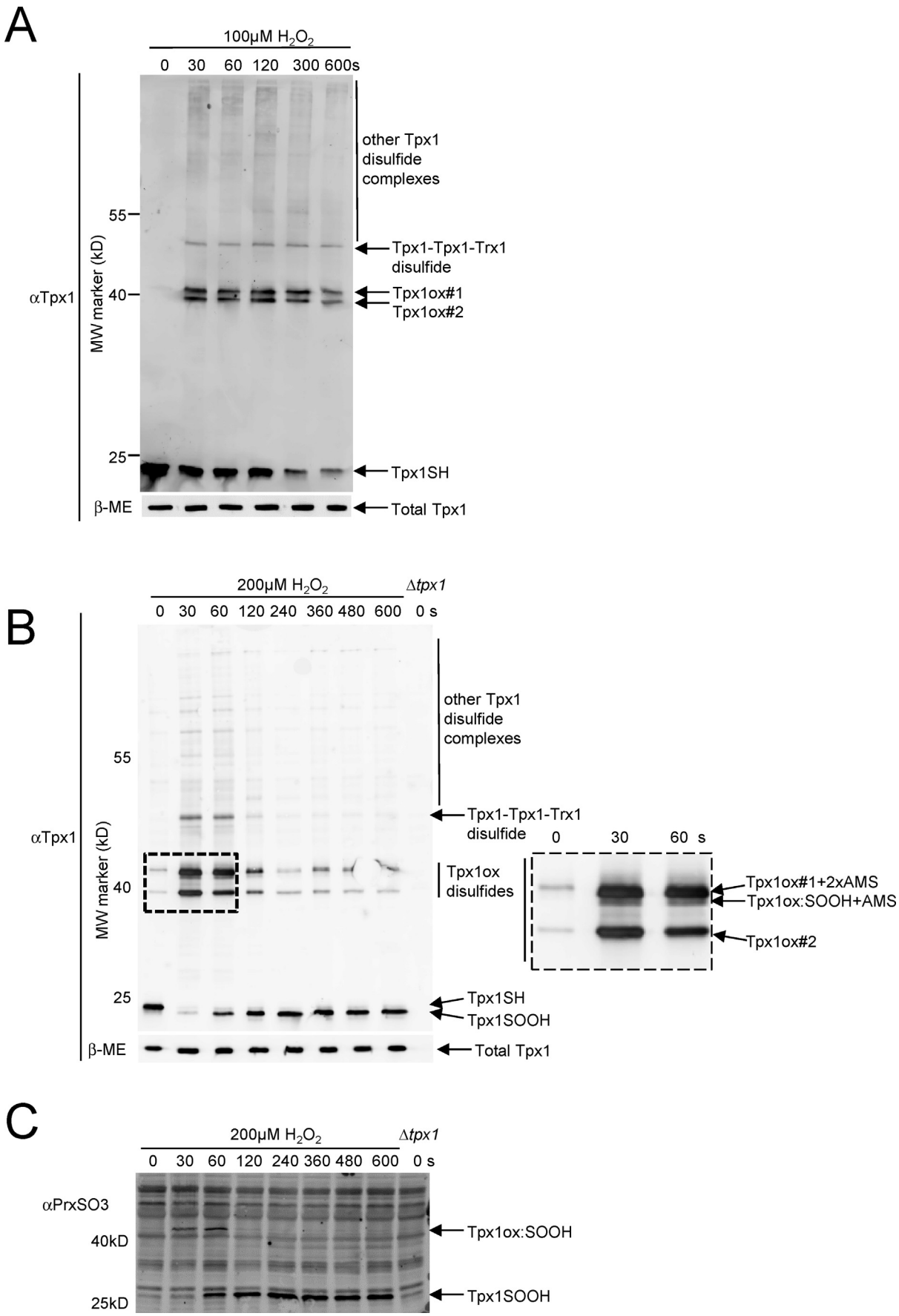

Fig. 2. Changes in Tpx1 oxidation over time following treatment with 100 or 200 μM H_2O_2. Western blot analysis with (A) and (B) anti-Tpx1 or (C) anti-PrxSO3 antibodies of AMS-treated protein extracts from wild-type (972) and Δ*tpx1* mutant (VX00) cells treated, as indicated with (A) 100 μM (B) and (C) 200 μM H_2O_2 for 0–600 s shows how the oxidation of Tpx1 changes with time. (B) and (C) shows that Tpx1ox:SOOH disulfide formation at 200 μM H_2O_2 precedes the formation of Tpx1-SOOH monomers. In (B) a section of the blot, outlined by the dotted line, is magnified and shown in the right hand panel to enable the additional Tpx1ox form present in cells treated with 200 μM H_2O_2 (Tpx1ox:SOOH) to be seen more clearly. Western blot analysis of beta-mercaptoethanol (βME)-treated samples, run on a separate gel (lower panel in (A) and (B)), in which a single band represents all Tpx1 redox states (eliminating any influence that differences in mobility might have on transfer to the membrane) allowing total Tpx1 levels to be compared (A) confirms that differences between lanes reflect changes in Tpx1 oxidation rather than total Tpx1 levels (see also Table S1 and Fig. S2).

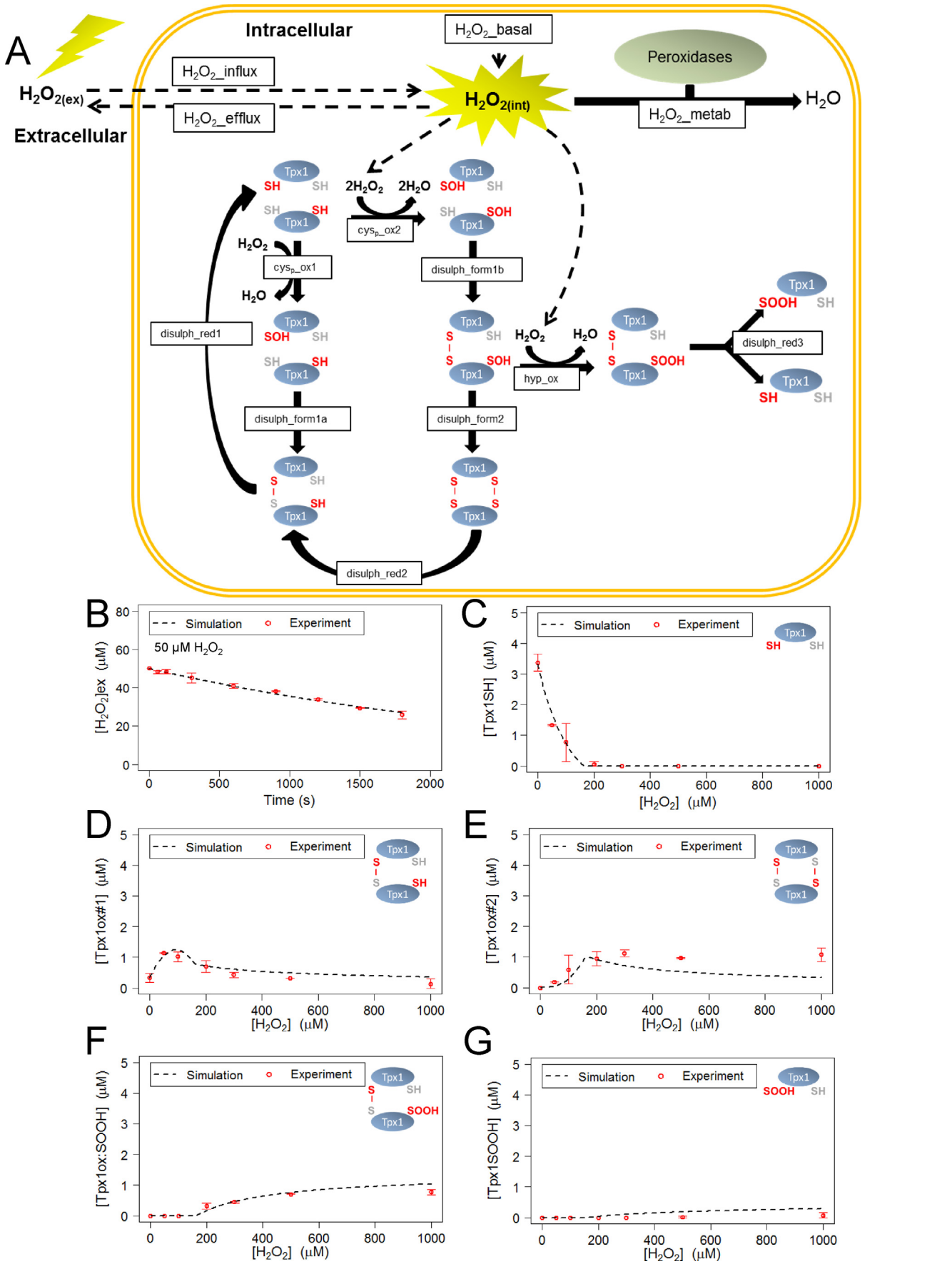

Fig. 3. Diagram representing the mathematical model describing the *in vivo* oxidation of Tpx1 and qualitative analysis of the fit of the model to the experimental data: (A) the model contains 9 different Tpx1 oxidation states which are interconverted by the indicated reactions. The rates of influx/efflux (H_2O_2 influx and H_2O_2 efflux) and removal of H_2O_2 (H_2O_2 metab) from the intracellular compartment were also included in the model. For rate laws see Table S2 and for parameters see Table S3. (B)–(G) Plots show simulated and experimentally determined concentrations of (B) extracellular H_2O_2 (C) reduced Tpx1; Tpx1SH (D) single Tpx1 disulfides; Tpx1ox#1 (E) double Tpx1 disulfides; Tpx1ox#2 (F) disulfide bonded hyperoxidized Tpx1; Tpx1ox:SOOH (G) hyperoxidized Tpx1 monomer; Tpx1SOOH in wild-type *S. pombe* following 20 s exposure to between 0 and 1000 μM H_2O_2. Simulated data derived from the model were plotted against the experimental data used in the parameter estimation (Table S1) (see also Tables S2 and S3, Figs. S3 and S4).

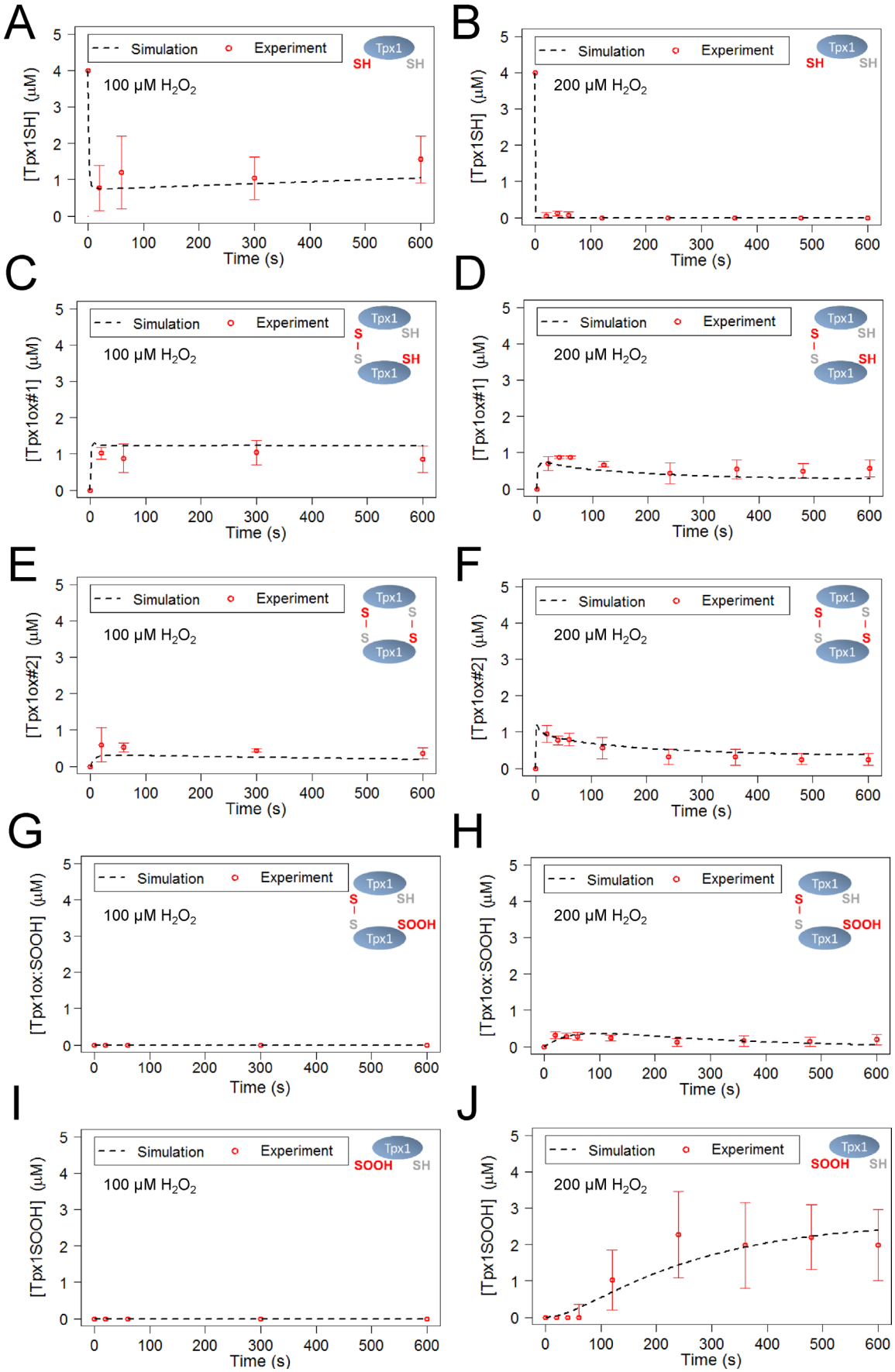

Fig. 4. Qualitative analysis of the fit of the model to the experimental data for between 0 and 600 s exposure to 100 or 200 μM H_2O_2. Plots show simulated and experimentally determined concentrations of (A) and (B) reduced Tpx1; Tpx1SH (C) and (D) single Tpx1 disulfides; Tpx1ox#1 (E) and (F) double Tpx1 disulfides; Tpx1ox#2 (G) and (H) disulfide bonded hyperoxidized Tpx1; Tpx1oxSOOH (I) and (J) hyperoxidized Tpx1 monomer; Tpx1SOOH in wild-type *S. pombe* following 0–600 s treatment with (A), (C), (E), (G) and (I) 100 μM or (B), (D), (F), (H) and (J) 200 μM H_2O_2. Simulated data derived from the model were plotted against the experimental data used in the parameter estimation (Table S1).

S2). In contrast, as expected (Fig. 1) Tpx1ox#1, Tpx1ox#2 and Tpx1ox:SOOH dimers were all detected in cells treated with 200 μM H_2O_2 (Fig. 2B and C). However, the intensity of the Tpx1 dimer bands decreased over time with the concomitant formation of a Tpx1-containing monomeric band (~20 kDa). The increased mobility, compared with the AMS-reactive Tpx1-SH monomer band detected before addition of H_2O_2, suggests this H_2O_2-induced band represents monomeric Tpx1 containing a single AMS-reactive cysteine thiol. This is consistent with the hyperoxidized Tpx1SOOH monomer previously observed following treatment of cells with higher H_2O_2 concentrations [9–12]. The formation of Tpx1-SOOH monomer was confirmed using antibodies specific to hyperoxidized Tpx1 (Figs. 2C and S2). The 200 μM time course data thus suggests that Tpx1ox:SOOH appears rapidly and is converted to Tpx1SOOH over time with the reaction essentially complete by 600 s. The detection of Prxox:SOOH dimers prior to PrxSOOH monomers is consistent with previous studies of Prx hyperoxidation [15,19]. At 500 μM and 1000 μM H_2O_2 the monomeric Tpx1SOOH form was maximal by 60 s, suggesting that increased H_2O_2 concentration results in an increased rate of formation of Tpx1SOOH (Fig. S2). Importantly, consistent with published studies [9,10,22], western blot analysis of beta-mercaptoethanol treated samples confirmed that differences in the intensity of different Tpx1-containing bands did not reflect changes in total Tpx1 levels (Fig. 2A and B). Thus quantitative analysis of images, obtained for multiple independent biological repeats of these experiments (Figs. 1 and 2), was used to estimate the concentrations of each Tpx1 oxidation state at each time point and level of H_2O_2 (Table S1).

2.3. A kinetic model of Tpx1 oxidation was developed that can replicate the experimental data

Computational models to describe Tpx1 oxidation were then constructed using reaction networks and parameters that were selected based on published mechanisms, *in vitro* kinetic data, and our *in vivo* experimental data (Figs. 1, 2 and Tables S1–S3). We carried out qualitative and quantitative assessments of the ability of each model to describe the experimental data. This led to the selection of a final model, depicted in Fig. 3A, that used the parameter set in Table S3. This final model was able to simulate the removal of H_2O_2 from the extracellular space, indicating that this model could effectively represent the peroxide-removing activity of the cells (Fig. 3B). The final model also simulated the changes in the concentrations of the different Tpx1 redox states following 20 s exposure to H_2O_2 concentrations between 0 and 1000 μM (Fig. 3C–G) or up to 600 s following exposure to 100 or 200 μM H_2O_2 (Fig. 4). Importantly, the parameters that were predicted for this model were similar to published values (Table S3). For instance, the parameters $k_{disulph\_red1}$, $k_{disulph\_red2}$ were predicted to be 0.190 and 0.143 $\mu M^{-1}\ s^{-1}$ respectively (Table S3, Figs. S3 and S4), broadly consistent with experimentally determined values [23,24]. This indicated that the model accurately represents the rapid Trx1-mediated reduction of the disulfide bonds in Tpx1ox#1 and Tpx1ox#2. Interestingly, the rate constant for the reduction of Tpx1ox:SOOH, $k_{disulph\_red3}$, was predicted, to be 0.029 $\mu M^{-1}\ s^{-1}$, 5 fold lower than either $k_{disulph\_red1}$ or $k_{disulph\_red2}$ (Table S3, Figs. S3 and S4). This suggests that Trx1 may be less efficient at reducing the disulfide bond in Tpx1ox:SOOH compared with the other Tpx1 disulfide dimers. Notably, the first order rate constant for Tpx1 disulfide formation (rate constant $k_{disulph\_form2}$) estimated by our model as 3.44 s^{-1} was in a similar range to the rates of disulfide formation estimated for human Prx1 and Prx3 (2 s^{-1} and 20 s^{-1} respectively) from *in vitro* experimental investigations [16]. This supports the use of our model and *in vitro* studies as complementary tools to understand the *in vivo* oxidation of yeast and human Prx.

2.4. Modeling suggests that oxidation of the peroxidatic cysteine thiol (Cys_P) in Tpx1ox#1 is not the major route for further oxidation of Tpx1

Having built and parameterized a dynamic model capable of simulating the *in vivo* oxidation of Tpx1 (Figs. 3 and 4), we tested which aspects of our model were important for simulation of the experimental data by comparing the ability of our final model and 2 alternative models to simulate the dynamics of Tpx1 oxidation. Although difficult to demonstrate experimentally, it seemed likely that the reaction of the free Cys_P in Tpx1ox#1 with H_2O_2 to form Tpx1ox:SOH would be involved in the formation of both the Tpx1ox#2 disulfide dimer and Tpx1ox:SOOH. However, unexpectedly, alternative Model A which included this additional reaction (Table S4) was less able to simulate the experimentally observed dynamics of Tpx1 oxidation (Fig. 5) and had an increased AIC compared with the final model (Table S5). Accordingly, this alternative model was rejected in favor of our final model (Fig. 3A) in which the simultaneous oxidation of neighboring Cys_P-SH (disulph_form1b) is the major route of Tpx1ox:SOH formation. Interestingly, this suggests that the reduced Cys_P in Tpx1ox#1 may be less sensitive to H_2O_2 and that, *in vivo*, the reaction of neighboring peroxidatic cysteines with H_2O_2, prior to disulfide bond formation, may be prerequisite for the generation of hyperoxidized SOOH derivatives.

Although an alternative route for the formation of hyperoxidized Tpx1 would be via the oxidation of the sulfenylated peroxidatic cysteine in Tpx1-SOH, the inclusion of this reaction was not required to fit the experimental data, and actually rendered models less able to simulate the experimentally observed dynamics of Tpx1 oxidation (data not shown). Thus, we conclude that this route makes a negligible contribution to the pool of hyperoxidized Tpx1SOOH detected at these H_2O_2 concentrations. This is consistent with previous work [19] suggesting that the hyperoxidation of Tpx1ox:SOH precedes the formation of Tpx1SOOH disulfide dimers and is the dominant route for Tpx1 sulfinylation *in vivo*.

2.5. The removal of H_2O_2 by an additional process/es (H_2O_2_metab) was required to explain the dynamics of Tpx1 hyperoxidation

The final model (Fig. 3A) accurately simulated our experimental observation that there was negligible formation of either of the hyperoxidized Tpx1 forms (Tpx1ox:SOOH and Tpx1-SOOH) at H_2O_2 concentrations below 200 μM (Figs. 1, 4 and S2). However, this particular feature of the experimental data was not captured by alternative Model B which did not contain the reaction 'H_2O_2_metab' (Table S4). Instead, alternative Model B predicted that Tpx1 would be hyperoxidized at all H_2O_2 concentrations, even below 200 μM (Alt Model B Fig. 5C and E). This suggests that, although Tpx1 reacts with extremely low H_2O_2 concentrations to generate Tpx1–Tpx1 disulfides, other components of the cell's H_2O_2-buffering capacity normally inhibit hyperoxidation *in vivo*. Together these results suggest that the sensitivity of peroxiredoxins to hyperoxidation is not just dependent on the kinetics of Prx reaction with H_2O_2 but is also heavily influenced by the other peroxide-reactive molecules present in their *in vivo* environment.

2.6. As predicted by our model, there is a two phase relationship between intracellular and extracellular H_2O_2 concentration

To further investigate the conditions which cause Prx to become hyperoxidized, we used our model to predict how increasing extracellular H_2O_2 concentrations ($[H_2O_2]_{ex}$) would affect the

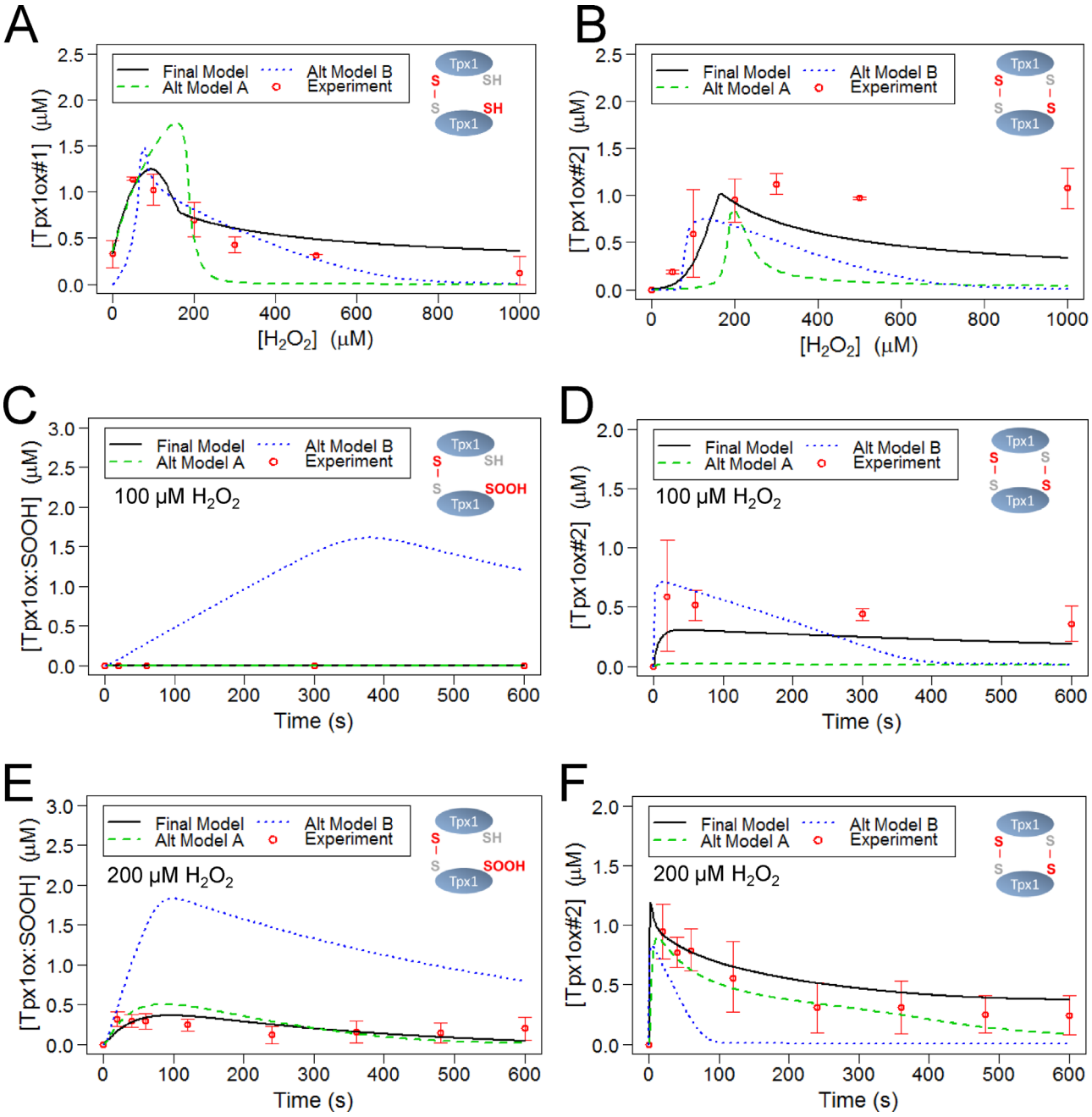

Fig. 5. Alternative models, Alt Model A and Alt Model B, were unable to simulate the experimentally determined changes in Tpx1 oxidation state following treatment of wild-type *S. pombe* with H_2O_2 as effectively as the final model. All 3 models were constructed using the same reaction network (Fig. 3A) and rate laws (Table S2) except that in alternative model A, Tpx1ox:SOH was also produced by the H_2O_2-induced oxidation of Tpx1ox#1 in a reaction governed by the rate law k_{cys_ox3} [Tpx1ox#1][H_2O_2]$_{int}$. Alternative model B was identical with the final model except that it lacked the peroxide-removing reaction, H_2O_2_metab. For parameters sets used in models see Tables S3 and S4. See also Table S5.

intracellular H_2O_2 concentration ([H_2O_2]$_{int}$) (Fig. 6A). Interestingly, the final model predicted that [H_2O_2]$_{ex} < 100$ μM would cause little net change in [H_2O_2]$_{int}$ but that at [H_2O_2]$_{ex} > 150$ μM the [H_2O_2]$_{int}$ increases linearly with increasing [H_2O_2]$_{ex}$ (Fig. 6A). This two phase relationship between intracellular and extracellular [H_2O_2] was dependent on the reaction H_2O_2_metab (Figs. 3A and 6A). This reaction, absent from alternative Model B, represents the cell's other peroxidase activities and is required for the model to accurately simulate the dynamics of Tpx1SOOH formation (Figs. 5C, E and 6B). Thus our model predicts that this peroxidase activity is saturated following treatment of wild-type cells with 150 μM H_2O_2. To test this prediction we used the H_2O_2 sensitive fluorescent dye, PF3, to measure the rate at which [H_2O_2]$_{int}$ increases in cells following exposure to different [H_2O_2]$_{ex}$ [25]. Although we detected a steady increase in the accumulation of intracellular H_2O_2 in cells exposed to low concentrations of H_2O_2, as predicted by our model, the rate of intracellular H_2O_2 accumulation was much faster in cells exposed to extracellular H_2O_2 concentrations greater than 150 μM (Fig. 6C). Notably, as predicted by the model, and experimentally confirmed, significant formation of hyperoxidized Tpx1 (Tpx1ox:SOOH) only begins to occur following exposure of cells to similar [H_2O_2]$_{ex}$ to those saturating H_2O_2_metab (Fig. 6B). Having established that our model was able to make accurate predictions in *S. pombe* we examined whether these findings held true in human cells.

To test whether there was also a biphasic effect of increasing

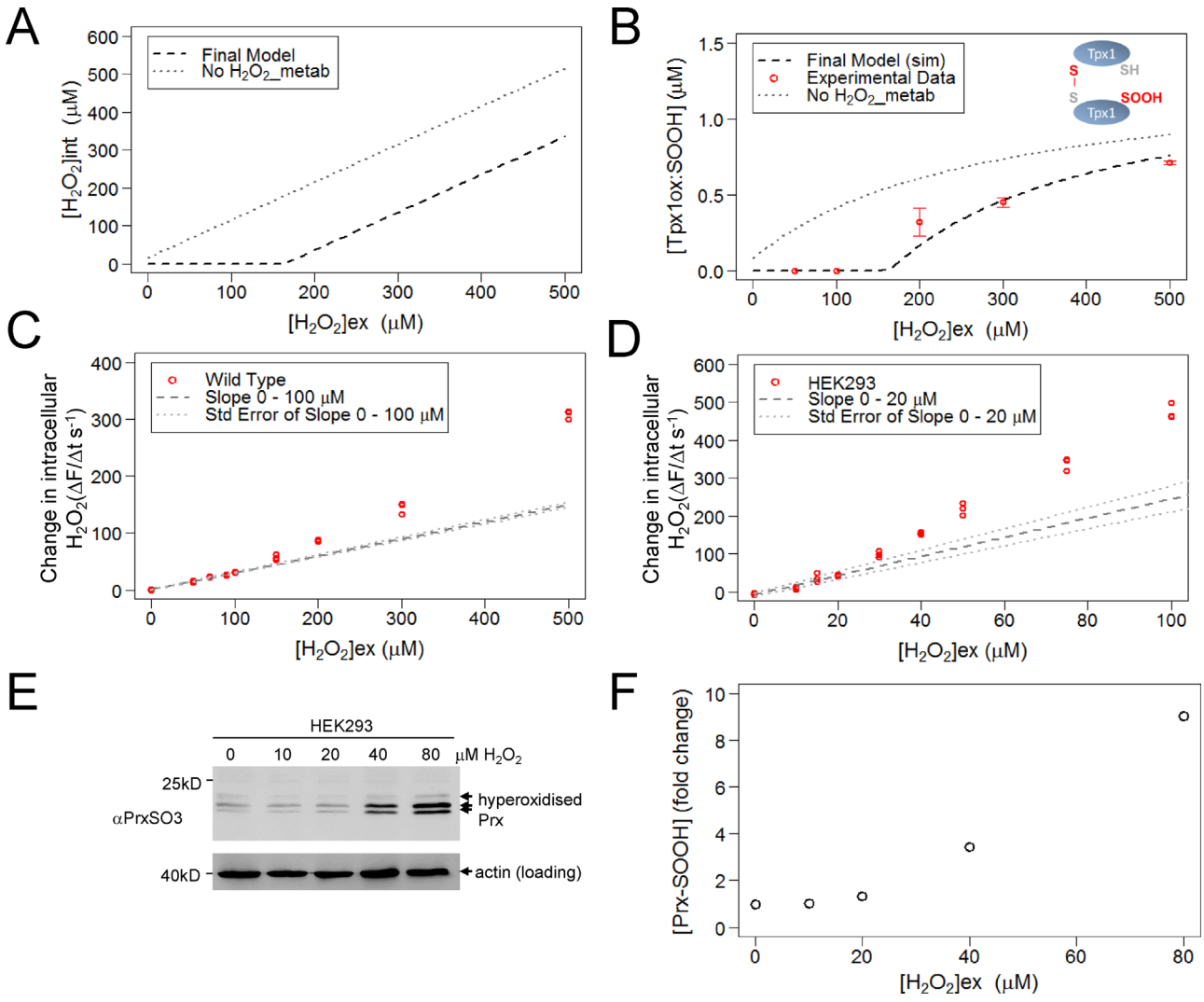

Fig. 6. As predicted by the model, hyperoxidation of Prx only occurs when the H_2O_2-removing capacity of cells is saturated. (A) and (B) The effect of increasing extracellular H_2O_2 on (A) intracellular H_2O_2 concentration (B) hyperoxidation of Tpx1 was simulated using the final model with the rate constant $V_{max\_H2O2\_metab}$ set as 59 μM s^{-1} (final model) or 0 μM s^{-1} (No H_2O_2_metab). In (B) the experimentally determined effects of increasing extracellular H_2O_2 concentrations on the hyperoxidation of Tpx1 are also shown. (C) and (D) Experimental measurements using a fluorescent H_2O_2-specific dye (PF3) (25) of the rate at which intracellular H_2O_2 increases ($\Delta F/\Delta t$) in (C) wild-type *S. pombe* (972) (D) human cells (HEK293) following exposure to increasing concentrations of H_2O_2. The results of three independent experiments are shown. The gradient (m ± SE) and intercept (c ± SE) were calculated using data points (C) 0–100 μM (*S. pombe*) (D) 0–20 μM (HEK293) and extrapolated to create the "Slope" and "Std. Error of Slope" lines that are shown. (E) and (F) The increase in hyperoxidized Prx in HEK293 cells treated with increasing concentrations of H_2O_2 was determined experimentally by (E) western blotting with anti-PrxSO3 antibodies of proteins extracted from HEK293 cells following 10 min exposure to the indicated concentration of H_2O_2. This revealed an increase in beta-mercaptoethanol-resistant hyperoxidized Prx (indicated by the arrows) which were (F) quantified as total hyperoxidized Prx relative to a loading control (actin).

$[H_2O_2]_{ex}$ on the rate at which intracellular H_2O_2 levels increase in human cells, we examined how exposure to different extracellular concentrations of H_2O_2 affected the intracellular H_2O_2 concentration in human embryonic kidney (HEK293) cells. A lower level of extracellular H_2O_2 was required to breach the H_2O_2-buffering capacity of HEK293 cells than *S. pombe*, possibly reflecting the increased H_2O_2-permeability of human cells (Fig. 6C and D). Nevertheless, we observed a similar 2 phase relationship between extracellular and intracellular H_2O_2 concentrations; human cells were able to maintain a low intracellular H_2O_2 concentration following exposure to lower concentrations of H_2O_2 but once this buffering capacity was exceeded (≥ 40 μM) the intracellular H_2O_2 concentration rose more rapidly (Fig. 6D). Furthermore, using anti-PrxSO3 antibodies that recognize the hyperoxidized forms of all 4 human 2-Cys Prx [18,26], we found that, similar to our findings in yeast (Fig. 6B), the *in vivo* hyperoxidation of human Prx only began to increase once the H_2O_2-buffering capacity of HEK293 cells was overwhelmed and intracellular H_2O_2 levels started to increase more rapidly (Fig. 6E and F). Together these data reveal that there is a biphasic increase in intracellular H_2O_2 in response to increases in extracellular H_2O_2 in yeast and human cells, with cells able to buffer exposure to low levels of extracellular H_2O_2 more effectively. Moreover, these data are consistent with the model's prediction that saturation of this buffering capacity triggers the hyperoxidation of Prx.

2.7. *Hyperoxidation of Prx detects the point at which other peroxide-removing processes (H_2O_2_metab) become saturated*

Accordingly, based on these modeling and experimental approaches, we propose that Prx hyperoxidation only occurs *in vivo* once the cell's peroxide-removing capacity becomes saturated and intracellular H_2O_2 levels start to increase more rapidly. This hypothesis, is consistent with *in vitro* work demonstrating that catalase is able to specifically inhibit the hyperoxidation of human Prx1 [16]. However, it was possible that the increased

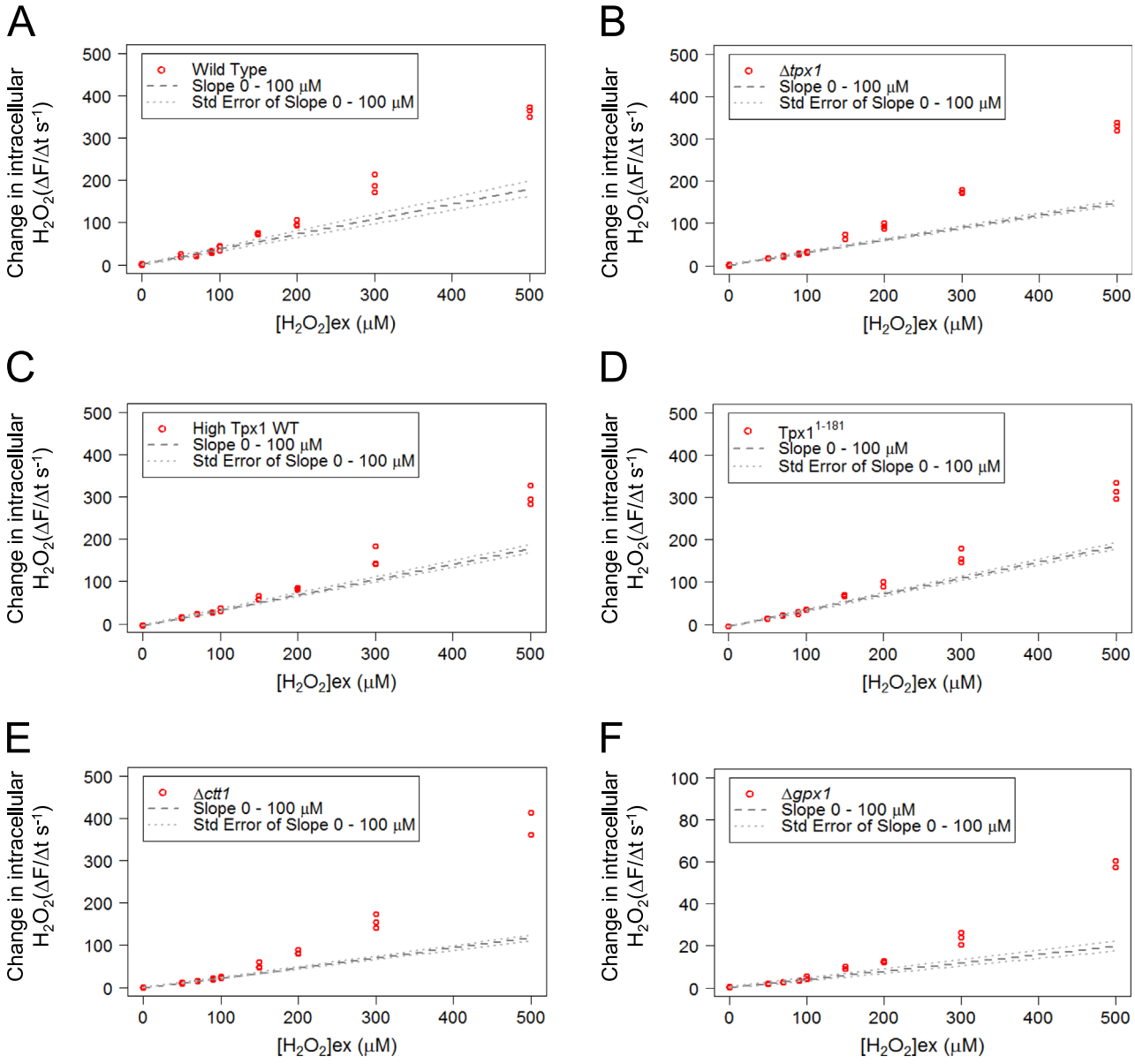

Fig. 7. Tpx1, Gpx1 and catalase activity, do not influence the biphasic increase in intracellular H_2O_2 in response to increasing extracellular H_2O_2. The rate of intracellular H_2O_2 accumulation, measured using a fluorescent H_2O_2-specific dye (PF3) [25], following exposure of (A) wild type (NT4) (B) Δ*tpx1* (VX00) mutant (C) cells expressing higher levels of wild-type Tpx1; High Tpx1 WT (JR68) or (D) truncated, hyperoxidation-resistant Tpx1; $Tpx1^{1-181}$ (JR20) (E) Δ*ctt1* (LT3) (F) Δ*gpx1* (SB13) to a range of H_2O_2 concentrations. The results of three independent experiments are shown. The gradient (m ± SE) and intercept (c ± SE) for the data points 0–100 μM were calculated and extrapolated to create the lines "Slope 0–100 μM" and "Std. Error of Slope 0–100 μM" (see "Methods").

accumulation of H_2O_2 observed in cells exposed to higher $[H_2O_2]_{ex}$ e.g. > 150 μM H_2O_2 in *S. pombe* (Fig. 6C) was due to the coincident hyperoxidation of Prx to peroxidase-inactive forms, rather than the saturation of other cellular peroxidases, To test this possibility we began by examining the effect of increasing $[H_2O_2]_{ex}$ on intracellular H_2O_2 in Δ*tpx1* mutant *S. pombe*. Notably, loss of Tpx1 had little effect on the H_2O_2-buffering capacity of cells (Fig. 7A and B). Furthermore, the peroxide-buffering capacity of cells expressing increased levels of either wild-type Tpx1 or a Tpx1 isoform that is 10× more resistant to hyperoxidation [12,27], was also saturated following exposure to 150 μM H_2O_2 (Fig. 7C and D). Together these data strongly suggest that the increase in the rate of H_2O_2 accumulation in cells exposed to $[H_2O_2]_{ex} > 150$ μM is due to the saturation of other cellular peroxide-buffering processes, rather than the inactivation of the thioredoxin peroxidase activity of Tpx1. Instead, this suggests that the hyperoxidation of Tpx1 *in vivo* actually detects the point at which the H_2O_2 buffering capacity of the cell is overcome and intracellular levels of H_2O_2 begin to rise more rapidly.

2.8. Thioredoxin is required to buffer low levels of extracellular H_2O_2

Having established that Tpx1 activity did not make an important contribution to the cell's ability to maintain low intracellular H_2O_2 levels following exposure to exogenous H_2O_2, we next investigated which other enzyme/s might be responsible for this H_2O_2-buffering capacity. Catalase has previously been demonstrated to protect Prx against hyperoxidation *in vitro* [16]. However, although Ctt1 appears to limit the increase in intracellular H_2O_2 at higher concentrations of H_2O_2 (Fig. 7E), the similar 2 phase relationship between extracellular and intracellular H_2O_2 concentrations in Δ*ctt1* mutant cells suggests that catalase does not make an important contribution to the cell's ability to buffer low levels of $H_2O_2 < 150$ μM (Fig. 7E). It was

possible that the Gpx/GSH system [28], or other subfamilies of Prx, contributed to the H_2O_2-buffering capacity of *S. pombe*, this seemed unlikely given the minimal effect that deletion of the genes encoding these enzymes (*gpx1*, *pmp20* or *dot5*) has on H_2O_2 resistance [10]. Indeed, loss of Gpx1 had no effect upon the bi-phasic relationship between extracellular and intracellular H_2O_2 (Fig. 7F).

Our previous studies have established that treatment with 0.2 mM H_2O_2 causes the majority of Trx1 and Txl1 to become rapidly oxidized [11,12]. As broad specificity oxidoreductases, thioredoxin family proteins are important cofactors for many enzymes and for the reduction of other oxidized proteins that may also impact on intracellular H_2O_2 levels [12,29,30]. Although, Tpx1 and Gpx1 were not important for buffering low levels of H_2O_2 (Fig. 7), it was still possible that the point at which the H_2O_2-buffering capacity is breached might reflect the point at which thioredoxin reductase activity becomes limiting for the removal of H_2O_2 by other thioredoxin-dependent activities. Hence, to test whether thioredoxin-dependent processes are important for inhibiting increases in intracellular H_2O_2 in cells exposed to $\leq$ 150 μM H_2O_2, we examined how extracellular H_2O_2 treatment affected intracellular H_2O_2 concentration in mutant *S. pombe* lacking, or ectopically expressing additional thioredoxin and/or Trr1. Strikingly, the bi-phasic relationship between extracellular [H_2O_2] and the rate of increase in intracellular [H_2O_2] was lost in Δ*trx1*Δ*txl1* cells in which both thioredoxin family proteins are absent (Fig. 8A). This linear relationship between intracellular and extracellular H_2O_2 concentrations up to 500 μM H_2O_2 in Δ*trx1*Δ*txl1* mutant cells indicated that the peroxide-removing activity that is normally saturated by low levels of H_2O_2 (H_2O_2_metab) requires thioredoxin (Fig. 8A).

Accordingly, we tested whether the point at which the H_2O_2-buffering capacity is breached might reflect the point at which thioredoxin reductase activity becomes limiting for the removal of H_2O_2 by thioredoxin-dependent processes. Importantly, overexpressing Trr1 prevented the rapid and sustained oxidation of Trx1 in cells treated with 0.2 mM H_2O_2, indicating that thioredoxin reductase activity, rather than NADPH levels, normally limits Trx1 reduction under these conditions (Fig. 8B). However, overexpressing Trx1 and/or Trr1 had a negligible effect on the relationship between extracellular [H_2O_2] and the rate of increase in intracellular [H_2O_2] (Fig. 8C–E). This suggests that the saturation of the cell's H_2O_2-buffering capacity is not due to the saturation of thioredoxin reductase activity.

Computational modeling and experimental studies have suggested that, although most protein thiols are relatively insensitive

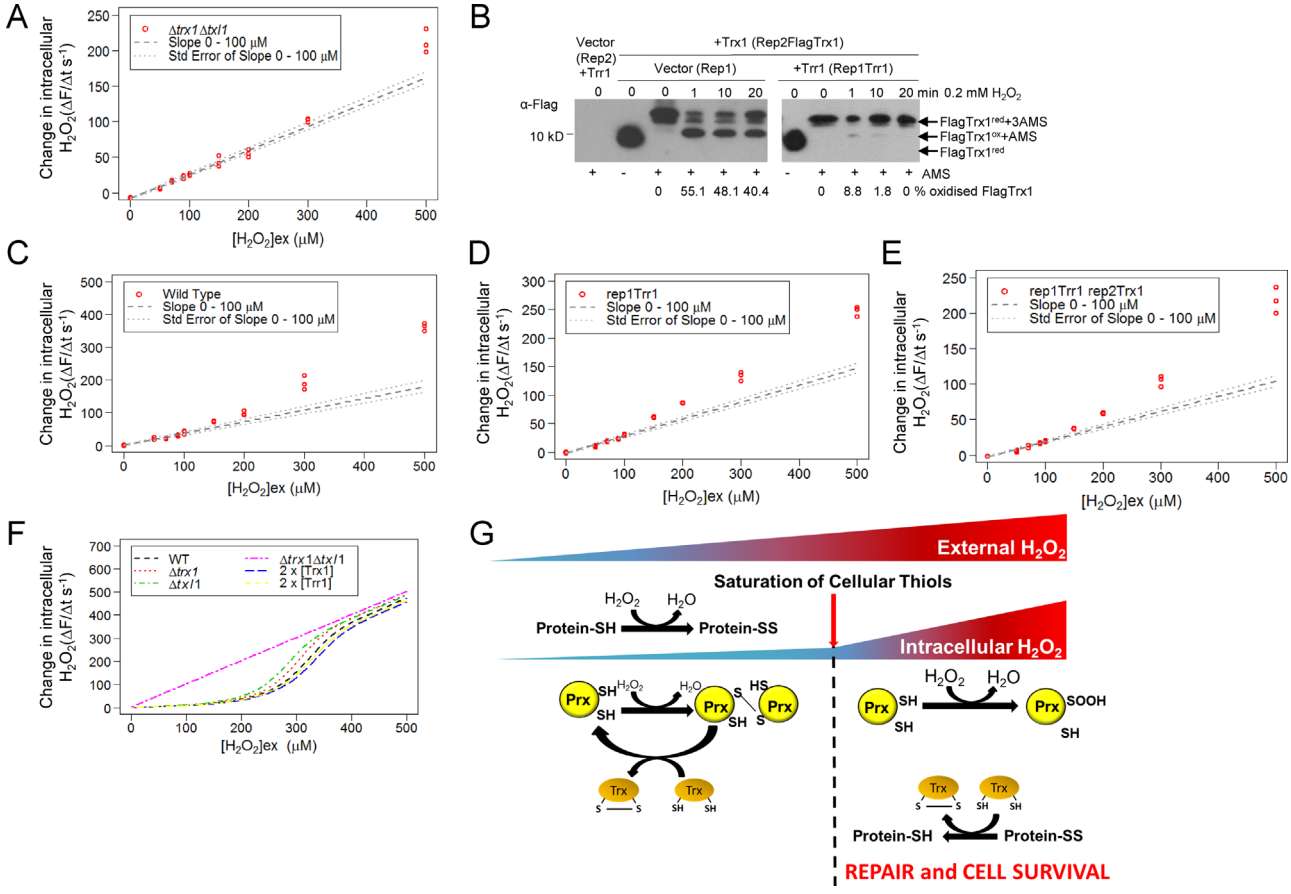

Fig. 8. Thioredoxin is required for the biphasic increase in intracellular H_2O_2 in response to increasing extracellular H_2O_2, consistent with the oxidation of protein-thiols limiting rises in intracellular H_2O_2 following exposure of *S. pombe* to low levels of extracellular H_2O_2 (A), (C)–(E) the rate of intracellular H_2O_2 accumulation, using a fluorescent H_2O_2-specific dye (PF3) [25], following exposure of (A) Δ*trx1*Δ*txl1* (AD140) (C)–(E) wild type (NT4) cells containing (C) vector control (Rep1) (D) and (E) ectopically expressing additional Trr1 (Rep1Trr1) [11] and (E) Flag-tagged Trx1 (Rep2Trx1), to a range of H_2O_2 concentrations. (B) Western blot analysis of FlagTrx1 redox state in cells containing vector control or overexpressing Trr1 (Rep1Trr1) before and following exposure for the indicated times to 0.2 mM H_2O_2. Image J quantification was used to determine the % FlagTrx1 oxidation. (F) The oxidation of protein thiols (Pr-SH) to protein disulfides (Pr-SS) with a low affinity for thioredoxin (Trx1/Txl1) is able to explain the H_2O_2-buffering capacity that is saturated following exposure to 150 μM H_2O_2. In this model (Tables S6 and S7) increasing oxidoreductase activity, by doubling the concentrations of Trx1 or Trr1, produces a negligible effect on the H_2O_2-buffering capacity, whereas loss of both Trx1 and Txl1 ablates the H_2O_2-buffering capacity. (G) We propose that reduced protein thiols (Protein-SH), act like a sponge, contributing to a buffer that prevents increases in intracellular accumulation of H_2O_2 but that, following maximal oxidation of these cellular protein-thiols to disulfides (Protein-SS), intracellular H_2O_2 concentrations increase, causing peroxidatic cysteines in Prx to become hyperoxidized to sulfinic derivatives (SOOH) and diverting thioredoxin towards the reduction of other protein disulfides. See also Tables S6, S7 and Fig. S5.

to oxidation, the reversible oxidation of H_2O_2-sensitive protein cysteine-thiols (PSH) (the thiol proteome) might still make an important contribution to the peroxide-buffering capacity of human cells [31,32]. Indeed, it has been estimated that the concentration of oxidant accessible protein thiols is around 13 mM, similar to the total concentration of glutathione [32]. Although most cellular thiols have a much lower reactivity with H_2O_2 than Prxs [33], the shear abundance of these H_2O_2-reactive thiols could mean that collectively they make a large contribution to the H_2O_2-buffering capacity of the cell. Moreover, previous work has shown that, like Trx1 and Txl1, the thiol proteome is also maximally oxidized following exposure of *S. pombe* to 200 μM H_2O_2 [29]. Hence, by causing constitutive, maximal oxidation of the thiol proteome [29], the absence of both cytosolic thioredoxin family proteins, Trx1 and Txl1, could potentially ablate the H_2O_2-buffering ability of this thiol pool. To test whether, despite their lower reactivity, the intracellular concentration of H_2O_2-oxidizable protein-thiols could be sufficient to make a significant contribution to the cell's capacity to buffer H_2O_2, we constructed a simple computer model, assuming 13 mM protein thiols with an average reactivity with H_2O_2 of 0.0005 $\mu M^{-1}\,s^{-1}$. This model was able to simulate the *in vivo* bi-phasic response in intracellular H_2O_2, illustrating the concept that the oxidation of 13 mM reduced protein-thiols (Tables S6 and S7), could prevent rises in intracellular H_2O_2 following treatment with up to 0.2 mM H_2O_2 (Fig. 8F). This model also predicted that, provided the thioredoxin-reactivity of the resulting protein disulfides is low, the initial concentration of reactive thiols, will have a greater influence on the buffering capacity than the availability of thioredoxin (Trx1) (Figs. 8F and S5). Accordingly, this model simulates the negligible effect of overexpressing Trx1 and/or Trr1 on the relationship between extracellular [H_2O_2] and the rate of increase in intracellular [H_2O_2] (Fig. 8C–F). This is consistent with the idea that the initial oxidation of protein thiols, rather than other thioredoxin-dependent enzymatic processes, could be responsible for the observed buffering of low levels of external H_2O_2 (Figs. 7 and 8C–E). Importantly, our model also recapitulated the effect of loss of Trx1 and Txl1 on intracellular H_2O_2 (Fig. 8A and F). Given that systems of redox-couples have previously been demonstrated to display 'apparent' Michaelis–Menten kinetics [34,35], this suggests that the V_{max} of the H_2O_2_metab, predicted in our model (Fig. 3 and Table S3), could represent the apparent V_{max} for removal of H_2O_2 by oxidation of the thiol proteome. Clearly the representation of the diverse protein-thiol pool in our model is a gross oversimplification and we note that the average reactivity we use requires a larger pool of protein thiols to react rapidly with H_2O_2 than might be expected from *in vitro* studies. Hence, although our experimental data indicate that thioredoxin is vital (Fig. 8A), it is possible that H_2O_2-reactants, such as glutathione or methionine, not investigated here, also make important contributions to the cell's capacity to buffer the intracellular environment against rises in extracellular H_2O_2. Nevertheless, our model and data are consistent with other studies that have suggested that the oxidation of the thiol proteome makes a major contribution to the *in vivo* removal of H_2O_2 (Fig. 8) [31,32]. Importantly, here we show that the H_2O_2-induced hyperoxidation of Prx only occurs once this peroxide-buffering capacity is saturated (Figs. 6 and 8G). Based on these findings, we propose that hyperoxidation is a response to increased intracellular H_2O_2, allowing downstream signaling, as well as protective chaperone functions of hyperoxidized peroxiredoxin [8,14]. These findings are also consistent with our previous studies which indicated that peroxiredoxin hyperoxidation is important for thioredoxin-mediated repair and cell survival (Fig. 8G) [12].

3. Discussion

The role of peroxiredoxins in cell responses to H_2O_2 has come under considerable scrutiny in recent years since the discovery that the thioredoxin peroxidase activity of Prx is sensitive to inactivation by H_2O_2. Several functions have been proposed for the H_2O_2-induced inactivation of this peroxidase activity. However, to assess if/when any or all of these functions are important, it is important to understand under which circumstances Prx become hyperoxidized (inactivated) *in vivo*. Here we have developed a mathematical model describing the kinetics of oxidation of the single *S. pombe* 2-Cys Prx in response to H_2O_2 as a tool to investigate the precise circumstances that cause Prx to become hyperoxidized *in vivo*. This model has made several unexpected predictions.

Firstly, our model suggested that there is a biphasic relationship between extracellular and intracellular H_2O_2 such that exposure to low levels of H_2O_2 produces only small increases in the intracellular H_2O_2 concentration, whereas above a certain threshold the cell's peroxide-removing capacity becomes overwhelmed and intracellular H_2O_2 concentrations increase at a much faster rate. Importantly, this prediction was experimentally confirmed in both yeast and human cells.

Secondly, our model reveals that this peroxide-removing activity protects Tpx1 from hyperoxidation. This explains why hyperoxidized Tpx1 is only detected following exposure to extracellular concentrations of H_2O_2 above 100 μM. Notably, this is consistent with work in mammalian cells, which can effectively buffer extracellular H_2O_2 concentrations of 10 μM that cause some hyperoxidation of Prx2 *in vitro* [16,36] but which require higher extracellular H_2O_2 concentrations to increase intracellular H_2O_2 levels and also cause *in vivo* hyperoxidation of Prx [6,36,37]. Indeed, not only do we confirm that the biphasic relationship between extracellular and intracellular H_2O_2 also holds true in HEK293 cells, but also that hyperoxidation of human Prx only occurs once the ability of these cells to buffer H_2O_2 becomes saturated (Fig. 6D–F).

Thirdly, our modeling suggests that the main route for formation of the hyperoxidized Prx involves reaction of 2 neighboring catalytic centers (Cys_P) with H_2O_2 prior to formation of Prx disulfides. Interestingly, this suggests that the reduced Cys_P in Tpx1ox#1 may be less sensitive to H_2O_2 than that in reduced Tpx1. This still needs to be experimentally validated, but could be explained by the propensity of disulfide formation to destabilize Prx decamers resulting in Prx dimers which are approximately 100 fold less reactive with H_2O_2 [38,39]. Intriguingly, this would provide an explanation as to why Prx hyperoxidation only occurs once the peroxide-buffering capacity of the cell is saturated, as the more rapid increase in intracellular H_2O_2 concentration would greatly increase the probability of neighboring Cys_P reacting with H_2O_2 prior to disulfide formation.

Fourthly, our modeling and experimental investigations together indicate that the peroxide-removing processes that are saturated in *S. pombe* are likely to include the reversible oxidation of the thiol proteome. Notably, although the H_2O_2-buffering capacity predicted by our model is eliminated in the absence of disulfide reductase activity, loss of Trx1 alone had little effect upon the ability of cells to buffer intracellular H_2O_2 (data not shown). Moreover, ectopically overexpressing Trr1 and Trx1 did not increase the intracellular H_2O_2-buffering capacity (Fig. 8C–E). This suggests that the maximum rate of H_2O_2-removal is independent of the availability of these disulfide reductases. Instead, this suggests that the limiting factor for H_2O_2-buffering is the initial availability of reduced protein thiols, with the low affinity of these protein disulfides for Trx1/Txl1 limiting the rate at which they are regenerated. It has been estimated that the concentration of

oxidant accessible protein thiols is around 13 mM, similar to the total concentration of glutathione [32]. Although it is possible that other activities, such as glutathione and methionine oxidation, also contribute, this is consistent with the saturation of this abundant pool of free protein-thiols making the most important contribution to the saturable H_2O_2 buffering capacity revealed by our computer model.

In response to 200 μM H_2O_2 both thioredoxin family proteins (Trx1 and Txl1) are completely oxidized in the reduction of Tpx1–Tpx1 disulfides [11,12]. This Tpx1-dependent inhibition of Txl1, allows the sustained activation of the Pap1 transcription factor which promotes the expression of a host of oxidative stress defense enzymes [11]. However, thioredoxin (Trx1) is also vital for the reduction of oxidized protein cysteine-thiols and the activity of methionine sulfoxide reductase enzymes. Indeed, the thiol proteome is maximally oxidized in cells where Trx1 and Txl1 are inhibited genetically, or as a result of Tpx1-dependent oxidation [29]. Hence, it is logical that, once reactive protein thiols have fully reacted with H_2O_2, it is important to target thioredoxin activity away from Prx disulfides, for which they have much greater affinity, towards reducing these oxidized cysteine and methionine residues. Hyperoxidized Prx cannot be reduced by thioredoxin. Accordingly, it has been proposed that, by converting Prx to a form that is no longer a thioredoxin substrate, Prx hyperoxidation enables thioredoxin to be targeted to other oxidized proteins instead [12]. Interestingly, our model predicts that Tpx1 disulfides are less efficiently reduced by thioredoxin if the non-bonded Cys_P is sulfinylated (Tpx1ox:SOOH). It is possible that, under conditions where thioredoxin reductase is limiting, this may also help redirect thioredoxin activity towards other substrates, for which it has a much lower affinity. Indeed, consistent with these findings, the hyperoxidation of Tpx1 is important to maintain thioredoxin activity, allowing the repair of oxidized proteins, and cell survival following exposure of cells to higher concentrations of H_2O_2 [12].

The high H_2O_2-scavenging activity of Prx, such as Tpx1, when recycling systems are provided in excess *in vitro*, supports previous reports suggesting that the thioredoxin peroxidase activity of Tpx1 is important for removing the low levels of endogenous H_2O_2 generated during normal aerobic growth and metabolism [16,40]. However, here we show that this thioredoxin peroxidase activity makes a negligible contribution to *S. pombe*'s capacity to buffer the internal environment against extracellular increases in H_2O_2 (Fig. 7A–D). Perhaps this is not surprising given that under these *in vivo* conditions thioredoxin reductase activity is limiting, preventing the efficient recycling of Tpx1 disulfides (Fig. 8B) [12]. Indeed, our previous work, has suggested that, rather than its H_2O_2-detoxifying capacity, the important role of the thioredoxin peroxidase activity of Tpx1 in cells exposed to these levels of exogenous H_2O_2 is to promote the oxidation of Txl1 and hence H_2O_2-induced gene expression and oxidative stress resistance [11]. Consistent with this, a model of Prx2 oxidation in human erythrocytes has also suggested that the abundance and peroxidase activity of the Prxs favors a signaling rather than a peroxide-detoxification role [41].

The hyperoxidation of 2-Cys Prx has been identified as a conserved feature of circadian rhythms in eukaryotes [42–44] (for a review see [7]). Our model suggests that hyperoxidation only occurs when the cell's capacity for H_2O_2-removal is breached, allowing the concerted reaction of 2 H_2O_2 molecules with adjacent peroxidatic cysteines. This raises the possibility that the hyperoxidized Prx detected in each of these organisms reflects a transient, daily increase in the intracellular H_2O_2 concentration above the cell's peroxide-buffering capacity. Consistent with the possibility that a cyclic increase in ROS might be important for circadian rhythms, Nrf2, the transcription factor controlling the levels of peroxidase-removing enzymes in mammals, was recently shown to be regulated in a circadian pattern [45]. If an increase in intracellular H_2O_2 is important for circadian control of cellular activities, then it is possible that loss of this regulation may contribute to the deleterious effects that can be associated with increased dietary antioxidants and constitutively activated stress defenses.

The inactivation of 2-Cys Prx by hyperoxidation has been proposed to allow H_2O_2 to act as a signal [5]. However, where the amount of hyperoxidized has been compared with the total Prx, only a small proportion of the total pool of 2-Cys Prx appears to be hyperoxidized under normal growth conditions/during circadian rhythms [6,8,46]. Moreover, hyperoxidation of Prx is undetectable in response to the low H_2O_2 levels produced in response to growth factor activated NADPH oxidases [6,37]. As 2-Cys Prx are highly abundant, and only 1 of a repertoire of peroxidase enzymes, it has seemed unlikely that inactivation of a small proportion would significantly impact on intracellular H_2O_2 levels. Indeed, as predicted by our model, our experimental data suggests that the complete inactivation of Tpx1, either by deletion or hyperoxidation, has minimal effect on *S. pombe*'s ability to prevent the intracellular accumulation of H_2O_2 (Fig. 7). Instead, our model is consistent with other work suggesting that hyperoxidation of Prx may have other functions in signaling or protein homeostasis [12,14,16,47,48].

In summary, our study provides new insight into the underlying causes and function of Prx hyperoxidation. Moreover, the discovery that extracellular increases in H_2O_2 produce non-linear increases in intracellular levels, which are dependent upon the levels of thioredoxin activity, has important implications for the host of studies which have used a bolus of H_2O_2 either as a stress or signaling stimulus. Indeed, the model we have developed provides an important new tool to predict responses to altered redox conditions. For example, our model reveals how differences between the thioredoxin or Prx activity in individual cells could precisely tailor the sensitivity/response of specific cells within a population to H_2O_2 signals and oxidative stress. Therefore, this has important implications for how dynamic redox changes initiate changes in cell function and behavior during normal physiology and in disease.

4. Materials and methods

4.1. Cell culture conditions

The *S. pombe* strains (Table S8) and human kidney (HEK293) cells used in this study were maintained using standard media and growth conditions. For experiments, *S. pombe* were grown with agitation at 30 °C in 50 ml Edinburgh minimal media (EMM) supplemented with 0.48 mM histidine, 0.56 mM adenine, 0.67 mM uracil, 1.91 mM leucine. In experiments involving Δ*trx1*Δ*txl1* cells, which are auxotrophic for cysteine, media was also supplemented with 0.52 mM cysteine. HEK293 cells were grown in a humidified CO_2 incubator at 37 °C in 24 ml Dulbecco's Modified Eagles Medium (DMEM) supplemented with 10% (v/v) fetal calf serum (FCS), 100 units/ml penicillin, 100 μg/ml streptomycin, 2 mM L-glutamine and 1% non-essential amino acids (NES).

4.2. Quantitative measurement of Prx or FlagTrx1 oxidation

S. pombe: 50 ml cultures of exponentially growing *S. pombe* (OD 0.4–0.5) were harvested before and after exposure to a range of H_2O_2 concentrations. At specific time points following addition of H_2O_2, 3 ml of culture ($2.4–4.0 \times 10^7$ cells) was harvested by adding an equal volume of 20% Trichloroacetic acid (TCA). Protein extracts were prepared essentially as described previously [49] but without phosphatase treatment. Proteins were re-suspended and

incubated in 100 mM Tris–HCl pH 8.0, 1% SDS, 1 mM EDTA, 1 mg/ml PMSF containing 25 mM AMS or 25 mM NEM for 30 min at 25 °C then 5 min at 37 °C. *Human embryonic kidney cells*: A 10 cm plate of confluent HEK293 cells was washed three times with Dulbecco's phosphate-buffered saline (DPBS) (Sigma), then incubated for 10 min at 37 °C in DPBS supplemented, as indicated, with H_2O_2 (Sigma). Cells were washed three times in DPBS and then re-suspended in 500 µl of lysis buffer (50 mM Tris–HCl pH 7.5, 150 mM NaCl, 0.5% NP40 (IGEPAL), 10 mM imidazole, 2 µg/ml pepstatin, 2 µg/ml leupeptin, 100 µg/ml PMSF and 1%(v/v) aprotinin). Western blotting: Insoluble material was pelleted by centrifugation (13,000 rpm, 3 min). The concentration of the solubilised proteins (supernatant) was determined using a Pierce® BCA protein assay kit (Thermo Scientific). Protein samples were mixed with an equal volume of 2 × SDS loading dye (625 mM Tris–HCl, pH 6.7, 50%(v/v) glycerol, 10% sodium dodecyl sulfate (SDS), 0.5% Bromophenol Blue) and sample volumes equivalent to 2 µg of protein were analyzed by 15% SDS-PAGE and western blotting. Tpx1 was detected using anti-Tpx1 polyclonal antibodies [12] and hyperoxidized Prx were detected with monoclonal anti-peroxiredoxin-SO3 antibodies (LabFrontiers) [26]. FlagTrx1 was detected with mononclonal anti-Flag (M2-Sigma) antibodies. For *S. pombe* anti-tubulin antibodies and for HEK293 cells anti-actin (Sigma) antibodies were used to confirm that gels were evenly loaded. Primary antibodies were diluted 1 in 1000 in TBST (1 mM Tris–HCl pH 8.0, 15 mM NaCl, 0.01%(v/v) Tween 20). As appropriate, HRP-conjugated anti-rabbit or anti-mouse IgG secondary antibodies (Sigma) were used, followed by the fluorescent substrate ECL Plus to visualize antibody-labeled proteins (Thermo Scientific). Digital images of western blots were acquired with a Typhoon™ 9400 (GE Healthcare) and densitometry analysis performed using ImageQuantTL (Version 7).

4.3. Hydrogen peroxide colorimetric quantitation in media

PeroXOquant Quantitative Peroxide Assay kit with aqueous compatible formulation (Thermo scientific) was used according to manufacturer's protocol. Briefly, *S. pombe* cells were grown in EMM media to OD_{600} 0.5. H_2O_2 was added to the growing cultures at a final concentration of 50 µM. 20 µl of media taken at various time points as indicated, were mixed in a 96-well microplate with 200 µl of working solution (freshly prepared according to manufacturer's instructions). The mix was incubated at room temperature for 20 min. Absorbance at 560 nm was measured using a TECAN infinite M200 plate reader. The blank value (EMM without H_2O_2) was automatically subtracted from all sample measurements.

4.4. Measuring changes in intracellular H_2O_2 concentration

The H_2O_2 sensor, acetylated Peroxyfluorescein 3 (PF3) [25], was added to 10 ml (2×10^7) exponentially growing *S. pombe* cells (OD_{595} 0.4–0.5) to a final concentration of 5 µM. Cells were incubated in the dark for 20 min, washed once then re-suspended in an equal volume of PBS (137 mM NaCl, 2.7 mM KCl, 10 mM Na_2HPO_4, and 1.8 mM KH_2PO_4 pH 7.4). HEK293 cells were incubated for 20 min in DPBS containing 5 µM PF3, washed three times then re-suspended in DPBS to a final concentration of 2×10^6 cells/ml. Following re-suspension, 200 µl aliquots (4×10^6 *S. pombe* cells, 4×10^5 HEK293 cells) of PF3-labeled cells, unlabeled cells or PBS controls were transferred to a 96-well plate. Fluorescence measurements were made at 529 nm following excitation at 495 nm using a TECAN Infinite M200PRO plate reader and the average fluorescence of the unlabeled cells was deducted to calculate fluorescence due to PF3 (F). Measurements were taken 0 and 60 s before addition of H_2O_2 to determine the basal rate of reaction of PF3 with endogenously produced H_2O_2

$$\left(\frac{\Delta F}{\Delta t}\right)_{no\_stress} = \frac{F_{t60} - F_{t0}}{60} \quad (1)$$

Fluorescence measurements were made 30, 60 and 120 s following addition of H_2O_2 (0–500 µM) and used to calculate the rate of change of fluorescence.

$$\left(\frac{\Delta F}{\Delta t}\right)_{stress} = \frac{F_{t120} - F_{t30}}{90} \quad (2)$$

The rate of fluorescence change due to exogenous H_2O_2 ($\Delta F/\Delta t$) was then calculated using Eq. (3) and plotted against H_2O_2 concentration using the graphics and statistics package R.

$$\left(\frac{\Delta F}{\Delta t}\right) = \left(\frac{\Delta F}{\Delta t}\right)_{stress} - \left(\frac{\Delta F}{\Delta t}\right)_{no\_stress} \quad (3)$$

The R linear model function [50] was used to calculate the derivative and 95% confidence interval for the change ($\Delta F/\Delta t$) when H_2O_2 is increased from 0 to 100 µM H_2O_2 (*S. pombe*) or increased from 0 to 20 µM (HEK293 cells). This gradient was extrapolated using the equation $y = mx + c$ and plotted on the same axis as the ($\Delta F/\Delta t$) data.

4.5. Computational method: Selection of a suitable reaction network for the kinetic model of Tpx1 oxidation

To find a set of reactions able to describe the formation of the Tpx1 monomers and disulfide homodimers detected in our experiments, we built a series of alternative models which contained different sets of biochemically feasible reactions. Parameter estimation was performed for each preliminary model, including preliminary models A and B (Fig. 5 and Table S4) (see below for details), and the model with parameters similar to published values that gave the lowest Akaike information criterion (AIC) parameter set [51] was selected for the final model (Fig. 3 and Table S5).

4.6. Computational Methods: Rate laws and measured parameters

The model contained two compartments, an extracellular compartment with volume Vol_{ex} (l) representing the growth media around the cells and an intracellular compartment of volume Vol_{int} (l) representing the total volume of all of the cells. The volume of the intracellular compartment was estimated using

$$Vol_{int} = Cell_{vol} \times Cell_{Num} \quad (4)$$

where $Cell_{Num} = 4 \times 10^8$ (the number of cells in 50 ml of an OD_{595} 0.4 culture) and $Cell_{Vol}$ is the mean volume of an *S. pombe* cell, measured for exponentially growing wild-type (972) cells (CASY®, Schärfe System) as 126 µM^3. The rate of movement of H_2O_2 between these compartments was modeled to move down its concentration gradient using the rate equations Eq. (5) (H_2O_2_influx) and Eq. (6) (H_2O_2_efflux).

$$v_{in} = k_{H2O2\_perm} \times \left[H_2O_2\right]_{ex} \quad (5)$$

$$v_{eff} = k_{H2O2\_perm} \times \left[H_2O_2\right]_{int} \quad (6)$$

where v_{in} is the rate of influx and v_{eff} = rate of efflux, $[H_2O_2]_{ex}$ and $[H_2O_2]_{int}$ represent the extracellular and intracellular H_2O_2 concentration and k_{H2O2_perm} is a constant representing all other factors that influence the rate of H_2O_2 movement between each compartment. The non-Tpx1 metabolism of H_2O_2 was modeled using Michaelis–Menten kinetics and all other reactions in the model were governed by mass action kinetics.

The parameters for the model were either derived from published work, measured experimentally or estimated from our experimental data. The initial concentrations of Tpx1 and Trx1 in the model were based on the global quantification of the *S. pombe* proteome [52]. The copy number per cell for these two proteins was used to calculate the concentration of each protein in the intracellular compartment using:

$$M = \frac{cpc}{N_A \times Cell_{Vol}} \quad (7)$$

where M is the molar protein concentration, cpc=copy number per cell [52] and N_A =Avagadro constant 6.02×10^{23} mol^{-1}.

Rate constants for the oxidation of the peroxidatic cysteine (Cys_P-SH) and the hyperoxidation of the sulfenic acid intermediate (Cys_P-SOH) were taken from a recent study of human Prx1 and Prx3 [16]. Michaelis–Menten parameters for the reduction of Trx1 by Trr1 were based on those experimentally determined for the orthologous *S. cerevisiae* enzymes [53]. All other parameters were estimated from our experimental data using parameter estimation.

4.7. Computational Methods: Parameter estimation, time course simulation, identifiability analysis and data representation

Parameter estimation was performed in COPASI 4.13 [54]. The data set used for the parameter estimation was calculated from the relative intensities of the Tpx1 monomer and disulfide homodimer bands detected in 2–5 independent biological replicates of Tpx1 oxidation experiments depicted in Fig. 1A and Fig. 2A, B (Table S1), and PeroXOquant measurements for the removal of extracellular H_2O_2 (Fig. 3B and Table S1). Based on a broad range of experimental evidence (reviewed in [55]), a mock data set assuming a steady-state intracellular H_2O_2 concentration of 1 nM in exponentially growing cells was also included in the parameter estimation.

Parameter estimation was performed 500 times from random initial parameter values using the Levenberg–Marquardt algorithm [56] for each model (Table S2). The parameter set used for the final model had an AIC of 77.6 and was found on 327 out of 500 estimations, each of these 327 parameter estimations converged on similar values as indicated by the frequency distributions for each parameter (Fig. S3). One-dimensional likelihood profiles for each parameter and 95% confidence intervals were calculated using a simple identifiability analysis [57]. This analysis demonstrated that the estimated parameters were identifiable (Fig. S4) with acceptable 95% percent confidence regions calculated for each parameter (Table S3 and Fig. S4). Time course simulation was performed in COPASI 4.10 [54] using the deterministic (LSODA) algorithm. All graphics and further analysis of the simulation and identifiability data were performed using R.

Conflict of interest

The authors declare that they have no conflict of interest.

Author contributions

L.T. designed and performed experiments under the supervision of A.D. and E.V., L.T. developed and tested mathematical models under the supervision of D.S. and E.V. with input from G.S. and P.D.P., Z.U. contributed data to Figs. 7,8 and S5 under the supervision of E.V. and L.T. W.P. assisted L.T. with the generation of data in Fig. 6D–F with advice from B.D. and E.V. Experiment in Fig. 3B was carried out by C.R. under the supervision of J.B., B.D., T.B. and C.C. synthesized PF3 and advised on its use in experiments in Figs. 6–8. L.T. and E.V. wrote the manuscript with input from all authors.

Acknowledgments

We are very grateful to Jonathon Brown for technical advice, Andy Karplus and Che Pillay for helpful discussions and Brian Morgan, Janet Quinn and Simon Whitehall for discussions and comments on the manuscript. Thanks to Michelle Wray for technical assistance, Peter Banks for providing the catalase mutant strain and Mike Gray the HEK293 cells. L.T., Z.U., W.P., A.D. and E.V. were funded by the BBSRC (BB/F015895/1, BB/F016980/1 and BB/F023065/1). Funding was also provided by a Wellcome Trust Senior Investigator Award (J.B.) #095598/Z/11/Z and NIH grant GM 79465 (C.J.C.). C.J.C. is an Investigator with the Howard Hughes Medical Institute. B.C.D. and T.F.B. were partially supported by a Chemical Biology Training Grant from the National Institutes of Health (T32 GM066698).

Appendix A. Supplementary material

Supplementary data associated with this article can be found in the online version at http://dx.doi.org/10.1016/j.freeradbiomed.2016.02.035.

References

[1] K.M. Holmstrom, T. Finkel, Cellular mechanisms and physiological consequences of redox-dependent signalling, Nat. Rev. Mol. Cell Biol. 15 (6) (2014) 411–421.
[2] S.G. Rhee, H.A. Woo, Multiple functions of peroxiredoxins: peroxidases, sensors and regulators of the intracellular messenger HO, and protein chaperones, Antioxid. Redox Signal. 15 (3) (2011) 781–794.
[3] T. Nystrom, J. Yang, M. Molin, Peroxiredoxins, gerontogenes linking aging to genome instability and cancer, Genes Dev. 26 (18) (2012) 2001–2008.
[4] K.S. Yang, et al., Inactivation of human peroxiredoxin I during catalysis as the result of the oxidation of the catalytic site cysteine to cysteine-sulfinic acid, J. Biol. Chem. 277 (41) (2002) 38029–38036.
[5] Z.A. Wood, L.B. Poole, P.A. Karplus, Peroxiredoxin evolution and the regulation of hydrogen peroxide signaling, Science 300 (5619) (2003) 650–653.
[6] H.A. Woo, et al., Inactivation of peroxiredoxin I by phosphorylation allows localized H(2)O(2) accumulation for cell signaling, Cell 140 (4) (2010) 517–528.
[7] A. Stangherlin, A.B. Reddy, Regulation of circadian clocks by redox homeostasis, J. Biol. Chem. (2013) 26505–26511.
[8] I.S. Kil, et al., Feedback control of adrenal steroidogenesis via H_2O_2-dependent, reversible inactivation of peroxiredoxin III in mitochondria, Mol. Cell 46 (5) (2012) 584–594.
[9] S.M. Bozonet, et al., Oxidation of a eukaryotic 2-Cys peroxiredoxin is a molecular switch controlling the transcriptional response to increasing levels of hydrogen peroxide, J. Biol. Chem. 280 (24) (2005) 23319–23327.
[10] A.P. Vivancos, et al., A cysteine-sulfinic acid in peroxiredoxin regulates H_2O_2-sensing by the antioxidant Pap1 pathway, Proc. Natl. Acad. Sci. USA 102 (25) (2005) 8875–8880.
[11] J.D. Brown, et al., A peroxiredoxin promotes H_2O_2 signaling and oxidative stress resistance by oxidizing a thioredoxin family protein, Cell Rep. 5 (5) (2013) 1425–1435.
[12] A.M. Day, et al., Inactivation of a peroxiredoxin by hydrogen peroxide is critical for thioredoxin-mediated repair of oxidized proteins and cell survival, Mol. Cell 45 (3) (2012) 398–408.
[13] M. Olahova, et al., A redox-sensitive peroxiredoxin that is important for longevity has tissue- and stress-specific roles in stress resistance, Proc. Natl. Acad. Sci. USA 105 (50) (2008) 19839–19844.
[14] H.H. Jang, et al., Two enzymes in one; two yeast peroxiredoxins display oxidative stress-dependent switching from a peroxidase to a molecular chaperone function, Cell 117 (5) (2004) 625–635.
[15] A.G. Cox, et al., Mitochondrial peroxiredoxin 3 is more resilient to hyperoxidation than cytoplasmic peroxiredoxins, Biochem. J. 421 (1) (2009) 51–58.
[16] A.V. Peskin, et al., Hyperoxidation of peroxiredoxins 2 and 3: rate constants for the reactions of the sulfenic acid of the peroxidatic cysteine, J. Biol. Chem. 288 (20) (2013) 14170–14177.
[17] A.C. Haynes, J. Qian, J.A. Reisz, C.M. Furdui, W.T. Lowther, Molecular basis for the resistance of human mitochondrial 2-Cys peroxiredoxin 3 to hyperoxidation, J. Biol. Chem. 288 (41) (2013) 29714–29723.

[18] Z. Cao, S. Subramaniam, N.J. Bulleid, Lack of an efficient endoplasmic reticulum-localized recycling system protects peroxiredoxin IV from hyperoxidation, J. Biol. Chem. 289 (9) (2014) 5490–5498.
[19] M. Jara, et al., The peroxiredoxin Tpx1 is essential as a H_2O_2 scavenger during aerobic growth in fission yeast, Mol. Biol. Cell 18 (6) (2007) 2288–2295.
[20] D. Chen, et al., Global transcriptional responses of fission yeast to environmental stress, Mol. Biol. Cell 14 (1) (2003) 214–229.
[21] D. Chen, et al., Multiple pathways differentially regulate global oxidative stress responses in fission yeast, Mol. Biol. Cell 19 (1) (2008) 308–317.
[22] D.H. Lackner, M.W. Schmidt, S. Wu, D.A. Wolf, J. Bahler, Regulation of transcriptome, translation, and proteome in response to environmental stress in fission yeast, Genome Biol. 13 (4) (2012) R25.
[23] H.Z. Chae, H.J. Kim, S.W. Kang, S.G. Rhee, Characterization of three isoforms of mammalian peroxiredoxin that reduce peroxides in the presence of thioredoxin, Diabetes Res. Clin. Pract. 45 (2–3) (1999) 101–112.
[24] B. Manta, et al., The peroxidase and peroxynitrite reductase activity of human erythrocyte peroxiredoxin 2, Arch. Biochem. Biophys. 484 (2) (2009) 146–154.
[25] B.C. Dickinson, C. Huynh, C.J. Chang, A palette of fluorescent probes with varying emission colors for imaging hydrogen peroxide signaling in living cells, J. Am. Chem. Soc. 132 (16) (2010) 5906–5915.
[26] H.A. Woo, et al., Reversible oxidation of the active site cysteine of peroxiredoxins to cysteine sulfinic acid. Immunoblot detection with antibodies specific for the hyperoxidized cysteine-containing sequence, J. Biol. Chem. 278 (48) (2003) 47361–47364.
[27] K.H. Koo, et al., Regulation of thioredoxin peroxidase activity by C-terminal truncation, Arch. Biochem. Biophys. 397 (2) (2002) 312–318.
[28] N. Makino, T. Mise, J. Sagara, Kinetics of hydrogen peroxide elimination by astrocytes and C6 glioma cells analysis based on a mathematical model, Biochim. Biophys. Acta 1780 (6) (2008) 927–936.
[29] S. Garcia-Santamarina, et al., Is oxidized thioredoxin a major trigger for cysteine oxidation? Clues from a redox proteomics approach, Antioxid. Redox Signal. 18 (13) (2013) 1549–1556.
[30] S. Garcia-Santamarina, S. Boronat, J. Ayte, E. Hidalgo, Methionine sulphoxide reductases revisited: free methionine as a primary target of H(2)O(2)stress in auxotrophic fission yeast, Mol. Microbiol. 90 (2013) 1113–1124.
[31] N.J. Adimora, D.P. Jones, M.L. Kemp, A model of redox kinetics implicates the thiol proteome in cellular hydrogen peroxide responses, Antioxid. Redox Signal. 13 (6) (2010) 731–743.
[32] R.E. Hansen, D. Roth, J.R. Winther, Quantifying the global cellular thiol-disulfide status, Proc. Natl. Acad. Sci. USA 106 (2) (2009) 422–427.
[33] C.C. Winterbourn, Reconciling the chemistry and biology of reactive oxygen species, Nat. Chem. Biol. 4 (5) (2008) 278–286.
[34] C.S. Pillay, J.H. Hofmeyr, B.G. Olivier, J.L. Snoep, J.M. Rohwer, Enzymes or redox couples? The kinetics of thioredoxin and glutaredoxin reactions in a systems biology context, Biochem. J. 417 (2009) 269–275.
[35] C.S. Pillay, J.H. Hofmeyr, J.M. Rohwer, The logic of kinetic regulation in the thioredoxin system, BMC Syst. Biol. 5 (2011) 15.
[36] E.W. Miller, B.C. Dickinson, C.J. Chang, Aquaporin-3 mediates hydrogen peroxide uptake to regulate downstream intracellular signaling, Proc. Natl. Acad. Sci. USA 107 (36) (2010) 15681–15686.
[37] S.L. Cuddihy, C.C. Winterbourn, M.B. Hampton, Assessment of redox changes to hydrogen peroxide-sensitive proteins during EGF signaling, Antioxid. Redox Signal. 15 (1) (2011) 167–174.
[38] Z.A. Wood, L.B. Poole, R.R. Hantgan, P.A. Karplus, Dimers to doughnuts: redox-sensitive oligomerization of 2-cysteine peroxiredoxins, Biochemistry 41 (17) (2002) 5493–5504.
[39] D. Parsonage, et al., Analysis of the link between enzymatic activity and oligomeric state in AhpC, a bacterial peroxiredoxin, Biochemistry 44 (31) (2005) 10583–10592.
[40] E. Paulo, et al., A genetic approach to study H_2O_2 scavenging in fission yeast—distinct roles of peroxiredoxin and catalase, Mol. Microbiol. 92 (2) (2014) 246–257.
[41] R. Benfeitas, G. Selvaggio, F. Antunes, P.M. Coelho, A. Salvador, Hydrogen peroxide metabolism and sensing in human erythrocytes: a validated kinetic model and reappraisal of the role of peroxiredoxin II, Free Radic. Biol. Med. 74 (2014) 35–49.
[42] R.S. Edgar, et al., Peroxiredoxins are conserved markers of circadian rhythms, Nature 485 (7399) (2012) 459–464.
[43] J.S. O'Neill, et al., Circadian rhythms persist without transcription in a eukaryote, Nature 469 (7331) (2011) 554–558.
[44] J.S. O'Neill, A.B. Reddy, Circadian clocks in human red blood cells, Nature 469 (7331) (2011) 498–503.
[45] V. Pekovic-Vaughan, et al., The circadian clock regulates rhythmic activation of the NRF2/glutathione-mediated antioxidant defense pathway to modulate pulmonary fibrosis, Genes Dev. 28 (6) (2014) 548–560.
[46] C.S. Cho, H.J. Yoon, J.Y. Kim, H.A. Woo, S.G. Rhee, Circadian rhythm of hyperoxidized peroxiredoxin II is determined by hemoglobin autoxidation and the 20S proteasome in red blood cells, Proc. Natl. Acad. Sci. USA 111 (33) (2014) 12043–12048.
[47] T.J. Phalen, et al., Oxidation state governs structural transitions in peroxiredoxin II that correlate with cell cycle arrest and recovery, J. Cell Biol. 175 (5) (2006) 779–789.
[48] B. Turner-Ivey, et al., Role for Prdx1 as a specific sensor in redox-regulated senescence in breast cancer, Oncogene 32 (45) (2013) 5302–5314.
[49] A. Delaunay, A.D. Isnard, M.B. Toledano, H_2O_2 sensing through oxidation of the Yap1 transcription factor, EMBO J. 19 (19) (2000) 5157–5166.
[50] G. Wilkinson, C.E. Rogers, Symbolic description of factorial models for analysis of variance, J. R. Stat. Soc. C—Appl. 22 (3) (1973) 392–399.
[51] Information Theory and An Extension of the Maximum Likelihood Principle, in: H.J. Akaike (Ed.), Akademia Kiado, Budapest, 1973, pp. 267–281.
[52] S. Marguerat, et al., Quantitative analysis of fission yeast transcriptomes and proteomes in proliferating and quiescent cells, Cell 151 (3) (2012) 671–683.
[53] M.A. Oliveira, et al., Insights into the specificity of thioredoxin reductase-thioredoxin interactions. A structural and functional investigation of the yeast thioredoxin system, Biochemistry 49 (15) (2010) 3317–3326.
[54] S. Hoops, et al., COPASI - a COmplex PAthway SImulator, Bioinformatics 22 (24) (2006) 3067–3074.
[55] J.R. Stone, S. Yang, Hydrogen peroxide: a signaling messenger, Antioxid. Redox Signal. 8 (3–4) (2006) 243–270.
[56] D.W. Marquadt, An algorithm for least squares estimation of nonlinear parameters, SIAM J. Algebra Discr. 11 (1963) 431–441.
[57] J. Schaber, Easy parameter identifiability analysis with COPASI, Biosystems 110 (3) (2012) 183–185.